Alkynyltrifluoroborate salts as versatile intermediates for heterocycle synthesis and a new entry into the synthesis of fluoroalkylated (hetero)aromatic compounds

David Lloyd Cousins

A thesis submitted in partial fulfilment of the requirements for the degree of
Doctor of Philosophy

The University of Sheffield
Faculty of Science
Department of Chemistry

September 2021

Abstract

Pyrimidines are amongst the most common heterocycles found in biological systems, they are constituents of nucleic acids and countless other biologically significant molecules, including many pharmaceutical and agrochemical products. They can be prepared by annulation or direct functionalisation of the preformed ring, but stable intermediate pyrimidines bearing organometallic functionality are rare in the literature. Such intermediates allow for potential production of numerous analogous pyrimidines for screening purposes *via* e.g. cross-coupling reactions without the need for a *de novo* synthesis each time.

We addressed this gap in the literature by preparing (amino)pyrimidin-6-yl trifluoroborate salts from the corresponding ynone trifluoroborate salts *via* an operationally simple and chromatography-free condensation procedure. The (amino)pyrimidin-6-yl trifluoroborate salts were amenable to classic boron chemistry at the trifluoroborate unit, including Suzuki-Miyaura cross coupling, oxidation and halodeboronation. In addition, transformations that were orthogonal to the trifluoroborate unit allowed the further elaboration of these intermediates while keeping the boron functionality intact for later derivatisation.

Fluorine is the most abundant halogen found in the Earth's crust. Despite this, organofluorine compounds are almost non-existent in biological systems and are created almost entirely by synthetic methods. Trifluoromethyl (CF_3) – substituted (hetero)aromatic compounds are a privileged substructure in medicinal chemistry and can be accessed by direct (C-H, "innate")) trifluoromethylation or by ("programmed") trifluoromethylation of an in-built functional group such as a halogen or organometallic. Less well-studied are cycloaddition approaches to their preparation, which sidestep limitations in both innate and programmed methods.

We developed a directed cycloaddition approach to fluoroalkyl-substituted (hetero)aromatic compounds that is mild, regiospecific and affords stabilised boronate products that are amenable to further functionalisation. This was achieved by preparing fluoroalkyl-substituted alkynyl trifluoroborate salts and subjecting them to substituted dienes/dipoles in the presence of a Lewis acid promoter. DFT calculations were conducted to investigate further the influence of the CF_3 group on this process.

Acknowledgements

List of abbreviations

AAD   – Acceptorless alcohol dehydrogenation

aHF   – Anhydrous hydrogen fluoride

BDC   – Boron-directed cycloaddition

Cbz   – Carboxybenzyl

ChOH   – Choline hydroxide

DAST   – Diethylaminosulfur trifluoride

DCB   – Dichlorobenzene

DFT   – Density functional theory

DHFR   – Dihydrofolate reductase

DMAD   – Dimethyl acetylenedicarboxylate

FDA   – Food and Drug Administration

F-TEDA   – *N*-Chloromethyl-*N'*-fluorotriethylenediammonium bis(tetrafluoroborate)

HALEX   – Halogen exchange

HFC   – Hydrofluorocarbon

HOMO   – Highest occupied molecular orbital

IEDDA   – Inverse electron demand Diels-Alder

IP   – Ionisation potential

KHMDS   – Potassium hexamethyldisilazide

LCMS   – Liquid chromatography-mass spectrometry

LDA   – Lithium diisopropylamide

LiTMP   – Lithium tetramethylpiperidide

LSF   – Late-stage functionalisation

LUMO   – Lowest unoccupied molecular orbital

MCR   – Multi-component reaction

MIDA   – Methyliminodiacetic acid

MRSA   – Methicillin-resistant Staphylococcus aureus

NBS   – *N*-bromosuccinimide

NCS   – *N*-chlorosuccinimide

NFOBS	–	*N*-fluoro-*o*-benzenedisulfonimide
NFSI	–	*N*-fluorobenzenesulfonimide
NHC	–	*N*-heterocyclic carbene
NMR	–	Nuclear magnetic resonance
PD	–	Pharmacodynamics
PET	–	Positron emission tomography
PK	–	Pharmacokinetics
PPHF	–	Pyridine-poly hydrogen fluoride
S$_E$Ar	–	Electrophilic aromatic substitution
S$_N$Ar	–	Nucleophilic aromatic substitution
TBAF	–	Tetra-*n*-butylammonium fluoride
TEMPO	–	(2,2,6,6-Tetramethylpiperidin-1-yl)oxyl
TES	–	Triethylsilyl
TIPS	–	Triisopropylsilyl
TFAA	–	Trifluoroacetic anhydride
TMEDA	–	Tetramethylethylenediamine
TMS	–	Trimethylsilyl

Declaration

I, the author, confirm that the Thesis is my own work. I am aware of the University's Guidance on the Use of Unfair Means (www.sheffield.ac.uk/ssid/unfair-means). This work has not previously been presented for an award at this, or any other, university.

Publications:

The data presented in chapter one were published here:

-    D. L. Cousins, P. Fricero, K. P. M. Kopf, E. J. McColl, C. Werngard, Y.-H. Lim, J. P. A. Harrity, *Angew. Chem. Int. Ed.*, **2021**, *60*, 9412 – 9415

Contents

Introduction & design of this thesis

The topics covered in this thesis fall into two main sections, each laying out and addressing the synthetic challenges associated with preparing two distinct, important molecular fragments. Both parts, however, fall under the theme of utilising reactions of alkynyl trifluoroborate salts to achieve this. The first section, comprised of **Chapter one**, introduces the importance of pyrimidines as a privileged class of heterocycle that is commonly found in life saving medicines and functional materials. It then goes on to concisely review part of the enormous research effort that has been put into accessing pyrimidines synthetically, covering a diverse range of strategies and exploring the advantages and disadvantages in each case. The Harrity group has recently investigated ynone trifluoroborate salts as powerful intermediates for the synthesis of valuable heterocyclic boronates which can be further functionalised under the right conditions. While investigating this strategy further, we envisaged the use of ynone trifluoroborates as a means to access novel (amino)pyrimidin-6-yl trifluoroborate salts, which might themselves offer a platform for efficient pyrimidine synthesis *via* cross coupling of the boronate moiety. The experimental work in this chapter thus focused on establishing the synthesis of (amino)pyrimidin-6-yl trifluoroborate salts and investigating the scope of this process, followed by an investigation into the capability of these intermediates for downstream functionalisation. An important aspect of the latter experiments was to learn more about the reactivity of the boronate moiety, as this underpins the functionalisation potential of these intermediates and, hence, their ultimate value to synthetic chemistry.

The second section of this thesis, comprised of chapters two and three, focuses on the synthesis of fluorinated small molecules *via* a mild cycloaddition process. **Chapter two** begins with a brief introduction to organofluorine chemistry: its virtually abiotic nature, the discovery of its importance to medicinal chemistry and the subsequent explosion of research interest that has taken it from a marginal pursuit to a vast industry of its own. This chapter then outlines the various ways in which organofluorine compounds can be prepared, from monofluorination, through to fluoroalkylation, then an overview of methods that employ intermediates already laden with fluoroalkyl substituents. The experiments presented come as part of an ongoing investigation in the Harrity group, namely, that of boron-directed cycloadditions which display phenomenally quick reaction times compared to related non-directed cycloadditions and some of the products of which have been investigated as dyes for confocal microscopy. Inspired by the apparent lack of mild cycloaddition routes to fluoroalkyl-substituted aromatic small molecules, we sought to address this gap in the literature by invoking the rate enhancements offered by the boron-directed cycloaddition by choosing, synthesising, and testing suitable fluoroalkyl-substituted precursors. **Chapter three** presents a computational approach to rationalising the disparities in reactivity in the boron-directed cycloaddition for different alkyne substituents, particularly those observed in the experiments presented in the preceding chapter, relating to the incorporation of a trifluoromethyl group in the alkyne starting materials.

Chapter four contains full experimental details for all procedures, alongside characterisation data, beginning with those for the (amino)pyrimidin-6-yl trifluoroborate salts before providing those obtained from directed cycloaddition studies of fluorinated alkynyl trifluoroborate salts.

1. Alkynyltrifluoroborates applied to (amino)pyrimidine synthesis

1.1. Introduction

1.1.1. Early isolation & significant history of pyrimidines
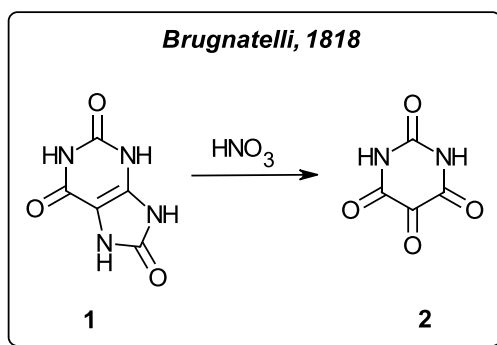
Figure 1: First recorded synthesis of a pyrimidine derivative

The pyrimidine ("m-diazine") ring is one of the oldest known and significant heterocyclic ring structures in organic chemistry, with the earliest isolation dating back to 1818[1] as an article by Luigi Gasper Brugnatelli published in the Italian *Journal of Physics, Chemistry, Natural History, Medicine, and Arts*. Brugnatelli treated uric acid (**1**, figure 1) with nitric acid and obtained a new acidic compound, which he dubbed "erythric acid" **2** due to the red hue it produced upon heating. The compound he isolated was alloxan, which was named by Wöhler[2] and Liebig while investigating the reactions of uric acid further, 20 years later. The discovery of alloxan was followed closely by further synthetic discoveries, such as the synthesis of 2,6-diethyl-5-methyl-4-pyrimidinamine **3** (figure 2) in 1848[3] by Frankland and Kolbe, who treated propionitrile with potassium metal and obtained the organic base which was named Cyanoethine (*Kyanäthin*) at the time due to its cyanoethyl parentage.
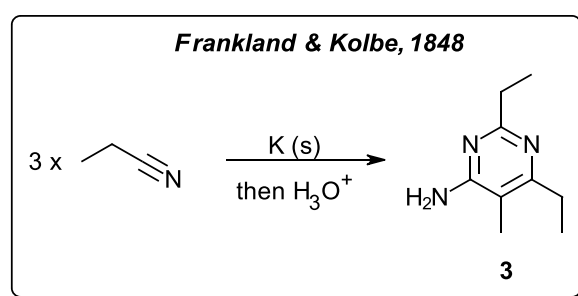
Figure 2: Early pyrimidine synthesis from propionitrile
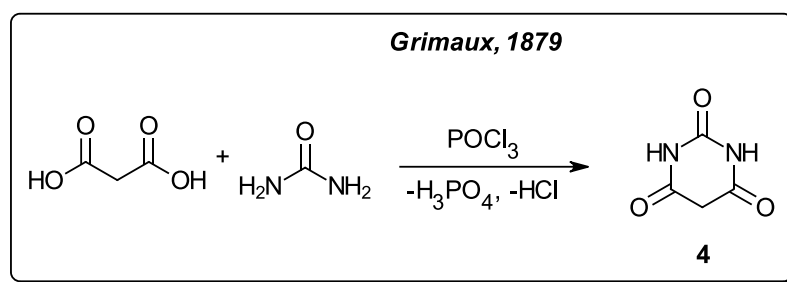
Figure 3: Earliest known example of a Pinner-type pyrimidine synthesis
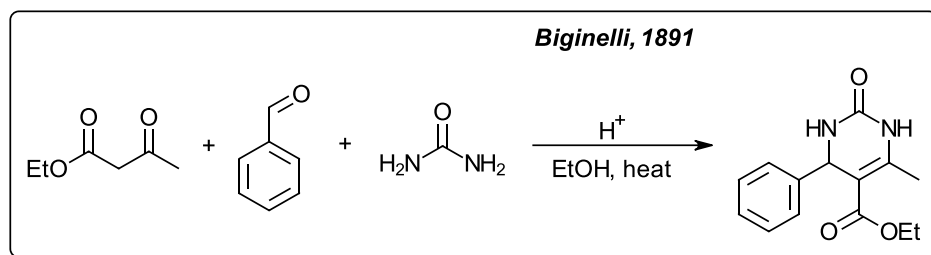
Figure 4: Biginelli's multicomponent pyrimidine synthesis

An important development in the synthesis of pyrimidine derivatives came in 1879, when Grimaux reported[4] a synthesis of barbituric acid (**4**, figure 3) by POCl$_3$-promoted condensation of urea with malonic acid. This pyrimidine formation strategy (N-C-N fragment + C-C-C fragment) is named after Pinner,[5] who proposed the name "pyrimidine" and was the first to appreciate the structure and reactivity of this important class of heterocycle. Soon after these developments, Biginelli reported his game-changing multi component synthesis,[6] comprising a mixture (in one pot) of a 1,3-dicarbonyl, an aldehyde and a urea/thiourea under Brønstead acid catalysis (figure 4). This reaction allowed the facile production of decorated dihydropyrimidinones/thiones from simple precursors, and it has been used and improved on continuously ever since it was discovered.[7–9] Recent reports have offered improvements in the reaction conditions including the development of novel catalysts,[10–12] and the discovery of alternative starting materials.[13] The Biginelli reaction has been used in total synthesis,[14,15] and it is used today as a means to access and develop promising therapeutic targets.[16–18]

1.1.2. Applications of pyrimidines today

Pyrimidines are constituents of nucleic acids and other important biological molecules that are found in abundance in the natural world, perhaps leading them to become convenient starting materials for use in further synthetic transformations and igniting the rich history introduced in the preceding paragraph. The synthesis of pyrimidine derivatives as nucleobases has gathered significant interest in recent years,[19] not just from a synthetic/chemical biology standpoint, but also as a means of understanding how these molecules could have been made abiotically,[20,21] probing life's chemical origins.

Despite a rich history of research, synthetic methods to access pyrimidines are still sought in order to satisfy demand in multiple fields of research and technology. The most common application of research in pyrimidine synthesis is medicinal chemistry. According to a 2014 study,[22] pyrimidines were

the 10th most common heterocycle in FDA approved pharmaceuticals and in 2019, 4 out of the 33 small molecule drugs that gained FDA approval contained a pyrimidine. This figure rose to 8 out of 35 for 2020, demonstrating the continued demand for this privileged substructure.

Pyrimidines are found in drugs and treatments that span a vast range of medical fields,[23–25]including antibiotics, antivirals, antifungals, anticancers, hypnotics, vasodilators and treatments for high cholesterol. One example of the way in which pyrimidine drugs are making a huge difference to lives today, is in the field of antibiotic-resistant infections. The family of antifolate and dihydrofolate reductase (DHFR) inhibiting drugs, consisting of 2,4-diaminopyrimidines, including Brodiprim (figure 5), Iclaprim, Trimethoprim and Pyrimethamine, have provided clinicians with an increased arsenal of antibiotic agents to tackle, for instance, methicillin-resistant Staphylococcus aureus (MRSA) infections. Additional to their ubiquity in the biomedical sciences, pyrimidines have also found numerous applications as building blocks for functional materials, including supramolecular assemblies,[26] non-linear optics[27,28] and organic electronics.[29]
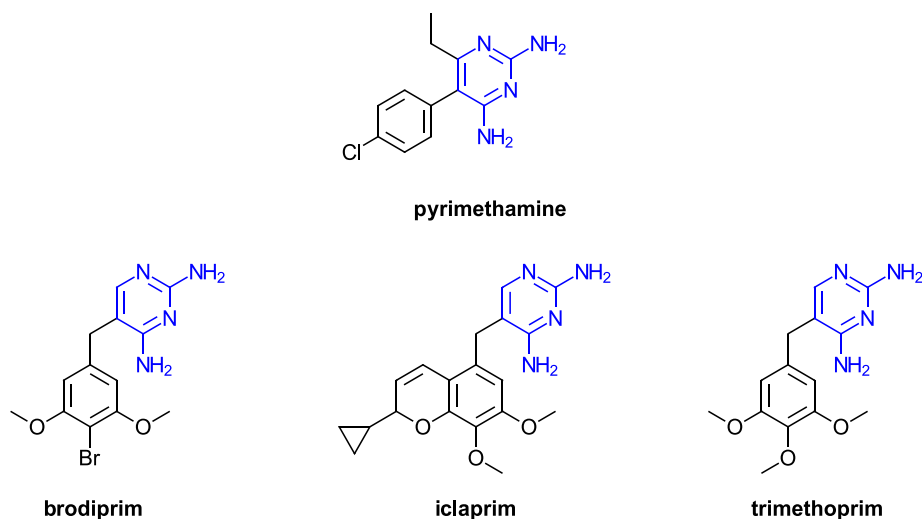
Figure 5: Dihydrofolate reductase-inhibiting (DHFR) antibiotic drugs

Due to the value of the pyrimidine substructure to numerus fields of technology as outlined in the previous section, synthetic studies have seen a proportionate amount of attention and the construction of highly substituted pyrimidine derivatives in an efficient manner is a constantly active area of research.[30–32] In order to concisely introduce the current state-of-the-art in pyrimidine synthesis, this part of the discussion will be separated into two sections: the first being a survey of the methods that have been discovered to construct the pyrimidine ring itself, and the second will deal with the reactivity of various pyrimidines and how this translates into their post-annulative functionalisation potential.

1.1.3. Current methods for pyrimidine ring synthesis

The number of ways to construct the pyrimidine ring from simple or acyclic precursors is commensurate with the amount of research effort, and commercial value, surrounding the product heterocycles. A retrosynthetic analysis such as that shown in figure 6 that represents literature routes to pyrimidines over the years will show that many of the possible strategies have been realised.
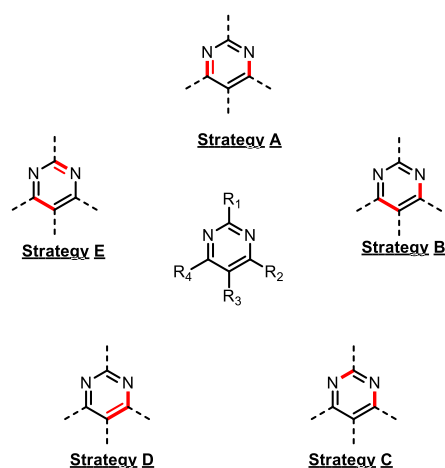
Figure 6: Possible retrosynthetic disconnections towards the pyrimidine ring

The most important route, however, is the Pinner synthesis (strategy A, figure 6). This includes condensation of an amidine with a 1,3-dicarbonyl (or appropriate electrophilic surrogate, *vide infra*) and constitutes the most common method[33,34] ("the principal synthesis")[34] of forming the pyrimidine ring. Recent developments in this type of process have centred[32] on increasing the scope of functional groups that can be attached to the pyrimidine core using the ring synthesis reaction, and increasing the availability or convenience of the precursor materials.

Pinner-type synthesis of pyrimidines ("route A")

While searching for an operationally simple procedure to obtain 2-aryl- and 2-alkylpyrimidines, Wang and Cloudsdale found[35] that by heating the corresponding amidine hydrochloride salt with the stable malondialdehyde surrogate: 1,1,3,3-tetramethoxypropane, in a sealed tube, they could obtain the desired pyrimidine in good yield (figure 7).
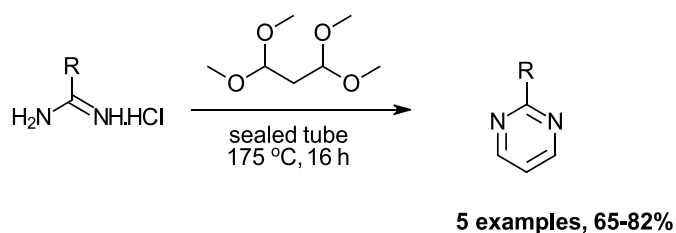
Figure 7: Use of malondialdehyde surrogate in Pinner pyrimidine synthesis

An intriguing class of alternative malondialdehyde surrogates, are vinamidinium salts **5** (figure 8), used in an elegant synthesis of 2,5-disubstituted pyrimidines[36] by condensation with amidines produced *in situ* from the corresponding nitrile. It is a powerful process for the synthesis of 2-alkyl and 2-heteroaryl pyrimidines (arising from reactive nitrile starting materials), but the scope suffers from a lack of electron-rich aryl groups (forming stabilised parent nitriles) in the 2-position and limited diversity in the 5-position (a result of the challenging production of the corresponding vinamidinium salt).
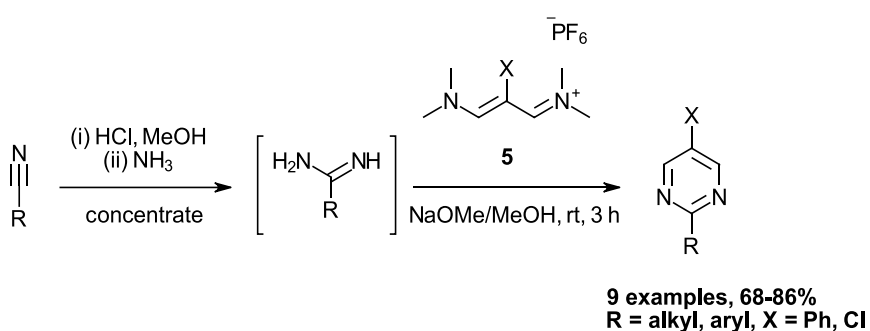
Figure 8: Vinamidinium salts as reactive 1,3-dicarbonyl surrogates

Another highly useful class of 1,3-dicarbonyl surrogates that have been used for Pinner-type pyrimidine syntheses,[37] are enaminones[38] (**6**, figure 9). These intermediates are easy to prepare and are easier to handle than β-ketoaldehyde derivatives. Although not strictly applicable to most Pinner-type reactions, enaminones also provide remarkable regioselectivity enhancements in heterocycle synthesis through amine dislocation or transamination.[39–42] Numerous recent reports of pyrimidine syntheses have utilised similar α,β-unsaturated carbonyl compounds to access highly substituted examples (*vide infra*).
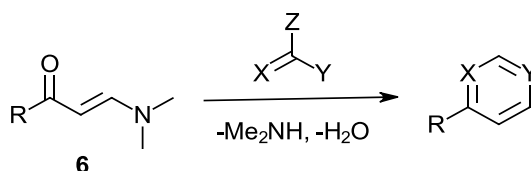
Figure 9: Enaminones as 1,3-dicarbonyl surrogates for heterocycle synthesis

Adapting conditions that efficiently produce quinazolines and quinazolinones from 2-halophenylcarbonyls and amidines,[43] Cho and coworkers showed that β-bromo-α,β-unsaturated ketones **7** (figure 10) can be reacted with amidine hydrochloride salts in the presence of copper powder and a base.[44]
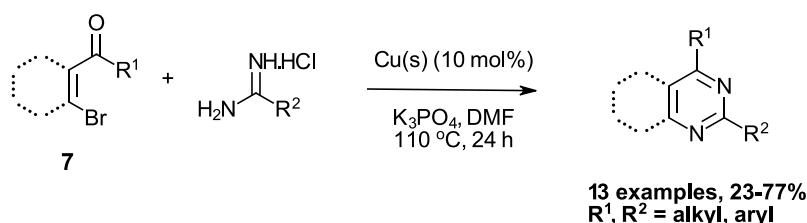
Figure 10: Cu-catalysed synthesis of fully substituted pyrimidines

The reaction is quite general for acetamidine and benzamidine with cyclic precursor ketones, affording the corresponding bicyclic pyrimidines in good yield, however, the yields when acyclic precursor ketones were used were moderate. Another α,β-unsaturated carbonyl class that has been employed recently in the synthesis of pyrimidine derivatives, are β-trichloromethyl-substituted α,β-unsaturated ketones **8** (figure 11) .[45,46] These intermediates react under mild conditions with amidines to afford a range of 2,4-diarylpyrimidines in good to excellent yield.
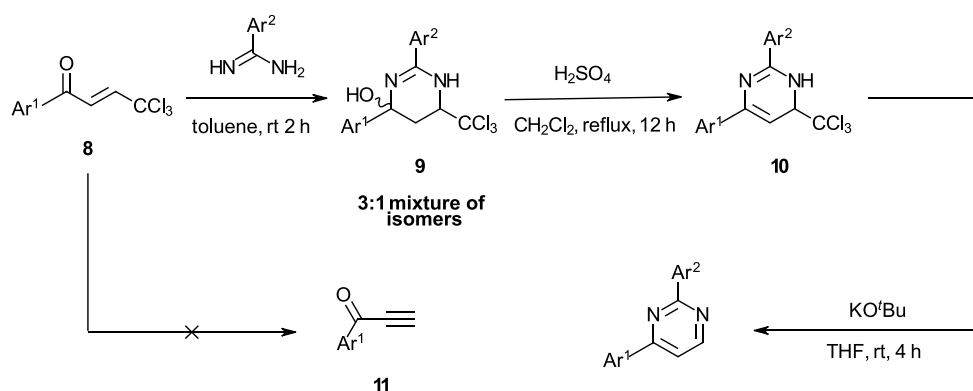
Figure 11: Synthesis of 2,4-disubstituted pyrimidines, using a trichloromethyl leaving group
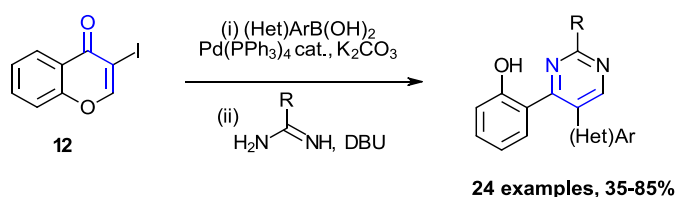
Figure 12: One-pot tandem Suzuki-condensation procedure for the synthesis of 2,4,6-trisubstituted pyrimidines

The isolation of intermediates **9** and **10** rule out a pre-cyclisation elimination of chloroform in the reaction mechanism, that would otherwise form the terminal ynone **11**.

A report describing the synthesis of the alternative 4,5-diarylpyrimidines utilises easily obtainable 3-iodochromone **12** (figure 12), in a tandem Suzuki-Miyaura/condensation process.[47] An extensive family of 2,4,5-trisubstituted (amino)pyrimidines were synthesised in a one-pot process and after minor modifications, were evaluated for inhibition against the human hepatocellular carcinoma BEL-7402 cancer cell line. A similar (acyclic) intermediate, β-*n*-butoxyenone **13** (figure 13) was synthesised by Skrydstrup and co-workers by a carbonylative Heck reaction[48] and was shown to react smoothly with benzamidine hydrochloride under mild conditions to afford the pyrimidine **14** in excellent yield.
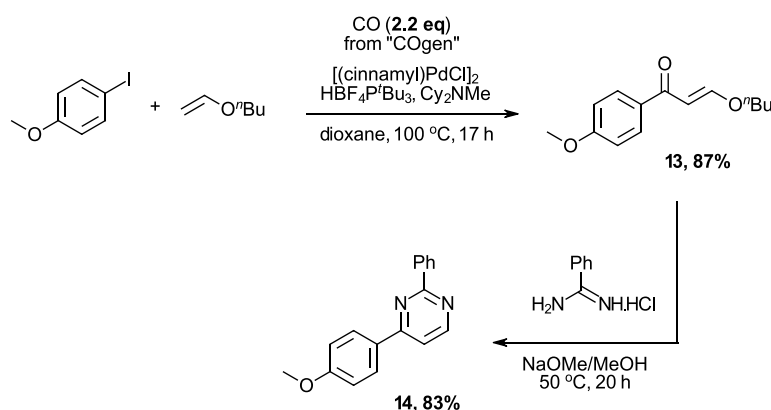
Figure 13: Carbonylative Heck reaction towards an α,β-unsaturated carbonyl compound for pyrimidine synthesis

An interesting way to access β-*n*-alkoxyenones for pyrimidine synthesis from saturated 3-ethoxycyclobutanones **15** (figure 14) was published recently by Song and coworkers.[49] The β-ethoxyenone **16** is released upon the Lewis acidic action of $BF_3.Et_2O$, which can then undergo a transamination-type process, leading to the enamine **17**, which may condense rapidly to the corresponding pyrimidine. Alternatively, the amidine may first react with the cyclobutanone (activated carbonyl), forming imine **18**, which is broken down under Lewis acidic conditions to intermediate **19**. This intermediate could feasibly produce the pyrimidine directly by trapping of a transient oxocarbenium by the second amidine nitrogen.
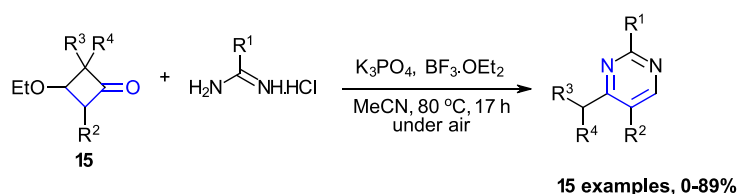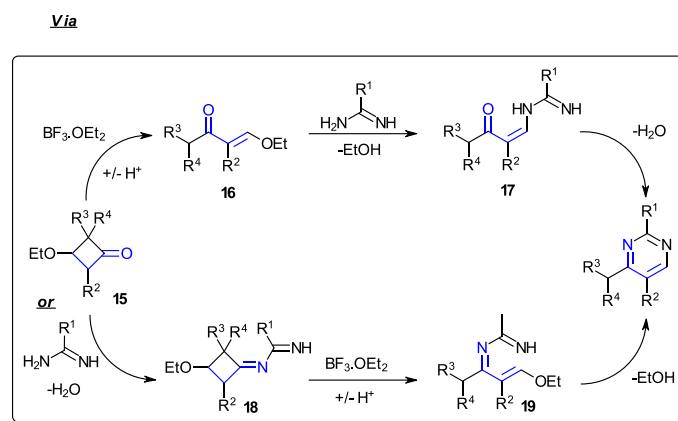
Figure 14: Lewis acid-mediated C-C bond cleavage of cyclobutanones towards pyrimidine precursors

Proton transfer and elimination of EtOH then provides the desired pyrimidine. Another important aspect of the Pinner synthesis that was realised recently by Dominguez and coworkers,[50] is that accessing pyrimidinols/pyrimidinones **21** (figure 15) by reacting β-ketoesters **20** instead of diketones/dialdehydes with amidines *via* sonication of the reaction mixture provides, through subsequent activation, a useful synthetic handle that can be transformed into a phenyl ring *via* e.g. cross coupling.

This strategy of transforming easily obtainable pyrimidinones ("pyrimidinols") and quinazolinones into the corresponding tosylate and performing catalytic reactions has been found to be applicable to: Suzuki-Miyaura cross coupling,[51–53] Kumada cross coupling,[54] Sonogashira cross coupling,[52] and C-H activation.[55]
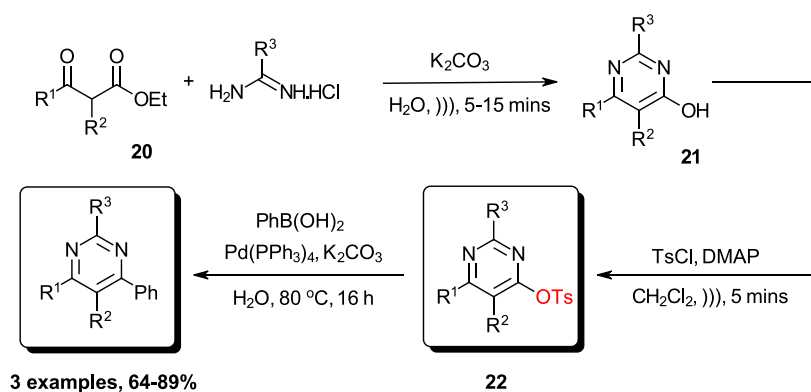
Figure 15: Transformation of pyrimidinone oxygen into useful handle for further synthesis

The final example of unsaturated β-dicarbonyl surrogates that have been exploited in pyrimidine synthesis to be presented in this section, are the highly versatile, and emerging,[56] α,β-acetylenic carbonyl compounds (ynones **23**, for the corresponding ketone, figure 16). There are numerous ways of making ynones, but the forging of the carbonyl-acetylene bond via a catalytic cross coupling reactions is among the most efficient.
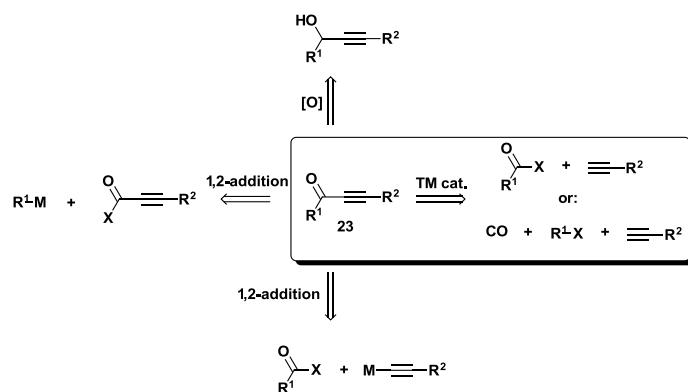
Figure 16: Summary of methods to obtain ynones, with the oxidant/harsh organometallic free catalytic method highlighted

This strategy of ynone synthesis represents one of the oldest applications of the Sonogashira reaction,[57,58] but was only recently used in an efficient (including the use of stoichiometric amounts of Et$_3$N, rather than as the reaction solvent) one-pot procedure to prepare pyrimidines by Müller *et al*. (figure 17).[59,60]
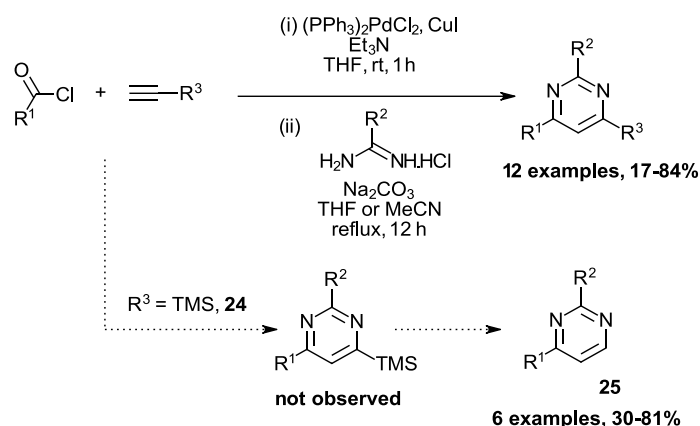
Figure 17: Catalytic access to ynones for pyrimidine synthesis

This procedure proved to be quite general, allowing the introduction of aliphatic, aromatic and heteroaromatic side chains in the resulting pyrimidine from every reaction component (acid chloride, terminal alkyne and amidine hydrochloride salt). Heteroatoms could also be incorporated *via* the use of *S*-methylisothiouronium chloride and guanidinium chloride in the ultimate cyclocondensation step. The products were obtained in moderate to excellent yields after purification. A noteworthy observation that was made by the authors was that when ethynyltrimethylsilane **24** (figure 17) was used in this one-pot procedure, the product that was obtained was the protodesilylated pyrimidine **25**. This procedure was extended to produce a small family of 2,4-disubstituted pyrimidines, which were obtained in moderate to very good yield.

An improved catalytic synthesis of ynones towards functionalised pyrimidines involves a carbonylative cross coupling between an aryl halide and a terminal alkyne. This avoids the need to prepare moisture sensitive acid chlorides and thus could improve the functional group tolerance and operational simplicity of the process. Carbon monoxide gas is commonly used as the carbonyl source in this type of process, such as that published by Feher and coworkers[61], where ferrocenyl pyrimidines **26** (figure 18) were prepared from ferrocenyl iodides *via* the carbonylative cross coupling procedure, followed by condensation with an amidine or guanidine.
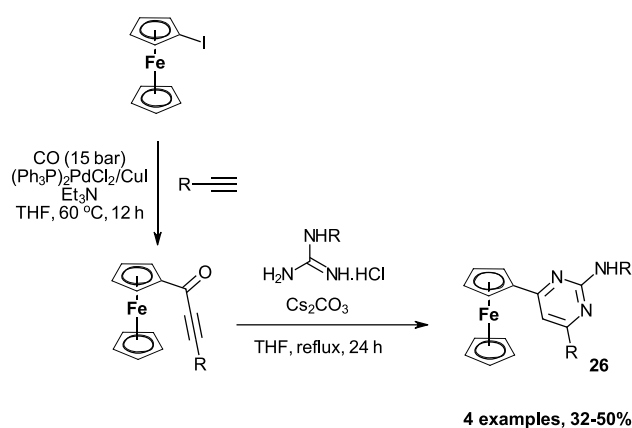
Figure 18: Preparation of ferrocenyl pyrimidines from the corresponding ynones

Alternatives to CO gas have been sought for carbonylative couplings in recent years, owing to the inherent toxicity and the potential requirement for special equipment in using the gas. Stonehouse and co-workers employed $Mo(CO)_6$ as the CO source for a related reaction,[62] which was successful in producing the desired pyrimidines by condensation of the intermediate ynone with amidines. However, the one-pot process was not amenable to the production of 2-aminopyrimidines or pyrimidin-2-ones *via* reaction with guanidine or urea, respectively. An important recent development in this chemistry came with the design of the CO generator molecule, COgen by Skrydstrup and co-workers. This commercially available and safe reagent was applied to the synthesis of ^{13}C labelled pyrimidine derivatives **27** (figure 19) by carbonylative cross coupling, using the ^{13}COgen reagent, followed by condensation with benzamidine.[63]

An interesting alternative to carbonylative production of ynone intermediates for pyrimidine synthesis was explored in a 2011 publication by Müller and co-workers.[64] Exploiting the nucleophilicity of azulenes **28** (figure 20), a glyoxyl chloride group was inserted at the 5-membered ring using oxalyl chloride to produce the corresponding glyoxalyl chloride derivatives **29**. These intermediates were subsequently found to undergo smooth decarbonylative alkynylation under Pd-catalysis to provide the ynone intermediates **30**, which could be transformed into pyrimidines by cyclocondensation with the appropriate amidine. This one-pot, four-component procedure was able to provide a range of disubstituted azulenylpyrimidines in moderate to good yield.
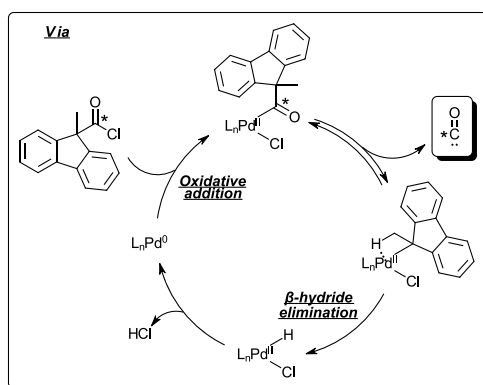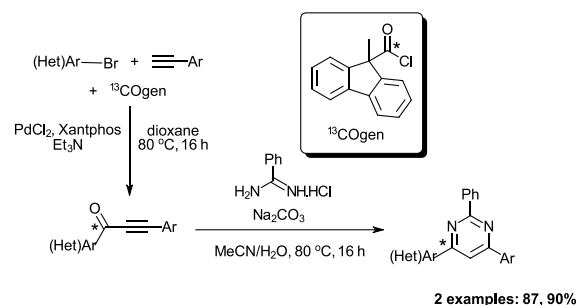
Figure 19: Synthesis of 13C-labelled pyrimidines via carbonylative Sonogashira cross coupling
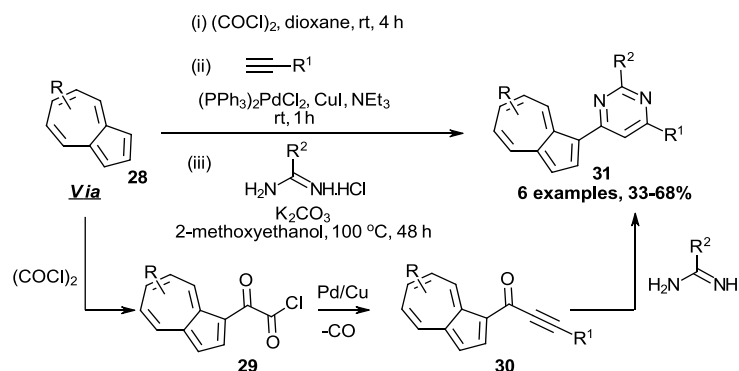
Figure 20: Preparation of azulenyl pyrimidines via decarbonylative cross coupling

Gevorgyan and co-workers discovered an elegant method to regioselectively produce a TIPS-alkyne substituted pyrimidine **34** (figure 21) from the 2,3,4,5-diynone **33**,[65] which was obtained by gold-catalysed *O*-transposition in the parent skipped diynone **32**. Pyrimidines bearing an acetal-protected aldehyde in the 4-position (**35** and **36**, figure 22) can be synthesised by reacting the acetal-substituted ynone with an amidine or guanidine. The acetal can be situated adjacent to the carbonyl[66,67] or attached directly to the alkyne.[68]
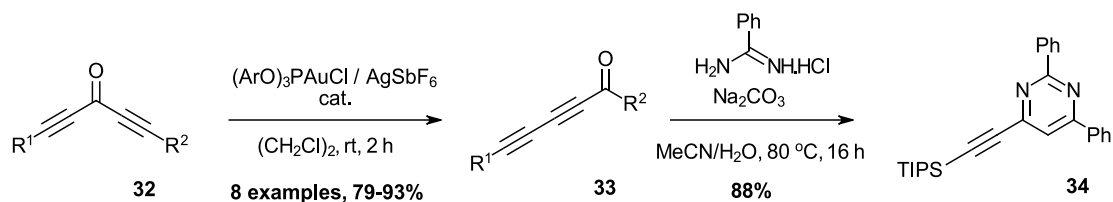
Figure 21:Preparation of a TIPS-alkyne substituted pyrimidine from a diynone
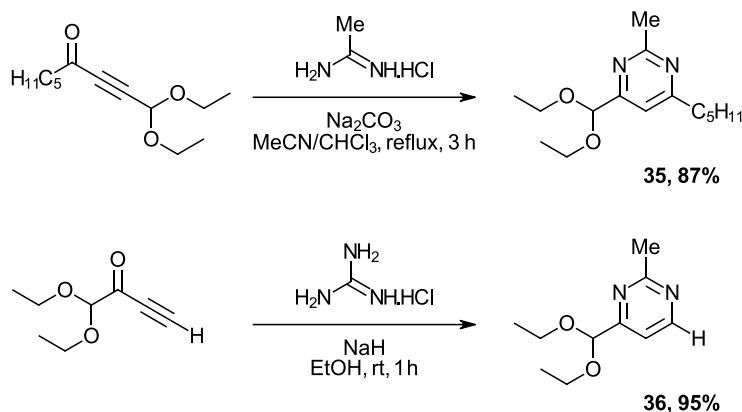
Figure 22: Preparation of pyrimidines with protected aldehyde substituents

Although not strictly a strategy A pyrimidine synthesis, Campagne *et al.* discovered that Cbz-protected propargylic hydroxylamines **37** (figure 23) could be transformed efficiently into the corresponding Cbz-β-enaminones **38** by a base-catalysed isomerisation.[69] These intermediates reacted with aromatic, heteroaromatic and also aliphatic amides in the presence of ^{t}BuOK to afford the expected pyrimidine product in good to excellent yield. Even acrylamide was a successful reaction partner (provided TEMPO was present as a polymerisation inhibitor/retarder), providing the corresponding 2-vinylpyrimidines in good yield. Interestingly, the unprotected β-enaminone (no Cbz group) did not produce any of the pyrimidine **39**. The authors suggest that final aromatisation of the pyrimidine may be facilitated by the elimination of Cbz-OH (rather than H_2O), by analogy to that proposed by Takai *et al.*[70] (potentially *via* the oxazetidine **40**) who were using similar systems to access pyridines.
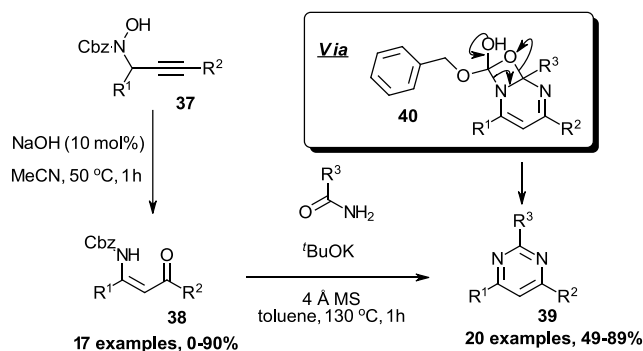
Figure 23: Synthesis of trisubstituted pyrimidines from Cbz-enaminones

Oxidative Pinner-type reactions based on saturated starting materials

Pinner 1,3-dicarbonyl surrogates need not begin at the required degree of saturation, provided that the means to produce them *in situ* are present. For instance, Bagley and co-workers have shown[71,72] that pyrimidines could be prepared from an oxidative procedure using the corresponding ynol **41** (figure 24) and an amidine, in the presence of a suitable oxidant (IBX,[71] MnO$_2$[71] or BaMnO$_4$[72]) under microwave irradiation. Overall, the optimised (BaMnO$_4$ promoted) reaction demonstrated a promising scope of tolerable aryl/heteroaryl side chains, however no aliphatic examples were shown. The potential of the principle of oxidising to the required Pinner intermediate *in situ* is an attractive prospect, and several oxidative Pinner pyrimidine syntheses have been published since.[32] Cai and co-workers demonstrated[73] that the same transformation (figure 25) could be carried out aerobically using a catalytic quantity of transition metal or post-transition metal Lewis acid. The catalyst that provided the desired pyrimidine in the highest yield was Cu(OTf)$_2$ (20 mol%) and the procedure was able to produce a range of aryl-, heteroaryl- and alkenyl- substituted pyrimidines in good yield however, the methyl substituted ynol (R^1=Me) failed to produce any of the expected product, presumably due to the high oxidation potential of the penultimate 1,6-dihydropyrimidine **46**, compared to the other successful substrates.
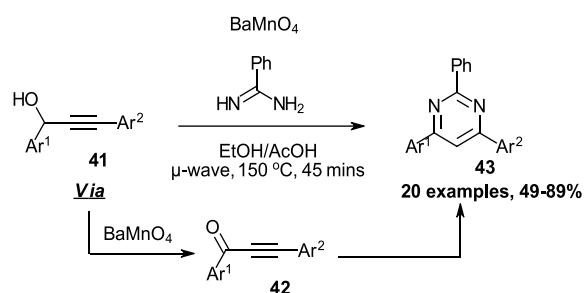
Figure 24: Oxidative pyrimidine synthesis starting from propargyl alcohols
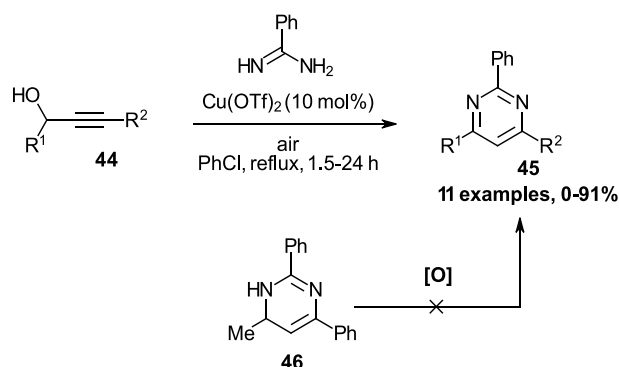
Figure 25: Catalytic aerobic synthesis of pyrimidines from propargylic alcohols

1,6-Dihydropyrimidines bearing aryl groups at the 6-position can be oxidised aerobically, this led to a series of papers demonstrating that pyrimidines could be produced from chalcone or cinnamaldehyde derivatives, under an air or O$_2$ atmosphere. Guo investigated the feasibility of this process, using an atmosphere of O$_2$ as the terminal oxidant (figure 26).[74] The reaction conditions were tolerated by an extensive range of cinnamaldehyde derivatives **47** and one chalcone (Ar = Ph, R^1 = H, R^2 = Ph, R^3 = Ph),
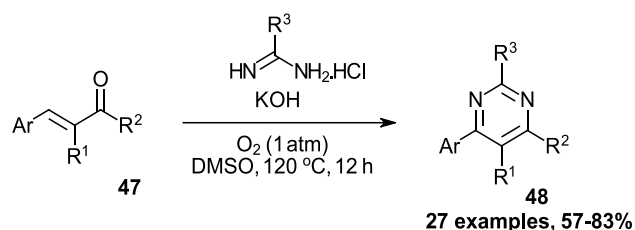
Figure 26: Aerobic pyrimidine synthesis starting from cinnamaldehyde and chalcone derivatives
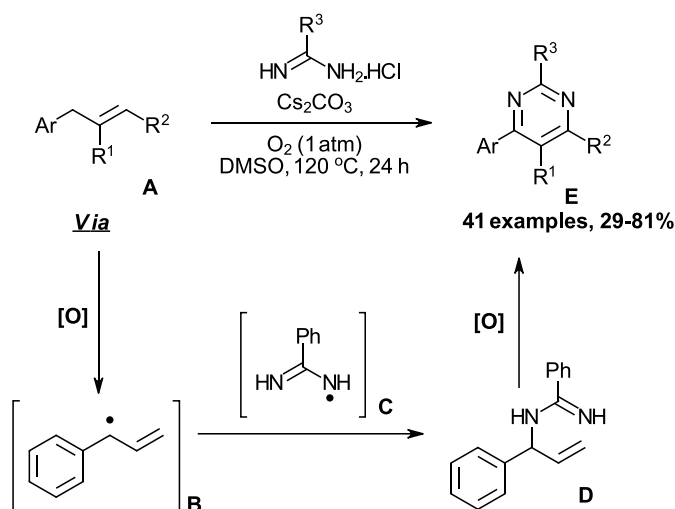
Figure 27: Aerobic pyrimidine synthesis starting from simple allylic compounds

producing di- or tri-substituted pyrimidines in good to excellent yield. The only alkyl substituents that were tolerated could be incorporated in the 2- and 5-positions. A more recent report by Jiang *et al.*[75] shows that a simple allyl fragment **A** (figure 27) can act as the 1,3-dicarbonyl surrogate in pyrimidine synthesis under an atmosphere of O_2. Control experiments suggest that the allyl radical that is formed by oxidation of **A** is trapped directly by an amidine species, such as the radical **C** forming the intermediate **D**, as opposed to initial oxygenation followed by amidine condensation. A set of reaction conditions using chalcones and aerobic oxygen, instead of a pure O_2 atmosphere, was published by Chaskar and co-workers (figure 28).[76] The reaction is promoted by choline hydroxide (ChOH), which is also used as the reaction solvent. Numerous aryl-substituted pyrimidines were successfully prepared but notably alkyl-substituted pyrimidines **51** and **52** were also prepared in excellent yield, suggesting that the ChOH plays a role in lowering the oxidation potential of the less reactive aliphatic 1,6-dihydropyrimidine intermediates.
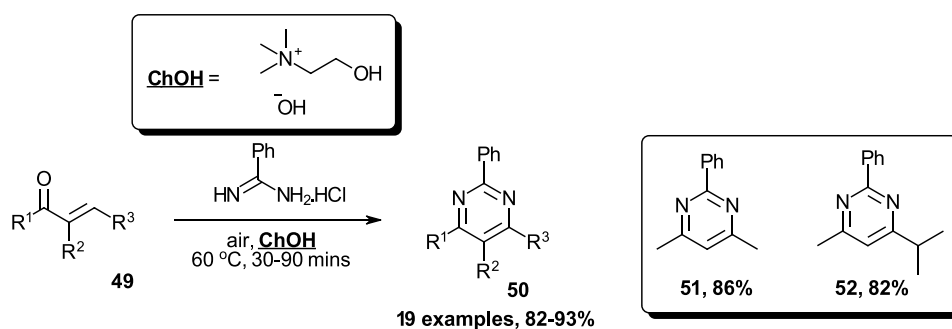
Figure 28: Aerobic pyrimidine synthesis, showing notable alkyl-substituted products

More recently, a report that uses propiophenones as reduced Pinner intermediates for pyrimidine synthesis[77] (figure 29) has been published. This procedure demonstrates a very extensive scope and functional group tolerance, including numerous aliphatic substituents that can decorate the product pyrimidine. The reaction is proposed to proceed *via* Cu-catalysed α-oxidation of the propiophenone, followed by elimination of TEMPO-H, providing the key chalcone **57**, which reacts quickly with the added amidine in a manner similar to that described above. The reaction temperature is rather high, but to start from such an inactive precursor as propiophenone is a highly desirable outcome in terms of starting material accessibility and represents a significant leap forward in the field of pyrimidine synthesis. A similar, iron-catalysed process has since been published by Han and co-workers.[78] A yet more attractive, recently developed Pinner-type synthetic strategy towards pyrimidine derivatives would be to assemble the carbon backbone *in situ* from simple building blocks in a multi-component reaction (MCR),[79–81] where the fragments that make up the 1,3-dicarbonyl surrogate are sequentially connected and the intermediate is raised to the required degree of unsaturation by a series of oxidative processes. The oxidised intermediate chalcone would then react with an amidine or guanidine, affording the desired pyrimidine as described above. A crucial development towards this goal came in 2015, when Kempe and co-workers invoked the versatile general oxidative ability of iridium catalysis[82] in an acceptorless alcohol dehydrogenative (AAD)[83] MCR involving 3 components towards trisubstituted pyrimidines, and 4 components towards tetrasubstituted pyrimidines (figure 30).[84]
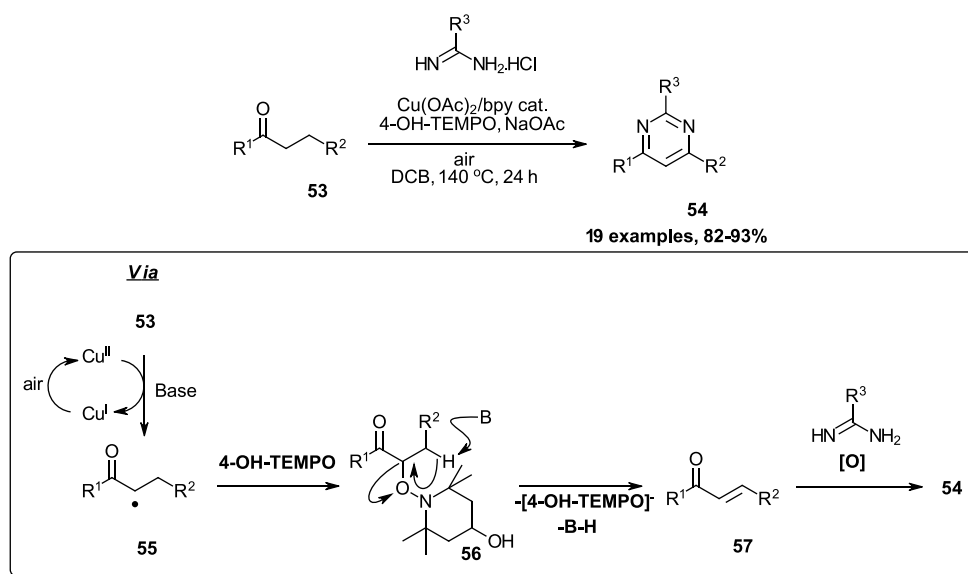
Figure 29: Aerobic pyrimidine synthesis starting from propiophenones

16

Since this report, numerous variations and improvements to this kind of process have been disclosed. Different transition- and post transition metal catalysts have been found to catalyse the dehydrogenative coupling of acetophenones and aldehydes for pyrimidine synthesis, including catalysts based on: Ru,[85,86] Pt,[87] Mn,[88,89] Re,[90] Cu,[91] Fe[92] and Ni.[93,94] These processes are efficient and allow the product pyrimidines to be isolated in good yields, showing good functional group tolerance and promising scope. The recent use of Earth-abundant Fe and Ni catalysts increases the value of these reactions and through experimentation of altering metal/ligand combinations, a promising reduction in the required temperature to 80 °C was realised.[94]
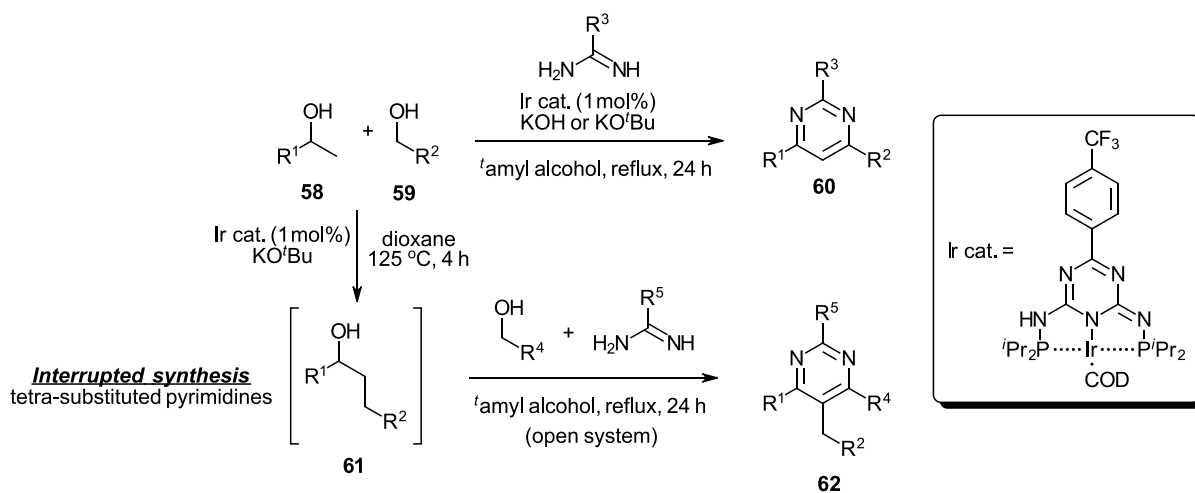
Figure 30: Ir-catalysed MCR synthesis of pyrimidines from alcohol precursors

Other oxidative Pinner syntheses

An interesting preparation of 2,4-diphenylpyrimidine from a propargylamine and benzamidine (figure 31) was reported by Starr and co-workers.[95] The propargylamine is transformed into an enaminone intermediate *via* oxidative rearrangement to the isoxazolinium intermediate, which then undergoes base-mediated N-O cleavage. Only one pyrimidine example was presented in the report but based on the efficient production of the key enaminone intermediate, this one-pot procedure is expected to be more generally applicable.
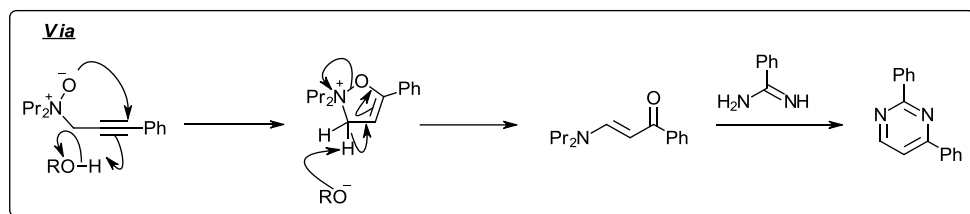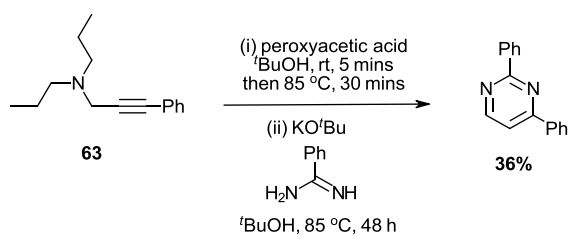
Figure 31: Oxidative rearrangement of porpargylamine towards 2,4-diphenylpyrimidine

Non-Pinner pyrimidine synthesis *via* strategy A, cycloaddition approach

In 2011, Boger *et al.* discovered that 1,2,3-triazines **64** (figure 32) underwent an extremely efficient inverse-electron-demand [4+2] cycloaddition with amidines, affording pyrimidines after elimination of nitrogen gas.[96] Imidates **66** were also amenable to the reaction conditions, providing the same pyrimidine product. This provides evidence for the mechanism of [4+2] cycloaddition, followed by elimination of NH_2/OR, however the temperature required for imidate cycloadditions was significantly higher than it was for amidines. A series of publications by Boger *et al.* followed,[96–99] including a systematic study of the effect that C-5 substitutents on the 1,2,3-triazine had on the rate of the [4+2] cycloaddition.[96]
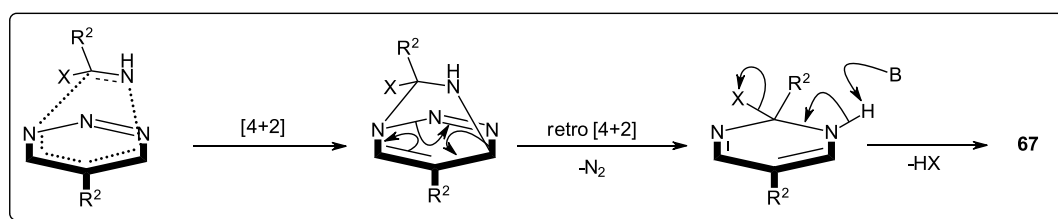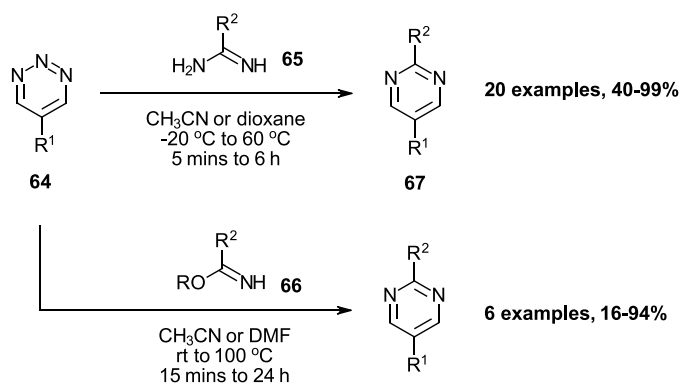
Figure 32: Cycloaddition approach to pyrimidine synthesis

In general, stronger electron-withdrawing substituents accelerated the reaction rate compared with less withdrawing examples, as is expected for an inverse-electron-demand Diels-Alder cycloaddition. 1,2,3-Triazines with ester substituents at C-4/C-6 were obtained in a subsequent publication[99] and found to undergo smooth cycloadditions at room temperature with amidines to afford the desired pyrimidines in moderate to excellent yields. A family of 1,2,3-triazines bearing electron-donating substituents (-SR, -OR, -NHAc) at C-5 were then prepared[97] and reacted with amidines, affording the corresponding pyrimidines in moderate to excellent yield albeit under slightly more forcing conditions. This chemistry has also been applied to the total synthesis of the pyrimidine subunit of the important anticancer agent Bleomycin A_2 (figure 33),[98] demonstrating the usefulness and functional group tolerance of this process. More recently, 5-nitro-1,2,3-triazine has been prepared and shown to undergo an extremely rapid cycloaddition with aryl-, heteroaryl- and alkylamidines at room temperature.[100]
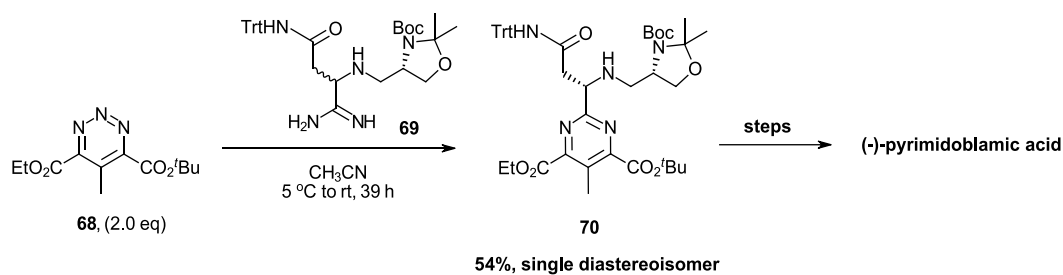
Figure 33: Cycloaddition of 1,2,3-triazine with amidine in the total synthesis of pyrimidoblamic acid

Pyrimidine synthesis *via* strategy B

An example of a pyrimidine synthesis following strategy B (figure 6) was disclosed by Muchowski and coworkers[101] (also separately, at a slightly earlier date by Ibnusaud and coworkers)[102] who found that isolable 1,3-diaza-1,3-butadienes **71** (figure 34) underwent a [4+2] cycloaddition with electron deficient alkynes, such as dimethylacetylenedicarboxylate (DMAD) and propiolate esters. After subsequent elimination of dimethylamine, the corresponding pyrimidine products could be obtained in moderate to excellent yield. DMAD underwent the most efficient cycloaddition in most cases, allowing the reaction to proceed at room temperature. The scope of this process was investigated further in a separate report,[103] demonstrating the usefulness of this reaction to obtain a range of fully functionalised pyrimidines, albeit in modest yields for some examples.
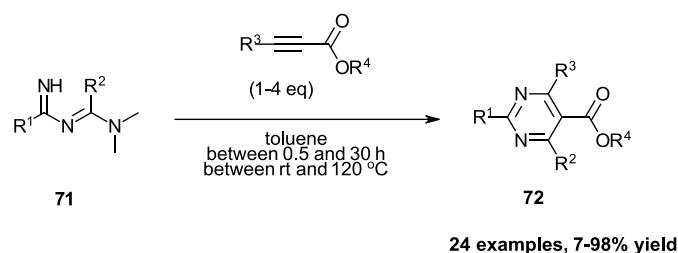
Figure 34: Alkyne cycloaddition approach to pyrimidines via disconnection strategy B
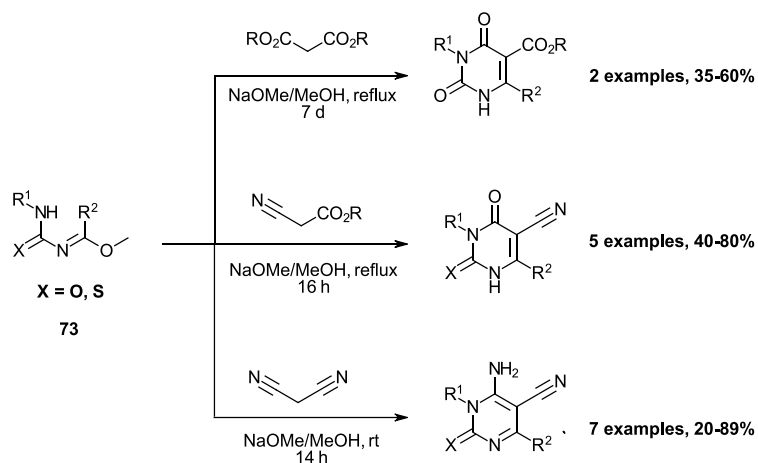
Figure 35: Condensation of N-amino(thio)carbonyl imidates with malonic acid derivatives towards pyrimidin(thi)ones

An example of pyrimidin-2-one synthesis *via* strategy B was realised by Krechl *et al.*,[104] who found that isolable *N*-amino(thio)carbonyl imidates **73** (figure 35) could function as the CNCN fragment for this strategy in condensation reactions with malonic acid derivatives including malonitrile, α-nitrile esters and malonic esters. This reaction allowed the isolation of a range of diversely substituted pyrimidinones, pyrimidin-diones, aminopyrimidinones and pyrimidin-thiones in moderate to excellent yield. However, the reactions often required extended periods of heating to reach high conversion. Nitriles are highly important precursors to pyrimidines and are often the source of one or more of the ring nitrogen atoms, not least as they are the precursors to amidines *via* the Pinner reaction.[105] A method to synthesise pyrimidines from nitriles and ketones/esters *via* strategy B was published by Martinez and co-workers, who utilised the Lewis acidity of trifluoromethanesulfonic anhydride (Tf$_2$O) to activate the carbonyl compounds **74** and **76** (figure 36) which reacted with 2 equivalents of a carbonitrile to form the corresponding 2,4,6-trisubstituted or 2,4,5,6-tetrasubstituted pyrimidines.[106]
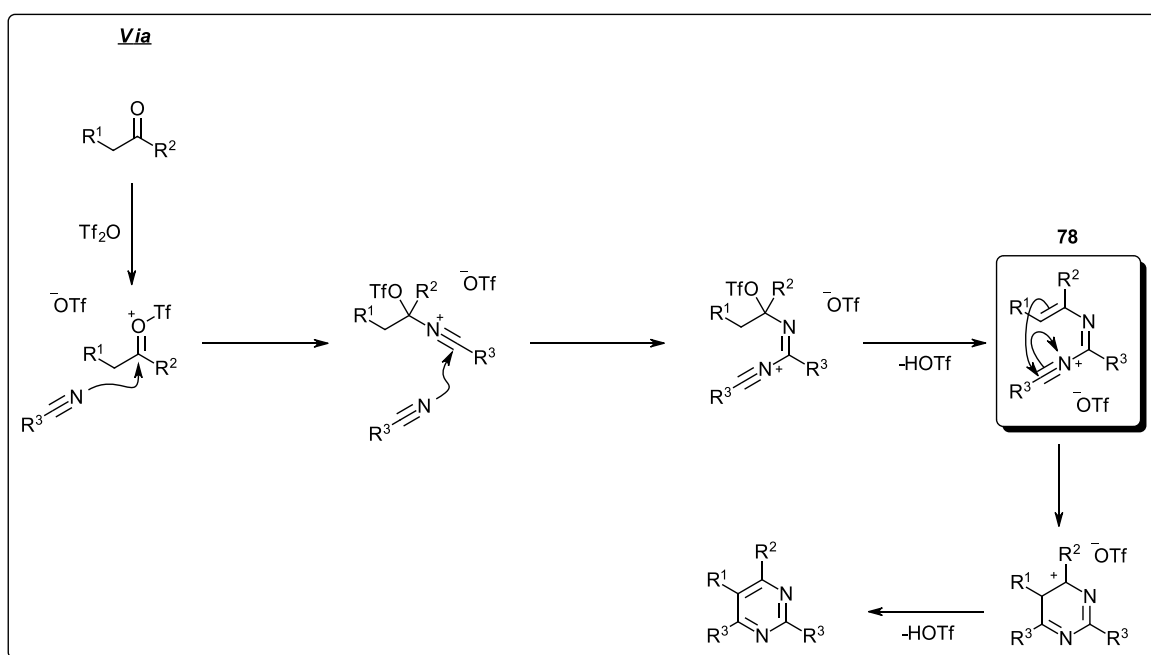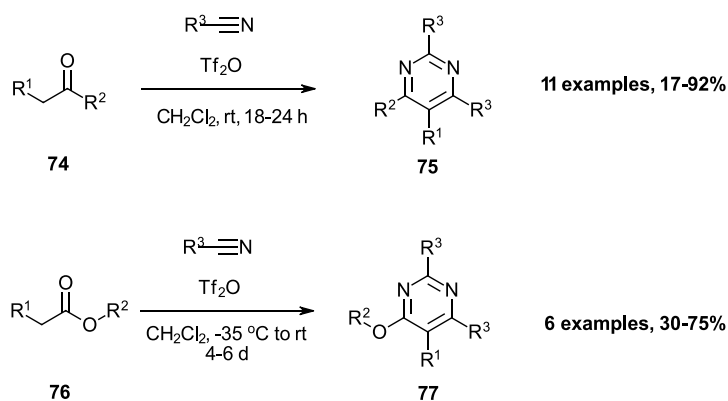
Figure 36: Lewis acid mediated synthesis of pyrimidines from ketones/esters and nitriles

The use of such a chemically powerful reagent as Tf_2O allowed the reaction to proceed efficiently at room temperature, providing a fair range of highly substituted pyrimidines in moderate to good yield. Notable in this study was the ability to produce alkoxypyrimidines upon the use of the corresponding ester, allowing a potential handle for further functionalisation. The reaction is believed to occur in a stepwise fashion, forming the nitrilium-type compound **78** after Lewis acid-mediated addition of two equivalents of nitrile.

Another efficient cycloaddition approach to pyrimidine synthesis *via* strategy B was realised by Neunhoeffer and Bachmann,[107] who discovered that 1,3,5-triazines acted as effective dienes that undergo [4+2] cycloadditions with ynamines and enamines, providing the expected pyrimidine regioselectively after elimination of HCN and the amine. The scope of this process was subsequently expanded by Boger et al.,[108] and an organocatalytic variant was disclosed recently by Wang and co-workers, allowing the process to begin from easily handled ketones (figure 37).[109]
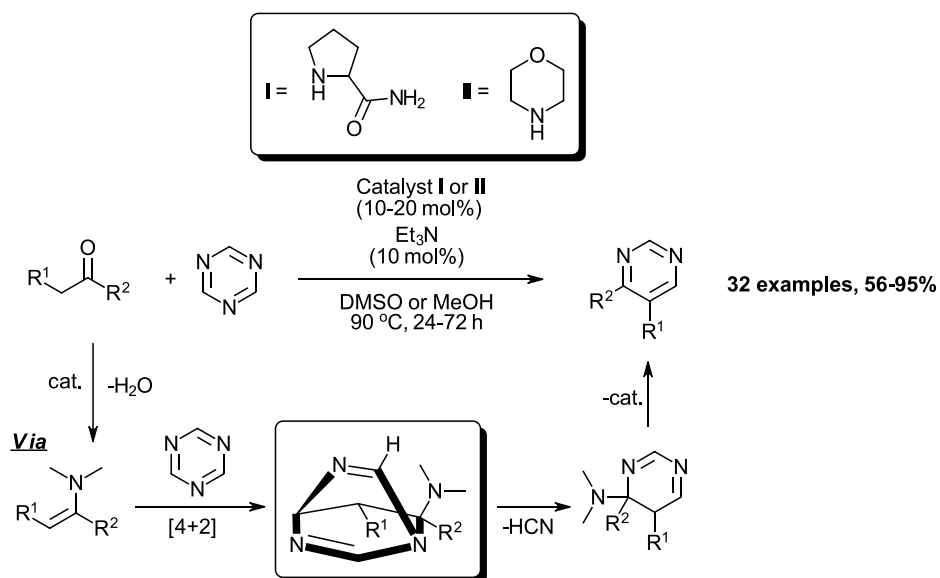
Figure 37: Organocatalytic synthesis of 4,5-disubstituted pyrimidines from ketones and 1,3,5-triazine

Pyrimidine synthesis *via* strategy C

An interesting procedure for obtaining 1,4-disubstituted pyrimidinones and pyrimidin-thiones from unsaturated thioamides and iso(thio)cyanates respectively, was developed by Deniaud and co-workers (figure 38).[110] The thioamide is first converted to the *S*-methyldiazadienium iodide salt **79**, then it is reacted with an isocyanate or isothiocyanate, which produces a molecule of Me$_2$NH. Formation of the urea **85** by the rapid reaction of *in situ* generated Me$_2$NH with the isocyanate was dealt with by using two equivalents of RNCO/RNCS. The reaction worked well for aromatic iso(thio)cyanates and aliphatic isothiocyanates, forming the corresponding pyrimidinones in good to excellent yield. However, when alkyl isocyanates were used under the same conditions, the intermediate adduct did not cyclise to the desired pyrimidinone. A second, NaH-mediated cyclisation step was adapted for these substrates to afford the alkyl-substituted pyrimidinones **84** from the acyclic species **83** in good yield. In the case of methyl isocyanate, the corresponding (commercially available) methyl isothiocyanate was employed to avoid the former's toxicity. The pyrimidin-thione **81** was obtained *via* the usual method, then it was transformed to the desired *O*-derivative **82** efficiently in 54% yield over two steps.
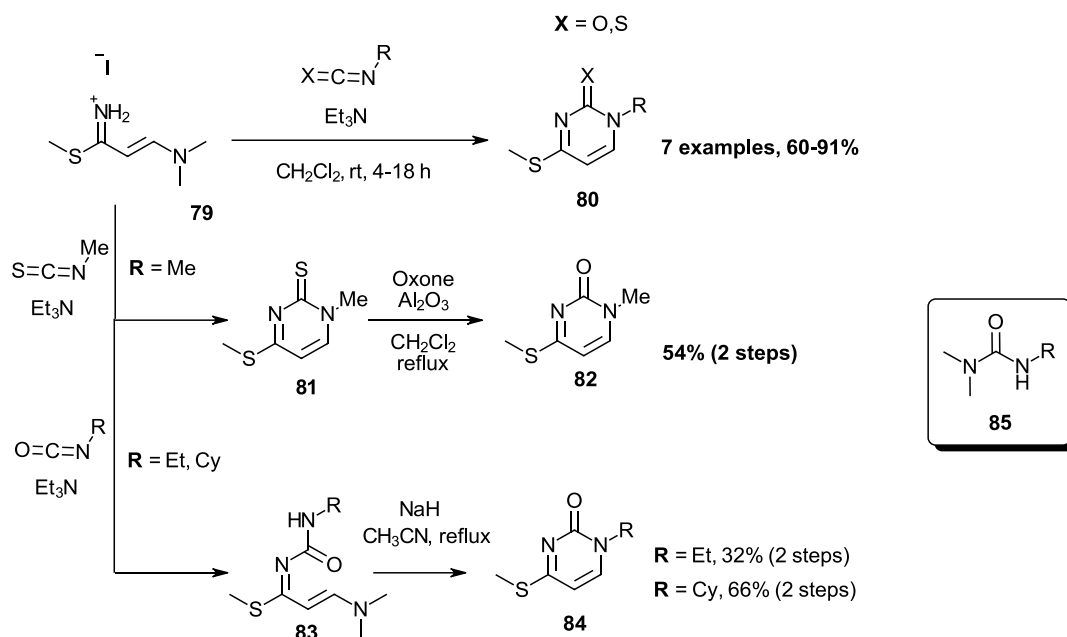
Figure 38: Synthesis of pyrimidinones and pyrimidinethiones from diazadienium iodides and iso(thio)cyanates:

Pyrimidine synthesis via strategy D
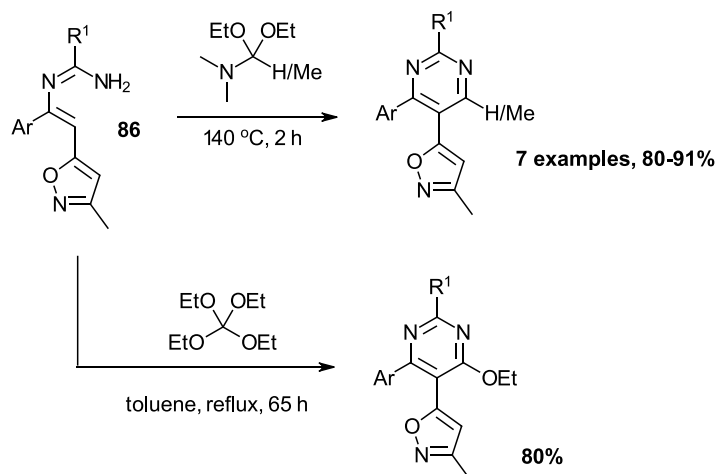
Figure 39: Condensation of olefinic amidines with orthoesters and formamides towards pyrimidines

Strategy D comprises one of the less well-studied approaches to pyrimidine synthesis, due to the exotic nature of the CCNCN fragment that is required. Nevertheless, Sakai *et al.* accessed olefinic amidines **86** (figure 39) to fit this purpose and published an efficient method to access pyrimidines by reacting these extended amidines with orthoesters or formamide surrogates.[111] This reaction was able to provide a small family of 2,4,5-triaryl pyrimidines in excellent yield, however aliphatic side chains were absent on the vinyl amidine component. Also, the optimised method to obtain the vinyl amidine allowed only an isoxazole side chain in the pyrimidine 5-position. The method was later expanded

upon[112] to include more examples and to investigate the potential of the isoxazole substituent for further organic synthesis.

Pyrimidine synthesis via strategy E

Another synthetic strategy for accessing pyrimidines *via* the only other possible combination of 3-atom synthons comes in the form of strategy E (figure 6). Holtschmidt *et al.* found that *N*-(dichloromethylene)trichloromethanimine **88** (figure 40, R^2 = Cl) could act as an effective CNC "acceptor" fragment and exploited the binucleophilicty of acetonitriles in an intriguing synthesis of 2,4,6-trichloro-5-substituted pyrimidines.[113] The reaction proceeded at a reaction temperature of 200 °C in the presence of a catalytic quantity of $FeCl_3$, affording a range of aromatic- and aliphatic-substituted 2,4,6-trichloropyrimidines in mostly good yield. Mechanistically, the acetonitrile is expected to react through the methylene to afford the adducts **89**, which were isolated in some instances, which then presumably underwent a 6π electrocyclization followed by elimination of HCl to afford the pyrimidine.
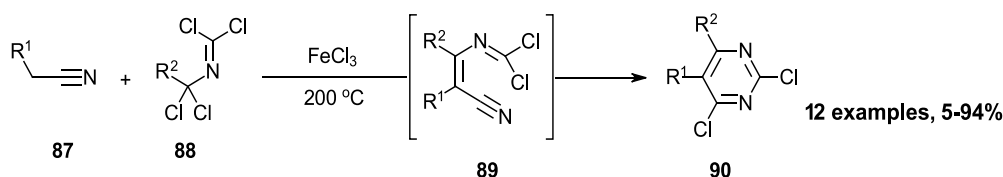
Figure 40: Lewis acid mediated cyclisation of (dichloromethylene)dichloromethanimines with substituted acetonitriles

Alternative binucleophiles that react with the dichloromethanimine **92** (figure 41) to produce pyrimidines include enamines **91**, which are easily accessed from the parent aldehyde/ketone. For instance, Heitzer and Grohe found that treatment of **92** with the enamine **91** under basic conditions afforded the corresponding pyrimidine **93** in good yield,[114] allowing additional diversity (R^1) compared to the previous synthesis.
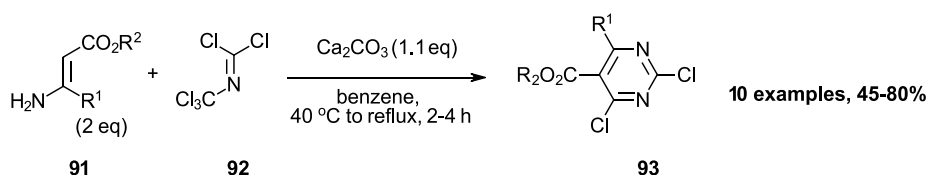
Figure 41: reaction of (dichloromethylene)dichloromethanimines with enamines under basic conditions

Enamines were also found to react with acyl isothiocyanates **95** (figure 42) by Dorfman *et al.*[115] to access a good range of fully substituted pyrimidin-4-thiones in moderate to good yield. The reaction of enamine **94** with benzoyl isocyanate (**95**, *O* instead of *S*) resulted only in the formation of the linear product **97** and none of the pyrimidin-4-one could be obtained, even after heating for extended

periods of time. In order to access highly substituted 2-aminopyrimidines, Maccioni *et al.* found that the enamines **98** (figure 43) reacted with cyanamides of type **99** to provide the products of type **100** with a range of alkylamino- or alkoxy-substituted aminopyrimidines in excellent yield.[116]
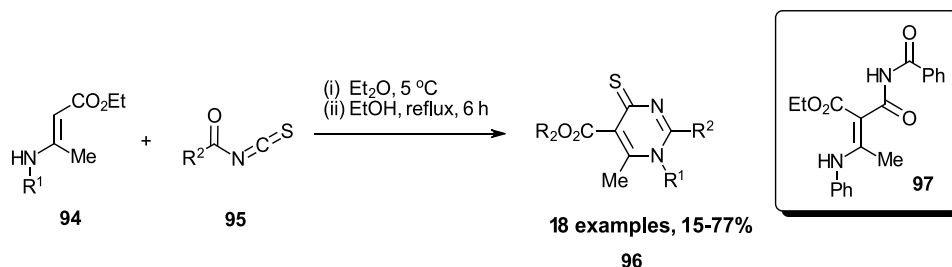
Figure 42: Reaction of enamines with acyl isothiocyanates
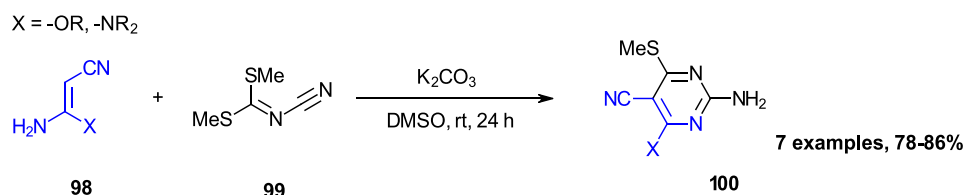
Figure 43: Reaction of enamines with cyanamide derivatives

1.1.4. Reactivity of pyrimidine derivatives

Transition metal-catalysed cross coupling reactions of functionalised pyrimidines

Traditionally, pre-formed pyrimidines with halide substituents (accessed by a considerable number of established transformations)[117] have been used to access highly substituted/arylated pyrimidines by Pd-catalysis.[118] Suzuki-Miyaura cross coupling has allowed the arylation of halopyrimidines at C2,[119,120] C4,[119] and C5.[120,121]Even allowing access to 5-arylated uracils through the use of suitable O-protecting groups.[121] The use of pyrimidinyl halides as the electrophilic component of Suzuki-Miyaura reactions dominates this particular strategy of ring functionalisation, with only very few successful examples of pyrimidin-(2 or 6)-yl boronates. Pyrimidin-5-yl boronates, however, are widely used and effective nucleophiles for the Suzuki-Miyaura reaction in the form of: boronic acids,[122,123] boronic esters,[124] organotrifluoroborates[125,126] and MIDA boronates[127,128] (*vide infra*).

Deprotonative functionalisation of pyrimidines[129]

A more attractive pyrimidine functionalisation strategy comprises the direct C-H activation of unsubstituted pyrimidines. Deprotonative metalation of pyrimidines has achieved this,[130] due to the lower pKa of pyrimidine hydrogens compared to azine or benzene derivatives.[131] This lowering of pKa is considered to be caused by the lower degree of aromaticity, and thus higher acidity compared to the latter.[130] The higher degree of electron withdrawal of diazines compared to azines or benzenes also provides further rationale for the higher acidity of ring protons. Metalation of diazines, although possible, is challenging due to the competing self-reaction/dimerisation that the metalated intermediates undergo (figure 44).
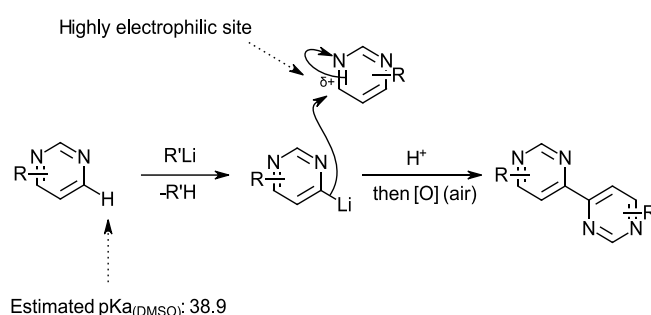
Figure 44: Issue of dimerisation when performing deprotonative[131] functionalisation reactions on pyrimidine

Early attempts[132,133] at pyrimidine C-H lithiation at the 4- and 6-positions were successful in producing the electrophile-trapped products, but in modest yields due to the competing inherent dimerisation reaction. Kondo *et al.* since published a highly selective and mild zincation of pyrimidine,[134] which employed a hindered phosphazene base, providing the C5 electrophile-trapped product in moderate to excellent yield with no mention of the formation of any pyrimidine dimer. A highly selective procedure for C4/6 deprotonative functionalisation of pyrimidine was disclosed by Mongin and coworkers.[135] This was achieved using an organolithium-mediated zincation reaction in the presence of TMEDA (figure 45).
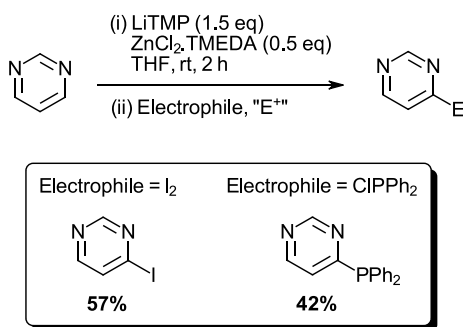
Figure 45: Selective C4/C6 deprotonation, followed by trapping with electrophiles. TMP = 2,2,6,6-tetramethylpiperidide, TMEDA = tetramethylethylenediamine

The reaction was extremely selective for C4/6 monofunctionalisation and only traces of the pyrimidine dimer was observed under the stated conditions, allowing the trapped products to be isolated in good yield. A highly significant deprotonative metalation procedure for the switchable C5 (magnesation) or C2 (zincation) functionalisation of pyrimidines was published more recently by Knochel *et al.*[136] (figure 46). The process is not limited to 4,6-disubstituted pyrimidines and the corresponding pyrimidin-2-yl zincates underwent smooth trapping reactions with a range of electrophiles and even participated in Pd-catalysed cross-coupling. The only example of C5 magnesation/iodination was on 4,6-dimethoxypyrimidine, suggesting that the selectivity is dictated by Mg-coordination of the adjacent pyrimidine alkoxy substituents, in a similar fashion to the directed cupration of arenes disclosed by Uchiyama and coworkers.[137] For the more general C2 selective zincation, BF_3 is expected to coordinate to the ring nitrogen, increasing the acidity of the adjacent C-H. However, selectivity between C2 and C4 deprotonation when feasible was not discussed. Further details pertaining to the direct (deprotonative) metalation of pyrimidines will be discussed later, in the context of the synthesis of stable pyrimidine organometallic intermediates.
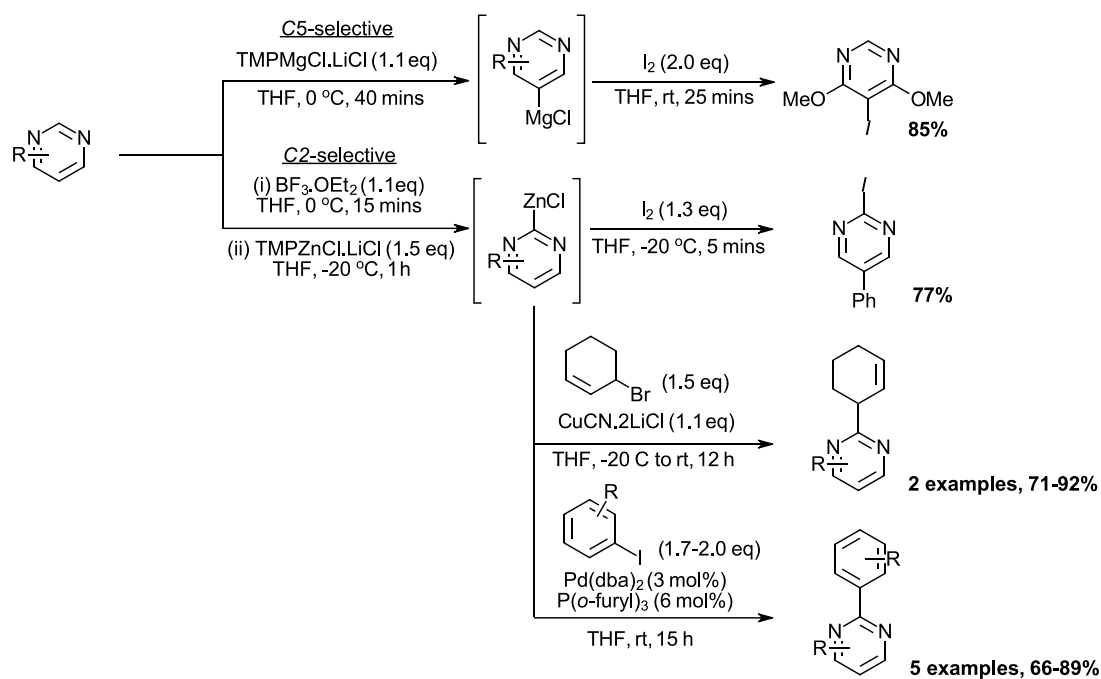
Figure 46: Deprotonative functionalisation reactions, allowing selective metalation of either C2 or C5

Radical C-H functionalisation of pyrimidines

A milder and more functional group-tolerant approach to C-H functionalisation comes in the form of radical addition. An example of heterocycle C-H functionalisation that utilises this is the powerful Minisci reaction, which is the reaction of a (*N*) heteroarene with a free radical under acidic conditions (figure 47).
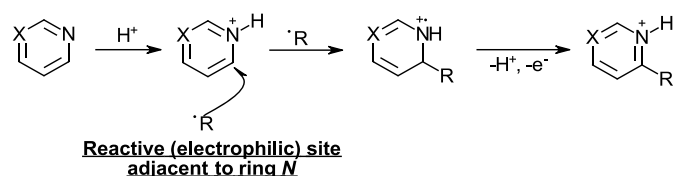
Figure 47: General scheme describing the concept of radical addition to a protonated (di)azine (the Minisci reaction)

The selectivity of radical addition is unique to each heterocycle (e.g., reactive sites on pyridine are the 2- and 4- positions) but is sometimes dictated by the identity of the attacking radical itself. The Minisci reaction has been widely studied in recent years and adopted in numerous fields for heterocycle functionalisation for its potential as a mild, rapid and selective tool for C-H diversification.[138] The pyrimidine ring is no exception to this, and has featured prominently in the development of this process. An interesting example of the Minisci reaction applied to the synthesis of pyrimidines in drug molecules was disclosed by Liu and Zhang,[139] who inserted the alkyl chains of a precursor of rosuvastatin **101** (figure 48) and pyrimethamine **102** efficiently, allowing the C6-alkylated products to be isolated in good yield.
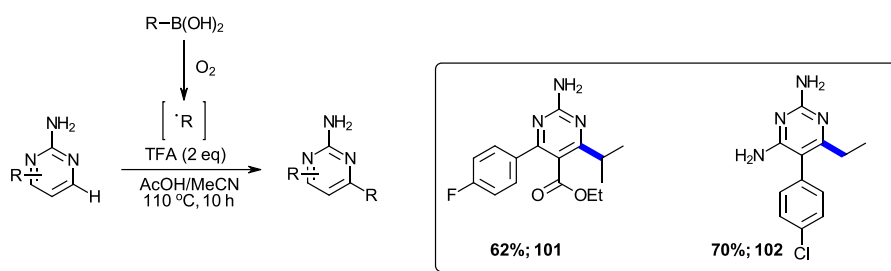
Figure 48: Minisci alkylation reaction applied to the synthesis of medicinally significant pyrimidines

Another highly useful feature of this type of process is the mild and functional group tolerant late-stage functionalisation (LSF) potential of unsubstituted heterocycle-containing drugs.[140] LSF provides the opportunity for creating drug analogues for testing, without the need for a *de novo* synthesis each time. For LSF viability, the chemical modification process must be mild and selective enough to only react at the desired site and not interfere much with other functional groups on the molecule in question. An example of a pyrimidine drug molecule that has been a case study for a lot of the development of LSF reactions is the antifungal voriconazole (Table 1),[140,141] which features two sites of potential pyrimidine C-H activation that are electron-deficient and so are expected to react with alkyl radicals. Indeed, several published Minisci-type procedures found that alkyl or hydroxyalkyl radicals react primarily with voriconazole to produce the C4-alkylated product, with some of the C4-C2 dialkylated product also observed. This is consistent with the innate C4 reactivity preference of alkyl radical addition to pyrimidine,[142] and is also predicted by the Fukui function, which describes the electron density of frontier molecular orbitals and has a large positive (LUMO) value at the pyrimidine C4 (figure 49).[143] This innate preference for reaction at C4 can be partially overridden by steric hindrance, exemplified by the alkylation of fenarimol (table 2) which provided a mixture of adducts for methyl and cyclopropyl radicals,[144] whereas in the case of the slightly more bulky isopropyl radical, only C2 was alkylated.[142]
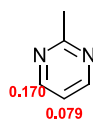
Figure 49: Calculated Fukui indices for 2-methylpyrimidine C4 and C5 for nucleophilic attack, indicating that the C4 is largely favoured over the C5
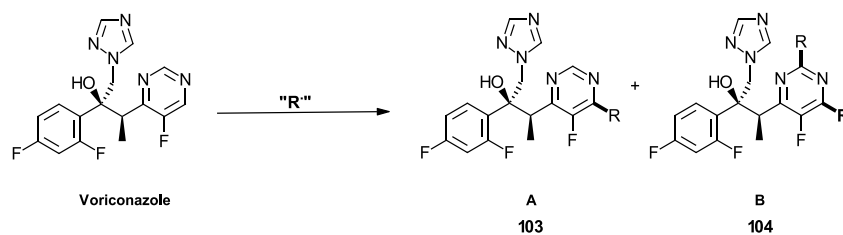
R	Yield A	Yield B	reference
—Me	37%	21%	(Tudge, 2014)
isopropyl	57%	-	(Baran, 2013)
cyclopropyl	38%	36%	(Tudge, 2014)
CH₂OH	44%	13%	Krska (2016)
CH(CH₃)CH₂CH₂OH	68%	-	Zhu (2018)

Table 1: LSF radical addition to voriconazole studies, displaying the preference of the pyrimidine for C4 alkylation
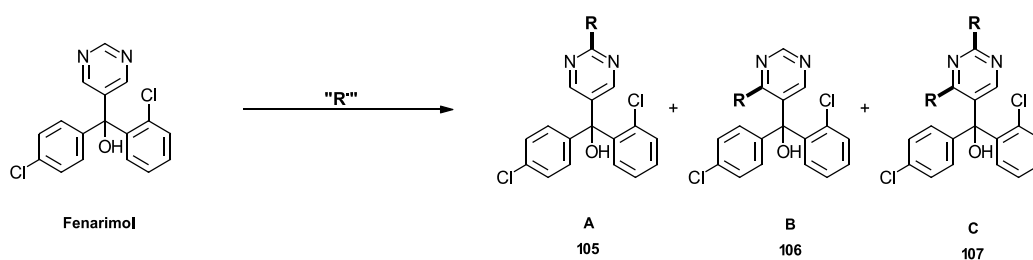
R	Yield A	Yield B	Yield C	reference
—Me	9%	6%	30%	(Tudge, 2014)
isopropyl	21%	-	-	(Baran, 2013)
cyclopropyl	-	-	49%	(Tudge, 2014)

Table 2: LSF radical addition to fenarimol, displaying the pyrimidine's mild C2 preference

In fact, Baran *et al.*[142] found that the presence of conjugated electron-withdrawing groups attached to the C2 or C5 position of pyrimidine scrambled the selectivity of isopropyl radical addition significantly. In an earlier publication,[145] other (fluoro)alkyl radicals were found to add to 2-cyanopyrimidine with marginal selectivity for C4 over C5 until the 1,1,1-trifluoroethyl radical was used, whereupon the addition was only at C5. The trifluoromethyl radical displays both electrophilic and nucleophilic behaviour, adding efficiently to the pyrimidine C4 where available, but also attacks other accessible nucleophilic sites on the compound when the pyrimidine C4 is not available or is less activated. This is exemplified by trifluoromethyl radical addition to trimethoprim (figure 50),[142] which occurs on the adjacent trimethoxybenzene instead of the diaminopyrimidine. An interesting, transition metal-free C-H arylation of (amino)pyrimidines and quinazolines believed to proceed via an aryl radical was published recently by Singh *et al.* (figure 51).[146] This reaction proceeded efficiently to produce the C4 arylated pyrimidines which were isolated in moderate to very good yield. When the position was unblocked, the C2-arylated pyrimidine was isolated in trace quantities.
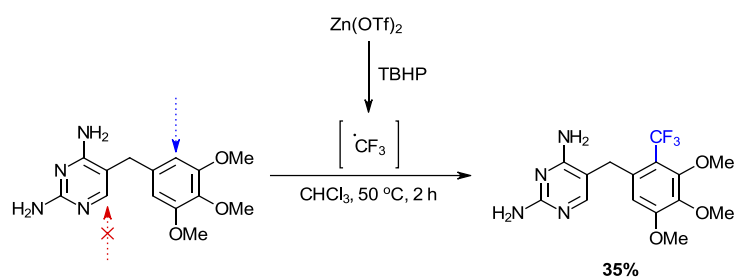
Figure 50: In the absence of a strongly electrophilic heterocycle, the trifluoromethyl radical can act as an electrophile itself
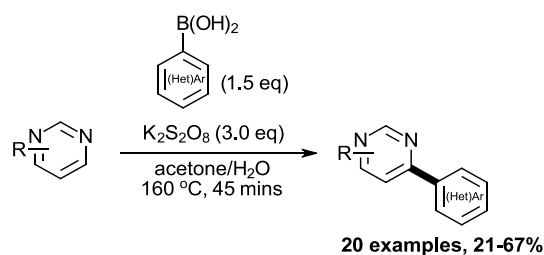
Figure 51: Radical C-H arylation of pyrimidines at C4

Preparation and functionalisation of stable pyrimidinyl metal species[147]

One way to avoid the selectivity problems posed by homolytic C-H functionalisation of pyrimidines, is to access a persistent/stable metalated pyrimidine which is poised to react only at that position. The advantage of having a bench-stable intermediate organometallic is the synthetic convenience of being

able to produce multiple analogous compounds from a common point, without the need for cryogenic or other special experimental conditions.

Stannylpyrimidines

Organotin reagents are known as easily prepared and stable organometallics, which undergo numerous useful transformations (e.g. Stille cross coupling). Despite their potential for synthetic chemistry, safety considerations surrounding their toxicity and that of their by-products have limited their use in certain applications, and so have been investigated considerably less in recent years.
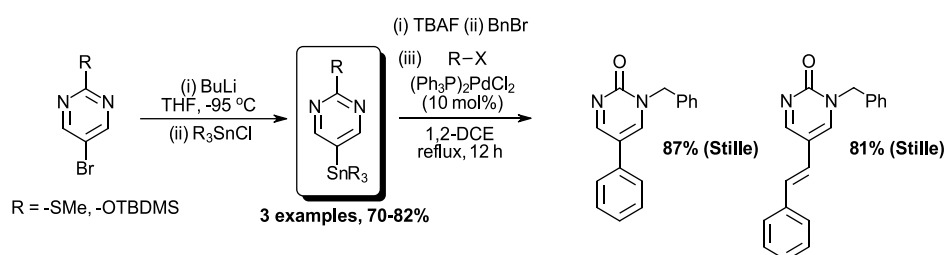
Figure 52: Nucleophilic stannylation of C5 bromopyrimidines, along with further functionalisation via Stille cross coupling
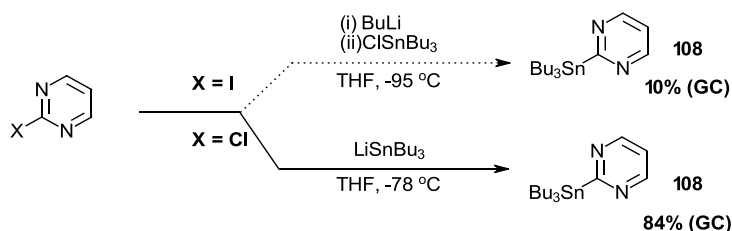
Figure 53: Electrophilic stannylation (bottom) provides an alternative means to access stannylpyrimidines regioselectively
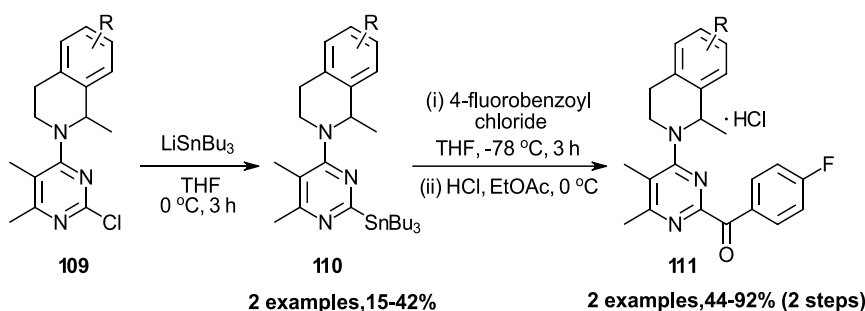
Figure 54: Pyrimidine stannylation applied to the synthesis of medicinally relevant compounds

Nevertheless, Undheim *et al.* prepared stannylpyrimidines by nucleophilic stannylation[148] from halopyrimidines *via* Li-halogen exchange, followed by quenching with trialkyltin chlorides (figure 52). This procedure allowed the isolation of C5-stannylated pyrimidines, which underwent smooth Stille coupling reactions with aryl- and vinyl bromides, as expected. This strategy was also successful in preparing a C4-stannylated pyrimidine in good yield *via* iodine-lithium exchange, followed by trapping with Bu₃SnCl.[149] Nucleophilic stannylation of 2-iodopyrimidine was less successful, with the product **108** being obtained in low yield (figure 53). However, electrophilic stannylation by Bu₃SnLi on 2-chloropyrimidine was comparatively more efficient, providing **108** in 84% yield. Pyrimidines bearing stannyl groups in the C2, C4 and C5 positions can be prepared by electrophilic stannylation and are amenable to tin-lithium exchange and Stille cross coupling. More recently, electrophilic stannylation of chloropyrimidines **109** (figure 54), followed by acylation was used in the synthesis of novel pyrimidines as potential treatments for Gastroesophageal Reflux Disease.[150]

Silylpyrimidines

Organosilicon functional groups have gained much interest and are researched widely, due to their stability, accessibility, versatility,[151] and the benign nature of their process by-products in terms of toxicity and sustainability. In recent years, aryl- and heteroarylsilicon compounds in particular have attracted attention as intermediates in polyaryl synthesis, thanks to a host of new transformations made possible by transition metal catalysis.[152]

Early methods to prepare silylpyrimidines relied upon the electrophilic trapping of an *in situ* generated pyrimidine organometallic with the corresponding chlorosilane. Sloan and Mattson published a method of directed deprotonation of methoxypyrimidines (figure 55)[153] by using LiTMP, that allowed the isolation of C4- and C5-silylated pyrimidines after trapping the intermediate organolithiums with TMS-Cl in moderate to excellent yield.
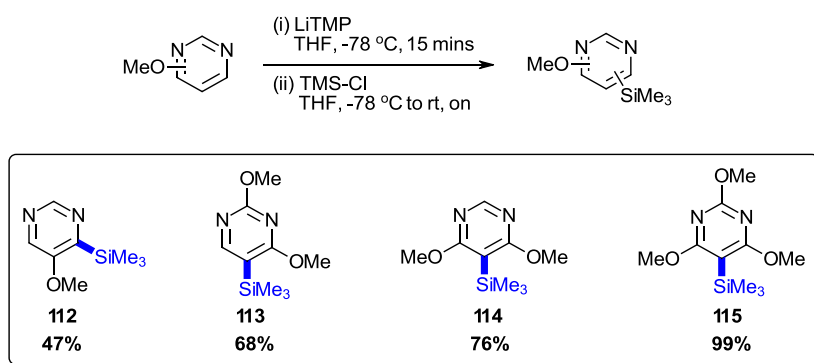
Figure 55: Silylation of methoxypyrimidines via directed lithiation

The lithiation-silylation example that was directed at the pyrimidine C4 provided the lowest yield of product (**112**, 47%). Radinov *et al.* disclosed a similar set of conditions, using LDA as the base, for polychlorinated pyrimidines. In this case, the major product was the C5-silylated pyrimidine. The yield was low for the C4-unsubstituted pyrimidines and improves upon addition of more chlorine atoms to

the ring, suggesting that the chlorine substituents stabilise the intermediate organolithium,[154] or block undesired potential reactivity at C4. While investigating the direct metalation of pyrimidines without pre-attached directing/stabilising groups Queguiner and co-workers noted the formation of significant levels of pyrimidine dimers (*vide supra*).[132] Nevertheless, they were able to obtain 2 C4-silylated pyrimidines in moderate yield after quenching the organolithium with TMS-Cl. In a later publication,[155] they found that simultaneous addition of the pyrimidine (figure 56) and TMS-Cl to the LiTMP solution suppressed the formation of dimers, allowing the C4-silylated pyrimidine to be isolated in 96% yield.
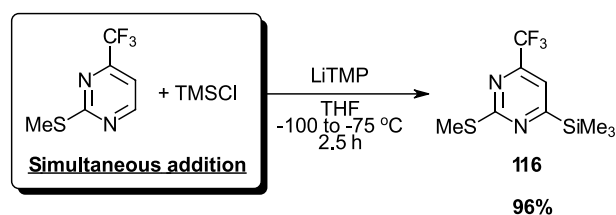
Figure 56: In situ quenching of reactive pyrimidinyl lithium species provides an efficient method of functionalisation

There are very few successful direct C-H metalation-silylation strategies at the C2 position, for this reason Yoshida *et al*. opted for a tin-lithium exchange procedure of the stannylpyrimidine **108** (figure 57), followed by quenching with the chlorosilane **117**.[156] The pyrimidin-2-yl silane product **118** was found to be a highly useful directing-activating group for Pauson-Khand type reactions with alkynes. A further example of C2-silylpyrimidines as directing groups was published more recently by Gevorgyan *et al.*,[157] who installed the silyl group onto the C2 of the pyrimidine **119** (figure 58) by magnesium-iodine exchange using ^{i}PrMgCl.LiCl. The silane was then further functionalised by a Rh-catalysed arylation,[158] affording a range of pyrimidin-2-yl(diisopropyl)arylsilanes **120** in up to 95% yield.
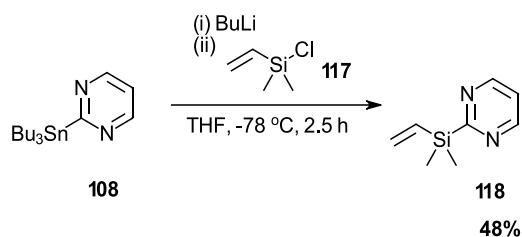
Figure 57: Tin-lithium exchange applied to the synthesis of a pyrimidin-2-yl silane
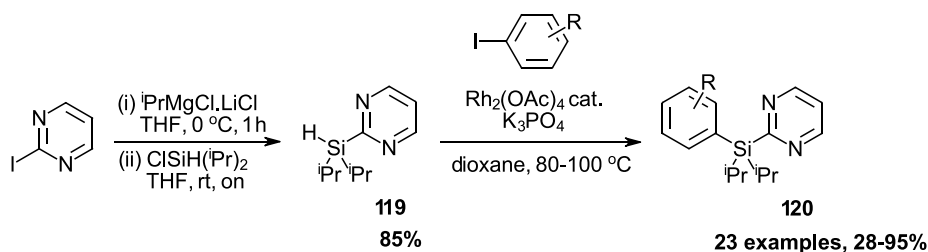
Figure 58: Pyrimidin-2-yl silane synthesis via magnesium-halogen exchange

In a significant development, Knochel *et al.* utilised the magnesium amide bases TMPMgCl·LiCl and TMP$_2$Mg·2LiCl as powerful and regio-/chemoselective reagents for the mild deprotonative functionalisation of pyrimidines.[159,160] By trapping the intermediate magnesiopyrimidine with TMS-CN, a range of C4-silylated pyrimidines could be isolated in very good to excellent yield. Even 2-bromo-6-iodopyrimidine was functionalised with a TMS group in 93% yield, indicating that the halogen substituents on the pyrimidine remained untouched. Recently, Martin and coworkers published an intriguing procedure for the mild, selective and functional group tolerant C-H silylation of (poly)azines, using a combination of TES-BPin and KHMDS (figure 59).[161] 3 Pyrimidine substrates, including the parent heterocycle and 2 currently marketed pyrimidine-based drugs were efficiently silylated at C4 with good yields of isolated product. In the case of unsubstituted pyrimidine, this process seemingly favoured C4 silylation over C2 or C5. It is thought that the TES group is rendered nucleophilic by the action of KHMDS on BPin.
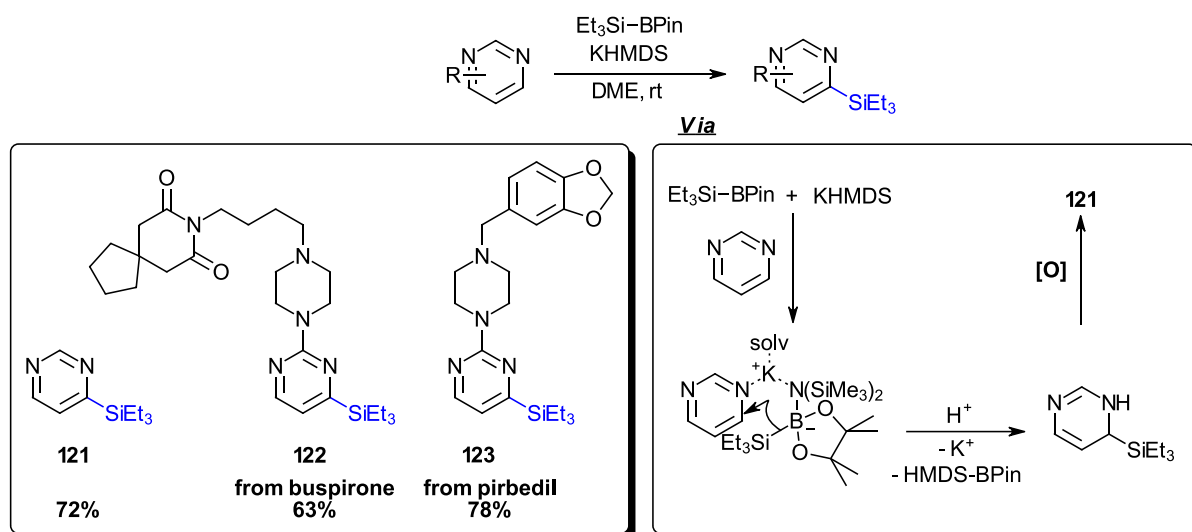
Figure 59: Mild silylation of pyrimidine C4, mediated by KHMDS and TES-BPin

Transition metal-catalysed C-H silylation has gathered much research interest in recent years,[162] An example of this in which a pyrimidine was used as a substrate was published by Hartwig *et al.*,[163] 2-methylpyrimidine was silylated selectively at the pyrimidine C5 over C4. A mild, photocatalytic C-H silylation of heteroarenes was recently disclosed by Zhang and coworkers, one pyrimidine substrate was silylated in the only accessible position in moderate yield (figure 60). [164]
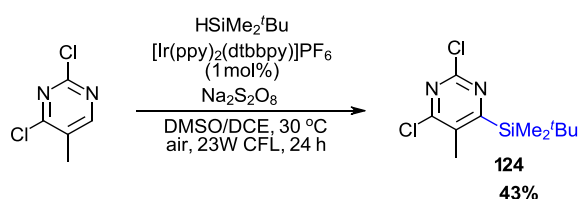
Figure 60: Photocatalytic C-H silylation of substituted pyrimidine
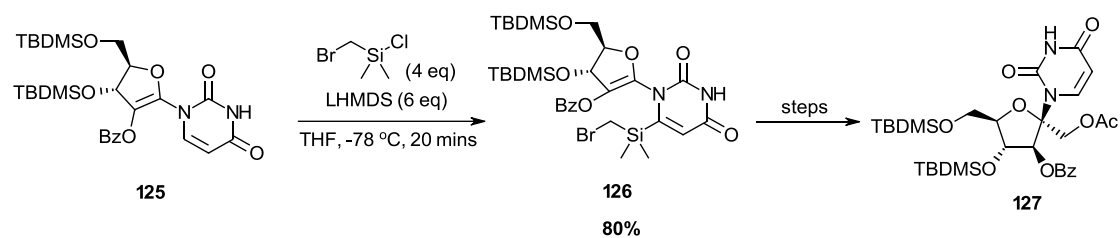
Figure 61: Application of pyrimidine silylation towards the synthesis of 1'-C-hydroxymethylated nucleosides

An interesting application of silylpyrimidine chemistry was investigated by Tanaka and coworkers,[165] who prepared the 2-(bromoalkyl)silyl uridine **126** (figure 61) by treating uridine **125** and the required chlorosilane with LiHMDS. The less basic LiHMDS was favoured over LDA due to potential competitive silane destruction by the latter. The products of type **126** were subsequently investigated for their intramolecular radical cyclisation reactions, leading to 1'-*C*-hydroxymethylated nucleosides **127** which were to be investigated for their antibacterial properties.

Recently, Garg *et al.* prepared pyrimidinyl silyl triflates **130** and **134** (figure 62) in an attempt to access pyrimidyne **131** for cycloaddition reactions.[166] 2-Silylpyrimidine **129** was obtained in good yield after deprotonating the parent heterocycle using LiTMP and *in situ* quenching with TES-Cl, whereas the 5-silylation only allowed the isolation of the product **133** in low yield (starting from pyrimidin-2-one). Pyrimidine silyl triflate **134** underwent non-specific decomposition, along with reversion to pyrimidin-2-one when subjected to typical benzyne cycloaddition conditions. The other silyl triflate **130** didn't react as an aryne either, but in this case it underwent a thia-Fries rearrangement to the sulphone **132**, which was isolated in 75% yield.

While many methods exist for the synthesis of silylated pyrimidines by functionalisation of the pre-formed heterocycle, accessing the same *via* annulation of silylated starting materials is significantly more challenging. As noted (*vide supra*), Müller *et al.* reacted TMS ynones (figure 17) with amidines and obtained the corresponding protodesilylated pyrimidines in quantitative yield.[59] This protodesilylation was also observed by Bagley *et al.*[167] However, a recent report by Agapie and coworkers detailing the catalytic cyclotrimerisation of nitriles with alkynes, prepared the C4 silylated pyrimidine **135** (figure 63) in 96% yield after chromatography on silica gel, by using ethynyltrimethylsilane as the alkyne.[168]
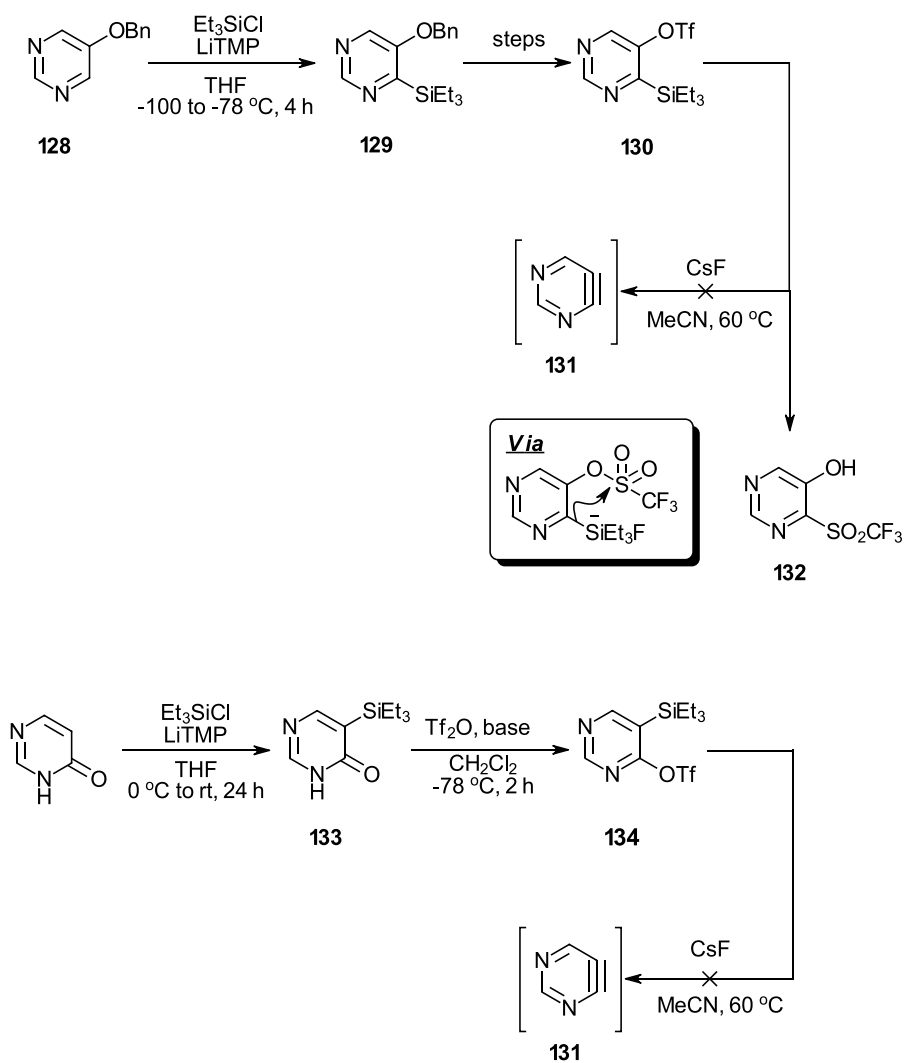
Figure 62: Preparation of silylpyrimidine precursors of pyrimidyne
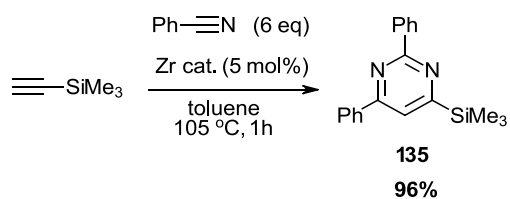
Figure 63: Zr-catalysed cotrimerisation of ethynyltrimethylsilane and benzonitrile

Borylpyrimidines

As noted previously, pyrimidinyl halides are by far the most common fragment used to functionalise pyrimidines *via* metal (Pd) catalysis,[118] however, the need for alternative reagents to produce similar products has driven research in the direction of accessing borylpyrimidines as versatile substitutes that display an umpolung character to the former. Among the borylpyrimidines that have been synthesised and studied in most detail are pyrimidin-5-yl boronic acid derivatives. These products are typically prepared by Li-halogen exchange with the corresponding pyrimidin-5-yl bromide (figure 64), followed by quenching of the organolithium with trialkyl borate esters (B(OR)$_3$, R = Me, ^{i}Pr, ^{n}Bu).[147,169–173]
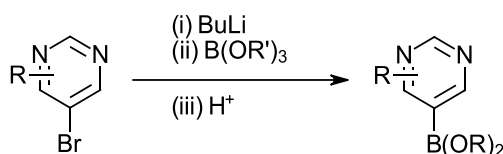
Figure 64: Generally successful strategy for the synthesis of pyrimidin-5-yl boronic acid derivatives

Reider *et al.* found that the synthesis of pyrimidin-5-yl boronic acid gave a higher yield when the organolithium was quenched *in situ* by simply adding butyllithium to a mixture of 5-bromopyrimidine and triisopropyl borate, as opposed to adding the borate electrophile after the butyllithium addition step. The yield of the corresponding boroxine anhydride was 76% when the *in situ* trapping method was used, and only 28% using a stepwise procedure.[170] Pyrimidin-5-yl boronic acids have been used in Suzuki-Miyaura cross coupling reactions extensively, usually producing the corresponding products in good yield.[174,175] They have also been successfully applied in other boron functionalisation studies, including oxidation,[176,177] Chan-Lam coupling[178,179] and alkene hydroarylation.[180]

Molander and co-workers prepared potassium pyrimidin-5-yl trifluoroborate salts from the corresponding boronic acids by the action of KHF$_2$ (figure 65) in good yield.[126] These salts were shown to undergo smooth Pd-catalysed cross coupling with aryl halides with excellent yields of biaryl products. The same trifluoroborate salts were also amenable to Ni-catalysed Suzuki-Miyaura cross coupling with aryl halides[125] and even alkyl halides,[181] providing the products in very good to excellent yield. Pyrimidin-2-yl boronates are rare in the literature, in comparison to the 5-borylated congeners. There is only a single, recent, report[182] that outlines the preparation of one such pyrimidin-2-yl boronate (figure 66). The boronic ester was subsequently shown to undergo smooth cross coupling with an aryl bromide to produce the pyrimidine **138**. The successful outcome of this coupling may originate from the slow addition of the aqueous base solution to the reaction mixture, potentially
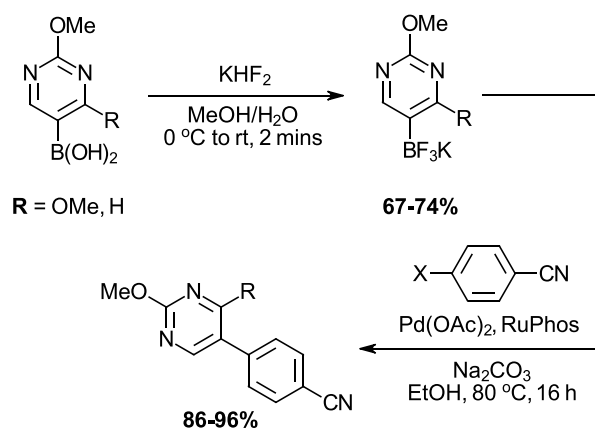
Figure 65: Pyrimidin-5-yl trifluoroborate salts as stable surrogates of the corresponding boronic acids
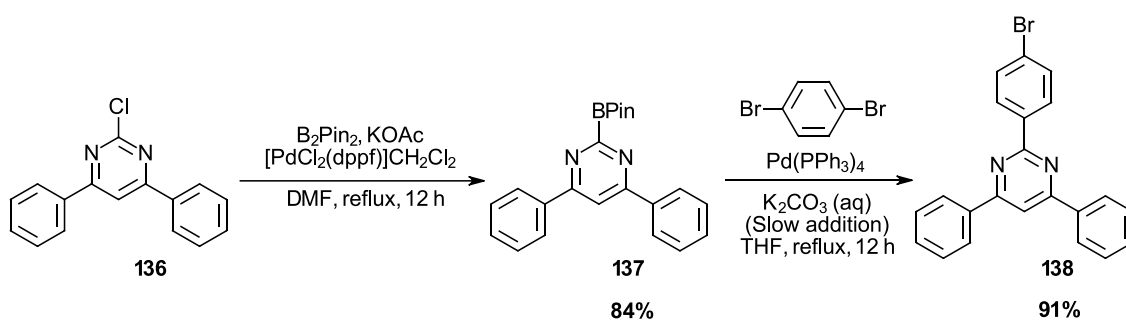
Figure 66: Rare example of the synthesis and cross couplng of pyrimidin-2-yl boronates

providing a controlled release of the reactive boronic acid, minimising protodeboronation.[183] There are only a handful of other publications that show successful functionalisation of pyrimidin-2-yl boronates, and few experimental details are typically provided.[184–188] Pyrimidin-6-yl boronates are similarly rare in the literature, present as intermediates where the source is unstated and few experimental details presented.[189,190,199–202,191–198] Although rare, they are not completely absent, and can be prepared from the corresponding 6-bromopyrimidine by Li-halogen exchange followed by quenching with B(OR)$_3$, as *per* the method of Prusoff *et al.*[172] 2,4-Bis(benzyloxy)pyrimidin-6-yl boronic acid **139** (figure 67) was obtained in 57% yield after the borylation/hydrolysis sequence, which had to be carried out at -95 °C. After catalytic hydrogenation, 6-(dihydroxyboryl)uracil **140** was obtained in 34% yield. The authors state that **140** was stable to acidic conditions, but decomposed in the presence of base or DMSO (occurrence of protodeborylation and oxidation, respectively). More recent, catalytic methods of borylation at the pyrimidine C6 that do not involve cryogenic metalation have been attempted without success, such as Miyaura borylation[203] and C-H activation.[204] Pyrimidin-6-yl boronic acid derivatives such as **139** have been used successfully in Suzuki-Miyaura cross coupling reactions,[205,206] but the reactions often require at least 2 equivalents of the boronic acid, and high catalyst loadings. The pyrimidin-6-yl trifluoroborate salt **141** (figure 68) was iododeboronated by an FeCl$_3$-mediated process published by Kabalka *et al.* but the product was obtained in modest yield.
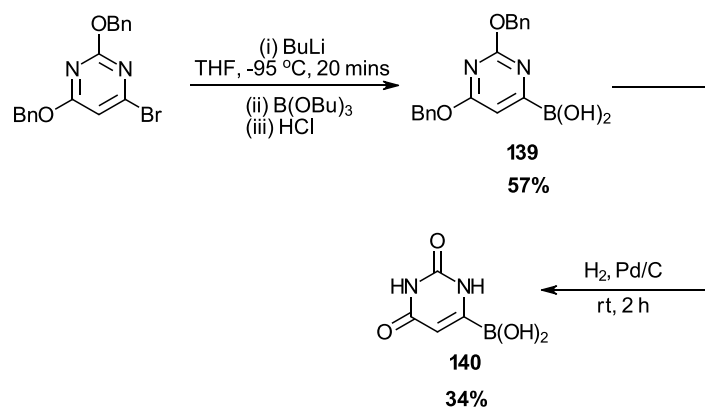
Figure 67: Synthesis of pyrimidin-6-yl boronic acid derivatives via Li-Br exchange
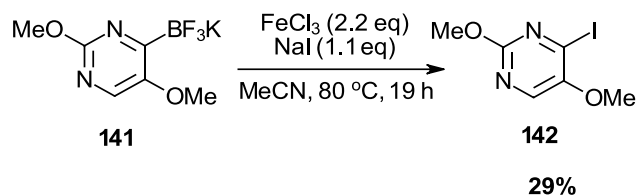
Figure 68: Elaboration of a pyrimidin-6-yl trifluoroborate salt by FeCl₃-promoted iododeboronation

The relative lack of pyrimidin-2-yl and pyrimidin-6-yl boronates in the literature, compared to other aryl boronates and to pyrimidin-5-yl boronates fits with the well-known instability of boronic acids and boronates in which the boron functionality lies adjacent to azine nitrogen atoms. In addition to potentially facile decomposition routes involving the α-nitrogen, there is some evidence that suggests pyrimidin-2-yl and pyrimidin-6-yl boronic acids are inherently less stable than pyrimidin-5-yl boronic acid, as their calculated homolytic bond dissociation energies are lower and equilibrium bond lengths longer (figure 69).[207]

	BDE (C-B), kJ mol^{-1}	Bond length, Å
pyrimidin-2-yl	472.8	1.591
pyrimidin-4-yl	480.1	1.584
pyrimidin-5-yl	508.1	1.57

Figure 69: Calculated C-B bond lengths and bond dissociation energies (BDE) for pyrimidinyl boronic acids

As a testament to how innovation solves long-standing technological problems, a paper was published very recently by Leonori *et al.* describing a novel strategy for C-H borylation of azines[208] and what looks to be a promising general solution to the synthesis and functionalisation of these otherwise-unworkable intermediates. The authors cited the selectivity and stability issues for accessing certain *N*-heterocyclic boronic acid derivatives by existing C-H borylation strategies *via* Ir/Ru and Pd catalysis, and how the product boronic esters are unstable to the very conditions that create them. As an intriguing solution, they proposed exploiting radical addition to azines (figure 70), which has been studied in great detail in recent years in the context of azine (fluoro)alkylation (*vide supra*), to the mild and selective synthesis of borylated azines. For this strategy to be realised, a boryl radical is required and this could be generated from several sources,[209–211] including NHC boranes,[212] phosphine boranes[213] or amine boranes.[214,215]
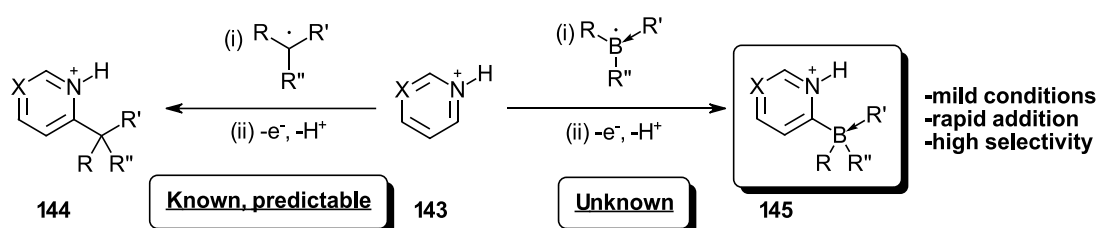
Figure 70: Concept of (Minisci) radical addition to azines applied to azinyl boronates
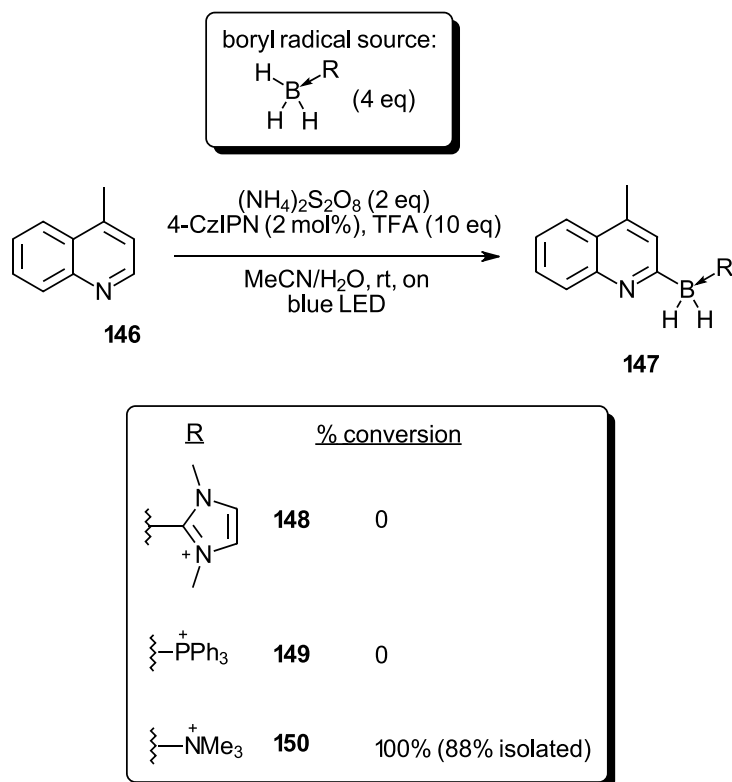
Figure 71: Radical borylation of lepidine using trimethylamine-borane

However, specifically for this application as a Minisci-type boryl radical addition to azine heterocycles, a highly nucleophilic radical is required. The widely studied NHC-boryl radicals are suggested to be of low nucleophilicity, due to the delocalisation of the unpaired electron into the NHC ligand. Indeed, attempts to borylate lepidine (figure 71, **a substrate that readily undergoes Minisci alkylation at C2**[216–218]) using NHC-borane **148** resulted in recovery of the starting material. Ph$_3$P-borane **149** was also subjected to the conditions to no avail. The amine borane **150** was then used, and the product was subsequently obtained in high yield. The reasons for the successful addition of the boryl-ammonium radical were investigated by a DFT study of the structure of the boryl radical **152** (figure 72) and an intriguing comparison with the isoelectronic neopentyl radical **151**.
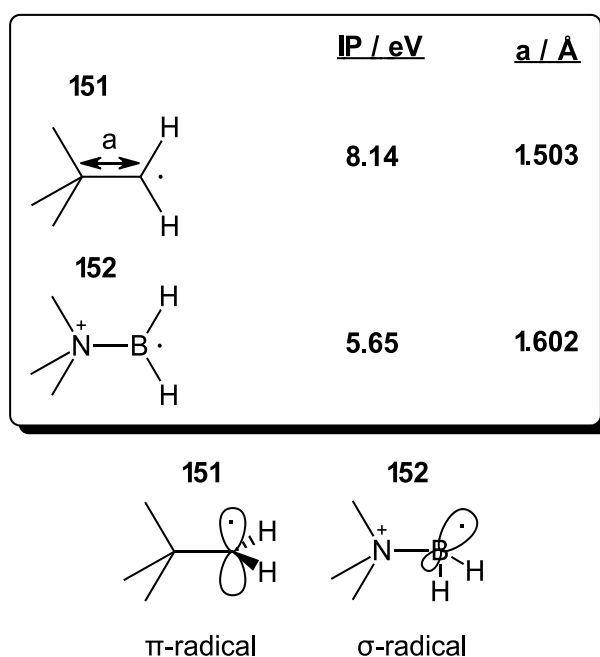
Figure 72: Calculated energetic and structural features of neopentyl and boryl radicals

Notably, the configuration of **152** was predicted as being a metalloid radical with a SOMO of high σ-character, whereas **151** resembles a π-radical, suggesting that **152** would display higher nucleophilicity. Another parameter that suggests **152** is a highly nucleophilic (more so than **151**) radical is the ionisation potential (IP). The higher IP of **151** (8.14 eV) compared to **152** (5.65 eV) suggests that **152** could donate an electron more readily, in e.g. radical addition to **146-H⁺**. The reaction of boryl **152** with **146-H⁺** was then studied by DFT and was found to have the lowest ΔG‡ by far, compared to the reaction of **146-H⁺** with neopentyl and NHC-boryl radicals. This is in agreement with the nucleophilicity arguments above, but also with the observation that the B-N bond distance of **152** (1.602 Å) is significantly longer than the C-C bond distance of **151** (1.503 Å) (figure 72), leading to minimal steric interference by the coordinated NMe$_3$ group. The Minisci-borylation process was applied to an impressive array of azine heterocycles, leading to high yields of the stable trimethylammonium coordinated boranes. Among the examples tested, were several (fused) pyrimidine rings (figure 73) which could be borylated at C2 (**153**-**157**) and C6 (**158**-**161**) in useful yields. Several challenging functional groups, such as phenols, anilines and alcohols were tolerated and the LSF potential of this procedure was demonstrated on pyrimidine medicines by selectively borylating voriconazole and famiclovir in good yield (see products **160** and **161**).
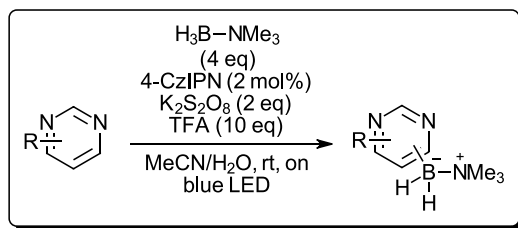
Pyrimidine C2 borylation

153	**154**
42%	32%

155	**156**	**157**
quant.	91%	72%
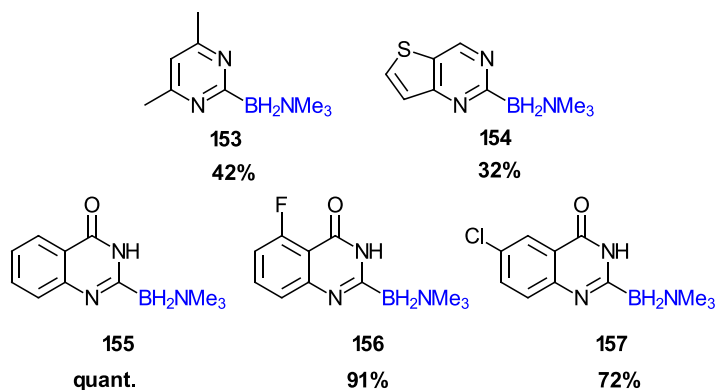
Pyrimidine C6 borylation

158	**159**
83%	57%

160	**161**
46%	51%
(from voriconazole)	(from famciclovir)
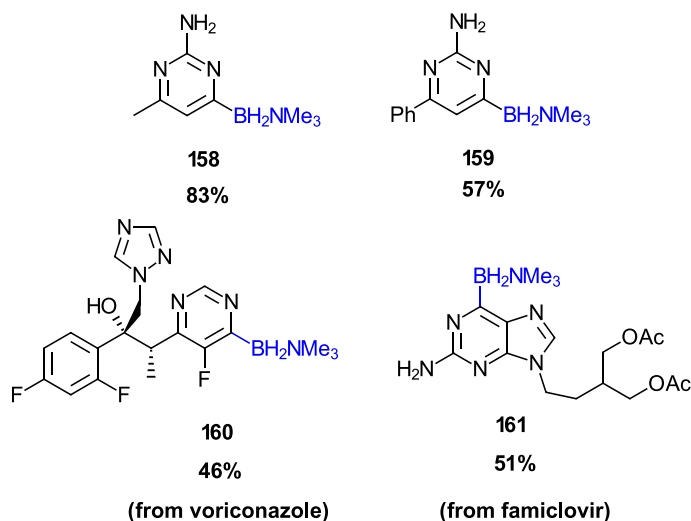
Figure 73: Radical C-H borylation applied to the synthesis of pyrimidin-2 and 6-yl boronates

Importantly, after the borylated heterocycles were obtained, their usefulness as synthetic intermediates was put to the test. Efficient procedures for Suzuki-Miyaura cross coupling, oxidation, Chan-Lam amination and Chan-Lam etherification were found for many of the products obtained. Of the (fused) pyrimidine products carried forward to the product elaboration section were the quinazolinone **155** (figure 74) and the aminopyrimidine **159**, which underwent oxidation and Suzuki-Miyaura cross coupling respectively, providing the products in useful yield.
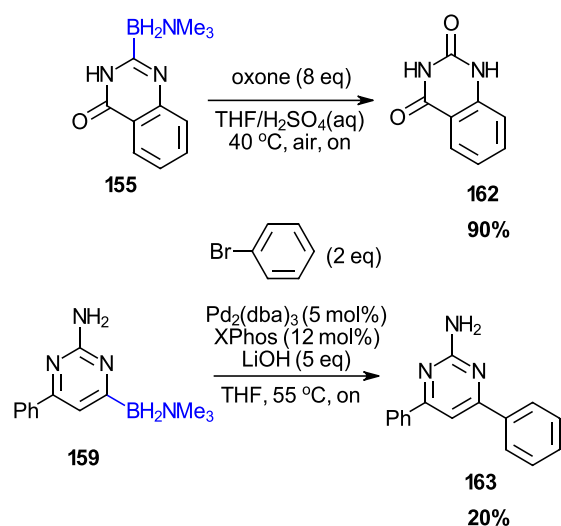
Figure 74: Functionalisation of pyrimidin-2 and -6-yl amine boranes via Suzuki-Miyaura cross coupling and oxidation

1.1.5. Experimental design & key objectives

The publication summarised in the context of pyrimidine synthesis above is an example of how well-known and established chemistry (Minisci alkylation) is used as a foundation to solve unrelated and pressing problems that research in synthetic chemistry is currently faced with (i.e. the incorporation of boron functionality α to azine nitrogen atoms). To address the specific problem of synthesising pyrimidin-6-yl boronic acid derivatives, which are rare in the literature, we sought to apply the same principle. Namely, to exploit classical condensation chemistry (Pinner-Müller synthesis) in a novel preparation of these elusive intermediates.
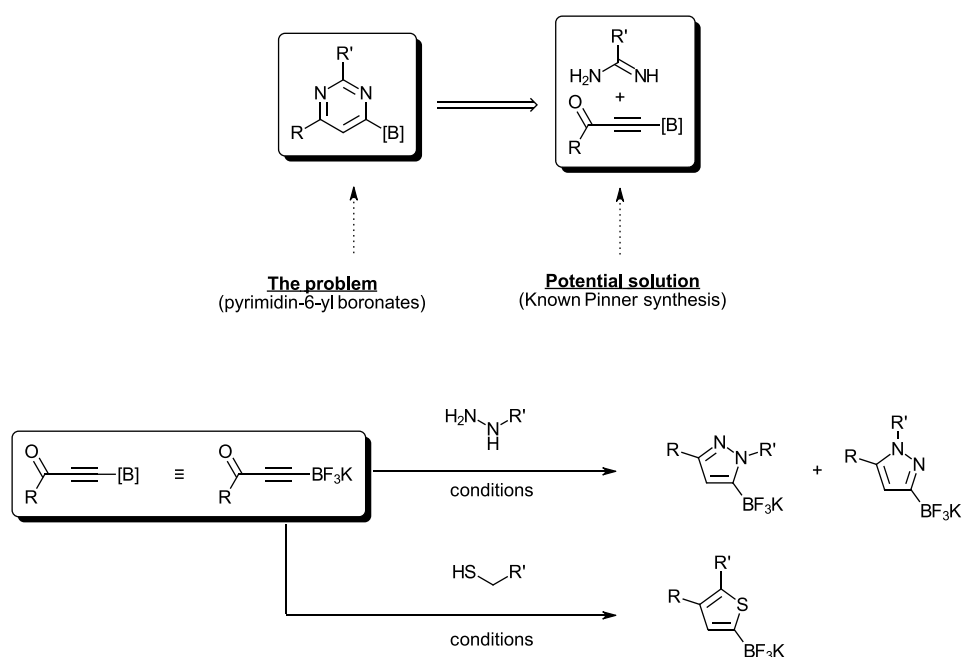
Figure 75: Proposal for approaching the problem of pyrimidin-6-yl boronate synthesis

To realise this, we required a boronic acid derivative that would survive the condensation step, but that could be activated under suitable conditions, allowing traditional boron chemistry to be carried out when desired on the resulting pyrimidine. Ynone trifluoroborates have proven themselves in recent years as the perfect candidate for this endeavour, allowing access to pyrazole[219–221] and thiophene[222] trifluoroborate salts that are amenable to standard boron functional group manipulation (figure 75). Trifluoroborate salts have allowed the isolation of stable pyridin-2-yl boronic acid derivatives (figure 76), however, their subsequent elaboration in Suzuki-Miyaura cross coupling reactions has met with mixed success. Molander *et al.* carried out an extensive screen for coupling conditions for potassium pyridine-2-yl trifluoroborate[126,223] but obtained none of the desired product. Wu and colleagues found suitable conditions for the Suzuki-Miyaura cross coupling of pyridin-2-yl trifluoroborate salts,[224] but the conditions were not so general, as a substituent at the 6-position was required. The Suzuki-Miyaura cross coupling of (amino)pyrimidin-6-yl trifluoroborate salts has not been disclosed and so we were keen to discover whether this could be a useful strategy for pyrimidine synthesis. The objectives in the following section are as follows (i) to establish an efficient and scalable

procedure for the production and purification of pyrimidin-6-yl trifluoroborate salts from ynone trifluoroborates and amidines/guanidines (ii) to assess the scope of the conditions by running substrates containing diverse functionality and substitution, and (iii) to explore the potential of these pyrimidin-6-yl trifluoroborate salts as intermediates for further organic synthesis, particularly to assess their viability in traditional boron functional group manipulation, e.g. oxidation, Suzuki-Miyaura cross coupling.
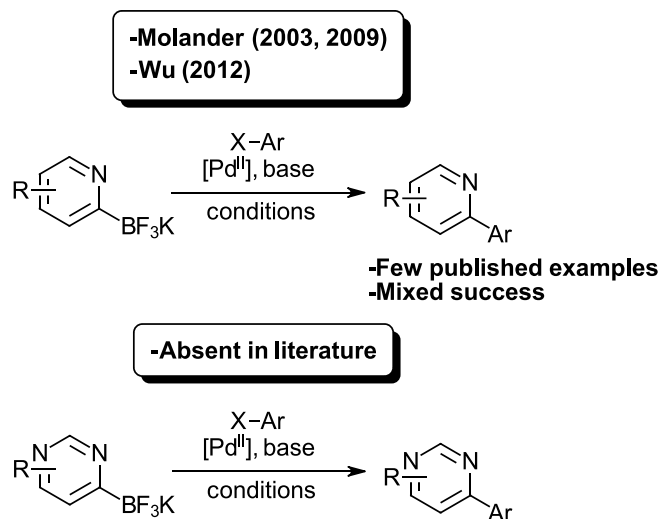
Figure 76: Azine trifluoroborate salts have been met with mixed success when their Suzuki-Miyaura cross coupling potential is explored, however this has not been attempted for pyrimidin-6-yl trifluoroborate salts specifically

1.2. Results and discussion

1.2.1. Synthesis of ynone trifluoroborates

Some of the experiments described in this chapter were performed in collaboration with Mr Elliot McColl during his MSc research project at the University of Sheffield

As shown, ynone trifluoroborates have proven themselves in recent years[219,220,222] as versatile and robust intermediates for heterocycle synthesis. In order to investigate the feasibility of producing useful pyrimidines *via* these intermediates, we applied the published 3-step procedure to obtain the model trifluoroborate **166** (figure 77). This is a convenient synthesis starting from widely accessible aldehydes, using commercially available reagents. While **166** and a number of other aryl-substituted ynones were smoothly produced, aliphatic- and heterocyclic- substituents on products **171** and **172** were more challenging to incorporate.
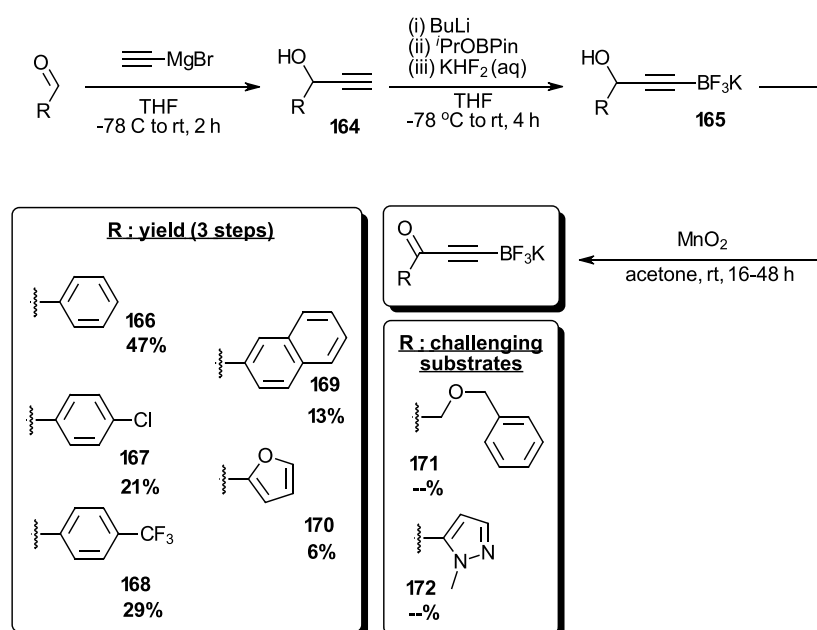
Figure 77: Synthesis of ynone trifluoroborate salts from aldehydes, following the three step literature procedure

The failure to obtain the ynone trifluorobrate **171** after MnO$_2$ oxidation of the corresponding ynol trifluoroborate stems from both the higher oxidation potential of the aliphatic (propargylic) alcohol (compared to benzylic substrates **166-170**) and the potential for undesired reactivity of any intermediate radical at the distal benzylic position. Potential undesired reactivity of the pyrazole ring in substrate **172** with butyllithium likely hindered access to the desired ynol trifluoroborate, which could not be obtained in high enough purity to continue. Nonetheless, the chemistry did allow us to produce a broad enough range of ynones to continue the study.

1.2.2. Synthesis of (amino)pyrimidin-6-yl trifluoroborate salts

With a range of ynone trifluoroborate salts in hand, we sought to subject them to commercially available benzamidine. Using conditions investigated by a co-worker, 100% conversion of **166** (figure 78, as judged by ^{19}F NMR spectroscopy) was observed and the pyrimidin-6-yl trifluoroborate salt **173** was obtained after precipitation from acetone in 73% yield. This reaction was subsequently scaled to 4.2 mmol, allowing analytically pure **173** to be obtained in 85% yield, The structure of which was unambiguously determined by single crystal X-ray analysis (figure 79 and appendix 6).
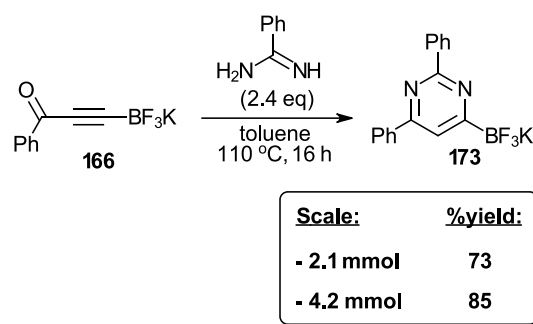
Figure 78: Preliminary investigations into the preparation of pyrimidin-6-yl trifluoroborate salts
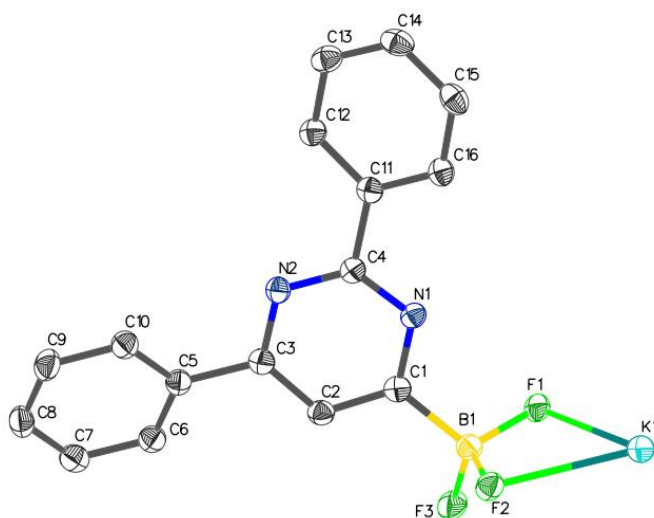
*Figure 79: ORTEP of the crystal structure for the pyrimidin-6-yl trifluoroborate potassium salt **173** (ellipsoids are shown at 50% probability)*

Encouraged by this result, further ynones (figure 80) were subjected to the same conditions, allowing pyrimidin-6-yl trifluoroborate salts **175**-**179** bearing a benzene ring at the 2-position to be isolated in moderate to excellent yield. To investigate the scope of this reaction with respect to the 2-position of the pyrimidine, we needed access to a range of amidines. Many of these are commercially available, but most are supplied cheaply as their HCl salts. The reaction of benzamidine hydrochloride with **166** (figure 81) proceeded with 0% conversion under the standard conditions. Addition of stoichiometric

quantities of bases NEt$_3$ and NaOEt resulted in complete conversion, but a mixture of compounds was obtained, comprising mostly the protodeborylated pyrimidine **180**.
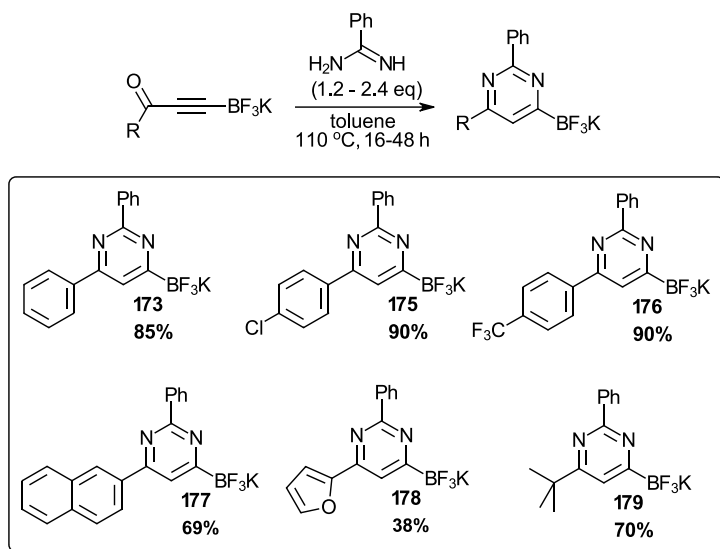
Figure 80: Scope of pyrimidine-forming reaction, from the ynone trifluoroborate perspective

Additive	% conv	%isol
-	0	-
NaOEt/EtOH	100	-
NEt$_3$	100	-
K$_2$CO$_3$	100	17
Cs$_2$CO$_3$	100	30
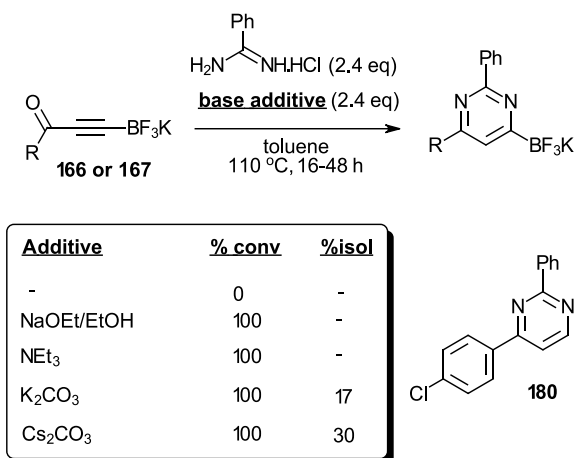
*Figure 81: Attempted in situ freebasing condensation of benzamidine hydrochloride with ynones **166** or **167***
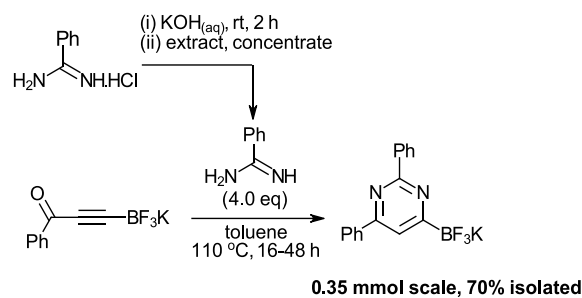
Figure 82: Isolation of amidine freebase prior to condensation

Next, carbonate bases K_2CO_3 and Cs_2CO_3 were investigated for *in situ* freebasing. The reactions using both bases proceeded with 100% conversion under the standard conditions, however the product pyrimidine was isolated in low yield in each case. The low yield is attributed to higher levels of product protodeborylation and the added purification step to remove insoluble salts. For the case of Cs_2CO_3, a slightly higher yield of the pyrimidine product was obtained after purification. Given the possibility of K^+/Cs^+ interchange between the trifluoroborate and carbonate salts and the significant characterisation challenge associated with this, we opted to freebase the amidine *ex situ* in a separate step (figure 82). The neutralisation was achieved by either reaction of the hydrochloride salt with NaOH/KOH then extraction & concentration, or elution of the freebase from a cation-exchange column using methanolic ammonia. Reaction of these freebased amidines with ynone **166** allowed pyrimidin-6-yl trifluoroborates **181-187** to be isolated in good to excellent yield (figure 83). The heteroaromatic amidine precursor to product **184** was obtained as a commercially available freebase. Subjecting urea to **166** under the standard conditions resulted in complete recovery of the starting materials, presumably due to poor solubility of urea in the reaction solvent along with a low nucleophilicity. A commercial sample of trifluoroacetamidine (figure 84) was subjected to **166** under slightly modified conditions (refluxing IPA inside a sealed tube), affording the pyrimidine **188** in 58% yield after purification.
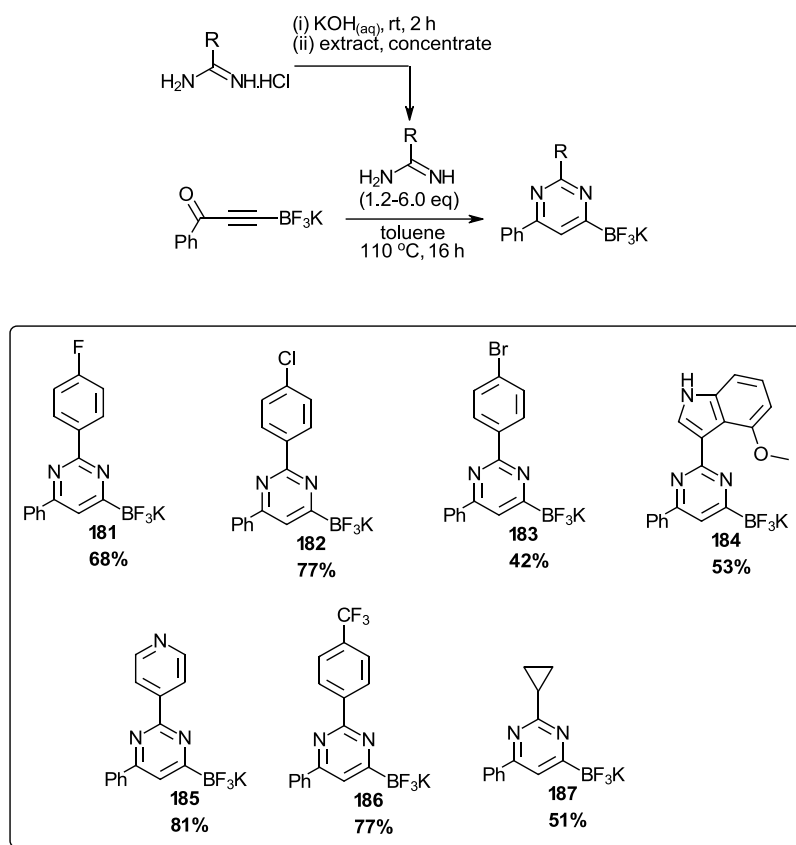
Figure 83: Neutralisation of amidine hydrochloride salts prior to condensation with ynone **166**
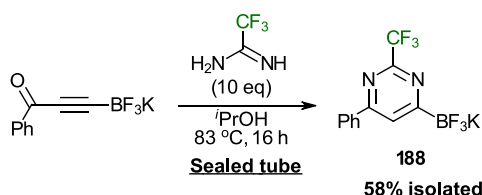
Figure 84: Condensation of trifluoroacetamidine with ynone **166**

A study by Castillo and Buchwald in 2016 noted that out of the FDA-approved pyrimidine-containing pharmaceuticals, 88% contained an amino group and out of these, 38% were 2-aminopyrimidines.[225] Given the prevalence of (2-)aminopyrimidines in currently marketed medicines, we sought to access this privileged scaffold by reaction of ynone trifluoroborates with guanidine derivatives (figure 85). As a convenient "free-guanidine" equivalent for these reactions, we used commercially available acetylguanidine. The reaction proceeded with 100% conversion to the acetylated aminopyrimidine-6-yl trifluoroborate **189**, which was isolated in 36% yield. Interestingly, changing the solvent from toluene to IPA, the acetyl group was cleaved to produce only the aminopyrimidine trifluoroborate **190**, which was isolated in 47% yield.
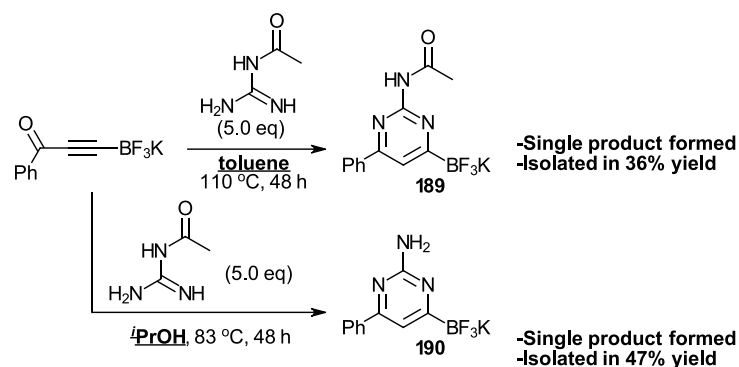
Figure 85: Condensation of acetylguanidine with ynone 166

Changing the guanidine equivalent to the pivaloyl guanidine **191** (figure 86), **190** was obtained as the sole product after refluxing in toluene and was isolated in 56% yield. Upon increasing the number of equivalents of **191** to 5.0 and scaling the reaction to 2 mmol, **190** was isolated in 91% yield. After finding optimal conditions for this condensation protocol, we applied it to a small family of ynone trifluoroborates, representing a diverse scope of substituents including aromatic (**193**, figure 87), heteroaromatic (**194**) and aliphatic (**195**) side chains. All of the 2-aminopyrimidin-6-yl trifluoroborates could be isolated in very good to excellent yield.
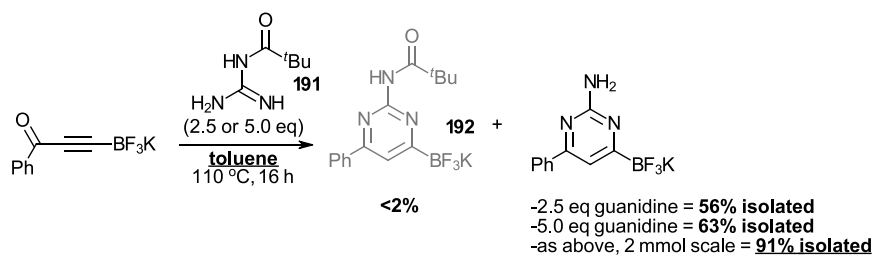
Figure 86: Condensation of pivaloyl guanidine with ynone 166
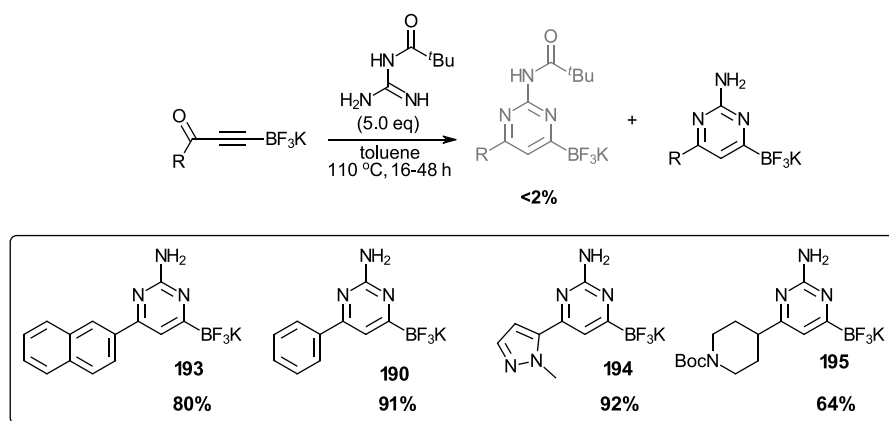
Figure 87: Scope of reaction of ynones with pivaloyl guanidine

Considering the loss of the pivaloyl group upon creation of the aminopyrimidine **190**, this may occur in two ways based on literature precedent. The first is *via* formation of the protected aminopyrimidine **196** (figure 88), followed by base-promoted hydrolysis. This is a known transformation for 2-aminopyrimidines[226] and 2-aminoquinazolines,[227] where the acyl/pivaloyl group is hydrolysed by gentle heating in the presence of NaOH(aq). An alternative mechanism for pivaloyl group loss may originate from the known acyl transfer process that occurs with acetylated guanidines.[228] Specifically, **191** could undergo a disproportionation-type process that would produce bis(pivaloyl)guanidine **198** (figure 88) and one molecule of guanidine, which would react rapidly with **166** under the reaction conditions due to its higher nucleophilicity. Limited evidence for the latter mechanism is provided by subjection of **191** to the reaction conditions without the ynone **166**. **191** was transformed in low conversion to a compound mixture from which **198** (figure 89) was isolated in **13% yield**.
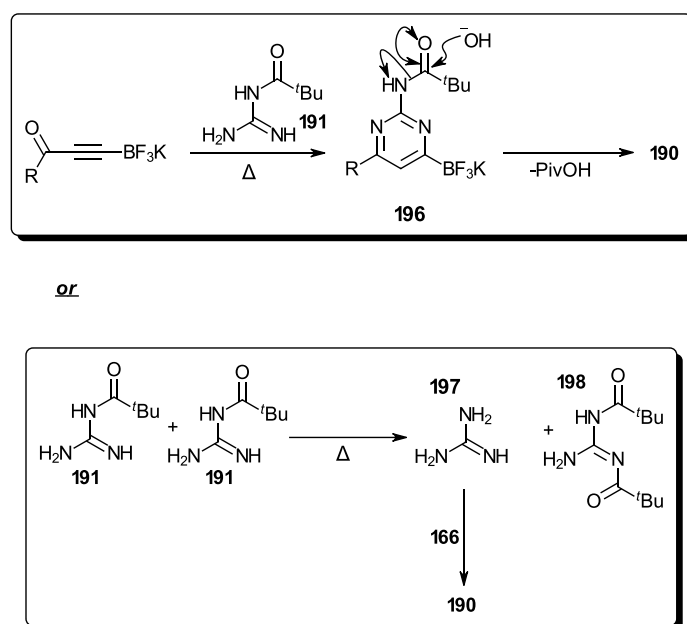
Figure 88: Rationale for the formation of the unsubstituted aminopyrimidine 192
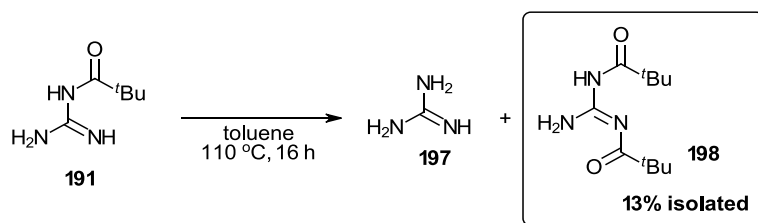
Figure 89: Subjection of pivaloyl guanidine 191 to the reaction conditions, isolation of bis(pivaloyl) guanidine 198

Having investigated the reactivity of acyl guanidines towards ynone trifluoroborates, we then turned our attention towards alkyl- and aryl-substituted guanidines. We began by testing commercially available (4-chlorophenyl)guanidine (figure 90) and found that two major products were formed (as

judged by the crude ^{1}H and ^{19}F NMR spectra, see appendix 1). LCMS analysis suggested the presence of two regioisomers of equal mass **200** and **201**, along with a product of imine hydrolysis **202** assigned tentatively in figure 90. Isomer **200** was successfully isolated by crystallisation and identified by correlating its ^{19}F NMR chemical shift to those of products **190**, **193-195** (figure 87, see appendix 2), isomer **201** was not isolated and so its identity remains unconfirmed.
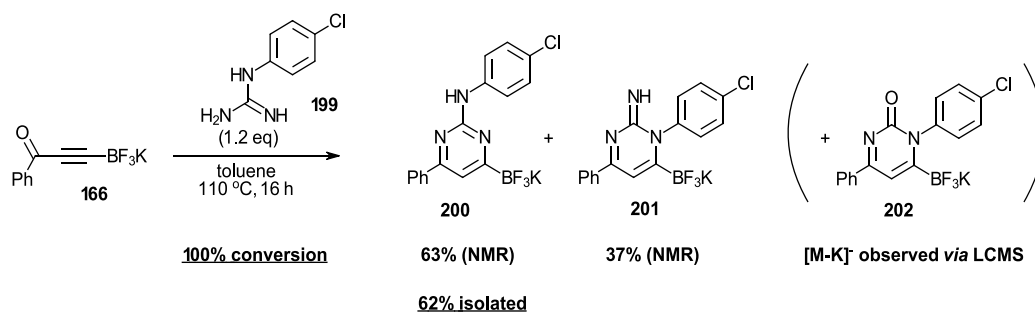
Figure 90: Condensation of (p-chloro)phenyl guanidine with the ynone 166

Some alkylguanidine hydrochloride salts are commercially available, but for the sample that we were interested in testing, a literature[229] procedure starting from cyanamide was employed (figure 91). After neutralising and purifying the obtained guanidine hydrochloride salts, we subjected the corresponding monosubstituted guanidine freebases **213-215** (figure 92) to the ynone **166** under the standard conditions (figure 93). A mixture of two organotrifluoroborate compounds was formed in each case, tentatively assigned as the regioisomers **X** and **Y**, analogous to the compounds **200** and **201** respectively, although in this case with a higher preference for the "aminopyrimidine-type" isomer **X** (on the basis of correlated ^{19}F NMR data, see appendix 2), which could be isolated from the mixture by crystallisation in modest yield. Pleasingly, a procedure for the *in situ* neutralisation of the guanidine hydrochloride salts followed by condensation with **166** was realised through the use of K_2CO_3. This procedure was successfully applied to commercially available methylguanidine hydrochloride and guanidine hydrochlorides **206** (figure 91), **208** and **210**. The regioselectivity was similar when comparing the use of either the guanidine freebase or hydrochloride, but the latter procedure was taken forward for further optimisation allowing the products **219**-**222** to be isolated in good yield after crystallisation from the crude mixture. In the case of compound **220**, the structure was unambiguously determined by single crystal X-ray analysis (figure 95), showing that the benzyl group resides on the exocyclic nitrogen atom. Interestingly, subjection of the dialkyl substituted guanidine freebases **211** and **212** to **166** under the standard conditions resulted in clean protodeborylation in each case (figure 94), providing the aminopyrimidines **223** and **224** exclusively, with only trace quantities of the expected pyrimidin-6-yl trifluoroborates observable *via* LCMS. The strongly basic dialkylamine portions of these guanidines may facilitate this undesired decomposition pathway, in a fashion similar to Et_3N (figure 81).
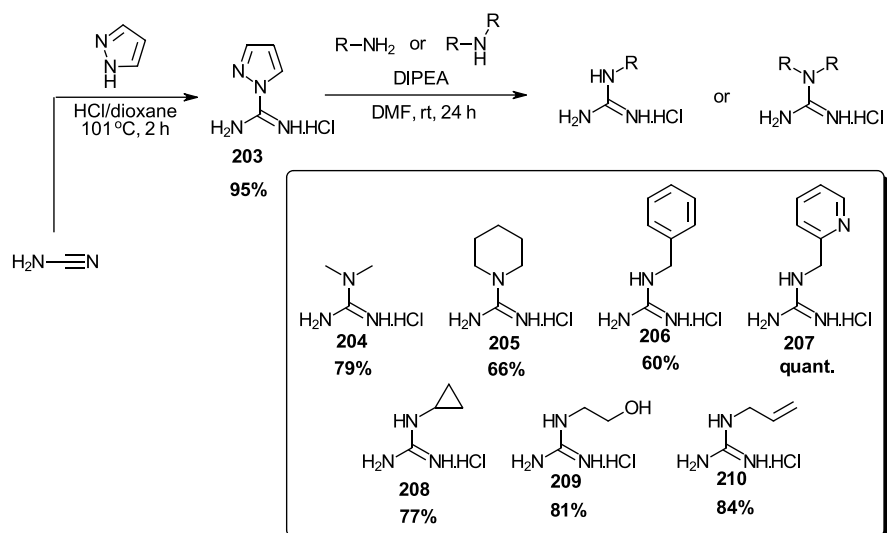
Figure 91: Method used in this work to obtain alkyl-substituted guanidine hydrochloride salts
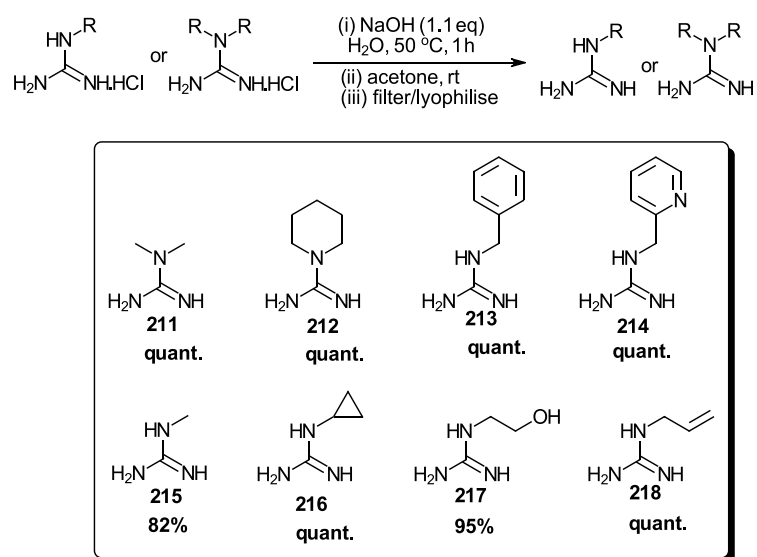
Figure 92: Neutralisation and purification of guanidine hydrochloride salts (methylguanidine hydrochloride was obtained from a commercial source)

Figure 93: Condensation reactions of alkyl-substituted guanidines with ynone **166**
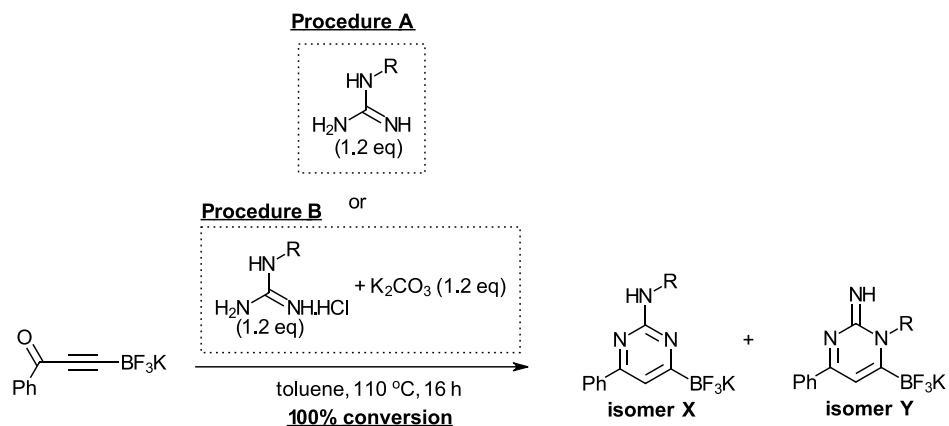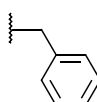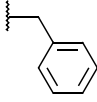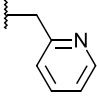
R	Procedure	Ratio X:Y	X isolated
Me	A	3:1	26%; 219
Me	B	2:1	25%; 219
benzyl	A	6:1	40%; 220
benzyl	B	4:1	72%; 220
pyridylmethyl	A	3:1	-
allyl	B	10:1	57%; 221
cyclopropyl	B	6:1	70%; 222
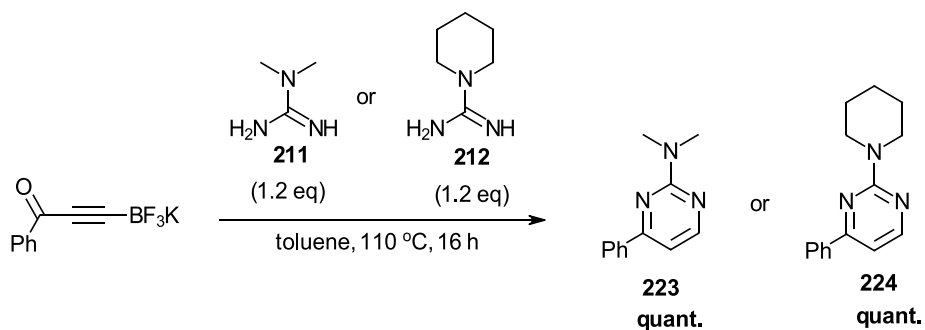
Figure 94: Observed incompatibility of the dialkyl-substituted guanidines with the production of the corresponding pyrimidin-6-yl trifluoroborate salts.
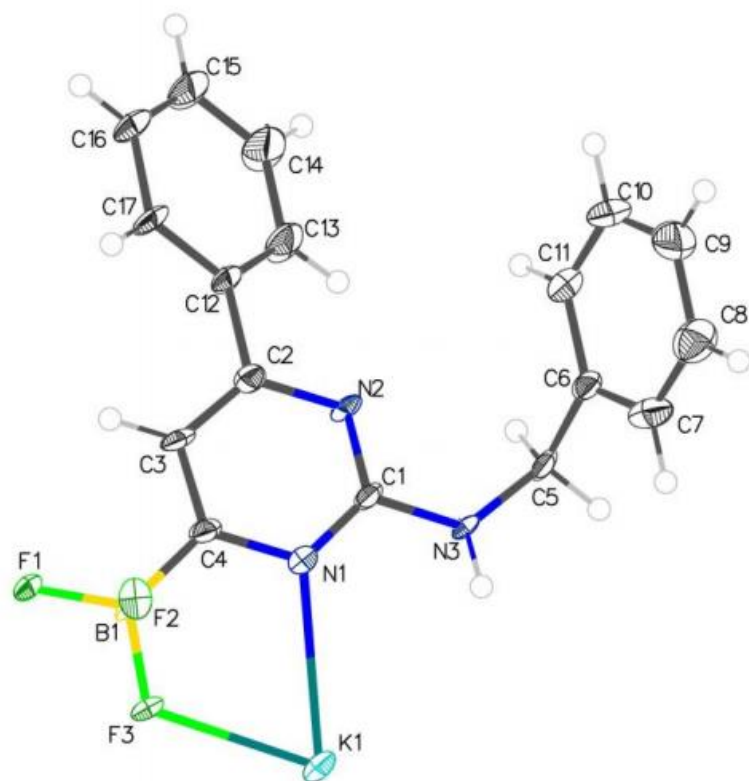
*Figure 95: ORTEP of compound **220**, ellipsoids are shown at 50% probability.*

Synthesis of pyrazolopyrimidinyl trifluoroborate salts

Inspired by the observation of "azopyrimidinone" type products **201** (figure 90), we wanted to explore the possibility of forming alternative heterocyclic trifluoroborate salts using the ynone **166**. 3-Aminopyrazole derivatives have been used extensively in reactions with 1,3-dicarbonyl compounds to form valuable fused pyrazolopyrimidines and pyrimidoindazoles, these heterocycles have a number of uses including as modular cores for luminescent materials[230–232] or important bioactive compounds.[233,234] We were pleased to find that treatment of **166** with 3-aminopyrazole in refluxing toluene resulted in complete conversion within 16 hours. Analysis of the crude reaction mixture by ^{1}H and ^{19}F NMR spectroscopy suggested that a mixture of 2 regioisomers were present (figure 96, *cf* appendix 3 for details). The structure of **225** was confirmed by performing a base-promoted protodeborylation reaction and comparing the data with those already published for the pyrazolopyrimidine **227**, it was assigned as the major isomer after the reaction of **166** with 3-aminopyrazole based on the high yield of isolated product after protodeborylation. In these initial experiments, only the deborylated pyrazolopyrimidine **227** was observed and confirmed, the presumed alternative isomer resulting from deborylation of **226** was not observed, highlighting the need for further experiments to confirm the presence of this salt as the second regioisomer in the condensation of 3-aminopyrazole with ynone **166**.
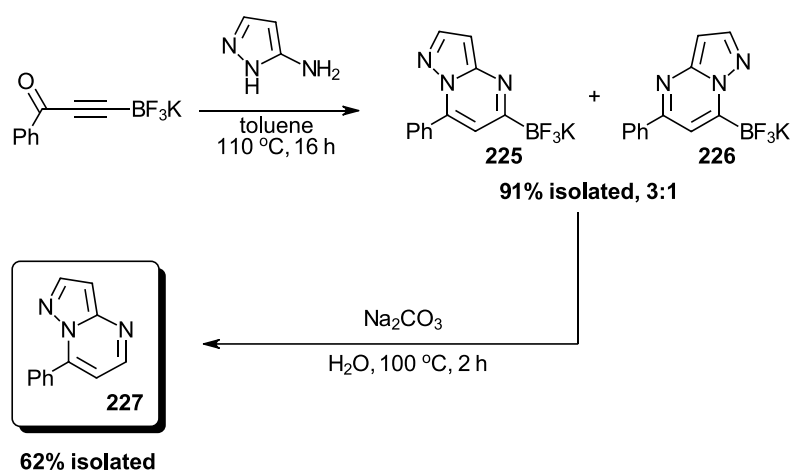
Figure 96: Synthesis of fused pyrimidinyl trifluoroborate salts through condensation of 3-aminopyrazole with 166

1.2.3. Elaboration of (amino)pyrimidin-6-yl trifluoroborate salts

With a range of pyrimidin- and aminopyrimidin-6-yl trifluoroborate salts in hand, we began exploring the potential of these intermediates for further organic synthesis and the production of valuable, highly-substituted pyrimidines. We were intrigued to investigate how we could exploit the borate functionality at C6, but also how the aminopyrimidine core of **190** could function as a template for modular reactivity, due to potentially reactive sites at the amino group and the nucleophilic C5 (figure 97).
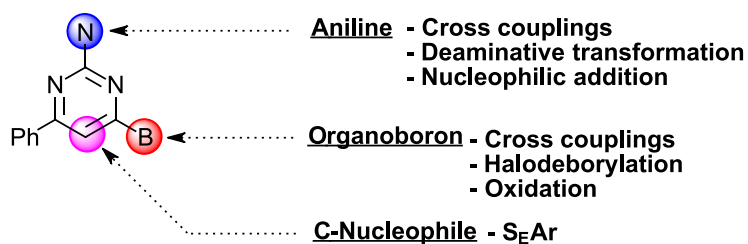
*Figure 97: Identification of reactive sites on **190** for further elaboration*

Functionalisation studies on the amino group of the aminopyrimidin-6-yl trifluoroborate salts
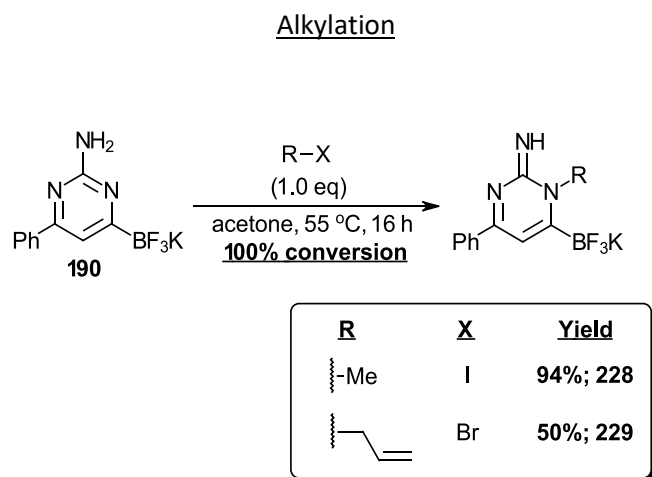
Alkylation

*Figure 98: Ring alkylation of **190** and isolation of the corresponding azopyrimidinone product*

We began functionalisation studies by considering the potential for reactivity at the aminopyrimidine -NH$_2$ of trifluoroborate salt **190** (figure 98). Exploitation of the nucleophilicity of the amino handle was first investigated through alkylation using traditional S$_N$2 chemistry with alkyl halides. Thus, treatment of **190** with iodomethane under established[235] conditions for methylation resulted in 100%
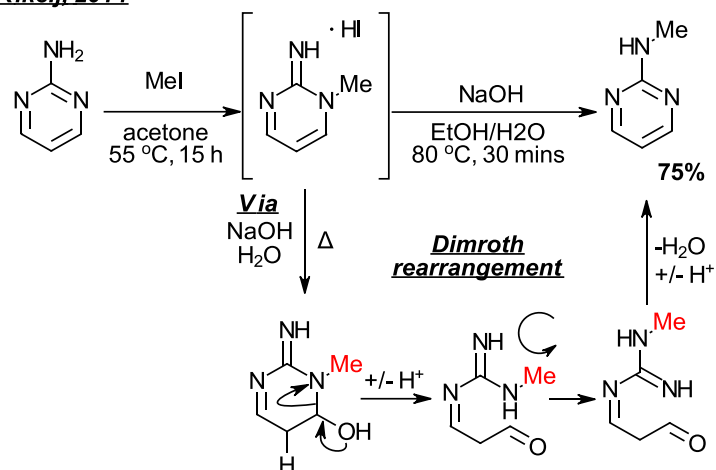
Figure 99: Published two-step method to obtain the product of exocyclic N-alkylation via base-catalysed (Dimroth) rearrangement
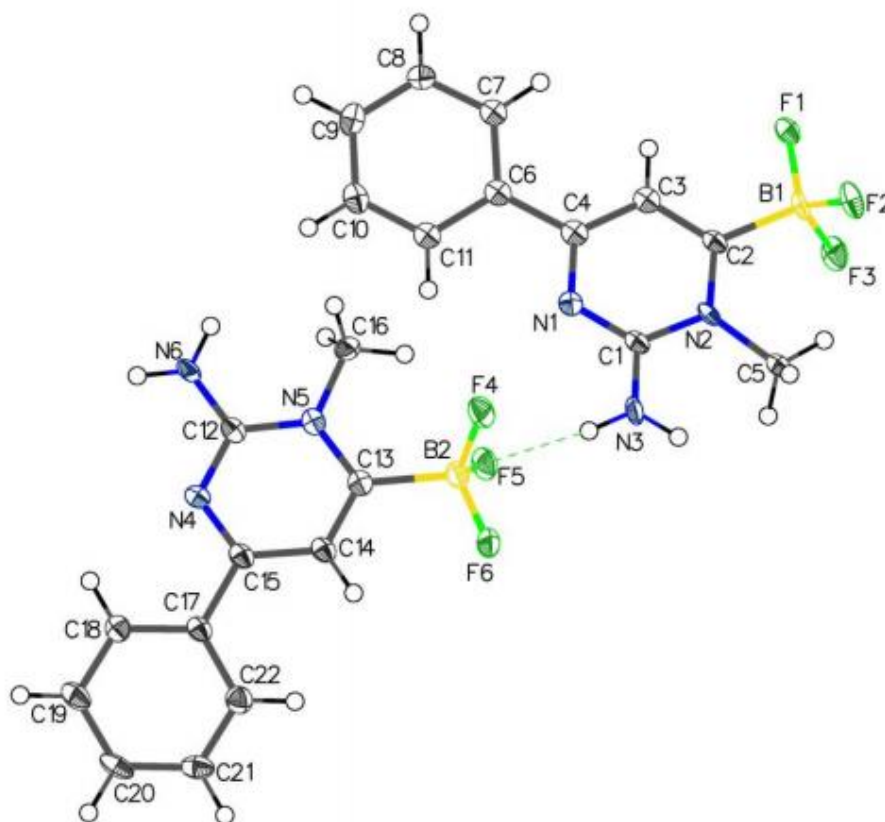
*Figure 100: ORTEP of azopyrimidinone **228***

conversion, providing the ring methylated azopyrimidinone **228**. While it is notable that *ring* alkylation of amino-heterocyclic compounds is known to occur in favour of methylation at the exocyclic nitrogen[236–241] (presumably due to a higher basicity and nucleophilicity residing on the ring nitrogen)[242] the product of exocyclic *N*-alkylation can be obtained *via* subsequent translocation of nitrogen atoms

by a base-catalysed (Dimroth) rearrangement[235,243,244] (figure 99). However, the harsh conditions necessary for *N*-translocation are not suitable for relatively sensitive boronate functionality, and substituted pyrimidines are known to undergo a slow Dimroth rearrangement.[245] In fact, attempts to protodeborylate the methylpyrimidine **228** by a base promoted procedure resulted in a complex mixture of products, due to the multitude of reactions that this product could feasibly undergo when subjected to such conditions (*cf* hydrolysis, protodeborylation, Dimroth rearrangement). Methods to alkylate the exocyclic nitrogen directly are more rare, but a few notable examples of radical[246] and transition metal-catalysed[247–249] alkylations have been published.

Pleasingly, the azopyrimidinone **228** could be isolated in excellent yield after recrystallisation. Single crystal X-ray analysis (figure 100) and an ensemble of 2D NMR experiments (*cf* appendix 4), respectively) confirmed the position of the methyl group to be adjacent to the trifluoroborate unit. The aminopyrimidine **190** could also be alkylated with allyl bromide under similar conditions, allowing the azopyrimidinone **229** to be isolated in good yield after recrystallisation (the regioselectivity was assigned by 2D NMR spectroscopic experiments, and by analogy to **228**). Interestingly, the products **228** and **229** (azopyrimidinones) were also observed in the crude reaction mixtures of alkylguanidine condensation with **166** (figure 93, see appendix 2 for a comparison of NMR data between condensation and methylation routes to **228**) as minor products. Given that no base was used during the formation of **228** and **229**, it was surprising that we did not obtain the corresponding HX salt (HI in the case of **228**, HBr in the case of **229**). Presumably, this is due to a universal lowering of the basicity of the pyrimidine ring by the trifluoroborate group *via* anion-anion repulsion from its conjugate acid (although there is limited evidence[250] to suggest that the trifluoroborate group is actually an electron-donor, which should *increase* the basicity of the heterocycle it is attached to). The question of alkylation selectivity with respect to the two ring *N* atoms remains (figure 101), but this is expected to be due to larger steric hindrance of the Ph group in comparison the the -BF$_3^-$ (*cf* a report published by Harper *et al.*,[243] the authors note that 2-amino-4,6-diphenylpyrimidine could not be alkylated under the tested conditions).
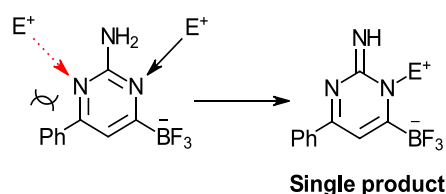
Figure 101: Steric hindrance of the Ph group could direct the electrophile to the other N

Other *N*-functionalisation reactions

With reliable access to pyrimidine alkylation products in hand, we then investigated whether the aminopyrimidin-6-yl trifluoroborate salt **190** could be selectively arylated at the exocyclic nitrogen. While traditionally *N*-arylation of aniline derivatives has been achieved by direct nucleophilic substitution with aryl halides, the conditions necessary for this transformation are often harsh and they typically require activated electrophilic arenes. Aminoheterocycles (e.g. aminopyrimidines) are particularly inert examples of anilines when it comes to reactivity of this sort.[225] In recent years, much

attention has been given to metal promoted/catalysed amine arylation as an alternative to S_NAr chemistry. Notable examples include the use of Pd catalysis,[225] which has revolutionised several fields where complex, highly substituted anilines are required. Another highly useful reaction that has allowed the formation of not only substituted amines/anilines, but also ethers and thioethers under mild, aerobic conditions is the Chan-Lam reaction.[251–253] We wanted to investigate whether the 2-amino handle of our pyrimidin-6-yl trifluoroborate salt could be arylated selectively while keeping the borate unit for later functionalisation. Given that our model substrate **190** is a trifluoroborate salt, we needed a reaction that meets a few requirements in order to provide useful results. Firstly, the reaction should proceed with 100% conversion, so that purification of the *N*-functionalised product may be achieved without the need for arduous recrystallisation protocols. Secondly, the reaction must proceed in a manner that is orthogonal to the activation of the trifluoroborate functional group, so as to avoid undesired side reactions causing the loss of potential for further functionalisation. Lastly, due to the polar nature of trifluoroborate salts, they are not amenable to column chromatography on silica gel and so the reaction must proceed to provide a mixture that can be separated without the need for such a purification method.

t	Comment	Conv
16 h	-	33%
16 h	portion-wise addition of RB(OH)$_2$	33%
16 h	4Å MS omitted	0%
60 h	-	33%
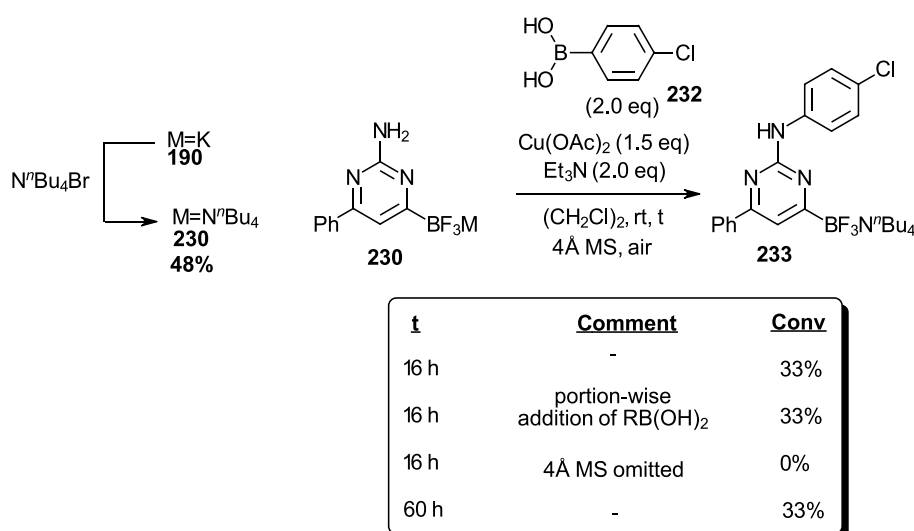
*Figure 102: Attempted Chan-Lam coupling of **230***

With the preceding requirements in mind, we attempted to functionalise the 2-amino handle using aerobic Chan-Lam-type conditions[253,254] (figure 102). We deployed the tetra-^{n}butylammonium salt **230** to eliminate the question of solubility of the starting material. The reaction proceeded to ~33% conversion overnight and unfortunately ceased at this point. No change in conversion was observed after leaving the reaction for 60 hours. It was expected that the boronic acid **232** would be degrading (*via* protodeborylation or oxidation) under the aerobic conditions, so we tried to maximise the chances of it reacting productively by adding it portion-wise over a period of 6 hours. Interestingly, the same result (~33% conversion) was observed, indicating that other factors were causing the reaction to slow down. Conducting the reaction without 4 Å MS resulted in recovery of **230**. The further optimisation of this *N*-functionalisation process will form part of future work for this project.
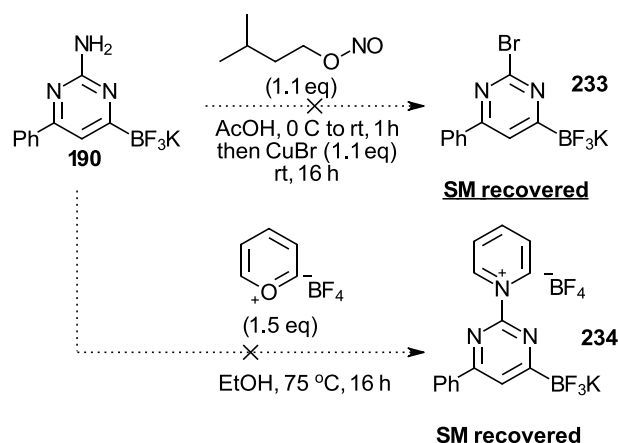
Figure 103: Attempted deaminative functionalisation reactions on the aminopyrimidine 190

Another attractive way to functionalise aminoheterocycles is by *N*-activation, followed by deamination. This is exemplified by the well-known Sandmeyer and Schiemann reactions, where the amino handle is first diazotised by a nitrite salt or an alkyl nitrite, then it is displaced by metal catalysis, S_NAr or homolytic fission. Another deaminative functionalisation principle has been developed by Katritzky and coworkers (figure 103), allowing the formation of highly useful pyridinium salts from simple amines/anilines. We attempted to transform the amino handle of **190** into the 2-bromopyrimidine **233** (figure 103) *in situ*, by treating **190** with isopentyl nitrite in AcOH at 0 °C, then adding CuBr followed by overnight stirring. The starting material was recovered, indicating that the diazo intermediate was not formed. The solubility of **190** in the reaction solvent at 0 °C was very low, thus further work on this transformation would include deployment of the corresponding tetra-*N*-alkylammonium salts of **190** (e.g. **230**, figure 102). In an attempt to access the *N*-activated pyridinium "Katritzky" salt **234**, we treated **190** with the required pyrylium tetrafluoroborate, however only unaltered starting material was recovered after overnight heating, indicating that the pyridinium didn't form, or that it subsequently reversed to **190** under the reaction conditions.

Functionalisation of the pyrimidine C5

2-aminopyrimidines are well known to be amenable to S_EAr reactions at the 5-position, driven by the strong directing effect of the amino group. A range of electrophiles can be used to forge new bonds at this position, including C-C and C-Halogen bonds. To begin our investigations on the potential of **190** to carry out established 2-aminopyrimidine S_EAr chemistry while preserving the borate functionality, we attempted to selectively formylate[255] it using traditional Vilsmeier-Haack conditions (figures 104 and 105). While high conversion of **190** was achieved, LCMS analysis of the crude reaction mixture (figure 105) gave two major assignable peaks, tentatively the formylation product **236**, and the intermediate dimethyliminium **235**. The apparent occurrence of **235** suggested that the aqueous workup consisting of 2 hours of stirring in the presence of K_2CO_3 was not sufficient to hydrolyse the iminium completely. Thus, the workup reaction was left to stir for 16 hours and pleasingly all trace of the intermediate **235** disappeared. After scrutinising the product left after workup, we concluded that
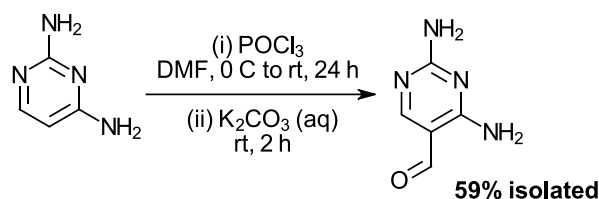
Figure 104: Literature formylation of 2,4-diaminopyrimidine using the Vilsmeier reagent
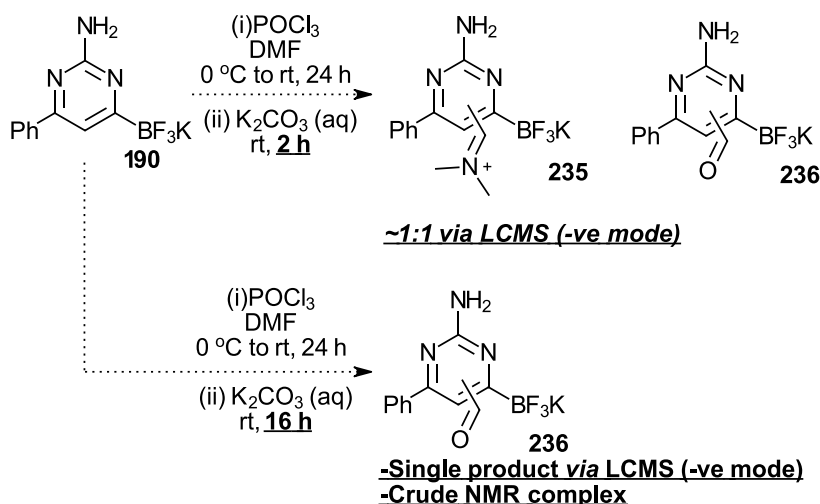
Figure 105: Attempted formylation of **190** using the literature procedure

although a formylation reaction had taken place, it was not at the expected C5 position (based on the observation of a pyrimidine *C*H peak in the ^{13}C NMR spectra). The material left over consisted of a complex mixture and regrettably, none of the desired product could be isolated. We turned our attention to C5 halogenation, which has been used extensively to perform diverse chemistry at this position in 2-aminopyrimidines. Accordingly, we subjected **190** to *N*-bromosuccinimide under conditions similar to those published[256] (figure 106) and were pleased to find that a very rapid reaction took place, reaching completion in less than 30 minutes. A single product was obtained, which was confirmed to be the bromopyrimidine **237**. It was subsequently found that **237** could be conveniently separated from the reaction mixture just by dilution with Et$_2$O and filtration, providing analytically pure material after drying the precipitate *in vacuo*. Encouraged by this result, we attempted to apply the same principle to other electrophilic halogenation reagents. Subjection of **190** to 1.1 equivalents of *N*-chlorosuccinimide resulted in low conversion after 3 hours of stirring, along with an unassignable mixture of products. The equivalent use of *N*-iodosuccinimide led to very low conversion of **190**.

In order to extend this principle to electrophilic fluorination at C5, we followed literature precedent by departing from less readily available *N*-fluorosuccinimide (one example of use[257]) in favour of the established bench-stable and cheaply available reagent Selectfluor. Armstrong *et al.*[258]

Figure 106: Screen of succinimide electrophilic halogenation reagents for reactivity at the aminopyrimidine C5
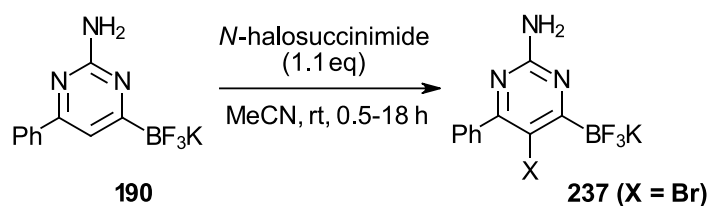
X	Time	Outcome
Cl	3 h	Complex
Br	30 mins	100% conv, 86% **237** isolated
I	18 h	<2% conversion
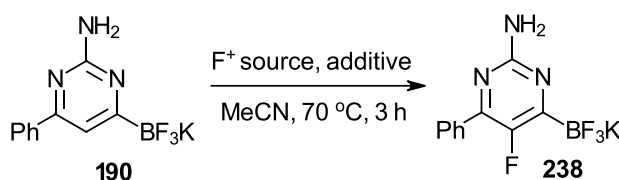
$F^{\pm}$ source	Equivs	Additive	Conversion
-Selectfluor	1.2	-	58%
-Selectfluor	2.5	-	48%
-Selectfluor	1.2	Ag_2CO_3 (0.5 eq)	71%
-Selectfluor	1.2	Ag_2CO_3 (1.0 eq)	78%
-Selectfluor	1.2	Ag_2CO_3 (2.0 eq)	100%
-NFSI	1.2	Ag_2CO_3 (2.0 eq)	<2%
-1-Fluoro-sym-collidinium tetrafluoroborate	1.2	Ag_2CO_3 (2.0 eq)	<2%

Figure 107: Optimisation of conversion in electrophilic fluorination of aminopyrimidine C5

found that 2,4-diaminopyrimidine was selectively fluorinated at C5 using 1.5 equivalents of Selectfluor at room temperature within 6 hours. The product was isolated in only 24% after chromatography on silica gel, reflecting the low conversion of the starting pyrimidine. We tried these conditions with pyrimidin-6-yl trifluoroborate **190** (figure 107) and found that a new trifluoroborate compound formed (as judged by new peaks in the crude ^{19}F NMR spectrum) that could correspond to the fluoropyrimidine **238** (figure 108), however, the new trifluoroborate peak was present in approximately equal intensity with the starting pyrimidine, so we sought ways to drive this reaction to completion. Use of silver carbonate as a promoter in this reaction has been shown to provide high yields of some 2-amino-5-fluoropyrimidines,[259] thought to form a silver complex which facilitates a
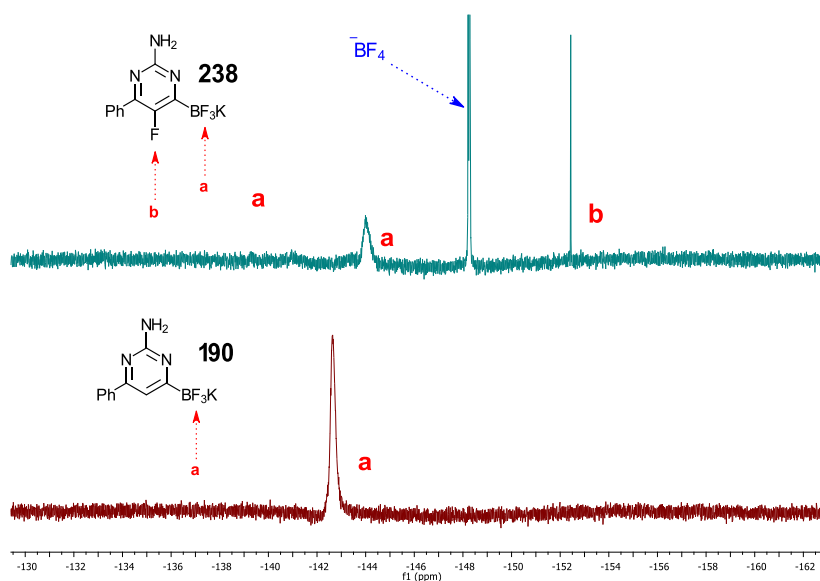
Figure 108: ^{19}F NMR (376 MHz, DMSO-d^6) overlay showing (top) the material obtained after optimisation of pyrimidine fluorination to 100% conversion, and (bottom) the starting material. -BF$_4$ is largely from Selectfluor derived salts.

redox event leading to the incorporation of fluorine at C5. Use of Ag$_2$CO$_3$ was indeed highly useful for the fluorination of **190** (figure 107), leading to full conversion within 3 hours. Both heat and Ag$_2$CO$_3$ were necessary for the reaction to reach completion and no reaction was observed when alternative "F$^+$" sources NFSI and 1-fluoro-*sym*-collidinium tetrafluoroborate were used.[260] Once the reaction had reached completion, our attention was turned to the purification of **238**. Regrettably, attempts to separate **238** from residual Selectfluor and byproduct salts including precipitation and recrystallisation were unsuccessful. Further work on this reaction would thus include a further optimisation of purification methods, and perhaps a review of the starting materials and reagents.

Functionalisation of the C6 trifluoroborate

Having explored the potential for **190** to undergo transformations at positions around the pyrimidine core while leaving the 6-boryl functionality intact, we then looked to how the borate itself can be successfully activated for functional group interconversion. Suzuki-Miyaura (SM) cross coupling has become a hugely important transition metal-catalysed process in industry and academia for synthesising biaryls and polyaryls and is synonymous with organoboron chemistry.

Thus, our first priority was to assess the reactivity of our pyrimidin-6-yl trifluoroborate salts under various cross-coupling conditions and work towards a viable procedure. We began by preparing the expected products of the cross coupling reaction of 4-bromobenzonitrile with the trifluoroborate salt **173** (figure 109) in order to obtain a complete picture of the reaction products by comparing TLC and NMR analytical data. Specifically, the cross coupling product **239** itself and the product of protodeborylation **240** were obtained *via* independent routes. Protodeborylation is a well-known undesired side reaction that was anticipated to occur on a significant scale during the optimisation of these reactions.
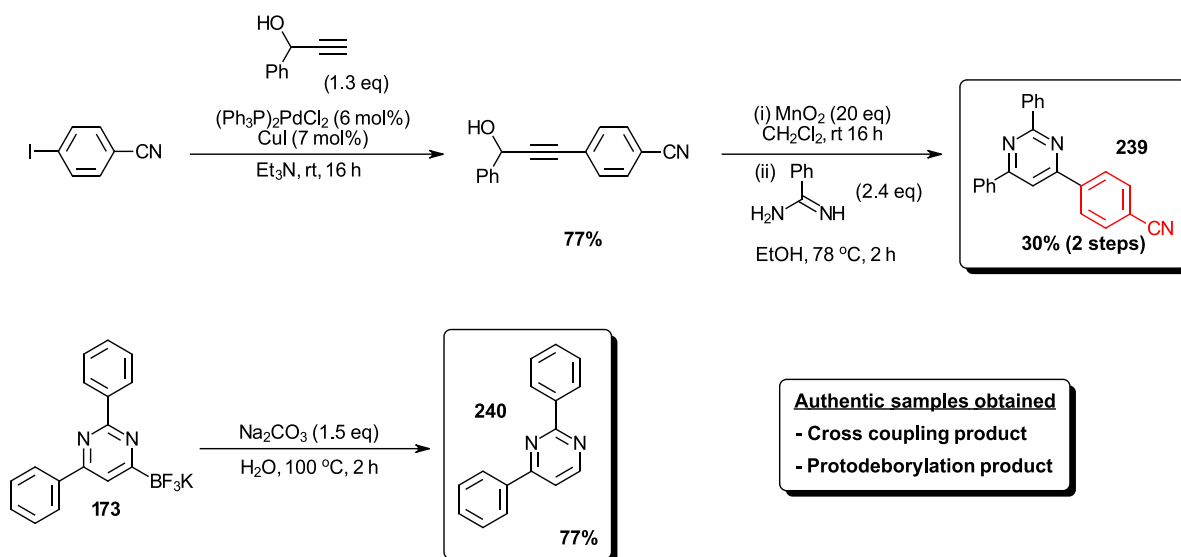
Figure 109: Preparation of expected products of Suzuki-Miyaura cross coupling as analytical references

Initial studies attempted to use Suzuki-Miyaura cross coupling conditions that were successful in coupling pyrazol-3-yl trifluoroborate salts[219,222] (figure 110). The conditions that were utilised in the cross coupling of pyrazolyl trifluoroborates resulted in low conversion of **173**, and where higher conversion was attained through changes to the conditions (entries **1-4**, **8-9**), the product of protodeboronation predominated with only trace quantities of desired coupling product being observed. Further examples of cross-coupling procedures of heterocyclic boronic acid derivatives from the literature[205,261] failed to provide high conversion of **173**. A procedure developed by Molander and coworkers for the SM coupling of potassium vinyltrifluoroborate with (hetero)aryl electrophiles[262] was then utilised for the coupling of **173** (figure 111), and the crude ^{1}H NMR spectrum seemed to show selectivity for the coupled product **239** over protodeborylation product **240** (albeit in low conversion).

This was a promising start and showed that to get productive conversion of **173** into **239** via Pd-catalysed cross coupling, the choice of solvent was crucial and water was likely a requirement. Upon increasing the proportion of water in the reaction solvent (figure 112), a higher conversion to **239** was

*Figure 110: Initial optimisation studies towards Suzuki-Miyaura cross coupling conditions for trifluoroborate salt **173**. Unless stated otherwise, yield was estimated by ^1H NMR spectroscopy*
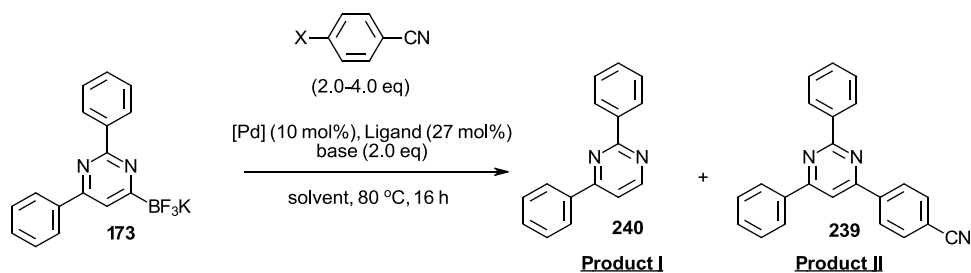
Entry	Pd source	Ligand	Base	Solvent	X	Conv	Yield I	Yield II
1	Pd(OAc)$_2$	XPhos	Et$_3$N	MeCN/EtOH	Br (2.0 eq)	38%	38%	-
2	PdCl$_2$	XPhos	Et$_3$N	MeCN/EtOH	Br (2.0 eq)	41%	41%	-
3	Pd(OAc)$_2$	RuPhos	Et$_3$N	MeCN/EtOH	Br (2.0 eq)	33%	33%	-
4	Pd(OAc)$_2$	SPhos	Na$_2$CO$_3$	^{i}PrOH	Br (2.0 eq)	64%	57%	7%
5	Pd(OAc)$_2$	XPhos	Na$_2$CO$_3$	MeCN/EtOH	Br (2.0 eq)	0%	-	-
6	Pd(OAc)$_2$	XPhos	K$_2$CO$_3$	MeCN/EtOH	Br (2.0 eq)	0%	-	-
7	Pd(OAc)$_2$	XPhos	Et$_3$N	MeCN	Br (2.0 eq)	0%	-	-
8	Pd(OAc)$_2$	XPhos	Et$_3$N	MeCN/EtOH	Br (4.0 eq)	33%	33%	-
9	Pd(OAc)$_2$	XPhos	Et$_3$N	MeCN/EtOH	I (2.0 eq)	17%	17%	-

Figure 111: Adaptation of Molander's organotrifluoroborate coupling conditions, affording a more product-selective procedure, as observed in the crude ^1H NMR spectrum (400 MHz, DMSO-d^6)
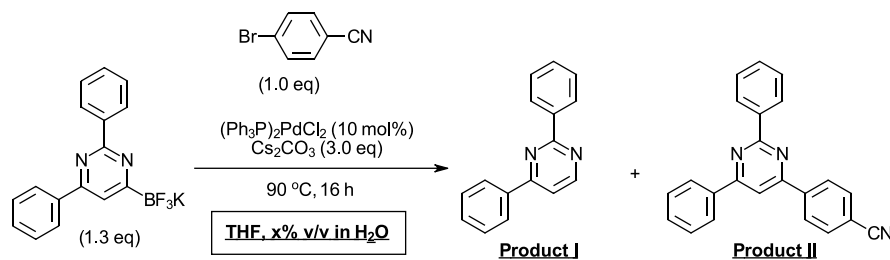
Figure 112: Investigation into the effect of H_2O concentration on conversion of the starting trifluoroborate salt. Unless stated otherwise, yield was estimated by ^1H NMR spectroscopy
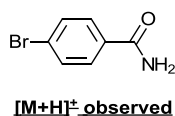
Figure 113: Product of substrate aryl bromide hydrolysis, observed in crude reaction mixture via LCMS

observed while keeping the relative amount of protodeborylation low. Use of 50% water in THF as the reaction solvent, **239** was subsequently isolated in a separate reaction with a yield of 36%. After scrutinising the crude material left over after subsequent (unsuccessful) optimisation attempts,[263], we noticed the formation of 4-bromobenzamide (figure 113) which is the hydrolysis product of 4-bromobenzonitrile. Assuming that this potential background process might interfere with product formation and isolation, we changed our aryl bromide substrate to one that is more resistant to hydrolysis, namely, 4-bromobenzotrifluoride (figure 114). Through employment of this electrophile and upon increasing the reaction time to 48 hours, we were able to isolate the desired cross coupling product in up to 64% yield after purification. Attempts to use microwave radiation to speed the reaction up resulted in complete conversion within 2 hours (figure 115). However, the product **241** was isolated in only 48%, along with a significant portion of protodeborylated pyrimidine **240** (23% isolated). Judging that the microwave heating compromised the selectivity between cross coupling and protodeborylation, we decided to proceed with conventional heating for a longer period instead. With this result in hand, we attempted to extend the conditions for cross-coupling to the aminopyrimidine **190** but obtained the desired coupling product in only 11% yield after purification. Along with the coupled product, the product of protodeborylation (aminopyrimidine **242**, figure 116) was obtained in 29%, indicating that **190** is more prone to decomposition than **173** under the present
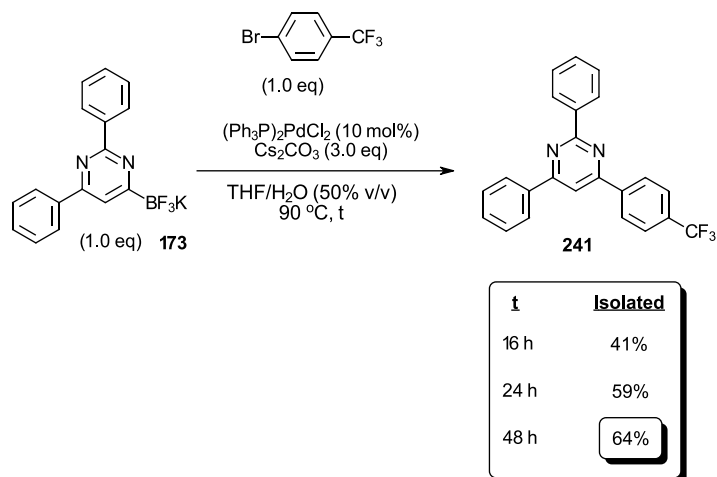
Figure 114: Use of an alternative, hydrolysis-resistant aryl bromide in Suzuki-Miyaura cross coupling reactions
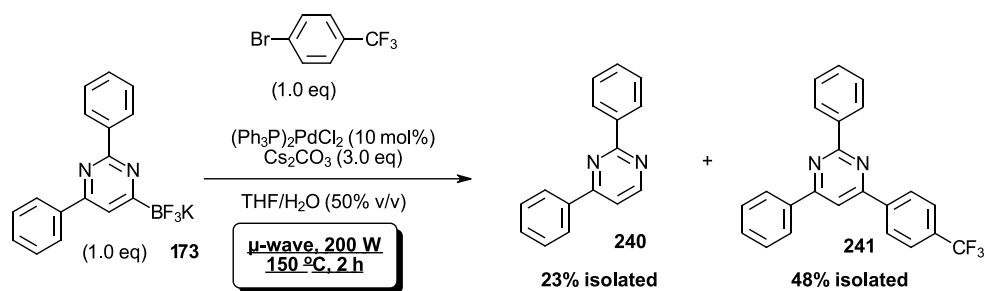
*Figure 115: Use of microwave heating in the Suzuki-Miyaura cross coupling reaction of **173** provides a significant shortening of reaction time, at the cost of a slightly diminished yield*
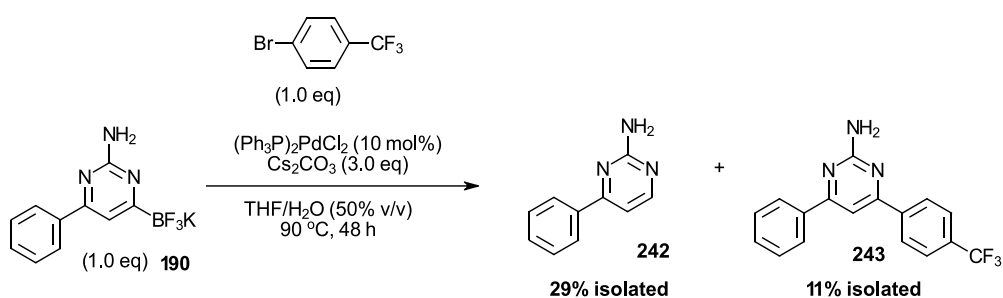
*Figure 116: Application of the optimised Suzuki-Miyaura cross-coupling conditions to aminopyrimidinyl trifluoroborate salt **190***

conditions. Next, 2.0 equivalents of the trifluoroborate **190** was used, and a screen of reaction condition parameters was undertaken (figure 117) to maximise cross coupling efficiency. Gratifyingly, the use of Ag_2O as an additive helped to suppress the undesired protodeborylation reaction (compare entries **1** and **2**), relative to productive cross coupling. The use of Ag_2O as an additive is common for

enabling the Suzuki coupling of challenging boronic acid derivatives.[264–267] The reason for this is believed to be due to a facilitation of the
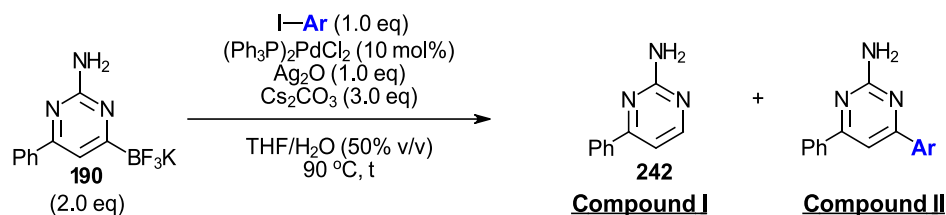
Entry	Ar	t	Conversion of trifluoroborate	Ratio I:II	NMR Yield II	Isolated yield II
1[a]	Ph	16 h	80%	5:1	20%	-
2	Ph	16 h	56%	1:4	28%	-
3[b]	Ph	16 h	63%	1:2	4%	-
4[c]	Ph	24 h	26%	1:3	18%	-
5	3,5-Me$_2$C$_6$H$_3$	16 h	100%	1:4	26%	-
6	3,5-Me$_2$C$_6$H$_3$	24 h	100%	1:3	72%	-
7[d]	3,5-Me$_2$C$_6$H$_3$	24 h	100%	1:5	42%	-
8	3,5-Me$_2$C$_6$H$_3$	48 h	100%	1:3	63%	56%
9[e]	3,5-Me$_2$C$_6$H$_3$	16 h	100%	nd	nd	11%
10	3,5-Me$_2$C$_6$H$_3$	48 h	100%	nd	nd	59%
11	Ph	48 h	100%	nd	nd	61%

[a] - Ag$_2$O additive was omitted, [b] - K$_2$CO$_3$ was used instead of Cs$_2$CO$_3$, [c] - Addition of PhI and **190** in 2 portions [d] - Addition of (Ph$_3$P)$_2$PdCl$_2$ in 2 portions, [e] - Reaction mixture more concentrated (0.24 M)

*Figure 117: Optimisation of reaction parameters for cross coupling of aminopyrimidine **190** with aryl iodides. Stated conversion and NMR yields were determined by H NMR spectroscopy, using 1,3,5-trimethoxybenzene as an internal standard*
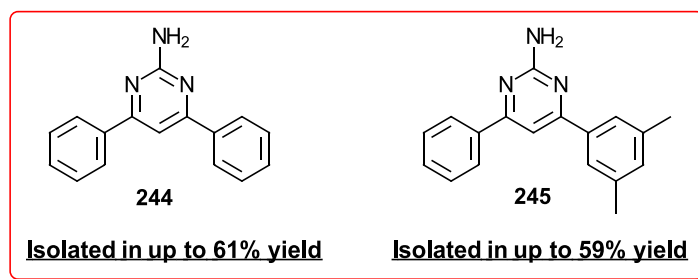
Figure 118: Cross coupling products obtained after optimisation pf reaction conditions

transmetallation event,[268,269] presumably by driving the formation of ArPd-OH (believed to be the key intermediate for transmetallation in Suzuki coupling under similar conditions)[270] *via* precipitation of AgI. Furthermore, this enhancement is expected to work better for Suzuki coupling of aryl iodides

70

compared to other aryl halides due to the decreased affinity that ArPd⁺ has for I⁻ compared with e.g. Br⁻,[271] along with the opposite preference for the softer Ag⁺ ion. Changing the base to K_2CO_3 caused the amount of protodeborylation to increase and the NMR yield of the desired product to decrease (entry **3**). To assess whether or not a slow addition of trifluoroborate and aryl iodide would be beneficial in terms of product formation over protodeborylation, we added these reagents in 2 portions with heating over a period of 24 h (entry **4**), in this case the protodeborylation rate was still sufficiently low but the conversion of the trifluoroborate was also diminished leading to a low yield of **II**. The most significant difference in product yield came by simply heating the reaction mixture for a longer period of time (compare entries **5** and **6**), when the reaction mixture was heated for 16 h, the product was observed in 26% yield however, when the same mixture was left for 24 h the yield increased to 72% (both judged by NMR spectroscopy). The high conversions of the trifluoroborate salt probably reflect formation of intermediate species, such as trifluoroborate hydrolysis products under the reaction conditions, thus compounding the accurate analysis of the conversion of this boronate. Addition of the catalyst in 2 portions over a period of 24 h resulted in a lower yield of the desired product (compare entries **6** and **7**), suggesting that the catalyst remains active throughout the reaction time period. Increasing the reaction time to 48 h allowed the isolation of the desired product in 56% yield (entry **8**) and increasing the scale of the reaction from 0.08 mmol to 0.24 mmol allowed the same product **245** (figure 118) to be isolated in 59% yield (entry **10**). In order to try and reduce the reaction time, a more concentrated reaction mixture was heated over a period of 16 h (entry **9**), the product was only isolated in 11% in this case, suggesting that higher dilution for longer time periods favours the formation of the desired cross coupling product. Under the optimised reaction conditions, iodobenzene also reacted in a similar fashion, allowing the product **244** to be isolated in 61% yield after purification (entry **11**).

With an acceptable protocol for cross-coupling in hand, we then sought to investigate further the potential of the trifluoroborate group for functionalisation at the pyrimidine C6. Another mainstay of organoboron chemistry is the potential for facile oxidation using simple reagents, leading to the corresponding alcohol or phenol. This has often been a strategy of choice when dealing with relatively sensitive boronic acids/esters, simply to work the reaction up with an oxidising agent such as H_2O_2 and recover the expected alcohol in its place.
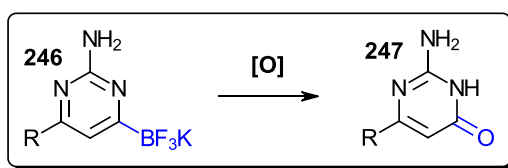
Figure 119: Investigation of known organoboron oxidation chemistry for the synthesis of medicinally significant pyrimidin-2-ones
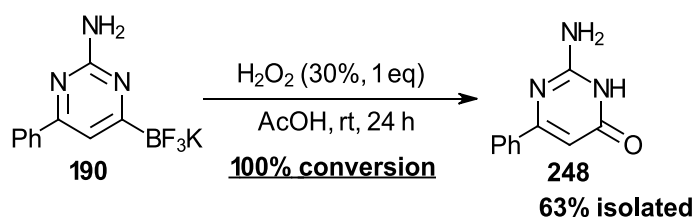
*Figure 120: Synthesis of 2-Amino-6-phenyl-3H-pyrimidin-4-one via oxidation of **190***

71
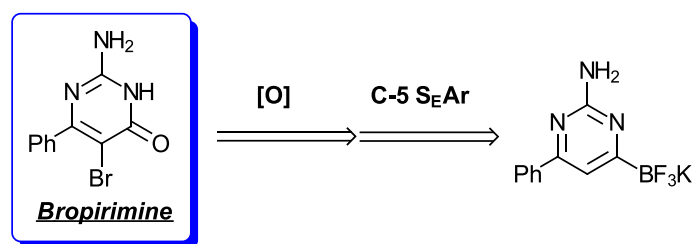
Figure 121: Proposed synthesis of the experimental anticancer drug, bropirimine from the trifluoroborate salt 190

There are numerous methods and reagents that have been shown to be useful for the oxidation of boronic acid derivatives and we wanted to establish a set of conditions that would facilitate this transformation in aminopyrimidin-6-yl trifluoroborate salts **246** (figure 119) to afford pyrimidinones **247**, which are constituents of important biological molecules, such as nucleobases and barbiturates. Beginning with an operationally straight forward procedure, we attempted to oxidise the pyrimidine **190** using H_2O_2/AcOH (figure 120).[272] Pleasingly, the oxidation was complete within 24 hours, furnishing the aminopyrimidinone **248** in 63% yield after purification. As an application of this chemistry, we envisaged a concise synthesis of the experimental anticancer bropirimine from **190** by C5 bromination (*vide supra*), followed by oxidation (figure 121). Thus, bromopyrimidin-6-yl trifluoroborate **237** was subjected to the H_2O_2/AcOH conditions (figure 122) but they were unsuitable due to the lower solubility of **237** in AcOH than **190** and the former was recovered unchanged.
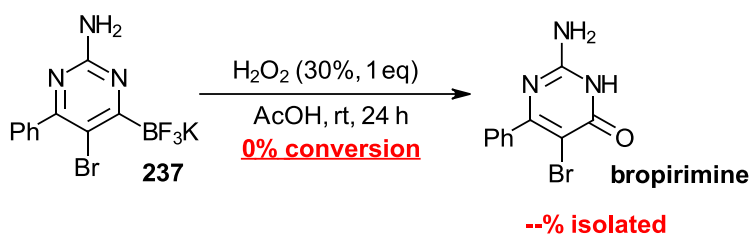
Figure 122: Unsuccessful oxidation of trifluoroborate salt 237 via the per-acetic acid procedure.
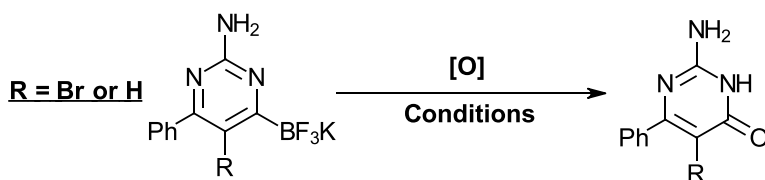
Entry	[O] reagent +Conditions	Outcome	Reference
1	NMO (1.2 eq) CH$_2$Cl$_2$, 40 °C, 16 h	<2% conversion	Falck (2012)
2	oxone (1.1 eq) acetone, rt, 16 h	<2% conversion	Molander (2011)
3	UHP (1.1 eq) MeOH, rt, 16 h	<2% conversion	Kandasamy (2016)
4	NaBO$_3$.4H$_2$O (4 eq) THF/H$_2$O, 40 °C, 16 h	33% conversion	Walsh (2009)
5	H$_2$O$_2$ (30%, 10.0 eq) Na$_2$CO$_3$ (1.1 eq) EtOH 50 °C, 16 h	low mass recovery **27% isolated**	Harrity (2017)

Figure 123: Screen of oxidation conditions towards bropirimine. NMO = N-methylmorpholine-N-oxide, UHP = Urea hydrogen peroxide adduct

After a brief survey of boronate oxidation conditions[273–275] for the aminopyrimidine trifluoroborates **190** and **237** (figure 123), we found that the use of excess hydrogen peroxide in a basic solution of warm EtOH provided bropirimine in 27% yield after silica gel chromatography (entry **5**).[276] Taking these conditions for further optimisation, it was found that extensive extraction (≥5 x) of the crude reaction mixture from water with ethyl acetate provided a significantly improved mass balance (figure 124), demonstrating bropirimine's high water solubility. Increasing the scale from 0.28 to 0.62 mmol and leaving the reaction to run for 24 h provided bropirimine after purification in a very good yield of **76%**.
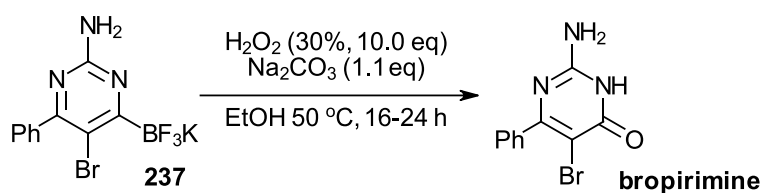
Figure 124: Adaptation and optimisation of oxidation conditions for the isolation of bropirimine. EA = ethyl acetate.

Heteroaryl halides are present in several naturally occurring molecules,[277] and the traditional methods of preparing them have often relied upon halogenation reagents that exploit the innate nucleophilicity of the arene in question. This has the disadvantage that if there are multiple nucleophilic sites on the substrate (hetero)aryl, then halogenated mixtures are inevitable and can lead to purification issues. An alternative to electrophilic halogenation is to replace a pre-existing functional group, which allows the halogen to be introduced selectively to the desired position on the substrate molecule. A useful functional group interconversion that has emerged in recent decades, is the halodeboronation of boronic acid derivatives. Kabalka and co-workers have undertaken significant research in this area, particularly, halodeboronation reactions of organotrifluoroborate salts.[278–282] Inspired by this work, Iododeboronation of **173** was attempted using the FeCl$_3$/NaI system[282] (figure 125). After 18 hours of heating, the reaction returned starting material, protodeborylation material and the iodopyrimidine **249**, which was isolated in 28% yield. In an attempt to drive the process to completion, the reaction was repeated with 24 hours of heating, but in this case, the product of protodeborylation/protodehalogenation[283] **240** dominated the crude mixture and was isolated in 77% yield, along with only 9% of **249**. At this point, we decided to explore alternative functionalisation processes
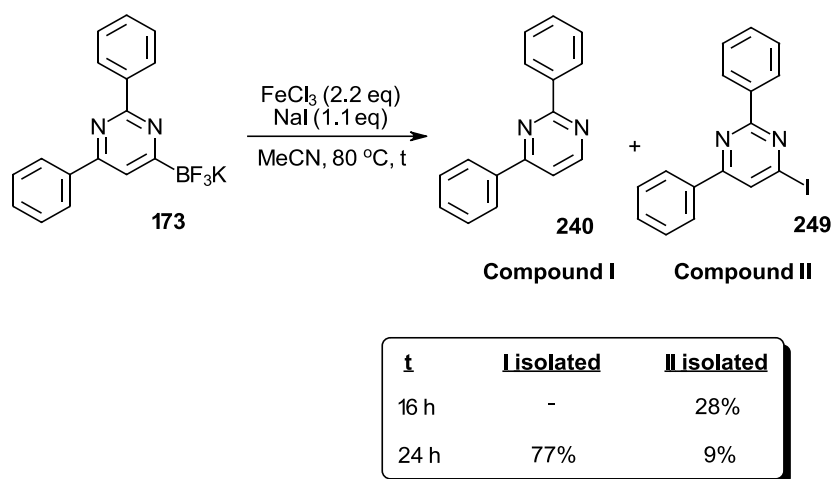
Figure 125: Iron(III) chloride-promoted iododeboronation of pyrimidin-6-yl trifluoroborate salt 173

Noting the prevalence of aminopyrimidines as a privileged heterocyclic core among FDA approved medicines,[225] we sought a transformation that would replace the trifluoroborate unit of 173 with a nitrogen-based functional group. Inspired by the established[284–287] reactivity of boranes and haloboranes towards organic azides forming secondary amines after aqueous workup, we attempted this transformation using 253 and 5.0 equivalents of $SiCl_4$, followed by addition of 1.3 equivalents of commercially available benzyl azide. After heating the reaction at 80 °C for 16 hours, the only products that were detected in the (NMR, LCMS) analysis of the crude mixture were the starting trifluoroborate salt and the product of protodeboronation. Given that the proposed intermediate required for the reaction to work is the difluoroborane resulting from a fluoride abstraction event by $SiCl_4$, further investigations into this transformation should include a screen of (less sensitive) fluoride abstractors (BX_3, TMSOTf, TMSCl, $TMSN_3$). An alternative, Cu-catalysed method for C6 azidonation was also attempted on the pyrimidine 173 (figure 126). This procedure has been shown to be successful in installing an amino group at the C5 of pyrazol-5-yl trifluoroborate salts[219] via azidonation then subsequent catalytic hydrogenation. Regrettably, the pyrimidin-6-yl trifluoroborate salt deborylated quantitatively under the same conditions and no trace of the desired azide 252 was observed.
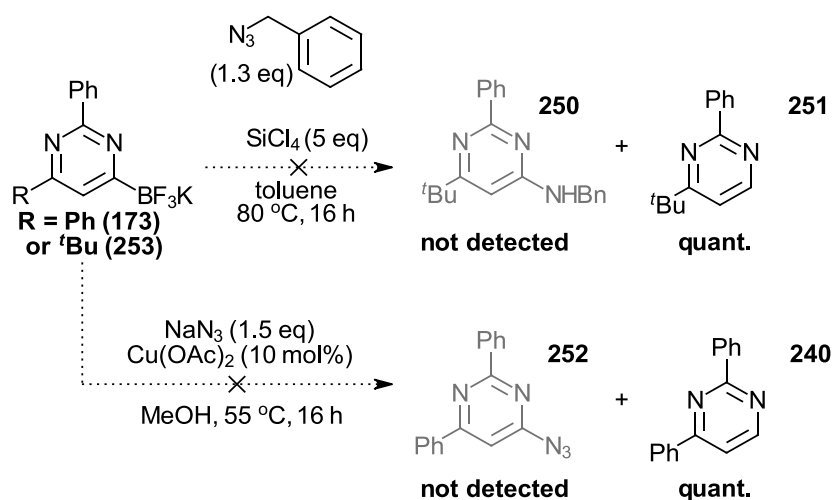
Figure 126: Attempted C6 amination and azidonation reactions, using known boron chemistry

1.3. Conclusions

Pyrimidines have been the subject of active investigation for over 200 years. They are seen extensively in medicinal applications and are also useful building blocks for functional materials. For these reasons, the development of new ways to access pyrimidines and novel pathways for their functionalisation is an ongoing field of research.

Thanks to this research interest, the number of established ways to synthesise the pyrimidine ring from simple precursors is enormous. The pyrimidine ring can also be readily functionalised and in this respect, pyrimidinyl halides are known to participate efficiently in cross-coupling reactions. In contrast, pyrimidinyl boronates have seen relatively little attention, particularly when borylated at C6.

Ynone trifluoroborates were found to be highly useful for the production of novel pyrimidin-6-yl trifluoroborate salts, which were stable under ambient conditions and could be stored without precaution. The aminopyrimidin-6-yl trifluoroborate salt **190** could also be prepared from **166** by reaction with an appropriate guanidine reagent, paving the way for a new intermediate with potentially useful modular reactivity. Substituted guanidines and even 3-aminopyrazole also reacted with the ynone **166** to provide regioisomeric mixtures of intriguing pyrimidin-6-yl type boronate products. Importantly, the pyrimidin-6-yl trifluoroborate salt **173** was found, after optimisation, to be amenable to Suzuki-Miyaura cross-coupling in good yield. The successful optimisation of this cross-coupling protocol was enabled by the discovery that a high water content in the reaction solvent was crucial for high conversion of the starting trifluoroborate. **190** was also amenable to cross-coupling under similar conditions and could be alkylated at the ring *N* selectively. Additionally, **190** could be efficiently brominated at the pyrimidine C5 and also oxidised at B to provide the experimental anticancer compound bropirimine in good yield.

Further studies on these systems should include a deeper study of the condensation reaction of **166** with substituted guanidines and 3-aminopyrazoles, aiming to gain a fuller understanding of the product composition and insight into the reaction selectivity. The elaboration of **190** has been investigated to an extent here, but further experimentation on its potential for modular reactivity including at the -NH$_2$ and also the pyrimidine C5 should be considered in order to maximise the application of this intermediate in the synthesis of valuable pyrimidine scaffolds.

2. Alkynyltrifluoroborates applied to organofluorine synthesis

2.1. Introduction

2.1.1. Occurrence and chemistry of fluorine

Fluorine is the 13th most common element and the most common halogen in the Earth's crust.[288] Despite this, organofluorine compounds are almost non-existent in nature, with only a handful of known fluorinated natural products discovered so far (figure 127). [289–293] The most simple example of a fluorine-containing naturally-occurring compound is the potent poison, fluoroacetic acid. This has been identified (sometimes highly concentrated) in tropical and sub-tropical plant species[294,295] and is potentially accumulated as a defence against insect pests.
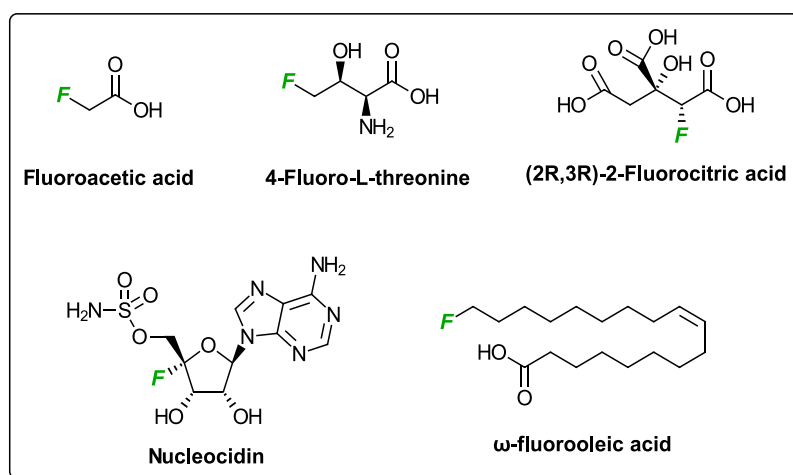
Figure 127: Fluorine-containing compounds of known biological origin

The reasons for this dearth in the natural occurrence of C-F bonds are fascinatingly linked to fluorine's properties, which distinguish it from the other halogens (table 3). The hydration energy of the fluoride ion is (at 117 kcal mol^{-1})[291] the highest of all the halogens by far and this has two main implications for its reactivity *in vivo*. Firstly, the nucleophilicity of aqueous fluoride is significantly attenuated due to its strong interaction with water. Secondly, the high energy of hydration is partially responsible for its prohibitively high oxidation potential (*in vivo*). The high oxidation potential restricts access to highly reactive species, such as "F$^+$" or "F$^•$", which may have otherwise facilitated the biosynthesis of fluorinated products.

X	BDE CH$_3$-X / kcal mol^{-1}	Bond length C-X / Å	Hydration energy, X$^-$ / kcal mol^{-1}	Pauling electronegativity	Standard oxidation potential, 2X$^-$ -> X$_2$ + 2e$^-$ / kcal mol^{-1}
F	110	1.39	117	4.0	-3.06
Cl	85	1.78	84	3.0	-1.36
Br	71	1.93	78	2.8	-1.07
I	57	2.14	68	2.5	-0.54
H	99	1.09	-	2.2	-

Table 3: Summary of key halogen properties,[291] *BDE = Bond Dissociation Energy*

Once incorporated inside organic compounds however, the other properties of fluorine that set it apart from later halogens, such as: electronegativity, Van der Waal's radius and C-F bond length/strength can affect the final properties of the compound enormously. Consequently, organofluorine compounds have been widely researched and used for their novel material properties.[296] For example, perfluoroalkyl chains can impart impressive thermal and chemical stability on the resulting substance and for this reason, such compounds have found application in numerous fields of material science as: Elastomers, non-stick/inert coatings, specialty lubricants, solvents and surfactants. The simplest perfluoroalkyl chain possible is the trifluoromethyl group (CF$_3$), which is a special case. The CF$_3$ group is hugely common in currently marketed medicines, and the incorporation of CF$_3$ and other C1 fluoroalkyl groups (CH$_2$F, CHF$_2$, OCF$_3$, SCF$_3$) into lead compounds during medicine development has come to be an indispensable tool for the modulation of key properties.[297–299] The explosion of organofluorine compounds within the field of medicinal chemistry in recent years can be rationalised by their scarcity in the natural world and the corresponding novelty of each organofluorine compound created henceforth. The properties of these novel organofluorine compounds turn out to be highly useful for lead development, and the main considerations in this regard are summarised below.

1.20 Å   1.47 Å   1.52 Å
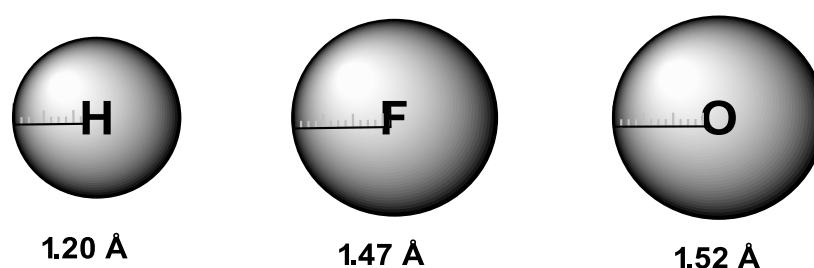
Figure 128: Van der Waals radii for H, F and O[297]

Fluorine, being the most electronegative of all the elements forms highly polarised C-F bonds and the resulting ionic attraction caused by this polarity contributes to the great strength of this bond. In fact, the C-F is the strongest single bond known in organic chemistry. The consequence of this, is that fluoroalkyl groups display high chemical stability towards metabolism (by e.g. C-P450) where a non-fluorine atom such as hydrogen would otherwise be transformed. Another consequence of the high electronegativity of fluorine, is that the pKa of nearby or adjacent acidic functional groups can be

lowered by its incorporation, due to inductive attenuation of the negative charge residing on the conjugate base, the opposite argument applies for basic functional groups. The size (figure 128) of a fluorine substituent (F, vdW radius: 1.47 Å)[297] is only slightly larger than that of hydrogen (H, VdW radius: 1.20 Å) and close to that of a hydroxyl group (oxygen, vdW radius: 1.52 Å), therefore the replacement of a substituent with F may cause only a minor steric disturbance while impacting the electronic nature of the compound significantly. Finally, another important consideration of organofluorine chemistry in lead development is that fluorine substituents may increase the lipophilicity of a lead compound.[300] One potential consequence is that if you were to replace a polar functional group such as O or NH with F, you may keep a degree of functional group polarity, but the lipophilicity of the compound would be greatly enhanced. Greater lipophilicity is important for the modulation of the PK/PD profile of the lead compound, potentially leading to e.g. enhanced cell penetration. The oldest and most famous example of the importance of medicine development by fluorine incorporation, was the introduction of a fluorine substituent at the 9α position of cortisol by Fried and Sabo in 1954 (figure 129).[301] This seemingly small change in the structure of cortisol resulted in a tenfold increase in glucocorticoid potency, massively improving the safety window for this treatment.
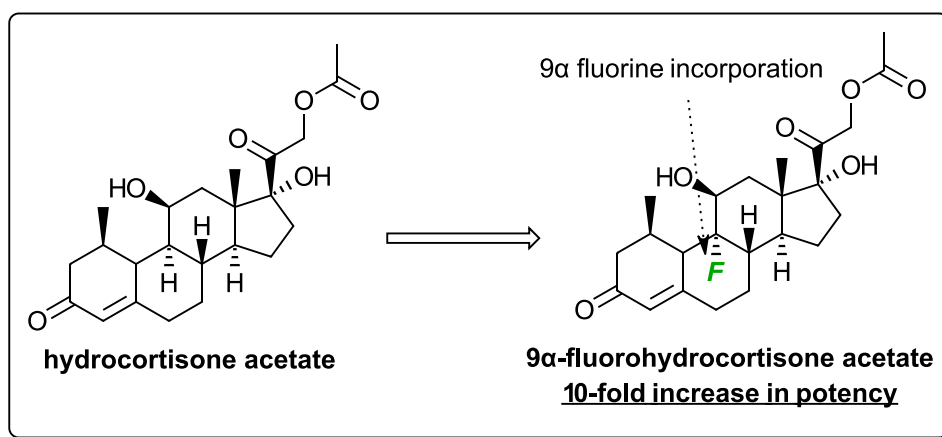
Figure 129: Fluorine incorporation into the hydrocortisone acetate backbone confers a tenfold increase in corticosteroid potency

2.1.2. Organofluorine synthesis *via* direct fluorination/fluoroalkylation

In 2010 it was found that approximately 20% of all prescribed medicines and 30% of the top 30 drugs by sales contained fluorine.[302] The percentage of all prescribed drugs containing fluorine was predicted to have risen to at least 30% by now, due to the number of those that were going through the later stages of approval.[303] Indeed, the portion of newly approved (small molecule) pharmaceutical products has risen significantly in recent years. In 2015 the portion of new approvals that contained fluorine was 34%,[304] in 2018 the number was 50% and in 2019 it was 43% These figures only help reveal the extent to which organofluorine chemistry has contributed, and continues to contribute, to curing disease and improving quality of life for millions.

The above expansion of medicinal organofluorine chemistry is of course a product of the immense research effort towards developing synthetic strategies to obtain such compounds. Due to its exceptional nature, fluorine is classically difficult to install selectively and conveniently and the development of reagents to achieve this has been the subject of much research. Nevertheless, the source of fluorine required to prepare these reagents must be considered as the foundation of this chemistry. Most fluorine insertion is achieved in one way or another using aqueous hydrofluoric acid (HF) or fluorine gas (F_2), which is obtained almost exclusively by processing naturally occurring CaF_2 (figure 130), which is found in the mineral Fluorspar.[305,306] Although useful for certain large scale and dedicated processes, HF is highly corrosive and hazardous, making it unsuitable for routine laboratory application. The same applies for F_2, which is extremely reactive and requires specialised equipment to work with safely. In the early days of organofluorine chemistry however, fluorinated precursor were more difficult to come by than they are today and so many interesting laboratory processes were developed using HF. For example, the Simons process includes the fluorinative electrolysis of organic compounds in HF solutions. Another, much older process using HF that was developed is the
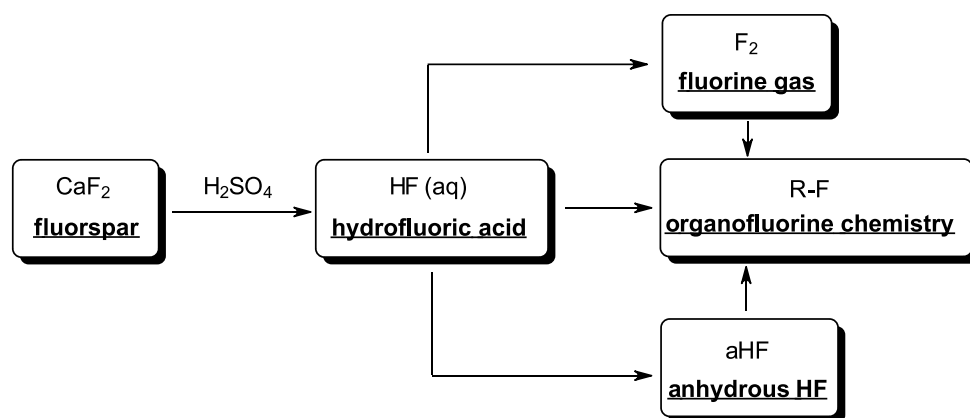
Figure 130: Processing of calcium fluoride, found in the mineral: fluorspar, for application to the field of organofluorine chemistry

Swarts fluorination,[307,308] which was invented to produce organofluorines from more easily obtainable organohalides such as bromides and chlorides (figure 131). The Swarts process can produce benzotrifluorides by the reaction of the appropriate substrate with HF or a Lewis acidic metal fluoride, such as SbF_3 (prepared by treating antimony trioxide with HF) and has since been a reliable method to obtain such compounds.[309] In fact, subsequent patents[310,311] obviated the need for SbF_3, allowing the procedure to be carried out using just HF.
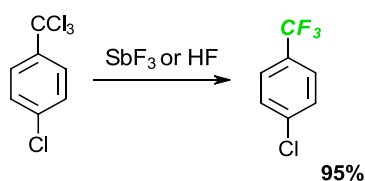
Figure 131: Swart's synthesis of benzotrifluorides from the corresponding benzotrichloride[308]

In recent decades, a host of new methods and reagents have been investigated to address the key issues of fluorination or fluoroalkylation chemistry, namely: safety, reactivity, selectivity and cost. The introduction of a single fluorine atom can be approached using different strategies, such as nucleophilic fluorination by the strategic use of fluoride (HALEX, deoxofluorination, Balz-Schiemann etc) and electrophilic/radical fluorination through the use of specialised reagents (Selectfluor, pyridinium fluorides, NFSI etc)

Nucleophilic fluorination strategies

Direct nucleophilic fluorination using fluoride is a common strategy for introducing radiofluorine (^{18}F) into tracers for minimally invasive imaging procedures, such as Positron Emission Tomography (PET).[312,313] Although an attractive strategy, fluoride typically displays low activity as a nucleophile in bimolecular displacements, due to two main factors. The first is that fluoride forms strong H-bonding interactions with protic solvents / impurities so in protic solvents, their lone pairs are lowered in energy compared to when aprotic solvents are employed. In some cases however, the presence of H-bonded ligands to the fluoride can be beneficial for reactivity and selectivity between nucleophilicity and basicity.[314–317] If care is taken to remove water from the aprotic solvents and the fluoride salt itself, the dissolved/slurried fluoride is considered "activated" due to the lack of competing solvent interactions. In this case however, fluoride is typically a much better base[318] than it is nucleophile and is thus only suitable for fluorination under certain circumstances.

When the reagents and solvents have been scrupulously dried, fluoride can be used to substitute chloride substituents in aromatic systems in a halogen-exchange (HALEX) process, provided a phase-transfer catalyst is present and enough thermal energy is supplied.[319] To address the prohibitively low solubility of most metal fluoride salts in organic solvents, tetraalkylammonium salts have emerged as convenient alternatives. Due to the fluoride hydration issue mentioned previously however, the most common use of one such reagent, TBAF, is not for nucleophilic fluorination but for silane deprotection (figure 132) *via* fluorination of the silicon leaving group.[320,321]
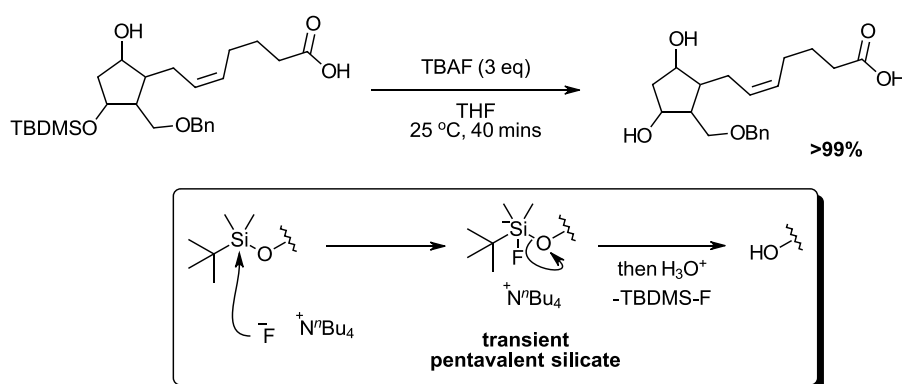
Figure 132: Mild deprotection of a bulky silane ether using soluble fluoride. TBDMSO = tert-butyldimethylsilyloxy, TBAF = tetra-n-butylammonium fluoride

For silane deprotections, hydrated or ill-defined samples are usually sufficient for most applications. Anhydrous TBAF and related alkylammonium fluorides are difficult to obtain, due to the inherent background Hofmann elimination which occurs upon attempting to dry the reagent after its synthesis.[322] Anhydrous TBAF can be prepared by carefully excluding water from its synthesis[323] and has been shown to perform much more effectively in S_NAr fluorinations under much milder conditions[324,325]

The nonviability of aHF for nucleophilic fluorination applications in the lab can be bypassed in some cases through its complexation with organic bases such as *N*-heterocycles and amines.[326,327] Reagents such as Et$_3$N.xHF (figure 133) and pyridine poly-HF (PPHF, also known as Olah's reagent) emerged as relatively convenient alternatives for nucleophilic fluorinations by aHF (figure). An example of the early application of these reagents is the fluorinative ring-opening of epoxides, which was found to be useful in the synthesis of fluorinated derivatives of shikimic acid (figure 134).[328]
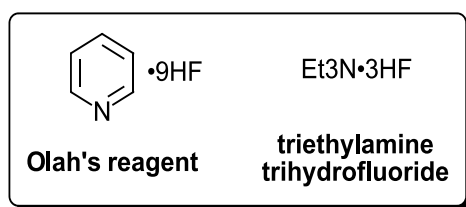
Figure 133: Examples of nucelophilic fluorination reagents
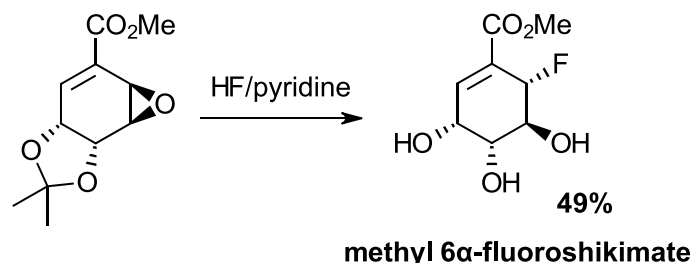
Figure 134: Utility of HF/pyridine ("Olah's reagent) as an effective nucleophilic fluorination reagent, here demonstrating fluorinative ring-opening of an epoxide

Several reagents for deoxofluorination (figure 135) have been developed, such as diethylaminosulphur trifluoride (DAST) and Bis(2-methoxyethyl)aminosulphur Trifluoride (Deoxofluor), the Ishikawa reagent and difluoroimidazole (figure 136). These reagents work by simultaneously activating the leaving O functionality, while providing a viable source of nucleophilic fluoride *in-situ*.[329]
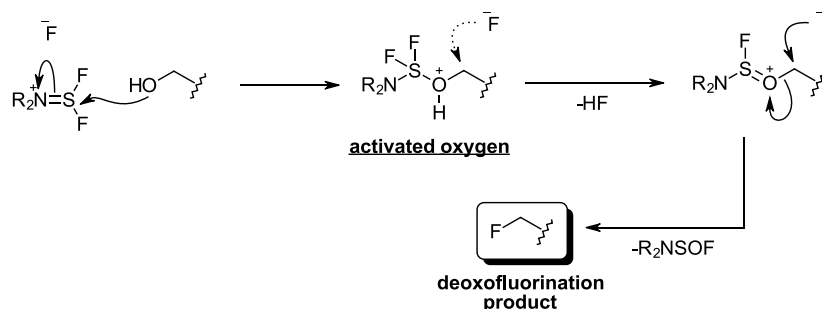
Figure 135: General mechanistic scheme for the S-based deoxofluorination of primary alcohols
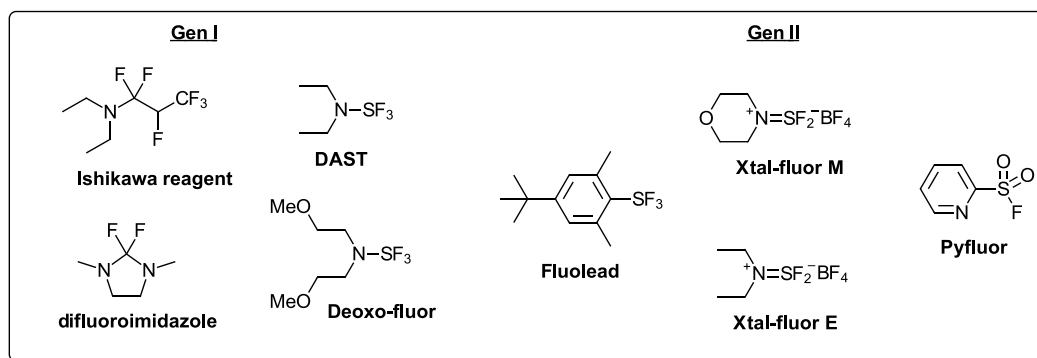
Figure 136: Selection of deoxofluorination reagents developed, with later generations possessing greater stability and selectivity

Such reagents have been very useful for selectively installing fluorine substituents under very mild conditions. Converting alcohols,[330,331] aldehydes,[330,332,333] ketones[330,334] and even thiocarbonyls[335] efficiently into the corresponding high-value organofluorine compound. Concerns surrounding the cost and thermal stability of DAST and related reagents[336] have been addressed by the later development of next generation reagents, such as Xtal-fluor, PhenoFluor, CpFluor, PyFluor and others.[337] Pyfluor (figure 136) can be prepared efficiently on multigram scale, from commercially available materials. It can be stored without precaution for extended periods without decomposition, in stark contrast to DAST. It has been deployed successfully for the radiofluorination of tetrabenzyl glucose by itself,[338] and redox active esters under visible light photocatalytic conditions.[339]

Electrophilic/radical fluorination

Another important strategy for selective fluorination is the use of electrophilic "F+" reagents, which have seen much development in parallel with the nucleophilic reagents described in the previous section. In order to replace the utility of fluorine gas, which displays extremely high reactivity with regards to electrophilic fluorination (figure 137)[340] but comes with significant practical issues including safety concerns.[341]
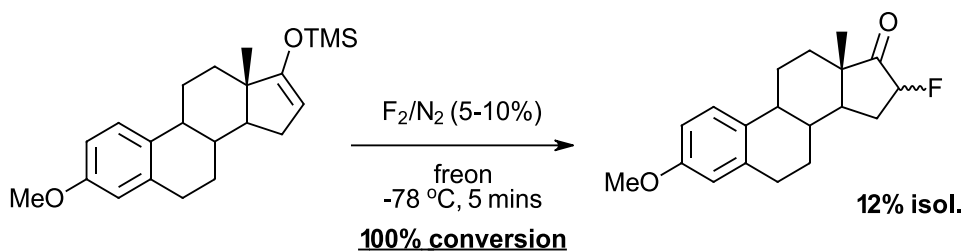
Figure 137: Example of electrophilic fluorination using fluorine gas. Fluorination of estrone enols using diluted F$_2$[340]

Considering the difficulty in handling F$_2$, alternative reagents were researched and prepared that could undergo the same electrophilic fluorination but were much more stable and safe. For example, a host of O-F reagents were investigated as F$_2$ surrogates, including acetyl hypofluorite (AcOF) which proved to be a useful "F$^+$" source for a variety of applications such as S$_E$Ar fluorination.[342] After research efforts to find more stable reagents for this transformation,[343,344] electrophilic N-F reagents emerged. Significant developments included the invention of: sulfonimide reagents NFSI and NFOBS (figure 138), F-TEDA (Selectfluor) and various *N*-fluoropyridinium salts.
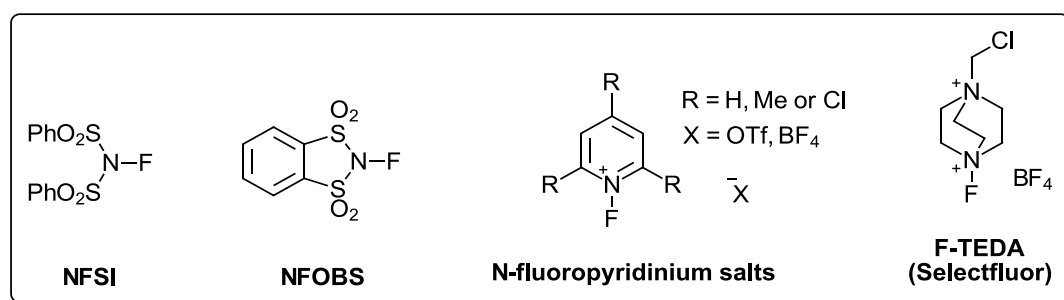
Figure 138: Selection of electrophilic fluorination reagents

The advantages that these reagents have over O-F fluorination reagents (greater stability, shelf-life) primarily originate from the stronger N-F bond compared to the O-F bond. So lower reactivity is seen for N-F reagents, but they can be stored quite safely and may not need to be produced *in-situ* as AcOF commonly is. The advantage of the *N*-fluoropyridinium salts shown in figure 138, is that modulation of the reactivity and thus selectivity can be achieved by altering the ring substituents.[345]

Due to the commonly weak F-X bond, some of the traditional "F$^+$" reagents were found in 2012 by Sammis and coworkers[346] to fluorinate alkyl radicals readily (figure 139), thus leading to the expanded utility of these reagents as potential "F$^•$" sources or F atom transfer reagents. Since these pioneering discoveries, methods for radical fluorination have seen huge interest and development, due to their potential for unprecedented mildness and selectivity of the fluorination reaction. These developments have been reviewed recently elsewhere for radical fluorinations[347,348] initiated by thermal energy,[349,350] visible/UV light[349,350] and more recently, by electrochemical means.[351]
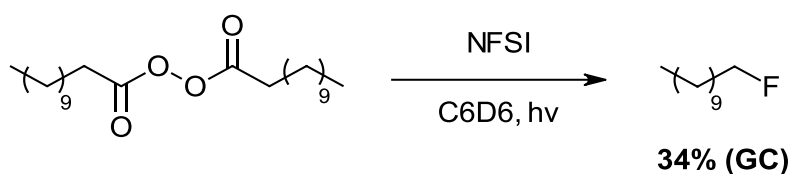
Figure 139: Preliminary experiments on radical fluorination using electrophilic fluorination reagent NFSI

Trifluoromethylation

The forms of fluorine most commonly seen in successful medicinal chemistry applications are single fluorine substituents or trifluoromethyl groups.[352] Longer chain perfluoroalkyl substituents are more rare, but still present.[353]

Trifluoromethylated arenes and heteroarenes are themselves privileged scaffolds in medicinal chemistry, this is reflected in the fact that they are the second-most common fluorinated chemotype of all fluoro pharmaceuticals registered between 1954 and 2019.[304]

They were traditionally accessed on a small scale by manipulation of the pre-trifluoromethylated aromatic compound, which was itself prepared by Swarts-type HALEX fluorination.[309] Given the atom-economy and environmental drawbacks associated with scaling up routes based on this strategy, much research has been devoted to the development of alternative methods for direct trifluoromethylation that address these concerns. Among the oldest methods of direct trifluoromethylation of arenes is through the reaction of [Cu-CF$_3$] complexes with haloarenes. This strategy first appeared in the open literature as a report by McLaughlin and Thrower in 1969 (figure 140),[354] in which a series of perfluoroalkyl iodides were found to selectively react at the arene halogen position in the presence of stoichiometric copper, to afford the expected perfluoroalkyl-substituted arenes. The reaction performed much more efficiently for iodoarenes than for bromoarenes, but this represented a significant leap forward in the field of organofluorine synthesis. Importantly, the reaction worked for CF$_3$I, providing the corresponding benzotrifluoride upon reaction with the iodoarene. The exact identity of the active [Cu-CF$_3$] reagent was not confirmed at the time.
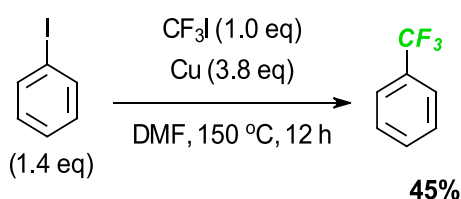
Figure 140: The McLaughlin-Thrower reaction is an early example of direct arene trifluoromethylation

This particular transformation was optimised soon after the report by McLaughlin *et al.* by Kumadaki and Kobayashi[355] to include several more examples of Ar-CF$_3$ products. This represented an important breakthrough in the field, as it opened the door to a potential contender to the Swarts reaction for the industrial synthesis of Ar-CF$_3$ compounds.
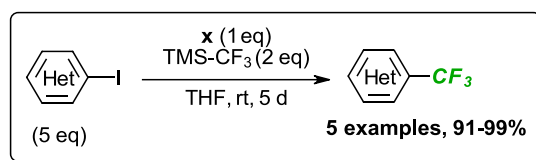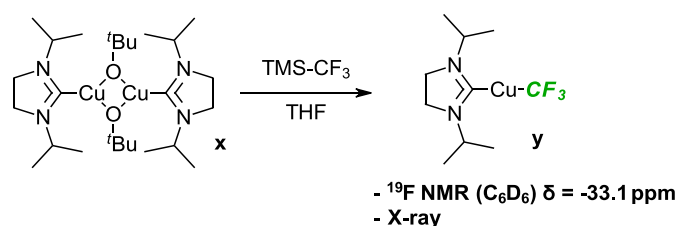
Figure 141: Preparation of a well-defined NHC-Cu-CF₃ complex and its application to iodoarene trifluoromethylation

Since these early discoveries, much progress has been made including the preparation of a highly defined [Cu(NHC)-CF₃] complex by Vicic *et al* (figure 141).[356] which could be prepared *in-situ*, providing a high-yielding and mild procedure for trifluoromethylation of iodoarenes. Building on the success of Cu-CF₃ as an effective strategy for trifluoromethylation, many different routes now exist and continue to be developed for the selective trifluoromethylation of aromatic compounds. This includes the investigation of nucleophilic and electrophilic CF₃ sources, the latter of which have also served as efficient CF₃ radical precursors for radical trifluoromethylation reactions. Nucleophilic sources of the trifluoromethyl group can be considered as "CF₃⁻"-transfer reagents and a key example is TMS-CF₃, known as the Ruppert-Prakash reagent, and related perfluoroalkyl silanes which have been used extensively for direct nucleophilic trifluoromethylation and also as precursors to various trifluoromethyl-metal complexes.

Nucleophilic trifluoromethylation using TMS-CF₃ and related agents is highly useful for addition to common electrophiles, such as carbonyl compounds. In particular, there has been much development on the use of this reagent in the field of asymmetric nucleophilic trifluoromethylation.[357] The favourable stability and modulated reactivity of TMS-CF₃ has lead to its widespread use as the CF₃ source for these applications. The CF₃ can be added diastereoselectively to an electrophile with an attached chiral auxiliary,[358] or the symmetry may be induced through the use of asymmetric ammonium fluoride activators such as the reactions investigated by Kobayashi[360] and also later by Larivée (figure 142).[359] These trifluoromethylation reactions have been reviewed,[357] and will not be
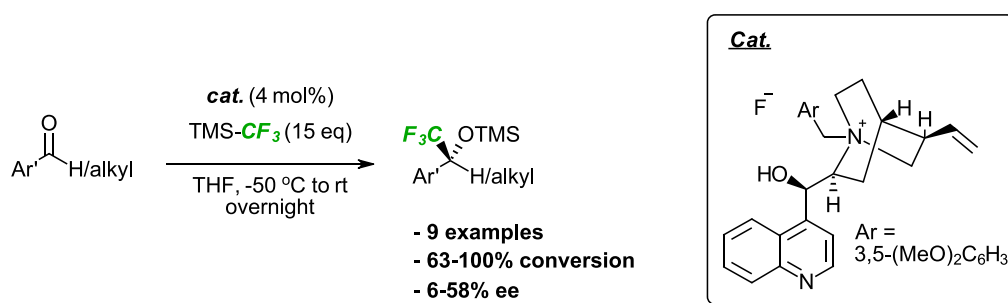
Figure 142: Asymmetric trifluoromethylation of carbonyl compounds using a chiral counterion for the fluoride catalyst[359]

discussed further in order to focus on (symmetric) trifluoromethylation reactions of aromatic and heteroaromatic compounds.

Returning to (hetero)arene trifluoromethylation, after Cu-mediated trifluoromethylation of (hetero)aryl halides became established as a highly useful alternative to the Swarts-type synthesis, the next stage of development for these processes was the move towards reactions that need only a catalytic quantity of Cu. Since then, numerous procedures for Cu-catalysed trifluoromethylation have been published. To achieve catalysis, the Cu species must remain active throughout the reaction time in order to re-form the active Cu-X catalyst ready for the next turnover. For example, Amii *et al* found that the amount of Cu could be reduced to just 10 mol% in their catalytic trifluoromethylation of (hetero)aryl iodides (figure 143).[361] The rationale for the apparent efficiency of the Cu species lies with its stabilisation by the phenanthroline (phen) ligand, slowing down its sequestration from the reaction mixture by decomposition.
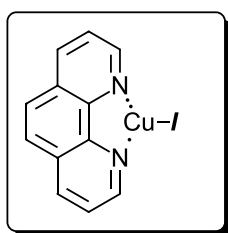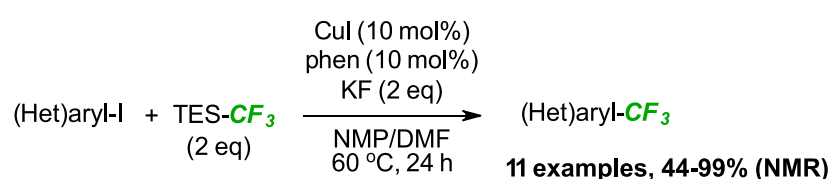
Figure 143: Cu-catalysed trifluoromethylation of (hetero)aryl iodides[361]

Since then, several permutations of Cu-catalysed trifluoromethylation reactions have been studied,[362] including the use of a silver(I) additive by Huang *et al.*[363] which allowed the use of the more widely available TMS-CF$_3$ rather than TES-CF$_3$ and produced a good scope of trifluoromethylated (hetero)arenes. The authors managed to support their hypothesis by obtaining X-ray crystal structures of both L-Cu-CF$_3$ and L-Ag-CF$_3$ complexes. Other improvements to Cu-catalysed trifluoromethylation include the use of CF$_3$ sources other than R$_3$Si-CF$_3$. Procedures have now been disclosed using CF$_3$B(OMe)$_3$K,[364] CF$_3$CO$_2$Na,[365] adducts of fluoral,[366] and even fluoroform[367,368] as the CF$_3$ donor. A fluoroform-derived [Cu-CF$_3$] reagent was used by Grushin *et al.* to prepare (Het)Ar-CF$_3$ compounds from anilines *via* a one-pot diazotisation-trifluoromethylation procedure (figure 144).[369] The reaction tolerated a good range of electron-withdrawing, electron-donating and protic arene substituents and several examples of challenging heterocycles were also trifluoromethylated as expected. The usefulness and orthogonality of this procedure is exemplified by its tolerance of even reactive halides, including aryl iodides, owing to its mild nature (0 °C 15 mins, after formation of diazonium salt).
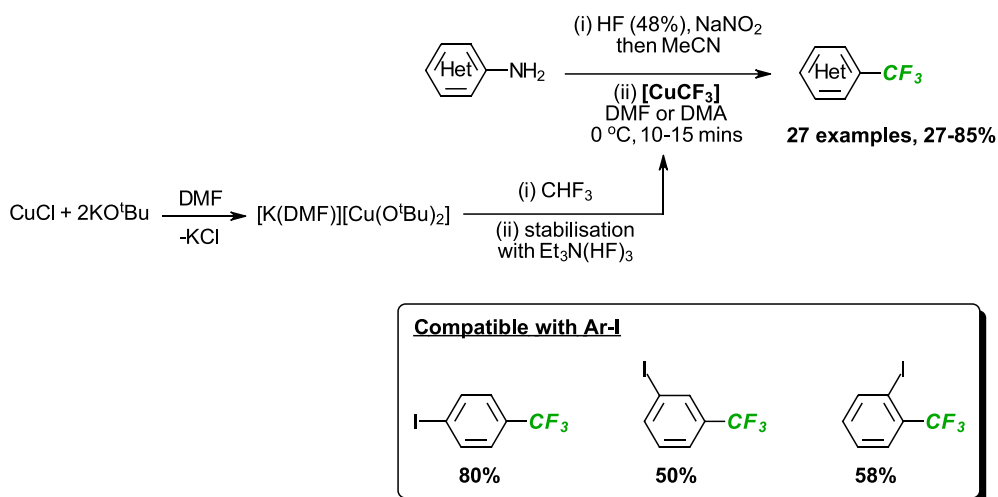
Figure 144: Trifluoromethylation of anilines via a tandem diazotisation-trifluoromethylation procedure, using CuCF₃ obtained from the cupration of fluoroform[369]

Boronic acids have also been shown by Qing *et al.* to be competent reaction partners in Cu-mediated arene trifluoromethylation.[370] In this report, 1,10-phenanthroline, TMS-CF₃ and [Cu(OTf)₂]•C₆H₆ were used to form a stabilised [Cu-CF₃] complex, which reacted under the conditions with the (hetero)arylboronic acids to form the Ar-CF₃. The reaction proceeded under mild conditions and was also amenable to alkenyl boronic acids

Pd catalysis has also been investigated for its potential in cross coupling the trifluoromethyl group with (hetero)arene substrates (figure 145). After formation of the Ar-Pd-CF₃ however, the strong Pd-CF₃ bond disfavours reductive elimination to provide the desired Ar-CF₃ and facilitate catalyst turnover. Indeed numerous Ar-Pd^{II}-CF₃ complexes have been prepared by transmetallation from TMS-CF₃, characterised and shown to be highly sluggish in Ar-CF₃ reductive elimination[371–375] when compared with their Ar-Pd^{II}-CH₃ counterparts in Ar-CH₃ reductive elimination.[376,377] Although sluggish, the reductive elimination of Ar-CF₃ does occur through judicious choice of wide bite-angle ligands for the Pd complex[373] (such as Xantphos) and has been shown to work as part of an
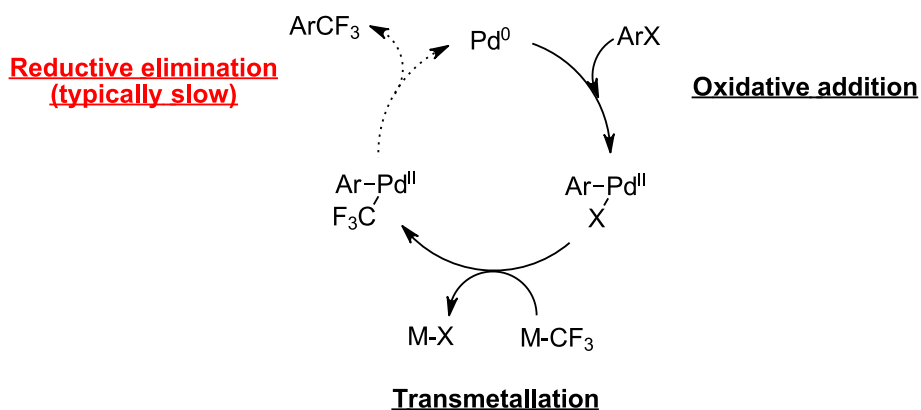
Figure 145: Catalytic cycle for the Pd-catalysed trifluoromethylation of aryl-(pseudo)halides. Reductive elimination of Ar-CF₃ is typically very slow and other undesired processes occur faster
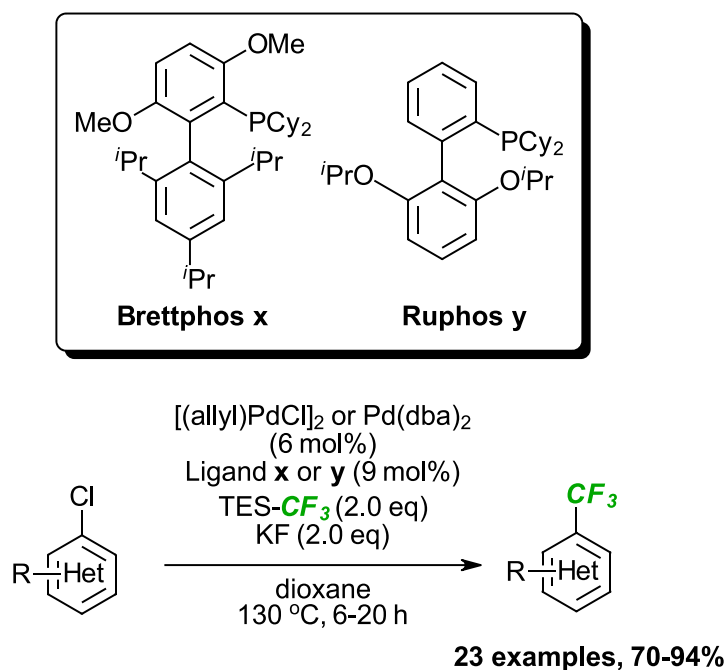
Figure 146: First general Pd-catalysed trifluoromethylation of (hetero)aryl chlorides, using TES-CF$_3$ as the CF$_3$ donor

efficient catalytic procedure that couples TES-CF$_3$ with (Het)Ar-Cl to produce (Het)Ar-CF$_3$ compounds in good to excellent yield (figure 146).[375] This is in stark contrast to the efforts to develop a Pd-catalytic approach to Ar-F bond formation *via* reductive elimination. Due to the polarised nature of the Pd-F bond, its electron density is not situated for ideal overlap with the Pd-Ar unit, making the barrier to reductive elimination very high. Indeed even Xantphos complexes of Ar-Pd^{II}-F[373,378] would not undergo reductive elimination where the corresponding Ar-Pd^{II}-CF$_3$ did. Reductive elimination of Ar-F from a high-valent Pd^{IV} center was subsequently shown to be possible by Ritter *et al*.[379,380]

More recently, there has been interest in the selective C-H trifluoromethylation of (hetero)aromatic compounds.[381–383] Yu *et al.* published a directed ortho-trifluoromethylation procedure, which exploited *N*-heterocyclic directing groups to facilitate C-H activation and provide the Ar-CF$_3$ compound after completion of the reaction (figure 147). [384]
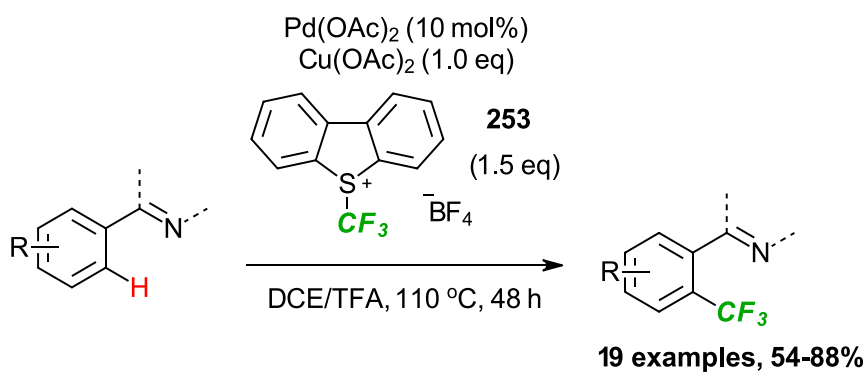
Figure 147: Pd-catalysed C-H ortho-directed trifluoromethylation

The source of the CF$_3$ group was the trifluoromethyl substituted dibenzothiophenium salt **253** (Umemoto reagent), which is among a class of "electrophilic" trifluoromethylation agents that have been developed as convenient sources of both "CF$_3^+$" and "CF$_3^\bullet$" and have been utilised in numerous trifluoromethylation procedures published in recent years (figure 148).[385–388]
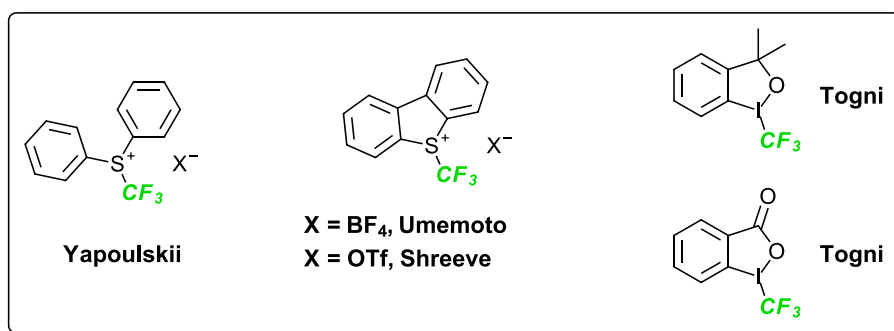
Figure 148: Selection of S- and hypervalent I-based "electrophilic" trifluoromethylation reagents

Although these reagents have proven themselves useful and valuable, as sources of CF$_3$, their cost per mole is high compared to many other more simple precursors. Beller *et al.* addressed this by developing a Pd-catalysed C-H trifluoromethylation procedure using CF$_3$Br,[389] an inexpensive and commercially available substance that was once used as a fire suppressant (figure 149). The production of CF$_3$Br has since been outlawed in accord with the Montreal Protocol[390] however, there may still be a large stock still in existence that could be used cheaply and
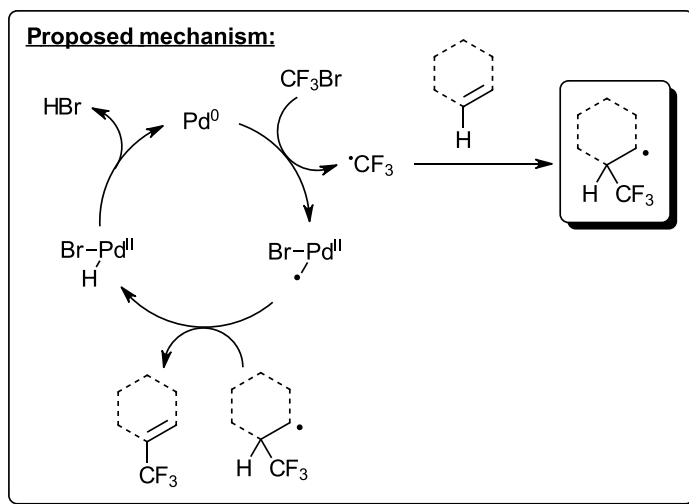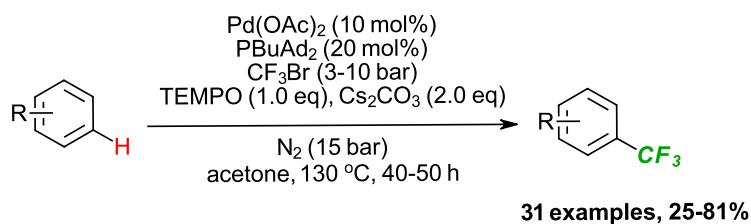
Figure 149: Pd-catalysed synthesis of CF₃ arenes via a proposed radical pathway

appropriately for chemical synthesis instead of risking future release into the atmosphere. Nonetheless, Beller found that the role of the Pd catalyst in this case was likely to be homolytic cleavage of the C-Br bond (figure 149), producing a CF₃• radical, which can add to the arene substrate. Despite the clear cost reduction by using such a simple CF₃ source, the process is still plagued with some issues, including the need for fairly harsh conditions (acetone, N₂ (15 bar), 130 °C, 40 hours) and the common problem of radical addition selectivity (*vide infra*). Addition of a "CF₃•" radical to an arene/heteroarene is of course a viable strategy for trifluoromethyl incorporation, provided that the C-H selectivity does not cause a problem with the yield of the process. Great advances in the controlled production of such radicals, followed by addition to interesting substrates have been achieved in recent years. For example, MacMillan *et al.* found that CF₃SO₂Cl (TfCl) was an efficient reservoir for the CF₃• radical in the presence of a ruthenium photocatalyst and a light bulb.[391] The procedure was proven a versatile strategy for (hetero)arene trifluoromethylation, proceeding at room temperature and providing an excellent sample of functionalised products in good to excellent yield. Significantly for pyrrole, which underwent facile bis-trifluoromethylation under the reaction conditions, the mono-trifluoromethylated product could also be isolated in very good yield by controlling the number of equivalents of TfCl. The procedure was amenable to the mild late-stage trifluoromethylation of numerous drugs and commercial products, often leading to regioisomeric mixtures.

Baran *et al.* made use of the stable and cheaply available CF₃SO₂Na (Langlois reagent)[392] as a CF₃• source,[393] the latter of which could be efficiently produced through the action of the initiator *t*BuOOH under the reaction conditions (figure 150). The conditions were mild and highly desirable as an aqueous solvent system that didn't require rigorous purification was used and a wide range of (protic) functionality
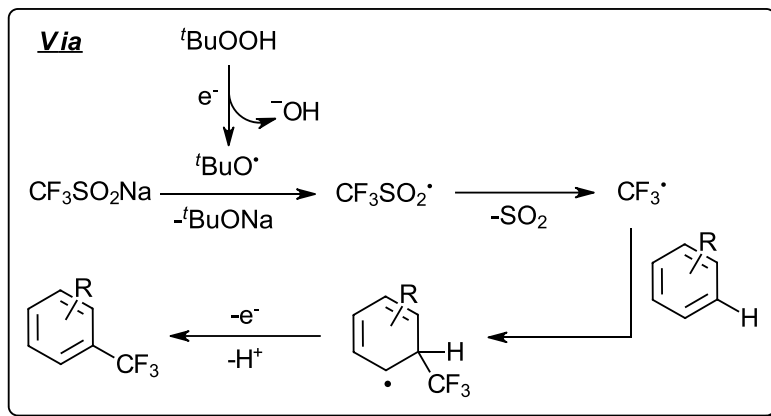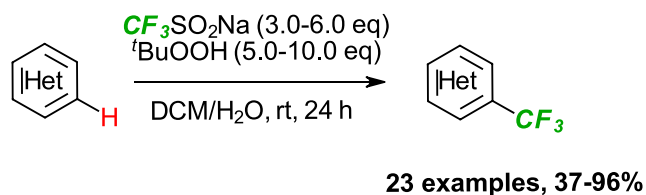
Figure 150: Radical trifluoromethylation using sodium triflinate (Langlois reagent)

was tolerated. However, the reaction often provided mixtures of products wherever there were multiple potential sites of reactivity and some substrates proceeded with only moderate conversion. Having said that, preliminary investigations into the influence of the solvent identity on the reaction selectivity showed promising results, suggesting that further optimisation of the selectivity of CF• addition to (hetero)arenes is possible. The principle was extended successfully to the CF$_2$H group in a subsequent publication[394] through the use of Zn(O$_2$SCF$_2$H)$_2$ as the fluoroalkyl radical precursor. Owing to the mildness of conditions and the promise of new reagents being developed, radical-based methods for trifluoromethylation have since become popular targets for research and many studies have been published in recent years.[395–397] For example, advances have been made in the field of Ni-catalysed/promoted radical C-H trifluoromethylation,[398,399] culminating in the development of a general procedure by Sanford *et al.* for the radical C-H trifluoromethylation of electron-rich benzenes and heteroaromatics catalysed by a Ni^{IV} complex,[399] fed by a thianthrenium similar to Umemoto's reagent as the CF$_3$ donor. The procedure is mild, tolerated by numerous protic and heterocyclic functionality and represents an intriguing first step into the field of trifluoromethylation by Ni-catalysis.

Another developing technique for radical-based trifluoromethylation methods is electrochemistry,[351,400–402] where the trifluoromethyl radical has been produced primarily by anodic oxidation of the CF$_3$ precursor, potentially obviating the need for chemical oxidants such as ^{t}BuOOH. For example in 2014, Baran *et al.* carried out their C-H trifluoromethylation of heterocycles using Zn(SO$_2$CF$_3$)$_2$ as in figure 150, but this time without TBHP and instead using a divided cell with an electrolyte solution to produce the CF$_3$• radical (figure 151). [403] The electrochemical route provided much better yields in most of the substrates tested, due to a slower and more controlled production of CF$_3$• limited by the delivery of charge as opposed to an excess of TBHP. Importantly, the reaction could be scaled to gram quantities without any depreciation in the product yield. A modified procedure was published subsequently by Zeng *et al.*,[404] who found that their reaction could be carried out at 50 °C, and a more straight-forward undivided cell could be used as opposed to the slightly more complicated cell devised by Baran *et al.* The proposed rationale for these advantages was that a
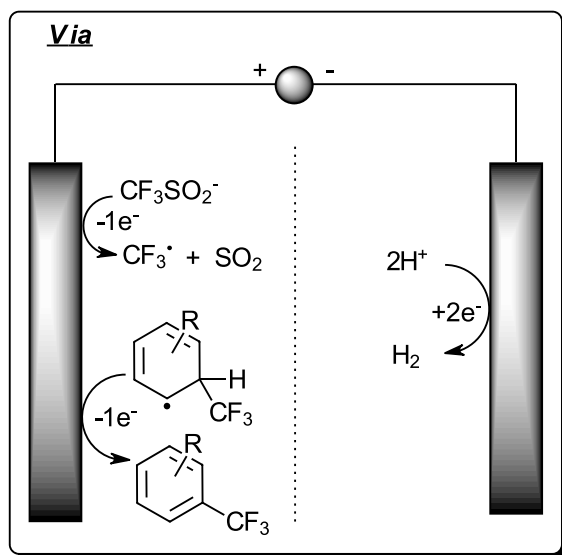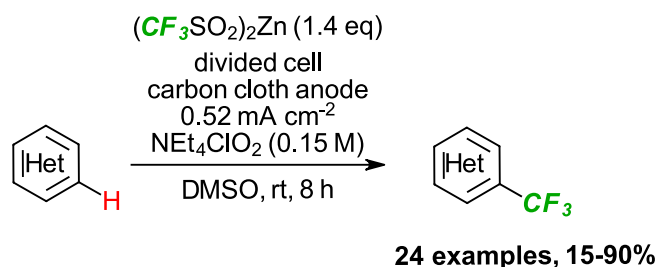
Figure 151: Electrochemical trifluoromethylation via anodic oxidation of the zinc triflinate CF$_3$ donor

different mechanism of CF$_3$$^•$ production could be contributing to the production of product. The bromide in solution was proposed to be oxidised preferentially at the anode, forming a molecule of molecular bromine which reacted with the triflinate salt to produce CF$_3$$^•$ upon either cathodic reduction or homolytic cleavage. This indirect/mediated electrolytic approach represented the first of its kind applied to (hetero)arene trifluoromethylation.

An intriguing development came in a publication by Ackermann *et al.*,[405] who devised an indirect electrolytic trifluoromethylation of (hetero)arenes (figure 152) based on the proposed oxidation of the Langlois reagent by an excited photoredox catalyst (according to Stern-Volmer quenching and cyclic Voltammetry studies). This electro-photocatalytic approach allowed efficient trifluoromethylation reactions to be carried out at room temperature, accessing numerous functionalised (hetero)aromatic products in moderate to excellent yield. The process could also be carried out in flow, revealing promise that it may be amenable to further scale up. Cantillo *et al.* found recently, that a mixture of TfCl and Et$_3$N (forming the ammonium salt **254**, figure 153) could efficiently produce CF$_3$$^•$ radicals for C-H trifluoromethylation of (hetero)arenes. The proposed mechanism in this case, however is a cathodic reduction of **254** which then breaks down and reforms Et$_3$N along with SO$_2$ and a CF$_3$$^•$ radical, the latter of which adds to the (hetero)arene substrate. This cathodic reduction pathway is expected to occur, due to the more positive reduction potential of **254** compared to TfCl, the values of which were estimated by DFT calculations in lieu of satisfactory cyclic voltammograms. One potential advantage of employing a cathodic reduction-focused strategy for CF$_3$$^•$ generation includes a higher tolerance of oxidation-sensitive functional groups in an electrochemical cell, such as thiols and thioethers.[406]
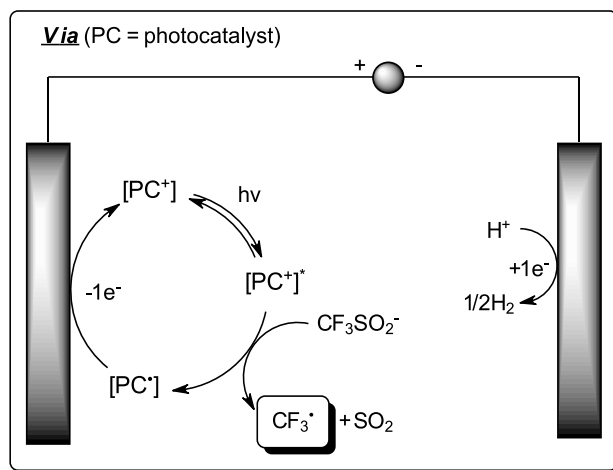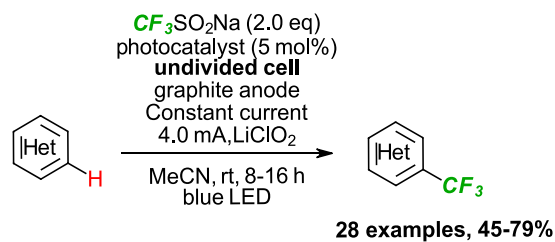
Figure 152: Ackermann's electrophotocatalytic C-H trifluoromethylation of (hetero)arenes, alongside a proposed mechanism for CF$_3$ radical formation
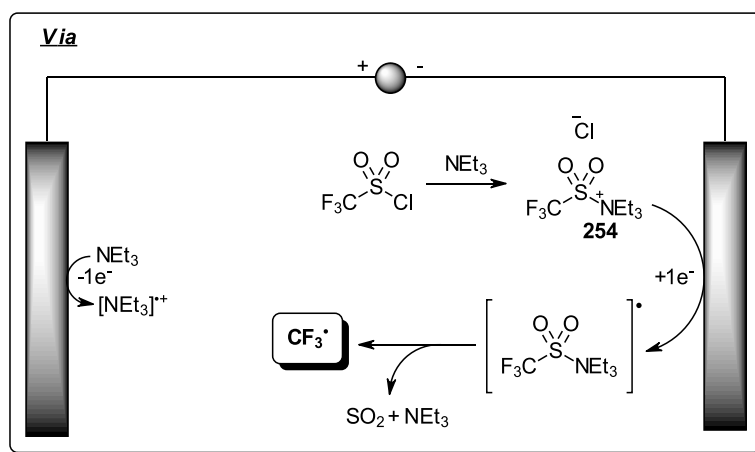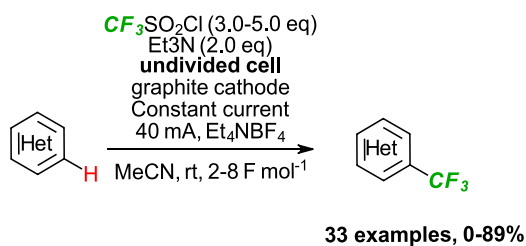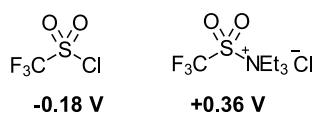
Figure 153: Cathodic reduction of a TfCl +Et$_3$N mixture leading to release of the CF$_3$ radical

2.1.3. Organofluorine synthesis *via* pre-fluorinated starting materials

The methods for obtaining CF_3-substituted (hetero)aromatic compounds outlined in the previous section detail the introduction of the CF_3 unit as a 1 carbon synthon. This has been achieved by trifluoromethylation of a pre-existing handle on the compound such as a halide or a boronate ("programmed functionalisation"), it has also been achieved through the exploitation of the innate reactivity of the (hetero)arene substrate towards $CF_3^{\bullet}$ radicals ("innate functionalisation"). These strategies complement one another, because while innate trifluoromethylation can be achieved under mild conditions (generation of highly reactive $CF_3^{\bullet}$), mixtures of products are sometimes obtained, the composition of which is unique/innate to the substrate under study. Programmed trifluoromethylation on the other hand, can provide access to products functionalised in non-innate positions, provided that the synthetic handle may be substituted in that position to begin with. Another strategy for the synthesis of CF_3-containing (hetero)arenes is *via* ring-forming annulation reactions of CF_3-containing starting materials. This strategy further complements the programmed/innate strategies outlined above, as the position of the CF_3 group is dictated neither by the presence of a synthetic handle, nor by the innate reactivity of the arene towards C-H trifluoromethylation. For annulation reactions, the position of the CF_3 in the product (hetero)arene is dictated solely by the selectivity (if any) of the particular reaction used, which complements both programmed and innate functionalisation strategies. The following is a selection of published works detailing annulation reactions of CF_3-containing starting materials towards trifluoromethylated (hetero)arenes.

Condensation approaches
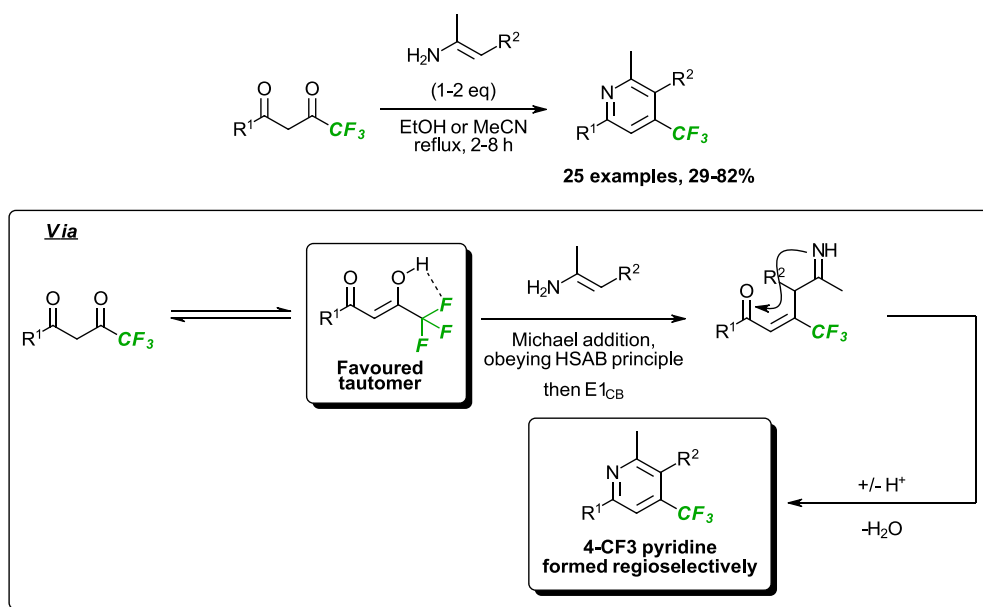
Figure 154: Regioselective synthesis of CF_3-substituted pyridines via condensation of enamines with 1,3-diketones

One common method for heterocycle formation is *via* the condensation of two substances with the extrusion of a small molecule, typically H_2O. Ketones are synonymous with condensation reactions and are a useful class of intermediate for the synthesis of carbo- and heterocycles. Having a CF_3 group attached to a ketone does not diminish its usefulness and allows the formation of CF_3-substituted (hetero)cycles. Among the carbonyl intermediates laden with fluoroalkyl groups[407] that have been studied for their condensation reactions to produce CF_3-substituted (hetero)arenes, are CF_3-substituted 1,3-diketones[408,409] and α,β-unsaturated ketones.[410–412] For instance, Shibata *et al.* discovered a convenient method of selectively obtaining 4-CF_3-substituted pyridines by reacting CF_3-substituted diketones (figure 154) with enamines.[413] The CF_3-substituted 1,3-diketones were prepared in good yield from ethyl trifluoroacetate and acetophenones with KO^tBu. The subsequent condensation reactions proceeded smoothly after refluxing in EtOH or MeCN, affording the corresponding 4-CF_3 pyridine in moderate to excellent yield, without the formation of isomeric 6-CF_3 products. The reaction was tolerant of numerous substituents on the diketone, such as various aliphatic, aromatic and heteroaromatic side chains (R^1). With regards to the enamine, 2 stabilising groups were tolerated including a nitrile (CN) and an ester (CO_2Et) group.

Much investigation into the reactions between CF_3-containing unsaturated ketones and (bis)nucleophiles has been carried out by Nenajdenko *et al.*, allowing access to numerous classes of CF_3-substituted (hetero)aromatic compounds.[414–419] While investigating the potential of CF_3 ynones **255** (figure 155) for fluoro-heterocycle synthesis, they published a series of papers detailing the reaction of the same with various reaction partners including hydrazines and amidines, affording CF_3-pyrazoles,[420] CF_3-pyrimidines[419] and others.[421–423] The CF_3-ynones were prepared by treatment of EtO_2CCF_3 with the corresponding terminal acetylide, providing the ynones **255** in mostly good yields. The condensation reactions of **255** with substituted hydrazines were found to proceed smoothly to provide a range of 3-CF_3 and 5-CF_3 pyrazoles in variable yield and sometimes as a mixture of regioisomers. Interestingly, the authors found that they could significantly influence the regioselectivity of the condensation by altering the solvent and order of reagent addition. When the reaction was carried out in HFIP (polar, protic), the products of condensation with phenylhydrazine were the 3-CF_3-pyrazoles, the products of condensation with other hydrazines in HFIP were also mostly composed of the 3-CF_3-pyrazole, although some substrates provided significant quantities of the 5-CF_3-pyrazole, too.
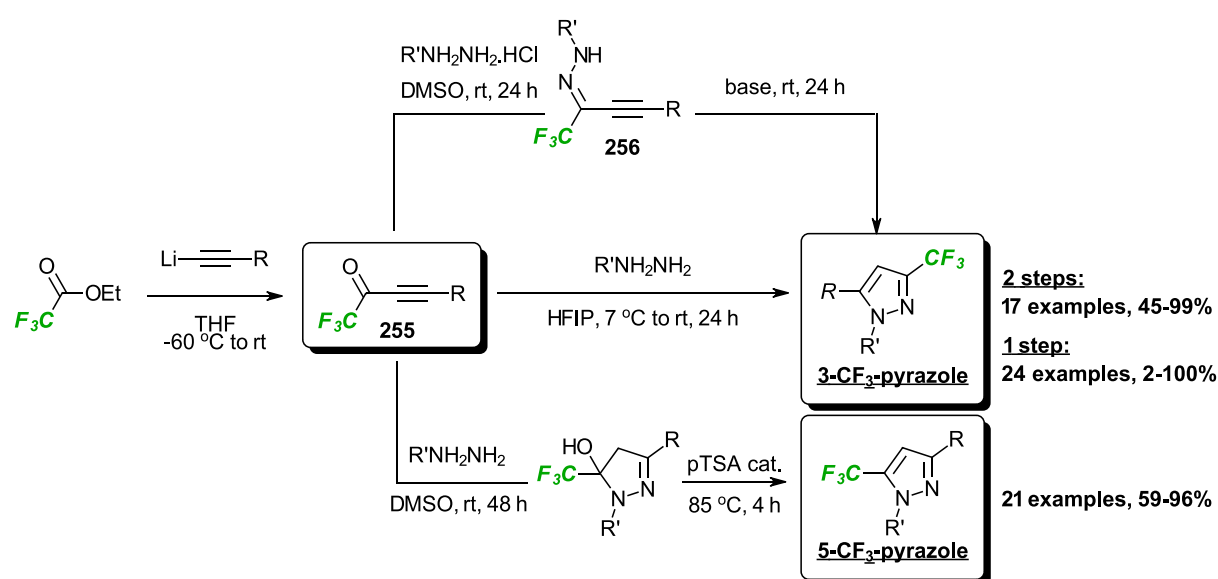
Figure 155:Regiocontrolled synthesis of CF₃-substituted pyrazoles

In contrast, when the reaction was carried out in DMSO, followed by an acid-mediated aromatisation, the 5-CF₃-pyrazoles were obtained with variously substituted phenylhydrazines. When the DMSO conditions were used with ethyl- or ^{t}butyl-hydrazine, the 3-CF₃-pyrazole was still obtained to a significant degree. To elicit further control on the reaction regioselectivity, the authors exploited the serendipitous formation of the (stable) hydrazone **256** upon condensation of **255** with hydrazines in acidic media. The hydrazones could be cyclised under basic conditions to afford the 3-CF₃-pyrazoles exclusively. The authors do not comment on the specific role (if any) played by the CF₃ group in directing the regioselectivity of the condensation, but it is likely that its electron-withdrawing nature facilitates each process by making the starting ynone **255** highly electrophilic. In a subsequent publication,[419] the CF₃-ynones **255** were found to react smoothly with amidines, guanidines and isothioureas to afford CF₃-substituted pyrimidines and aminopyrimidines in good to excellent yield (figure 156).

Z = H, Me, Ph, NH₂, SEt

base = KOBu, NaOMe, NaOAc, NEt3
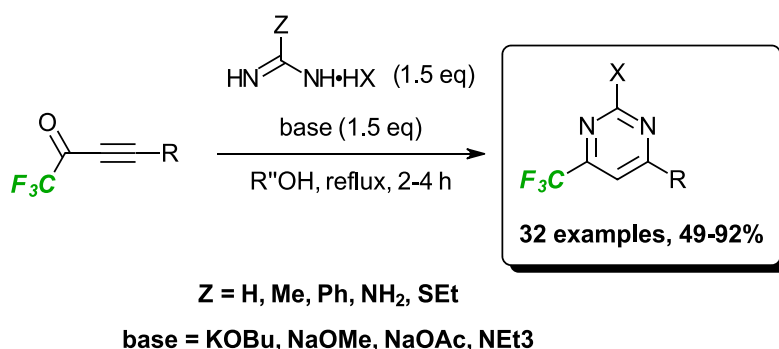
Figure 156: Condensation of CF₃-ynones with amidine/guanidine derivatives to afford CF₃-substituted pyrimidines
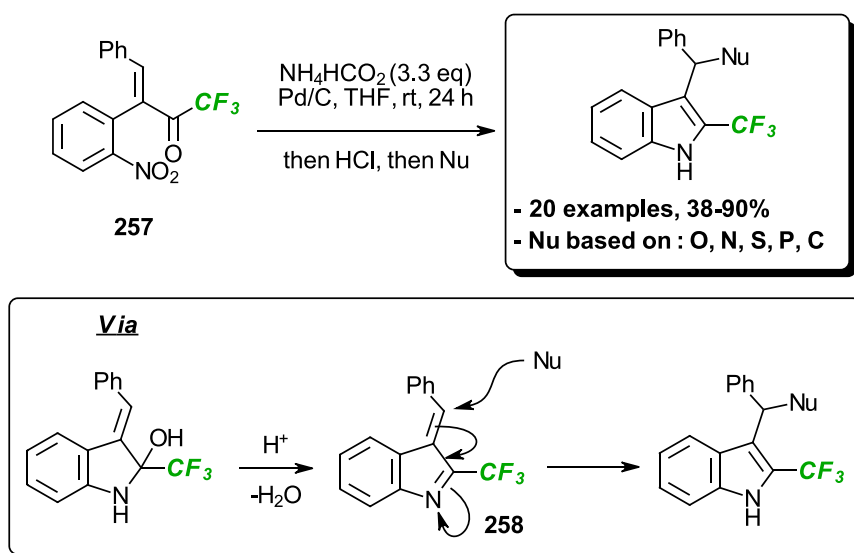
Figure 157:One-pot reductive condensation of CF₃-ketones, providing nucleophile-trapped products after elimination of H₂O

More recently, nitro-substituted α,β-diaryl-CF3-enones **257** (figure 157) were prepared and found to cyclise efficiently upon reduction of the nitro group to the corresponding 2-CF₃-substituted indole.[424] After some optimisation, the authors found a reduction procedure that appeared to be selective for

nitro group reduction over ketone reduction. After reducing the number of equivalents of the "H$_2$" surrogate (NH$_4$HCO$_2$) and investigating various nucleophiles, numerous 2-CF$_3$-substituted indoles were prepared by the same method in moderate to excellent yield. The intermediate unsaturated imine **258** could be trapped with an impressive array of nucleophiles in this one-pot reduction-cyclisation procedure, including those based on C, O, N, S and P.

Han *et al.* recently disclosed[425–427] a series of organocatalytic benzannulation reactions of fluoroalkyl-substituted alkenes with various nucleophilic substrates (figure 158). For instance, **259** reacted with α,β-unsaturated aldehydes in the presence of a secondary amine catalyst to afford highly functionalised benzenes **261** in good to excellent yield. The reaction displayed an impressive scope of application, allowing the incorporation of numerous cinnamaldehyde derivatives and amenable to CF$_3$, CF$_2$H and C$_2$F$_5$ incorporation as the fluoroalkyl substituent. When ketone-stabilised **260** was used, alternative benzaldehyde products **262** were formed, resulting from the participation of the ketone carbonyl in the final cyclisation ([4+2] annulation) as opposed to the aldehyde carbonyl ([3+3] annulation). The same perfluoroalkyl-substituted intermediates were shown in a separate publication to react with Michael acceptor alkenes such as dicyanoalkenes and nitroalkenes in the presence of a nucleophilic catalyst to afford anilines and other substituted benzenes, respectively. The method represents a useful addition to the arsenal of techniques for obtaining fluoroalkyl-substituted benzenes from simple acyclic precursors.
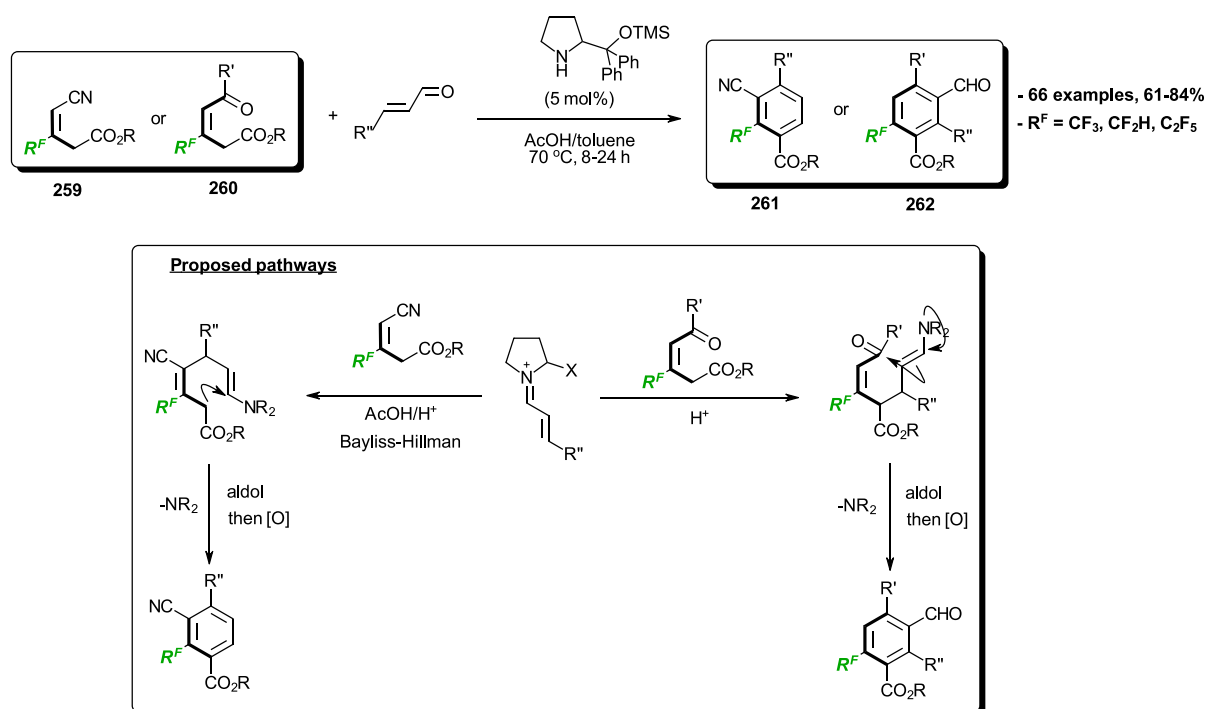
Figure 158: Organocatalytic regiocontrolled synthesis of tetra- or penta-substituted CF$_3$-containing benzenes from simple precursors

Diels-Alder and 1,3-dipolar cycloaddition approaches

To complement the numerous powerful methods for the benzannulation of fluoroalkyl-substituted precursors *via* condensation reactions, reactions such as [4+2] (Diels-Alder) and dipolar cycloadditions have also been used to great effect over many decades for the synthesis of fluorinated / fluoroalkyl-substituted (hetero)arenes.[428] The materials required to achieve such transformations are fluoroalkylated dienes or dipoles and/or dienophiles or dipolarophiles. Much progress has been made in the synthesis of such materials, and the following few paragraphs will lay out some examples of how this strategy has been applied to the problem of preparing CF_3-substituted (hetero)arenes.

For example, Sato and Hiyama prepared aryl trifluoropropynes **264** (figure 159) and reacted them with Danishefsky's diene **263** at 150 °C for 6 hours and obtained, after a SiO_2-mediated aromatising workup, the CF_3-substituted phenol **265** as a single regioisomer. The procedure could be applied to 6 examples, affording the expected products in good to excellent yield.[429]
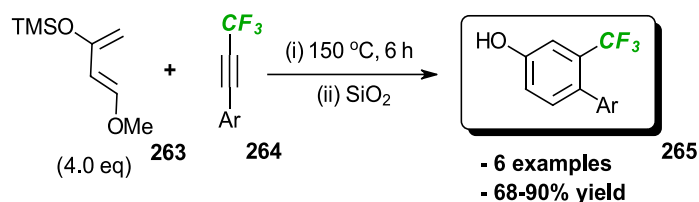
Figure 159: [4+2] Diels-Alder reaction of trifluoropropynes with danishefsky's diene, affording CF$_3$-substituted benzenes
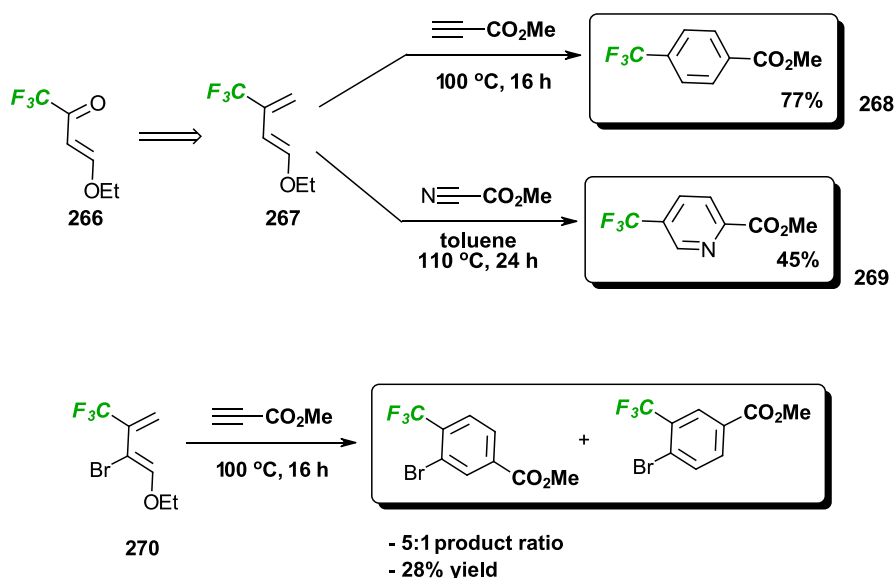
Figure 160: [4+2] Diels-Alder reactions of CF$_3$-substituted butadienes with propiolate esters, affording CF$_3$-substituted (hetero)arenes

At the turn of the century, Schlosser *et al.* prepared the CF₃-substituted 1,3-butadienes **267** and **270** (figure 160) first by a tedious 5-step procedure from 3,3,3-trifluoroacetone, then in a later publication by Wittig methylenation of the corrresponding CF_3 enone **266**, which is prepared from TFAA in one step.[430,431] Upon subjection of **267** to methyl propiolate and heating, a single product **268** was obtained regioselectively in very good yield.

266 was also found to react with the less active dienophile: methyl cyanoformate to produce, again regioselectively, the pyridine **269** in moderate yield. The corresponding Br-substituted buta-1,3-diene **270** was also prepared and reacted with methyl propiolate, although in this case the regioselectivity was compromised, affording a 5:1 mixture of regioisomers in only moderate yield. The rationale for regioselectivity (if any) for the preceding examples of cycloadditions of Danishefsky's diene **263** and diene **267** is that the lowest energy transition state will be the one that matches the biggest HOMO and LUMO coefficients, with 1-alkoxy-substituted 1,3-butadienes the HOMO typically has its largest coefficient on the 2- and 4-positions of the diene. For alkyne dienophiles, the largest coefficient of the LUMO lies on the most electron-poor atom and the CF_3 group of alkynes **264** is expected to cause the *ipso* carbon atom to fulfil this role.[429] If the Diels-Alder reaction is inverse in electron demand (LUMO of diene, HOMO of dienophile), then the converse argument applies, leading to the same regiochemistry.

2-pyrones are convenient and versatile diene equivalents that have been used to prepare aromatic compounds for a long time.[432,433] Due to a degree of aromaticity, they are less reactive in [4+2] cycloadditions than standard cyclic conjugated dienes such as cyclohexa-1,3-dienes, but still undergo reactions readily with alkenes and alkynes (figure 161). After [4+2] cycloaddition, 2-pyrones form unstable bicycloocta-1,4-dienes **271** which decompose quickly by extrusion of CO_2 to either the aromatic compound **272** directly or the dihydrobenzene **273**, which may be transformed to **272** *via* elimination of a built-in leaving group such as HX, or by oxidation.
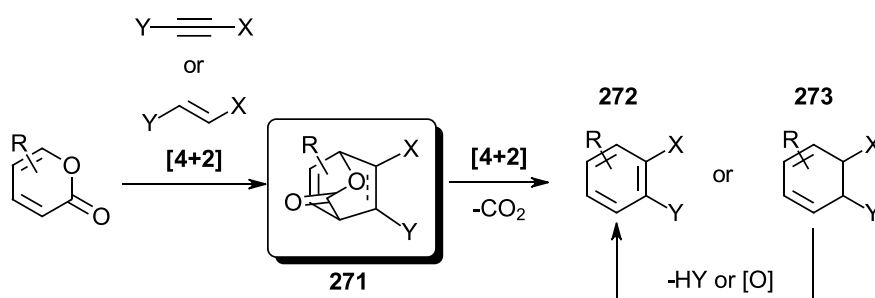
Figure 161: General reactivity pattern of 2-pyrones towards alkenes and alkynes
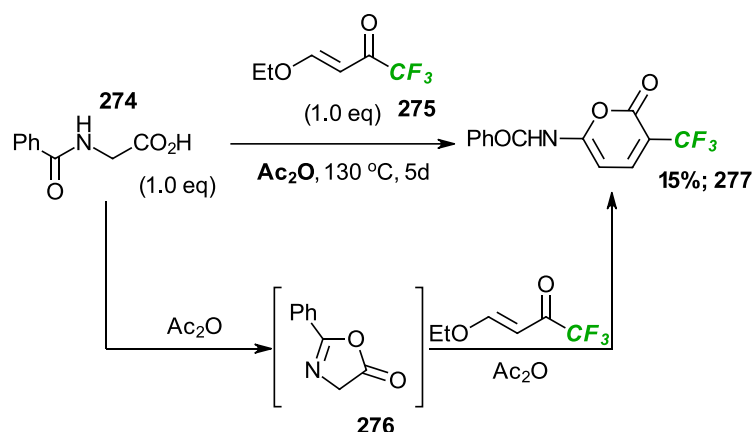
Figure 162: Synthesis of CF₃-substituted 2-pyrone via anhydride mediated condensation of hippuric acid

Despite this, here have only been a handful of reports in the literature detailing the synthesis and cycloaddition reactivity of CF$_3$-contining 2-pyrones[434–438] Haufe *et al.* prepared protected 3-amino-6-CF$_3$-pyrones **277** (figure 162) for the synthesis of 4-trifluoromethylanilines *via* a cycloaddition strategy.[439,440] It is notable that, at the time, trifluoromethylation *via* a radical addition pathway to anilines lead only to *o/p* trifluoromethylated mixtures or bis(trifluoromethylated) anilines were obtained.[441] There was thus a need for synthetic procedures that allowed the selective incorporation of CF$_3$ at the para position of anilines. The pyrone **277** was prepared by treatment of hippuric acid **274** with Ac$_2$O, followed by reaction of the intermediate azlactone **276** with the CF$_3$-enone **275**. Additional to a CF$_3$ group, CF$_2$Cl and C$_3$F$_7$ could also be incorporated into the 2-pyrone. The prepared CF$_3$-substituted pyrones reacted smoothly with terminal alkynes in the absence of solvent (figure 163), albeit at temperatures in excess of 100 $^{\circ}$C and over extended reaction times.
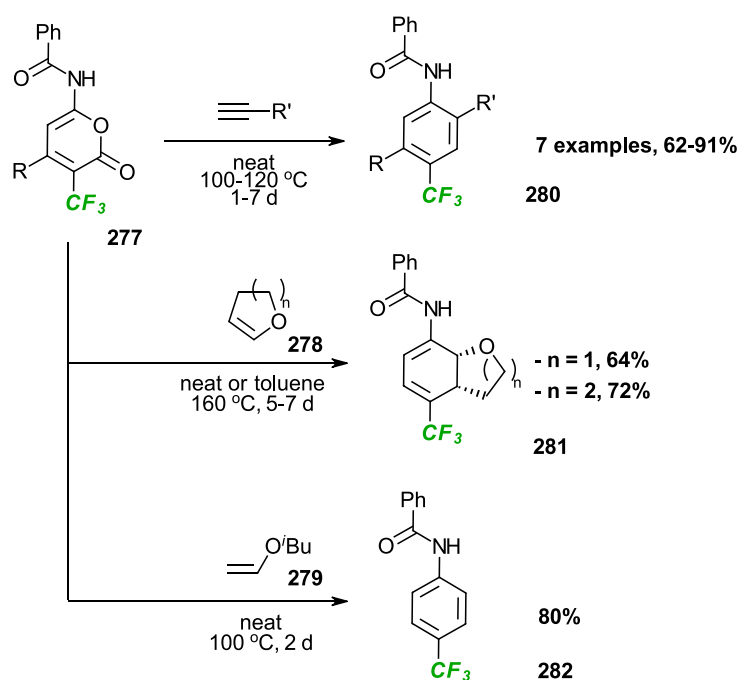
Figure 163: Diels-Alder reactions of CF₃-substituted 2-pyrones with various dienophiles

The regioselectivity of this cycloaddition was, however, very good: affording the ortho-substituted anilines **280** in good to excellent yield. The regioselectivity of this cycloaddition is expected to be due to the high steric demand of the CF$_3$ group (thought to be of a similar size to the ^{i}Pr group)[442] compared to the anilide moiety, thereby causing a preference for the alkyne substituent to be adjacent to the latter in the transition state. The pyrone **277** was then reacted with alkyl vinyl ethers **278** and **279**, affording cyclohexa-1,3-diene **281** or benzene **282** in good yield. Despite reports suggesting vinyl ethers react smoothly under mild conditions with 2-pyrones,[443,444] The cycloadditions of **278** with **277** proceeded only at elevated temperatures, but the cyclohexa-1,3-dienes **281** were obtained regioselectively.

In order to access substituted indolines, Snyder *et al.* prepared alkyne-tethered pyrones (**283**, figure 164)[445] by mono-amine substitution of 4,6-dichloropyrone and heated them at 140 °C to afford the corresponding indoline. Among the substrates prepared was CF$_3$-acetylene **283** (figure 164) which, after [4+2]/retro [4+2] afforded CF$_3$-substituted indoline **284** in excellent yield.
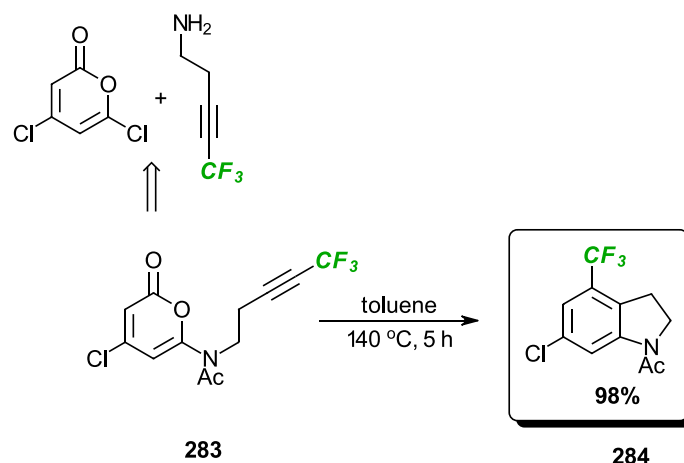
Figure 164: Diels-Alder reaction of a CF$_3$-substituted alkyne-tethered 2-pyrone

This represents a convenient way to enforce regioselectivity in [4+2] cycloadditions of CF$_3$-alkynes with 2-pyrones however, the ethylene tether in **283** does not seem to confer benefits in terms of reducing the harshness of the cycloaddition conditions as 140 °C heat is still required for the reaction to proceed.

While [4+2] cycloadditions are an established means for obtaining 6-membered fluoroalkyl-containing (hetero)aromatic rings, 5-membered rings can also be accessed through [3+2] cycloadditions. In this context, CF$_3$ or other fluoroalkyl-substituted pyrazoles are a privileged subclass,[446] owing to their widespread application as pharmaceutical products such as Celecoxib,[447] And important agrochemicals including herbicides,[448] fungicides[449] and pesticides.[450,451] While pyrazoles have been prepared by a huge number of methods in recent years,[452] an important example is the 1,3-dipolar cycloaddition of alkynes with NNC dipoles, such as sydnones and diazomethane derivatives (figure 165).

1,3-dipolar cycloadditions
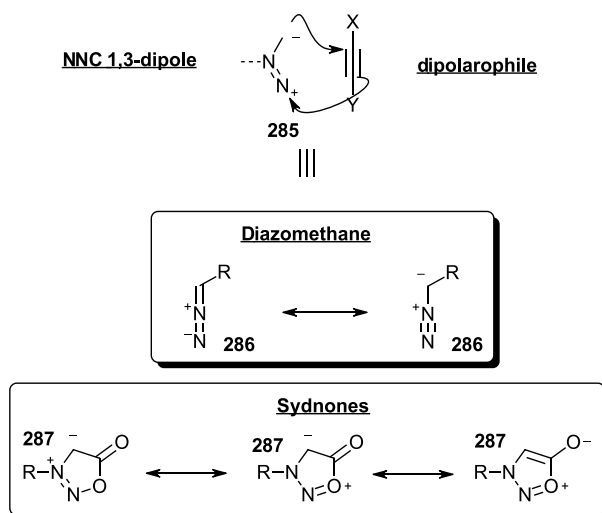
Figure 165: General scheme for 1,3-dipolar cycloadditions of NNC dipoles towards functionalised pyrazoles

- 15 examples, 43-94%
- Regioselective when R" = H
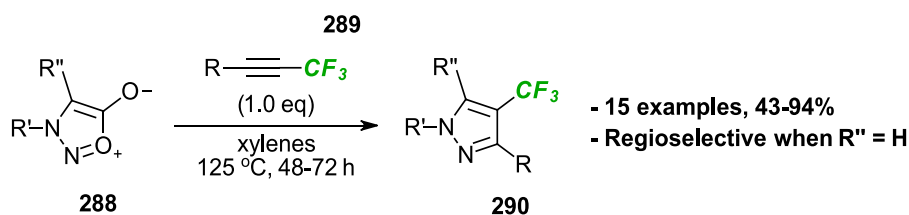
Figure 166: Dipolar cycloaddition reactions of sydnones with trifluoropropynes, affording CF₃-substituted pyrazoles

Sydnones **287** are a member of the family of mesoionic heterocycles that function as 1,3-dipoles for [3+2] cycloadditions with alkynes, in this case forming pyrazoles after extrusion of the embedded CO_2 leaving group. These fascinating intermediates are easily prepared from amino acid derivatives using easily obtainable chemicals and are largely stable to bench conditions and column chromatography.

Piccardi *et al.* exploited this reactivity to synthesise CF_3-substituted pyrazoles **290** (figure 166) by reaction of sydnones **288** with 3,3,3-trifluoropropynes **289**.[453] Several examples of CF_3-substituted pyrazoles could be accessed and were highly regioselective for 4-CF_3-5-H-pyrazoles. It is only when substituents other than H at the 4-position of the sydnone (R'') did the reaction begin to favour the 5-CF_3-pyrazole slightly more and reduce the overall selectivity. Based on this observation, the selectivity is expected to be dictated by the degree of steric hindrance (or lack of) in the cycloaddition transition state. The procedure also suffered from the need for harsh conditions, requiring xylenes at reflux over a period of at least 48 hours.
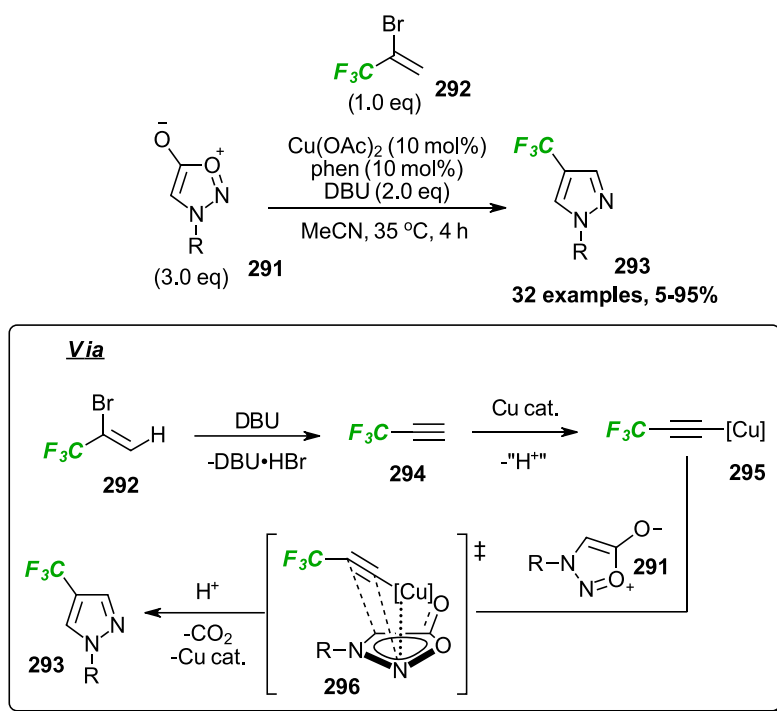
Figure 167: Cu-catalysed synthesis of 4-CF₃ pyrazoles. The regioselectivity is thought to arise due to a Cu-N interaction in the corresponding transition state

Recently, Weng *et al.* reported a mild, selective and convenient Cu-catalysed synthesis of 4-CF₃-pyrazoles, using 2-bromo-3,3,3-trifluoropropene **292** as a 3,3,3-trifluoropropyne precursor.[454] The reaction is expected to proceed *via* initial base-promoted elimination of HBr to the terminal alkyne **294**. The Cu(I) catalyst (formed presumably by disproportionation of 2 equivalents of Cu(II), then coordination of phen) coordinates to the alkyne **294** and forms a Cu(I)-acetylide **295**, which coordinates the sydnone **291** and undergoes the regioselective [3+2] cycloaddition followed by reversion and extrusion of CO_2 to furnish the Cu(I)-pyrazole. After protodemetalation, the pyrazole **293** is released along with the regenerated Cu(I) catalyst. The selectivity of this reaction towards the 4-CF₃ regioisomer **293** is expected to be because of a relative lowering in energy of the required transition state **296** due in part to a potential Cu-N interaction.[455]

While investigating methods to obtain 5-trifluoromethylated pyrazoles selectively, Harrity *et al.* prepared CF₃-substituted sydnone **299** (figure 168) in a 6-step synthesis from phenyl azide using methyl trifluoromethyl pyruvate as the CF₃ precursor.[456] Realising that trifluoromethylation at a later stage would be beneficial for the continuation of the scope, the authors developed a direct Cu-mediated trifluoromethylation of iodosydnone **297** (numerous examples of iodosydones have been prepared easily from commercially available reagents)[457] using the reagent: methyl fluorosulphonyl difluoroacetate **298** as the CF₃ precursor, a cheap and widely available reagent. The CF₃-substituted sydnone **299** was found to undergo smooth cycloaddition reactions with terminal alkynes, affording the 3,5-disubstituted pyrazoles regioselectively[458] in very good to excellent yield.
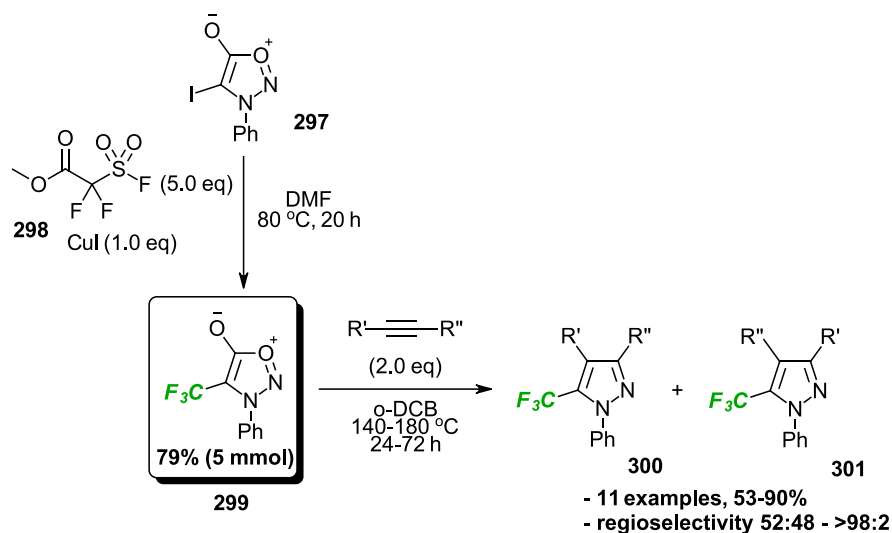
Figure 168: Synthesis and reactivity of a CF₃-substituted sydnone

Upon switching to internal alkynes, fully substituted pyrazoles were obtained but with the expected poorer regioselectivity than that observed for terminal alkynes. Interestingly, alkynyl boronates could also undergo cycloaddition with **299**, providing the 3- or 4-borylated pyrazole in good yield. The regioselectivity of this particular alkyne class was good in all cases, and reversed upon switching from an internal to a terminal alkyne. Although the cycloaddition reactions provide valuable CF₃-substituted pyrazoles selectively in good yield, they require temperatures in excess of 140 °C and reaction times of at least 24 hours to reach completion.

An alternative dipole used to prepare CF₃-substituted pyrazoles *via* dipolar cycloadditions is 2,2,2-trifluorodiazoethane **303** (figure 169), which may react with alkynes to afford the 5-CF₃-pyrazole directly.[459,460] Among the issues with using **303** as a reactant is its explosive nature, utmost caution must be used when isolating or manipulating it. Mykhailiuk *et al.* attempted to address this issue by preparing it *in-situ* by oxidation of 2,2,2-trifluoroethylamine **302** (figure169) with NaNO₂, then adding the appropriate alkyne to produce the pyrazole **304** or **305** without the need to generate and isolate **303** separately.[460] The reaction was effective at forming the desired 3,5-disubstituted pyrazole for a number of terminal alkynes bearing electron-withdrawing groups (ketone, ester, phosphonate) in excellent yield.
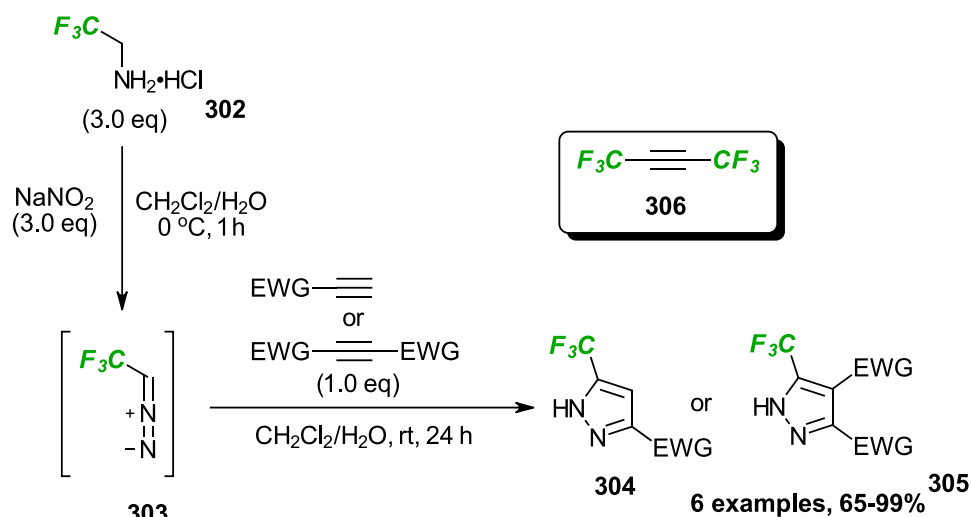
Figure 169: In-situ preparation of 2,2,2-trifluorodiazoethane for 1,3-dipolar cycloadditions with alkynes, affording CF₃-substituted pyrazoles

The reaction also worked for disubstituted alkynes, including hexafluorobut-2-yne **306**, providing access to tris(trifluoromethyl)pyrazole in excellent yield. Although the cycloaddition reaction conditions were mild (CH$_2$Cl$_2$/H$_2$O, rt, 24 h), the reaction failed to proceed with any alkynes that did not bear strongly electron-withdrawing substituents (such as phenylacetylene and trimethylsilylacetylene).

2.1.4. A directed cycloaddition approach to fluorinated small molecules

Reflecting on the vast research effort that has gone into investigating annulation reactions of fluorinated precursors to access fluorinated (hetero)arenes, there have been many different permutations leading to numerous valuable fluorinated products. However, in the case of Diels-Alder and 1,3-dipolar cycloaddition reactions, many of these processes require heating to temperatures in excess of 100 °C and require extended lengths of time to reach completion.[428] Recent work in the Harrity group has focused on developing efficient annulation reactions that offer benefits over existing methods, including the use of mild conditions and enhanced regioselectivity. To that end, the boron-directed cycloaddition reaction of an alkynyl trifluoroborate salt **308** (figure 170) with a substituted
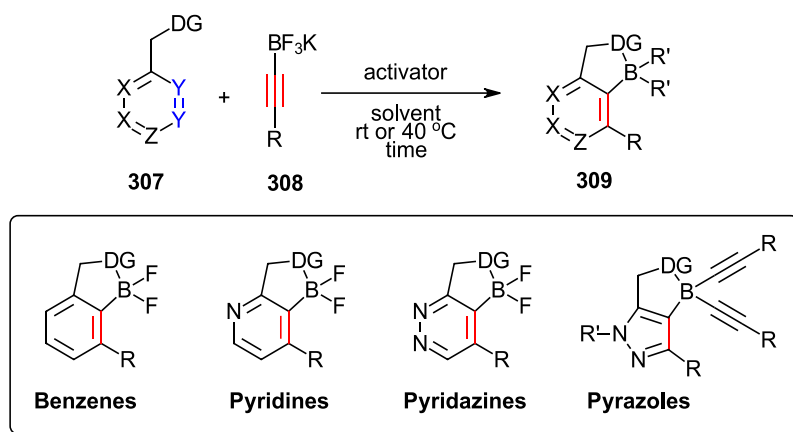
Figure 170: General scheme and current scope of the boron-directed cycloaddition reaction. DG = Directing Group
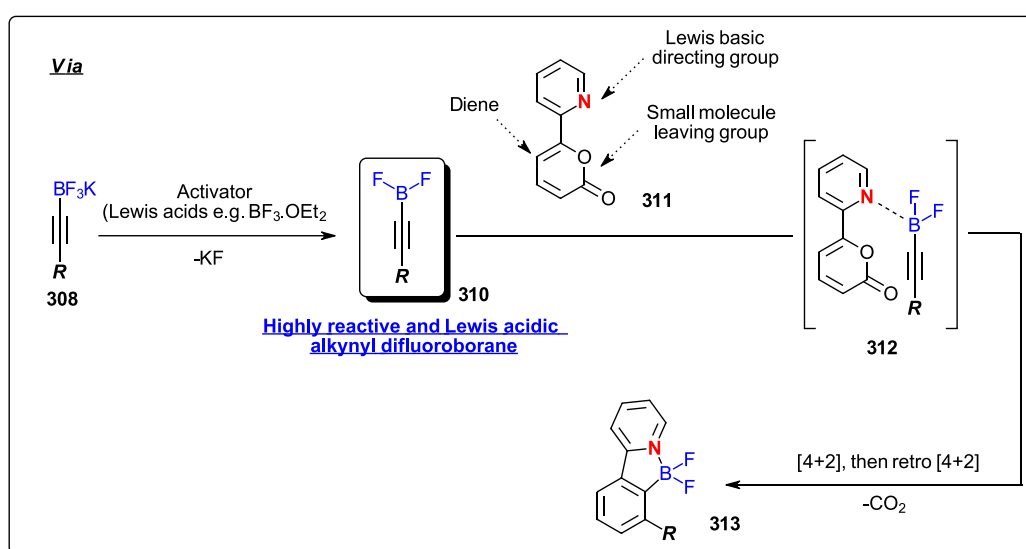
Figure 171: Mechanistic scheme outlining the boron-directed cycloaddition of substituted 2-pyrones with alkynyl trifluoroborate salts

diene/dipole **307** in the presence of a Lewis-acidic promoter (BF$_3$.OEt$_2$, TMS-Cl etc) has emerged as a highly potent method for the preparation of (hetero)aromatic boronic acid derivatives regiospecifically. The advantages, including rate enhancement and regiospecificity stem from the coordination of a Lewis-basic directing group attached to the diene/dipole to a Lewis-acidic alkynyl borane **310** (figure 171, produced *in-situ* from the alkynyl trifluoroborate **308**), forming a complex such as **312**. The cycloaddition rate is enhanced by the acid-base interaction, bringing the two reacting compounds together. The regiospecificity originates also from the acid-base interaction, specifically, in that it is only possible while in one particular orientation of the alkyne (borane group *cis* to the directing group). After the cycloaddition and the following cycloreversion (with elimination of CO$_2$ or N$_2$), Lewis base coordinated (hetero)aromatic boranes **313** are produced, which have been shown to undergo expected boronate functional group interconversions (ligand exchange, Suzuki-Miyaura cross coupling, halodeboronation etc).

This principle has been successfully applied to the regiospecific synthesis of functionalised pyridazines,[461] benzenes,[462–464] pyridines,[465,466] and pyrazoles.[276] In each case, reaction conditions much milder than the equivalent non-directed reaction were realised and a single

a	b	T / ºC	Yield	Ratio 315:316:317
1	1	40	62%	100:0:0
3	3	40	92%	90:5:5
3	3	25	95%	80:10:10
3	3	0	81%	50:25:25
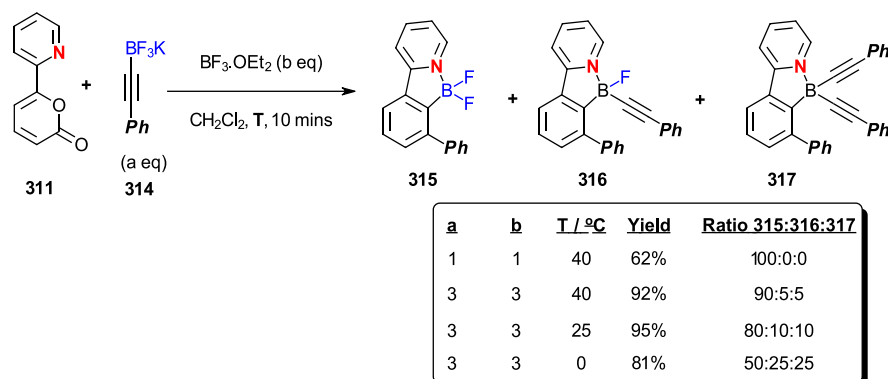
Figure 172: Directed cyclaoddition studies on substituted 2-pyrones, formation of unexpected products

cycloaddition regioisomer was obtained. For the BF$_3$.OEt$_2$-promoted cycloaddition reactions of 2-pyrones, 1,3,4-triazines and sydnones, products other than the (hetero)aryl difluoroborane such as **315** (figure 172) were obtained. These were determined as the alkynylated boranes of the form **316** and **317**, and were obtained as mixtures, the composition of which depended on the ratio of alkyne **314** to BF$_3$.OEt$_2$ and also the reaction temperature.[462,464] Realising that the products **316** and **317** could originate from a pre-cycloaddition disproportionation reaction of the intermediate alkynyl difluoroborane **310**, a detailed computational analysis of this reaction and the subsequent cycloaddition processes was undertaken.[464] The conclusions from this study, were that although the major product was usually the difluoroborane **315**, this was not solely due to a directed cycloaddition of **310** with 2-pyrone **311**. In fact, alkynyl boranes such as **319** (figure 173) and **320** that were also present in the reaction mixture as a result of the aforementioned disproportionation process also underwent directed cycloadditions to products such as **325** and **326**, respectively. Furthermore, the activation enthalpies of directed [4+2] cycloaddition of the acid-base complexes **321**, **322** and **323** were calculated and it was found that the lowest barrier to cycloaddition was for **323**.
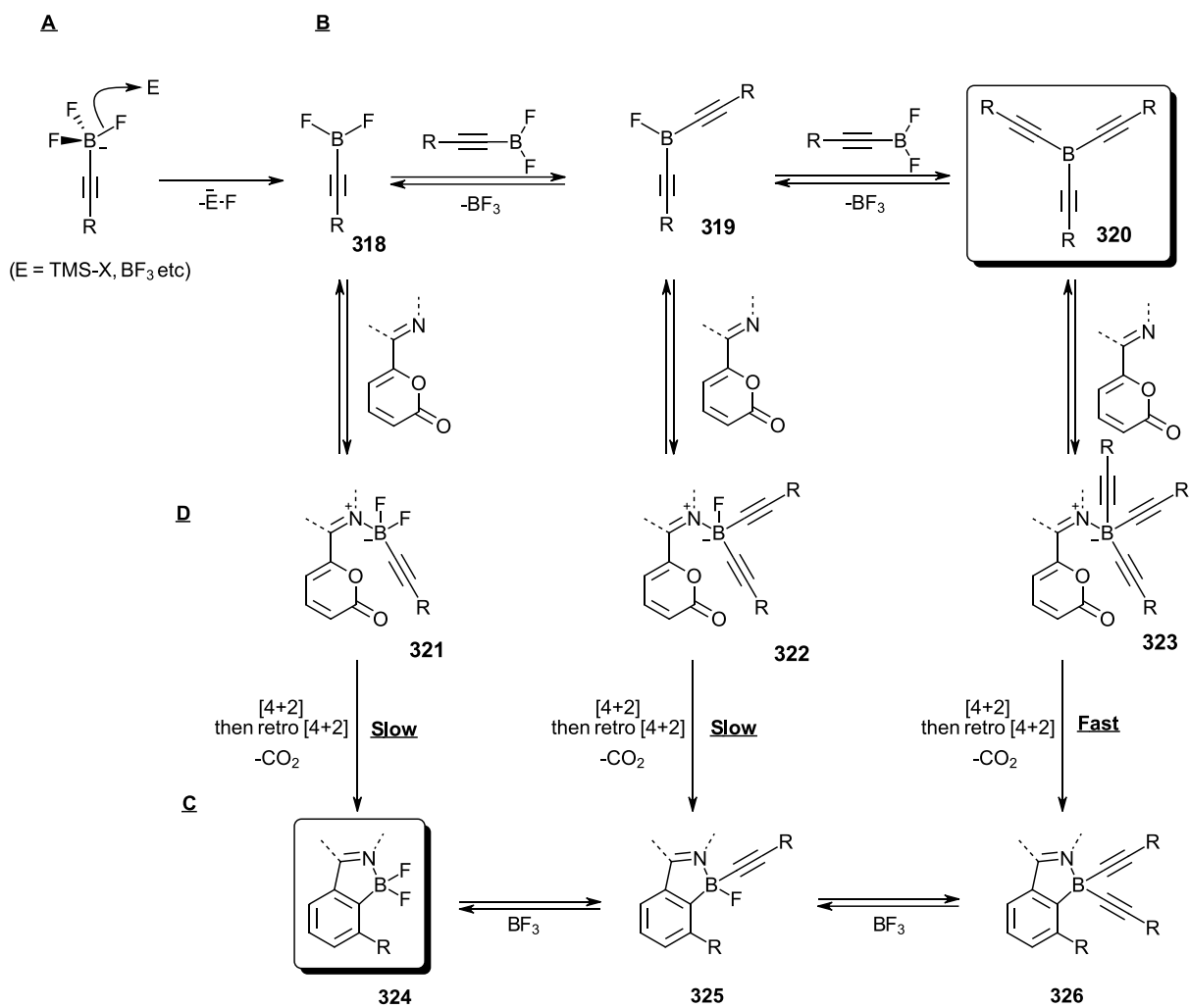
*Figure 173: Mechanistic rationale for the origin of products **325** and **326**, also why the major product is usually **324***

To reconcile the seemingly contradictive observations that **315** (figure 172) is the major product while the complex **323** (figure 173) has the lowest barrier to cycloaddition (assuming borane
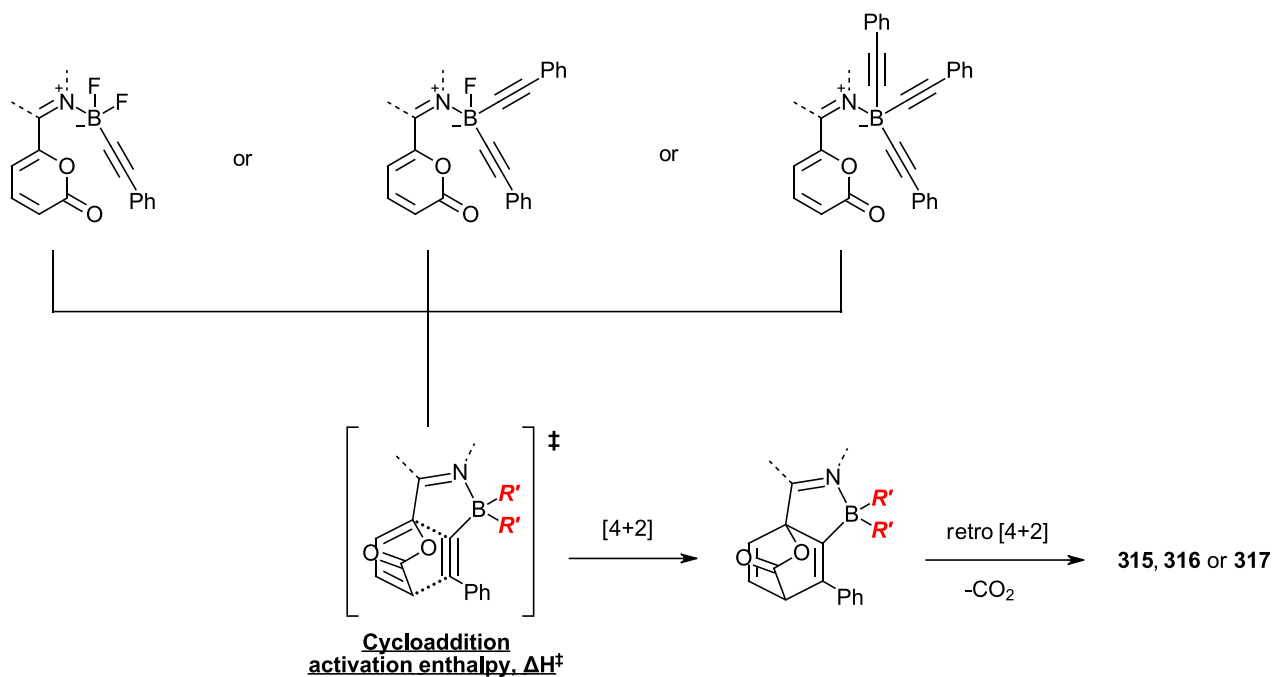
R^1	R^2	ΔH‡ / kJ mol^{-1}	Rel rate (298 K)
F	F	+101.4	1
F	C≡CPh	+90.6	78
C≡CPh	C≡CPh	+81.8	2727

Table 4: Influence of the boron centre's ligands on the activation enthalpy for directed cycloaddition
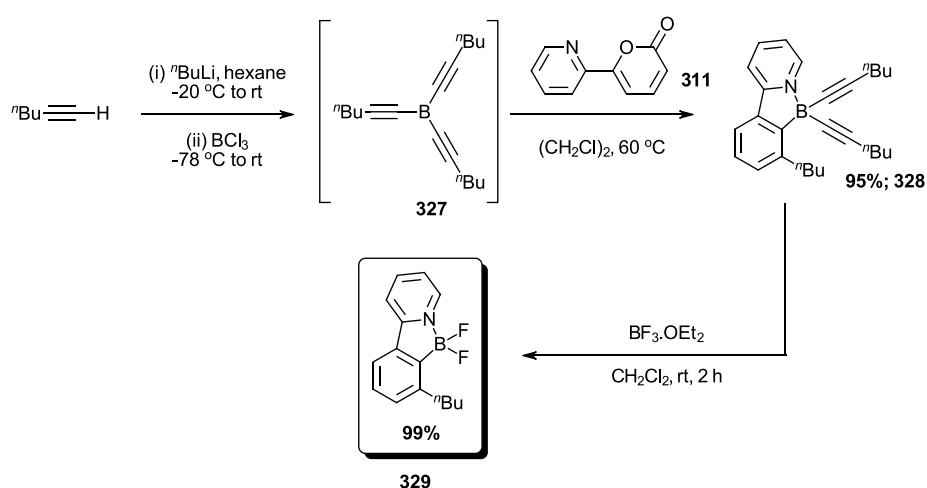
Figure 174: Independent synthesis of bis(alkynyl) borane cycloadduct and BF$_3$.OEt$_2$-mediated ligand exchange, leading to the convergence upon the corresponding difluoroborane product

disproportionation is rapid), the authors proposed and calculated a post-cycloaddition ligand exchange reaction, converting **326** to **324** by the action of BF₃.OEt₂. This process was verified experimentally verified by treating **328** (figure 174) with BF₃.OEt₂ under the reaction conditions and obtaining the difluoroborane **329** in excellent yield. The cycloaddition of the independently generated tris(alkynyl)borane **327** with the 2-pyrone **311** confirmed that the proposed mechanism was valid. Namely, after fluoride abstraction by BF₃.OEt₂, the alkynyl difluoroborane **318** (figure 173) is obtained, which undergoes a slow background cycloaddition with the 2-pyrone **311**, forming **324**. **318** also undergoes a bimolecular disproportionation forming **319**, and then **320**. The latter of which performs a rapid cycloaddition to the borane **326** which is subsequently converted to **324** *via* the BF₃.OEt₂-promoted ligand exchange process. The combined theoretical and experimental approach provides remarkable insights into the reaction mechanism and the study just mentioned is an example of how the comparison of calculated activation energies can help to reclaim potential mechanistic pathways that may otherwise have been discarded.

2.1.5. Experimental design & key objectives

Fluorinated (hetero)aromatic small molecules are highly valuable fragments to numerous industries owing to their useful properties. In addition, their production is entirely abiotic which has lead to huge research interest and the birth of the field of synthetic organofluorine chemistry. Among the methods of obtaining e.g. trifluoromethylated (hetero)aromatic compounds are direct trifluoromethylations of pre-activated functional groups or appropriate C-H bonds, alternatively, (hetero)benzannulation of CF₃-containing acyclic precursors is another widely explored method. Regarding the latter, numerous procedures now exist for the production of CF₃-substituted (hetero)arenes by cycloaddition reactions however, a common theme among most of these is the requirement for high temperatures and long reaction times. Even the CF₃-alkyne-tethered 2-pyrone **283** (figure 164)[445] required heating at 140 °C over a period of 5 h to reach completion. Given the scarcity of mild cycloaddition-based syntheses of CF₃-substituted (hetero)arenes, we were keen to explore this gap in the literature further. With the directed cycloaddition chemistry outlined in the previous section being developed by the Harrity group, we envisaged that this strategy may provide the necessary workaround to the harsh and sometimes unselective cycloaddition conditions that exist for the non-directed synthesis of CF₃-substituted (hetero)arenes.
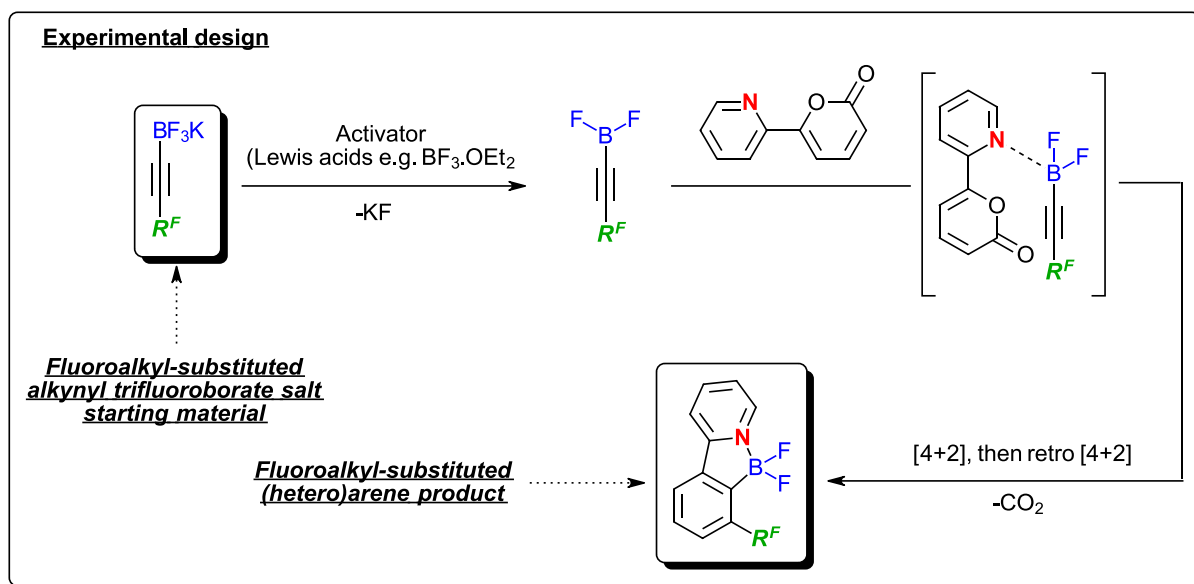
Figure 175: Design of the experimental investigations in this thesis - boron-directed cycloaddition reactions of fluoroalkyl-substituted alkynyl trifluoroborate salts with substituted dienes and dipoles, towards fluoroalkyl-substituted (hetero)arenes

To realise this, we needed to access CF_3(or other fluoroalkyl) -substituted alkynyl trifluoroborate salts (figure 175) and then test its reactivity against various dienes, starting with 2-pyrone **311**, in the presence of Lewis-acidic promoters such as $BF_3.OEt_2$. The reactions were expected to be regiospecific and proceed under mild conditions, providing CF_3-substituted (hetero)arene boronic acid derivatives. Fluorinated aryl boronic acid derivatives have emerged in recent years as powerful intermediates in the preparation of complex organofluorine compounds, due to the rich potential for further functionalisation at the C-B position.[467] Challenges in their preparation, such as a higher propensity to protodeborylate or oxidise compared to non-fluorinated aryl boronic acids, have been addressed by advances in catalytic borylation. Nonetheless, we envisaged that this directed cycloaddition approach would also make a welcome addition to the arsenal of methods available to prepare this class of intermediate.

2.2. Results and discussion

2.2.1. Synthesis of fluorinated alkynyl trifluoroborate salts

We began our studies by considering the synthesis of CF_3-substituted alkynyl trifluoroborate salt **357** (figure 176), to investigate their potential in directed cycloaddition reactions. There are only a few publications that detail the synthesis of such fluorinated trifluoroborate salts, and until recently have required HF or KHF_2 in the final fluorination of boron. We were interested in pursuing a route that could be carried out safely at large enough scale in the lab and preferably one that avoids the use of glassware-etching substances such as HF or KHF_2. We thus decided to repeat the work of Ramachandran and co-workers,[468] who took inspiration from Brisdon *et al.*[469,470] in the use of the hydrofluorocarbon (HFC): R-245fa (1,1,1,3,3-pentafluoropropane, **330**) as a convenient trifluoromethylacetylide **331** precursor.
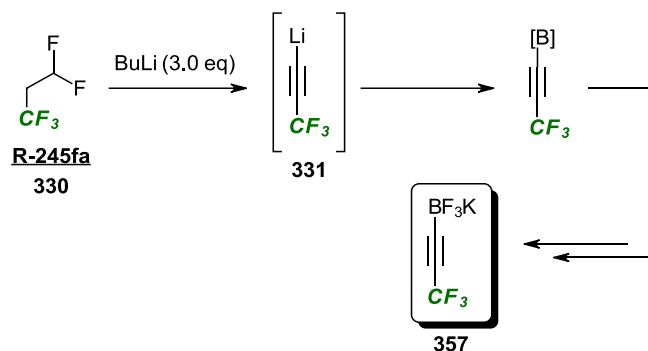
*Figure 176: Cheap and convenient access to lithium trifluoromethylacetylide for the synthesis of **357***

Bardin *et al.* prepared the salt **357** by trapping **331** with $B(OMe)_3$,[471] followed by fluorodemethoxylation using KHF_2 dissolved in aqueous HF. Ramachandran prepared **357** instead by trapping **331** with $BF_3 \cdot OEt_2$ (forming the lithium trifluoroborate salt) and performing a counter ion exchange using K_3PO_4 to provide **357** in moderate yield. The latter procedure avoids the use of hazardous HF and removes one step from the synthesis, it is also a non-etching process. Repeating the synthesis in our hands (figure 177) involved first condensing out a sample of commercially obtained R-245fa, which was then diluted with anhydrous Et_2O to a concentration of 0.5 M. This solution was subjected to the published conditions, which afforded the desired trifluoroborate salt in 30% yield.
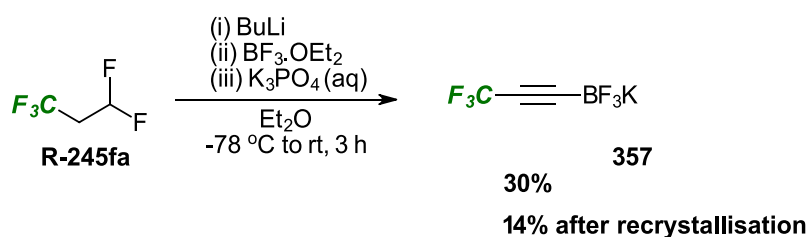
*Figure 177: Preparation and purification of the trifluoromethyl-substituted alkynyl trifluoroborate salt **357***

The material obtained after precipitation from acetone was soluble in many common solvents (Et$_2$O, EtOH, MeOH, H$_2$O) under ambient conditions, but eventually a solvent composition of toluene:MeCN (4:1 *v/v*) was used to recrystallise the salt effectively, leading to a total yield of 14%. The recrystallisation of **357** was necessary in order to obtain consistent results for later directed cycloadditions. The reasons for this may include the presence of byproduct inorganic salts or the undesired formation of more highly substituted borate salts such as the difluoroborate equivalent of **333** (figure 178), as observed in small quantities by Bardin and co-workers.
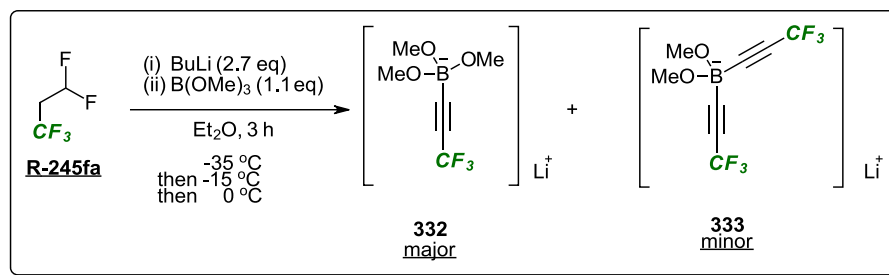
Bardin *et al.*, *Organometallics*, **2005**, *24*, 5311-5317

*Figure 178: Observation of bis(alkynyl) dimethoxyborate salt **333** en-route to the trifluoroborate **357***

A procedure that was found to be important for high conversion in later directed cycloadditions, was the final drying step. It was found that leaving the salt **357** to dry over P$_2$O$_5$ inside an evacuated desiccator overnight was sufficient to provide consistently high conversion, although once prepared they were typically stored inside the same desiccator and taken out when required.
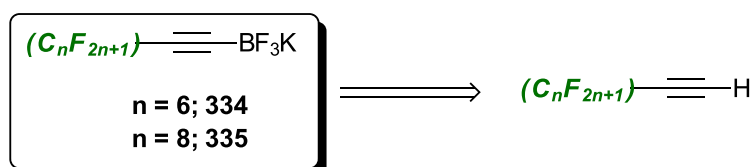
Figure 179: Synthesis of longer chain perfluoroalkyl alkynyl trifluoroborate salts starting from the required terminal alkyne

An easier set of targets to access, were perfluoroalkyl chain-substituted alkynyl trifluoroborates **334** and **335** (figure 179), as the required terminal alkynes were more widely available, commercially. Some of the product salts have also been prepared previously by Bardin. Although some are known (e.g. **334**), none have been prepared *via* Ramachandran's non-etching route[468] before, so we were keen to subject the terminal alkynes to these conditions, on the basis that they would behave in a similar fashion to the trifluoromethyl acetylene produced *in-situ* for the production of **357** previously. Pleasingly, both salts could be prepared in good yield (figure 180) and were fully characterised.
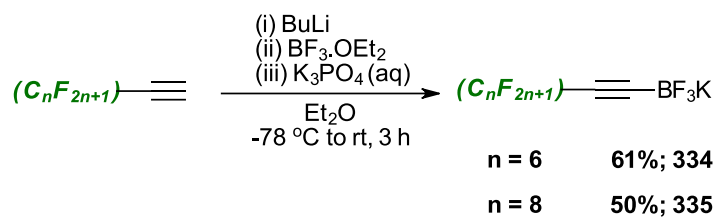
Figure 180: Preparation of longer chain perfluoroalkyl-substituted alkynyl trifluoroborate salts

The salts **334** and **335** were dried over P_2O_5 in the usual way, but not recrystallised before their application to directed cycloadditions. After the successful synthesis of the three salts **357**, **334** and **335**, we wanted to explore the possibility of counter ion exchange to enable the chemistry of **357** in dichloromethane. Thus, applying the usual procedure (figure 181), we could prepare the corresponding tetra-ethylammonium salt of **357** in excellent yield
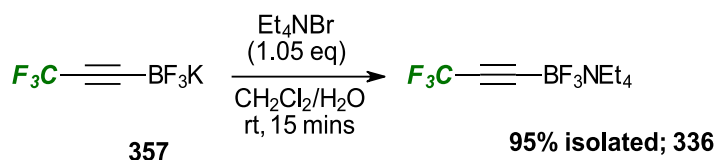
*Figure 181: Counter ion exchange of **357***

2.2.2. Selection and synthesis of substituted dienes & dipoles

In order to investigate the cycloaddition efficacy of the trifluoroborate salts prepared as shown in the previous section, we needed to access a set of dienes / 1,3-dipoles that were substituted with appropriate directing groups. The boron-directed cycloaddition has been studied extensively by our

Diene:	2-pyrones	1,3,4-triazines	1,2,4,5-tetrazines	Sydnones
Expected products:	phenylboranes	pyridylboranes	pyridazinylboranes	pyrazoleboranes
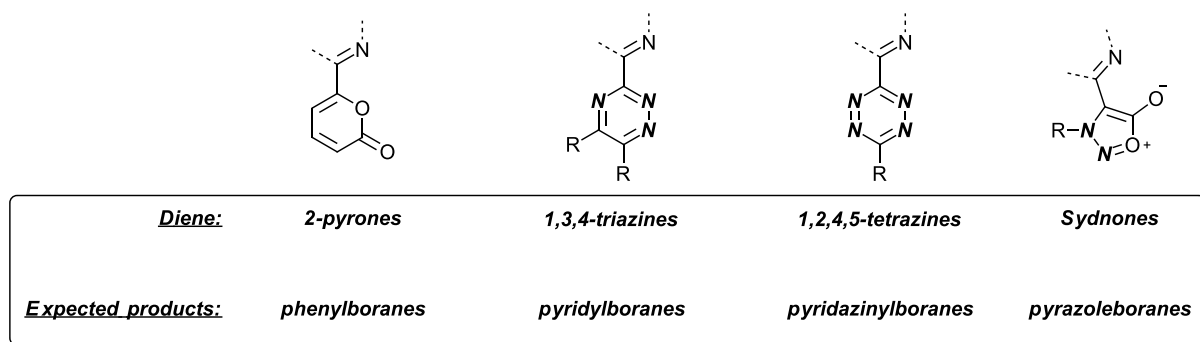
Figure 182: Selection of substituted dienes to be tested in this work

group for non-fluorinated alkynyl trifluoroborate salts and continues to be investigated for its application prospects. For this reason, we wanted to attempt directed cycloadditions using **357** on each of the dienes used so far for other alkynyl trifluoroborates, namely: 2-Pyrones, 1,3,4-triazines,

115

1,2,4,5-tetrazines and sydnones (figure 182). Preparation and testing of each of these classes of cycloaddition partner with **357** would provide good proof-of-concept and allow access to both aromatic and heteroaromatic fluorinated products, both of which are molecular fragments of high value. To begin with, 2-pyrones with a pendant *N*-heterocyclic directing group (e.g. 2-pyridyl) were prepared from the corresponding (2-heterocyclic) aldehyde and ethyl 2,3-butadienoate **337** (figure 183) in a phosphine catalysed process.[462]
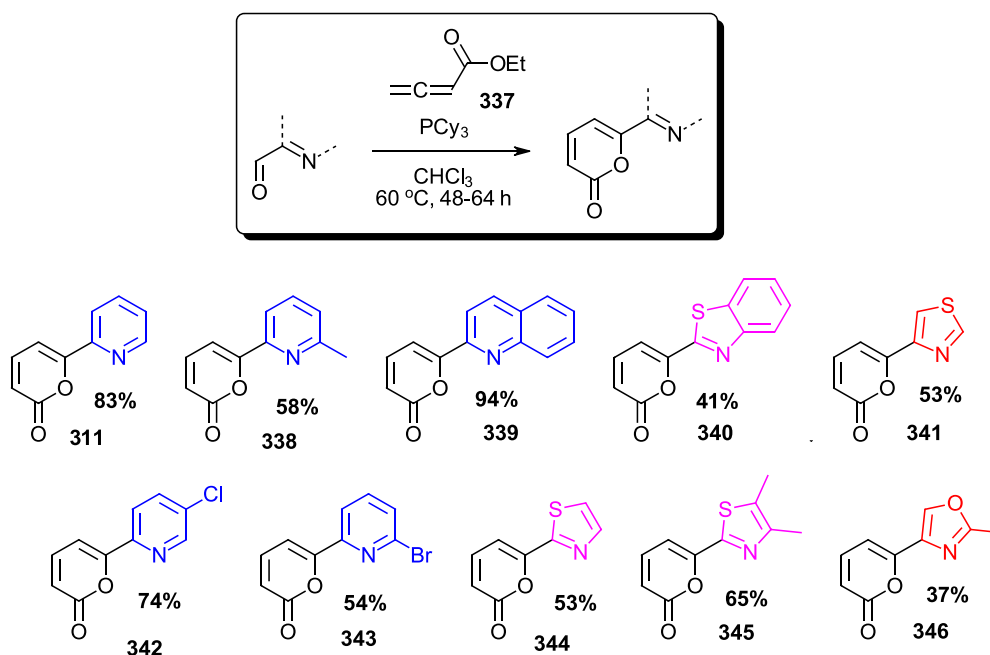
Figure 183: Preparation of 2-pyrones containing a pendant N-heterocyclic directing group

Due to the oxygen-sensitive nature of PCy$_3$ and its wide availability, we elected to use it in superstoichiometric amounts, to maximise the yield of the product. Thus, applying the standard procedure to various commercially available (2-heterocyclic) aldehydes allowed access to the desired (2-heterocyclic)-2-pyrones in moderate to excellent yield. As for the preparation of the alkyne **357,** the pyrones were recrystallised and dried over P$_2$O$_5$ prior to use in cycloadditions. To investigate the possibility of further diversity in the identity of the directing group, we wanted to access amide-substituted 2-pyrones of the form **347** (figure 184). For the synthesis of these 2-pyrones, we first prepared the required carboxylic acid by the published Claisen condensation route (figure 185),[472,473] then reacted it further with SOCl$_2$ followed by dialkylamines to afford **348** and **349**.
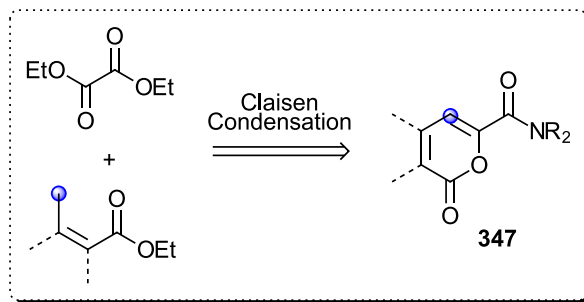
Figure 184: Retrosynthetic strategy towards amide-substituted 2-pyrones followed in this work
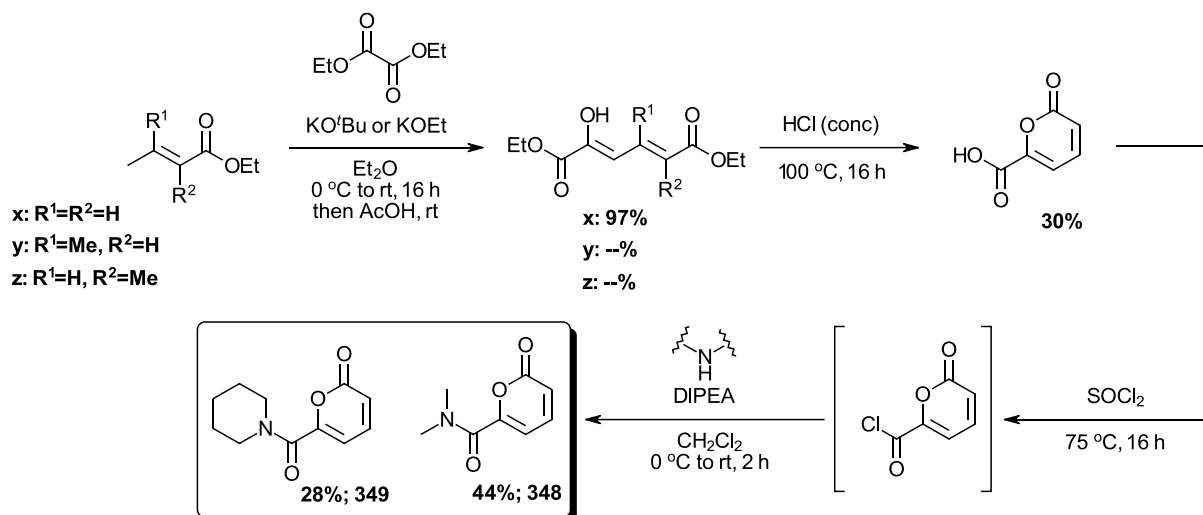
Figure 185: Synthesis of amide-substituted 2-pyrones[472,473]

Regrettably in our hands, attempts to access ring-substituted 2-pyrones by the same route, starting with the required substituted crotonate or tiglate esters (**y, z** figure 185) were unsuccessful.

The preparation of substituted sydnones was achieved using the literature route, namely, nitrosation then cyclodehydration of *N*-phenylglycine[276] to afford *N*-phenylsydnone (figure 186) then Pd-catalysed C-H arylation with 2-bromopyridine, providing the (2-pyridyl) substituted sydnone **350** in good yield. 2-pyridyl substituted triazine **351** (figure 187) was obtained after following a literature procedure[474] *via* the 2-pyridyl amidrazone and substituted tetrazines **352** (figure 188) and **353** were obtained from commercial sources.
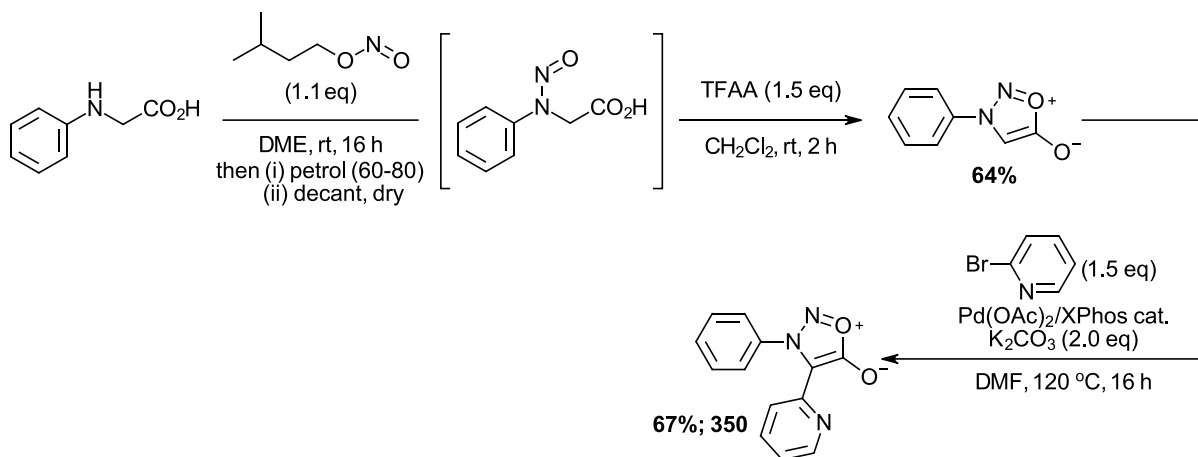
*Figure 186: Synthesis of substituted sydnone **350**[276]*
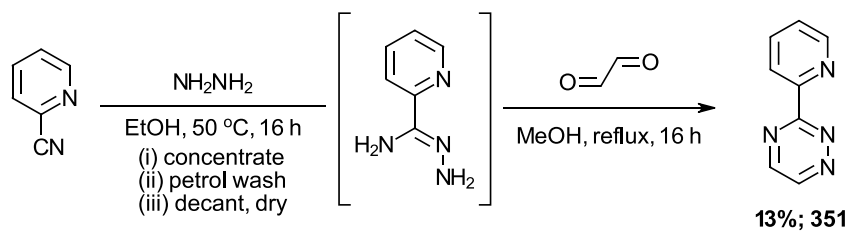
Figure 187: Synthesis of substituted 1,3,4-triazines

352 **353**
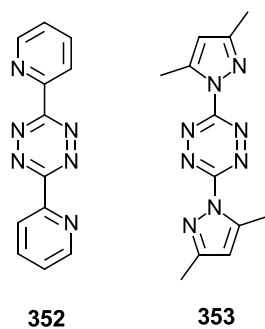
Figure 188: Commercially available substituted 1,2,4,5-tetrazines used in this work

2.2.3. BF₃.OEt₂ promoted cycloadditions of substituted 2-pyrones

Figure 189: Optimisation of conversion for the directed cycloaddition of 357 with substituted 2-pyrone 311
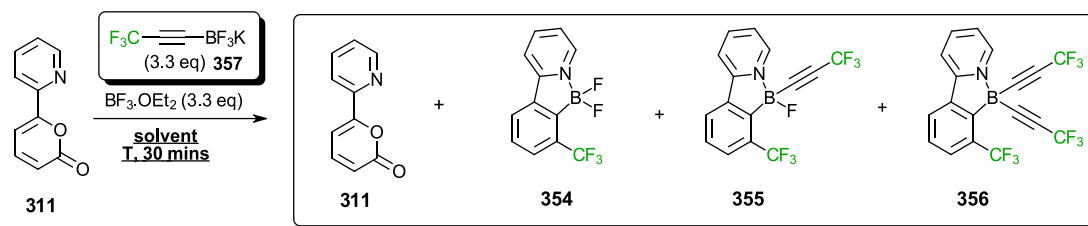
Entry	Solvent	T	conv	354	355	356
1	CH₂Cl₂	40 °C	5%	5%	-%	-%
2	(CH₂Cl)₂	80 °C	100%	63%	29%	8%

To commence studies on the cycloaddition reactions of substituted 2-pyrones, we subjected the pyrone **311** and **357** to the conditions optimised in the literature for non-fluorinated alkynyl trifluoroborate salts.[462] The reaction proceeded with ~5% conversion of to a single compound after 30 minutes of stirring with BF₃.OEt₂ in refluxing CH₂Cl₂. The identity of the major product was determined as the difluoroborane **354**, which was the expected product at this stage based on literature precedent. Pleasingly, upon the use of the higher boiling 1,2-dichlorethane ((CH₂Cl)₂) and heating the mixture of at 80 °C for 30 mins resulted in complete conversion of **311**. However, we did not observe **354** as the only product in this case and an additional two other products, assigned as **355** and **356** were obtained.
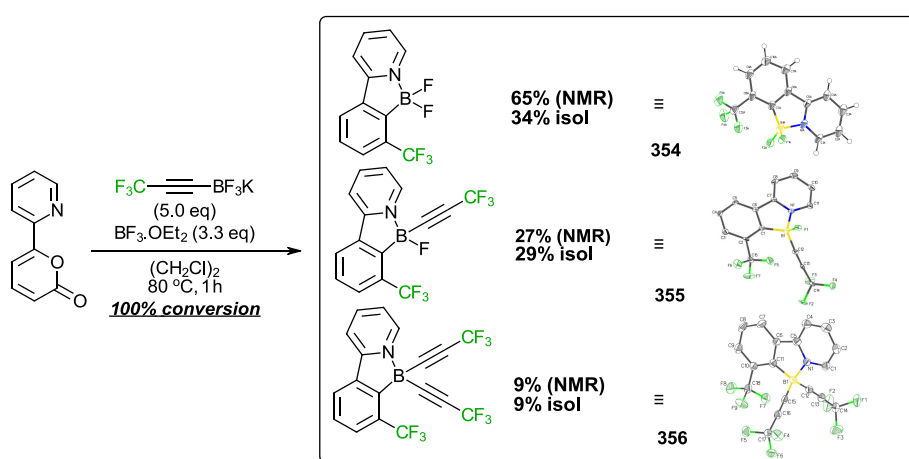
Figure 190: Isolation of the adducts obtained from the cycloaddition along with ORTEPs of their crystal structures

Gratifyingly, each of the adducts **354**, **355** and **356** could be separated and isolated by careful chromatography on silica gel, leading to their full characterisation and structure elucidation by single crystal X-ray analysis (figure 190). The presence of products: **355** and **356** was anticipated based on previous investigations of the reaction and its mechanism,[462,464] but the relative amount of **355** was a little higher than expected. Regardless of the observed ratio of adducts, we were expecting to be able to converge to the difluoroborane **354** simply by the addition of further equivalents of BF$_3$.OEt$_2$.
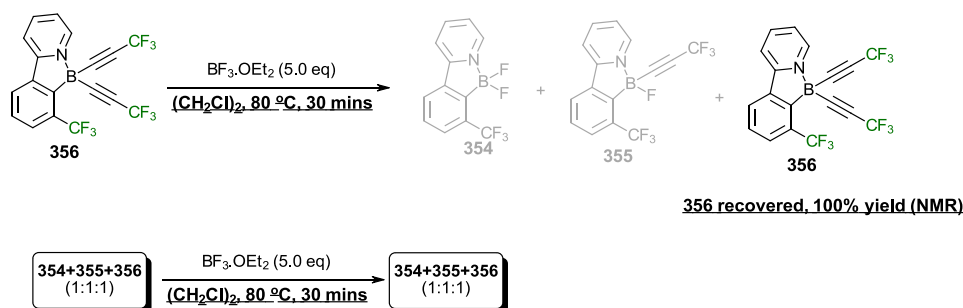
*Figure 191: Treatment of adducts with BF$_3$.OEt$_2$ in an attempt to converge to the difluoroborane **354***
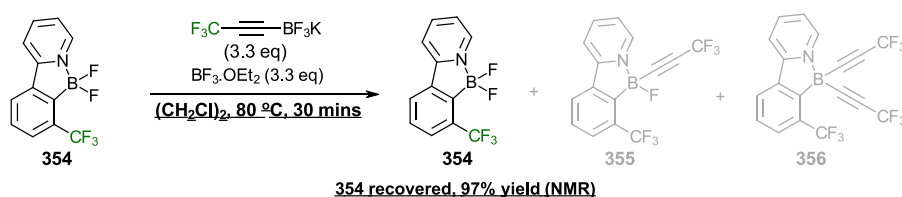
*Figure 192: Treatment of the difluoroborane with **357** and BF$_3$.OEt$_2$ under the reaction conditions to check for post-cycloaddition formation of **355** and/or **356***

To our surprise however, treatment of either pure **356** or an equimolar mixture of **354/355/356** with an excess quantity of BF$_3$.OEt$_2$ (figure 191) under the reaction conditions ((CH$_2$Cl)$_2$, 80 °C, 30 mins) lead to the recovery of **356** (100%, NMR) or no change in the ratio **354/355/356** after workup. For other systems, with alternative side chains such as Ph and ^{t}Bu,[464] the alkyne substituents on boron are labile in the presence of BF$_3$.OEt$_2$ however in this case, for the CF$_3$ side chain, the ratio appears to be fixed after the cycloaddition. An alternative explanation for the presence of **355** and **356** comes from the reaction of **354** with further equivalents of the trifluoroborate **357** in the presence of BF$_3$.OEt$_2$. To test this, we subjected pure **354** to the reaction conditions (**357** and BF$_3$.OEt$_2$, figure 192) to see if any **355** or **356** would be formed. No change to **354** was observed after workup, again suggesting that the ratio of products is set before the cycloaddition and that no product interconversion takes place under the reaction conditions. With this in mind, we decided to screen various parameters of the reaction conditions in order to establish whether the product distribution could be influenced from that direction, the results are summarised in table 6.
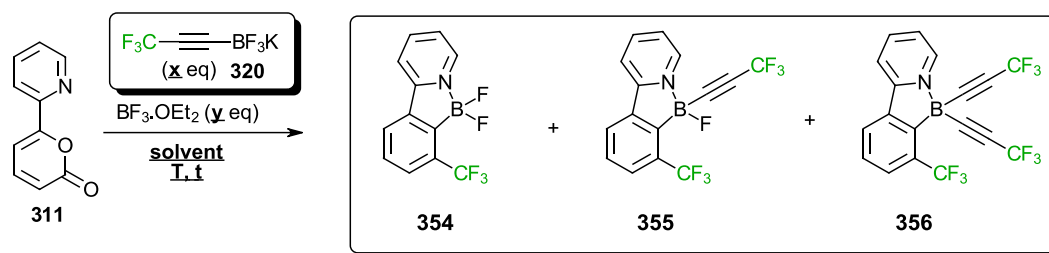
Entry	x	y	Solvent	T	Time / mins	conv[a]	354[a]	355[a]	356[a]
1	3.3	3.3	CH₂Cl₂	40 °C	30	5%	5%	-%	-%
2	3.3	3.3	(CH₂Cl)₂	80 °C	30	100%	63%	29%	8%
3	5.0	3.3	(CH₂Cl)₂	80 °C	30	100%	65%	27%	9%
4	5.0	3.3	(CH₂Cl)₂	80 °C	60	90%	54%	30%	6%
5	5.0	2.0	(CH₂Cl)₂	80 °C	30	98%	77%	15%	6%
6	5.0	2.0	(CH₂Cl)₂	80 °C	180	99%	64%	21%	13%
7	3.3	3.3	toluene	80 °C	30	98%	63%	29%	6%
8	5.0	3.3	toluene	80 °C	30	99%	57%	34%	8%
9	5.0	2.0	toluene	80 °C	30	95%	76%	16%	3%
10	5.0	2.0	toluene	80 °C	180	100%	68%	26%	5%

Table 5: Assessment of variations to reaction conditions and their impact on the selectivity outcome (a) Conversion and yield estimated by ¹H NMR spectroscopy

After the initial result of switching solvents to 1,2-dichloroethane and increasing the reaction temperature to 80 °C resulted in complete conversion after 30 mins (entry 2), we increased the concentration of **357** to 5.0 equivalents and then further decreased the concentration of BF₃.OEt₂ to 2.0 equivalents (entry 5). The change in the ratio of **357**:BF₃.OEt₂ resulted in no significant drop in conversion, and surprisingly, only a small change in reaction selectivity was observed. Increasing the reaction time twofold (compare entries 3 and 4) and fourfold (compare entries 5 and 6) had little impact on the reaction selectivity, when the same proportion of **357** and BF₃.OEt₂ were used. Interestingly, switching the solvent to toluene also had virtually zero impact on reaction selectivity (entries 7-10). In summary, the boron-directed cycloaddition of **357** with the 2-pyrone **311** proceeded with full conversion to a mixture of adducts, differentiated by the ligands attached to boron. Once formed, the products did not interconvert under the reaction conditions and reaction selectivity between the adducts could not be altered significantly by modifying some of the reaction condition parameters.

Based on current mechanistic understanding,[464,475] once the trifluoroborate is transformed into the difluoroborane **358** (figure 193), it reacts with itself to form a molecule of BF₃ and a molecule of the bis(alkynyl) borane **359** which can react further to form tris(alkynyl) borane **360**. The origin of the adducts **364**, **365** and **366** is then considered to be due to the directed cycloaddition reactions of **358**, **359** and **360** respectively. Once the cycloaddition reactions have taken place to form each product, they do not interconvert on the reaction timescale and so the observed selectivity is the result of a superposition of the rates of both the directed cycloaddition and the borane interconversion. So even
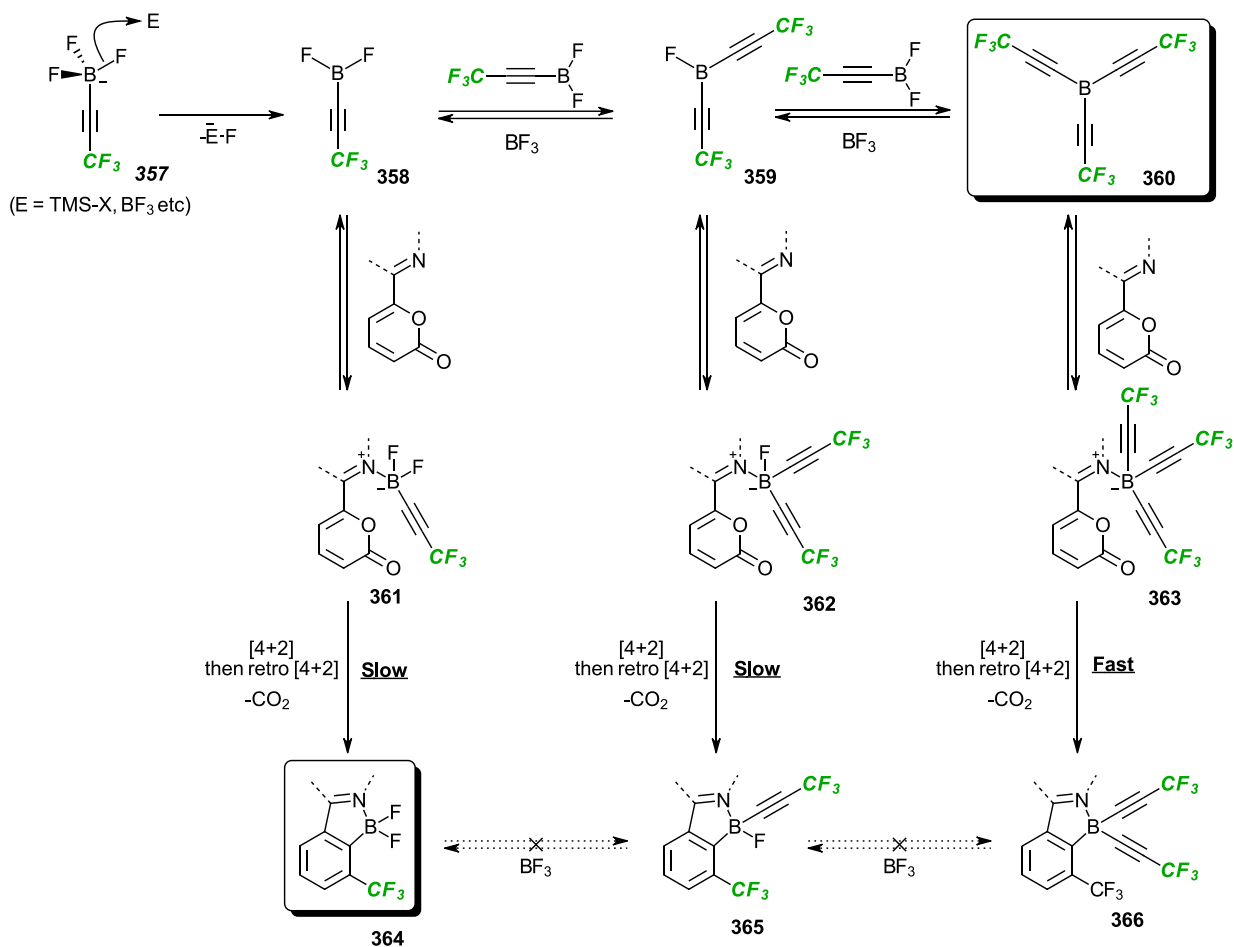
*Figure 193: Current mechanistic understanding for boron-directed cycloadditions with 2-pyrones from the alkynyl trifluoroborate salt **357** to the aryl difluoroborane*

though we may have **358** as the major borane to begin with (directly after fluoride abstraction by BF$_3$.OEt$_2$), if the directed cycloaddition of the complex **361** is slow enough for the borane interconversion to compete, then we will see a mixture of products and not just **364**. To investigate this further, we performed the reaction in the absence of the 2-pyrone **311** and monitored the progress by ^{11}B and ^{19}F NMR, in an attempt to observe the borane interconversion. So, after performing the reaction according to figure 194 for the stated quantity of time, it was cooled and an aliquot was taken for ^{11}B NMR analysis. After allowing the reaction to proceed for only 2 mins, 4 tentative signals were observed in the ^{11}B NMR spectrum (figure 195) corresponding to BF$_3$.OEt$_2$ (δ_B 0.1 ppm, singlet), **358** (δ_B -0.1 ppm, triplet, J = 31 Hz), **359** (δ_B -1.6 ppm, very broad doublet), **360** (δ_B 10.8 ppm, singlet). Interestingly, after 1 hour of stirring, another peak at δ_B -33.8 ppm appeared in the ^{11}B NMR spectra, indicating a highly shielded environment. This peak may correspond to traces of the tetrakis(alkynyl) borate **367** (figure 196), but it is unclear as to how a species of this kind could form. Regrettably, due to the quick relaxation time of the excited ^{11}B nucleus and the long pulse sequence required for background suppression, the resulting ^{11}B NMR spectra cannot be accurately quantified. ^{19}F-^{11}B correlation experiments could not be carried out due to hardware constraints. After repeating the experiment with 15 mins, 1 hour, 2 hours and 3 hours of heating it was apparent that the triplet
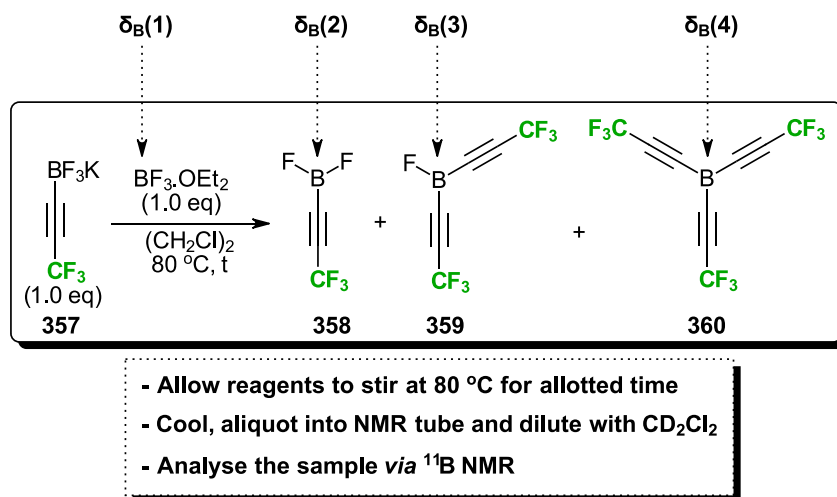
Figure 194: Attempted experimental monitoring of the reaction from **358** to **360** via ^{11}B and ^{19}F NMR
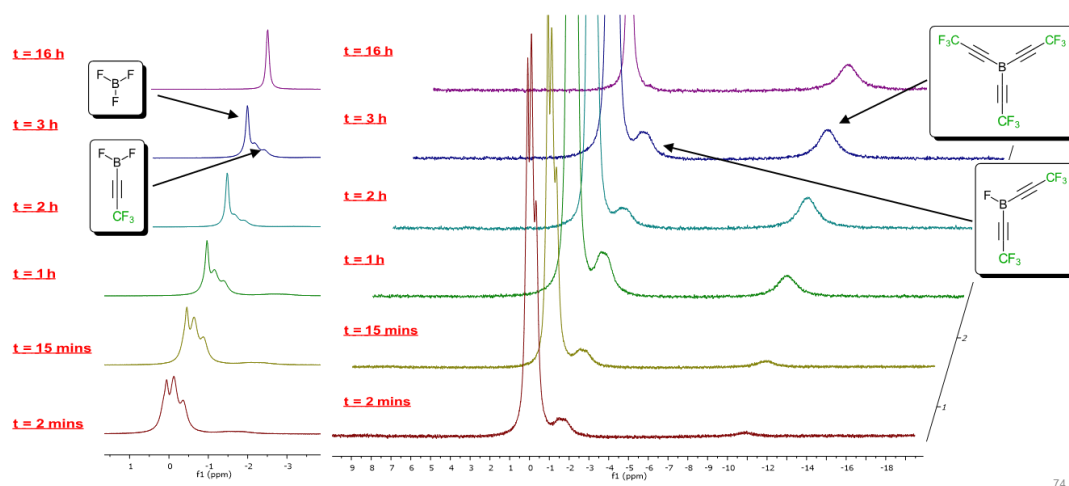
Figure 195: Overlayed B NMR spectra of samples from the reaction shown in figure 19, showing the borane interconvervsion from **357** to **360**
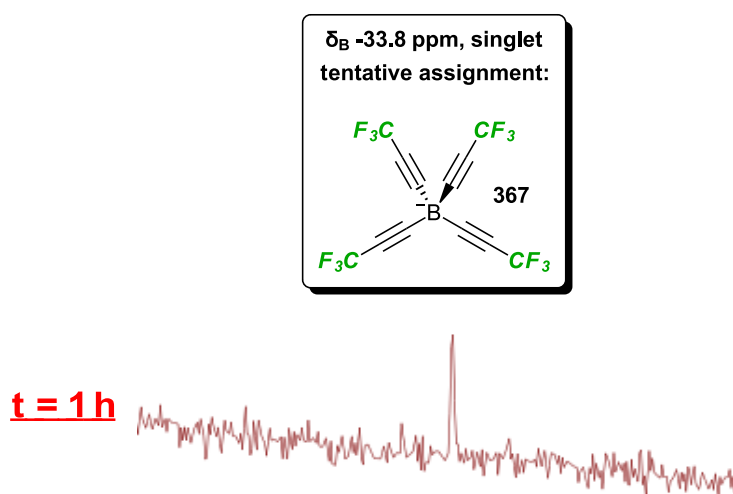
Figure 196: Upfield region of ^{11}B NMR spectrum of the reaction of **357** with BF₃.OEt₂ after 1 h of stirring
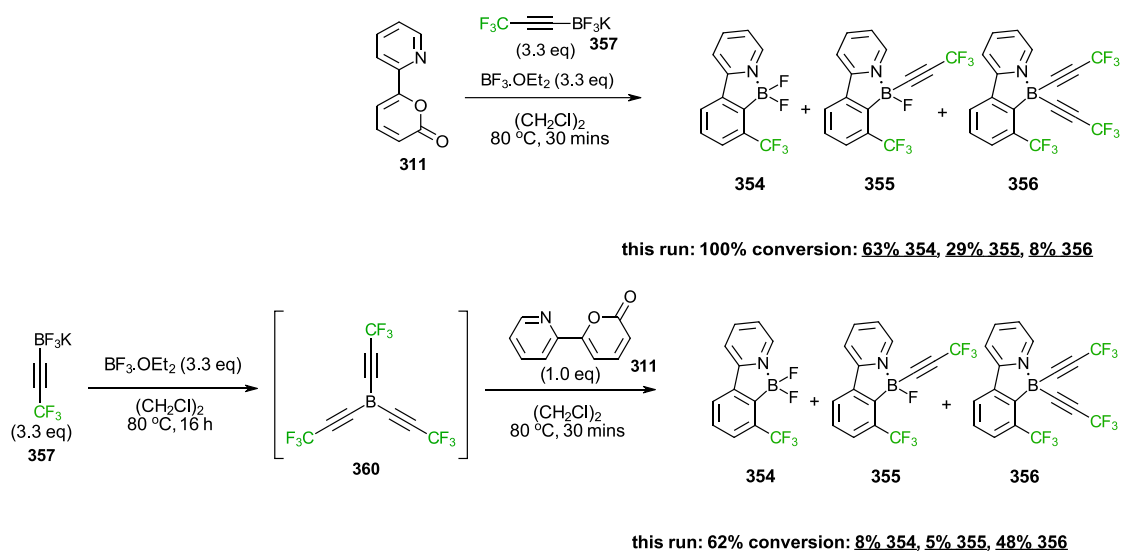
Figure 197: Investigation of the borane interconversion by changing the order of reactant addition. Conversion and yield were estimated by ^{1}H NMR spectroscopy

assigned as **358** became more and more depleted with respect to the other peaks, the longer the reaction was left to stir. Upon leaving the reaction to stir overnight (16 hours), **358** and the broad doublet assigned as **359** disappeared, leaving only the singlet assigned as **360** alongside BF$_3$.OEt$_2$ remaining. The preceding experiments suggest that the borane equilibration may occur under the reaction conditions, and that the position of equilibrium lies towards the tris(alkynyl) borane **360**. To confirm this, we devised an experiment (figure 197) to directly trap **360** by injecting a solution of the pyrone **311** into the equilibrating borane solution after heating for 16 hours. Thus, heating a mixture of the salt **357** and BF$_3$.OEt$_2$ at 80 °C for 16 hours, then injecting a solution of **311** in CH$_2$Cl$_2$ followed by heating for an additional 30 mins resulted in 62% (NMR) conversion of **311**, along with 8% (NMR) of **354**, 5% (NMR) of **355** and 48% (NMR) of **356**. The lower cycloaddition conversion in this case may be attributed to partial hydrolysis or other decomposition of the intermediate boranes. So performing the cycloaddition *after* the borane mixture has been allowed to equilibrate for the appropriate amount of time reverses the selectivity (*i.e.* **356** is the major product, not **354**) of the final product mixture, since the product **356** does not convert to **354** under the reaction conditions.

Conclusions from experimental studies on BF$_3$.OEt$_2$ promoted cycloaddition process

To conclude this section on BF$_3$.OEt$_2$-promoted cycloadditions of trifluoromethyl-substituted alkynyl trifluoroborate salt **357** with substituted 2-pyrones, the following observations are summarised with the aim of introducing further improvements to the process on the way to a milder and more selective set of conditions. **(1) The process requires extra heat in order to reach high conversion**. When subjected to the literature conditions (figure 189, entry 1), TFB salt **357** provided only a small portion of the expected cycloaddition product with high selectivity for the difluoroborane **354**. Only when extra heat is delivered, in the form of refluxing DCE, do we observe complete conversion of the 2-pyrone within the same time period. The reasons for this are discussed further alongside DFT calculations in chapter 3. **(2) Upon completion of the reaction, a mixture of adducts is formed**. A 6:3:1

mixture of **354**, **355** and **356** was observed (figure 189, entry 2), changes to the conditions including solvent, reactant ratio and reaction time resulted in minimal change to this product distribution. The changes that were observed could not be rationalised based on the established mechanism **(3) The adducts 354, 355 and 356 do not interconvert under the reaction conditions**. Subjection of **354** to the TFB salt **357** and $BF_3.OEt_2$ under the reaction conditions lead to a complete recovery of **354**. Similarly, treatment of **356** or a 1:1:1 mixture of **354**, **355** and **356** with $BF_3.OEt_2$ under the reaction conditions (without the TFB salt **357**) resulted in no change in composition. These observations imply that the products do not interconvert under the reaction conditions, suggesting that the final selectivity between the products is set <u>before</u> the cycloaddition takes place, presumably as a result of the expected borane interconversion process **(4) The selectivity between 354, 355 and 356 can be <u>reversed</u> upon changing the order of reagent addition**. After tentatively observing the progression of borane **358** through intermediate borane **359** to borane **360** *via* ^{11}B NMR, we confirmed the enrichment of borane **360** in solution after allowing the interconversion to proceed for 16 h by subsequently adding a solution of the 2-pyrone and observing **356** as the major product after workup. This observation adds weight to the tentative assignment of the 2 peaks in the ^{11}B NMR spectrum of the mixture of TFB salt **357** and $BF_3.OEt_2$ after 16 h (**360** + $BF_3.OEt_2$). A discussion of the borane interconversion process alongside DFT calculations is given in chapter 3.

2.2.4. Alternative Lewis-acidic promoters
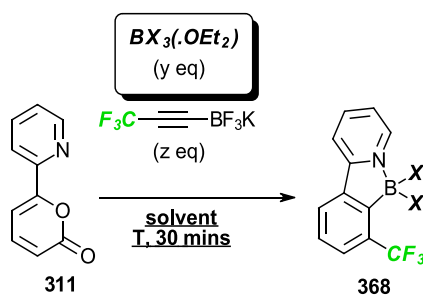
Entry	Solvent	X	y / eq	z / eq	T	Conv[a]	Yield 368[a]	Isolated prod
1	(CH$_2$Cl)$_2$	F	3.3	3.3	80 °C	100%	63%	34%; **354**
2	CH$_2$Cl$_2$	F	3.3	3.3	**40 °C**	5%	5%	-
3	CH$_2$Cl$_2$	Cl	1.1	1.1	**19 °C**	100%	96%	92%; **369**
4	CH$_2$Cl$_2$	Br	1.5	1.5	**19 °C**	82%	82%	60%; **370**

Table 6: Investigation of the efficacy of alternative Lewis acidic reaction promoters (a) Conversion and yield were estimated by ^{1}H NMR spectroscopy
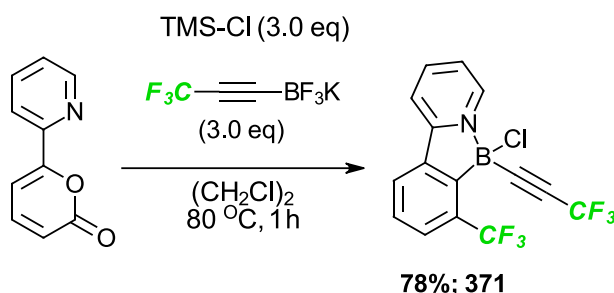
Figure 198: Implementation of a TMS-Cl promoted cycloaddition, providing 371 as the sole product

With this set of results in hand, we sought to improve the outlook and usefulness of the boron-directed cycloaddition reactions of **357** with 2-pyrones by seeking a more selective and milder process. Thus, use of the more Lewis-acidic BCl$_3$ in the place of BF$_3$.OEt$_2$ (table 7, entry 3) allowed the reaction to proceed at room temperature with as little as 1.1 equivalents of both **357** and BCl$_3$ to provide a single product, which was the expected dichloroborane **369** isolated in 92% yield. Use of BBr$_3$ proved also to be highly effective, consuming 82% of **311** after 30 minutes of stirring at room temperature, affording 60% of the dibromoborane **370** after purification. For TMS-Cl to successfully promote the process, heating at 80 °C was required (figure 198) however, the reaction was complete within one hour and provided a single product determined as the chloroborane **371** which was isolated in 78% yield. With an acceptable protocol for the production of CF$_3$-substituted aryl dichloroboranes at room temperature, we sought to investigate its scope. Subjection of the 2-pyrone **311** to the longer fluoroalkyl chain trifluoroborate salts **334** and **335** and BCl$_3$ provided the expected products in each case (**373** and **374**, respectively, figure 199). For **334**, the reaction reached completion within 30 minutes and the pure dichloroborane **373** was obtained after workup without the need for further

purification. For the perfluorooctyl substituted **335**, the conversion reached 85% within 30 mins, allowing the dichloroborane **374** to be isolated after recrystallisation in 57% yield. In the case of the salt **335**, the low solubility of the product **374** in CH_2Cl_2 leading to precipitation and thus diminished stirring capacity probably accounts for the lower conversion of **311** in this case. After exploring the scope of the alkyne component with the trifluoroborate salts prepared thus far, we then sought to investigate the scope with respect to the 2-pyrone component, particularly, the identity of the directing group. Thus, subjection of the 3-chloropyridine substituted 2-pyrone **342** to the same conditions afforded the expected product **376** with 100% conversion after stirring at room temperature for 30 mins. **376** was isolated in 91% yield directly after the reaction workup, as further purification was not deemed necessary. 2-methyl- (**338**) and 2-bromopyridine (**343**) substituted 2-pyrones were also tested, with **338** proceeding to 85% conversion after 30 minutes of heating at 40 °C and **343** proceeding to 38% conversion after stirring at room temperature (19 °C) for 30 minutes. Both expected products **377** and **375** were isolated in excellent yield (based on the recovery of the starting 2-pyrone), the lower conversions in this case could be caused by the steric/electronic deactivation effect on the directing group by having ortho substituents. Additionally, the structure of **377** was determined unambiguously by single crystal X-ray analysis. Quinoline-substituted 2-pyrone **339** was also tested, reaching full conversion after heating at 40 °C for 30
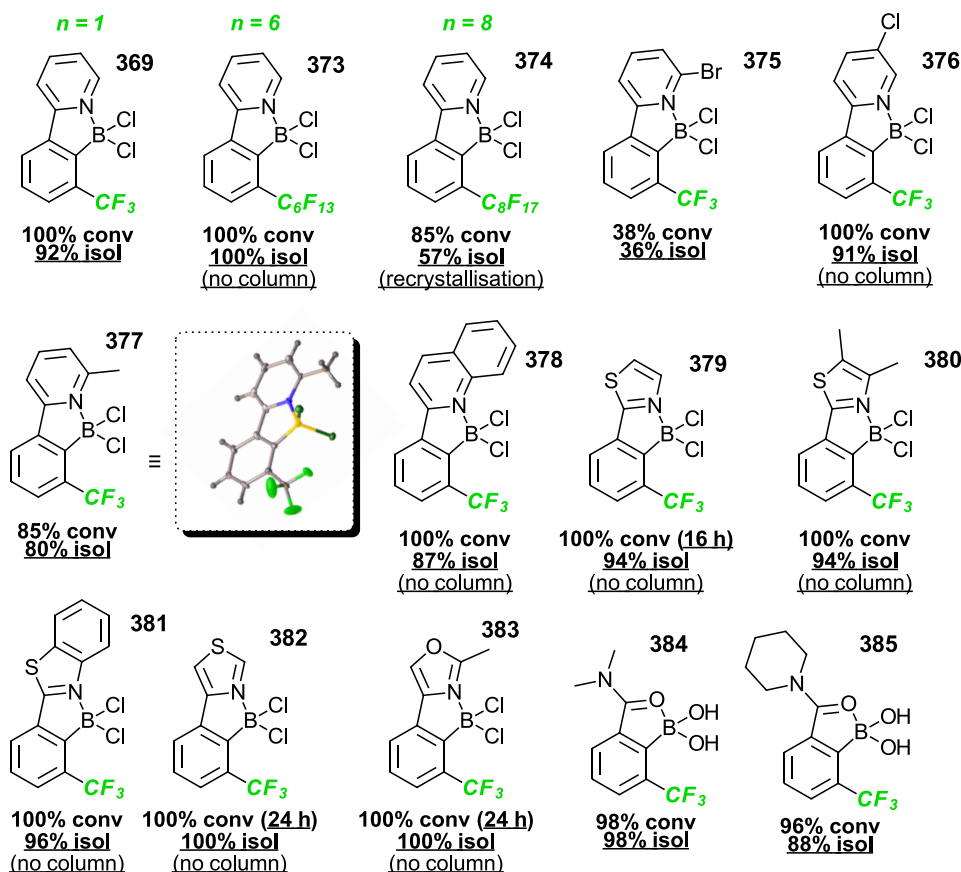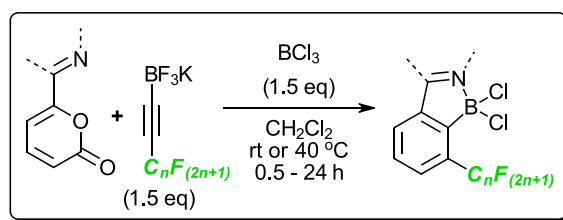
Figure 199: Scope of the BCl₃-promoted cycloaddition of fluorinated alkynyl trifluoroborate salts with substituted 2-pyrones

minutes and providing the expected product **378** in excellent yield, without the need for a purification step. After a brief exploration of pyridine-based directing groups, we then moved on to test the efficacy of other *N*-heterocycle based systems. 2-Thiazolium substituted 2-pyrone **344** reacted significantly slower than the preceding examples, reaching completion only after 16 hours of stirring at 40 °C however, once complete, the product **379** was obtained in high purity after workup without purification. Interestingly, dimethyl substituted thiazole- and benzothiazole-substituted 2-pyrones **345** and **340**, proceeded to 100% conversion with only 30 minutes of stirring at 40 °C. It was unclear at this stage why the 2-pyrones **345** and **340** should react quicker with **357** than **344**. Nevertheless, the expected products **380** and **381** were also obtained without the need for specific purification. 4-Thiazolium- and 4-oxazolium-substituted 2-pyrones **341** and **346** reacted at a similar speed to **344**, requiring 24 hours of stirring at 40 °C to reach completion and providing the expected products in excellent yield, without the need for column chromatography. After verifying the generality of the BCl₃ promoted cycloaddition between alkynyl trifluoroborate salts **357**, **334** and **335** with various *N*-heterocycle substituted 2-pyrones, we then sought to extend the same principle to the amide substituted pyrones **348** and **349**. Pleasingly, the reactions proceeded smoothly to high conversion

after heating at 40 °C for 30 minutes. The cycloaddition products however, were not the expected dichloroboranes but the coordinated boronic acids **384** and **385**, which were isolated by precipitation in excellent yield.
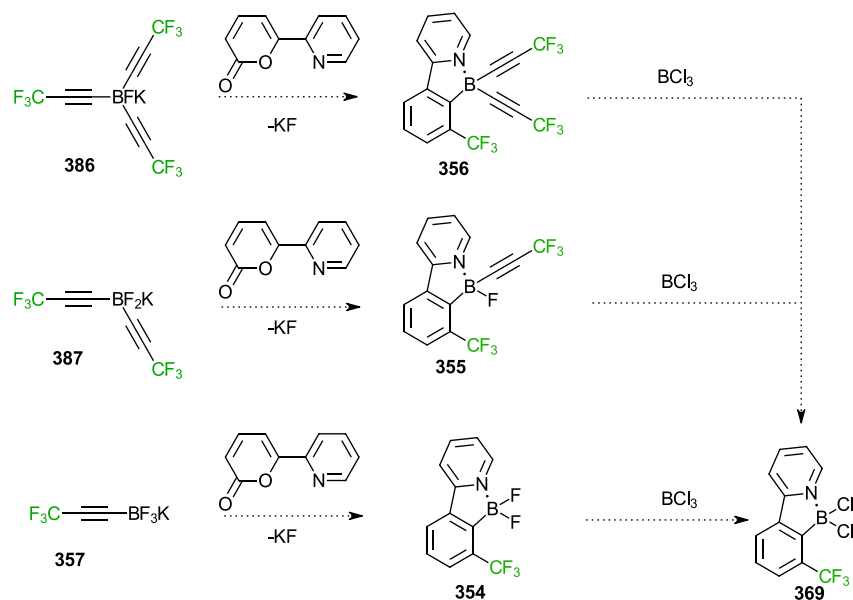
*Figure 200: Potential further rationale for the observation of adducts **354**, **355** and **356**, and the required reactivity of the same in order to be in agreement with the clean production of dichloroboranes as in fig. 199*

To return to the discussion of selectivity in the BF$_3$.OEt$_2$ promoted cycloaddition of **357** with **311** (figure 190), one possible mechanism for the formation of the adducts **355** and **356** would be the directed cycloaddition of the precursor boranes **359** and **360** produced directly from the corresponding fluoroborate salts **387** (figure 200) and **386** respectively, which may be present in the sample of **357**. However, given the extremely clean nature of the BCl$_3$ promoted cycloadditions of the same sample of **357** presented in the preceding section (only one observed product), the presence of these extra fluoroborate salts is highly unlikely *unless* the products **355** (or Cl derivative) and **356** can be converted to **369** under the reaction conditions by BCl$_3$.
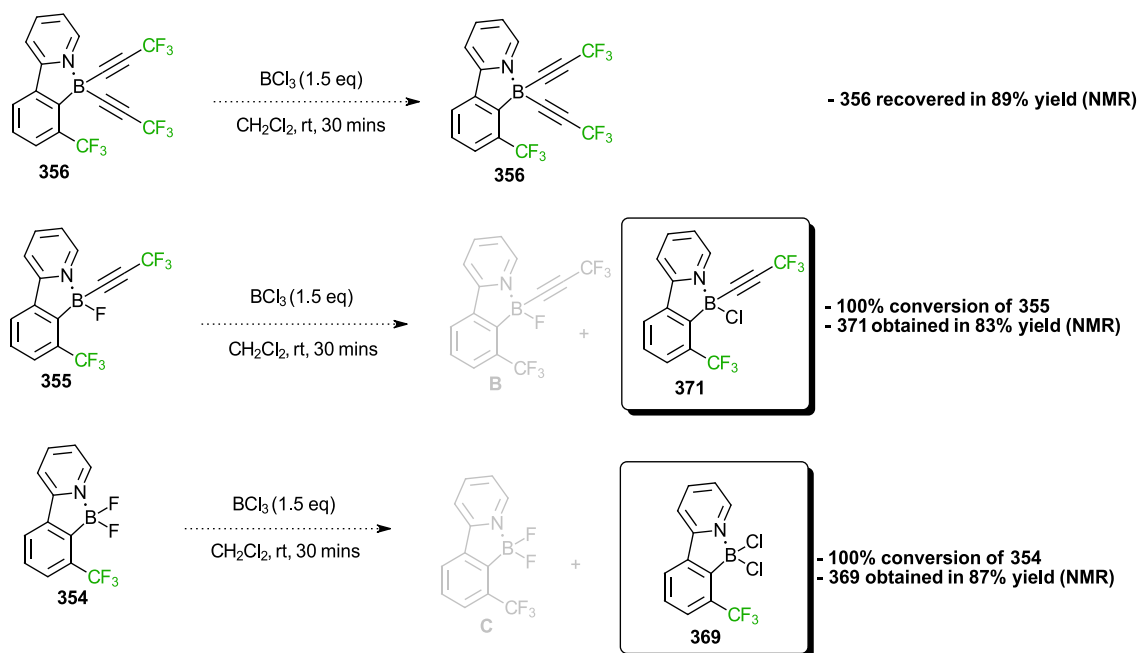
Figure 201: Control experiments using BCl₃ to probe the lability of the alkyne ligands on the adducts **355** *and* **356** *under the reaction conditions*
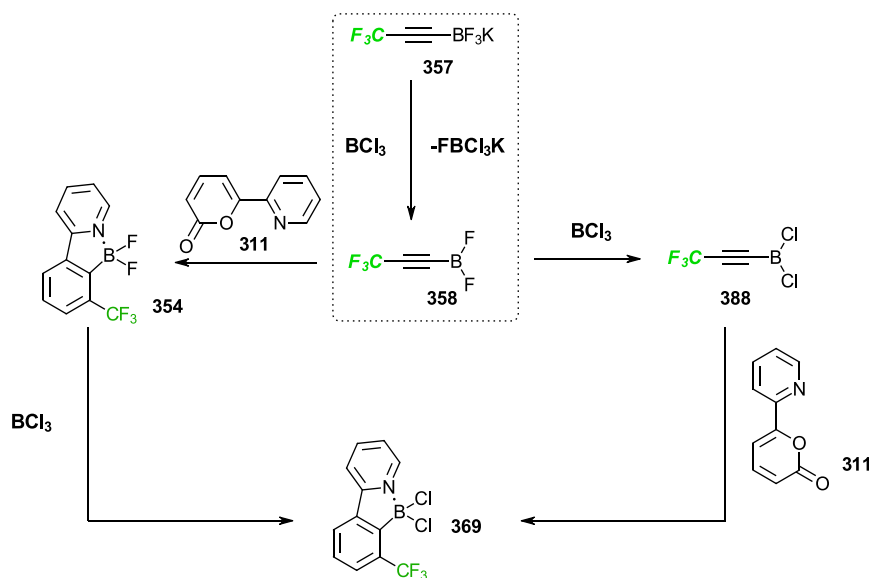
Figure 202: Possible mechanistic pathways for the production of dichloroboranes from the reaction of **357** *with* **311** *by the action of BCl₃*

To test this, we subjected purified samples of **354**, **355** and **356** separately to the BCl₃ promoted reaction conditions. It was found, that **356** did not react at all with BCl₃ and was recovered in 89% (NMR) yield, the F ligand on **355** was exchanged with Cl upon reaction with BCl₃ but was otherwise unchanged giving the chloroborane **371** in 83% (NMR) yield and both F ligands on **354** were exchanged quantitatively to provide **369** in 87% (NMR) yield. These experiments rule out the presence of fluoroborate salts **386** (figure 200) or **387** in the samples of **357** tested, which adds weight to the borane interconversion route. Furthermore, the readily exchangeable nature of the F ligands of **354**

and **355** in the presence of BCl₃ suggests that the initial product of the reaction could be the difluoroborane **354** which is then quickly converted to **369**. This mechanism may compete with pre-cycloaddition ligand scrambling to the alkynyl dichloroborane **388** (figure 202), followed by directed cycloaddition to form **369** directly.

Conclusions for 2-pyrone cycloaddition reactions using alternative Lewis acid promoters

The boron-directed cycloaddition reaction between fluoroalkyl-substituted alkynyl trifluoroborate salts and substituted 2-pyrones can be effectively promoted with reagents other than BF₃.OEt₂. Provided the reaction is heated at 80 °C, TMS-Cl can promote the reaction, affording a single product that suggests borane interconversion, which can be isolated in excellent yield. Upon switching the promoter to the more Lewis-acidic BCl₃ or BBr₃, the reaction can be performed smoothly at room temperature. The reaction showed good tolerance towards the heterocyclic/amidic directing groups tested, and the product dichloro- / dibromoboranes could be isolated in excellent yield.

2.2.5. Product elaboration
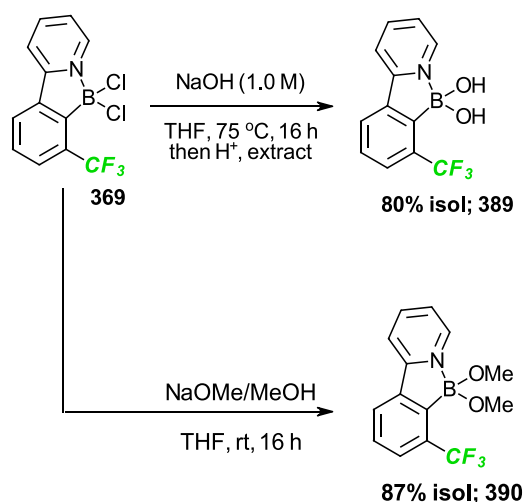
Figure 203: Ligand exchange from **369** to the corresponding boronic acid/ester via base-promoted hydrolysis/alcoholysis

With reliable access to fluorinated benzenes *via* the boron directed cycloaddition of fluorinated trifluoroborate salts with substituted 2-pyrones, we wanted to explore the potential synthetic advantage of having the boron functionality delivered at the same time. To begin with, we examined how the dichloroborane **369** could undergo ligand exchange reactions to afford alternative boron functional groups. Pleasingly, we found hydrolysis conditions (figure 203) that allowed the isolation of the boronic acid **389** in excellent yield. Due to the low solubility of **369** and **389** in common organic solvents, we then wanted to investigate whether the corresponding boronic esters could also be accessed. Drawing on the literature precedent[476] of ligand exchange reactions of Cl-BODIPYs, we

subjected **369** to NaOMe at room temperature and observed an immediate colour change. After stirring the reaction for 16 h, **369** was fully consumed affording the boronic ester **390** in excellent yield after purification. To increase the usefulness of the ligand exchange procedure on products such as **369**, we wanted to explore the feasibility of a one-pot cycloaddition-ligand exchange procedure to afford the corresponding boronic ester without the need for an intermediate purification step. After allowing the BCl₃ promoted cycloaddition of **311** with **357** to proceed as usual (figure 204) to completion the alkoxide solution was added (R = Me or Et). The intermediate **369** was found by TLC analysis to be consumed after only 15 minutes of stirring, and following celite filtration, the desired boronic esters were obtained in excellent yield, without the need for further purification. After investigating the efficacy of **369** to undergo ligand exchange, we then sought to investigate how it or related products could undergo further elaboration at the C-B bond. Attempts to oxidise **369** were unsuccessful, this was suspected to be due to its sparing solubility in the solvents tested. Switching to the boronic ester **391** allowed full dissolution in EtOH, but low conversion was observed, even after gentle heating of the oxidising solution and none of the phenol **392** (figure 205) was obtained. To verify the boron-directed cycloaddition approach as a useful means to obtain fluorinated aromatic compounds, we wanted to explore the ability of the boronate handle in **391** to undergo cross coupling in the presence of a suitable catalyst.
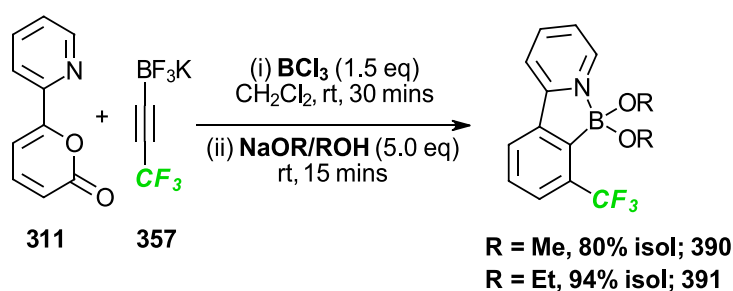
Figure 204: One-pot cycloaddition-ligand exchange procedure to afford boronic esters
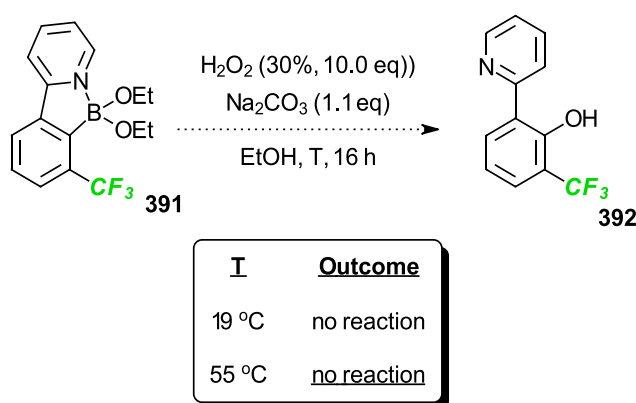
Figure 205: Unsuccessful attempts at boronate oxidation
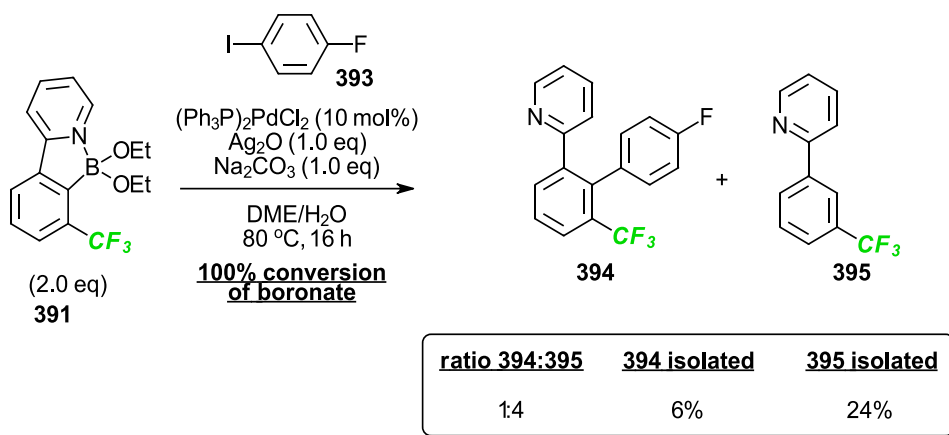
Figure 206: Low-yielding initial cross coupling attempt of the boronate 391

Thus, we subjected it to the aryl iodide **393** (figure 206) under conditions that were successful in coupling similar systems[462] and found that the major product was that of protodeboronation **395**, which was isolated in 24% yield. Nevertheless, the desired product **394** was also formed, albeit as a minor component and it was isolated in 6% yield. After a brief assessment of coupling conditions from the literature,[477,478] we attempted the reaction again under modified conditions and found initially low conversion of the boronate **391** (table 8, entry 1).
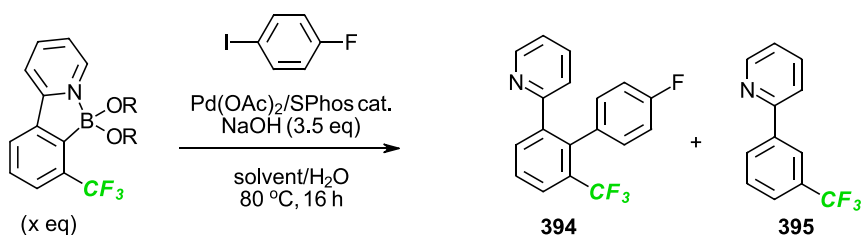
Entry	R	x	solvent	Boronate conversion	Ratio 394:395	394 isolated
1	Et	1.1	THF	30%	- (~13% 395)	-
2	Me	1.2	toluene	100%	1:1	41%
3	Me	1.6	toluene	50%	1:1	25%

Table 7: Brief investigation of conditions for boronate cross coupling

Upon switching the boronate ester starting material to the Me homologue **390** and the solvent to the higher-boiling toluene, a much higher conversion of the boronate was achieved (entry 2). The product mixture composed of an almost equal quantity of **394** and **395**, but the desired product was isolated in 41% yield after column chromatography. Further attempts to optimise these conditions failed to produce a higher yield of **394**.

Starting product elaboration studies from the dichloroborane **369** produced from the BCl₃ promoted cycloaddition reaction stated, we were pleased to find that it underwent smooth ligand exchange with water and methanol to afford the corresponding boronic acid **389** and the boronic ester **390** in excellent yield. The alcoholysis of **369** to form boronic esters could be performed as part of a one-pot process starting from the 2-pyrone **311**. This allowed the isolation of **390** and **391** in excellent yield and also increased the versatility of the entire process, opening the door to these products which turned out to be more soluble in organic solvents than **369** itself. Attempts to oxidise **369** or **391** and obtain the phenol **392** were unsuccessful. Literature methods[276,479] even with added heat failed to provide high conversion of the boronate in each case and the optimisation of this transformation should form part of future studies. Suzuki-Miyaura cross coupling of the boronate **390** was achieved with 4-fluoro iodobenzene, allowing the product to be obtained in moderate yield after purification. Further investigations into the yield optimisation for this cross coupling alongside the scope of coupling partners should also be included in further work for this project.

2.2.6. Cycloadditions of heterodienes & dipoles

Conditions	Outcome
CH₂Cl₂, 40 °C, 30 mins	17% conv, 17% **397**
(CH₂Cl)₂, 80 °C, 30 mins	
run 1	95% conv, 63% **397** (27% isol), 30% **398** (16% isol), 2% **399**
run 2	95% conv, 50% **397** (20% isol), 37% **398** (16% isol), 9% **399** (9% isol)
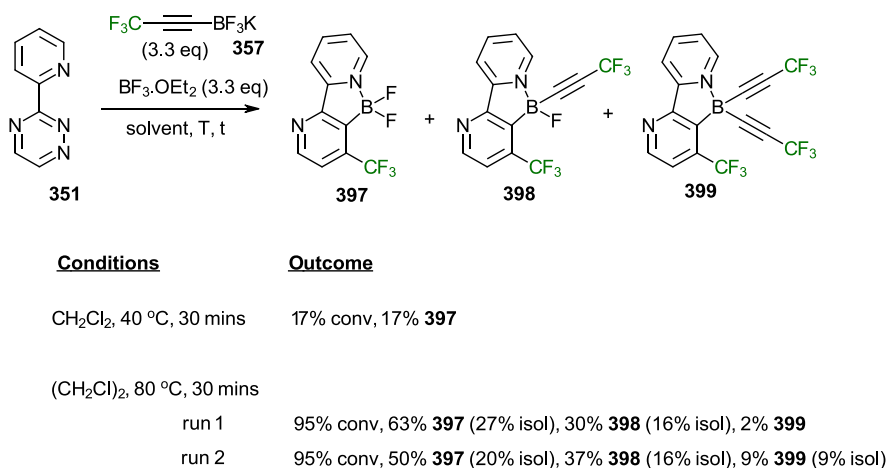
Figure 207: Directed cycloadditions of salt 357 with substituted 1,3,4-triazines

Having completed detailed investigations into the boron-directed cycloaddition reactions of **357** with 2-pyrones to produce trifluoromethylated benzenes, we were keen to establish proof-of-concept for its reactivity with other dienes to broaden the scope of this strategy. To begin with, the triazine **351** (figure 207) was tested against **357** under BF₃.OEt₂ promoted conditions and was found to react in a similar fashion to the 2-pyrone **311** (figure). When heated at 40 °C for 30 mins, the reaction proceeded with 17% conversion to the difluoroborane **397**. Upon heating the reaction to 80 °C in (CH₂Cl)₂ for 30 mins, the triazine was fully consumed and a mixture of the three expected adducts was obtained, all of which could be separated on silica gel and characterised.
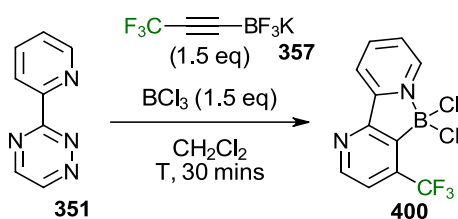
Entry	T	Conv	**400** isolated
1	19 °C	74%	51%
2	40 °C	88%	54%

Table 8: Cycloadditions performed under milder conditions through the use of BCl₃

After these promising results, we then subjected **351** and **357** to BCl₃ in CH₂Cl₂ at room temperature for 30 minutes (table 10, entry 1) and found that the reaction proceeded with 74% conversion of **351** to the dichloroborane **400** which was isolated in 51% yield. Marginal improvements in the reaction conversion and yield of **400** were seen upon heating at 40 °C for the same amount of time (table 10, entry 2).

In order to access trifluoromethylated pyrazoles, pyridine-substituted sydnone **350** (figure) was subjected to the literature[276] conditions using **357** as the alkyne. After stirring at room temperature for 4 hours, **350** was recovered quantitatively highlighting the need for more forcing conditions.
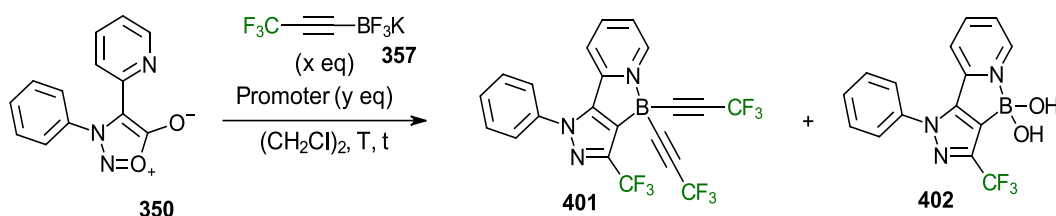
Entry	x	y	Promoter	T	t / h	Conv	Ratio 401:402	401 isolated	402 isolated
1	5.0	2.0	BF₃.OEt₂	19 °C	4	0%	-	-	-
2	5.0	2.0	BF₃.OEt₂	80 °C	4	100%	2:1	52%	-
3	5.0	2.0	BF₃.OEt₂	80 °C	16	100%	2:1	39%	38%
4	3.3	3.3	TMS-Cl	80 °C	2	100%	20:1	66%	-

*Table 9: Directed cycloadditions between the salt **357** and substituted sydnones*

Pleasingly, increasing the temperature to 80 °C and stirring the reaction for 4 hours led to complete conversion of **350** to the pyrazole product **401** which was isolated in 52% yield. Another major product was observed in the crude ¹H NMR spectrum of this reaction, and in a separate experiment where the reaction was heated for 16 hours, **401** was obtained in 39% alongside this other product: the boronic acid **402** which was isolated in 38% yield. Access to the boronic acid derivatives of these pyrazole boranes has been observed previously[276] under certain circumstances. Interestingly, the reaction can also be promoted by TMS-Cl, which drove the reaction to completion within 2 hours and provided **401**

in 66% yield after purification. While it is plausible that the borane interconversion towards **360** (figure 194) may not require BF$_3$.OEt$_2$ specifically (any means to obtain the alkynyl difluoroborane **358** along with sufficient energy), ligand exchange using further equivalents of difluoroborane has not been ruled out either at this stage, as it was for the 2-pyrone cycloadditions.
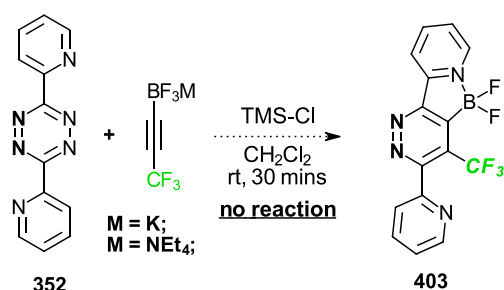
*Figure 208: Demonstrated unreactivity of **357** with substituted 1,2,4,5-tetrazine **352** in the presence of TMS-Cl*

Finally, we wanted to test the feasibility of accessing CF$_3$-substituted pyridazines *via* this strategy and acquired the commercially available pyridine-disubstituted 1,2,4,5-tetrazine **352** for this purpose. Attempting the literature[461] conditions (figure 208), no noticeable reaction occurred with either the potassium salt **357** nor with the tetraethylammonium salt **336** and **352** was recovered. Upon switching the promoter to the powerful Lewis acid, TMS-OTf (figure 209), a vigorous reaction took place using **336**, which consumed **352** within 30 minutes. The difluoroborane **403** was hence isolated as the only product in excellent yield. Building on this result, we tried the pyrazole-disubstituted 1,2,4,5-tetrazine **353** under the same conditions and found that the reaction proceeded to only 61% conversion, allowing the product **404** to be isolated in 56%. The reaction could be driven to completion by gentle heating, increasing the isolated yield of **404** to 76%.
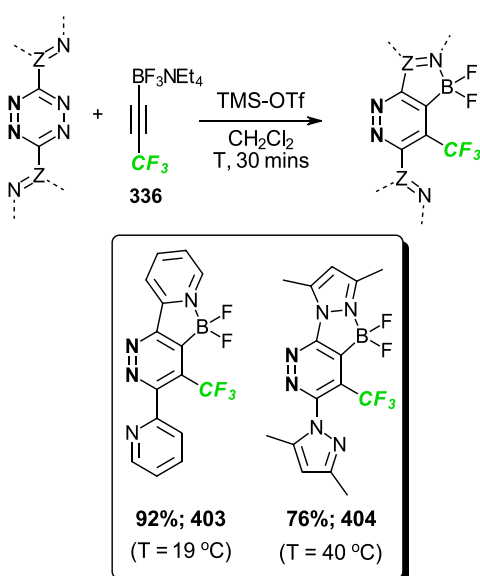
*Figure 209: Smooth reactivity of **336** with substituted 1,2,4,5-tetrazines in the presence of TMS-OTf*

2.3. Conclusions

The boron-directed cycloadditions of the salt **357** with substituted 1,3,4-triazines proceeded in a similar fashion to those attempted with the 2-pyrone **311**. Specifically, low conversion of **351** to **397** as the only product was observed when the BF$_3$.OEt$_2$ promoted reaction was conducted in refluxing CH$_2$Cl$_2$, but when the conditions were switched to refluxing (CH$_2$Cl)$_2$, full conversion to a mixture of the 3 products **397**, **398** and **399** was achieved. When the promoter was switched to BCl$_3$, high conversion of the triazine **351** was seen even at room temperature to the dichloroborane **400**, which could be isolated in good yield. Only marginal improvements to the yield of **400** were achieved by heating the reaction mixture at 40 °C. The BF$_3$.OEt$_2$ promoted reaction of **357** with substituted sydnones did not proceed at room temperature but when heated at 80 °C, was found to go to completion within 4 hours. The product mixture consisted of the expected **401** and the boronic acid **402**, which were both isolated in a separate experiment in moderate yield. This 1,3-dipolar cycloaddition process was found also to be promoted by TMS-Cl, which fully consumed the sydnone **350** within 2 hours affording **401**, which was isolated in good yield. The salts **357** and **336** did not react with the substituted 1,2,4,5-tetrazine **352** at room temperature when TMS-Cl was used as a promoter. Upon switching to the more Lewis-acidic TMS-OTf, full conversion of **352** was achieved, affording the CF$_3$-substituted pyridazine boranes **403** and **404** in good to excellent yield. Further work on the reactions of hetero-dienes/dipoles with the salts **357** and **336** should include a deeper investigation into the scope of each process and an analysis of the application prospects of such transformations.

3. Computational investigations for directed cycloadditions

3.1. Context & design of the investigation

It was not immediately obvious to us why the $BF_3.OEt_2$-promoted Boron-Directed Cycloaddition (BDC) should require harsher conditions when **357** (figure 210) is employed as opposed to other alkynyl trifluoroborate salts, such as **314** (figure 210). Upon consideration of the reaction mechanism for the BDC reaction (figure 173) with substituted 2-pyrones, a number of key processes emerge as potentially significant in terms of impeding the reaction progress due to higher energetic barriers of the transition states. For this reason, we decided to undertake a comparative study utilising DFT calculations of each process and how the nature of the alkyne side chain affects the corresponding energetic barriers in each case.

- Destabilisation of RBF_3^- by electron-donating contributions of side chain
- Low barrier to fluoride abstraction?
- Known to occur readily under mild conditions

- Stabilisation of RBF_3^- by inductive electron-withdrawal by CF_3 side chain
- Higher barrier to fluoride abstraction?
- Predicted to occur more slowly than than for R = Ph
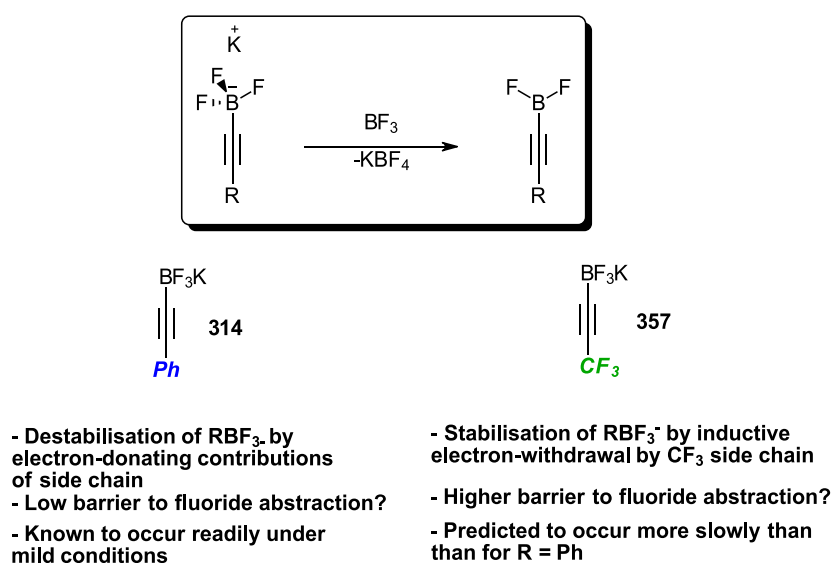
Figure 210: Initiation of BDC process: abstraction of fluoride using Lewis-acidic activator, such as BF_3

Intuitively, the first of these to occur is the abstraction of a fluoride ion from the trifluoroborate unit by the fluorophile (TMS-Cl, BF_3, BCl_3, BBr_3 etc) to produce the highly reactive alkynyldifluoroborane. Qualitative comparison of side chains of **357** (figure 210) and **314** leads to the suggestion that **357** would undergo a slower fluoride abstraction than **314**, due to the enhanced attenuation of the negative charge residing on the boron centre by the more electron-withdrawing CF_3 group. However, given how little has been published specifically on processes of this kind,[480] and the transient nature of the difluoroborane products, a computational investigation was appropriate to establish the significance of the side-chain's identity and was expected to provide useful mechanistic insights.

The second key process of the BDC reaction of alkynyl trifluoroborates with substituted 2-pyrones that drew our attention, was the borane interconversion (figure 211) from **318** to **319** and ultimately **320**. This process is predicted to be highly significant for the overall rate of the reaction (*vide infra*) and also describes how products **324** (figure 212), **325** and **326** can be formed. It is less easy to predict intuitively how the nature of the alkyne side chain would affect the rate of this interconversion, but due to how crucial it appears to be for the rate of the BDC, it was likewise a worthy target for computational investigation.
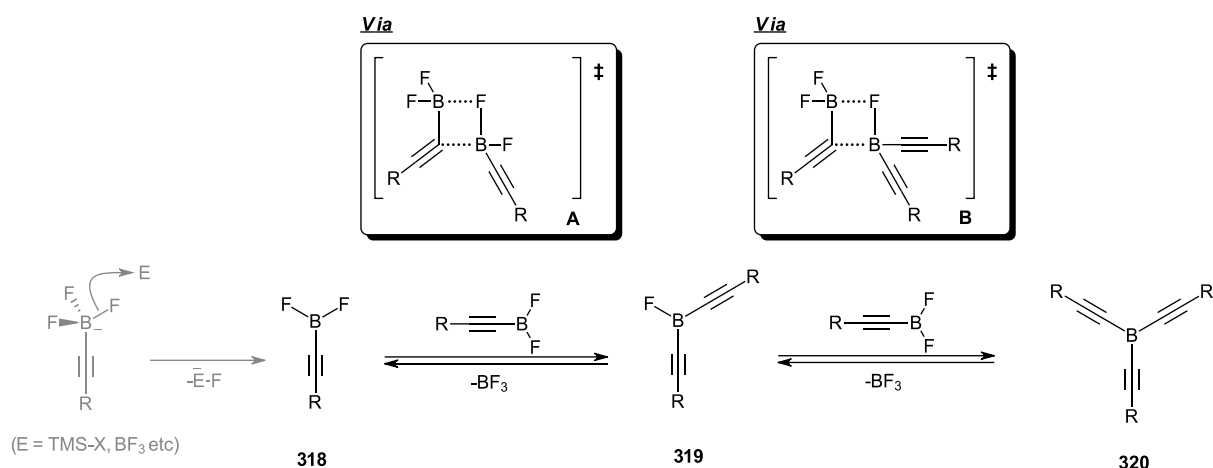
Figure 211: The second process to consider for computational investigation: the borane equilibration
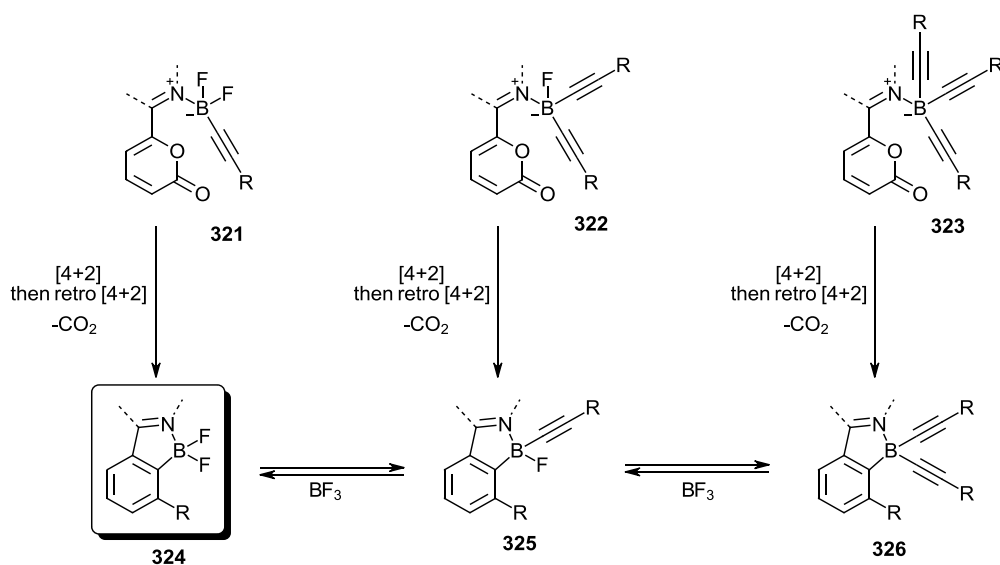
Figure 212: The third process to consider: directed cycloadditions of the three borane types and how the nature of the R group affects activation energies

The third process in this series that we decided to scrutinise was the directed [4+2] cycloaddition itself (figure 212). With this being an inverse-electron-demand Diels-Alder reaction (IEDDA), it was considered that electronic factors such as increased electron-withdrawal of the alkyne side-chain could have an impact on the barrier to cycloaddition.
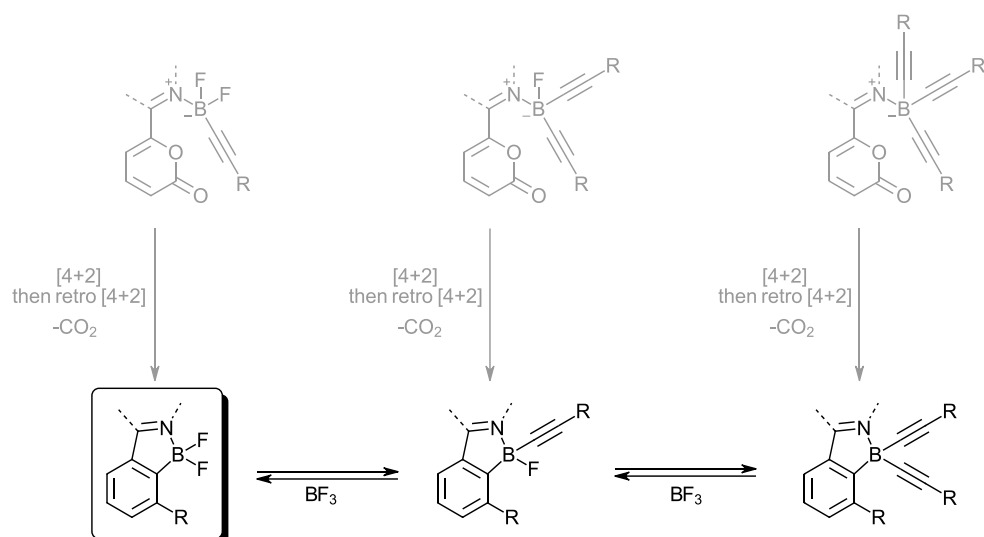
Figure 213: The fourth and final process to consider: how easily the three possible products interconvert under the reaction conditions for different R groups

There are only two published examples[445,481] containing cycloadditions between 2-pyrones and CF_3-substituted alkynes, both require temperatures exceeding 100 °C and no systematic study of the effect of the CF_3 group on the cycloaddition was included. Thus, the IEDDA reaction part of the BDC was also prioritised as a target for computational study.

The final process to consider was the post-cycloaddition ligand exchange process that links the bis(alkynyl)borane product **326** (figure 212) to the difluoroborane **324** through the action of $BF_3.OEt_2$. Given that experiments have shown that, while for R = Ph the deliberate convergence of a mixture of the three products **324**, **325** and **326** to **324** by the action of $BF_3.OEt_2$ is possible, the same cannot be said for when R = CF_3. Indeed for R = CF_3, the product composition did not change upon addition of extra $BF_3.OEt_2$ by itself nor upon addition of a mixture of $BF_3.OEt_2$ and the alkynyl trifluoroborate salt **357**. Thus, we wanted to interrogate this process computationally to help rationalise this difference in reactivity of the products where R = Ph or CF_3.

3.1.2. General considerations for calculations

All of the calculations were performed using DFT with the B3LYP hybrid functional[482–484] as implemented in Gaussian 09.[485] The 6- 311G(d,p) basis set was used for H, C, N, O, B, F, and Cl atoms. All dispersion corrections were included through the GD3BJ method.[486] All reactant, intermediate, transition state, and product structures were optimised with symmetry contributions ignored. Transition states were located using the QST3[487,488] or Berny[489] algorithms. Frequency calculations were carried out to characterise all optimised structures as local minima or transition states. Transition states were identified by having one imaginary frequency. Solvent effects were included in all of the calculations *via* the PCM method[490,491] as implemented in Gaussian 09 with the default parameters for dichloromethane (CH_2Cl_2). All enthalpies and free energies quoted below were evaluated at 298.15 K.

3.2. Fluoride abstraction

We began computational studies by identifying a fluoride abstraction reaction that could be used as a model to compare the influence of side chains on the rate of reaction. Regrettably, efforts to obtain transition states for the reaction of BF_3 or $BF_3.OEt_2$ with the trifluoroborate of **357** were unsuccessful, so alternative processes needed to be explored in order to assess the difference in reactivity. Inspired by the apparent inertness of **357** to fluoride abstraction by TMS-Cl, where **314** undergoes a vigorous reaction at room temperature,[461] we found a transition state that could describe this particular abstraction and calculated reaction coordinates for the trifluoroborate components of both **357** and **314** (figure 214). Inspection of figure 214 shows that the barrier to fluoride loss for the trifluoroborate of **357** is larger enthalpically than that for **314** by +17.9 kJ mol^{-1}.
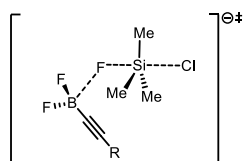
R	$\Delta H^{\ddagger}$ / kJ mol^{-1}	Rel rate (298 K)	$\Delta G^{\ddagger}$ / kJ mol^{-1}	Rel rate (298 K)
-CF$_3$	59.5	1	59.5	1
-Ph	41.4	1489	43.7	588

Table 10: Summary of activation parameters for the key fluoride abstraction transition state and relative rates of reaction, as determined by the Eyring equation
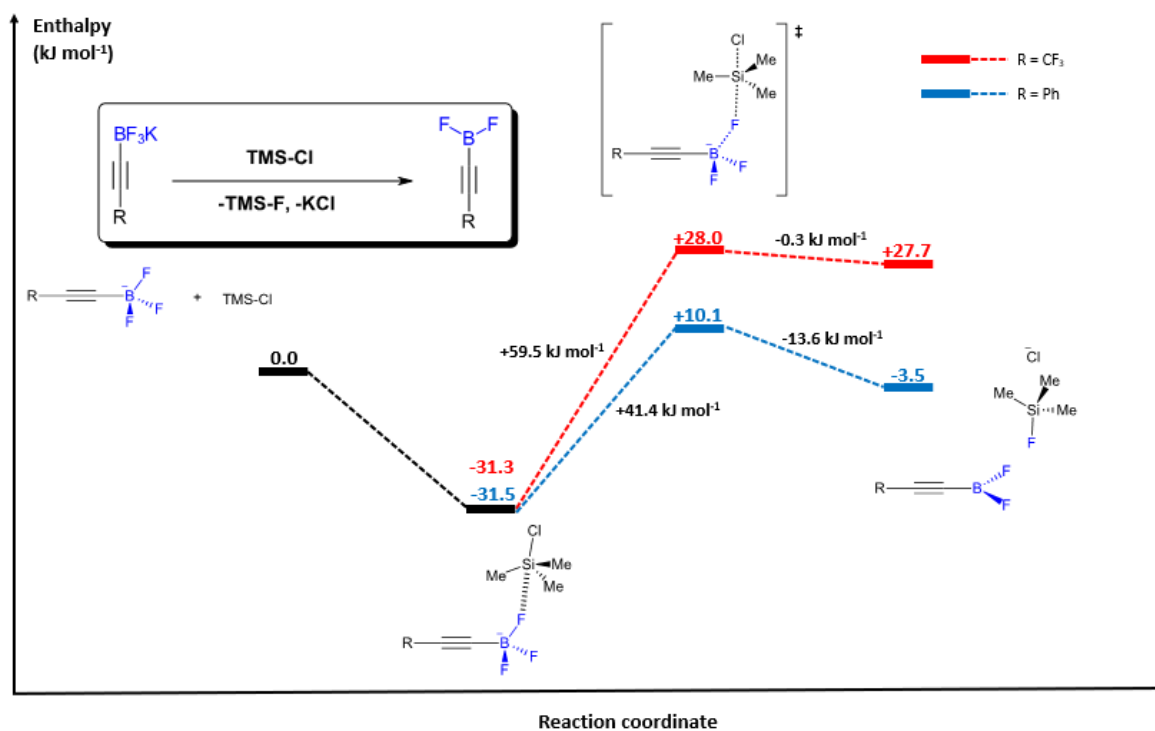
Figure 214: Energy profile for the fluoride abstraction of alkynyl trifluoroborate salts with TMS-Cl

R	σ (para)	$\Delta H^{\ddagger}$ / kJ mol^{-1}
-OMe	-0.27	31.8
-CH$_2$TMS	-0.21	34
-^{t}Bu	-0.2	35.8
-Me	-0.17	35.6
-Ph	-0.01	41.4
-butenone	-0.01	44.2
-H	0	44.2
-SMe	0	35.9
-C$_6$F$_5$	0.27	50.9
-CO$_2$Me	0.45	53.1
-CF$_3$	0.54	59.5
-NO$_2$	0.78	66
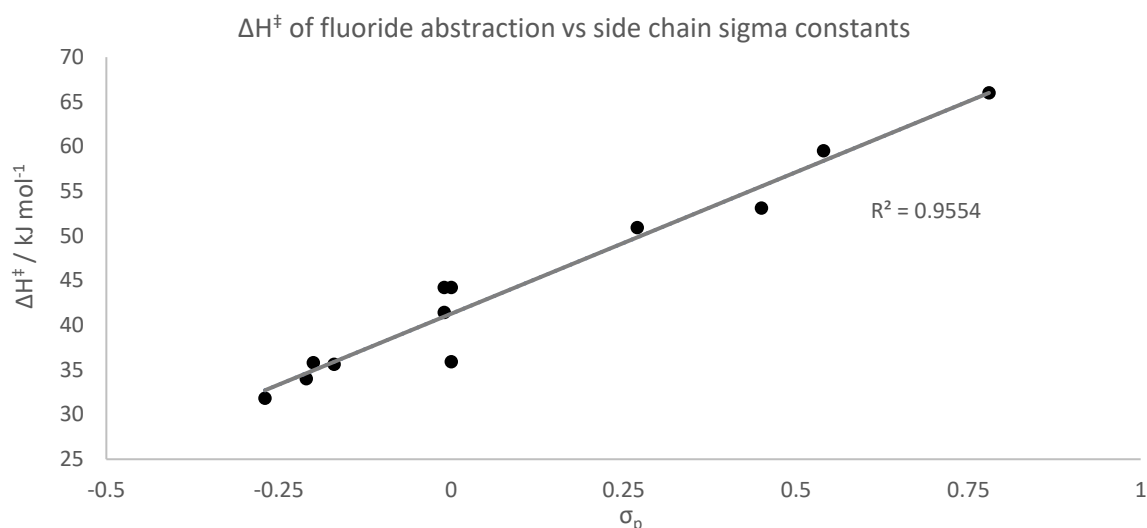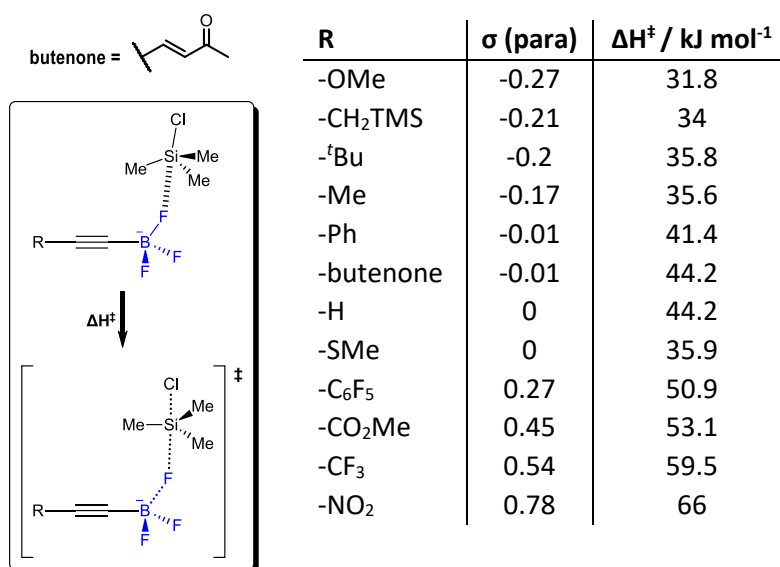
Figure 215: Calculated activation enthalpies for fluoride abstraction by TMS-Cl for a series of substituted alkynyl trifluoroborates, plotted against the corresponding Hammett para-substituent constant[492]

Processing these figures using the Eyring equation (table 10, *cf* appendix 5) allowed us to estimate the relative rates of fluoride abstraction at 298K. With the trifluoroborate of **357** undergoing a fluoride abstraction that is 1489 times slower than for **314**, we reasoned that the fluoride abstraction may well be a significant process when considering the rate/conversion of the BDC as a whole, and whether or not it is possible under the tested conditions. TMS-Cl was shown (section 2.2.4) to work as a promoter for the BDC reaction of **357** with substituted 2-pyrones and sydnones only at the elevated temperature of refluxing 1,2-dichloroethane, this observation, along with the fact that **357** is inert to TMS-Cl at room temperature shows that the fluoride abstraction can still occur but only if enough thermal energy is supplied (agreeing with calculation). To investigate whether or not this was a general pattern, we calculated the same fluoride abstraction reaction for a number of examples of alkynyl trifluoroborates with electronically diverse side chains (figure 215). As a measure of the electron

withdrawing/donating ability of each side chain, we used Hammett para-substituent constants (σ_p) which have been determined experimentally and have been conveniently tabulated by Taft and colleagues.[492] The results of this calculation series are shown in figure 215, the substrates are listed downwards in the table from low σ_p to high σ_p (electron-donating with respect to H, to electron-withdrawing with respect to H) and it is apparent that highly electron-withdrawing substrates (R = NO$_2$, CF$_3$) have a relatively high barrier to fluoride abstraction compared to highly electron-donating substrates (R = OMe, SMe, CH$_2$TMS). This correlation becomes clear once the variables are plotted, describing succinctly that alkynyl trifluoroborates bearing electron-withdrawing side chains undergo a slower fluoride abstraction by TMS-Cl than those bearing electron-donating side chains.

While **357** may be much less willing to undergo the fluoride abstraction than other alkynyl trifluoroborates such as **314** using TMS-Cl, an important principle that needed to be confirmed was whether the use of more powerful fluorophiles would enable this transformation at ambient temperatures. Realisation of this useful strategy was found during the optimisation of the BDC reaction of **336** with substituted tetrazines (figure 209, 2.2.6).
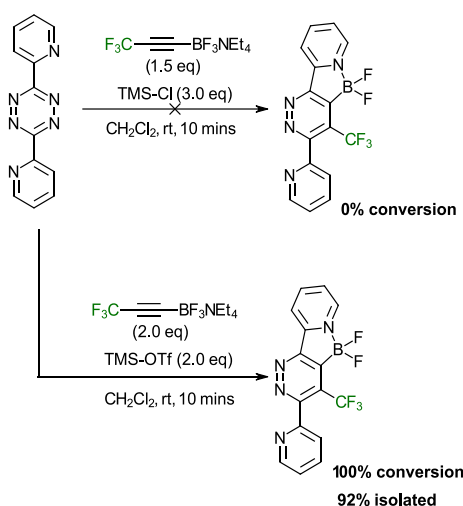
Figure 216: Switching from TMS-Cl to TMS-OTf in the boron-directed cyclaoddition of **336** with substituted tetrazines allows the reaction to take place at ambient temperature

No reaction occurs when the literature[461] conditions are used (room temperature, TMS-Cl promoter), but upon the use of TMS-OTf (a stronger fluorophile, can be considered an equivalent of " TMS$^+$ ") as a promoter, a vigorous reaction takes place allowing the desired pyridazine difluoroborane to be isolated in good yield. The juxtaposition of these experimental findings complement the calculated correlation of fluoride abstraction barrier with σ_p for the side chain, because it shows that although the trifluoroborates with more electron-withdrawing side chains may undergo a slow fluoride abstraction at room temperature with TMS-Cl, changing to a stronger fluorophile allows this abstraction to take place rapidly. It is this same tunability that allowed further success in promoting the BDC with 2-pyrones and also triazines (*cf* BCl$_3$, BBr$_3$ as fluorophile, section 2.2.4).

The fluoride ion affinity (FIA, denoted pF$^-$), defined as the negative enthalpy change (in kcal mol^{-1}) of a Lewis acid with a fluoride donor divided by 10, has been calculated for numerous reagents and species and has become a convenient scale for measuring Lewis acidity.[480,493–495] A collection of these calculated values is shown in figure 217.

Fluoride ion affinity (pF⁻) of Lewis acidic boranes
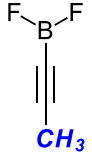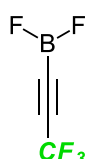
Level of theory	CH₃		CF₃			
B3LYP	6.89	7.88	8.90	-	-	-
BP86/SV(P)	-	8.08	-	9.68	10.35	10.71

Figure 217: Published values of the calculated fluoride ion affinity for some Lewis acidic boranes[480,494,495]
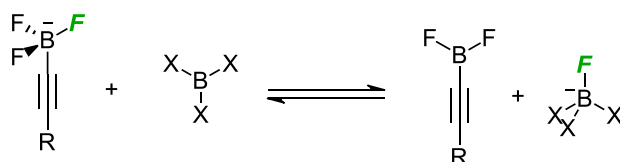
R	X	ΔH / kJ mol⁻¹	ΔG / kJ mol⁻¹	K_{eq}(298 K)
Ph	F	-27.9	-25.2	$2.61×10^4$
CF₃	F	+14.2	+13.9	$3.66×10^{-3}$
CF₃	Cl	-43.2	-44.7	$6.85×10^7$
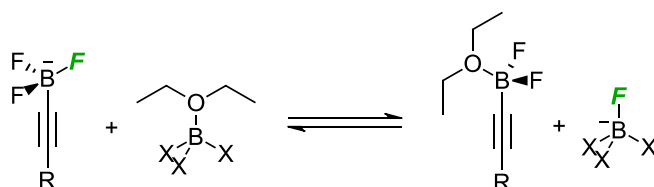
R	X	ΔH / kJ mol⁻¹	ΔG / kJ mol⁻¹	K_{eq}(298 K)
Ph	F	-3.2	-0.5	$1.20×10^0$
CF₃	F	+13.5	+17.1	$1.02×10^{-3}$
CF₃	Cl	-43.0	-47.2	$1.88×10^8$

Figure 218: Calculated values of ΔH and ΔG for fluoride abstraction reactions by BX₃ and BX₃.OEt₂

Although care must be taken when juxtaposing pF⁻ values that are calculated using different levels of theory, what becomes clear when these values are compared, is that BF₃ (not BF₃.OEt₂), which has a pF⁻ value of 7.88 according to Westphal *et al.*[480] reacts exothermically with the CH₃-substituted alkynyl trifluoroborate (pF⁻ value of the difluoroborane = 6.89) but *not* with the CF₃-substituted alkynyl trifluoroborate (pF⁻ value of the difluoroborane = 8.90, suggests a higher fluoride affinity than BF₃). Furthermore, the published values for alternative boranes such as BCl₃ and BBr₃ suggest, quite

intuitively, that they would react exothermically with the trifluoroborate of **357** (and are thus stronger Lewis acids than the corresponding difluoroborane). With this thermodynamic rationale in mind, in lieu of suitable transition states to assess kinetic feasibility, we compared the relative stability of Ph- and CF$_3$-substituted trifluoroborates with their corresponding difluoroboranes after reaction with BX$_3$ or BX$_3$.OEt$_2$ (X = F or Cl, figure 218). Our results corroborate the conclusions drawn above regarding the feasibility of fluoride abstraction by BF$_3$ or BCl$_3$ (or the corresponding etherate). Specifically, while the fluoride abstraction of the Ph-substituted alkynyl trifluoroborate by BF$_3$ is spontaneous with a change in free energy of -25.2 kJ mol^{-1} (figure 218), the same reaction on the CF$_3$-substituted alkynyl trifluoroborate was not, with a change in free energy of +13.9 kJ mol^{-1} upon going to the difluoroborane. Interestingly, upon switching from BF$_3$ to BF$_3$.OEt$_2$ as the Lewis acid and forming the corresponding difluoroborane etherate, the driving force for the abstraction of the Ph-substituted alkynyl trifluoroborate was diminished (from ΔG = -25.2 kJ mol^{-1} to ΔG = -0.5 kJ mol^{-1}), but the process was still exergonic. This effect was not as pronounced for the same abstractions on the CF$_3$-substituted alkynyl trifluoroborate, as the changes in free energy were similar regardless of whether BX$_3$ or BX$_3$.OEt$_2$ was used.

3.3. Alkyne transfer
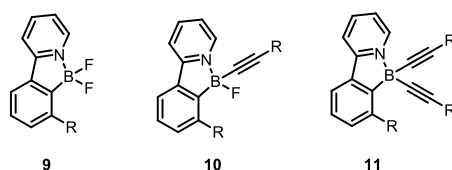
Figure 219: Observed product mixture of the BF$_3$.OEt$_2$ promoted BDC

It has been shown in the 2014 study[464] through a combination of theoretical and experimental investigations, that a pre-cycloaddition alkyne transfer reaction[475] (figure 173) could be a mechanism for the formation of products **9** and **10** (figure 219). Given, in the studied case, that this process was found to be rather significant to the success of the BDC with 2-pyrones because the precursor coordination complexes have significantly different cycloaddition activation enthalpies, we decided to investigate further the effect of the alkyne side-chain on this transfer reaction. Thus, we began by comparing enthalpy profile diagrams representing the borane transfer reactions for the difluoroboranes of **357** and **314**, the results are summarised in figures 220 and 221. The rate-determining transition states for the two processes were the four-membered cyclic structures **405** (figure 220) and **406** (figure 221), the activation enthalpies of which, for the -CF$_3$ substituted alkynes, were 45.5 kJ mol^{-1} and 33.9 kJ mol^{-1} greater than those for the -Ph substituted alkynes, respectively. Depending on the significance of the bis- and tris(alkynyl)boranes for the speed of the subsequent cycloadditions, this could serve as rationale for why **357** reacts sluggishly in the BDC at ambient temperatures using BF$_3$.OEt$_2$ as promoter. After discovering the stark difference between the calculated values **ΔH$^{‡}_{CF3}$** and **ΔH$^{‡}_{Ph}$**, we wanted to determine whether there was a general pattern between reactivity and the nature of the alkyne side-
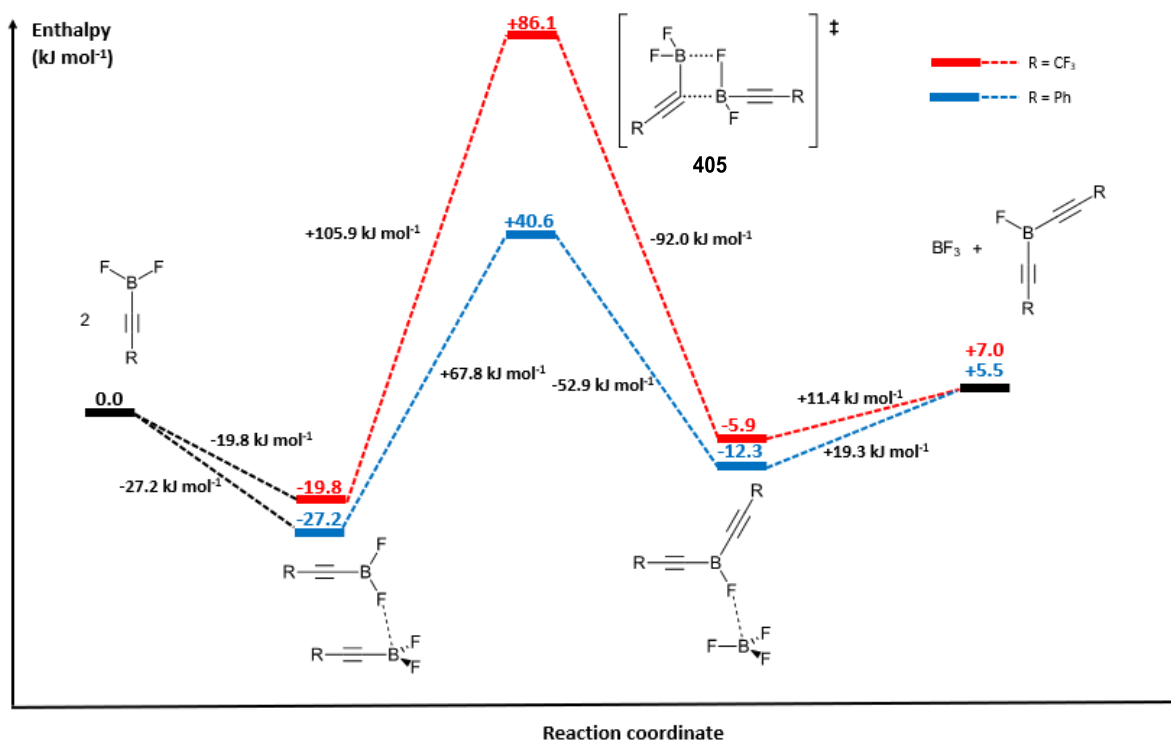
Figure 220: Enthalpy profile diagram comparing side chains -Ph and -CF₃ for the borane equilibration process
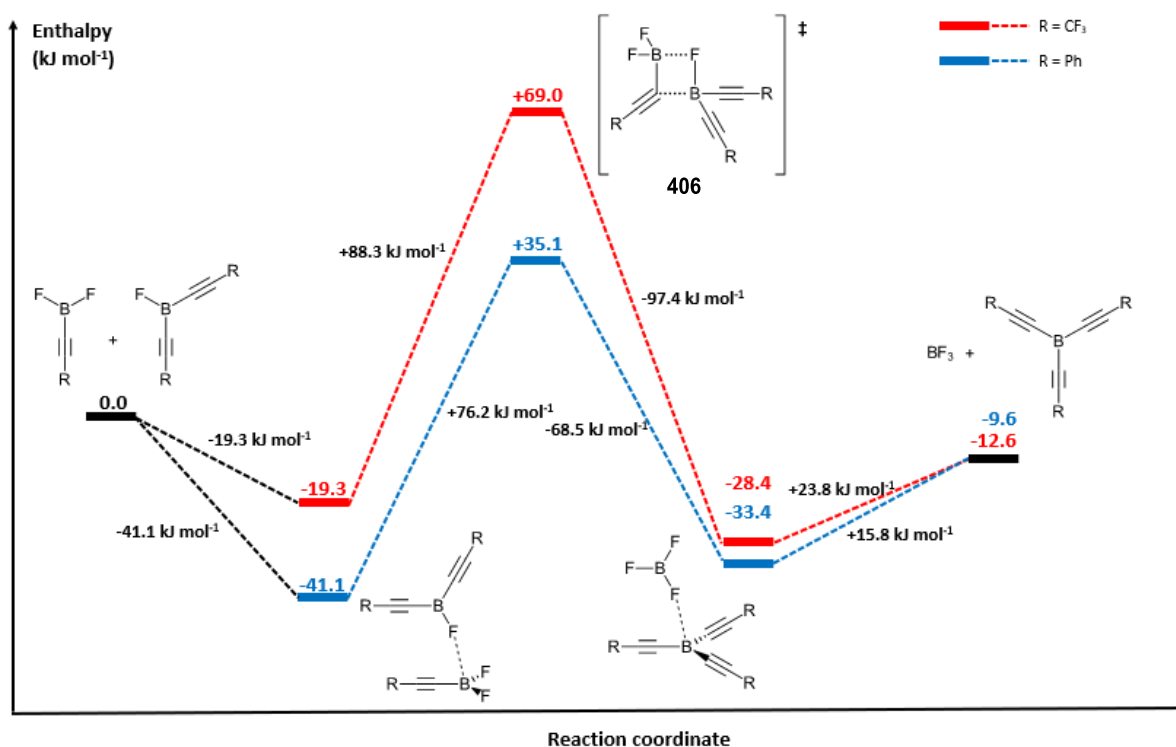
Figure 221: Enthalpy profile diagram comparing side chains -Ph and -CF3 for the borane equilibration process

146

R	σ (para)	σ⁺ (para)	$\Delta H^{\ddagger}$ / kJ mol⁻¹
-OMe	-0.27	-0.78	51.4
-CH$_2$TMS	-0.21	-0.62	52.5
-SMe	0	-0.6	54.8
-Me	-0.17	-0.31	67.6
-Ph	-0.01	-0.18	67.8
-^{t}Bu	-0.2	-0.26	73.9
-H	0	0	87
-C$_6$F$_5$	0.27	0.23	94.8
-butenone	-0.01	0.39	88.6
-CO$_2$Me	0.45	0.49	98.4
-NO$_2$	0.78	0.79	101.7
-CF$_3$	0.54	0.61	105.9
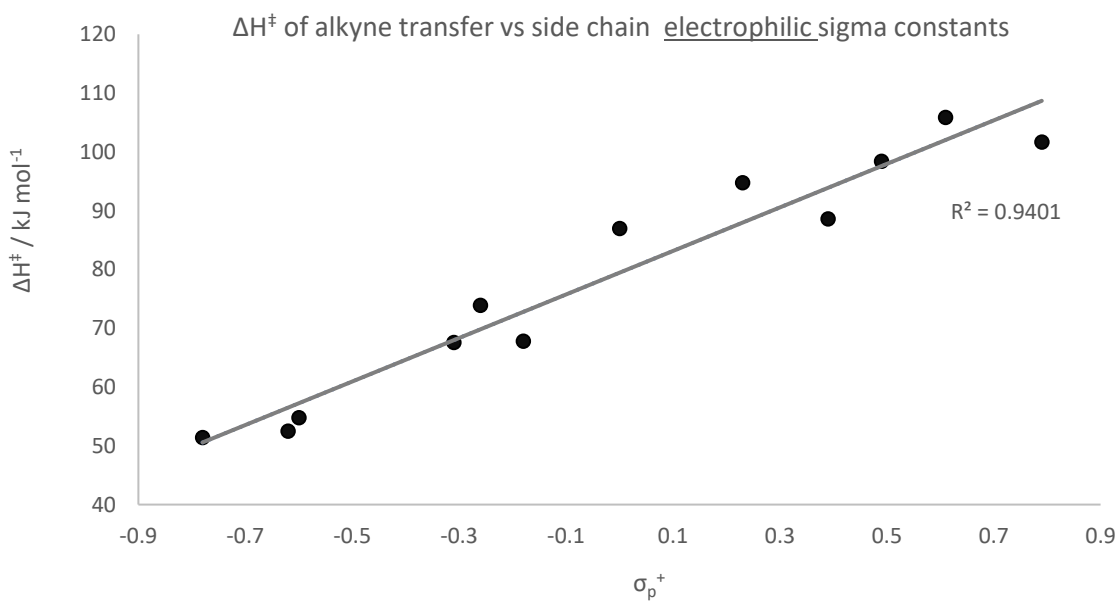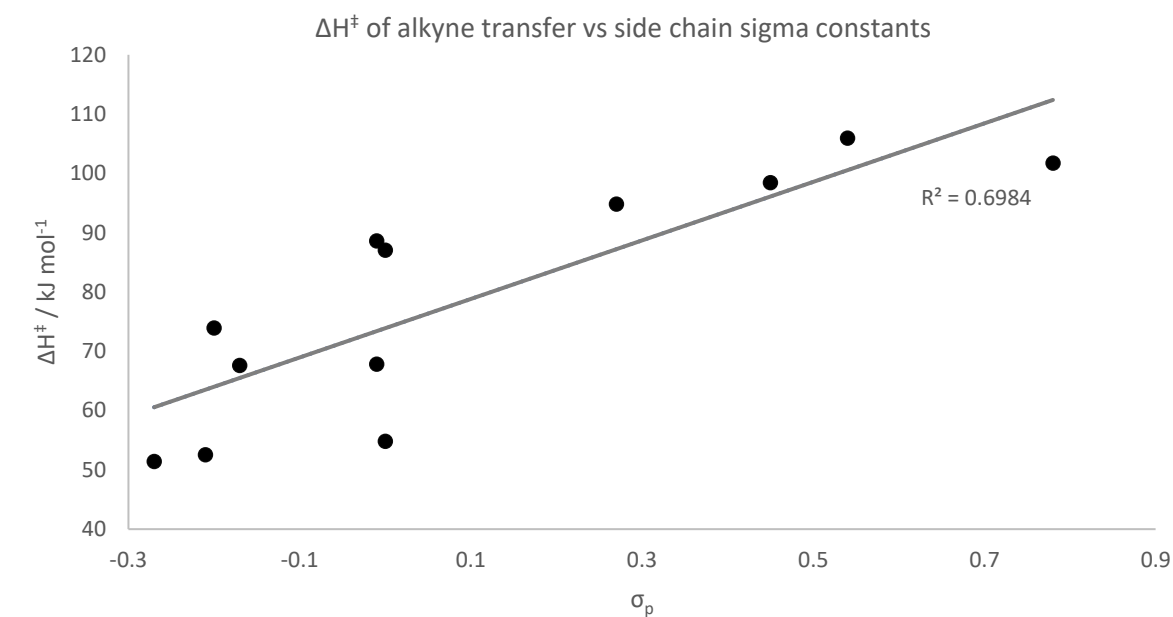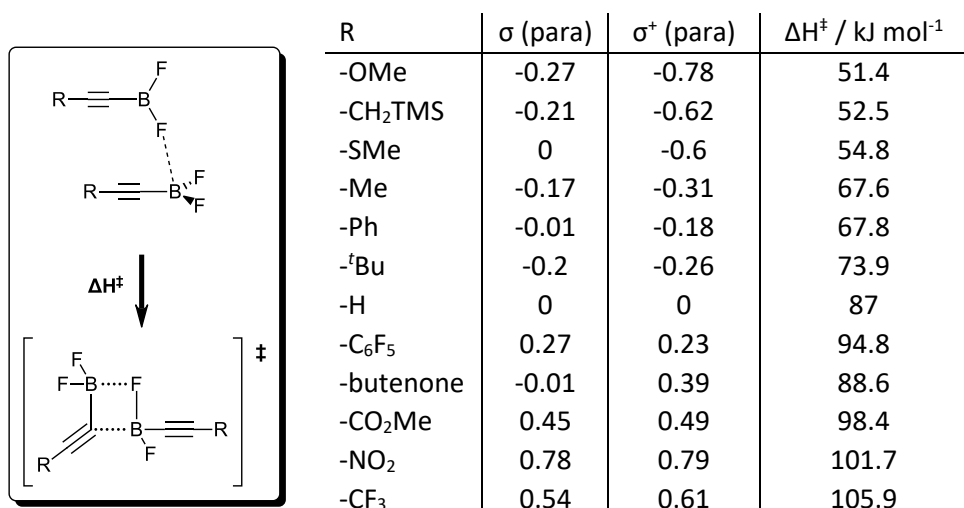
*Figure 222: Values of the activation energy for the borane disproportionation reaction linking **318** to **319** and plots of these values against para-substituent constants and <u>electrophilic</u> para-substituent constants*

chain, as was found for the fluoride abstraction in the previous section. To explore this possibility, the model alkyne transfer reaction linking **318** to **319** (figure 173) was calculated for the same series of alkyne substituents investigated previously (broad range of σ values, figure 222) and the activation enthalpy for each substrate is shown in figure 222. A plot of $\mathbf{\Delta H^{\ddagger}_R}$ for alkyne transfer against $\mathbf{\sigma_p}$ is shown in figure 222, and it displays broad correlation between the two variables. Use of the electrophilic para substituent constant, σ_p^+, instead of σ_p provides a better fit to a linear relationship between these variables. This observation can be rationalised by the fact that included in the series of substituents shown in figure 222 are those that withdraw/donate electron density mostly *via* either resonance (e.g. -NO$_2$, -OMe, -SMe) or induction (e.g. -CF$_3$, -CH$_2$TMS, -^{t}Bu), and for those that contribute *via* resonance, the linear relationship between $\mathbf{\Delta H^{\ddagger}_R}$ and σ_p does not fit as well as for those that contribute mostly *via* induction (an exception being the -CH$_2$TMS group, which comprises a special case of hyperconjugation, *cf* β-Si effect).[496] Electrophilic and nucleophilic substituent constants are obtained by comparing relative rates for reactions that are influenced heavily by substituents that communicate with the reaction centre directly by resonance, e.g. hydrolysis reactions of cumyl halides[497,498] (the rate of the reaction depends on the extent to which the transient carbocation is (de-)stabilised). So again, we see in the pre-cycloaddition alkyne transfer reaction, a process that occurs slower for alkynes that bear electron-withdrawing side-chains. This finding is thus highly important for rationalising why **357** requires more heat in the BF$_3$.OEt$_2$-promoted BDC than **314**.

Another alkyne transfer process that is likely to occur, is the post-cycloaddition ligand exchange, which provides an explanation for the BF$_3$.OEt$_2$-promoted interconversion of the three compounds **324**, **325**, and **326** (figure 173) after the BF$_3$.OEt$_2$-promoted BDC of alkynyl trifluoroborate salts with substituted 2-pyrones. The authors[462] record **315** (figure 172) as the major product in this process, and it was the same for all the alkynyl trifluoroborates tested. This is rationalised on the basis that the products **315**, **316** and **317** (figure 172) are (in the presence of BF$_3$.OEt$_2$) in equilibrium and thus favour **315** when an excess of BF$_3$.OEt$_2$ is used. After calculating the total enthalpy of **315**, **316** and **317** alongside the expected other reagents and products (figure 223), we realised that all three products are similar in total enthalpy, this provides no obvious inherent driving force towards any single product, thus causing the main determinant of ultimate selectivity to be the concentration of BF$_3$.OEt$_2$ (so long as the reactions are kinetically feasible, *vide infra*) as is confirmed by experiment. If we compare these structures with **354** (figure 224), **355** and **356**, the situation is rather different, with the highly substituted borane **356** being lower in total enthalpy than **354** by 60.9 kJ mol^{-1}. This magnitude of exothermicity suggests that there should be a driving force towards **356**, alienating the ability of BF$_3$.OEt$_2$ to manage selectivity. After we optimised the BDC reaction using **357** to obtain full conversion of the 2-pyrone (figure 189 and table 6) by applying heat, **354** was typically the major product, although significant amounts of **355** and **356** were also observed. Attempts to converge to **354** by using an excess of BF$_3$.OEt$_2$ on the mixture of adducts resulted in no conversion (figure 191), demonstrating the enhanced stability of **356** compared to **354**. However, **354** was not converted to **356** when treated with both BF$_3$.OEt$_2$ and **357** (figure 192). This suggests a more complex relationship between the three compounds and mechanism for their interconversion. The apparent increase in stability for **356** compared to **354** and **355** and the apparent lack of this stabilisation when R = Ph, may be rationalised by the increased attenuation of the negative charge on B caused by a greater electron-withdrawing ability of C≡C-CF$_3$ (σ_p = **0.51**)[492] compared to F (σ_p = 0.06)[492] and C≡C-Ph (σ_p = 0.16).[492] This is supported by the fact that an inverse relationship exists between the three types of complex when R = OMe (figure 225), compared to those where R = CF3.
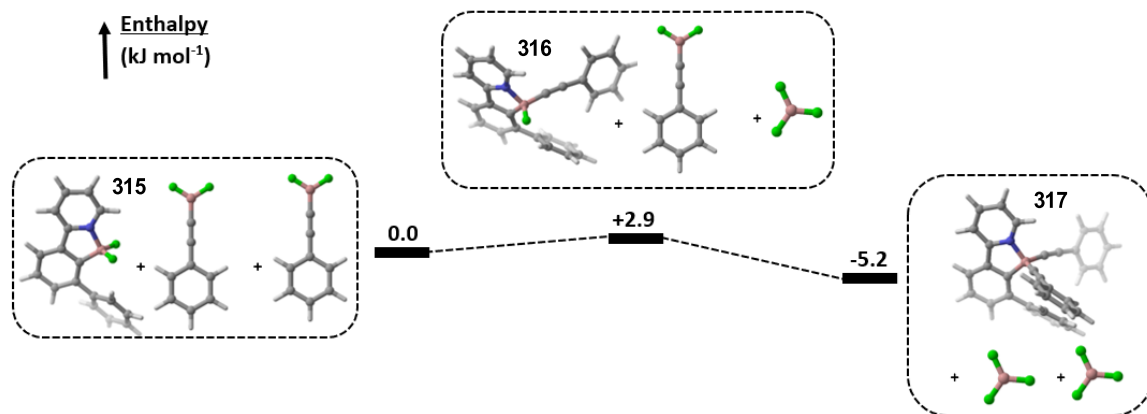
Figure 223: Calculated enthalpies of each possible product structure from the BF₃.OEt₂ promoted BDC reaction using -Ph substituted alkyne
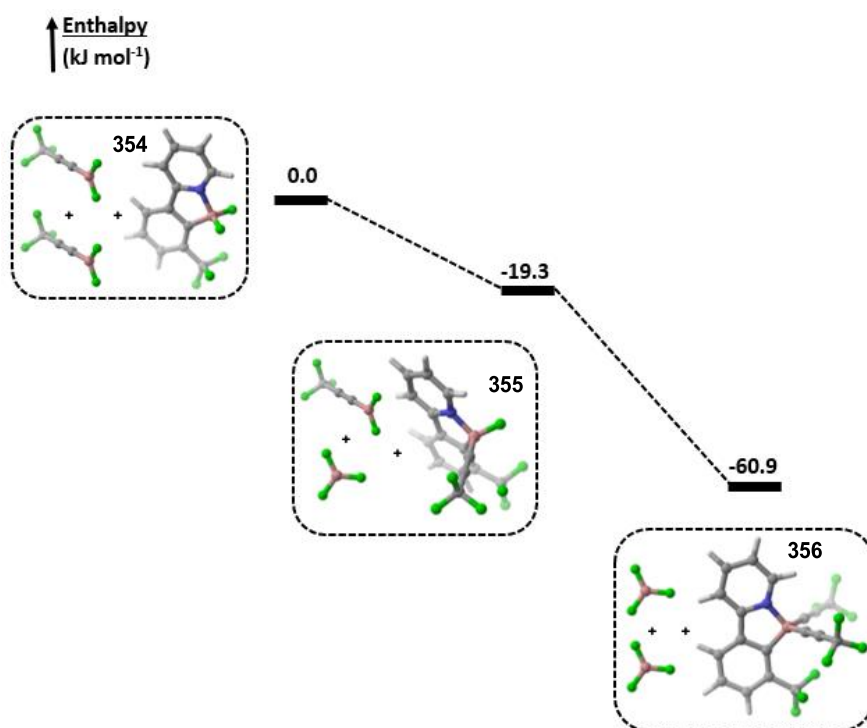
Figure 224: Calculated enthalpies of each possible product structure from the BF3.OEt2 promoted BDC reaction using -CF₃ substituted alkyne
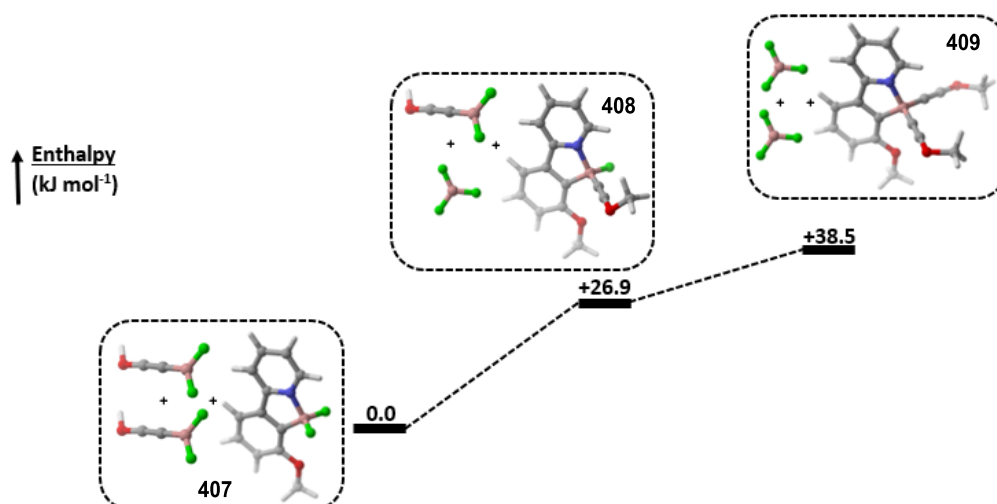
Figure 225: Calculated enthalpies of each possible product structure from the BF$_3$.OEt$_2$ promoted BDC reaction using -OMe substituted alkyne

After establishing the thermodynamic stability of each product, we wanted to assess the kinetic feasibility of their interconversion under the reaction conditions. For this, we calculated reaction coordinates for the expected mechanism of interconversion based on data already published.[464] The coordinates for the products where R = Ph are shown in figures 226 and 227. On going from product **317** to product **316** (figure 227), the highest activation enthalpy that was calculated was +31.5 kJ mol^{-1}. This is a rather low value, and the pattern of low activation enthalpy for this process agrees with the published results for this particular substrate.[464] For R = CF$_3$ however (figures 228 and 229), the enthalpy profiles are considerably different. The calculated activation enthalpies for interconversion are much higher in this case, with the highest at +92.3 kJ mol^{-1}, linking **356** to **355** (figure 229). The thermodynamic driving force towards **356** and the relatively high barriers to interconversion (compared to the R = Ph substrate) may help to explain why the attempted convergence to either **354** or **356** (figures 191 and 192, respectively) through the addition of further equivalents of BF$_3$.OEt$_2$ and/or alkyne **357** resulted in no change in the product composition.
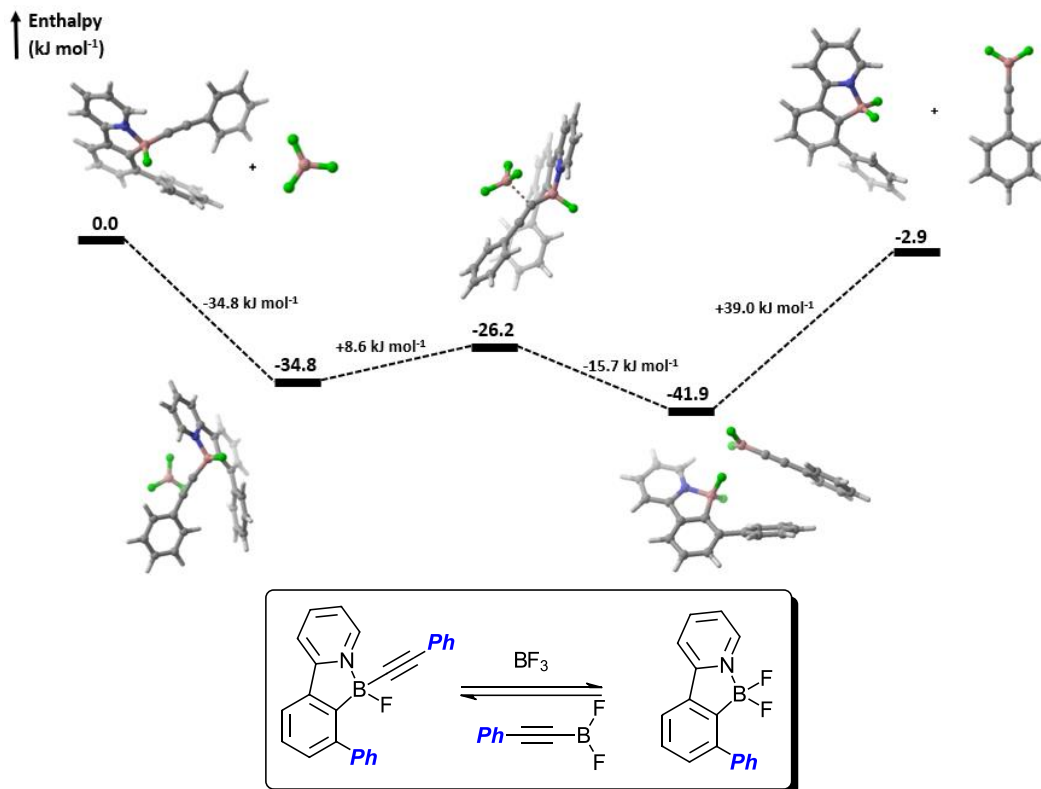
*Figure 226: Enthalpy profile diagram linking product **316** (left) to product **315** (right)*
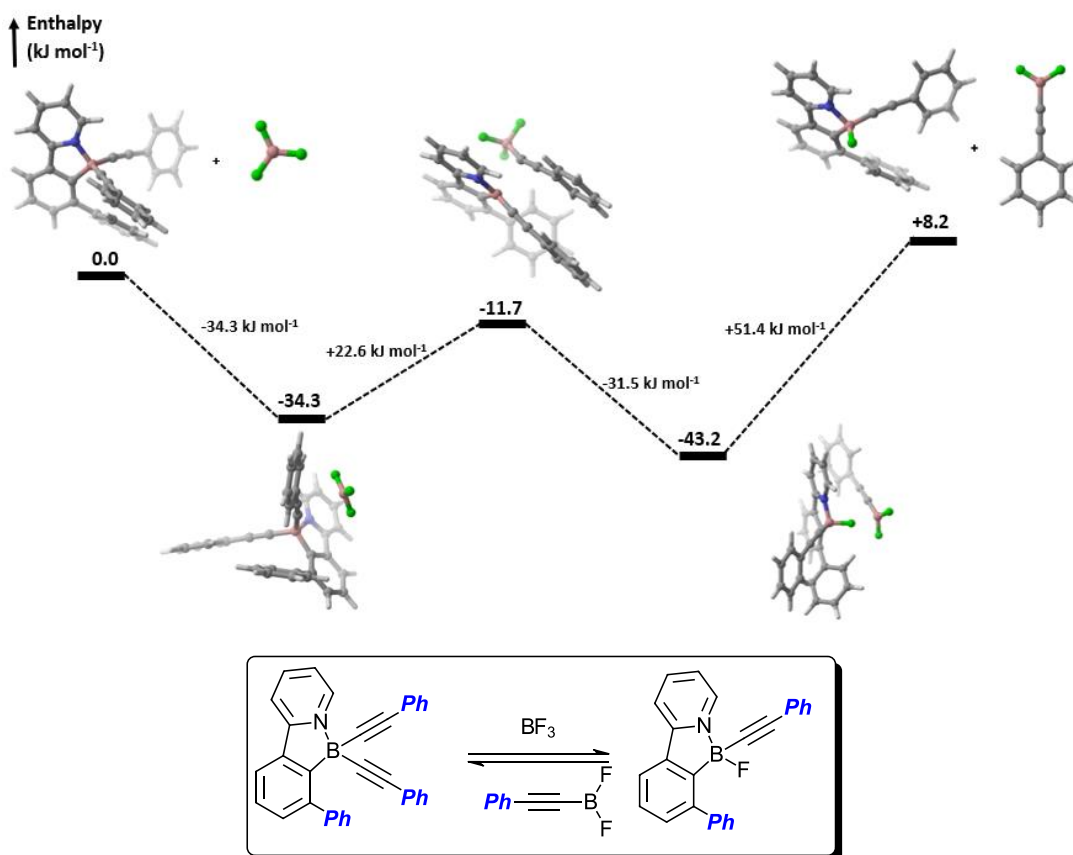
*Figure 227: Enthalpy profile diagram linking product **317** (left) to product **316** (right)*

151
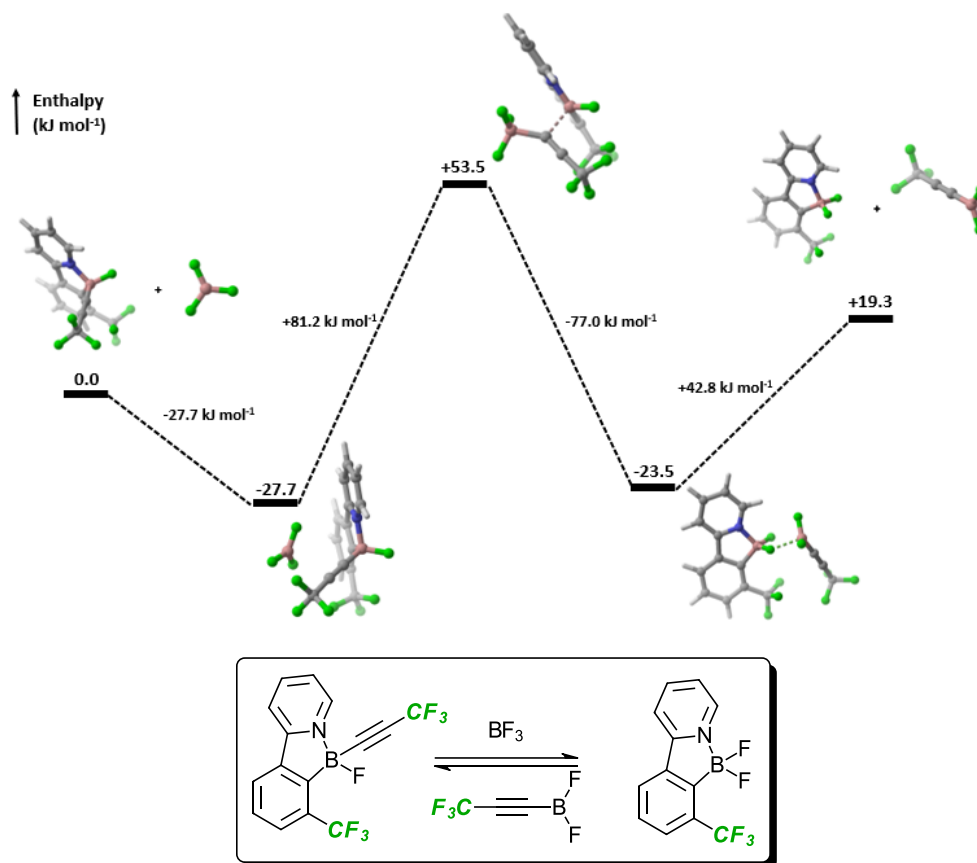
*Figure 228: Enthalpy profile diagram linking product **355** (left) to product **354** (right)*
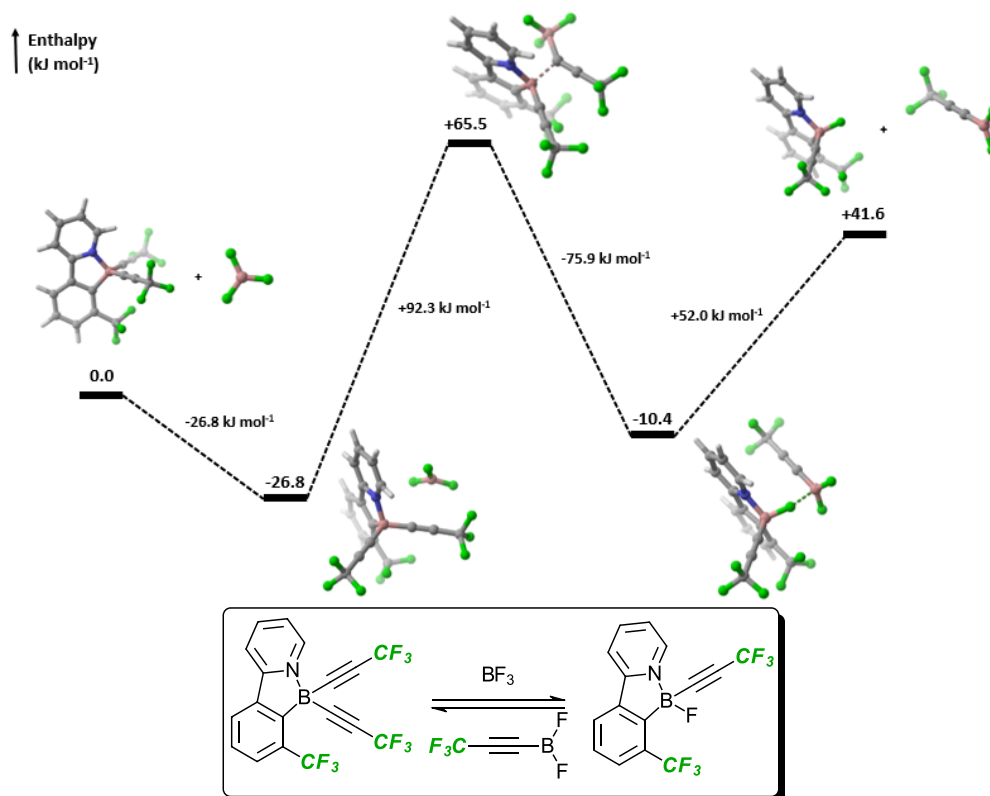
*Figure 229: Enthalpy profile diagram linking product **356** (left) to product **355** (right)*

3.4. Directed [4+2] cycloaddition

The final major step in the BDC process that we sought to investigate computationally is the [4+2] cycloaddition itself (figure 14), expected to occur after formation of the acid-base complex between the pyrone and the borane. In order to assess the impact that the side-chain "R" had on the barrier to [4+2] cycloaddition, we conducted calculations for R = CF_3 and Ph and obtained transition states for the compounds **321**, **322** and **323** (table 13) to compare energetic barriers to cycloaddition relative to the respective acid-base complexes.

Activation energies for directed [4+2] cycloaddition

Entry	R^1	R^2	$\Delta H^{\ddagger}$ / kJ mol^{-1}	$\Delta G^{\ddagger}$ / kJ mol^{-1}	Rel rate (298 K)	Rel rate (353 K)
			R = Ph			
1	F	F	+89.0	+97.4	1	1
2	F	C≡CR	+78.5	+85.5	122	58
3	C≡CR	C≡CR	+73.9	+80.7	846	296
			R = CF$_3$			
4	F	F	+84.2	+95.9	2	2
5	F	C≡CR	+75.3	+85.3	132	62
6	C≡CR	C≡CR	+72.1	+78.4	2141	648

Table 11: Calculated activation energies of directed cycloadditions for R = Ph and CF$_3$

For transition structures of type **321** (table 11, entries 1 and 4), the activation enthalpies are only ~ 5 kJ mol^{-1} apart, suggesting that the identity of the side chain has only limited impact on the barrier to cycloaddition in this case. For transition structures of type **322** (entries 2 and 5), the activation enthalpies are only 3.2 kJ mol^{-1} apart. The barriers to cycloaddition for transition states of type **323** (entries 3 and 6) are similar to those of type **322**. Based on these data, which show a relationship between activation enthalpies of the complexes **321**, **322** and **323** that is consistent with published data (complex type **323** has the lowest activation enthalpy), we can conclude that it is unlikely that
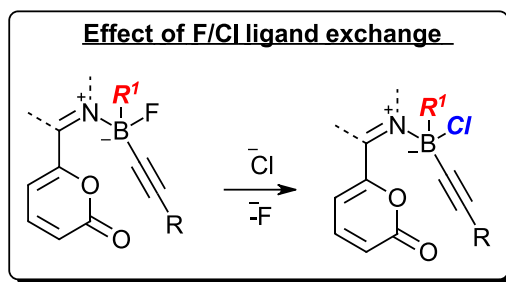
Figure 230: Theoretical scheme summarising the species that were next to be investigated for their cycloaddition activation energies: F/Cl exchanged boranes

Entry	R^1	X	$\Delta H^{\ddagger}$ / kJ mol^{-1}	$\Delta G^{\ddagger}$ / kJ mol^{-1}	Rel rate (298 K)	Rel rate (353 K)
			R = Ph			
1	F	F	+89.0	+97.4	1	1
2	C≡CR	F	+78.5	+85.5	122	58
3	Cl	Cl	+71.1	+79.1	1614	511
4	C≡CR	Cl	+71.1	+80.7	846	296
			R = CF$_3$			
5	F	F	+84.2	+95.9	2	2
6	C≡CR	F	+75.3	+85.3	132	62
7	Cl	Cl	+64.2	+74.6	9922	2365
8	C≡CR	Cl	+67.3	+77.0	3766	1044

Table 12: Activation parameters for directed cycloadditions of fluoro- or chloro-borane dienophiles

the directed cycloaddition portion of the BDC process would cause there to be a large discrepancy in reactivity between alkynes **357** and **314**.Given the success of the use of BCl$_3$ as an activator for the BDC reaction of **357** with substituted 2-pyrones, forming dichloroboranes as single products (figure 199), we wanted to investigate what the consequences on cycloaddition activation energy were upon Cl/F exchange in the starting difluoroboranes. Our results are summarised, alongside selected data from table 13, in table 14. The key finding from this was that the replacement of F by Cl had a significant effect on cycloaddition activation energies. The effect was a drastic reduction in activation enthalpy upon going from the F- to the Cl-substituted borane, and it was greatest for the change from difluoroboranes to dichloroboranes (compare entries 1 and 3 for R = Ph, entries 5 and 7 for R = CF$_3$), although reductions in activation energy were also observed for bisalkynyl fluoroboranes (compare

entries 2 and 4 for R = Ph, entries 6 and 8 for R = CF$_3$). For R = Ph, upon exchanging both F for Cl, the activation enthalpy was reduced from +81.0 kJ mol^{-1} (entry 1) to +71.1 kJ mol^{-1} (entry 3). The effect was more pronounced for R = CF$_3$, where exchange of both F for Cl reduced the activation enthalpy from +84.2 kJ mol^{-1} (entry 5) to +64.2 kJ mol^{-1} (entry 7). The corresponding activation Gibbs energy was also obtained in each case, showing a similar pattern. From the activation Gibbs energies, we determined that the rate enhancement provided by the exchange of both F for Cl spanned 2 orders of magnitude for both R = Ph and R = CF$_3$.
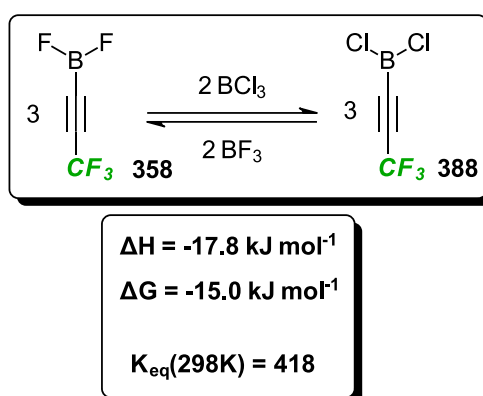
Figure 231: Calculated enthalpy and free energy change upon F/Cl exchange of difluoroborane **358** by the action of BCl$_3$, showing an exothermic and spontaneous process at 298 K

Furthermore, the exchange of fluoride for chloride in the CF$_3$-substituted intermediate difluoroborane by the action of BCl$_3$ is calculated (figure 231) to be moderately exothermic. So if the fluoride abstraction from alkyne **357** by BCl$_3$ proceeds smoothly under the conditions, then we can expect a considerable amount of dichloroborane **388** to be present in solution soon after, due to F/Cl scrambling of the difluoroborane **358** with further equivalents of BCl$_3$.

Based on these observations, it is plausible that the mechanism for the BCl$_3$-promoted cycloaddition of alkyne **357** with 2-pyrones proceeds *via* fluoride abstraction (figure 232), followed by F/Cl exchange to the alkynyl dichloroborane **388**, then directed cycloaddition to **369**. Alternatively, the difluoroborane **358** may also undergo the directed cycloaddition, followed by rapid F/Cl exchange *after* the cycloaddition. This latter mechanism has been shown to be possible by the treatment of products **354** and **355** with BCl$_3$ under the reaction conditions (figure 201), leading to quantitative replacement of F for Cl. However, due to the high driving force towards the alkynyl dichloroborane **388** from **358** (figure 231), and the much lower barrier to cycloaddition of the complex **410** (figure 232) compared to **361** (*vide supra*, table 14), it is expected that the dichloroborane does the cycloaddition to obtain the product directly and not the difluoroborane.
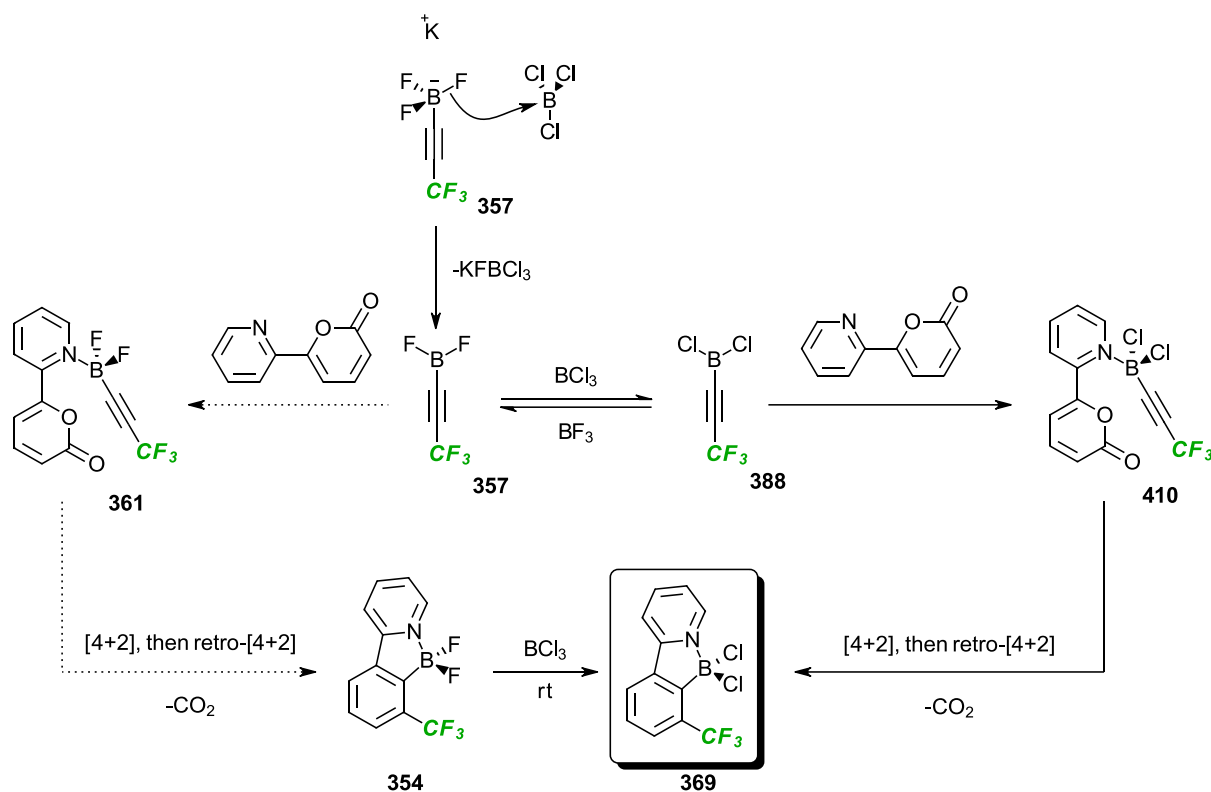
*Figure 232: Proposed mechanistic pathways for the BCl$_3$-promoted cycloaddition of alkyne **357** with 2-pyrone **311***

3.5. Conclusions

In summary, the BDC process is deeply influenced by the nature of the alkyne side chain. Particularly if the side chain is strongly electron withdrawing, judging from increased barriers to fluoride abstraction and alkyne transfer. For both of these reactions, relationships between electron donating/withdrawing ability and activation enthalpy were established. Namely, more electron-withdrawing substituents had higher activation enthalpies for both the fluoride abstraction and the first step of the alkyne transfer. The reaction in the BDC that appears to be less strongly affected by the identity of the side chain is, surprisingly, the [4+2] cycloaddition itself. This was unexpected, because of the proximity of the side chain to the reaction centre(s) - and the harsh conditions typically required for IEDDA reactions of fluoroalkyl-substituted alkynes.[445,481] The Ligands attached to B appeared to have greatest influence on the barrier to cycloaddition. Based on the calculated thermodynamic and kinetic data, along with selected experimental results, the failure of BF$_3$.OEt$_2$ and the success of BCl$_3$ as a promoter for the mild boron directed cycloaddition of alkynyl trifluoroborate salt **357** with 2-pyrones was rationalised.

4. Experimental methods & compound characterisation

4.1. General considerations

All reactions were conducted in flame-dried glassware under ambient conditions unless otherwise stated. THF and toluene were dried before use over an alumina column. All commercially available solvents and reagents were used as supplied or purified using standard laboratory techniques according to methods described by Perrin and Armarego.[499]

Thin layer chromatography was performed on aluminium-backed plates pre-coated with silica (Merck silica Kieselgel 60 F254), which were developed using standard visualizing agents: ultraviolet light or potassium permanganate. Flash chromatography was performed on silica gel (60 Å, mesh 40-63 µm). Melting points were obtained using either a Stuart or Büchi apparatus and are uncorrected.

^{1}H spectra were recorded on a Bruker AVIII HD-400 (400 MHz), Bruker AVI-400 (400 MHz), Bruker AMX-400 (400 MHz) or DPX-400 (400 MHz). Proton magnetic resonance chemical shifts are reported from tetramethylsilane with the residual protic solvent resonance as the internal standard (DMSO: δ = 2.50 ppm). Data are reported as follows: chemical shift (ppm), multiplicity (s = singlet, d = doublet, t = triplet, q = quartet, quint = quintet, br = broad, m = multiplet), normalised peak integral (arbitrary units) then coupling constant (Hz). ^{13}C NMR spectra were recorded on a Bruker AVIII HD-400 (101 MHz), Bruker AVI-400 (101 MHz), Bruker AMX-400 (101 MHz) or DPX-400 (101 MHz). Carbon magnetic resonance chemical shifts are reported from tetramethylsilane with the solvent as the internal reference (DMSO: δ = 2.50 ppm). ^{19}F NMR spectra were recorded on a Bruker AMX-400 (376 MHz) or Bruker AVIII HD-400 (376 MHz) and the chemical shifts are uncorrected. ^{11}B NMR spectra were recorded on a Bruker AVIII HD-400 (128 MHz), and the chemical shifts are uncorrected.

Note that the ^{13}C NMR signal for the carbon atom attached to boron is not typically observed due to quadrupolar relaxation broadening.[500]

Infrared spectra were recorded on a Perkin-Elmer Paragon 100 FTIR spectrometer. Spectra were obtained from neat compounds through the use of a standard ATR attachment, and the most structurally relevant bands are quoted in cm^{-1}. Bands are characterized as broad (br), strong (s), medium (m) or weak (w). High-resolution mass spectra (HRMS) were recorded on a MicroMass LCT operating in Electrospray mode (TOF ES).

4.2. (amino)pyrimidin-6-yl trifluoroborate salts

4.2.1 Synthesis of (amino)pyrimidin-6-yl trifluoroborate salts

General procedure A: Preparation of terminal alkynes
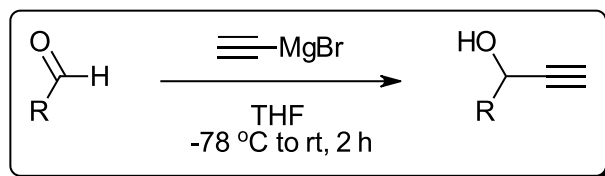
To a stirring solution of ethynylmagnesium bromide (0.27 M in THF) at -78 °C was added dropwise aldehyde. The reaction mixture was stirred for 10 minutes before warming to room temperature over 2 hours. Upon completion (as judged by TLC analysis), NH$_4$Cl (sat. aq.) was added and the solvent phases separated. The aqueous phase was extracted with EtOAc and the combined organic phases dried over anhydrous MgSO$_4$ then concentrated *in vacuo*. The resulting dark mixture was purified by flash column chromatography on silica gel to afford the terminal alkyne.

1-Phenylprop-2-yn-1-ol[501]
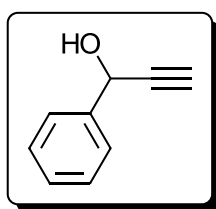
Following general procedure A, using benzaldehyde (6.1 mL, 60 mmol) and ethynylmagnesium bromide (0.5 M in THF, 180 mL, 90 mmol), the title compound was obtained as a gold-coloured oil (7.4 g**, 93%); **^{1}H NMR (400 MHz, CDCl$_3$)** δ_H ppm 2.29 (d, 1H, J = 2.0 Hz), 2.70 (d, 1H, J = 6.0 Hz), 5.50 (dd, 1H, J = 2.0, 6.0 Hz), 7.46 – 7.43 (m, 3H), 7.62 – 7.55 (m, 2H); **^{13}C NMR (101 MHz, CDCl$_3$)** δ_C ppm 64.3, 74.9, 83.7, 126.7, 128.5, 128.7, 140.1. (The data were in agreement with those published)

1-(4-Chlorophenyl)prop-2-yn-1-ol[220]
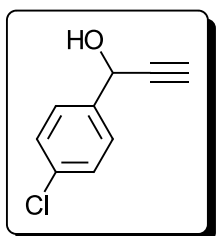
Following general procedure A, using 4-chlorobenzaldehyde (8.4 g, 60 mmol) and ethynylmagnesium bromide (0.5 M in THF, 180 mL, 90 mmol), the title compound was obtained as a gold-coloured oil (10.2 g**, >99%); **^{1}H NMR (400 MHz, CDCl$_3$)** δ_H ppm 2.31 (d, 1H, J = 5.0 Hz), 2.71 (d, 1H, J = 2.0 Hz), 5.47 (dd, 1H, J = 2.0, 5.0 Hz), 7.36 – 7.41 (m, 2H), 7.49 – 7.54 (m, 2H); **^{13}C NMR (101 MHz, CDCl$_3$)** δ_C ppm 63.6, 75.2, 83.2, 128.1, 128.8, 134.3, 138.5. (The data were in agreement with those published)

1-(4-(Trifluoromethyl)phenyl)prop-2-yn-1-ol[502]
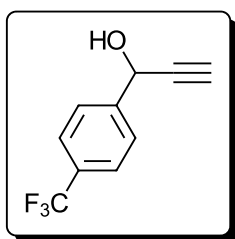
Following general procedure A, using 4-(trifluoromethyl)benzaldehyde (2.0 mL, 14.6 mmol) and ethynylmagnesium bromide (0.5 M in THF, 44.0 mL, 22.0 mmol), the title compound was obtained as a gold-coloured oil (2.8 g**,** 94%); **¹H NMR (400 MHz, CDCl₃)** δ_H ppm 2.68 (d, 1H, J = 6.0 Hz), 2.73 (d, 1H, J = 2.0 Hz), 5.54 (dd, 1H, J = 2.0, 6.0 Hz), 7.71 – 7.65 (m, 4H); **¹⁹F NMR (376 MHz, CDCl₃)** δ_F ppm -62.6; **¹³C NMR (101 MHz, CDCl₃)** δ_C ppm 63.7, 75.5, 82.8, 124.0 (q, J = 272.0 Hz), 125.6 (q, J = 3.5 Hz), 126.9, 130.7 (q, J = 32.0 Hz), 143.7. (The data were in agreement with those published)

1-(naphthalen-3-yl)-prop-2-yn-1-ol[503]
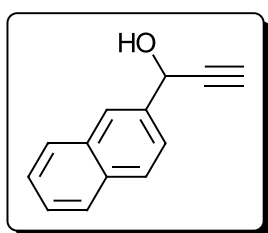
Following general procedure A, using 2-naphthaldehyde (4.7 g, 30 mmol) and ethynylmagnesium bromide (0.5 M in THF, 75 mL, 38 mmol), the title compound was obtained as a pale yellow solid (5.3 g**,** 96%); **M.p.** = 56 – 57 °C (lit[503] = 53 – 55 °C); **¹H NMR (400 MHz, CDCl₃)** δ_H ppm 8.02 (s, 1H), 7.91 – 7.85 (m, 3H), 7.67 (dd, J = 8.5, 1.5 Hz, 1H), 7.56 – 7.51 (m, 2H), 5.65 (s, 1H), 2.75 (d, J = 2.0 Hz, 1H), 2.62 (s, 1H). **¹³C NMR (101 MHz, CDCl₃)** δ_C ppm 137.4, 133.3, 133.2, 128.7, 128.3, 127.7, 126.4, 126.4, 125.5, 124.5, 83.5, 75.1, 64.6. (The data were in agreement with those published)

1-(Furan-2-yl)prop-2-yn-1-ol[504]
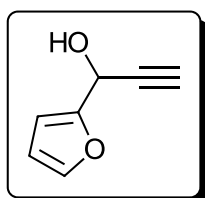
Following general procedure A, using furfural (2.0 mL, 24.0 mmol) and ethynylmagnesium bromide (0.5 M in THF, 72.0 mL, 36 mmol), the title compound was obtained as a dark oil (2.8 g**,** 95%); **¹H NMR (400 MHz, CDCl₃)** δ_H ppm 2.64 (d, 1H, J = 2.0 Hz), 2.72 (d, 1H, J = 7.0 Hz), 5.48 (dd, 1H, J = 2.0, 7.0 Hz), 6.37 (dd, 1H, J = 2.0, 3.0 Hz), 6.48 – 6.50 (m, 1H), 7.43 (dd, 1H, 1.0, 2.0 Hz); **¹³C NMR (101 MHz, CDCl₃)** δ_C ppm 57.9, 74.1, 81.0, 108.0, 110.5, 143.2, 152.4. (The data were in agreement with those published)

1-(1-Methyl-1H-pyrazol-5-yl)prop-2-yn-1-ol[220]
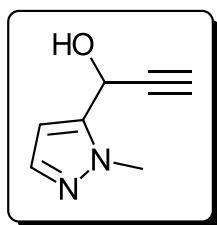
Following general procedure A, using 1-methyl-1*H*-pyrazole-5- carboxaldehyde (2.0 mL, 20.0 mmol) and ethynylmagnesium bromide (0.5 M in THF, 50.0 mL, 25 mmol), the title compound was obtained and used before column chromatography as a brown solid (3.1 g, >99%) . **M.p.** = 106 – 107 °C (lit[220] = 107 °C); **¹H NMR (400 MHz, DMSO-d⁶)** δ_H ppm 3.58 (d, 1H, J = 2.0 Hz), 3.83 (s, 3H), 5.57 (dd, 1H, J = 2.0, 6.0 Hz), 6.24 (d, 1H, J = 6.0 Hz), 6.26 (d, 1H, J = 1.5 Hz), 7.32 (d, 1H, J = 1.5 Hz); **¹³C NMR (101 MHz, DMSO-d⁶)** δ_C ppm 37.2, 55.2, 76.1, 83.0, 105.3, 137.5, 142.1. (The data were in agreement with those published)

1-(Benzyloxy)but-3-yn-2-ol[220]
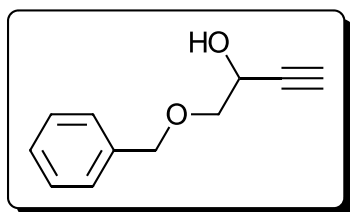
Following general procedure A, using benzyloxyacetaldehyde (1.0 g, 6.7 mmol) and ethynylmagnesium bromide (0.5 M in THF, 27.0 mL, 13.3 mmol), the title compound was obtained as a pale-yellow oil (747 mg, 63%); **^{1}H NMR (400 MHz, CDCl$_3$)** δ_H ppm 2.49 (d, 1H, J = 2.0 Hz), 2.70 (d, 1H, J = 5.0 Hz), 3.61 (dd, 1H, J = 7.0, 10.0 Hz), 3.68 (dd, 1H, J = 3.5, 10.0 Hz), 4.55 – 4.69 (m, 3H), 7.30 – 7.42 (m, 5H); **^{13}C NMR (101 MHz, CDCl$_3$)** δ_C ppm 61.3, 73.4, 73.6, 74.0, 82.3, 128.0, 128.0, 128.6, 137.7. (The data were in agreement with those published)

General procedure B: Preparation of potassium ynol trifluoroborate salts
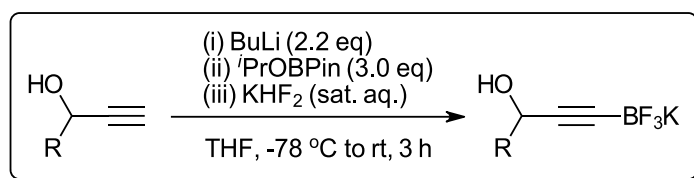
To a solution of terminal alkyne in THF (0.2-0.3 M) at -78 °C, ^{n}butyllithium (~2.5 M in hexanes, 2.2 eq) was added dropwise. The mixture was stirred for 1 hour before adding 2-isopropoxy-4,4,5,5-tetramethyl-1,3,2-dioxaborolane (^{i}PrOBPin) (3 eq) dropwise and allowing it to warm to $^-$20 °C over a period of 2 hours. Potassium hydrogen difluoride (aq, 12 eq) was added slowly and the flask was allowed to warm to room temperature. The resulting mixture was concentrated to dryness *in vacuo* and the product was separated from excess inorganic material by addition of acetone and vigorous stirring for 1 hour followed by filtration. The filtrate was concentrated *in vacuo* and redissolved in the minimum amount of acetone affording a saturated solution. The product was precipitated by adding diethyl ether and isolated by filtration followed by washing with diethyl ether. The precipitate was dried *in vacuo* to give the ynol trifluoroborate salt.

Potassium (3-hydroxy-3-phenylprop-1-yn-1-yl)trifluoroborate[219]
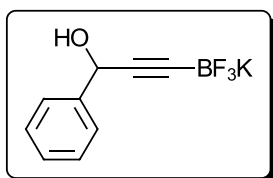
Following general procedure B, using the terminal alkyne (5.0 g, 38 mmol), ^{n}butyllithium (~2.5 M in hexanes, 33.2 mL, 83 mmol), 2-isopropoxy-4,4,5,5-tetramethyl-1,3,2-dioxaborolane (24.0 mL, 113 mmol), potassium hydrogen difluoride (35.0 g, 454 mmol) dissolved in H$_2$O (130 mL) and THF (190 mL), the title compound was obtained as a colourless solid (8.3 g, 92%). **M.p. =** 234 °C (dec) (lit^{219} = 232 – 235 °C); **^{1}H NMR (400 MHz, DMSO-d^6)** δ_H ppm 5.16 (d, J = 5.5 Hz, 1H), 5.59 (d, J = 5.5 Hz, 1H), 7.20 – 7.27 (m, 1H), 7.28 – 7.35 (m, 2H), 7.41 – 7.48 (m, 2H); **^{19}F NMR (376 MHz, DMSO-d^6)** δ_F ppm -131.6; **^{11}B NMR (128 MHz, DMSO-d^6)** δ_B ppm -2.0; **^{13}C NMR (101 MHz, DMSO-d^6)** δ_C ppm 64.0, 90.8, 127.0, 127.4, 128.3, 144.1. (The data were in agreement with those published)

Potassium (3-hydroxy-3-(4-chlorophenyl)prop-1-yn-1-yl)trifluoroborate[220]
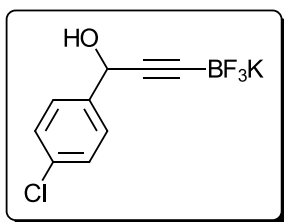
Following general procedure B, using the terminal alkyne (3.0 g, 18 mmol), ^{n}butyllithium (2.41 M in hexanes, 16.5 mL, 39.6 mmol), 2-isopropoxy-4,4,5,5-tetramethyl-1,3,2-dioxaborolane (11.5 mL, 54.0 mmol), potassium hydrogen difluoride (16.9 g, 216.1 mmol) dissolved in H_2O (60 mL) and THF (100 mL), the title compound was obtained as a colourless solid (3.5 g, 71%). **M.p.** = 198 – 200 °C (dec) (lit[220] = >290 °C); **^{1}H NMR (400 MHz, DMSO-d^6)** δ_H ppm 5.18 (s, 1H), 5.73 (s, 1H), 7.36 – 7.41 (m, 2H), 7.44 – 7.49 (m, 2H); **^{19}F NMR (376 MHz, DMSO-d^6)** δ_F ppm -131.7; **^{11}B NMR (128 MHz, DMSO-d^6)** δ_B ppm -2.0; **^{13}C NMR (101 MHz, DMSO-d^6)** δ_C ppm 62.9, 90.4, 128.3, 128.8, 131.9, 143.1. (The data were in agreement with those published)

Potassium (3-hydroxy-3-(4-trifluoromethylphenyl)prop-1-yn-1-yl)trifluoroborate[219]
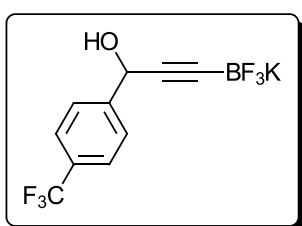
Following general procedure B, using the terminal alkyne (2.5 g, 12.5 mmol), ^{n}Butyllithium (~2.5 M in hexanes, 11.0 mL, 27.5 mmol), 2-isopropoxy-4,4,5,5-tetramethyl-1,3,2-dioxaborolane (7.3 mL, 37.5 mmol), potassium hydrogen difluoride (11.7 g, 150 mmol) dissolved in H_2O (30 mL) and THF (55 mL), the title compound was obtained as a colourless solid (2.3 g, 64%). **M.p.** = 237 - 238 °C (dec) (lit[219] = 238 °C); **^{1}H NMR (400 MHz, DMSO-d^6)** δ_H ppm 5.28 (d, 1H, J = 6.0 Hz), 5.86 (d, 1H, J = 6.0 Hz), 7.66 (d, 2H, J = 8.5 Hz), 7.70 (d, 2H, J = 8.5 Hz); **^{19}F NMR (376 MHz, DMSO-d^6)** δ_F ppm -60.7 (s), -131.3 (m); **^{11}B NMR (128 MHz, DMSO-d^6)** δ_B ppm -2.0; **^{13}C NMR (101 MHz, DMSO-d^6)** δ_C ppm 63.0, 90.2, 124.9 (q, J = 272.0 Hz), 125.3 (q, J = 3.5 Hz), 127.6, 128.1 (q, J = 31.5 Hz), 148.7. (The data were in agreement with those published)

Potassium (3-hydroxy-3-(naphthalen-2-yl)prop-1-yn-1-yl)trifluoroborate
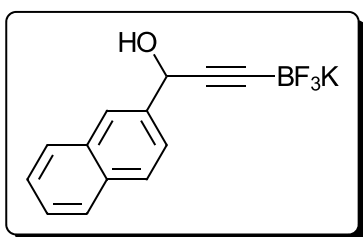
Following general procedure B, using the terminal alkyne (1.8 g, 10 mmol), ^{n}butyllithium (~2.5 M in hexanes, 8.6 mL, 22 mmol), 2-isopropoxy-4,4,5,5-tetramethyl-1,3,2-dioxaborolane (6.0 mL, 29 mmol), potassium hydrogen difluoride (9.0 g, 118 mmol) dissolved in H_2O (30 mL) and THF (41 mL), the title compound was obtained as a colourless solid (0.8 g, 29%). **M.p.** = 210 – 212 °C (dec) **^{1}H NMR (400 MHz, DMSO-d^6)** δ_H ppm 7.94 – 7.86 (m, 4H), 7.63 (dd, J = 8.5, 1.5 Hz, 1H), 7.54 – 7.46 (m, 2H), 5.79 (d, J = 5.5 Hz, 1H), 5.36 (d, J = 4.5 Hz, 1H); **^{19}F NMR (376 MHz, DMSO-d^6)** δ_F ppm -131.5; **^{11}B NMR (128 MHz, DMSO-d^6)** δ_B ppm -1.8; **^{13}C NMR (101 MHz, DMSO-d^6)** δ_C ppm 141.7, 133.2, 132.8, 129.5, 128.3, 128.0, 126.5, 126.2, 125.9, 124.8, 83.6, 63.7. **FTIR** (v_{max}/ cm^{-1}) : 3544 (w), 3465 (w), 3297 (br, w), 3057 (w), 2207 (w), 1601 (m), 1508 (w), 992 (s); **HRMS: (ESI-TOF)** m/z [M-K]$^-$ Calculated for $C_{13}H_9BF_3O$, 249.0704 found 249.0710.

Potassium (3-hydroxy-3-(2-furyl)prop-1-yn-1-yl)trifluoroborate
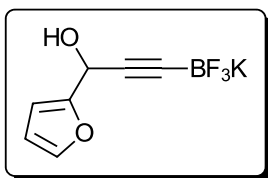
Following general procedure B, using the terminal alkyne (3.0 g, 25 mmol), ^{n}butyllithium (~2.5 M in hexanes, 21.6 mL, 54 mmol), 2-isopropoxy-4,4,5,5-tetramethyl-1,3,2-dioxaborolane (14.4 mL, 74 mmol), potassium hydrogen difluoride (23 g, 300 mmol) dissolved in H_2O (60 mL) and THF (110 mL), the title compound was obtained as a brown solid (1.2 g, 17%). **M.p.** = 153 - 155 °C (dec); **^{1}H NMR (400 MHz, DMSO-d^6)** δ_H ppm 5.15 (d, 1H, J = 6.5 Hz), 5.67 (d, 1H, J = 6.5 Hz), 6.28 (dt, 1H, J = 1.0, 3.0 Hz), 6.38 (dd, 1H, J = 2.0, 3.0 Hz), 7.56 (dd, 1H, J = 1.0, 2.0 Hz); **^{19}F NMR (376 MHz, DMSO-d^6)** δ_F ppm -131.4 (m); **^{11}B NMR (128 MHz, DMSO-d^6)** δ_B ppm -2.1; **^{13}C NMR (101 MHz, DMSO-d^6)** δ_C ppm 57.4, 88.4, 106.6, 110.6, 142.5, 156.2; **FTIR** (v_{max}/ cm^{-1}) 3366, (w), 1970 (w), 1502 (m), 1088 (s), 951(s); **HRMS: (ESI-TOF)** m/z [M-K]$^-$ Calculated for $C_7H_5BF_3O_2$, 189.0335 found 189.0342

Potassium (4-benzyloxy-3-hydroxybut-1-yn-1yl)trifluoroborate[220]
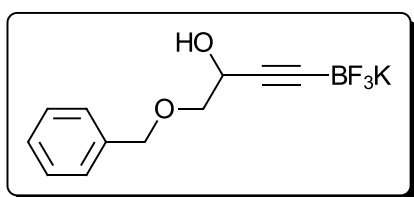
Following general procedure B, using the terminal alkyne (630 mg, 3.6 mmol), ^{n}Butyllithium (~2.5 M in hexanes, 3.2 mL, 7.9 mmol), 2-isopropoxy-4,4,5,5-tetramethyl-1,3,2-dioxaborolane (2.1 mL, 10.7 mmol), potassium hydrogen difluoride (3.4 g, 43 mmol dissolved in H_2O (30 mL)) and THF (16 mL), the title compound was obtained as a colourless solid (623 mg, 61 %). **M.p.** = 168 - 170 °C (dec) (lit[220] = 86 °C); **^{1}H NMR (400 MHz, DMSO-d^6)** δ_H ppm 3.36 – 3.44 (m, 2H), 4.17 – 4.28 (m, 1H), 4.53 (s, 2H), 5.09 (d, 1H, J = 5.5 Hz) 7.25 – 7.40 (m, 5H); **^{19}F NMR (376 MHz, DMSO-d^6)** δ_F ppm -131.7; **^{11}B NMR (128 MHz, DMSO-d^6)** δ_B ppm -2.1; **^{13}C NMR (101 MHz, DMSO-d^6)** δ_C ppm 61.2, 72.4, 75.3, 89.4, 127.8, 128.0, 128.6, 139.0. (The data were in agreement with those published)

General procedure C: Preparation of potassium ynone trifluoroborate salts
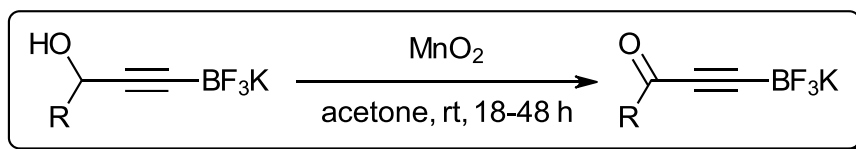
To a stirring suspension of manganese(IV) oxide (5-11 eq) in acetone (0.3 M) was added portion-wise ynol trifluoroborate **3** at room temperature. Upon completion (determined by ^{19}F NMR spectroscopy), the reaction mixture was filtered through a bed of Celite and the filtrate concentrated *in vacuo*. The solid residue was redissolved in the minimum amount of acetone affording a saturated solution. The product was precipitated by adding diethyl ether and isolated by filtration followed by washing with diethyl ether. The precipitate was dried *in vacuo* to give the ynone trifluoroborate salt.

Potassium (3-oxo-3-phenylprop-1-yn-1-yl)trifluoroborate **166**[219]
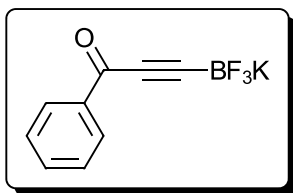
Following general procedure C, using the ynol trifluoroborate (3.5 g, 14.7 mmol), manganese(IV) oxide (12.8 g, 148 mmol) and acetone (50 mL), the reaction was complete after 48 hours giving the title compound as a colourless solid (2.5 g, 71%). **M.p.** = 169 - 170 °C (lit[219] = 143 – 145 °C); **^{1}H NMR (400 MHz, DMSO-d^6)** δ_H ppm 7.53 – 7.60 (m, 2H), 7.64 – 7.71 (m, 1H), 8.04 – 8.10 (m, 2H) ; **^{19}F NMR (376 MHz, DMSO-d^6)** δ_F ppm -133.1 (m); **^{11}B NMR (128 MHz, DMSO-d^6)** δ_B ppm -1.9 (q, J = 33.0 Hz) **^{13}C NMR (101 MHz, DMSO-d^6)** δ_C ppm 88.6, 129.2, 129.4, 134.3, 137.2, 178.7. (The data were in agreement with those published)

Potassium (3-oxo-3-(4-chorophenyl)prop-1-yn-1-yl)trifluoroborate **167**[220]
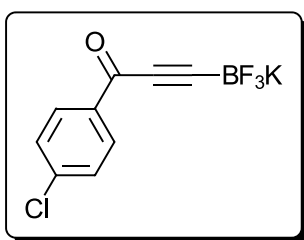
Following general procedure C, using the ynol trifluoroborate (3.0 g, 11 mmol), manganese(IV) oxide (7.7 g, 88 mmol) and acetone (37 mL), the reaction was complete after 18 hours giving the title compound as a colourless solid (2.5 g, 83%). **M.p.** = 251 – 252 °C (lit[220] = >300 °C); **^{1}H NMR (400 MHz, DMSO-d^6)** δ_H ppm 7.63 – 7.68 (m, 2H), 8.03 – 8.08 (m, 2H); **^{19}F NMR (376 MHz, DMSO-d^6)** δ_F ppm -133.2; **^{11}B NMR (128 MHz, DMSO-d^6)** δ_B ppm -1.9 (q, J = 32.0 Hz); **^{13}C NMR (101 MHz, DMSO-d^6)** δ_C ppm 88.5, 129.4, 131.2, 135.9, 139.4, 177.4. (The data were in agreement with those published)

Potassium (3-oxo-3-(4-trifluoromethylphenyl)prop-1-yn-1-yl)trifluoroborate **168**[219]
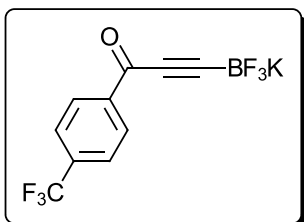
Following general procedure C, using the ynol trifluoroborate (2.0 g, 6.5 mmol), manganese(IV) oxide (6.2 g, 71.5 mmol) and acetone (22 mL), the reaction was complete after 24 hours giving the title compound as a colourless solid (1.0 g, 51%). **M.p.** = 248 °C (dec) (lit[219] = 205 °C); **^{1}H NMR (400 MHz, DMSO-d^6)** δ_H ppm 7.96 (d, 2H, J = 8.0 Hz), 8.24 (d, 2H, J = 8.0 Hz); **^{19}F NMR (376 MHz, DMSO-d^6)** δ_F ppm -61.6 (s), -133.3 (m); **^{11}B NMR (128 MHz, DMSO-d^6)** δ_B ppm -2.0 (q, J = 31.0 Hz) **^{13}C NMR (101 MHz, DMSO-d^6)** δ_C ppm 88.6, 124.2 (q, J = 272.5 Hz), 126.4 (q, J = 3.5 Hz), 130.1, 133.5 (q, J = 32.0 Hz), 140.1, 177.5. (The data were in agreement with those published)

Potassium (3-oxo-3-(naphthalen-2-yl)prop-1-yn-1-yl)trifluoroborate **169**
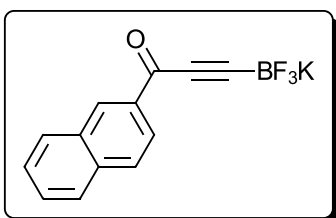
Following general procedure C, using the ynol trifluoroborate (0.6 g, 2.1 mmol), manganese(IV) oxide (0.9 g, 10.4 mmol) and acetone (7 mL), the reaction was complete after 24 hours giving the title compound as a colourless solid (290 mg, 49%). **M.p.** = 155 – 156 °C; **^{1}H NMR (400 MHz, DMSO-d^6)** δ_H ppm 8.70 (s, 1H), 8.17 (d, J = 8.0 Hz, 1H), 8.11 – 8.00 (m, 3H), 7.74 – 7.62 (m, 2H); **^{19}F NMR (376 MHz, DMSO-d^6)** δ_F ppm -132.9 (m); **^{11}B NMR (128 MHz, DMSO-d^6)** δ_B ppm -2.1 (m); **^{13}C NMR (101 MHz, DMSO-d^6)** δ_C ppm 178.5, 135.9, 134.8, 132.4, 131.8, 130.2, 129.5, 129.0, 128.3, 127.7, 124.2, 84.2; **FTIR** (neat, ν_{max} / cm^{-1}) 3637 (w), 3467 (w), 3052 (w), 2188 (w), 1618 (m), 977 (s); **HRMS: (ESI-TOF)** m/z [M-K]$^-$ Calculated for $C_{13}H_7{}^{11}B^{19}F_3O$ 247.0548, found 247.0551.

Potassium (3-oxo-3-(2-furyl)prop-1-yn-1-yl)trifluoroborate **170**
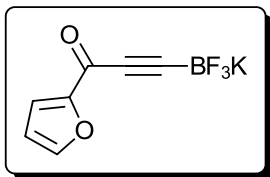
Following general procedure C, using the ynol trifluoroborate (1.0 g, 4.4 mmol), manganese(IV) oxide (3.8 g, 43.9 mmol) and acetone (15 mL), the reaction was complete after 24 hours giving the title compound as a brown solid (381 mg, 38%). **M.p.** = 160 – 165 °C; **^{1}H NMR (400 MHz, DMSO-d^6)** δ_H ppm 6.73 (dd, 1H, J = 1.5, 3.5 Hz), 7.33 (dd, 1H, J = 1.0, 3.5 Hz), 8.02 (dd, 1H, J = 1.0, 1.5 Hz); **^{19}F NMR (376 MHz, DMSO-d^6)** δ_F ppm -133.2 (m); **^{11}B NMR (128 MHz, DMSO-d^6)** δ_B ppm -2.1 (q, J = 32.0 Hz); **^{13}C NMR (101 MHz, DMSO-d^6)** δ_C ppm 88.2, 113.3, 121.0, 149.1, 153.4, 165.7; **FTIR** (neat, v_{max} / cm^{-1}) 1900 (m), 1631 (s), 1572 (s), 1462 (s), 1066 (s), 977 (s); **HRMS: (ESI-TOF)** m/z [M-K]$^-$ Calculated for $C_7H_3BF_3O_2$, 187.0184, found 187.0187.

General procedure D: Preparation of pyrimidin-6-yl trifluoroborates
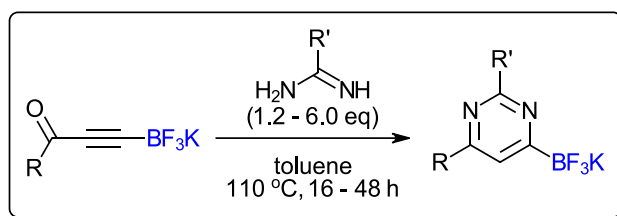
To a stirring suspension of ynone trifluoroborate salt (1.0 eq) in toluene (0.07 M) was added amidine (1.2 – 6.0 eq) and the mixture was heated at reflux for 16-48 hours. Upon completion (determined by ^{19}F NMR spectroscopy), the reaction mixture was cooled and concentrated *in* vacuo. The solid residue was re-dissolved in the minimum amount of acetone affording a saturated solution. The product was precipitated by adding diethyl ether and isolated by filtration or decantation followed by further washing with diethyl ether. The resulting solid was dried thoroughly *in vacuo*, to provide the desired pyrimidin-6-yl trifluoroborate salt.

Potassium (2,6-diphenylpyrimidin-6-yl)trifluoroborate **173**
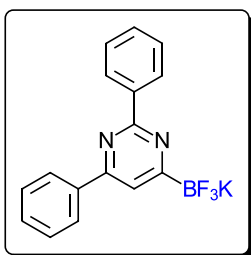
Following general procedure D using **166** (1.00 g, 4.23 mmol) and benzamidine (1.23 g, 10.20 mmol). The reaction was complete within 16 hours, giving **173** as a colourless solid (1.22 g, 85%). **M.p.** = 294 °C (dec); **^{1}H NMR (400 MHz, DMSO-d$_6$)** δ_H ppm 7.48 – 7.59 (m, 6H), 7.78 (s, 1H), 8.24 (dd, 2H, J = 8.0, 1.5 Hz), 8.54 (dd, 2H, J = 8.0, 1.5 Hz); **^{13}C NMR (101 MHz, DMSO-d^6)** δ_C ppm 116.7, 126.7, 127.8, 128.3, 128.9, 129.8, 130.1, 137.9, 139.1, 159.5, 161.8; **^{19}F NMR (376 MHz, DMSO-d^6)** δ_F ppm -142.6; **^{11}B NMR (128 MHz, DMSO-d^6)** δ_B ppm 1.5; **FTIR (neat)** v_{max} / cm^{-1} 3000 (w), 1572 (s), 1514 (s); **HRMS (ESI-TOF)** m/z [M-K]$^-$ calculated for $[C_{16}H_{11}{}^{11}BF_3N_2]^-$ 299.0973, found 299.0985; **Single crystal X-ray analysis**, see appendix 6.

Potassium (2-phenyl-4-(4-chlorophenyl)pyrimidin-6-yl)trifluoroborate **175**
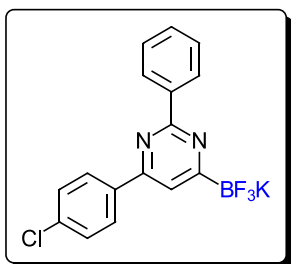
Following general procedure D using **167** (1.00 g, 3.70 mmol) and benzamidine (1.07 g, 8.87 mmol). The reaction was complete within 24 hours, giving **175** as a colourless solid (1.24 g, 90%). **M.p.** = >300 °C; ^{1}**H NMR (400 MHz, DMSO-d$_6$)** δ_H ppm 7.45 – 7.57 (m, 3H), 7.60 (d, 2H, J = 8.5 Hz), 7.78 (s, 1H), 8.29 (d, 2H, J = 8.5 Hz), 8.53 (dd, 2H, J = 8.0, 1.5 Hz); ^{13}**C NMR (101 MHz, DMSO-d^6)** δ_C ppm 116.6, 127.8, 128.3, 128.5, 128.9, 129.9, 134.9, 136.7, 138.9, 158.3, 161.8; ^{19}**F NMR (376 MHz, DMSO-d^6)** δ_F ppm -142.6; ^{11}**B NMR (128 MHz, DMSO-d^6)** δ_B ppm 1.4; **FTIR (neat)** ν_{max} / cm^{-1} 3096 (w), 1513 (m), 972 (s); **HRMS (ESI-TOF)** *m/z* [M-K]$^-$ calculated for [C$_{16}$H$_{10}$^{11}B^{35}ClF$_3$N$_2$]$^-$ 333.0583, found 333.0594.

Potassium (2-phenyl-4-(4-trifluoromethylphenyl)pyrimidin-6-yl)trifluoroborate **176**
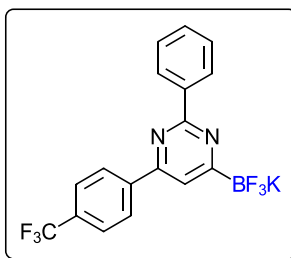
Following general procedure D using **168** (900 mg, 2.96 mmol) and benzamidine (1.35 g, 11.24 mmol). The reaction was complete within 16 hours, giving **176** as a colourless solid (1.08 g, 90%). **M.p.** = 297 °C (dec); ^{1}**H NMR (400 MHz, DMSO-d^6)** δ_H ppm 7.49 – 7.57 (m, 3H), 7.88 (s, 1H), 7.91 (d, 2H, J = 8.0 Hz), 8.48 (d, 2H, J = 8.0 Hz), 8.56 (dd, 2H, J = 8.0, 1.5 Hz); ^{13}**C NMR (101 MHz, DMSO-d^6)** δ_C ppm 117.3, 124.3 (q, J = 272.0 Hz), 125.8 (q, J = 3.5 Hz), 127.6, 127.8, 128.4, 130.0, 130.1 (q, J = 32.0 Hz), 138.8, 141.8, 158.1, 162.0; ^{19}**F NMR (376 MHz, DMSO-d^6)** δ_F ppm -142.7, -61.2; ^{11}**B NMR (128 MHz, DMSO-d^6)** δ_B ppm 1.7; **FTIR (neat)** ν_{max} / cm^{-1} 3393 (w), 1512 (m), 1328 (m), 978 (s); **HRMS (ESI-TOF)** *m/z* [M-K]$^-$ calculated for [C$_{17}$H$_{10}$^{11}BF$_6$N$_2$]$^-$ 367.0847, found 367.0855.

Potassium (2-phenyl-4-(naphthalen-2-yl)pyrimidin-6-yl)trifluoroborate **177**
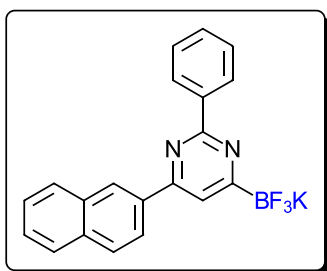
Following general procedure D using **169** (100 mg, 0.35 mmol) and benzamidine (84 mg, 0.70 mmol). The reaction was complete within 40 hours, giving **177** as a colourless solid (94 mg, 69%). **M.p.** = 255-256 °C (dec); ^{1}**H NMR (400 MHz, DMSO-d^6)** δ_H ppm 7.48 – 7.64 (m, 5H), 7.95 – 8.03 (m, 2H), 8.09 (d, 1H, J = 8.5 Hz), 8.14 – 8.21 (m, 1H), 8.44 (d, 1H, J = 8.5 Hz), 8.61 (d, 2H, J = 7.0 Hz), 8.85 (s, 1H); ^{13}**C NMR (101 MHz, DMSO-d^6)** δ_C ppm 117.5, 124.5, 126.9 (x2C), 127.5, 128.0, 128.3, 128.8, 128.9, 129.4, 130.2, 133.5, 134.3, 135.8, 139.5, 159.9, 162.3; ^{19}**F NMR (376 MHz, DMSO-d^6)** δ_F ppm -142.6; ^{11}**B NMR (128 MHz, DMSO-d^6)** δ_B ppm 1.8; **FTIR (neat)** ν_{max} / cm^{-1} 3064 (w), 1572 (w), 1519 (m), 1365 (m), 969 (s); **HRMS (ESI-TOF)** *m/z* [M-K]$^-$ calculated for [C$_{20}$H$_{13}$^{11}BF$_3$N$_2$]$^-$ 349.1129, found 349.1140.

Potassium (2-phenyl-4-(2-furyl)pyrimidin-6-yl)trifluoroborate **178**
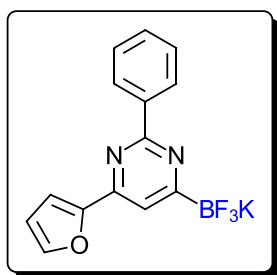
Following general procedure D using **170** (280 mg, 1.24 mmol) and benzamidine (744 mg, 6.19 mmol). The reaction was complete within 16 hours, giving **178** as a dark brown solid (154 mg, 38%). **M.p.** = 246 °C (dec); **^{1}H NMR (400 MHz, DMSO-d^6)** δ_H ppm 6.71 (dd, 1H, J = 3.5, 2.0 Hz), 7.38 (dd, 1H, J = 0.5, 3.5 Hz), 7.47 – 7.55 (m, 3H), 7.58 (s, 1H), 7.93 (dd, 1H, J = 0.5, 1.5 Hz), 8.47 – 8.51 (m, 2H); **^{13}C NMR (101 MHz, DMSO-d^6)** δ_C ppm 111.3, 112.9, 115.1, 128.2, 128.7, 130.3, 139.2, 145.6, 152.5, 153.1, 162.1; **^{19}F NMR (376 MHz, DMSO-d^6)** δ_F ppm -142.9; **^{11}B NMR (128 MHz, DMSO-d^6)** δ_B ppm 1.6; **FTIR (neat)** v_{max} / cm^{-1} 3095 (w), 1522 (s), 970 (s); **HRMS (ESI-TOF)** m/z [M-K]- calculated for [C$_{14}$H$_9$^{11}BF$_3$N$_2$O]$^-$ 289.0766 found 289.0771.

Potassium (2-phenyl-4-tert-butylpyrimidin-6-yl)trifluoroborate **179**
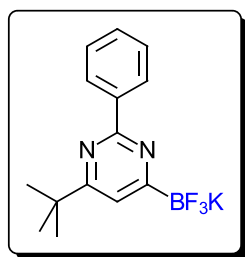
Following general procedure D using potassium (3-tert-butyl-3-oxoprop-1-yn-1-yl)trifluoroborate[219] (obtained from Prisca Fricero, used without further purification) (1.00 g, 4.63 mmol) and benzamidine (1.30 g, 10.82 mmol). The reaction was complete within 16 hours, giving **179** as a colourless solid (1.03 g, 70%). **M.p.** >300 °C; **^{1}H NMR (400 MHz, DMSO-d^6)** δ_H ppm 1.34 (s, 9H), 7.32 (s, 1H), 7.43 – 7.51 (m, 3H), 8.44 (dd, 2H, J = 8.0, 1.5 Hz); **^{13}C NMR (101 MHz, DMSO-d^6)** δ_C ppm 29.4, 64.9, 116.4, 127.6, 128.2, 129.4, 139.5, 160.8, 172.9; **^{19}F NMR (376 MHz, DMSO-d^6)** δ_F ppm -142.4; **^{11}B NMR (128 MHz, DMSO-d^6)** δ_B ppm 1.4; **FTIR (neat)** v_{max} / cm^{-1} 2962 (w), 2922 (w), 2903 (w), 2870 (w), 1569 (w), 1516 (m); **HRMS (ESI-TOF)** m/z [M-K]$^-$ calculated for [C$_{14}$H$_{15}$^{11}BF$_3$N$_2$]$^-$ 279.1286, found 279.1288.

Potassium 2-(4-trifluoromethylphenyl)-4-phenylpyrimidin-6-yl)trifluoroborate **186**
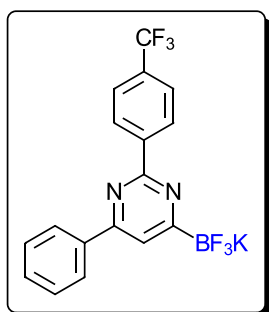
Following general procedure D using **166** (50 mg, 0.21 mmol) and (4-trifluoromethyl)benzamidine (80 mg, 0.51 mmol). The reaction was complete within 16 hours, giving **186** as a colourless solid (66 mg, 77%). **M.p.** 243-244 °C (dec); **^{1}H NMR (400 MHz, CD$_3$CN)** δ_H ppm 7.49 – 7.58 (m, 3H), 7.80 (d, 2H, J = 8.0 Hz), 7.96 (s, 1H), 8.26 – 8.33 (m, 2H), 8.70 (d, 2H, J = 8.0 Hz); **^{13}C NMR (101 MHz, CD$_3$CN)** δ_C ppm 118.6, 125.6 (q, J = 271.0 Hz), 126.3 (q, J = 3.5 Hz), 128.1, 129.5, 129.8, 131.3, 131.6 (q, J = 32.0 Hz), 139.0, 144.3, 162.0, 162.6; **^{19}F NMR (376 MHz, CD$_3$CN)** δ_F ppm -63.0, -145.6; **^{11}B NMR (128 MHz, CD$_3$CN)** δ_B ppm 1.6; **FTIR (neat)** v_{max} / cm^{-1} 3145 (w), 1573 (m), 1513 (s), 1318 (s), 980 (s), 971 (s); **HRMS (ESI-TOF)** m/z [M-K]$^-$ calculated for [C$_{17}$H$_{10}$^{11}BF$_6$N$_2$]$^-$ 367.0841, found 367.0855.

Potassium 2-(4-fluorophenyl)-4-phenylpyrimidin-6-yl)trifluoroborate 181
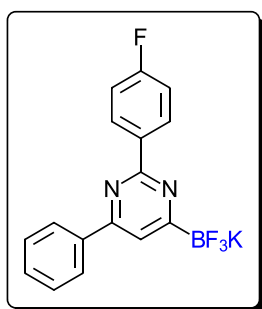
Following general procedure D using **166** (83 mg, 0.35 mmol) and (4-fluoro)benzamidine (97 mg, 0.70 mmol). The reaction was complete within 24 hours giving **181** as a colourless solid (88 mg, 68%). **M.p.** 292-293 °C (dec); **^{1}H NMR (400 MHz, DMSO-d^6)** δ$_H$ ppm 7.28 – 7.40 (m, 2H), 7.49 – 7.61 (m, 3H), 7.79 (s, 1H), 8.24 (dd, 2H, J = 8.0, 1.0 Hz), 8.59 (dd, 2H, J = 8.5, 6.0 Hz); **^{13}C NMR (101 MHz, DMSO-d^6)** δ$_C$ ppm 115.2 (d, J = 21.5 Hz), 116.7, 126.7, 128.9, 130.0 (d, J = 8.5 Hz), 130.2, 135.6 (d, J = 2.5 Hz), 137.8, 159.6, 161.0, 163.5 (d, J = 246.5 Hz); **^{19}F NMR (376 MHz, DMSO-d^6)** δ$_F$ ppm -112.3, -142.7; **^{11}B NMR (128 MHz, DMSO-d^6)** δ$_B$ ppm 1.6; **FTIR (neat)** ν$_{max}$ / cm^{-1} 3596 (w), 3146 (w), 1668 (w), 1603 (w), 1574 (w), 1507 (w), 1349 (w), 997 (s); **HRMS (ESI-TOF)** *m/z* [M-K]$^-$ calculated for [C$_{16}$H$_{10}$^{11}BF$_4$N$_2$]$^-$ 317.0873, found 317.0887.

Potassium 2-(4-chlorophenyl)-4-phenylpyrimidin-6-yl)trifluoroborate 182
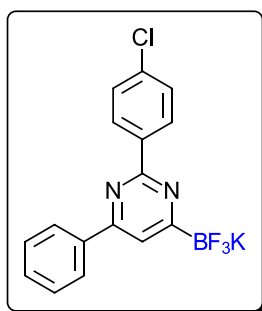
Following general procedure D using **166** (83 mg, 0.35 mmol) and (4-chloro)benzamidine (110 mg, 0.70 mmol). The reaction was complete within 24 hours, giving **182** as a colourless solid (100 mg, 77%). **M.p.** 280-281 °C (dec); **^{1}H NMR (400 MHz, DMSO-d^6)** δ$_H$ ppm 7.46 – 7.68 (m, 5H), 7.80 (s, 1H), 8.24 (dd, 2H, J = 7.5, 1.0 Hz), 8.56 (d, 2H, J = 8.5 Hz); **^{13}C NMR (101 MHz, DMSO-d^6)** δ$_C$ ppm 116.9, 126.7, 128.4, 128.9, 129.5, 130.2, 134.7, 137.7, 137.9, 159.6, 160.8; **^{19}F NMR (376 MHz, DMSO-d^6)** δ$_F$ ppm -142.7; **^{11}B NMR (128 MHz, DMSO-d^6)** δ$_B$ ppm 1.7; **FTIR (neat)** ν$_{max}$ / cm^{-1} 3070 (w), 1591 (w), 1514 (s), 1350 (s), 974 (s); **HRMS (ESI-TOF)** *m/z* [M-K]$^-$ calculated for [C$_{16}$H$_{10}$^{11}B^{35}ClF$_3$N$_2$]$^-$ 333.0578, found 333.0594.

Potassium 2-(4-bromophenyl)-4-phenylpyrimidin-6-yl)trifluoroborate 183
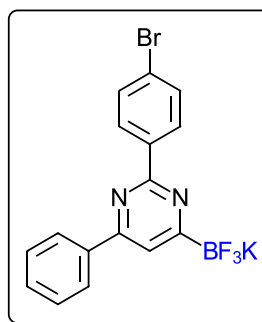
Following general procedure D using **166** (83 mg, 0.35 mmol) and (4-bromo)benzamidine (139 mg, 0.70 mmol). The reaction was complete within 24 hours, giving **183** as a colourless solid (62 mg, 42%). **M.p.** 234 – 235 °C (dec); **^{1}H NMR (400 MHz, DMSO-d^6)** δ$_H$ ppm 7.59 – 7.50 (m, 3H), 7.76 – 7.70 (m, 2H), 7.80 (s, 1H), 8.24 (dd, J = 8.0, 1.5 Hz, 2H), 8.52 – 8.47 (m, 2H); **^{13}C NMR (101 MHz, DMSO-d^6)** δ$_C$ ppm 117.4, 124.0, 127.2, 129.4, 130.3, 130.7, 131.8, 138.1, 138.7, 160.1, 161.4; **^{19}F NMR (376 MHz, DMSO-d^6)** δ$_F$ ppm -142.7; **^{11}B NMR (128 MHz, DMSO-d^6)** δ$_B$ ppm 1.5; **FTIR (neat)** ν$_{max}$ / cm^{-1} 3066 (w), 1636 (w), 1589 (m), 1513 (s), 1350 (s), 973 (s); **HRMS (ESI-TOF)** *m/z* [M-K]$^-$ calculated for [C$_{16}$H$_{10}$^{11}B^{79}BrF$_3$N$_2$]$^-$ 377.0078, found 377.0084.

Potassium 2-cyclopropyl-4-phenylpyrimidin-6-yl)trifluoroborate **187**
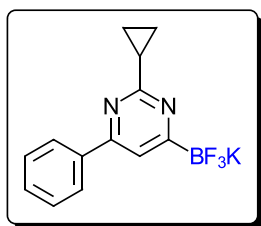
Following general procedure D using **166** (250 mg, 1.06 mmol) and (4-cyclopropyl)benzamidine (535 mg, 6.36 mmol). The reaction was complete within 16 hours, giving **187** as a tan solid (163 mg, 51%). **M.p.** 295 °C (dec); **^{1}H NMR (400 MHz, DMSO-d^6)** δ_H ppm 0.93 – 0.99 (m, 2H), 1.02 – 1.07 (m, 2H), 2.22 (tt, 1H, J = 8.0, 5.0 Hz), 7.43 – 7.55 (m, 3H), 7.60 (s, 1H), 8.04 – 8.10 (m, 2H); ^{13}**C NMR (101 MHz, DMSO-d^6)** δ_C ppm 9.9, 18.5, 116.0, 127.0, 129.2, 130.3, 138.5, 159.6, 169.3; ^{19}**F NMR (376 MHz, DMSO-d^6)** δ_F ppm -142.6; ^{11}**B NMR (128 MHz, DMSO-d^6)** δ_B ppm 1.5; **FTIR (neat)** v_{max} / cm^{-1} 3096 (w), 1575 (s), 1520 (s), 1009 (s), 981 (s); **HRMS (ESI-TOF)** m/z [M-K]$^-$ calculated for [C$_{13}$H$_{11}$^{11}BF$_3$N$_2$]$^-$ 263.0973, found 263.0981.

Potassium (2-(4-methoxy-1H-indol-3-yl)-4-phenylpyrimidin-6-yl)trifluoroborate **184**
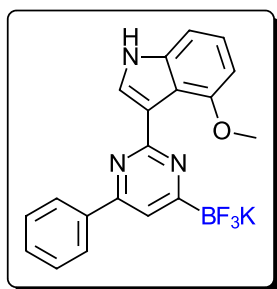
Following general procedure D using **166** (83 mg, 0.35 mmol) and 4-methoxy-1*H*-indole-3-carboximidamide (80 mg, 0.42 mmol), added portion-wise. The reaction was complete within 16 hours, giving **184** as a light brown solid (75 mg, 53%). **M.p** = 174-175 °C (dec); ^{1}**H NMR (400 MHz, DMSO-d$_6$)** δ_H ppm 3.93 (s, 3H), 6.72 (d, 1H, J = 5.5 Hz), 7.09 – 7.18 (m, 2H), 7.51 – 7.60 (m, 3H), 7.73 – 7.82 (s, 1H), 8.18 (s, 1H), 8.30 – 8.38 (m, 2H); ^{13}**C NMR (101 MHz, DMSO-d^6)** δ_C ppm 55.7, 102.0, 103.4, 106.1, 114.3, 114.8, 123.3, 124.5, 127.5, 128.9, 131.0, 138.8, 139.1, 151.6, 153.1, 160.3; ^{19}**F NMR (376 MHz, DMSO-d^6)** δ_F ppm -143.3; ^{11}**B NMR (128 MHz, DMSO-d^6)** δ_B ppm 1.3; **FTIR (neat)** v_{max} / cm^{-1} 3351 (w), 3069 (w), 1576 (s), 1525 (m), 1509 (s), 1485 (w), 1086 (s); **HRMS (ESI-TOF)** m/z [M-K]$^-$ calculated for [C$_{19}$H$_{14}$^{11}B^{19}F$_3$N$_3$O]$^-$ 368.1188, found 368.1196.

Potassium (2-(4-pyridyl)-4-phenylpyrimidin-6-yl)trifluoroborate **185**
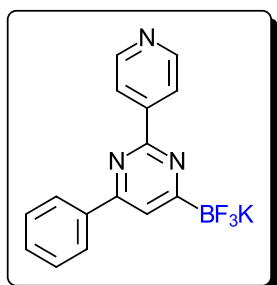
Following general procedure D using **166** (100 mg, 0.42 mmol) and isonicotinamidine (103 mg, 0.85 mmol). The reaction was complete within 16 hours, giving **185** as a colourless solid (117 mg, 81%). **M.p** = 272-273 °C (dec); ^{1}**H NMR (400 MHz, DMSO-d$_6$)** δ_H ppm 7.51 – 7.61 (m, 3H), 7.90 (s, 1H), 8.27 (dd, 2H, J = 8.0, 1.5 Hz), 8.42 (dd, 2H, J = 4.5, 1.5 Hz), 8.76 (dd, 2H, J = 4.5, 1.5 Hz); ^{13}**C NMR (101 MHz, DMSO-d^6)** δ_C ppm 118.0, 121.8, 126.8, 129.0, 130.4, 137.4, 146.1, 150.2, 159.9, 160.1; ^{19}**F NMR (376 MHz, DMSO-d^6)** δ_F ppm -142.7; ^{11}**B NMR (128 MHz, DMSO-d^6)** δ_B ppm 1.7; **FTIR (neat)** v_{max} / cm^{-1} 3042 (w), 2966 (w), 1555 (m), 1507 (s), 1004 (s), 963 (s); **HRMS (ESI-TOF)** m/z [M-K]$^-$ calculated for [C$_{15}$H$_{10}$^{11}B^{19}F$_3$N$_3$]$^-$ 300.0925, found 300.0932.

Preparation of potassium (2-trifluoromethyl-4-phenylpyrimidin-6-yl)trifluoroborate 188
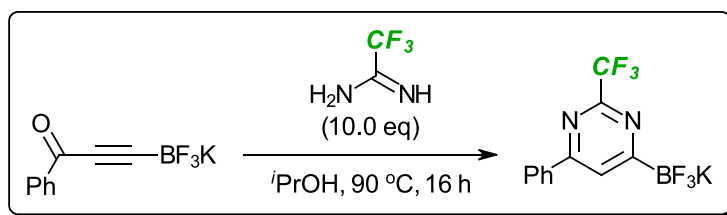
A sealable tube charged with **166** (100 mg, 0.4 mmol) was flushed with argon three times, isopropanol (4 mL) and trifluoroacetamidine (325 µL, 4.2 mmol) were then added via syringe and the mixture was sealed. The reaction mixture was heated at reflux for 16 hours, before being cooled to room temperature and concentrated *in vacuo*. The residue was dissolved in the minimum amount of acetone and the product precipitated by addition of Et$_2$O. The product was isolated by filtration, giving the title compound as a colourless solid (81 mg, 58%). **M.p.** = 167 °C (dec); **^{1}H NMR (400 MHz, DMSO-d^6)** δ_H ppm 7.55 – 7.58 (m, 3H), 8.08 (s, 1H), 8.15 – 8.21 (m, 2H); **^{13}C NMR (101 MHz, DMSO-d^6)** δ_C ppm 120.87 (q, J = 276.0 Hz), 120.91, 127.4, 129.6, 131.5, 136.4, 155.0 (q, J = 33.5 Hz), 161.2; **^{19}F NMR (376 MHz, DMSO-d^6)** δ_F ppm -68.7 (s), -143.1 (m); **^{11}B NMR (128 MHz, acetone-d^6)** δ_B ppm 1.6; **FTIR** (ν_{max}/cm^{-1}) 3301 (w), 3213 (w), 1594 (m), 1353 (m), 986 (s), 775 (s); **HRMS (ESI-TOF)** *m/z* [M-K]$^-$ calculated for [C$_{11}$H$_6$BF$_6$N$_2$]$^-$ 291.0534, found 291.0546.

General procedure E: Preparation of 2-aminopyrimidin-6-yl trifluoroborates
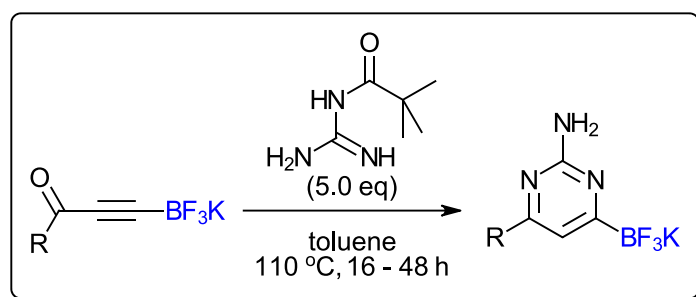
To a stirring suspension of ynone in toluene (0.07 M) at room temperature was added *N*-carbamimidoyl pivalamide[4] (5 eq) in one portion. The mixture was heated at reflux until the reaction was complete, then cooled to room temperature and concentrated *in vacuo*. The residue was then suspended in acetone, and Et$_2$O was added slowly from a dropping funnel (typically ~10 times the volume of acetone). The mixture was then filtered and the resultant solid was washed with Et$_2$O then dried *in vacuo* to provide the corresponding potassium (aminopyrimidine)trifluoroborate salt **3**.

Potassium (2-amino-4-phenylpyrimidin-6-yl)trifluoroborate **190**
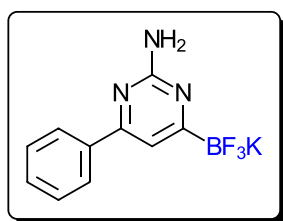
Following general procedure E using **166** (500 mg, 2.12 mmol) and *N*-carbamimidoyl pivalamide (1.52 g, 10.59 mmol). The reaction was complete within 16 hours, giving **190** as a tan solid (534 mg, 91%). **M.p.** = 262-263 °C; **^{1}H NMR (400 MHz, DMSO-d$_6$)** δ_H ppm 6.12 (s, 2H), 7.07 (s, 1H), 7.35 – 7.56 (m, 3H), 7.90 – 8.06 (m, 2H); ^{13}**C NMR (101 MHz, DMSO-d^6)** δ_C ppm 108.7, 126.3, 128.5, 129.3, 138.8, 160.1, 163.2; **^{19}F NMR (376 MHz, DMSO-d^6)** δ_F ppm -142.7; **^{11}B NMR (128 MHz, DMSO-d^6)** δ_B ppm 1.4; **FTIR (neat)** v_{max} / cm^{-1} 3474 (m), 3308 (m), 3193 (m), 3064 (m), 1619 (m), 1577 (s), 1527 (s), 969 (s); **HRMS (ESI-TOF)** *m/z* [M-K]$^-$ calculated for [C$_{10}$H$_8$^{11}BF$_3$N$_3$]$^-$ 238.0769, found 238.0772.

Potassium (2-amino-4-(naphthalen-2-yl)pyrimidin-6-yl)trifluoroborate **193**
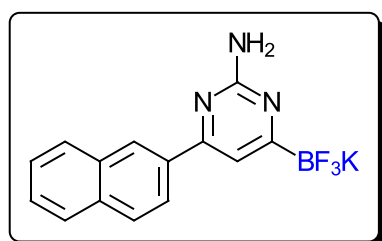
Following general procedure E using **169** (100 mg, 0.35 mmol) and *N*-carbamimidoyl pivalamide (250 mg, 1.75 mmol). The reaction was complete within 48 hours, giving **193** as a tan solid (92 mg, 80%). **M.p.** = 235-236°C (dec); **^{1}H NMR (400 MHz, DMSO-d$_6$)** δ_H ppm 6.16 (br, 2H), 7.27 (s, 1H), 7.55 (m, 2H), 7.87 – 8.12 (m, 3H), 8.16 (d, 1H, J = 7.5 Hz), 8.58 (s, 1H); ^{13}**C NMR (101 MHz, DMSO-d^6)** δ_C ppm 109.0, 124.2, 125.8, 126.4, 126.7, 127.5, 128.0, 128.7, 133.0, 133.6, 136.1, 160.1, 163.2; **^{19}F NMR (376 MHz, DMSO-d^6)** δ_F ppm -142.6; **^{11}B NMR (128 MHz, DMSO-d^6)** δ_B ppm 1.5; **FTIR (neat)** v_{max} / cm^{-1} 3467 (w), 3305 (w), 3189 (w), 1526 (s), 954 (s); **HRMS (ESI-TOF)** *m/z* [M-K]$^-$ calculated for [C$_{14}$H$_{10}$^{11}BF$_3$N$_3$]$^-$ 288.0925, found 288.0930.

Potassium (2-amino-4-(1-methyl-1*H*-pyrazol-5-yl)pyrimidin-6-yl)trifluoroborate **194**
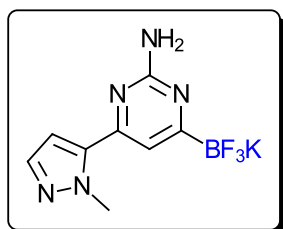
Following general procedure E using potassium (3-(1-methylpyrazol-5-yl)-3-oxoprop-1-yn-1-yl)trifluoroborate[220] (obtained from Prisca Fricero, used without further purification) (400 mg, 1.67 mmol) and *N*-carbamimidoyl pivalamide (1.20 g, 8.35 mmol). The reaction was complete within 16 hours, giving **194** as a tan solid (427 mg, 92%). **M.p.** = 288-289 °C (dec); **^{1}H NMR (400 MHz, DMSO-d$_6$)** δ_H ppm 4.15 (s, 3H), 6.21 (br, 2H), 6.67 (d, 1H, J = 1.0 Hz), 6.85 (s, 1H), 7.43 (d, 1H, J = 1.0 Hz); ^{13}**C NMR (101 MHz, DMSO-d^6)** δ_C ppm 39.4, 106.7, 110.7, 137.7, 140.5, 153.7, 162.5; **^{19}F NMR (376 MHz, DMSO-d^6)** δ_F ppm -142.9; **^{11}B NMR (128 MHz, DMSO-d^6)** δ_B ppm 1.4; **FTIR (neat)** v_{max} / cm^{-1} 3469 (m), 3325 (m), 3212 (m), 3114 (w), 2951 (w), 1633 (m), 1526 (m), 974 (s); **HRMS (ESI-TOF)** *m/z* [M-K]$^-$ calculated for [C$_8$H$_8$^{11}BF$_3$N$_5$]$^-$ 242.0825, found 242.0832.

Potassium (2-amino-4-(1-Boc-piperidin-4-yl)pyrimidin-6-yl)trifluoroborate **195**
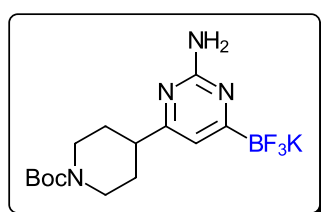
Following general procedure E using potassium (3-((1-tert-butylcarboxylato)piperidin-4-yl)-3-oxoprop-1-yn-1-yl)trifluoroborate[220] (obtained from Prisca Fricero, used without further purification) (160 mg, 0.47 mmol) and *N*-carbamimidoyl pivalamide (334 mg, 2.33 mmol). The reaction was complete within 16 hours, giving **195** as a tan solid (115 mg, 64%). **M.p.** = 207-208 °C (dec); **^{1}H NMR (400 MHz, DMSO-d$_6$)** δ_H ppm 1.26 – 1.52 (m, 11H), 1.71 (dd, 2H, J = 13.0, 2.0 Hz), 2.40 – 2.48 (m, 1H), 2.62 – 2.89 (m, 2H), 3.90 – 4.10 (m, 2H), 5.84 (br, 2H), 6.44 (s, 1H); ^{13}**C NMR (101 MHz, DMSO-d^6)** δ_C ppm 28.1, 30.7, 42.9, 59.8, 78.5, 110.3, 153.9, 162.7, 169.1; **^{19}F NMR (376 MHz, DMSO-d^6)** δ_F ppm -142.7; **^{11}B NMR (128 MHz, DMSO-d^6)** δ_B ppm 1.5; **FTIR (neat)** v_{max} / cm^{-1} 3461 (m), 3319 (m), 3174 (m), 2975 (m), 1628 (s), 1531

(s), 1428 (m), 963 (m); **HRMS (ESI-TOF)** *m/z* [M-K]⁻ calculated for [C₁₄H₂₁ ¹¹BF₃N₄O₂]⁻ 345.1715, found 345.1726.

Preparation of Potassium (2-acetamido-4-phenylpyrimidin-6-yl)trifluoroborate 189
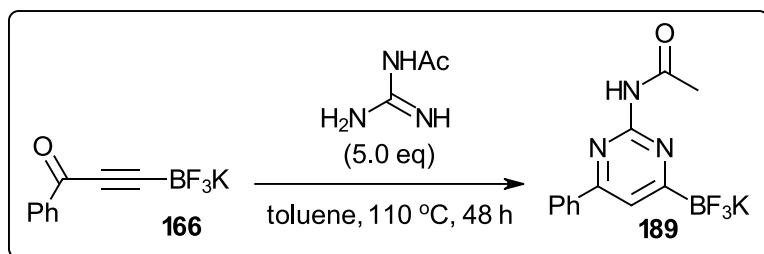
To a slurry of **166** (83 mg, 0.35 mmol) in toluene at reflux was added portion-wise *N*-acetylguanidine (177 mg, 1.75 mmol). The mixture was heated with stirring until completion (within 48 h) then cooled to rt and concentrated *in vacuo*. The crude residue was dissolved in a minimal quantity of acetone and Et₂O was added. The resultant precipitate was collected and dried thoroughly *in vacuo*, affording the title compound as a colourless solid (41 mg, 36%). **M.p. =** 199 – 200 °C; **¹H NMR (400 MHz, DMSO-d⁶)** δ_H ppm 2.28 (s, 3H), 7.54 – 7.48 (m, 3H), 7.56 (s, 1H), 8.11 (dd, J = 2.0, 7.5 Hz, 2H); ¹³**C NMR (101 MHz, DMSO-d⁶)** δ_C ppm 25.2, 114.2, 127.2, 129.3, 130.7, 137.9, 157.7, 159.3, 160.9; **¹⁹F NMR (376 MHz, DMSO-d⁶)** δ_F ppm -142.8; **¹¹B NMR (128 MHz, DMSO-d⁶)** δ_B ppm 1.2; **FTIR (neat)** ν_max / cm⁻¹ 2704 (w), 1672 (m), 1595 (s), 1578 (s), 1522 (s); **HRMS (ESI-TOF)** *m/z* [M-K]⁻ calculated for [C₁₂H₁₀¹¹B¹⁹F₃N₃O]⁻ 280.0875, found 280.0883.

Preparation of *N*-(amino(pivalamido)methylene)pivalamide 198
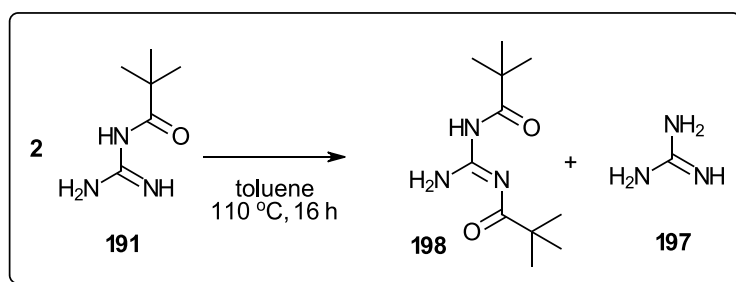
To a flask charged with *N*-carbamimidoylpivalamide (1.25 g, 8.75 mmol) under argon was added toluene (25 mL). The resultant slurry was heated at reflux with stirring for 16 hours, then cooled to ambient temperature and concentrated *in vacuo*. The crude product was then purified by flash column chromatography on silica gel (eluting with 10% MeOH in CH₂Cl₂), affording the title compound as a colourless solid (131 mg, 13%). **M.p. =** 109 – 110 °C; **¹H NMR (400 MHz, DMSO-d₆)** δ_H ppm 1.15 (s, 18H), 8.69 (s, 2H), 12.48 (s, 1H); ¹³**C NMR (101 MHz, DMSO-d⁶)** δ_C ppm 27.1, 40.5, 158.3, 180.6, 192.6;

FTIR (neat) v_{max} / cm^{-1} 3377 (m), 3166 (w), 2971 (m), 2931 (m), 2868 (w), 1697 (s), 1640 (s), 1566 (s); **HRMS (ESI-TOF)** *m/z* [M+H]$^+$ calculated for [C$_{11}$H$_{22}$N$_3$O$_2$]$^+$ 228.1706, found 228.1706.

Preparation of tetra-*n*-butylammonium (2-amino-4-phenylpyrimidin-6-yl)trifluoroborate
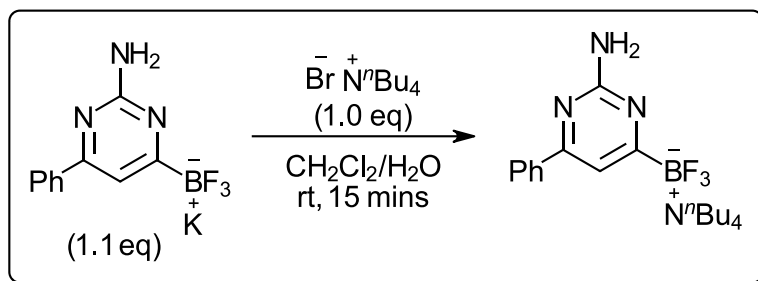
To a slurry of **190** (500 mg, 1.80 mmol) and tetra-*n*-butylammonium bromide (529 mg, 1.60 mmol) in CH$_2$Cl$_2$ (4 mL) was added dropwise H$_2$O (1 mL). The solution was stirred rapidly for 15 minutes then allowed to settle. The layers were separated and the aqueous layer was extracted with CH$_2$Cl$_2$ (5 x 4 mL), the combined organic layers were then dried over anhydrous MgSO$_4$ and concentrated *in vacuo*, affording the title compound as a tan solid (677 mg, 88%). **M.p. =** 125 − 126 °C; **^{1}H NMR (400 MHz, CDCl$_3$)** δ_H ppm 0.90 (t, 12H, J = 7.5 Hz), 1.24 − 1.37 (m, 8H), 1.41 − 1.54 (m, 8H), 2.99 − 3.14 (m, 8H), 5.61 (s, 2H), 7.36 − 7.44 (m, 4H), 7.97 − 8.05 (m, 2H); ^{13}**C NMR (101 MHz, DMSO-d^6)** δ_C ppm 163.6, 160.4, 139.3, 129.7, 128.9, 126.8, 109.2, 58.0, 23.5, 19.7, 14.0; **^{19}F NMR (376 MHz, DMSO-d^6)** δ_F ppm -142.6; **^{11}B NMR (128 MHz, DMSO-d^6)** δ_B ppm 1.3; **FTIR (neat)** v_{max} / cm^{-1} 3505 (w), 3272 (w), 3114 (w), 2960 (w), 2875 (w), 1624 (m), 1567 (m), 1524 (s); **HRMS (ESI-TOF)** *m/z* [M-N^{n}Bu$_4$]$^-$ calculated for [C$_{10}$H$_8$^{11}B^{19}F$_3$N$_3$]$^-$ 238.0769, found 238.0771.

Condensation of *N*-aryl/alkyl guanidines

Preparation of 2-((4-chorophenyl)amino)-4-phenylpyrimidin-6-yl trifluoroborate 200
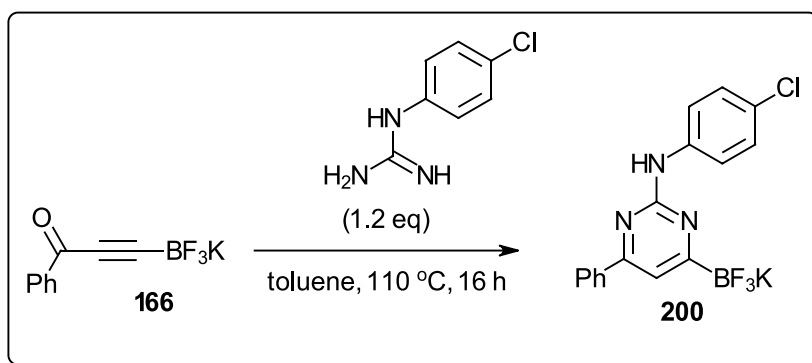
To a slurry of **166** (174 mg, 0.74 mmol) in toluene (11 mL) was added (4-chlorophenyl)guanidine (150 mg, 0.88 mmol). The mixture was heated at reflux for 16 h then cooled to room temperature and concentrated *in vacuo*. The crude mixture was dissolved in acetone, and Et$_2$O was added. The resultant precipitate was collected. Cooling the mixture to 0 $^{\circ}$C provided a second crop of product. The solids were combined, washed with Et$_2$O and dried *in vacuo* to give **200** as a yellow solid (178 mg, 62%). **M.p. = 156-157 $^{\circ}$C (dec); ^{1}H NMR (400 MHz, DMSO-d^6)** δ_H ppm 7.31 (d, 2H, J = 9.0 Hz), 7.33 (s, 1H), 7.29 – 7.32 (m, 3H), 7.98 (d, 2H, J = 9.0 Hz), 8.08 (dd, 2H, J = 8.0, 1.0 Hz), 9.53 (br, 1H); ^{13}**C NMR (101 MHz, DMSO-d^6)** δ_C ppm 110.9, 119.4, 123.4, 126.6, 128.2, 128.8, 129.9, 138.3, 140.9, 159.6, 160.0; ^{19}**F NMR (376 MHz, DMSO-d^6)** δ_F ppm -142.7; ^{11}**B NMR (128 MHz, DMSO-d^6)** δ_B ppm 1.5; **FTIR (neat)** v_{max} / cm^{-1} 3414 (w), 3338 (br), 3338 (w), 1522 (s), 1490 (s), 1059 (m); **HRMS (ESI-TOF)** *m/z* [M-K]$^-$ calculated for [C$_{16}$H$_{11}$^{11}B^{35}ClF$_3$N$_3$]$^-$ 348.0692, found 348.0702.

General procedure F: Freebasing and condensation of *N*-alkyl guanidine hydrochloride salts
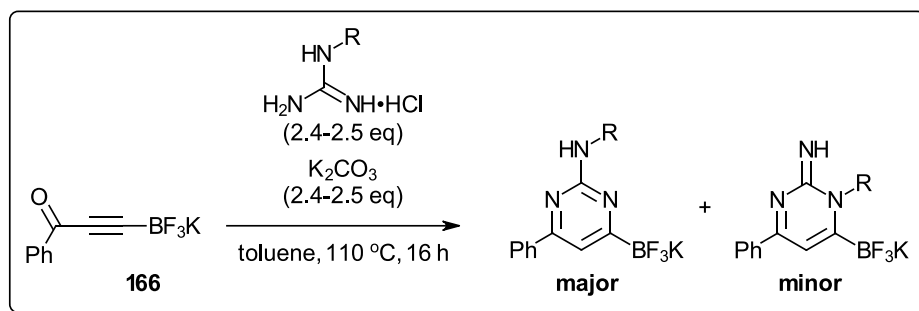
To a stirring suspension of alkylguanidine hydrochloride (2.4-2.5 eq) in toluene was added potassium carbonate (2.4-2.5 eq). The mixture was heated at 80 °C for 2 h, then **166** (1.0 eq) was added and the mixture was heated at reflux for 16 h. The mixture was cooled to room temperature and concentrated *in vacuo*, followed by dissolving in acetone and filtering to remove residual salts. The resultant acetone solution was concentrated to afford a saturated solution and Et$_2$O was added slowly. The aminopyrimidine trifluoroborate precipitate was then collected by filtration and dried thoroughly *in vacuo*.

Preparation of 2-(benzylamino)-4-phenylpyrimidin-6-yl trifluoroborate 220
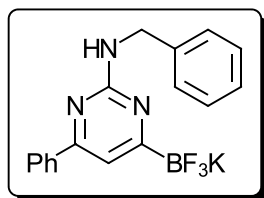
Following general procedure F using benzylguanidine hydrochloride (200 mg, 1.08 mmol), potassium carbonate (147 mg, 1.06 mmol), **166** (100 mg, 0.42 mmol) and toluene (10 mL). The title compound was obtained as a colourless solid (114 mg, 74%). **M.p. =** 234-235 °C (dec); **¹H NMR (400 MHz, DMSO-d⁶)** δ$_H$ ppm 4.61 (d, 2H, J = 6.0 Hz), 7.09 (s, 1H), 7.10 − 7.25 (m, 2H), 7.29 (t, 2H, J = 7.5 Hz), 7.37 − 7.47 (m, 5H), 7.99 (dd, 2H, J = 8.0, 1.5 Hz); **¹³C NMR (101 MHz, DMSO-d⁶)** δ$_C$ ppm 44.2, 108.5, 126.3 (x2C), 127.3, 128.0, 128.5, 129.4, 138.7, 141.5, 159.6, 162.1; **¹⁹F NMR (376 MHz, DMSO-d⁶)** δ$_F$ ppm -142.6; **¹¹B NMR (128 MHz, DMSO-d⁶)** δ$_B$ ppm 1.3; **FTIR (neat)** v$_{max}$ / cm⁻¹ 3432 (m), 3063 (w), 3033 (w), 2945 (w), 1534 (s), 1026 (s), 953 (s); **HRMS (ESI-TOF)** *m/z* [M-K]⁻ calculated for [C$_{17}$H$_{14}$¹¹BF$_3$N$_3$]⁻ 328.1238, found 328.1251; **Single crystal X-ray analysis**, see appendix 6.

Preparation of 2-((*N*-allyl)amino)-4-phenylpyrimidin-6-yl trifluoroborate 221
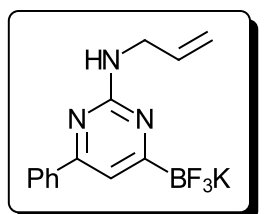
Following general procedure F using allylguanidine hydrochloride (115 mg, 0.85 mmol), potassium carbonate (117 mg, 0.85 mmol), **166** (82 mg, 0.35 mmol) and toluene (6 mL). The title compound was obtained as a colourless solid (60 mg, 54%). **M.p.** = 204-205 °C (dec); **¹H NMR (400 MHz, DMSO-d⁶)** δ$_H$ ppm 3.97 − 4.06 (m, 2H), 5.00 − 5.08 (m, 1H), 5.16 − 5.25 (m, 1H), 5.98 (ddt, 1H, J = 17.0, 10.5, 5.5 Hz), 6.69 (s, 1H), 7.08 (s, 1H), 7.40 − 7.51 (m, 3H), 8.02 (dd, 2H, J = 8.0, 1.5 Hz); **¹³C NMR (101 MHz, DMSO-d⁶)** δ$_C$ ppm 43.7, 109.0, 114.8, 116.4, 126.8, 129.0, 129.8, 139.1, 159.9, 162.3; **¹⁹F NMR (377 MHz, DMSO-d⁶):** δ$_F$ ppm -142.6; **¹¹B NMR (128 MHz, DMSO-d⁶)** δ$_B$ ppm 1.6; **FTIR (neat)** v$_{max}$ / cm⁻¹ 3383, 1645, 1601, 1534, 1033; **HRMS (ESI-TOF)** *m/z* [M-K]⁻ calculated for [C$_{13}$H$_{12}$¹¹BF$_3$N$_3$]⁻ 278.1082, found 278.1091.

Preparation of 2-((*N*-cyclopropyl)amino)-4-phenylpyrimidin-6-yl trifluoroborate **222**
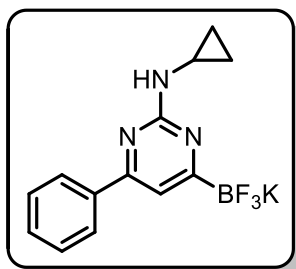
Following general procedure F using cyclopropylguanidine hydrochloride (145 mg, 1.07 mmol), potassium carbonate (147 mg, 1.06 mmol), **166** (100 mg, 0.42 mmol) and toluene (10 mL). The title compound was obtained as a pale yellow solid (100 mg, 75%). **M.p.** = 168-170 °C (dec); **^{1}H NMR (400 MHz, DMSO-d^6)** δ_H ppm 0.44 – 0.57 (m, 2H), 0.65 – 0.77 (m, 2H), 2.77 – 2.85 (m, 1H), 6.80 (s, 1H), 7.11 (s, 1H), 7.42 – 7.49 (m, 3H), 8.03 – 8.10 (m, 2H); **^{13}C NMR (101 MHz, DMSO-d^6)** δ_C ppm 6.9, 24.4, 106.4, 127.2, 129.2, 131.0, 137.5, 159.3, 163.9; **^{19}F NMR (377 MHz, DMSO-d^6)** δ_F ppm -142.6; **^{11}B NMR (128 MHz, DMSO-d^6)** δ_B ppm 1.5; **FTIR (neat)** ν_{max} / cm^{-1} 3373, 1672, 1532, 1347, 1058; **HRMS: (ESI-TOF)** *m/z* [M-K]$^-$ calculated for [C$_{13}$H$_{12}$^{11}BF$_3$N$_3$]$^-$ 278.1082, found 278.1094.

Preparation of 2-((*N*-methyl)amino)-4-phenylpyrimidin-6-yl trifluoroborate **219**
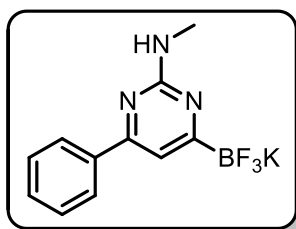
Following general procedure F using methylguanidine hydrochloride (116 mg, 1.06 mmol), potassium carbonate (147 mg, 1.06 mmol), **166** (100 mg, 0.42 mmol) and toluene (10 mL). The title compound was obtained as a pale yellow solid (30 mg, 25%). **M.p.** = 154-155 °C (dec); **^{1}H NMR (400 MHz, DMSO-d^6)** δ_H ppm 2.83 – 2.91 (m, 3H), 6.48 (s, 1H), 7.06 (s, 1H), 7.37 – 7.52 (m, 3H), 7.97 – 8.10 (m, 2H); **^{13}C NMR (101 MHz, DMSO-d^6)** δ_C ppm 28.5, 108.7, 126.8, 129.0, 129.8, 139.3, 160.1, 163.2; **^{19}F NMR (377 MHz, DMSO-d^6)** δ_F ppm -142.6; **^{11}B NMR (128 MHz, DMSO-d^6)** δ_B ppm 1.8; **FTIR (neat)** ν_{max} / cm^{-1} 3357, 1662, 1542, 1308, 1080; **HRMS: (ESI-TOF)** *m/z* [M-K]$^-$ calculated for [C$_{11}$H$_{10}$^{11}BF$_3$N$_3$]$^-$ 252.0925, found 252.0936.

4.2.2. Elaboration of products

General procedure G: Ring alkylation of 190
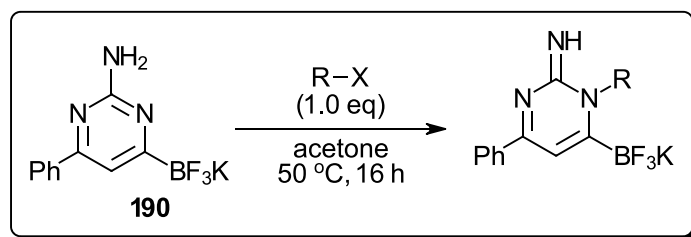
To a stirring suspension of **190** (1.0 eq) in acetone at room temperature was added alkyl halide (1.0 eq). The reaction mixture was heated at 50 °C for 16 h, then cooled to room temperature and concentrated *in vacuo*, giving a saturated solution. Et$_2$O was added and the resultant precipitate was collected, washed with Et$_2$O and dried thoroughly *in vacuo* to afford the corresponding alkylated pyrimidine trifluoroborate salt.

For regiochemical assignments of compounds **228** and **229**, see appendix 4

1-methyl-2-(1*H*)-4-phenylpyrimidinimin-6-yl trifluoroborate **228**
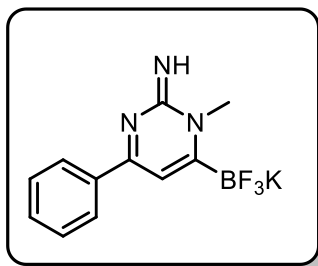
Following general procedure G, using **190** (70 mg, 0.25 mmol), iodomethane (15 µL, 0.25 mmol) and acetone (8 mL) The title compound was obtained as a colourless solid (68 mg, 93%). **M.p** = 175-177 °C (dec); **^{1}H NMR (400 MHz, DMSO-d^6)** δ_H ppm 3.77 (s, 3H), 6.90 (s, 1H), 7.45 (s, 1H), 7.55 – 7.67 (m, 3H), 8.11 – 8.21 (m, 2H); **^{13}C NMR (101 MHz, DMSO-d^6)** δ_C ppm 38.6, 109.4, 127.8, 129.2, 132.5, 134.6, 156.5, 166.3; **^{19}F NMR (377 MHz, DMSO-d^6)** δ_F ppm -141.5; **^{11}B NMR (128 MHz, DMSO-d^6)** δ_B ppm 0.6; **FTIR (neat)** v_{max} / cm^{-1} 3367, 1639, 1599, 1562, 1360; **HRMS: (ESI-TOF)** *m/z* [M-K]$^-$ calculated for [C$_{11}$H$_{10}$^{11}BF$_3$N$_3$]$^-$ 252.0925, found 252.0932; **Single crystal X-ray analysis**, see appendix 6.

1-allyl-2-(1*H*)-4-phenylpyrimidinimin-6-yl trifluoroborate **229**
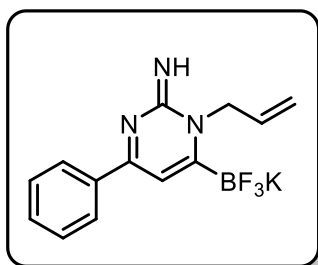
Following general procedure D, using **4a** (70 mg, 0.25 mmol), allyl bromide (22 µL, 0.25 mmol) and acetone (8 mL). The title compound was obtained as a colourless solid (40 mg, 50%). **M.p** = 173-174 °C (dec); **^{1}H NMR (400 MHz, DMSO-d^6)** δ_H ppm 4.96 (d, 2H J = 3.0 Hz), 5.21 (d, 1H, J = 17.5 Hz), 5.26 (d, 1H, J = 11.0 Hz), 5.83 – 5.95 (m, 1H), 7.04 (s, 1H), 7.48 (s, 1H), 7.54 – 7.67 (m, 3H), 8.08 – 8.22 (m, 2H); **^{13}C NMR (101 MHz, DMSO-d^6)** δ_C ppm 52.1, 109.9, 118.5, 128.0, 129.3, 130.4, 132.8, 134.5, 155.7, 166.8; **^{19}F NMR (377 MHz, DMSO-d^6)** δ_F ppm -140.7; **^{11}B NMR (128 MHz, DMSO-d^6)** δ_B ppm 0.6; **FTIR (neat)** v_{max} / cm^{-1} 3367, 1636, 1597, 1556, 1362; **HRMS: (ESI-TOF)** *m/z* [M-K]$^-$ calculated for C$_{13}$H$_{12}$^{11}BF$_3$N$_3$. 278.1082, found 278.1096.

Bromination of 190 using *N*-bromosuccinimide
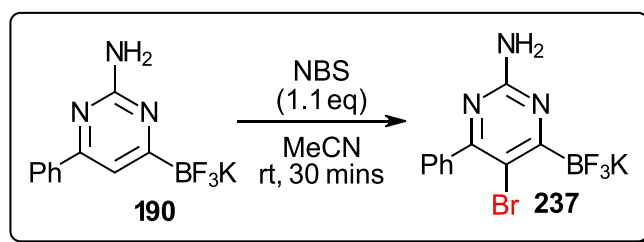
To a stirring slurry of **190** (300 mg, 1.08 mmol) in MeCN (5 mL) in the absence of light was added *N*-bromosuccinimide (212 mg, 1.19 mmol) in one portion. The mixture was stirred rapidly in the dark at room temperature for 30 minutes, then Et$_2$O (20 mL) was added and the resulting suspension was allowed to stand undisturbed for 10 minutes. The mixture was filtered and the collected solid was washed with Et$_2$O (3 x 10 mL) then dried *in vacuo* to give **237** (329 mg, 86%) as a tan solid. **M.p.** 285-286 °C (dec); **^{1}H NMR (400 MHz, DMSO-d^6)** δ_H 6.28 (s, 2H), 7.29 – 7.58 (m, 5H); **^{13}C NMR (101 MHz, DMSO-d^6)** δ_C ppm 110.4, 127.5, 128.2, 128.8, 140.0, 161.1, 162.5; **^{19}F NMR (376 MHz, DMSO-d^6)** δ_F ppm -139.8; **^{11}B NMR (128 MHz, DMSO-d^6)** δ_B ppm 1.1; **FTIR (neat)** v_{max} / cm^{-1} 3486 (m), 3330 (m), 3204 (w), 1626 (s), 1515 (s), 991 (s); **HRMS (ESI-TOF)** *m/z* [M-K]$^-$ calculated for [C$_{10}$H$_7$N$_3$^{11}B^{79}BrF$_3$]$^-$ 315.9874, found 315.9878.

General procedure H: Suzuki-Miyaura coupling of 173
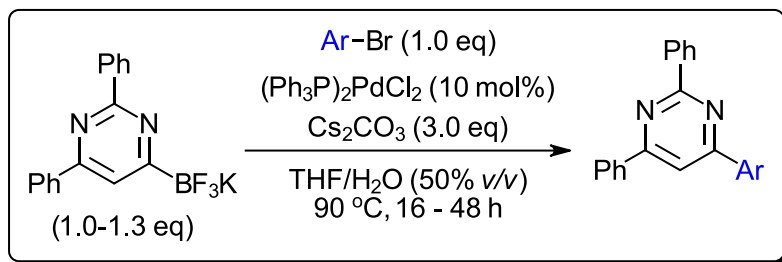
A 10 mL Biotage microwave vial was charged with **173** (1.0-1.3 eq), $(Ph_3P)_2PdCl_2$ (10 mol%), Cs_2CO_3 (3.0 eq), the aryl halide (1.0 eq) and then H_2O/THF (50% vv, diluting ArX to a concentration of 0.05-0.08 M) were added. The tube was sealed and the reaction mixture was heated with vigorous stirring for 16-48 h, then cooled to room temperature. The layers were separated and the aqueous layer was extracted with CH_2Cl_2 (3 x 3 mL). The combined organic layers were dried over anhydrous $MgSO_4$, concentrated *in vacuo* then purified by flash column chromatography on silica gel.

2,4-Diphenyl-6-(4-cyanophenyl)pyrimidine **239**
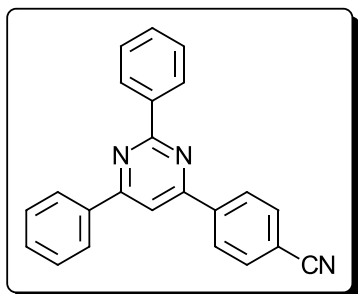
Following general procedure H, using **173** (45 mg, 0.13 mmol), 4-bromobenzonitrile (19 mg, 0.10 mmol), $(Ph_3P)_2PdCl_2$ (7 mg, 0.01 mmol), Cs_2CO_3 (98 mg, 0.3 mmol) and H_2O/THF (50% v/v, 2 mL), heating for 16 hours. The title compound was obtained after flash column chromatography (70 % petroleum ether in EtOAc) as a colourless solid (12 mg, 36%). **M.p.** = 182 – 185 °C; **^{1}H NMR (400 MHz, CDCl$_3$)** δ_H ppm 7.54 – 7.64 (m, 6H), 7.84 – 7.91 (m, 2H), 8.04 (s, 1H), 8.28 – 8.35 (m, 2H), 8.38 – 8.45 (m, 2H), 8.69 – 8.76 (m, 2H); **^{13}C NMR (101 MHz, CDCl$_3$)** δ_C ppm 110.6, 114.2, 118.5, 127.3, 127.9, 128.5, 128.6, 129.1, 131.0, 131.2, 132.7, 137.0, 137.6, 141.7, 162.7, 164.8, 165.4; **FTIR** (v_{max}/ cm^{-1}) 3063 (w), 2226 (m), 1568 (s), 1525 (s); **HRMS (ESI-TOF)** m/z [M+H]$^+$ calculated for [$C_{23}H_{15}N_3$]$^+$ 334.1339, found 334.1344.

2,4-Diphenyl-6-(4-(trifluoromethyl)phenyl)pyrimidine **241**[505]
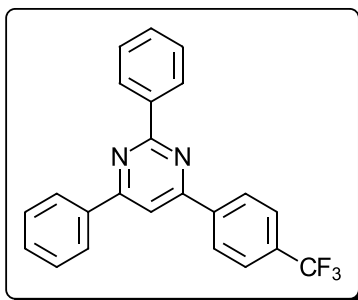
Following general procedure H, using **173** (50 mg, 0.15 mmol), $(Ph_3P)_2PdCl_2$ (11 mg, 0.015 mmol), Cs_2CO_3 (145 mg, 0.45 mmol), aqueous THF (50% v/v, 2 mL), with 4-bromo, α, α, α, trifluorotoluene (21 μL, 0.15 mmol) added last, the mixture was heated for 48 hours. The title compound was obtained after flash column chromatography (90 % petroleum ether in EtOAc) as a colourless solid (36 mg, 64%). **M.p.** = 128 – 135 °C (lit^{505} = 147 – 149 °C); **^{1}H NMR (400 MHz, CDCl$_3$)** δ_H ppm 7.54 – 7.63 (m, 6H), 7.84 (d, 2H, J =

8.0 Hz), 8.04 (s, 1H), 8.29 – 8.35 (m, 2H), 8.41 (d, 2H, J = 8.0 Hz), 8.71 – 8.77 (m, 2H); **¹³C NMR (101 MHz, CDCl₃)** δ_C ppm 110.6, 124.0 (q, J = 272.5 Hz), 125.9 (q, J = 3.5 Hz), 127.3, 127.7, 128.5, 128.6, 129.0, 130.9, 131.1, 132.4 (q, J = 32.5 Hz), 137.2, 137.8, 140.9, 163.3, 164.8, 165.2; **¹⁹F NMR (376 MHz, DMSO-d⁶)** δ_F ppm -62.7; (the data were in agreement with those published)[505]

General procedure I: Suzuki-Miyaura cross coupling of 190
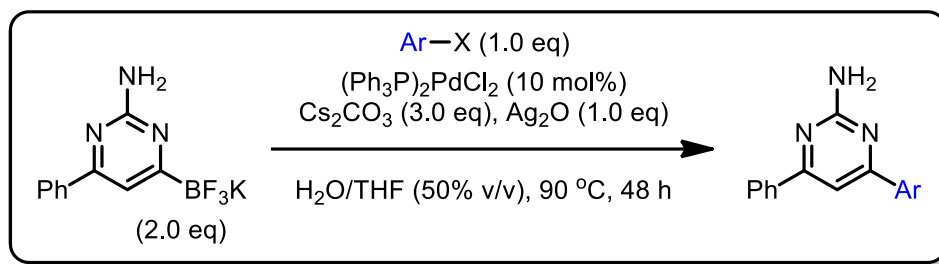
A 10 mL Biotage microwave vial was charged with **190** (2.0 eq), (Ph₃P)₂PdCl₂ (10 mol%), Cs₂CO₃ (3.0 eq) and Ag₂O (1.0 eq). The tube was then capped and purged with argon before the aryl halide (1.0 eq) and then H₂O/THF (50% vv, diluting ArX to a concentration of 0.13 M) were added. The tube was sealed and the reaction mixture was heated with vigorous stirring for 48 h, then cooled to room temperature and concentrated *in vacuo*. The crude mixture was suspended in a small quantity of DMSO and subjected to flash column chromatography on silica gel (gradient elution, 0-50% EtOAc in petroleum ether).

4,6-diphenylpyrimidin-2-amine **244**[506]
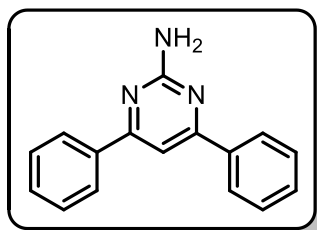
Following general procedure I, using **190** (133 mg, 0.48 mmol), iodobenzene (27 µL, 0.24 mmol), (Ph₃P)₂PdCl₂ (17 mg, 0.02 mmol), Cs₂CO₃ (235 mg, 0.72 mmol), Ag₂O (56 mg, 0.24 mmol) and H₂O/THF (50% v/v, 1.8 mL). The title compound was obtained (36 mg, 61%) as a colourless solid. **M.p.** 135 °C (lit[506] = 134-136 °C); **¹H NMR (400 MHz, CDCl₃)** δ_H ppm 5.41 (s, 2H), 7.46 (s, 1H), 7.47 – 7.52 (m, 6H), 8.03 – 8.09 (m, 4H); **¹³C NMR (101 MHz, CDCl₃)** δ_C ppm 104.4, 127.3, 128.9, 130.6, 137.9, 163.8, 166.4; (the data were in agreement with those published)[506]

4-(3,5-dimethylphenyl)-6-phenylpyrimidin-2-amine, **245**
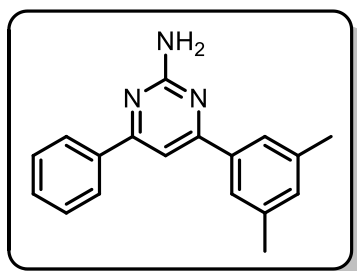
Following general procedure I, using **190** (133 mg, 0.48 mmol), 1-iodo-3,5-dimethylbenzene (35 µL, 0.24 mmol), (Ph$_3$P)$_2$PdCl$_2$ (17 mg, 0.02 mmol), Cs$_2$CO$_3$ (235 mg, 0.72 mmol), Ag$_2$O (56 mg, 0.24 mmol) and H$_2$O/THF (50% v/v, 1.8 mL). The title compound was obtained (39 mg, 59%) as a colourless solid. **M.p.** 155 °C; **^{1}H NMR (400 MHz, CDCl$_3$)** δ$_H$ ppm 2.42 (s, 6H), 5.37 (s, 2H), 7.13 (m, 1H), 7.44 (s, 1H), 7.47 – 7.52 (m, 3H), 7.66 (m, 2H), 8.03 – 8.09 (m, 2H); ^{13}**C NMR (101 MHz, CDCl$_3$)** δ$_C$ ppm 21.5, 104.6, 125.1, 127.3, 128.9, 130.5, 132.2, 137.9, 138.0, 138.5, 163.8, 166.2, 166.8; **FTIR (neat)** ν$_{max}$ / cm^{-1} 3420(m), 3158(m), 2986(m), 1624(m), 1572(s), 1541(s); **HRMS: (ESI-TOF)** *m/z* [M+H]$^+$ calculated for [C$_{18}$H$_{18}$N$_3$]$^+$ 276.1495, found 276.1492.

Preparation of 2-Amino-6-phenyl-4(3H)-pyrimidinone 248
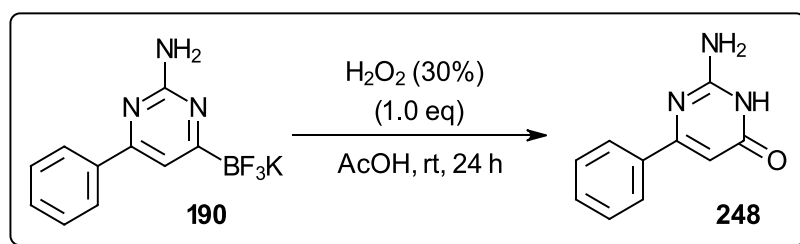
To a solution of **190** (139 mg, 0.5 mmol) in AcOH (1.0 mL) was added dropwise H$_2$O$_2$ (30%, 51 µL, 0.5 mmol). The mixture was stirred at rt for 24 hours, then concentrated *in vacuo* and the residue was subjected to flash column chromatography on silica gel (eluting with 10% methanol in CH$_2$Cl$_2$), affording the title compound as a colourless solid (59 mg, 63%). **^{1}H NMR (400 MHz, DMSO-d^6)** δ$_H$ 6.10 (s, 1H), 6.60 (s, 2H), 7.38 – 7.49 (m, 3H), 7.89 – 7.99 (m, 2H), 10.80 (s, 1H). (The spectral data were in agreement with those published)[507]

Preparation of Bropirimine *via* oxidation of 237
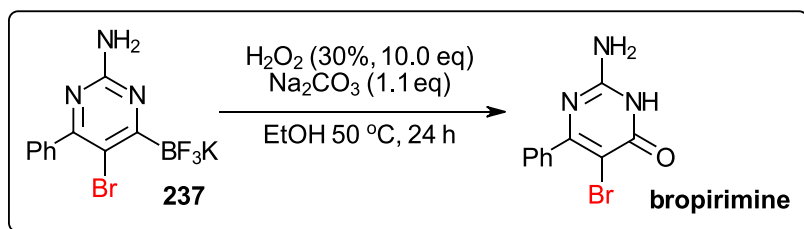
A solution of **237** (220 mg, 0.62 mmol), H$_2$O$_2$ (30% aq, 631 µL, 6.18 mmol), Na$_2$CO$_3$ (72 mg, 0.68 mmol) in ethanol (7 mL) behind a precautionary blast shield was heated at 55 °C for 24 hours then cooled to room temperature and diluted with EtOAc (25 mL) then H$_2$O (10 mL). The phases were separated and

the aqueous phase was extracted with EtOAc (5 x 20 mL). The combined organic phases were dried over anhydrous MgSO$_4$ then concentrated *in vacuo*. The crude product was purified by flash column chromatography on silica gel (eluting with EtOAc) to give bropirimine (125 mg, 76%) as a colourless solid. **M.p.** 269-270 °C (lit[5] = 275-277 °C); **^{1}H NMR (400 MHz, DMSO-d^6)** δ$_H$ ppm 6.76 (s, 2H), 7.34 – 7.49 (m, 3H), 7.49 – 7.60 (m, 2H), 11.42 (s, 1H); ^{13}**C NMR (101 MHz, DMSO-d^6)** δ$_C$ ppm 96.0, 127.7, 128.5, 128.9, 139.1, 154.2, 159.2, 163.5.

Preparation of 4-iodo-2,6-diphenylpyrimidine 249[508]
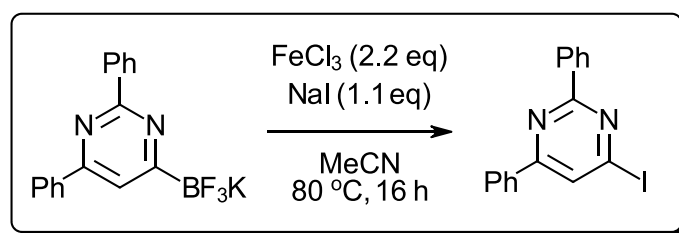
A sealed tube charged with **173** (47 mg, 0.14 mmol), FeCl$_3$ (50 mg, 0.31 mmol) and NaI (22 mg, 0.15 mmol) was flushed with argon, and MeCN (5 mL) was added. The mixture was heated to 80 °C for 16 hours, then allowed to cool to room temperature and diluted with CH$_2$Cl$_2$ (10 mL). The mixture was washed with a saturated aqueous solution of NaHCO$_3$ (5 mL), the layers were separated and the aqueous layer extracted with CH$_2$Cl$_2$ (3 x 5 mL). The combined organic layers were dried over MgSO$_4$ and concentrated *in vacuo*. The crude mixture was submitted to flash column chromatography on silica gel (eluting 10% EtOAc in petrol), affording **249** as a colourless solid (14 mg, 28%). **M.p.** = 104 – 106 °C (lit[508] = 98 °C); **^{1}H NMR (400 MHz, CDCl$_3$)** δ$_H$ ppm 7.50 – 7.60 (m, 6H), 8.07 (s, 1H), 8.16 – 8.24 (m, 2H), 8.53 – 8.61 (m, 2H); ^{13}**C NMR (101 MHz, CDCl$_3$)** δ$_C$ ppm 125.6, 127.4, 128.56, 128.62, 129.0, 130.8, 131.4, 131.5, 135.6, 136.4, 163.5, 164.7. (The data were in agreement with those published)[508]

4.3. Fluorinated alkynyltrifluoroborate salts

4.3.1. Synthesis of fluorinated alkynyltrifluoroborate salts

Preparation of potassium (1,1,1-trifluoroprop-2-yn-3-yl)trifluoroborate 357
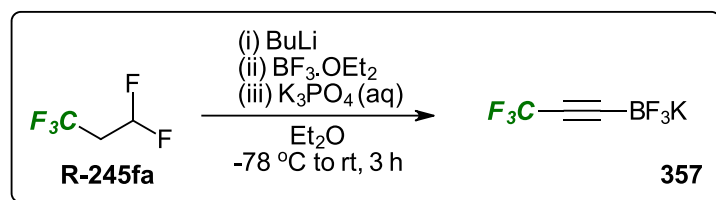
This method was adapted from that published by Ramachandran *et al.*[468]

A 3-neck round-bottomed flask under argon was charged with a solution of R-245fa in anhydrous Et_2O (90.0 mL, 45 mmol) and cooled to -35 °C. ^{n}BuLi in cyclohexane (66.3 mL, 128 mmol) was added slowly to the flask and the mixture was stirred at -35 °C for 1 hour. The mixture was then cooled to -78 °C by exchanging the cooling bath and allowing 15 minutes stirring to acclimatise. $BF_3.OEt_2$ (5.6 mL, 45 mmol) was added, dropwise, to the mixture which was then stirred for 15 minutes at -78 °C. The mixture was warmed to -20 °C by exchanging cooling baths and allowing 15 minutes of stirring to acclimatise, then a solution of K_3PO_4 (12.5 g, 59 mmol) in H_2O (14 mL) was added slowly *via* syringe. The mixture was allowed to warm to room temperature then concentrated *in vacuo* to dryness. Acetone (500 mL) was added to the flask and the product was extracted by vigorous stirring and agitation over a period of 20 minutes, followed by filtration and concentration of the filtrate *in vacuo*. The crude product was purified by dissolving the residue in acetone (10 mL) and adding dropwise CH_2Cl_2 (250 mL) without stirring. The resultant precipitate was collected and dried *in vacuo*, providing the crude **357** as a colourless solid (2.6 g, 30%). Prior to recrystallisation, the precipitate was dissolved in acetone and the solution was dried over anhydrous $MgSO_4$ then concentrated *in vacuo*. The product was dispersed in toluene (200 mL) inside a flask fitted with a reflux condenser and heated at 80 °C, whereupon MeCN (50 mL) was added slowly. After cooling the mixture to ambient temperature, the mixture was further cooled to -20 C over a period of 1 hour. The cold mixture was filtered and the collected crystals were dried inside an evacuated desiccator over anhydrous P_2O_5 for 60 hours, affording **357** as a colourless powder (1.2 g, 14%). **M.p.** 182 – 183 °C; ^{13}**C NMR (101 MHz, CD$_3$CN)** δ_C ppm 74.5 – 77.7 (m), 115.2 (q, J = 255.5 Hz); ^{19}**F NMR (376 MHz, CD$_3$CN)** δ_F ppm -49.8, -137.5 (q, J = 32.0 Hz); ^{11}**B NMR (128 MHz, CD$_3$CN)** δ_B ppm -2.4 (q, J = 32.0 Hz). (The data were in agreement with those published).[471]

General procedure J: Preparation of perfluoroalkyl-substituted alkynyltrifluoroborate salts

$$(C_nF_{2n+1})—\!\!\!=\!\!\!— \quad \xrightarrow[\substack{Et_2O \\ \text{-78 °C to rt, 3 h}}]{\substack{\text{(i) BuLi} \\ \text{(ii) BF}_3.\text{OEt}_2 \\ \text{(iii) K}_3\text{PO}_4\text{ (aq)}}} \quad (C_nF_{2n+1})—\!\!\!=\!\!\!—BF_3K$$
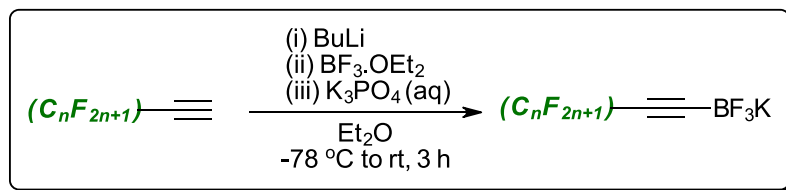
This method was adapted from that published by Bardin $et\ al.$,[471] deploying aspects of Ramachandran's[468] HF-free approach.

To a solution of the terminal alkyne (1.2 eq) in anhydrous Et_2O (0.3 M) at -60 °C was added dropwise ^{n}BuLi in cyclohexane (1.0 eq). The mixture was stirred, keeping the temperature between -55 and -60 °C for 1 hour then cooled to -78 °C. The resultant cold acetylide solution was transferred via cannula into a flask containing $BF_3.OEt_2$ (1.4 eq) in Et_2O (0.3 M) at -78 °C and stirred at this temperature for 1 hour. The mixture was warmed to -20 °C by exchanging cooling baths, allowing 15 minutes of stirring to acclimatise, then a solution of K_3PO_4 (1.3 eq) in H_2O (4.0 M) was added slowly via syringe. The mixture was allowed to warm to room temperature then concentrated $in\ vacuo$ to dryness, the desired product was then extracted by vigorous stirring and agitation in acetone for 15 minutes followed by filtration and concentration $in\ vacuo$. The crude product was dissolved in acetone and CH_2Cl_2 was added, leading to precipitation. The precipitate was collected and dried inside an evacuated desiccator over anhydrous P_2O_5 for 24 hours, affording the desired product as a colourless powder.

Potassium (perfluorohexylethynyl)trifluoroborate 334

$$F_{13}C_6—\!\!\!=\!\!\!—BF_3K$$
$$n = 6$$
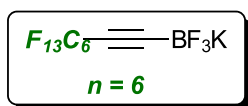
Following general procedure J, using (perfluorohexyl)acetylene (1.0 g, 2.9 mmol), ^{n}BuLi in cyclohexane (1.5 mL, 2.5 mmol), $BF_3.OEt_2$ (0.4 mL, 3.4 mmol) and K_3PO_4 (0.7 g, 3.2 mmol). The title compound was obtained as a colourless solid (676 mg, 61%). **M.p.** 214 – 215 °C; **^{13}C NMR (101 MHz, acetone-d^6)** δ_C ppm 74.2, 104.5 – 114.2 (m, multiple signals), 118.1 (qt, J = 33.0, 288.0 Hz); **^{19}F NMR (376 MHz, acetone-d^6)** δ_F ppm -81.8 – -81.7 (m), -94.1 – -94.0 (m), -121.9 – -121.5 (m), -123.1 – -122.8 (m), -123.6 – -123.3 (m), -126.9 – -126.7 (m), -137.4 (q, J = 30.5 Hz); **^{11}B NMR (128 MHz, acetone-d^6)** δ_B ppm -2.3 (q, J = 30.5 Hz); **FTIR (neat)** v_{max} / cm^{-1} 2227 (w), 1366 (w), 1227 (s), 1194 (s), 1144 (s), 706 (s); **HRMS (ESI-TOF)** m/z [M-K]$^-$ calculated for $[C_8{}^{11}B^{19}F_{16}]^-$ 410.9844, found 410.9839. (the data were in agreement with those published)[471]

Potassium (perfluorooctylethynyl)trifluoroborate 335

$$F_{17}C_8—\!\!\!=\!\!\!—BF_3K$$
$$n = 8$$
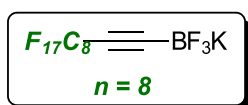
Following general procedure J, using (perfluorooctyl)acetylene (1.0 g, 2.3 mmol), ^{n}BuLi in cyclohexane (1.1 mL, 1.9 mmol), $BF_3.OEt_2$ (0.3 mL, 2.6 mmol) and K_3PO_4 (0.5 g, 2.4 mmol). The title compound was obtained as a colourless solid (513 mg, 50%). **M.p.** 241 – 244 °C; **^{13}C NMR (101 MHz, acetone-d^6)** δ_C ppm 74.1, 104.6 – 105.3 (m, multiple signals), 118.0 (qt, J = 33.0, 288.0); **^{19}F NMR (376 MHz, acetone-d^6)** δ_F ppm -81.7 (t, J =

9.5 Hz), -94.1 – -93.9 (m), -121.6 – -121.2 (m), -122.7 - -122.3 (m), -123.1 – -122.8 (m), -123.5 – -123.1 (m), -126.8 – -126.6 (m), -137.4 (q, J = 30.5 Hz); **^{11}B NMR (128 MHz, acetone-d^6)** δ_B ppm -2.3 (q, J = 30.5 Hz); **FTIR (neat)** v_{max} / cm^{-1} 2227 (w), 1371 (w), 1201 (s), 1146 (s), 1015 (m), 710 (m); **HRMS (ESI-TOF)** *m/z* [M-K]$^-$ calculated for [C$_{10}$^{11}BF$_{20}$]$^-$ 510.9780, found 510.9779.

Preparation of tetra-*N*-ethylammonium (1,1,1-trifluoroprop-2-yn-3-yl)trifluoroborate 336
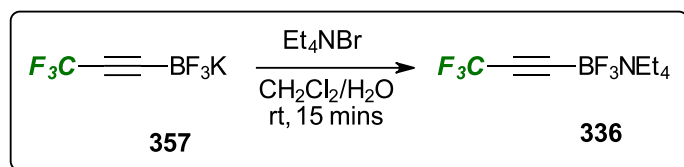
To a rapidly stirring surry of **357** (1.0 g, 5.0 mmol) and tetra-*n*-ethylammonium bromide (1.0 g, 5.3 mmol) in CH$_2$Cl$_2$ (13.6 mL) was added dropwise H$_2$O (6.6 mL). The mixture was stirred rapidly for a further 15 minutes, then allowed to settle and the layers were separated. The aqueous layer was extracted with CH$_2$Cl$_2$ (3 x 25 mL) and the combined organic layers were dried over anhydrous MgSO$_4$ and concentrated *in vacuo*. The product obtained was dried dried inside an evacuated desiccator over anhydrous P$_2$O$_5$ for 24 hours, affording **336** as a colourless powder (1.4 g, 95%). **M.p.** 48 – 49 °C; **^{1}H NMR (400 MHz, CDCl$_3$)** δ_H ppm 1.30 – 1.38 (m, 12H), 3.28 (q, 8H, J = 7.5 Hz); **^{13}C NMR (101 MHz, CDCl$_3$)** δ_C ppm 7.7 (q, J = 11.0 Hz), 52.9 – 53.3 (m), 75.3 – 77.3 (m), 115.2 (q, J = 252.0 Hz); **^{19}F NMR (376 MHz, CDCl$_3$)** δ_F ppm -48.8, -136.6 (q, J = 33.5 Hz); **^{11}B NMR (128 MHz, CDCl$_3$)** δ_B ppm -2.2 (q, J = 33.5 Hz); **FTIR (neat)** v_{max} / cm^{-1} 3000 (w), 2213 (w), 1491 (w), 1397 (w), 1255 (m), 1123 (s), 1031 (s), 787 (w); **HRMS (ESI-TOF)** *m/z* [M-NEt$_4$]$^-$ calculated for [C$_3$^{11}BF$_6$]$^-$ 160.9997, found 161.0007

4.3.2. Synthesis of 2-pyrones

General procedure K, synthesis of *N*-heterocycle-substituted 2-pyrones from aldehydes[462]
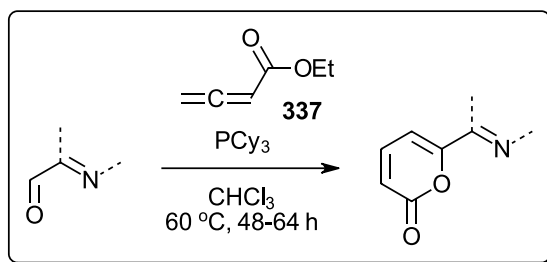
To a stirring solution of aldehyde (3.0 – 3.6 eq) and PCy$_3$ (1.0 – 1.1 eq) in anhydrous CHCl$_3$ under argon was added dropwise **337** (1.0 eq). The mixture was sealed inside the reaction tube and heated at 60 °C with stirring for 48-64 hours, then cooled to room temperature and concentrated *in vacuo*. The crude residue was purified by flash column chromatography on silica gel (eluting with EtOAc in hexanes) then recrystallised from CH$_2$Cl$_2$/hexanes. The purified product was then dried over P$_2$O$_5$ inside an evacuated desiccator for a period of 24 hours.

Products **311**, **338**, **341**, **344** and **346** were prepared according to the general procedure and their data were in agreement with those published.[462]

Preparation of 6-(6-bromo-2-pyridyl)-2-pyrone, 343
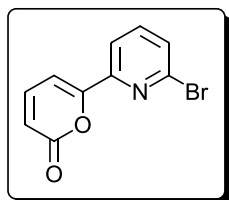
Following general procedure K, using 6-Bromo-2-pyridinecarboxaldehyde (930 mg, 5.0 mmol), PCy$_3$ (430 mg, 1.5 mmol), **337** (160 µL, 1.4 mmol) and CHCl$_3$ (10 mL). The crude product was purified by flash column chromatography on silica gel (gradient elution, 0-30% EtOAc in hexanes) followed by recrystallisation and drying, to afford **343** as yellow crystals (189 mg, 54%). **M.p.** = 104 – 105 °C; **^{1}H NMR (400 MHz, CDCl$_3$)** δ_H ppm 6.39 (dd, 1H, J = 1.0, 9.5 Hz), 7.33 (dd, 1H, J = 1.0, 7.0 Hz), 7.44 – 7.54 (m, 2H), 7.66 (t, 1H, J = 8.0 Hz), 7.93 (dd, 1H, J = 1.0, 8.0 Hz); **^{13}C NMR (101 MHz, CDCl$_3$)** δ_C ppm 103.9, 116.9, 119.2, 129.5, 139.5, 142.2, 143.7, 149.9, 157.7, 161.1; **FTIR (neat)** v_{max} / cm^{-1} 3101 (w), 2808 (w), 2568 (w), 2047 (w), 1743 (s), 1561 (m), 1108 (m), 789 (s); **HRMS (ESI-TOF)** *m/z* [M+H]$^+$ calculated for [C$_{10}$H$_7$^{79}BrNO$_2$]$^+$ 251.9655, found 251.9651.

Preparation of 6-(5-chloro-2-pyridyl)-2-pyrone, 342
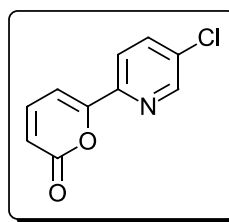
Following general procedure K, using 5-chloro-2-pyridinecarboxaldehyde (600 mg, 4.2 mmol), PCy$_3$ (390 mg, 1.4 mmol), **337** (160 µL, 1.4 mmol) and CHCl$_3$ (10 mL). The crude product was purified by flash column chromatography on silica gel (gradient elution, 0-30% EtOAc in hexanes) followed by recrystallisation and drying, to afford **342** as colourless crystals (216 mg, 74%). **M.p.** = 180 – 181 °C; **^{1}H NMR (400 MHz, CDCl$_3$)** δ_H ppm 6.39 (dd, 1H, J = 1.0, 9.5 Hz), 7.32 (dd, 1H, J = 1.0, 7.0 Hz), 7.49 (dd, 1H, J = 7.0, 9.5 Hz), 7.80 (dd, 1H, J = 2.5, 8.5 Hz), 7.95 (dd, 1H, J = 0.5, 8.5 Hz), 8.58 (dd, 1H, J = 0.5, 2.5 Hz); **^{13}C NMR (101 MHz, CDCl$_3$)** δ_C ppm 103.4, 116.5, 121.2, 133.6, 137.1, 143.8, 147.0, 148.9, 158.4, 161.3; **FTIR (neat)** v_{max} / cm^{-1} 3081 (w), 2832 (w), 1735 (s), 1630 (w), 1546

(m), 1103 (m), 805 (s); **HRMS (ESI-TOF)** *m/z* [M+H]⁺ calculated for [C$_{10}$H$_7$^{35}ClNO$_2$]⁺ 208.0160, found 208.0157.

Preparation of 6-(2-quinolinyl)-2-pyrone, 339
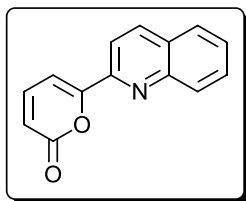
Following general procedure K, using 2-quinolinecarboxaldehyde (790 mg, 5.0 mmol), PCy$_3$ (420 mg, 1.5 mmol), **337** (160 µL, 1.4 mmol) and CHCl$_3$ (10 mL). The crude product was purified by flash column chromatography on silica gel (gradient elution, 0-30% EtOAc in hexanes) followed by recrystallisation and drying, to afford **339** as brown crystals (293 mg, 94%). **M.p.** = 160 – 161 °C; **¹H NMR (400 MHz, CDCl$_3$)** δ$_H$ ppm 6.40 – 6.47 (m, 1H), 7.53 – 7.64 (m, 3H), 7.76 (ddd, 1H, J = 1.5, 7.0, 8.5 Hz), 7.86 (dd, 1H, J = 1.0, 8.0 Hz), 8.10 (ddd, 1H, J = 1.0, 1.5, 8.5 Hz), 8.14 (d, 1H, J = 8.5 Hz), 8.30 (d, 1H, J = 8.5 Hz); **¹³C NMR (101 MHz, CDCl$_3$)** δ$_C$ ppm 103.7, 116.4, 117.7, 127.9, 128.6, 129.9, 130.4, 137.5, 144.0, 148.0, 149.0, 159.7, 161.8; **FTIR (neat)** ν$_{max}$ / cm⁻¹ 3063 (w), 2855 (w), 2758 (w), 1723 (s), 1500 (m), 1072 (m), ; **HRMS (ESI-TOF)** *m/z* [M+H]⁺ calculated for [C$_{14}$H$_{10}$NO$_2$]⁺ 224.0706, found 224.0702.

Preparation of 6-(4,5-dimethyl-1,3-thiazol-2-yl)-2-pyrone, 345
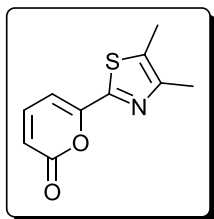
Following general procedure K, using 4,5-Dimethyl-1,3-thiazole-2-carbaldehyde (590 mg, 4.2 mmol), PCy$_3$ (390 mg, 1.4 mmol), **337** (160 µL, 1.4 mmol) and CHCl$_3$ (10 mL). The crude product was purified by flash column chromatography on silica gel (gradient elution, 0-30% EtOAc in hexanes) followed by recrystallisation and drying, to afford **345** as yellow crystals (188 mg, 65%). **M.p.** = 184 – 185 °C; **¹H NMR (400 MHz, CDCl$_3$)** δ$_H$ ppm 2.37 (s, 3H), 2.43 (s, 3H), 6.30 (dd, 1H, J = 0.5, 9.5 Hz), 7.01 (dd, 1H, J = 0.5, 7.0 Hz), 7.41 (dd, 1H, J = 7.0, 9.5 Hz); **¹³C NMR (101 MHz, CDCl$_3$)** δ$_C$ ppm 11.8, 14.9, 101.0, 115.6, 131.6, 143.7, 151.4, 154.2, 155.4, 160.8; **FTIR (neat)** ν$_{max}$ / cm⁻¹ 3307 (w), 3078 (w), 2928 (w), 1713 (s), 1619 (m), 1524 (s), 1269 (m); **HRMS (ESI-TOF)** *m/z* [M+H]⁺ calculated for [C$_{10}$H$_{10}$NO$_2$S]⁺ 208.0427, found 208.0423.

Preparation of 6-(1,3-benzothiazol-2-yl)-2-pyrone, 340
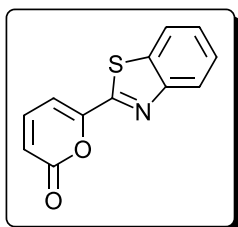
Following general procedure K, using 1,3-Benzothiazole-2-carbaldehyde (690 mg, 4.2 mmol), PCy$_3$ (390 mg, 1.4 mmol), **337** (160 µL, 1.4 mmol) and CHCl$_3$ (10 mL). The crude product was purified by flash column chromatography on silica gel (gradient elution, 0-30% EtOAc in hexanes) followed by recrystallisation and drying, to afford **340** as orange crystals (133 mg, 41%). **M.p.** = 205 – 206 °C; **¹H NMR (400 MHz, CD$_2$Cl$_2$)** δ$_H$ ppm 6.42 (dd, 1H, J = 1.0, 9.5 Hz), 7.30 (dd, 1H, J = 1.0, 6.5 Hz), 7.46 – 7.54 (m, 2H), 7.57 (ddd, 1H, J = 1.0, 7.0, 8.5 Hz), 8.01 (ddd, 1H, J = 0.5, 1.0, 8.0 Hz), 8.09 (ddd, 1H, J = 0.5, 1.0, 8.5 Hz); **¹³C NMR (101 MHz, CD$_2$Cl$_2$)** δ$_C$ ppm 103.9, 117.5, 122.2, 124.0, 126.5, 127.1, 135.7, 143.2, 153.8, 154.8, 159.4, 159.9; **FTIR (neat)** ν$_{max}$ / cm⁻¹ 3078 (w), 2828 (w), 2354 (w), 1728 (s), 1630 (w), 1546 (m), 1315 (m), 1258 (m), 1106 (m); **HRMS (ESI-TOF)** *m/z* [M+H]⁺ calculated for [C$_{12}$H$_8$NO$_2$S]⁺ 230.0270, found 230.0266.

General procedure L, synthesis of amide-substituted 2-pyrones from carboxylic acids
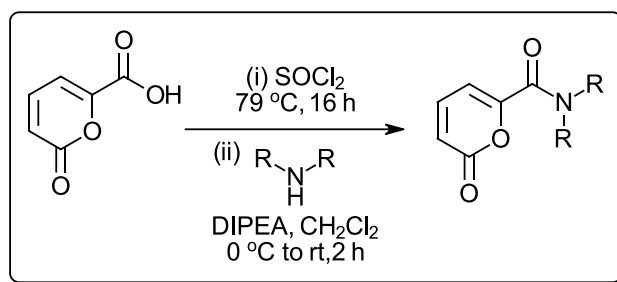
A solution of 6-(hydroxycarbonyl)-2-pyrone[473] (1.0 eq) in $SOCl_2$ was heated at reflux for 16 hours, then concentrated *in vacuo*. The resultant residue was dissolved in CH_2Cl_2 (10 mL) and cooled to 0 °C, whereupon the secondary amine (1.0 eq) then DIPEA 1.0 eq) were added slowly. The mixture was allowed to warm to room temperature over 2 hours, then washed with saturated aqueous $NaHCO_3$ (10 mL), followed by H_2O (10 mL), followed by brine (10 mL). The layers were separated and the organic layer was dried over anhydrous $MgSO_4$ then concentrated *in vacuo*. The crude product was purified by flash column chromatography on silica gel, then dried over P_2O_5 inside an evacuated desiccator for a period of 24 hours.

6-(*N*,*N*-dimethylformamido)-2-pyrone **348**
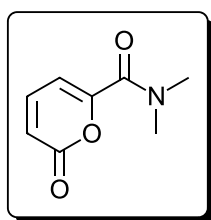
Following general procedure L, using 6-(hydroxycarbonyl)-2-pyrone (300 mg, 2.1 mmol), $SOCl_2$ (2.8 mL), dimethylamine (2.0 M in THF, 1.1 mL, 2.1 mmol) and DIPEA (370 µL, 2.1 mmol). The crude product was purified by flash column chromatography on silica gel (gradient elution, 50 – 100% EtOAc in hexanes), followed by drying, to afford the title compound **348** as a colourless solid (157 mg, 44%). **M.p. = 62 – 63 °C; ¹H NMR (400 MHz, CDCl₃)** δ_H ppm 3.03 (s, 3H), 3.12 (s, 3H), 6.36 (dd, 1H, J = 1.0, 9.5 Hz), 6.66 (dd, 1H, J = 1.0, 6.5 Hz), 7.39 (dd, 1H, J = 6.5, 9.5 Hz); **¹³C NMR (101 MHz, CDCl₃)** δ_C ppm 36.3, 38.5, 107.2, 117.7, 143.0, 155.8, 159.9, 161.5. (The data were in agreement with those published)[464]

6-(piperidinocarbonyl)-2-pyrone **349**
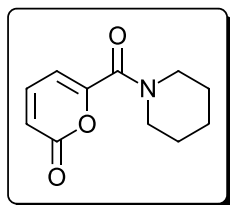
Following general procedure L, using 6-(hydroxycarbonyl)-2-pyrone (250 mg, 1.78 mmol), $SOCl_2$ (10 mL), piperidine (180 µL, 1.78 mmol) and DIPEA (310 µL, 1.78 mmol). The crude product was purified by flash column chromatography on silica gel (eluting with EtOAc), followed by recrystallisation from CH_2Cl_2/hexanes then drying, to afford the title compound **349** as colourless crystals (104 mg, 28 %). **M.p. = 79 – 80 °C; ¹H NMR (400 MHz, CDCl₃)** δ_H ppm 1.56 – 1.65 (m, 4H), 1.65 – 1.75 (m, 2H), 3.46 – 3.61 (m, 4H), 6.34 (dd, 1H, J = 1.0, 9.5 Hz), 6.56 (dd, 1H, J = 1.0, 6.5 Hz), 7.58 (dd, 1H, J = 6.5, 9.5 Hz); **¹³C NMR (101 MHz, CDCl₃)** δ_C ppm 25.1, 26.2, 27.2, 43.8, 48.5, 106.3, 117.4, 144.3, 157.0, 160.4, 161.0; **FTIR (neat)** ν_max / cm⁻¹ 3086 (w), 2942 (w), 2866 (w), 1721 (s), 1638 (s), 1618 (m), 1448 (m), 1274 (m), 1089 (m); **HRMS (ESI-TOF)** *m/z* [M+H]⁺ calculated for $[C_{11}H_{14}NO_3]^+$ 208.0968, found 208.0965.

4.3.3. Directed cycloadditions promoted by BF₃.OEt₂

BF₃.OEt₂-promoted cycloaddition between potassium 1,1,1-trifluoropropynyl trifluoroborate 357 and 2-pyrone 311, synthesis of adducts 354, 355 and 356
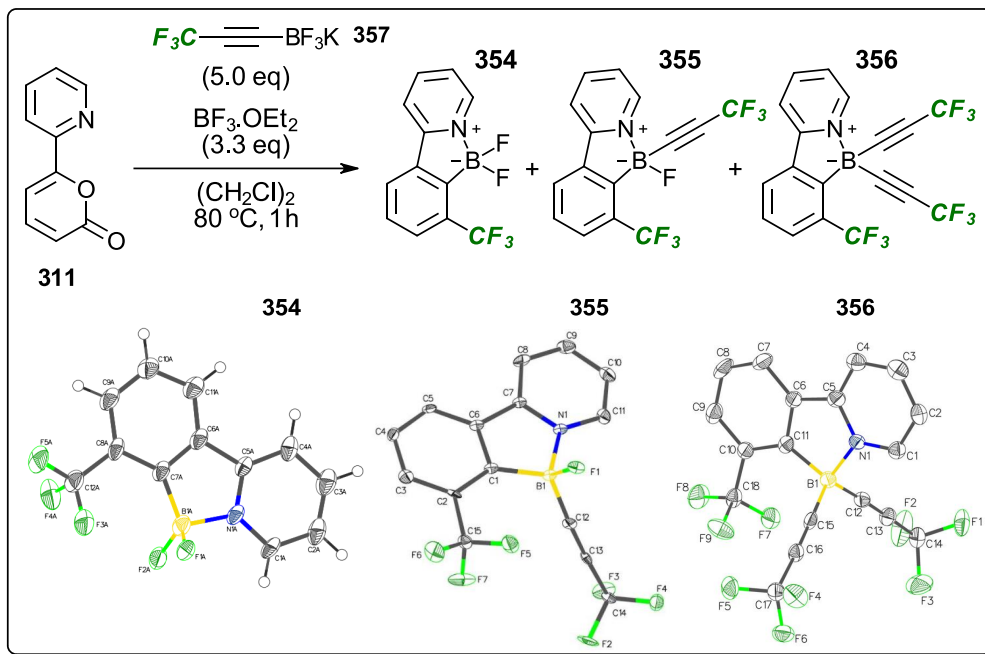
To a suspension of **311** (19 mg, 0.11 mmol) and **357** (110 mg, 0.55 mmol) in (CH₂Cl)₂ (1 mL) at 80 °C was added dropwise BF₃.OEt₂ (44 μL, 0.36 mmol). The mixture was allowed to stir at 80 °C for 1 hour, then cooled to room temperature and diluted with CH₂Cl₂ (10 mL). The mixture was then washed with NaHCO₃ (sat. aq., 4 mL) and the layers were separated. The aqueous layer was extracted with CH₂Cl₂ (3 x 5 mL) and the combined organic layers were dried over anhydrous MgSO₄ and concentrated *in vacuo*. The compounds **354**, **355** and **356** were purified by flash column chromatography on silica gel (gradient elution, 0-50% ethyl acetate in petroleum ether (60-80)), providing; **354** as a colourless solid (10 mg, 34%), **M.p. =** 217-218 °C (dec), **355** as a colourless solid (11 mg, 29%), **M.p. =** 153-154 °C and **356** as a colourless solid (4 mg, 9%), **M.p. =** 210 °C.

[2-(2-Pyridyl)-6-(trifluoromethyl)phenyl]difluoroborane **354**
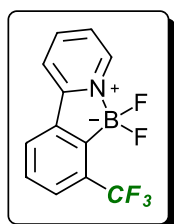
¹H NMR (400 MHz, acetone-d⁶) δ_H ppm 7.66 (t, 1H, J = 7.5 Hz), 7.78 (d, 1H, J = 8.0 Hz), 7.87 (ddd, 1H, J = 1.5, 5.5, 7.5 Hz), 8.26 (d, 1H, J = 7.5 Hz), 8.40 (d, 1H, J = 8.0 Hz), 8.49 (dt, 1H, J = 1.5, 7.5 Hz), 8.71 (d, 1H, J = 5.5 Hz); **¹³C NMR (101 MHz, acetone-d⁶)** δ_C ppm 120.0, 125.6 (q, J = 273.0 Hz), 126.2, 126.5, 129.0 (q, J = 4.5 Hz), 130.5, 133.4 (q, J = 33.0 Hz), 139.3 (t, J = 4.0 Hz), 142.9, 145.9, 154.5; **¹⁹F NMR (376 MHz, acetone-d⁶)** δ_F ppm -62.0 (t, J = 6.0 Hz), -159.1 − -158.6 (m); **¹¹B NMR (128 MHz, acetone-d⁶)** δ_B ppm 7.67 (t, J = 49.5 Hz); **FTIR (neat)** ν_{max} / cm⁻¹ 2925 (w), 2851 (w), 1626 (m), 1496 (m), 1117 (s), 775 (s); **HRMS (ESI-TOF)** *m/z* [M+Na]⁺ calculated for [C₁₂H₇¹¹BF₅NNa]⁺ 294.0484, found 294.0484; **Single crystal X-ray analysis** see appendix 6.

[2-(2-Pyridyl)-6-(trifluoromethyl)phenyl](3,3,3-trifluoro-1-propynyl)fluoroborane **355**
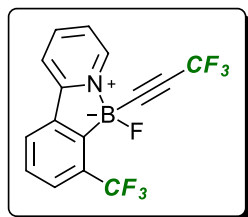
¹H NMR (400 MHz, acetone-d⁶) δ_H ppm 7.73 (t, 1H, J = 7.5 Hz), 7.84 (d, 1H, J = 8.0 Hz), 7.93 – 7.99 (m, 1H), 8.34 (d, 1H, J = 7.5 Hz), 8.49 (dd, 1H, J = 1.5, 8.0 Hz), 8.57 (dt, 1H, J = 1.5, 8.0 Hz), 8.92 (d, 1H, J = 5.5 Hz); **¹³C NMR (101 MHz, acetone-d⁶)** δ_C ppm 80.9 (q, J = 49.5 Hz), 114.8 (q, J = 255.0 Hz), 120.6, 125.7 (q, J = 273.5 Hz), 126.5, 127.0, 129.5 (q, J = 4.5 Hz), 130.8, 133.6 (q, J = 33.0 Hz), 139.5 (d, J = 3.0 Hz), 144.3, 146.2, 155.8; **¹⁹F NMR (376 MHz, acetone-d⁶)** δ_F ppm -50.3 (d, J = 2.5 Hz), -61.1 (d, J = 6.5 Hz), -187.0 – -186.4 (m); **¹¹B NMR (128 MHz, acetone-d⁶)** δ_B ppm 2.8 (d, J = 56.5 Hz); **FTIR (neat)** v_{max} / cm⁻¹ 2919 (w), 2850 (w), 2238 (w), 2213 (w), 1626 (m), 1496 (m), 1257 (s), 1136 (s), 1115 (s), 769 (s); **HRMS (ESI-TOF)** m/z [M+Na]⁺ calculated for $[C_{15}H_7{}^{11}BF_7NNa]^+$ 368.0453, found 368.0453. **Single crystal X-ray analysis** see appendix 6.

[2-(2-Pyridyl)-6-(trifluoromethyl)phenyl]bis(3,3,3-trifluoro-1-propynyl)borane **356**
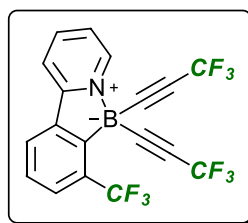
¹H NMR (400 MHz, acetone-d⁶) δ_H ppm 7.78 (dt, 1H, J = 8.0, 1.0 Hz), 7.92 (d, 1H, J = 8.0 Hz), 8.02 (ddd, 1H, J = 6.5, 6.0, 2.0 Hz), 8.44 (d, 1H, J = 8.0 Hz), 8.55 – 8.65 (m, 2H), 9.09 (d, 1H, J = 5.5 Hz); **¹³C NMR (101 MHz, acetone-d⁶)** δ_C ppm 82.4 (q, J = 57.5 Hz), 114.8 (q, J = 255.0 Hz), 121.1, 125.6 (q, J = 274.0 Hz), 126.7, 127.5, 130.0 (q, J = 4.5 Hz), 130.5, 133.1 (q, J = 33.0 Hz), 139.6, 145.0, 145.8, 157.0; **¹⁹F NMR (376 MHz, acetone-d⁶)** δ_F ppm -50.4 (s), -60.5 (s); **¹¹B NMR (128 MHz, acetone-d⁶)** δ_B ppm -11.1; **FTIR (neat)** v_{max} / cm⁻¹ 2927 (w), 2227 (m) 1627 (m), 1497 (m), 1254 (s), 1124 (s), 772 (s); **HRMS (ESI-TOF)** m/z [M+Na]⁺ calculated for $[C_{18}H_7{}^{11}BF_9NNa]^+$ 442.0421, found 442.0426. **Single crystal X-ray analysis** see appendix 6.

BF₃.OEt₂-promoted cycloaddition between potassium 1,1,1-trifluoropropynyl trifluoroborate 357 and 1,3,5-triazine 351
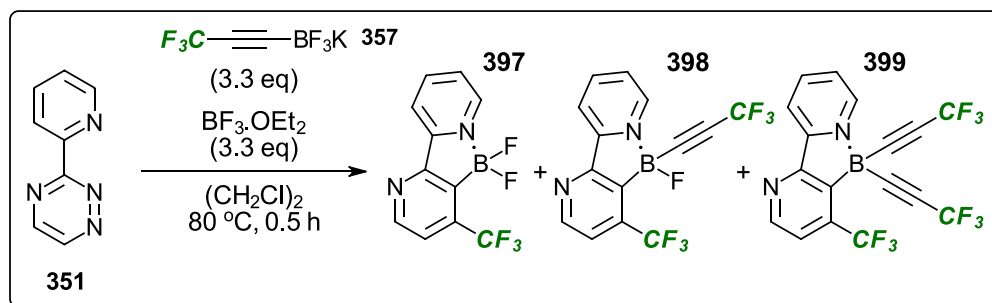
To a suspension of **351** (17 mg, 0.11 mmol) and **357** (72 mg, 0.36 mmol) in (CH₂Cl)₂ (1 mL) at 80 °C was added dropwise BF₃.OEt₂ (44 µL, 0.36 mmol). The mixture was allowed to stir at 80 °C for 30 minutes, then cooled to room temperature and diluted with CH₂Cl₂ (10 mL). The mixture was then washed with

NaHCO$_3$ (sat. aq., 4 mL) and the layers were separated. The aqueous layer was extracted with CH$_2$Cl$_2$ (3 x 5 mL) and the combined organic layers were dried over anhydrous MgSO$_4$ and concentrated *in vacuo*. The compounds **397**, **398** and **399** were purified by flash column chromatography on silica gel (gradient elution, 0-55% ethyl acetate in petroleum ether (60-80)), providing; **397** as a colourless solid (6 mg, 20%), **M.p. =** 189 – 190 °C, **398** as a colourless oil (6 mg, 16%) and **399** as a colourless solid (4 mg, 9%), **M.p. =** 131 – 132 °C (dec).

[4-(Trifluoromethyl)-2,2'-bipyridyl-3-yl]difluoroborane **397**
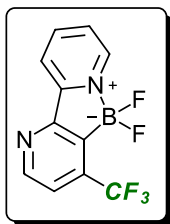
^{1}H NMR (400 MHz, acetone-d^6) δ$_H$ ppm 7.63 (d, 1H, J = 5.0 Hz), 8.05 (ddd, 1H, J = 1.0, 5.5, 7.5 Hz), 8.50 (d, 1H, J = 8.0 Hz), 8.64 (dt, 1H, J = 1.5, 8.0 Hz), 8.84 (d, 1H, J = 5.5 Hz), 8.90 (d, 1H, J = 5.0 Hz); ^{13}**C NMR (101 MHz, acetone-d^6)** δ$_C$ ppm 120.4, 122.1 (q, J = 4.0 Hz), 124.5 (q, J = 273.5 Hz), 128.2, 141.1 (q, J = 33.5 Hz), 143.1, 146.6, 152.5, 153.8, 158.5; ^{19}**F NMR (376 MHz, acetone-d^6)** δ$_F$ ppm -64.5 (t, J = 4.5 Hz), -158.8 (q, J = 49.5 Hz); ^{11}**B NMR (128 MHz, acetone-d^6)** δ$_B$ ppm 7.2 (t, J = 48.0 Hz); **FTIR (neat)** v$_{max}$ / cm^{-1} 3090 (w), 2927 (w), 2855 (w), 1630 (w), 1577 (w), 1315 (m), 1157 (s), 1155 (s), 1127 (s); **HRMS (ESI-TOF)** *m/z* [M+H]$^+$ calculated for [C$_{11}$H$_7$^{11}BF$_5$N$_2$]$^+$ 273.0617, found 273.0619.

[4-(Trifluoromethyl)-2,2'-bipyridyl-3-yl](3,3,3-trifluoro-1-propynyl)fluoroborane **398**
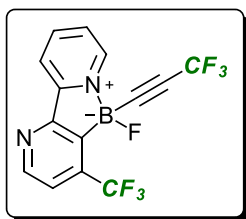
^{1}H NMR (400 MHz, acetone-d^6) δ$_H$ ppm 7.79 (d, 1H, J = 5.0 Hz), 8.13 (ddd, 1H, J = 5.5, 7.5 Hz), 8.56 (td, 1H, J = 1.0, 8.0 Hz), 8.70 (dt, 1H, J = 1.5, 8.0 Hz), 8.95 (d, 1H, J = 5.0 Hz), 9.04 (d, 1H, J = 5.5 Hz); ^{13}**C NMR (101 MHz, acetone-d^6)** δ$_C$ ppm 79.6 – 81.4 (q, low intensity and unresolved, J ≈ 43.5 Hz), 114.8 (q, J = 255.0 Hz), 121.0, 122.5 (q, J = 4.0 Hz), 124.5 (q, J = 274.0 Hz), 128.5, 141.2 (q, J = 34.5 Hz), 144.6, 146.9, 152.9, 154.8, 158.4 (d, J = 3.0 Hz); ^{19}**F NMR (376 MHz, acetone-d^6)** δ$_F$ ppm -50.6 (d, J = 2.5 Hz), -63.6 (d, J = 5.5 Hz), -186.0 – -187.7 (m); ^{11}**B NMR (128 MHz, acetone-d^6)** δ$_B$ ppm 2.3 (d, J = 53.0 Hz); **FTIR (neat)** v$_{max}$ / cm^{-1} 2930 (w), 2241 (w), 1630 (w), 1573 (w), 1316 (m), 1260 (s), 1125 (s); **HRMS (ESI-TOF)** *m/z* [M+H]$^+$ calculated for [C$_{14}$H$_7$^{11}BF$_7$N$_2$]$^+$ 347.0585, found 347.0585.

[4-(Trifluoromethyl)-2,2'-bipyridyl-3-yl]bis(3,3,3-trifluoro-1-propynyl)borane **399**
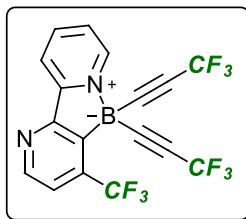
^{1}H NMR (400 MHz, acetone-d^6) δ$_H$ ppm 7.87 (d, 1H, J = 5.0 Hz), 8.18 (ddd, 1H, J = 1.5, 6.0, 7.5 Hz), 8.64 (td, 1H, J = 1.0, 8.0 Hz), 8.73 (dt, 1H, J = 1.5, 8.0 Hz), 9.01 (d, 1H, J = 5.0 Hz), 9.20 (d, 1H, J = 5.5 Hz); <u>399 was obtained in insufficient quantity for full characterisation by ^{13}C NMR spectroscopy</u>; ^{19}**F NMR (376 MHz, acetone-d^6)** δ$_F$ ppm -50.6, -63.1; ^{11}**B NMR (128 MHz, acetone-d^6)** δ$_B$ ppm -11.7; **FTIR (neat)** v$_{max}$ / cm^{-1} 2929 (w), 2856 (w), 2233 (w), 1631 (w), 1313 (w), 1255 (s), 1125 (s); **HRMS (ESI-TOF)** *m/z* [M+H]$^+$ calculated for [C$_{17}$H$_7$^{11}BF$_9$N$_2$]$^+$ 421.0554, found 421.0559.

4.3.4. Directed cycloadditions promoted by alternative Lewis acids

General procedure M, boron trihalide promoted directed cycloadditions of fluoroalkyl-substituted potassium alkynyltrifluoroborate salts with 2-pyrones and 1,3,4-triazines
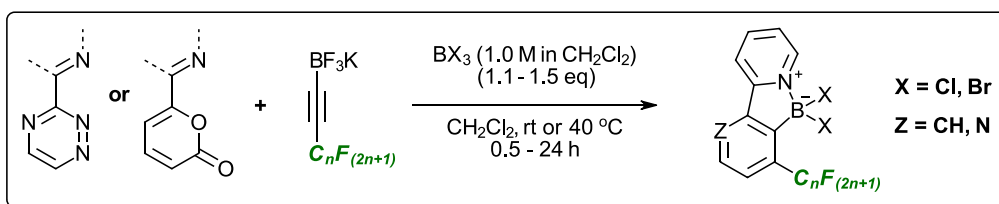
To a stirring suspension of the diene (1.0 eq) and the fluoroalkyl-substituted potassium alkynyl trifluoroborate salt (1.1 – 1.5 eq) in CH_2Cl_2 (0.11 M) at room temperature (19 °C) or 40 °C was added dropwise BX_3 (1.0 M in CH_2Cl_2, 1.1 – 1.5 eq). The reaction mixture was stirred at the starting temperature for the stated amount of time, then cooled (if necessary) and diluted tenfold with CH_2Cl_2. The crude mixture was washed with $NaHCO_3$ (sat. aq., 4 mL per 10 mL diluting CH_2Cl_2) and the layers were separated. The aqueous layer was extracted with CH_2Cl_2 (3 x 5 mL per 10 mL diluting CH_2Cl_2, unless otherwise stated) and the combined organic layers were dried over anhydrous $MgSO_4$ then concentrated *in vacuo*. If necessary, the compound was purified by flash column chromatography on silica gel (gradient elution, 0-80% EtOAc in petroleum ether), precipitation from acetone *via* addition of petroleum ether or recrystallised from hot acetone.

2-(2-(Dichloroboryl)-3-(trifluoromethyl)phenyl)pyridine **369**
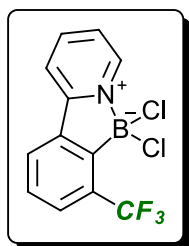
Following general procedure M, using pyrone **311** (114 mg, 0.66 mmol), potassium 1,1,1-trifluoroprop-2-ynyltrifluoroborate (144 mg, 0.72 mmol) and BCl_3 solution (0.72 mL, 0.72 mmol) stirring at room temperature (19 °C) for 30 minutes, the product was purified by flash column chromatography on silica gel (gradient elution, 0-80% EtOAc in petroleum ether), providing **369** as a colourless solid (185 mg, 92%) **M.p.** = 279-280 °C; **^{1}H NMR (400 MHz, acetone-d_6)** δ_H ppm 7.74 (td, 1H, J = 8.0, 1.0 Hz), 7.87 (d, 1H, J = 8.0 Hz), 7.99 (ddd, 1H, J = 7.5, 6.0, 1.0 Hz), 8.37 (d, 1H, J = 7.5 Hz), 8.46-8.53 (m, 1H), 8.54-8.61 (m, 1H), 8.99 (d, 1H, J = 6.0 Hz); **^{13}C NMR (101 MHz, acetone-d_6)** δ_C ppm 120.3, 125.53 (q, J = 274.0 Hz), 126.6, 127.1, 130.4 (q, J = 4.5 Hz), 130.7, 132.8 (q, J = 33.5), 137.4, 144.2, 146.3, 154.2; **^{19}F NMR (376 MHz, acetone-d_6)** δ_F ppm -59.5; **^{11}B NMR (128 MHz, acetone-d_6)** δ_B ppm 6.6; **FTIR (neat)** v_{max} / cm^{-1} 3095 (w), 1626 (m), 1307 (s), 1165 (s), 1145 (s), 763 (s), 701(s); **HRMS (ESI-TOF)** *m/z* [M+Na]$^+$ calculated for $[C_{12}H_7{}^{11}B^{35}Cl_2F_3NNa]^+$ 325.9893, found 325.9893.

2-(2-(Dichloroboryl)-3-(perfluorohexyl)phenyl)pyridine **373**
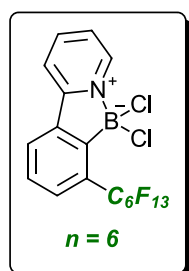
Following general procedure M, using pyrone **311** (19 mg, 0.11 mmol), potassium (perfluorohexylethynyl)trifluoroborate (76 mg, 0.17 mmol) and BCl_3 solution (0.17 mL, 0.17 mmol) stirring at 40 °C for 30 minutes, further purification was not deemed necessary, providing **373** as a colourless solid (61 mg, 100%) **M.p.** = 228 – 229 °C; **^{1}H NMR (400 MHz, acetone-d_6)** δ_H ppm 7.76 – 7.85 (m, 2H), 7.99 (ddd, 1H, J = 1.0, 6.0, 7.5 Hz), 8.43 (dd, 1H, J = 1.0, 7.5 Hz), 8.49 – 8.54 (m, 1H), 8.58 (ddd, 1H, J = 1.5, 7.5, 8.0 Hz), 8.96 – 9.04 (m, 1H); **^{13}C NMR (101 MHz, acetone-d_6)** δ_C ppm 105.4 –

123.0 (m, multiple peaks), 120.3, 126.7, 127.4, 130.6, 131.4 (t, J = 25.5 Hz), 132.1 – 132.4 (m), 137.7, 144.1, 146.3, 154.1; **^{19}F NMR (376 MHz, acetone-d^6)** δ_F ppm -81.6 – -81.7 (m), -105.4 – -105.6 (m), -119.3 – -119.7 (m), -121.7 – -122.2 (m), -123.2 – -123.4 (m), -126.6 – -126.9 (m); **^{11}B NMR (128 MHz, acetone-d^6)** δ_B ppm 6.8; **FTIR (neat)** ν_{max} / cm^{-1} 3086 (w), 2981 (w), 1626 (w), 1497 (w), 1215 (s), 1143 (s), 714 (s); **HRMS (ESI-TOF)** *m/z* [M-Cl]$^+$ calculated for [C$_{17}$H$_7$^{11}B^{35}ClF$_{13}$N]$^+$ 518.0148, found 518.0144.

2-(2-(Dichloroboryl)-3-(perfluorooctyl)phenyl)pyridine **374**
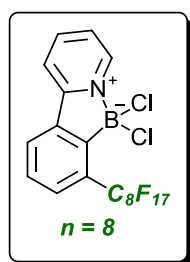
Following general procedure M, using pyrone **311** (19 mg, 0.11 mmol), potassium (perfluorooctylethynyl)trifluoroborate (91 mg, 0.17 mmol) and BCl$_3$ solution (0.17 mL, 0.17 mmol) stirring at room temperature (19 °C) for 30 minutes, the product was recrystallised from acetone, providing **374** as a colourless solid (41 mg, 57%) **M.p.** = 242 – 243 °C; **^{1}H NMR (400 MHz, acetone-d$_6$)** δ_H ppm 7.75 – 7.86 (m, 2H), 7.99 (ddd, 1H, J = 1.0, 6.0, 7.5 Hz), 8.40 – 8.46 (m, 1H), 8.52 (dt, 1H, J = 1.0, 8.0 Hz), 8.59 (ddd, 1H, J = 1.5, 7.5, 8.0 Hz), 9.00 (d, 1H, J = 6.0 Hz); **^{13}C NMR (101 MHz, acetone-d^6)** δ_C ppm 107.0 – 121.0 (m, multiple signals), 120.3, 126.7, 127.4, 130.6, 131.4 (t, J = 25.5 Hz), 132.1 – 132.5 (m), 137.7, 144.1, 146.3, 154.1; **^{19}F NMR (376 MHz, acetone-d^6)** δ_F ppm -81.7 – 81.6 (m), -105.6 – -105.4 (m), -119.6 – -119.2 (m), -121.7 – -121.5 (m), -122.6 – -122.1 (m), -123.4 – -123.0 (m), -126.9 – -126.5 (m); **^{11}B NMR (128 MHz, acetone-d^6)** δ_B ppm 6.8; **FTIR (neat)** ν_{max} / cm^{-1} 3091 (w), 2924 (w), 2853 (w), 1626 (w), 1497 (w), 1220 (s), 1207 (s), 1146 (s), 761 (s); **HRMS (ESI-TOF)** *m/z* [M+H]$^+$ calculated for [C$_{19}$H$_7$^{11}B^{35}ClF$_{17}$N]$^+$ 618.0085, found 618.0073.

2-(2-(Dibromoboryl)-3-(trifluoromethyl)phenyl)pyridine **370**
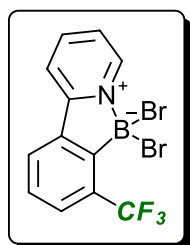
Following general procedure M, using pyrone **311** (19 mg, 0.11 mmol), potassium 1,1,1-trifluoroprop-2-ynyltrifluoroborate (34 mg, 0.17 mmol) and BBr$_3$ solution (0.17 mL, 0.17 mmol) stirring at 40 °C for 30 minutes, the product was purified by flash column chromatography on silica gel (gradient elution, 0-80% EtOAc in petroleum ether), providing **370** as a colourless solid (26 mg, 60%) **M.p.** = 218 – 219 °C (dec); **^{1}H NMR (400 MHz, acetone-d$_6$)** δ_H ppm 7.76 (ddd, 1H, J = 1.0, 1.5, 8.5 Hz), 7.9 (d, 1H, J = 8.0 Hz), 8.00 (ddd, 1H, J = 1.0, 6.0, 7.5 Hz), 8.41 (d, 1H, J = 7.5 Hz), 8.48 – 8.53 (m, 1H), 8.58 (ddd, 1H, J = 1.5, 7.5, 8.0 Hz), 9.15 (d, 1H, J = 6.0 Hz); **^{13}C NMR (101 MHz, acetone-d^6)** δ_C ppm 119.7, 124.7 (q, J = 274.5 Hz), 125.8, 126.4, 129.85, 129.88 (q, J = 4.5 Hz), 131.9 (q, J = 33.0 Hz), 135.8, 144.4, 145.5, 152.9; **^{19}F NMR (376 MHz, acetone-d^6)** δ_F ppm -58.5; **^{11}B NMR (128 MHz, acetone-d^6)** δ_B ppm -1.9; **FTIR (neat)** ν_{max} / cm^{-1} 3088 (w), 2927 (w), 2855 (w), 1628 (m), 1495 (m), 1306 (m), 1132 (m), 780 (m); **HRMS (ESI-TOF)** *m/z* [M-Br]$^+$ calculated for [C$_{12}$H$_7$^{11}B^{79}BrF$_3$N]$^+$ 311.9802, found 311.9802.

2-(2-(Dichloroboryl)-3-(trifluoromethyl)phenyl)-6-methylpyridine 377
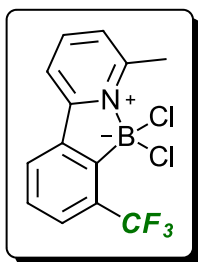
Following general procedure M, using pyrone **338** (21 mg, 0.11 mmol), potassium 1,1,1-trifluoroprop-2-ynyltrifluoroborate (34 mg, 0.17 mmol) and BCl_3 (0.17 mL, 0.17 mmol) stirring at 40 °C for 30 minutes, the product was purified by flash column chromatography on silica gel (gradient elution, 0-80% EtOAc in petroleum ether), providing **377** as a colourless solid (28 mg, 80%) **M.p.** = 288-289 °C; **^{1}H NMR (400 MHz, acetone-d6)** δ_H ppm 3.21 (s, 3H), 7.66-7.77 (m, 2H), 7.85 (d, 1H, J = 8.0 Hz), 8.27-8.34 (m, 2H), 8.38 (t, 1H, J = 8.0 Hz); **^{13}C NMR (101 MHz, acetone-d6)** δ_C ppm 21.0, 117.6, 125.6 (q, J = 274.0 Hz), 126.5, 128.6, 130.50, 130.51 (q, J = 4.5 Hz), 132.3 (q, J = 33.0 Hz), 137.1, 145.5, 155.2, 158.6; **^{19}F NMR (376 MHz, acetone-d6)** δ_F ppm -58.8; **^{11}B NMR (128 MHz, acetone-d6)** δ_B ppm 7.4; **FTIR (neat)** v_{max} / cm^{-1} 3072 (w), 2926 (w), 1492 (m), 1312 (s), 1167 (s), 1109 (s), 707 (s), 698 (s); **HRMS (ESI-TOF)** *m/z* [M+Na]$^+$ calculated for $[C_{13}H_9{}^{11}B^{35}Cl_2F_3NNa]^+$ 340.0049, found 340.0053. **Single crystal X-ray analysis** see appendix 6.

5-Chloro-2-(2-(dichloroboryl)-3-(trifluoromethyl)phenyl)pyridine 376
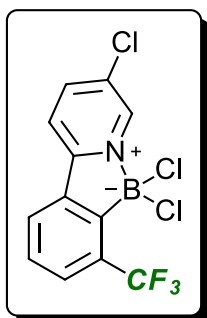
Following general procedure M, using pyrone **342** (23 mg, 0.11 mmol), potassium 1,1,1-trifluoroprop-2-ynyltrifluoroborate (34 mg, 0.17 mmol) and BCl_3 (0.17 mL, 0.17 mmol) stirring at room temperature (19 °C) for 30 minutes, further purification was not deemed necessary, providing **376** as a brown solid (34 mg, 91%) **M.p.** = 297-298 °C; **^{1}H NMR (400 MHz, acetone-d6)** δ_H ppm 7.72-7.78 (m, 1H), 7.89 (d, 1H, J = 8.0 Hz), 8.38 (d, 1H, J = 8.0 Hz), 8.54 (dd, 1H, J = 8.5, 0.5 Hz), 8.63 (dd, 1H, J = 8.5, 2.0 Hz), 9.02 (dd, 1H, J = 2.0, 0.5 Hz); **^{13}C NMR (101 MHz, acetone-d6)** δ_C ppm 121.6, 125.4 (q, J = 274.0 Hz), 127.3, 130.6 (q, J = 4.5 Hz), 130.9, 132.8 (q, J = 33.5 Hz), 133.7, 136.7, 142.8, 146.2, 153.2; **^{19}F NMR (376 MHz, acetone-d6)** δ_F ppm -59.6; **^{11}B NMR (128 MHz, acetone-d6)** δ_B ppm 6.8; **FTIR (neat)** v_{max} / cm^{-1} 3128 (w), 3070 (w), 1494 (m), 1312 (s), 1131 (s), 815 (s), 778 (s), 751 (s), 707 (s); **HRMS (ESI-TOF)** *m/z* [M+Na]$^+$ calculated for $[C_{12}H_6{}^{11}B^{35}Cl_3F_3NNa]^+$ 359.9503, found 359.9505.

2-Bromo-6-(2-(dichloroboryl)-3-(trifluoromethyl)phenyl)pyridine, 375
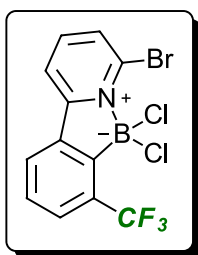
Following general procedure M, using pyrone **343** (28 mg, 0.11 mmol), potassium 1,1,1-trifluoroprop-2-ynyltrifluoroborate (34 mg, 0.17 mmol) and BCl_3 (0.17 mL, 0.17 mmol) stirring at room temperature (19 °C) for 30 minutes, the product was purified by flash column chromatography on silica gel (gradient elution, 0-80% EtOAc in petroleum ether), providing **375** as a colourless solid (15 mg, 36%) **M.p.** = 253 °C; **^{1}H NMR (400 MHz, DMSO-d6)** δ_H ppm 7.71-7.78 (m, 1H), 7.89 (d, 1H, J = 8.0 Hz), 8.17 (dd, 1H, J = 8.0, 1.0 Hz), 8.36 (t, 1H, J = 8.0 Hz), 8.44 (d, 1H, J = 8.0 Hz), 8.59 (dd, 1H, J = 8.0, 1.0 Hz); **^{13}C NMR (101 MHz, DMSO-d6)** δ_C ppm 118.9, 124.3 (q, J = 275.0 Hz), 126.8, 130.1, 130.2 (q, J = 5.0 Hz), 130.3 (q, J = 32.5 Hz), 132.3, 135.1, 137.9, 146.3, 156.6; **^{19}F NMR (376 MHz, acetone-d6)** δ_F ppm -58.7; **^{11}B NMR (128 MHz, acetone-d6)** δ_B ppm 8.8; **FTIR (neat)** v_{max} / cm^{-1} 3128 (w), 3071 (w), 1494 (m), 1312 (s), 1131 (s), 815 (s), 708 (s); **HRMS (ESI-TOF)** *m/z* [M+Na]$^+$ calculated for $[C_{12}H_6{}^{11}B^{79}Br^{35}Cl_2F_3NNa]^+$ 403.8998, found 403.9001.

2-(2-(Dichloroboryl)-3-(trifluoromethyl)phenyl)quinoline, 378
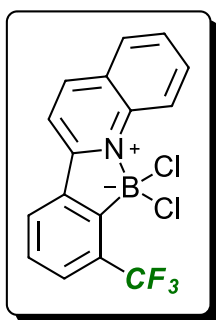
Following general procedure M, using pyrone **339** (25 mg, 0.11 mmol), potassium 1,1,1-trifluoroprop-2-ynyltrifluoroborate (34 mg, 0.17 mmol) and BCl_3 (0.17 mL, 0.17 mmol) stirring at 40 °C for 30 minutes. The aqueous layer was extracted first with CH_2Cl_2 (7 x 5 mL), then with EtOAc (3 x 5 mL). Further purification was not deemed necessary, providing **378** as a brown solid (34 mg, 87%) **M.p.** = >300 °C; **^{1}H NMR (400 MHz, DMSO-d$_6$)** δ$_H$ ppm 7.79-7.86 (m, 1H), 7.92 (ddd, 1H, J = 8.0, 7.0, 1.0 Hz), 7.98 (d, 1H, J = 8.0 Hz), 8.20 (ddd, 1H, J = 8.5, 7.0, 1.5 Hz), 8.38 (dd, 1H, J = 8.0, 1.5 Hz), 8.66 (d, 1H, J = 8.0 Hz), 8.74 (d, 1H, J = 8.5 Hz), 8.95 (d, 1H, 9.0 Hz), 9.22 (d, 1H, J = 8.5 Hz); ^{13}C NMR (101 MHz, DMSO-d^6) δ$_C$ ppm 116.3, 122.5, 124.4 (q, J = 274.5 Hz), 128.0, 128.4, 129.0, 130.2 (2 x C), 130.4 (q, J = 4.5 Hz), 130.4 (q, J = 33.0 Hz), 133.8, 136.3, 138.4, 147.4, 155.4; **^{19}F NMR (376 MHz, DMSO-d^6)** δ$_F$ ppm -57.3; **^{11}B NMR (128 MHz, DMSO-d^6)** δ$_B$ ppm 6.9; **FTIR (neat)** v$_{max}$ / cm^{-1} 3125 (w), 3070 (w), 3046 (w), 1494 (m), 1312 (s), 1130 (s), 815 (s), 707 (s); **HRMS (ESI-TOF)** m/z [M+Na]$^+$ calculated for [$C_{16}H_9^{11}B^{35}Cl_2F_3NNa$]$^+$ 376.0049, found 376.0055.

2-(2-(Dichloroboryl)-3-(trifluoromethyl)phenyl)-4,5-dimethylthiazole 380
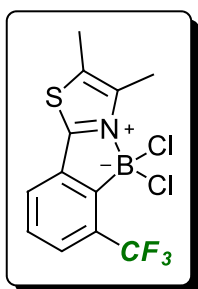
Following general procedure M, using pyrone **345** (23 mg, 0.11 mmol), potassium 1,1,1-trifluoroprop-2-ynyltrifluoroborate (34 mg, 0.17 mmol) and BCl_3 (0.17 mL, 0.17 mmol) stirring at 40 °C for 30 minutes, further purification was not deemed necessary, providing **380** as a brown solid (35 mg, 94%) **M.p.** = >300 °C; **^{1}H NMR (400 MHz, acetone-d$_6$)** δ$_H$ ppm 2.59 (q, 3H, J = 1.0 Hz), 2.70 (q, 3H, J = 1.0 Hz), 7.65-7.70 (m, 1H), 7.83 (d, 1H, J = 8.0 Hz), 8.07 (d, 1H, J = 7.5 Hz; **^{13}C NMR (101 MHz, acetone-d$_6$)** δ$_C$ ppm 11.9 (q, J = 4.0 Hz), 12.1 (q, J = 4.0 Hz), 125.4 (q, J = 274.5 Hz), 126.7, 130.2 (q, J = 4.5 Hz), 130.6, 132.5 (q, J = 33.5 Hz), 133.1, 134.0, 142.8, 168.2; **^{19}F NMR (376 MHz, acetone-d^6)** δ$_F$ ppm -59.3; **^{11}B NMR (128 MHz, acetone-d^6)** δ$_B$ ppm 5.0; **FTIR (neat)** v$_{max}$ / cm^{-1} 3092 (w), 3029 (w), 1570 (w), 1305 (s), 1169 (s), 1112 (s), 815 (s), 717 (s); **HRMS (ESI-TOF)** m/z [M+Na]$^+$ calculated for [$C_{12}H_9^{11}B^{35}Cl_2F_3NNaS$]$^+$ 359.9770, found 359.9773.

2-(2-(Dichloroboryl)-3-(trifluoromethyl)phenyl)benzo[d]thiazole 381
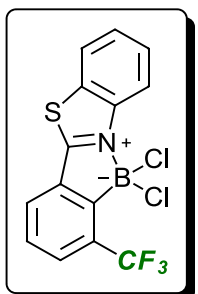
Following general procedure M, using pyrone **340** (25 mg, 0.11 mmol), potassium 1,1,1-trifluoroprop-2-ynyltrifluoroborate (34 mg, 0.17 mmol) and BCl_3 (0.17 mL, 0.17 mmol) stirring at 40 °C for 30 minutes, further purification was not deemed necessary, providing **381** as a brown solid (38 mg, 96%) **M.p.** = >300 °C; **^{1}H NMR (400 MHz, DMSO-d$_6$)** δ$_H$ ppm 7.76 (ddd, 1H, J = 8.5, 7.5, 1.0 Hz), 7.79-7.84 (m, 1H), 7.89 (ddd, 1H, J = 8.5, 7.5, 1.0 Hz), 8.01 (d, 1H, J = 8.0 Hz), 8.29 (d, 1H, J = 8.5 Hz), 7.74-7.79 (m, 2H); **^{13}C NMR (101 MHz, DMSO-d^6)** δ$_C$ ppm 118.5, 124.1 (q, J = 275.0 Hz), 125.6, 127.6, 128.9, 129.3, 130.5, 130.6 (q, J = 33.0 Hz), 130.8 (q, J = 5.0 Hz), 133.0, 134.2, 139.2, 173.5; **^{19}F NMR (376 MHz, DMSO-d^6)** δ$_F$ ppm -57.9; **^{11}B NMR (128 MHz, DMSO-d^6)** δ$_B$ ppm 4.9; **FTIR (neat)** v$_{max}$ / cm^{-1} 3074 (w), 2926 (w), 1425 (m), 1302 (s), 1124 (s), 755 (s), 710 (s), 714 (s); **HRMS (ESI-TOF)** m/z [M+Na]$^+$ calculated for [$C_{14}H_7^{11}B^{35}Cl_2F_3NNaS$]$^+$ 381.9614, found 381.9623.

2-(2-(Dichloroboryl)-3-(trifluoromethyl)phenyl)thiazole 379
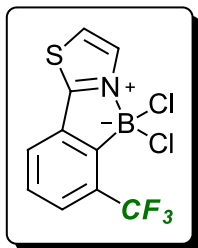
Following general procedure M, using pyrone **344** (20 mg, 0.11 mmol), potassium 1,1,1-trifluoroprop-2-ynyltrifluoroborate (34 mg, 0.17 mmol) and BCl_3 (0.17 mL, 0.17 mmol) stirring at 40 °C for 16 hours inside a sealed tube, further purification was not deemed necessary, providing **379** as a brown solid (32 mg, 94%) **M.p. =** 250-251 °C (dec); **^{1}H NMR (400 MHz, acetone-d$_6$)** δ_H ppm 7.70-7.75 (m, 1H), 7.88 (d, 1H, J = 8.0 Hz), 8.17 (d, 1H, J = 3.5 Hz), 8.24 (d, 1H, J = 7.5 Hz), 8.30 (d, 1H, J = 3.5 Hz); **^{13}C NMR (101 MHz, acetone-d^6)** δ_C ppm 125.3 (q, J = 274.0 Hz), 126.3, 127.6, 130.5 (q, J = 4.5 Hz), 130.7, 132.7 (q, J = 33.5 Hz), 134.0, 134.3, 171.7; **^{19}F NMR (376 MHz, acetone-d^6)** δ_F ppm -59.6; **^{11}B NMR (128 MHz, acetone-d^6)** δ_B ppm 4.5; **FTIR (neat)** v_{max} / cm^{-1} 3123 (w), 1312 (s), 1166 (s), 1130 (s), 816 (s), 709 (s), 701 (s); **HRMS (ESI-TOF)** *m/z* [M+Na]$^+$ calculated for [C$_{10}$H$_5$^{11}B^{35}Cl$_2$F$_3$NNaS]$^+$ 331.9457, found 331.9460.

4-(2-(Dichloroboryl)-3-(trifluoromethyl)phenyl)thiazole 382
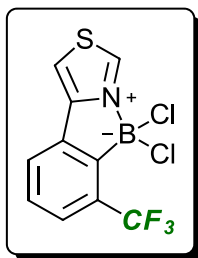
Following general procedure M, using pyrone **341** (20 mg, 0.11 mmol), potassium 1,1,1-trifluoroprop-2-ynyltrifluoroborate (34 mg, 0.17 mmol) and BCl_3 (0.17 mL, 0.17 mmol) stirring at 40 °C for 24 hours inside a sealed tube, further purification was not deemed necessary, providing **382** as a brown solid (34 mg, 100%) **M.p. =** 209-210 °C (dec); **^{1}H NMR (400 MHz, acetone-d$_6$)** δ_H ppm 7.62-7.68 (m, 1H), 7.75 (d, 1H, J = 8.0 Hz), 8.14 (d, 1H, J = 7.5 Hz), 8.36 (d, 1H, J = 2.0 Hz), 10.02 (d, 1H, J = 2.0 Hz); **^{13}C NMR (101 MHz, acetone-d^6)** δ_C ppm 113.9, 125.5 (q, J = 274.0 Hz), 126.3, 128.6 (q, J = 4.5 Hz), 130.5, 133.1 (q, J = 33.0 Hz), 134.3, 153.4, 157.2; **^{19}F NMR (376 MHz, acetone-d^6)** δ_F ppm -59.2; **^{11}B NMR (128 MHz, acetone-d^6)** δ_B ppm 4.4; **FTIR (neat)** v_{max} / cm^{-1} 3122 (w), 1319 (s), 1165 (s), 1165 (s), 1115 (s), 1077 (s), 815 (s), 756 (s); **HRMS (ESI-TOF)** *m/z* [M+Na]$^+$ calculated for [C$_{10}$H$_5$^{11}B^{35}Cl$_2$F$_3$NNaS]$^+$ 331.9457, found 331.9460.

4-(2-(Dichloroboryl)-3-(trifluoromethyl)phenyl)-2-methyloxazole 383
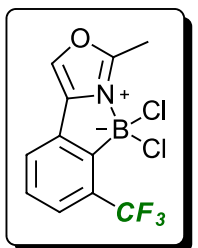
Following general procedure M, using pyrone **346** (19 mg, 0.11 mmol), potassium 1,1,1-trifluoroprop-2-ynyltrifluoroborate (34 mg, 0.17 mmol) and BCl_3 (0.17 mL, 0.17 mmol) stirring at 40 °C for 16 hours inside a sealed tube, further purification was not deemed necessary, providing **383** as a brown solid (34 mg, 100%) **M.p. =** 252-253 °C (dec); **^{1}H NMR (400 MHz, acetone-d$_6$)** δ_H ppm 2.98 (s, 3H), 7.59-7.68 (m, 1H), 7.74 (d, 1H, J = 8.0 Hz), 7.97 (d, 1H, J = 7.5 Hz), 8.55 (s, 1H); **^{13}C NMR (101 MHz, acetone-d^6)** δ_C ppm 12.8, 125.5 (q, J = 274.0 Hz), 126.7, 128.6 (q, J = 5.0 Hz), 130.5, 130.9, 133.1 (q, J = 33.0 Hz), 133.4, 139.6, 164.6; **^{19}F NMR (376 MHz, acetone-d^6)** δ_F ppm -59.0; **^{11}B NMR (128 MHz, acetone-d^6)** δ_B ppm 4.0; **FTIR (neat)** v_{max} / cm^{-1} 3174 (w), 1302 (s), 1174 (s), 1123 (s), 823 (s), 762 (s); **HRMS (ESI-TOF)** *m/z* [M+Na]$^+$ calculated for [C$_{11}$H$_7$^{11}B^{35}Cl$_2$F$_3$NNaO]$^+$ 329.9842, found 329.9845.

(2-(Dimethylcarbamoyl)-6-(trifluoromethyl)phenyl)boronic acid **384**
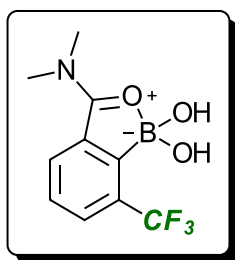
Following general procedure M, using pyrone **348** (18 mg, 0.11 mmol), potassium 1,1,1-trifluoroprop-2-ynyltrifluoroborate (34 mg, 0.17 mmol) and BCl$_3$ (0.17 mL, 0.17 mmol) stirring at 40 $^\circ$C for 30 minutes, the product was purified by precipitation from a saturated acetone solution *via* the addition of petroleum ether (5 x V$_{acetone}$) followed by agitation, then chilling to -20 $^\circ$C over 30 minutes. The precipitation was performed two times providing **384** as a colourless solid (28 mg, 98%) **M.p.** = 208-209 $^\circ$C (dec); **^{1}H NMR (400 MHz, acetone-d$_6$)** δ$_H$ ppm 3.62 (s, 3H), 3.98 (s, 3H), 7.73-7.80 (m, 1H), 8.01 (d, 1H, J = 8.0 Hz), 8.47 (d, 1H, J = 8.0 Hz); ^{13}**C NMR (101 MHz, acetone-d$_6$)** δ$_C$ ppm 41.5, 42.2, 125.2 (q, J = 274.0 Hz), 130.2, 132.0, 132.1 (q, J = 34.0), 132.2, 132.5 (q, J = 4.5 Hz), 171.8; ^{19}**F NMR (376 MHz, acetone-d$_6$)** δ$_F$ ppm -59.2; ^{11}**B NMR (128 MHz, acetone-d$_6$)** δ$_B$ ppm 9.6; **FTIR (neat)** v$_{max}$ / cm^{-1} 3394 (br), 3092 (w), 2957 (w), 2899 (w), 2878 (w), 1655 (s), 1429 (w), 1392 (s), 3120 (s), 1169 (s), 1125 (s), 733 (s), 701 (s); **HRMS (ESI-TOF)** *m/z* [M+Na]$^+$ calculated for [C$_{10}$H$_{11}$^{11}BF$_3$NNaO$_3$]$^+$ 284.0676, found 284.0677.

(2-(Piperidine-1-carbonyl)-6-(trifluoromethyl)phenyl)boronic acid **385**
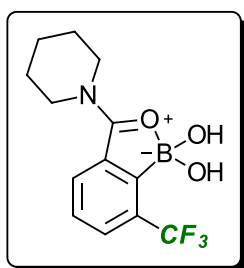
Following general procedure M, using pyrone **349** (23 mg, 0.11 mmol), potassium 1,1,1-trifluoroprop-2-ynyltrifluoroborate (34 mg, 0.17 mmol) and BCl$_3$ (0.17 mL, 0.17 mmol) stirring at 40 $^\circ$C for 30 minutes, the product was purified by precipitation from a saturated acetone solution *via* the addition of petroleum ether (5 x V$_{acetone}$) followed by agitation, then chilling to -20 $^\circ$C over 30 minutes. The supernatant was decanted, and the resultant solid was washed once with petroleum ether and the remaining solid was dried thoroughly *in vacuo*. The precipitation was performed two times providing **385** as a colourless solid (29 mg, 88%) **M.p.** = 195-196 $^\circ$C (dec); **^{1}H NMR (400 MHz, acetonitrile-d$_3$)** δ$_H$ ppm 1.76-1.86 (m, 4H), 1.87-1.92 (m, 2H), 3.97-4.05 (m, 2H), 4.17-4.25 (m, 2H), 7.65-7.72 (m, 1H), 7.98 (d, 1H, J = 8.0 Hz), 8.28 (d, 1H, J = 8.0 Hz); ^{13}**C NMR (101 MHz, acetone-d$_6$)** δ$_C$ ppm 22.9, 25.5, 25.6, 49.4, 124.2 (q, J = 274.0 Hz), 129.3, 130.8, 131.0, 131.3 (q, J = 33.5 Hz), 131.6 (q, J = 4.5 Hz), 168.9; ^{19}**F NMR (376 MHz, acetone-d$_6$)** δ$_F$ ppm -59.2; ^{11}**B NMR (128 MHz, acetone-d$_6$)** δ$_B$ ppm 9.5; **FTIR (neat)** v$_{max}$ / cm^{-1} 3484 (br), 3224 (br), 3023 (w), 2975 (w), 2947 (w), 2949 (w), 2864 (w), 1633 (s), 1456 (m), 1385 (s), 1318 (s), 1174 (s), 1093 (s), 734 (s), 701 (s); **HRMS (ESI-TOF)** *m/z* [M+Na]$^+$ calculated for [C$_{13}$H$_{15}$^{11}BF$_3$NNaO$_3$]$^+$ 324.0989, found 324.0989.

2-(3-(Dichloroboryl)-4-(trifluoromethyl)pyridin-2-yl)pyridine **400**
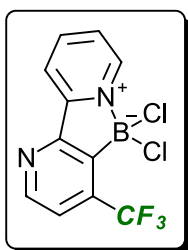
Following general procedure M, using triazine **351** (17 mg, 0.11 mmol), potassium 1,1,1-trifluoroprop-2-ynyltrifluoroborate (33 mg, 0.17 mmol) and BCl$_3$ solution (0.17 mL, 0.17 mmol) stirring at 40 $^\circ$C for 30 minutes, the product was purified by passing through a small plug of silica gel (eluting with EtOAc), providing **400** as a colourless solid (18 mg, 54%) **M.p.** = 177 – 178 $^\circ$C; **^{1}H NMR (400 MHz, acetone-d$_6$)** δ$_H$ ppm 7.82 (d, 1H, J = 5.0 Hz), 8.16 (ddd, 1H, J = 2.5, 5.5, 9.5 Hz), 8.52 – 8.58 (m, 1H), 8.71 (dt, 1H, J = 1.5, 8.0 Hz), 8.97 (dd, 1H, J = 0.5, 5.0 Hz), 9.10 (d, 1H, J = 5.5 Hz); ^{13}**C NMR (101 MHz, acetone-d$_6$)** δ$_C$ ppm 120.8, 123.3 (q, J = 4.5 Hz), 124.4 (q, J = 124.5 Hz), 128.6, 140.3 (q, J = 35.0 Hz), 144.3, 147.1, 152.9, 153.3, 156.0; ^{19}**F NMR (376 MHz, acetone-d$_6$)** δ$_F$ ppm -62.1; ^{11}**B NMR (128 MHz, acetone-d$_6$)** δ$_B$ ppm 6.1; **FTIR (neat)** v$_{max}$ / cm^{-1} 3085 (w), 2926 (w), 2855 (w), 1630 (w), 1482 (w), 1314 (s), 1134 (s), 1087 (m), 772 (s); **HRMS (ESI-TOF)** *m/z* [M+Na]$^+$ calculated for [C$_{11}$H$_6$^{11}B^{35}Cl$_2$F$_3$N$_2$Na]$^+$ 326.9846, found 326.9849.

TMS-Cl promoted reaction of 357 with 2-pyrone 311, synthesis of 371
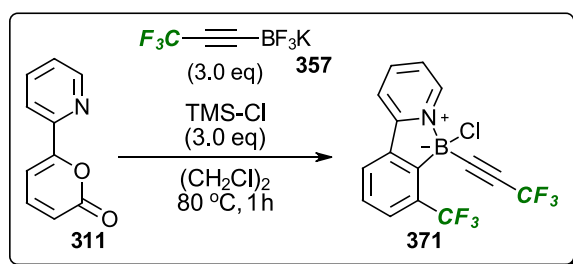
To a suspension of **311** (19 mg, 0.11 mmol) and **357** (68 mg, 0.34 mmol) in $(CH_2Cl)_2$ (1.0 mL) at 50 °C was added dropwise TMS-Cl (43 μL, 0.34 mmol). The mixture was heated at 80 °C for 1 hour, then cooled to room temperature and diluted with CH_2Cl_2 (10 mL). The resultant solution was washed with saturated aqueous $NaHCO_3$ (4 mL) and the layers were separated. The aqueous layer was extracted with CH_2Cl_2 (3 x 5 mL) and the combined organic layers were dried over anhydrous $MgSO_4$ then concentrated *in vacuo*. The crude product was purified by flash column chromatography on florisil (gradient elution, 0 – 50% EtOAc in hexanes), affording **371** as a colourless solid (31 mg, 78%). **M.p. =** 205 – 206 °C (dec); **^{1}H NMR (400 MHz, acetone-d$_6$)** δ_H ppm 7.77 (ddt, 1H, J = 1.0, 1.5, 8.0 Hz), 7.89 (d, 1H, J = 8.0 Hz), 8.01 (ddd, 1H, J = 1.5, 6.0, 7.5 Hz), 8.41 (d, 1H, J = 7.5 Hz), 8.55 (d, 1H, J = 8.0 Hz), 8.61 (dt, 1H, J = 1.5, 8.0 Hz), 9.03 (d, 1H, J = 6.0 Hz); **^{13}C NMR (101 MHz, acetone-d^6)** δ_C ppm 82.3 (q, J = 49.0 Hz), 114.9 (q, J = 255.0 Hz), 120.8, 125.5 (q, J = 273.5 Hz), 126.7, 127.3, 130.1 (q, J = 4.0 Hz), 130.8, 133.0 (q, J = 33.0 Hz), 138.8, 144.8, 146.3, 155.8; **^{19}F NMR (376 MHz, acetone-d^6)** δ_F ppm -50.5, -60.0; **^{11}B NMR (128 MHz, acetone-d^6)** δ_B ppm -2.4; **FTIR (neat)** v_{max} / cm^{-1} 2917 (w), 2849 (w), 2219 (w), 1628 (w), 1497 (w), 1255 (m), 1136 (s); **HRMS (ESI-TOF)** *m/z* [M+Na]$^+$ calculated for [$C_{15}H_7^{11}BClF_6NNa$]$^+$ 384.0157, found 384.0161.

4.3.5. Directed cycloadditions of sydnones and tetrazines

BF$_3$.OEt$_2$-promoted reaction of 357 with sydnone 350, synthesis of 401 and 402
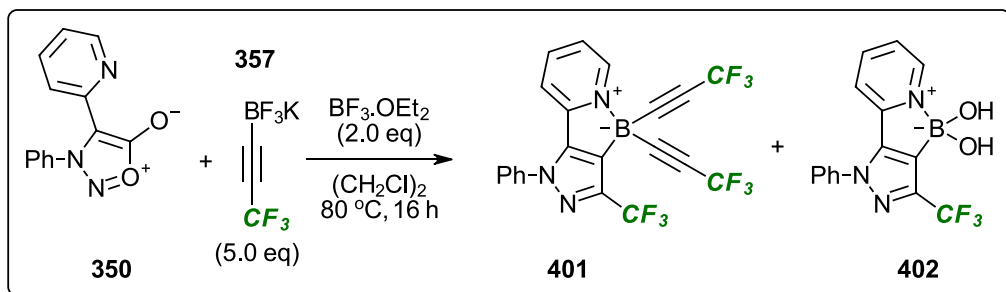
To a slurry of **350** (48 mg, 0.2 mmol) and **357** (200 mg, 1.0 mmol) in $(CH_2Cl)_2$ (2 mL) at 50 °C under argon was added dropwise BF$_3$.OEt$_2$ (49 L, 0.4 mmol). The mixture was heated at 80 °C for 16 hours, then cooled to room temperature and washed with brine (5 mL). The layers were separated and the aqueous layer was extracted with CH_2Cl_2 (3 x 10 mL), the combined organic layers were dried over

anhydrous MgSO₄ and concentrated *in vacuo*. The crude product was purified by flash column chromatography on silica gel (gradient elution 0 – 100% EtOAc in hexanes, then 10% MeOH in CH₂Cl₂), affording **401** as a tan solid (38 mg, 39%) **m.p.** 180 – 183 °C and **402** as a colourless solid (25 mg, 38%). **M.p.** 197 – 198 °C.

[1-Phenyl-5-(2-pyridyl)-3-(trifluoromethyl)-4-pyrazolyl]bis(3,3,3-trifluoro-1-propynyl)borane **401**
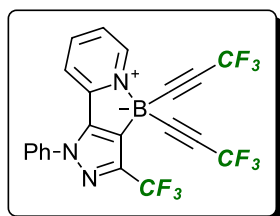
¹H NMR (400 MHz, CDCl₃) δ_H ppm 7.49 (td, 1H, J = 1.0, 8.0 Hz), 7.58 – 7.73 (m, 6H), 8.14 (dt, 1H, J = 1.5, 8.0 Hz), 8.73 – 8.81 (m, 1H); **¹³C NMR (101 MHz, CDCl₃)** δ_C ppm 83.1 (q, J = 50.5), 113.8 (q, J = 256.5), 118.5, 121.2 (q, J = 269.5 Hz), 122.6, 124.1, 125.1, 130.1, 130.3, 138.4, 143.8 (q, J = 40.0 Hz), 143.9, 146.1, 146.5; **¹⁹F NMR (376 MHz, CDCl₃)** δ_F ppm -50.0, -62.4; **¹¹B NMR (128 MHz, CDCl₃)** δ_B ppm -13.3; **FTIR (neat)** ν_max / cm⁻¹ 2918 (w), 2230 (w), 1629 (m), 1506 (m), 1250 (s), 1113 (s); **HRMS (ESI-TOF)** *m/z* [M+H]⁺ calculated for [C₂₁H₁₀BF₉N₃]⁺ 486.0819, found 486.0829.

[1-Phenyl-5-(2-pyridyl)-3-(trifluoromethyl)-4-pyrazolyl]boronic acid **402**
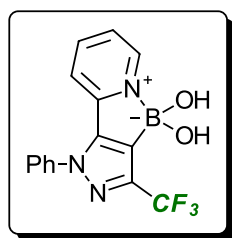
¹H NMR (400 MHz, CDCl₃) δ_H ppm 6.90 (d, 1H, J = 8.0 Hz), 7.26 – 7.30 (m, 2H), 7.34 (ddd, 1H, J = 1.0, 5.0, 7.5 Hz), 7.38 – 7.44 (m, 3H), 7.56 (dt, 1H, J = 2.0, 8.0 Hz), 7.62 (s, 2H), 8.71 (ddd, 1H, J = 1.0, 1.5, 5.0 Hz); **¹³C NMR (101 MHz, acetone-d⁶)** δ_C ppm 121.6 (q, J = 270.0 Hz), 124.1, 126.2, 126.4, 129.4, 129.7, 137.4, 139.3, 147.8, 147.9 (q, J = 37.0 Hz), 148.7, 148.8; **¹⁹F NMR (376 MHz, acetone-d⁶)** δ_F ppm -60.9; **¹¹B NMR (128 MHz, acetone-d⁶)** δ_B ppm 27.9; **FTIR (neat)** ν_max / cm⁻¹ 3327 (br), 2932 (w), 2855 (w), 1598 (w), 1139 (s); **HRMS (ESI-TOF)** *m/z* [M+H]⁺ calculated for [C₁₅H₁₂BF₃N₃O₂]⁺ 334.0969, found 334.0972.

General procedure N, TMS-OTf-promoted reactions of 336 with 1,2,4,5-tetrazines, synthesis of (pyridazine-4-yl)difluoroboranes 403 and 404
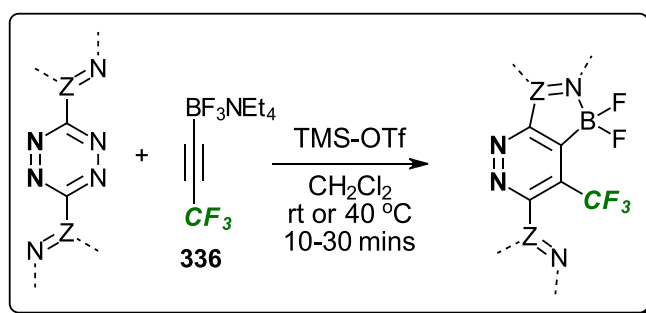
To a solution of the tetrazine (0.14 mmol, 1.0 eq) and **336** (0.19 – 0.28 mmol, 1.3 – 2.0 eq) in CH₂Cl₂ (1.0 mL) at room temperature (19 °C) or 40 °C under argon was added dropwise TMS-OTf (0.19 – 0.28 mmol, 1.3 – 2.0 eq). The mixture was stirred at room temperature or 40 °C for 10-30 minutes then cooled (if applicable) and diluted with CH₂Cl₂ (10 mL). The mixture was washed with saturated aqueous

NaHCO₃ (2.5 mL) and the layers were separated, the aqueous layer was extracted with CH$_2$Cl$_2$ (3 x 5 mL) and the combined organic layers were dried over anhydrous MgSO$_4$ then concentrated *in vacuo*. The crude product was then purified by flash column chromatography on florisil.

[3,6-Bis(2-pyridyl)-5-(trifluoromethyl)-4-pyridazinyl]difluoroborane 403
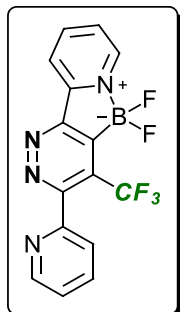
Following general procedure N, using 3,6-di-2-pyridyl-1,2,4,5-tetrazine (33 mg, 0.14 mmol), **336** (81 mg, 0.28 mmol) and TMS-OTf (52 µL, 0.28 mmol). The reaction mixture was stirred at room temperature for 10 minutes and the product was purified by passing through a small plug of florisil (eluting with EtOAc, 50 mL), affording **403** as a colourless solid (45 mg, 92%). **M.p.** = 201 °C; **¹H NMR (400 MHz, CD₃CN)** δ$_H$ ppm 7.54 (ddd, 1H, J = 1.0, 5.0, 7.5 Hz), 7.86 (td, 1H, J = 1.0, 8.0 Hz), 7.96 – 8.05 (m, 2H), 8.56 (dt, 1H, J = 1.5, 8.0 Hz), 8.68 – 8.75 (m, 2H), 8.80 (d, 1H, J = 5.5 Hz); ¹³C **NMR (101 MHz, CD₃CN)** δ$_C$ ppm 121.6, 124.3 (q, J = 274.5 Hz), 125.4, 125.5, 129.6, 131.2 (q, J = 35.5 Hz), 138.0, 143.6, 147.1, 150.0, 151.4, 156.1, 158.5, 160.7;
¹⁹F NMR (376 MHz, CD₃CN) δ$_F$ ppm -59.2 (t, J = 7.0 Hz), -156.4 – -157.0 (m); **¹¹B NMR (128 MHz, CD₃CN)** δ$_B$ ppm 6.9 (t, J = 44.0 Hz); **FTIR (neat)** v$_{max}$ / cm^{-1} 3042 (w), 1633 (w), 1572 (w), 1394 (w), 1168 (m), 1046 (w); **HRMS (ESI-TOF)** *m/z* [M+H]$^+$ calculated for [C$_{15}$H$_9$^{11}BF$_5$N$_4$]$^+$ 351.0835, found 351.0838.

[3,6-Bis(3,5-dimethyl-1-pyrazolyl)-5-(trifluoromethyl)-4-pyridazinyl]difluoroborane 404
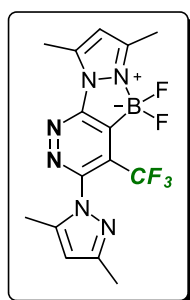
Following general procedure N, using 3,6-Bis(3,5-dimethyl-1H-pyrazol-1-yl)-1,2,4,5-tetrazine (38 mg, 0.14 mmol), **336** (54 mg, 0.19 mmol) and TMS-OTf (34 µL, 0.19 mmol). The reaction mixture was stirred at 40 °C for 30 minutes and the product was purified by flash column chromatography on florisil (eluting with 50% EtOAc in hexanes), affording **404** as a colourless solid (41 mg, 76%). **M.p.** = 206 – 207 °C; **¹H NMR (400 MHz, CD₃CN)** δ$_H$ ppm 2.23 (s, 3H), 2.23 – 2.25 (m, 3H), 2.51 (s, 3H), 2.87 (s, 3H), 6.13 (s, 1H), 6.53 (s, 1H); ¹³C **NMR (101 MHz, CD₃CN)** δ$_C$ ppm 11.4, 11.6, 13.1, 13.6, 108.2, 114.4, 122.8 (q, J = 275.0), 131.6 (q, J = 36.5 Hz), 143.6,
144.8, 150.8, 151.6, 151.7, 159.6; **¹⁹F NMR (376 MHz, CD₃CN)** δ$_F$ ppm -61.7 (t, J = 7.0 Hz), -153.3 – -154.1 (m); **¹¹B NMR (128 MHz, CD₃CN)** δ$_B$ ppm 3.7 (t, J = 33.5 Hz); **FTIR (neat)** v$_{max}$ / cm^{-1} 3146 (w), 2930 (w), 1538 (w), 1483 (w), 1428 (w), 1190 (m), 1148 (s); **HRMS (ESI-TOF)** *m/z* [M+H]$^+$ calculated for [C$_{15}$H$_{15}$^{11}BF$_5$N$_6$]$^+$ 385.1366, found 385.1367.

4.3.6. Elaboration of products

Hydrolysis of 369, synthesis of [2-(2-Pyridyl)-6-(trifluoromethyl)phenyl]boronic acid 389
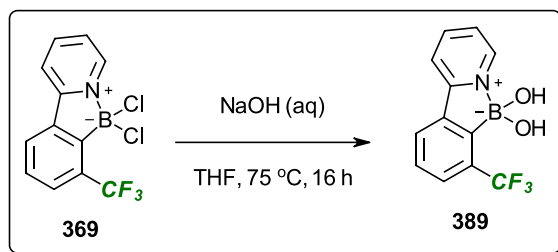
To a suspension of **369** (21 mg, 0.1 mmol) in THF (1.0 mL) at room temperature was added $NaOH_{(aq)}$ (0.7 mL, 0.7 mmol). The mixture was heated at 75 °C for 16 hours then cooled to room temperature and the layers were separated. The aqueous layer was acidified with aqueous HCl, then extracted with EtOAc (3 x 3 mL). The combined organic layers were dried over anhydrous $MgSO_4$ then concentrated *in vacuo*, affording **389** as a colourless solid (15 mg, 80%). **M.p. = 230 – 231 °C; ^{1}H NMR (400 MHz, acetone-d_6)** δ_H ppm 7.52 (dt, 1H, J = 0.5, 7.5 Hz), 7.64 – 7.73 (m, 2H), 8.17 (d, 1H, J = 7.5 Hz), 8.20 – 8.31 (m, 2H), 8.72 (d, 1H, J = 5.0 Hz); ^{13}**C NMR (101 MHz, acetone-d^6)** δ_C ppm 118.8, 125.2, 125.8, 126.2 (q, J = 273.5 Hz), 128.3 (q, J = 4.5 Hz), 128.6, 133.4 (q, J = 32.0 Hz), 139.4, 143.0, 143.1, 153.6; ^{19}**F NMR (376 MHz, acetone-d^6)** δ_F ppm -60.4; ^{11}**B NMR (128 MHz, acetone-d^6)** δ_B ppm 10.1; **FTIR (neat)** v_{max} / cm^{-1} 3395 (w), 3244 (br), 3048 (w), 2930 (w), 1619 (m), 1301 (s), 1114 (s); **HRMS (ESI-TOF)** *m/z* [M+H]$^+$ calculated for $[C_{12}H_{10}{}^{11}BF_3NO_2]^+$ 268.0751, found 268.0754.

General procedure O, one-pot cycloaddition-ligand exchange from 311 to boronic esters 390 and 391
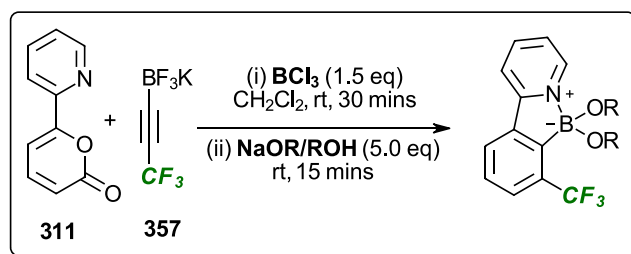
To a slurry of **311** (1.0 eq) and **357** (1.5 eq) in CH_2Cl_2 (0.11 M) at room temperature under argon was added dropwise a solution of BCl_3 in CH_2Cl_2 (1.0 M, 1.5 eq). The mixture was stirred at room temperature for 30 minutes before adding dropwise NaOR/ROH (5.0 eq). The mixture was stirred for a further 10 minutes before being filtered through a bed of activated charcoal and celite. The filtrate was then concentrated *in vacuo*, affording the desired boronic ester.
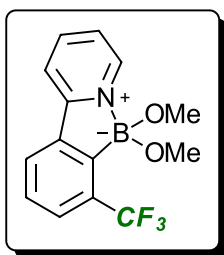
Following general procedure O, using **311** (19 mg, 0.11 mmol), **357** (34 mg, 0.17 mmol), BCl₃ solution (0.17 mL, 0.17 mmol) and NaOMe/MeOH (0.12 mL, 0.55 mmol). The boronate ester **390** was obtained as a light brown solid (26 mg, 80%). **M.p.** = 100 – 101 °C (dec); **¹H NMR (400 MHz, acetone-d₆)** δ_H ppm 2.92 (s, 6H), 7.60 (dt, 1H, J = 1.0, 7.5 Hz), 7.71 – 7.80 (m, 2H), 8.26 (d, 1H, J = 7.5 Hz), 8.32 – 8.39 (m, 2H), 8.58 (td, 1H, J = 1.0, 5.5 Hz); ¹³**C NMR (101 MHz, acetone-d₆)** δ_C ppm 50.1, 119.1, 125.5, 125.9 (q, J = 273.5 Hz), 126.1, 128.4 (q, J = 4.5 Hz), 129.4, 134.0 (q, J = 32.5 Hz), 140.1, 143.1, 143.9, 154.3; ¹⁹**F NMR (376 MHz, acetone-d₆)** δ_F ppm -61.9; ¹¹**B NMR (128 MHz, acetone-d₆)** I_b. ppm 11.5; **FTIR (neat)** v_{max} / cm⁻¹ 3073 (w), 2939 (w), 2903 (w), 2824 (w), 1619 (m), 1314 (m), 1304 (m), 1155 (s), 1132 (s); **HRMS (ESI-TOF)** *m/z* [M+H]⁺ calculated for [C₁₄H₁₄¹¹BF₃NO₂]⁺ 296.1064, found 296.1066.
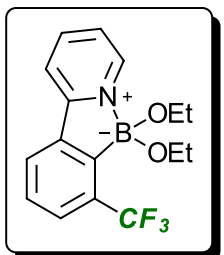
Following the general procedure using **311** (114 mg, 0.66 mmol), **357** (198 mg, 0.99 mmol), BCl₃ solution (0.99 mL, 0.99 mmol) and NaOEt/EtOH (1.23 mL, 3.30 mmol). The boronate ester **391** was obtained as a colourless solid (200 mg, 94%). **M.p.** = 104 – 105 °C; **¹H NMR (400 MHz, acetone-d₆)** δ_H ppm 0.93 (t, 6H, J = 7.5 Hz), 3.00 (qd, 2H, J = 7.0, 9.5 Hz), 3.21 (qd, 2H, J = 7.0, 9.5 Hz), 7.59 (dt, 1H, J = 1.0, 8.0 Hz), 7.70 – 7.79 (m, 2H), 8.25 (d, 1H, J = 7.5 Hz), 8.29 – 8.38 (m, 2H), 8.62 (td, 1H, J = 1.0, 5.5 Hz); ¹³**C NMR (101 MHz, acetone-d₆)** δ_C ppm 18.3, 57.7, 119.0, 125.5, 125.9 (q, J = 274.0 Hz), 126.1, 128.4 (q, J = 4.5 Hz), 129.3, 134.0 (q, J = 32.0 Hz), 140.0, 143.2, 143.7, 154.1; ¹⁹**F NMR (376 MHz, acetone-d₆)** δ_F ppm -61.5; ¹¹**B NMR (128 MHz, acetone-d₆)** δ_B ppm 11.0; **FTIR (neat)** v_{max} / cm⁻¹ 3048 (w), 2979 (w), 2866 (w), 1618 (m), 1491 (m), 1314 (m), 1305 (m), 1168 (s), 1137 (s); **HRMS (ESI-TOF)** *m/z* [M+H]⁺ calculated for [C₁₆H₁₈¹¹BF₃NO₂]⁺ 324.1378, found 324.1379.

Suzuki-Miyaura cross coupling of boronate 391, synthesis of triaryl 394
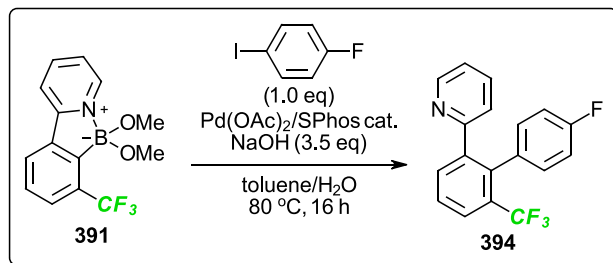
A 10 mL Biotage microwave vial under argon was charged with **391** (36 mg, 0.12 mmol), 4-fluoroiodobenzene (12 µL, 0.10 mmol), Pd(OAc)₂ (1 mg, 0.005 mmol), SPhos (2 mg, 0.005 mmol) and toluene (1.0 mL). 1.4 M Aqueous NaOH (0.25 mL, 0.35 mmol) was then added and the mixture was degassed by bubbling argon for 30 minutes. The mixture was then heated with stirring at 80 °C for 16 hours, then cooled to room temperature and concentrated *in vacuo*. The crude product was purified

by flash column chromatography on silica gel (gradient elution, 0 – 50% EtOAc in hexanes), affording the cross-coupled product **394** as a colourless solid (13 mg, 41%). **M.p.** = 73 – 74 °C; **^{1}H NMR (400 MHz, acetone-d^6)** δ$_H$ ppm 6.97 – 7.05 (m, 3H), 7.12 – 7.22 (m, 3H), 7.53 (dt, 1H, J = 2.0, 7.5 Hz), 7.72 (dt, 1H, J = 1.0, 8.0 Hz), 7.85 (d, 1H, J = 7.5 Hz), 7.92 (dd, 1H, J = 1.0, 8.0 Hz), 8.48 (ddd, 1H, J = 1.0, 2.0, 5.0 Hz); ^{13}**C NMR (101 MHz, acetone-d^6)** δ$_C$ ppm 114.8 (d, J = 22.0 Hz), 122.6, 125.2 (q, J = 273.5 Hz), 125.7, 126.7 (q, J = 5.5 Hz), 128.9, 129.8 (q, J = 29.0 Hz), 133.3 (qd, J = 1.5, 8.0 Hz), 134.2 (d, J = 3.5 Hz), 134.7, 136.2, 139.3, 144.4, 150.0, 158.8, 163.0 (d, J = 245.0 Hz); ^{19}**F NMR (376 MHz, acetone-d^6)** δ$_F$ ppm -57.1, -116.4; **FTIR (neat)** ν$_{max}$ / cm^{-1} 3054 (w), 2927 (w), 2855 (w), 1609 (w), 1515 (m), 1327 (m), 1169 (m), 1124 (s); **HRMS (ESI-TOF)** *m/z* [M+H]$^+$ calculated for [C$_{18}$H$_{12}$F$_4$N]$^+$ 318.0901, found 318.0899.

Conclusions and outlook

Reactions of ynone trifluoroborates towards novel pyrimidin-6-yl trifluoroborates

The aim of the work presented in this section was to establish a preparative procedure for obtaining novel pyrimidin-6-yl trifluoroborate salts *via* condensation reactions of the corresponding ynone trifluoroborate salts. This was indeed achieved, with numerous examples of the desired salts prepared and isolated in useful yields alongside their full characterisation. Importantly, aminopyrimidine-6-yl salts could also be accessed and isolated by condensation of the ynone trifluoroborate with a guanidine reagent. Furthermore, following considerable optimisation efforts, efficient procedures for the elaboration of these (amino)pyrimidin-6-yl trifluoroborate salts *via* Suzuki-Miyaura cross coupling was achieved. The aminopyrimidin-6-yl trifluoroborates were also amenable to other synthetic manipulations that left the boronate moiety intact, culminating in a concise synthesis of the experimental anticancer pyrimidine drug Bropirimine. It is hoped that ynone trifluoroborate salts continue to be of use for the synthesis of valuable, highly substituted pyrimidines, and that the scope of their application for the synthesis of other heterocycles will continue to grow.

Reactions of fluorinated alkynyl trifluoroborates towards fluorinated (hetero)aromatic compounds

As a novel entry into the enormously high-value field of organofluorine chemistry, the boron-directed cycloaddition was expected to provide an efficient platform for the mild and regiospecific synthesis of fluorinated (hetero)aromatic compounds. With the CF_3 example alone, such mild cycloadditions would have made a welcome addition to the literature, where the non-directed conditions could be harsh and unselective. After preparing CF_3- and longer chain perfluoroalkyl-substituted alkynyl trifluoroborate salts *via* a non-etching procedure, the $BF_3.OEt_2$-promoted boron-directed cycloadditions with 2-pyrones proceeded as expected, albeit at a higher temperature than for the examples already published. Control experiments and NMR studies provided further insight into the complex interplay between the different processes occurring simultaneously, while DFT calculations provided some rationale as to why the CF_3 substituent may require higher temperatures. Nevertheless, after further optimisation, a milder, BCl_3-promoted procedure for the boron-directed cycloaddition was discovered and was shown to be broadly applicable to numerous examples of substituted 2-pyrones. The CF_3-substituted borane products were amenable to efficient ligand exchange to boronic esters, which themselves underwent Suzuki-Miyaura cross coupling providing the biaryl product in useful yield. The boron-directed cycloaddition of the CF_3-substituted alkynyl trifluoroborate was also shown to occur for substituted heterodienes, such as: 1,3,4-triazines, 1,2,4,5-tetrazines and sydnones, affording the expected CF_3-substituted pyridines, pyridazines and pyrazoles, respectively. It is hoped that the scope boron-directed cycloaddition of fluorinated alkynyl trifluoroborate salts with heterodienes can be improved and that it continues to provide efficient access to valuable fluorinated (hetero)aromatic compounds.

References

1   L. G. Brugnatelli, *G. di Fis. Chim. Stor. Nat. Med. ed Arti*, 1818, **Series 2**, 117–129.

2   J. L. F. Wöhler, *Ann. der Chemie und Pharm.*, 1838, **26**, 241–340.

3   E. Frankland and H. Kolbe, *Ann. der Chemie und Pharm.*, 1848, **65**, 269–287.

4   E Grimaux, *C. R. Hebd. Seances Acad. Sci.*, 1879, **87**, 752–753.

5   A. Pinner, *Berichte der Dtsch. Chem. Gesellschaft*, 1884, **17**, 2519–2520.

6   P. Biginelli, *Berichte der Dtsch. Chem. Gesellschaft*, 1891, **24**, 1317–1319.

7   M. M. Heravi and V. Zadsirjan, *Curr. Org. Chem.*, 2020, **24**, 1331–1366.

8   L. V. Chopda and P. N. Dave, *ChemistrySelect*, 2020, **5**, 5552–5572.

9   C. O. Kappe, *Acc. Chem. Res.*, 2000, **33**, 879–888.

10   H. S. Oboudatian, H. Naeimi and M. Moradian, *RSC Adv.*, 2021, **11**, 7271–7279.

11   L. V Chopda and P. N. Dave, *ChemistrySelect*, 2020, **5**, 14161–14167.

12   T. Krishna, E. Laxminarayana and D. Kalita, *Eur. J. Chem.*, 2020, **11**, 206–212.

13   F. Krauskopf, K. N. Truong, K. Rissanen and C. Bolm, *Org. Lett.*, 2021, **23**, 2699–2703.

14   Z. Gao, J. Li, Y. Song, X. Bi, X. Meng and Y. Guo, *RSC Adv.*, 2020, **10**, 39266–39270.

15   F. Cohen, L. E. Overman and S. K. Ly Sakata, *Org. Lett.*, 1999, **1**, 2169–2172.

16   L. Ismaili, J. Monnin, A. Etievant, R. L. Arribas, L. Viejo, B. Refouvelet, O. Soukup, J. Janockova, V. Hepnarova, J. Korabecny, T. Kucera, D. Jun, R. Andrys, K. Musilek, A. Baguet, E. M. García-Frutos, A. De Simone, V. Andrisano, M. Bartolini, C. De Los Ríos, J. Marco-Contelles and E. Haffen, *ACS Chem. Neurosci.*, 2021, **12**, 1328–1342.

17   G. S. Mhaske, R. H. Khiste, S. A. Shinde and S. A. Jadhav, *Int. J. Pharm. Sci. Res.*, 2021, **12**, 963–972.

18   A. El-Malah, Z. Mahmoud, H. Hamed Salem, A. M. Abdou, M. M. H. Soliman and R. A. Hassan, *Green Chem. Lett. Rev.*, 2021, 14, 220–232.

19   M. Yadav, R. Kumar and R. Krishnamurthy, *Chem. Rev.*, 2020, 120, 4766–4805.

20   J. W. Szostak, *Nature*, 2009, 459, 171–172.

21   W. Gilbert, *Nature*, 1986, **319**, 618.

22   E. Vitaku, D. T. Smith and J. T. Njardarson, *J. Med. Chem.*, 2014, **57**, 10257–10274.

23   V. Sharma, N. Chitranshi and A. K. Agarwal, *Int. J. Med. Chem.*, 2014, **2014**, 202784.

24   I. Tomar and R. Mishra, *Int. J. Pharm. Sci. Res.*, 2011, **2**, 758–771.

25   I. M. Lagoja, *Chem. Biodivers.*, 2005, **2**, 1–50.

26   J. A. R. Navarro, E. Barea, M. A. Galindo, J. M. Salas, M. A. Romero, M. Quirós, N. Masciocchi, S. Galli, A. Sironi and B. Lippert, *J. Solid State Chem.*, 2005, **178**, 2436–2451.

27   H. Akdas-Kilig, T. Roisnel, I. Ledoux and H. Le Bozec, *New J. Chem.*, 2009, **33**, 1470–1473.

28   H. Akdas-Kilig, M. Godfroy, J. L. Fillaut, B. Donnio, B. Heinrich, P. Kędziora, J. P. Malval, A. Spangenberg, S. Van Cleuvenbergen, K. Clays and F. Camerel, *J. Phys. Chem. C*, 2015, **119**, 3697–3710.

29   Y. K. Chen, H. H. Kuo, D. Luo, Y. N. Lai, W. C. Li, C. H. Chang, D. Escudero, A. K. Y. Jen, L. Y. Hsu and Y. Chi, *Chem. Mater.*, 2019, **31**, 6453–6464.

30   G. W. Rewcastle, in *Heterocyclic Chemistry III*, eds. A. R. Katritzky, C. A. Ramsden, E. F. V. Scriven and R. J. K. Taylor, Elsevier, 2008, pp. 117–272.

31   M. Radi, S. Schenone and M. Botta, *Org. Biomol. Chem.*, 2009, **7**, 2841–2847.

32   M. Mahfoudh, R. Abderrahim, E. Leclerc and J.-M. Campagne, *European J. Org. Chem.*, 2017, **2017**, 2856–2865.

33   S. Von Angerer, in *Science of Synthesis*, eds. D. E. Kaufmann and D. S. Matteson, Thieme, Stuttgart, 2004, pp. 379–572.

34   D. J. Brown, R. F. Evans, W. B. Cowden and M. D. Fenn, in *Chemistry of Heterocyclic Compounds*, Wiley, New York, 1994, p. 1.

35   T. Wang and I. S. Cloudsdale, *Synth. Commun.*, 1997, **27**, 2521–2526.

36   R. P. Frutos, X. Wei, N. D. Patel, T. G. Tampone, J. A. Mulder, C. A. Busacca and C. H. Senanayake, *J. Org. Chem.*, 2013, **78**, 5800–5803.

37   E. Bejan, H. Haddou, J. C. Daran and G. G. A. Balavoine, *Synthesis (Stuttg).*, 1996, **8**, 1012–1018.

38   J. V. Greenhill, *Chem. Soc. Rev.*, 1977, 6, 277–294.

39   L. Chang, T. Guo, Z. Wang, S. Wang and Z. J. Yao, *J. Org. Chem.*, 2017, **82**, 1567–1574.

40   W. Huang, C. Zhu, M. Li, Y. Yu, W. Wu, Z. Tu and H. Jiang, *Adv. Synth. Catal.*, 2018, **360**, 3117–3123.

41   Y. Li, X. Cao, Y. Liu and J. P. Wan, *Org. Biomol. Chem.*, 2017, **15**, 9585–9589.

42   S. Hernández, I. Moreno, R. SanMartin, G. Gómez, M. T. Herrero and E. Domínguez, *J. Org. Chem.*, 2010, **75**, 434–441.

43   C. Huang, Y. Fu, H. Fu, Y. Jiang and Y. Zhao, *Chem. Commun.*, 2008, 6333–6335.

44   Y. Jiao, S. L. Ho and C. S. Cho, *Synlett*, 2015, **26**, 1081–1084.

45   A. Guirado, E. Alarcón, Y. Vicente, R. Andreu, D. Bautista and J. Gálvez, *Tetrahedron*, 2016, **72**, 3922–3929.

46   A. Guirado, E. Alarcón, Y. Vicente and R. Andreu, *Tetrahedron Lett.*, 2013, **54**, 5115–5117.

47   F. Xie, H. Zhao, L. Zhao, L. Lou and Y. Hu, *Bioorganic Med. Chem. Lett.*, 2009, **19**, 275–278.

48   T. M. Gøgsig, D. U. Nielsen, A. T. Lindhardt and T. Skrydstrup, *Org. Lett.*, 2012, **14**, 2536–2539.

49   Y. Zhou, Z. Tang and Q. Song, *Adv. Synth. Catal.*, 2017, **359**, 952–958.

50   M. Vidal, M. García-Arriagada, M. C. Rezende and M. Domínguez, *Synth.*, 2016, **48**, 4246–4252.

51   D. Guay, C. Beaulieu, M. Belley, S. N. Crane, J. DeLuca, Y. Gareau, M. Hamel, M. Henault, H. Hyjazie, S. Kargman, C. C. Chan, L. Xu, R. Gordon, L. Li, Y. Mamane, N. Morin, J. Mancini, M.

Thérien, G. Tranmer, V. L. Truong, Z. Wang and W. C. Black, *Bioorganic Med. Chem. Lett.*, 2011, **21**, 2832–2835.

52 P. Benderitter, J. X. de Araújo Júnior, M. Schmitt and J. J. Bourguignon, *Tetrahedron*, 2007, **63**, 12465–12470.

53 J. Yang, S. Liu, J.-F. Zheng and J. S. Zhou, *European J. Org. Chem.*, 2012, **2012**, 6248–6259.

54 X. Ye, Z. Yuan, Y. Zhou, Q. Yang, Y. Xie, Z. Deng and Y. Peng, *J. Heterocycl. Chem.*, 2016, **53**, 1956–1962.

55 S. Fan, J. Yang and X. Zhang, *Org. Lett.*, 2011, **13**, 4374–4377.

56 C. Nájera, L. K. Sydnes and M. Yus, *Chem. Rev.*, 2019, 119, 11110–11244.

57 R. Chinchilla and C. Nájera, *Chem. Rev.*, 2007, 107, 874–922.

58 Y. Tohda, K. Sonogashira and N. Hagihara, *Synth.*, 1977, 1977, 777–778.

59 A. S. Karpov and T. J. J. Müller, *Org. Lett.*, 2003, **5**, 3451–3454.

60 A. S. Karpov and T. J. J. Müller, *Synthesis (Stuttg).*, 2003, **2003**, 2815–2826.

61 C. Fehér, Á. Kuik, L. Márk, L. Kollár and R. Skoda-Földes, *J. Organomet. Chem.*, 2009, **694**, 4036–4041.

62 J. P. Stonehouse, D. S. Chekmarev, N. V. Ivanova, S. Lang, G. Pairaudeau, N. Smith, M. J. Stocks, S. I. Sviridov and L. M. Utkina, *Synlett*, 2008, **2008**, 0100–0104.

63 K. T. Neumann, S. R. Laursen, A. T. Lindhardt, B. Bang-Andersen and T. Skrydstrup, *Org. Lett.*, 2014, **16**, 2216–2219.

64 C. F. Gers, J. Rosellen, E. Merkul, T. J. J. Müller, J. Rosellen@uni, -Duesseldorf De;, -E Merkul@uni, T. Mueller@uni and -Duesseldorf De, *Beilstein J. Org. Chem*, 2011, **7**, 1173–1181.

65 R. Kazem Shiroodi, M. Soltani and V. Gevorgyan, *J. Am. Chem. Soc.*, 2014, **136**, 9882–9885.

66 M. Sengee and L. K. Sydnes, *Synthesis (Stuttg).*, 2011, **2011**, 3899–3907.

67 I. Nes and L. K. Sydnes, *Synth.*, 2015, **47**, 89–94.

68 P. Bannwarth, A. Valleix, D. Grée and R. Grée, *J. Org. Chem.*, 2009, **74**, 4646–4649.

69 E. Gayon, M. Szymczyk, H. Gérard, E. Vrancken and J. M. Campagne, *J. Org. Chem.*, 2012, **77**, 9205–9220.

70 S. I. Yamamoto, K. Okamoto, M. Murakoso, Y. Kuninobu and K. Takai, *Org. Lett.*, 2012, **14**, 3182–3185.

71 M. C. Bagley, D. D. Hughes, H. M. Sabo, P. H. Taylor and X. Xiong, *Synlett*, 2003, **2003**, 1443–1446.

72 M. C. Bagley, Z. Lin and S. J. A. Pope, *Tetrahedron Lett.*, 2009, **50**, 6818–6822.

73 M. Lin, Q. Z. Chen, Y. Zhu, X. L. Chen, J. J. Cai, Y. M. Pan and Z. P. Zhan, *Synlett*, 2011, **2011**, 1179–1183.

74 W. Guo, *Chinese Chem. Lett.*, 2016, **27**, 47–50.

75 W. Guo, C. Li, J. Liao, F. Ji, D. Liu, W. Wu and H. Jiang, *J. Org. Chem.*, 2016, **81**, 5538–5546.

76   K. S. Vadagaonkar, H. P. Kalmode, S. Prakash and A. C. Chaskar, *New J. Chem.*, 2015, **39**, 3639–3645.

77   J. L. Zhan, M. W. Wu, F. Chen and B. Han, *J. Org. Chem.*, 2016, **81**, 11994–12000.

78   X. Q. Chu, W. Bin Cao, X. P. Xu and S. J. Ji, *J. Org. Chem.*, 2017, **82**, 1145–1154.

79   D. M. D. D' Souza and T. J. J. Müller, *Chem. Soc. Rev.*, 2007, **36**, 1095–1108.

80   B. A. Arndtsen, *Chem. - A Eur. J.*, 2009, **15**, 302–313.

81   B. Jiang, T. Rajale, W. Wever, S.-J. Tu and G. Li, *Chem. - An Asian J.*, 2010, **5**, 2318–2335.

82   T. Suzuki, *Chem. Rev.*, 2011, 111, 1825–1845.

83   R. H. Crabtree, *Chem. Rev.*, 2017, 117, 9228–9246.

84   N. Deibl, K. Ament and R. Kempe, *J. Am. Chem. Soc.*, 2015, **137**, 12804–12807.

85   R. Mondal and D. E. Herbert, *Organometallics*, 2020, **39**, 1310–1317.

86   M. Maji and S. Kundu, *Dalt. Trans.*, 2019, **48**, 17479–17487.

87   S. Sultana Poly, S. M. A. H. Siddiki, A. S. Touchy, K. W. Ting, T. Toyao, Z. Maeno, Y. Kanda and K. I. Shimizu, *ACS Catal.*, 2018, **8**, 11330–11341.

88   N. Deibl and R. Kempe, *Angew. Chemie Int. Ed.*, 2017, **56**, 1663–1666.

89   M. Mastalir, M. Glatz, E. Pittenauer, G. Allmaier and K. Kirchner, *J. Am. Chem. Soc.*, 2016, **138**, 15543–15546.

90   M. Mastalir, M. Glatz, E. Pittenauer, G. Allmaier and K. Kirchner, *Org. Lett.*, 2019, **21**, 1116–1120.

91   T. Shi, F. Qin, Q. Li and W. Zhang, *Org. Biomol. Chem.*, 2018, **16**, 9487–9491.

92   R. Mondal, S. Sinha, S. Das, G. Chakraborty and N. D. Paul, *Adv. Synth. Catal.*, 2020, **362**, 594–600.

93   G. Chakraborty, R. Sikari, R. Mondal, S. Mandal and N. D. Paul, *Asian J. Org. Chem.*, 2020, **9**, 431–436.

94   A. K. Bains and D. Adhikari, *Catal. Sci. Technol.*, 2020, **10**, 6309–6318.

95   J. Chen, R. Properzi, D. P. Uccello, J. A. Young, R. G. Dushin and J. T. Starr, *Org. Lett.*, 2014, **16**, 4146–4149.

96   E. D. Anderson and D. L. Boger, *J. Am. Chem. Soc.*, 2011, **133**, 12285–12292.

97   C. M. Glinkerman and D. L. Boger, *Org. Lett.*, 2015, **17**, 4002–4005.

98   A. S. Duerfeldt and D. L. Boger, *J. Am. Chem. Soc.*, 2014, **136**, 2119–2125.

99   E. D. Anderson, A. S. Duerfeldt, K. Zhu, C. M. Glinkerman and D. L. Boger, *Org. Lett.*, 2014, **16**, 5084–5087.

100   C. M. Glinkerman and D. L. Boger, *Org. Lett.*, 2018, **20**, 2628–2631.

101   A. Guzmán, M. Romero, F. X. Talamás and J. M. Muchowski, *Tetrahedron Lett.*, 1992, **33**, 3449–3452.

102   I. Ibnusaud, E. J. Padma Malar and N. Sundaram, *Tetrahedron Lett.*, 1990, **31**, 7357–7358.

103   A. Guzmán, M. Romero, F. X. Talamás, R. Villena, R. Greenhouse and J. M. Muchowski, *J. Org. Chem.*, 1996, **61**, 2470–2483.

104   J. Krechl, M. A. Pérez, F. J. Cuadrado and J. L. Soto, *Synth.*, 1988, **1988**, 122–124.

105   A. Pinner, *Berichte der Dtsch. Chem. Gesellschaft*, 1883, **16**, 1643–1655.

106   A. García Martínez, A. Herrera Fernández, R. Martínez Álvarez, M. D. Molero Vilchez, M. L. Laorden Gutiérrez and L. R. Subramanian, *Tetrahedron*, 1999, **55**, 4825–4830.

107   H. Neunhoeffer and M. Bachmann, *Chem. Ber.*, 1975, **108**, 3877–3882.

108   D. L. Boger, J. Schumacher, M. D. Mullican, M. Patel and J. S. Panek, *J. Org. Chem.*, 1982, 47, 2673–2675.

109   G. Yang, Q. Jia, L. Chen, Z. Du and J. Wang, *RSC Adv.*, 2015, **5**, 76759–76763.

110   A. Robin, K. Julienne, J.-C. Meslin and D. Deniaud, *European J. Org. Chem.*, 2006, **2006**, 634–643.

111   N. Sakai, Y. Aoki, T. Sasada and T. Konakahara, *Org. Lett.*, 2005, **7**, 4705–4708.

112   T. Sasada, Y. Aoki, R. Ikeda, N. Sakai and T. Konakahara, *Chem. - A Eur. J.*, 2011, **17**, 9385–9394.

113   R. Braden, K. Findeisen and H. Holtschmidt, *Angew. Chemie Int. Ed. English*, 1970, **9**, 65–66.

114   K. Grohe and H. Heitzer, *Justus Liebigs Ann. Chem.*, 1973, **5–6**, 1025–1035.

115   G. deStevens, B. Smolinsky and L. Dorfman, *J. Org. Chem.*, 1964, **29**, 1115–1119.

116   M. T. Cocco, C. Congiu, V. Onnis and A. Maccioni, *Synthesis (Stuttg.)*, 1991, 529–530.

117   S. Von Angerer, in *Science of Synthesis*, eds. D. S. Matteson and D. E. Kaufmann, Thieme, Stuttgart, 2004, pp. 379–572.

118   L. Wimmer, L. Rycek, M. Koley and M. Schnürch, in *Top. Heterocycl. Chem.*, Springer, Cham, 2014, pp. 61–157.

119   T. J. Delia and J. M. Schomaker, *J. Org. Chem.*, 2001, **66**, 7125–7128.

120   Y. Yang and A. R. Martin, *Heterocycles*, 1992, **34**, 1395–1398.

121   D. Peters, A.-B. Hörnfeldt and S. Gronowitz, *J. Heterocycl. Chem.*, 1990, **27**, 2165–2173.

122   N. Kudo, M. Perseghini and G. C. Fu, *Angew. Chemie - Int. Ed.*, 2006, **45**, 1282–1284.

123   Z. Fu, T. Li, X. He, J. Liu, W. Xu and Y. Wu, *J. Mol. Catal. A Chem.*, 2014, **395**, 293–299.

124   J. B. Liu, H. Yan, H. X. Chen, Y. Luo, J. Weng and G. Lu, *Chem. Commun.*, 2013, **49**, 5268–5270.

125   G. A. Molander and F. Beaumard, *Org. Lett.*, 2010, **12**, 4022–4025.

126   G. A. Molander, B. Canturk and L. E. Kennedy, *J. Org. Chem.*, 2009, **74**, 973–980.

127   C. P. Seath, J. W. B. Fyfe, J. J. Molloy and A. J. B. Watson, *Angew. Chemie - Int. Ed.*, 2015, **54**, 9976–9979.

128   G. Aridoss, B. Zhou, D. L. Hermanson, N. P. Bleeker and C. Xing, *J. Med. Chem.*, 2012, **55**, 5566–5581.

129   A. Turck, N. Plé, F. Mongin and G. Quéguiner, *Tetrahedron*, 2001, 57, 4489–4505.

130   F. Chevallier and F. Mongin, *Chem. Soc. Rev.*, 2008, **37**, 595–609.

131   K. Shen, Y. Fu, J. N. Li, L. Liu and Q. X. Guo, *Tetrahedron*, 2007, **63**, 1568–1576.

132   N. Plé, A. Turck, K. Couture and G. Quéguiner, *J. Org. Chem.*, 1995, **60**, 3781–3786.

133   T. J. Kress, *J. Org. Chem.*, 1979, **44**, 2081–2082.

134   T. Imahori and Y. Kondo, *J. Am. Chem. Soc.*, 2003, **125**, 8082–8083.

135   A. Seggio, F. Chevallier, M. Vaultier and F. Mongin, *J. Org. Chem.*, 2007, **72**, 6602–6605.

136   K. Groll, S. M. Manolikakes, X. M. Du Jourdin, M. Jaric, A. Bredihhin, K. Karaghiosoff, T. Carell and P. Knochel, *Angew. Chemie - Int. Ed.*, 2013, **52**, 6776–6780.

137   S. Usui, Y. Hashimoto, J. V. Morey, A. E. H. Wheatley and M. Uchiyama, *J. Am. Chem. Soc.*, 2007, **129**, 15102–15103.

138   R. S. J. Proctor and R. J. Phipps, *Angew. Chemie - Int. Ed.*, 2019, 58, 13666–13699.

139   L. Zhang and Z. Q. Liu, *Org. Lett.*, 2017, **19**, 6594–6597.

140   T. Cernak, K. D. Dykstra, S. Tyagarajan, P. Vachal and S. W. Krska, *Chem. Soc. Rev.*, 2016, 45, 546–576.

141   A. C. Sun, R. C. McAtee, E. J. McClain and C. R. J. Stephenson, *Synth.*, 2019, 51, 1063–1072.

142   F. O'Hara, D. G. Blackmond and P. S. Baran, *J. Am. Chem. Soc.*, 2013, **135**, 12122–12134.

143   Y. Ma, J. Liang, D. Zhao, Y. L. Chen, J. Shen and B. Xiong, *RSC Adv.*, 2014, **4**, 17262–17264.

144   D. A. DiRocco, K. Dykstra, S. Krska, P. Vachal, D. V. Conway and M. Tudge, *Angew. Chemie - Int. Ed.*, 2014, **53**, 4802–4806.

145   Y. Fujiwara, J. A. Dixon, F. O'hara, E. D. Funder, D. D. Dixon, R. A. Rodriguez, R. D. Baxter, B. Herlé, N. Sach, M. R. Collins, Y. Ishihara and P. S. Baran, *Nature*, 2012, 492, 95–99.

146   T. Thatikonda, U. Singh, S. Ambala, R. A. Vishwakarma and P. P. Singh, *Org. Biomol. Chem.*, 2016, **14**, 4312–4320.

147   P. C. Gros, in *Metalation of Azines and Diazines*, eds. M. Schnürch and M. D. Mihovilovic, Springer Berlin Heidelberg, Berlin, Heidelberg, 2013, pp. 1–20.

148   J. Arukwe, T. Benneche and K. Undheim, *J. Chem. Soc. Perkin Trans. 1*, 1989, 255–259.

149   J. Sandosham and K. Undheim, *Tetrahedron*, 1994, **50**, 275–284.

150   Y. A. Yoon, C. S. Park, M. H. Cha, H. Choi, J. Y. Sim and J. G. Kim, *Bioorganic Med. Chem. Lett.*, 2010, **20**, 5735–5738.

151   G. G. Furin, O. A. Vyazankina, B. A. Gostevsky and N. S. Vyazankin, *Tetrahedron*, 1988, 44, 2675–2749.

152   T. Komiyama, Y. Minami and T. Hiyama, *ACS Catal.*, 2017, 7, 631–651.

153   R. J. Mattson and C. P. Sloan, *J. Org. Chem.*, 1990, **55**, 3410–3412.

154   R. Radinov, C. Chanev and M. Haimova, *J. Org. Chem.*, 1991, **56**, 4793–4796.

155   N. Plé, A. Turck, A. Heynderickx and G. Quéguiner, *J. Heterocycl. Chem.*, 1997, **34**, 551–556.

156   K. Itami, K. Mitsudo, K. Fujita, Y. Ohashi and J. I. Yoshida, *J. Am. Chem. Soc.*, 2004, **126**,

11058–11066.

157   A. V. Gulevich, F. S. Melkonyan, D. Sarkar and V. Gevorgyan, *J. Am. Chem. Soc.*, 2012, **134**, 5528–5531.

158   C. Huang, N. Chernyak, A. S. Dudnik and V. Gevorgyan, *Adv. Synth. Catal.*, 2011, **353**, 1285–1305.

159   M. Mosrin, N. Boudet and P. Knochel, *Org. Biomol. Chem.*, 2008, **6**, 3237–3239.

160   M. Mosrin and P. Knochel, *Org. Lett.*, 2008, **10**, 2497–2500.

161   Y. Gu, Y. Shen, C. Zarate and R. Martin, *J. Am. Chem. Soc.*, 2019, **141**, 127–132.

162   C. Cheng and J. F. Hartwig, *Chem. Rev.*, 2015, 115, 8946–8975.

163   C. Cheng and J. F. Hartwig, *J. Am. Chem. Soc.*, 2015, **137**, 592–595.

164   S. Liu, P. Pan, H. Fan, H. Li, W. Wang and Y. Zhang, *Chem. Sci.*, 2019, **10**, 3817–3825.

165   J. Ogamino, H. Mizunuma, H. Kumamoto, S. Takeda, K. Haraguchi, K. T. Nakamura, H. Sugiyama and H. Tanaka, *J. Org. Chem.*, 2005, **70**, 1684–1690.

166   J. M. Medina, M. K. Jackl, R. B. Susick and N. K. Garg, *Tetrahedron*, 2016, **72**, 3629–3634.

167   M. C. Bagley, D. D. Hughes, M. C. Lubinu, E. A. Merritt, P. H. Taylor and N. C. O. Tomkinson, *QSAR Comb. Sci.*, 2004, **23**, 859–867.

168   C. H. Low, J. N. Rosenberg, M. A. Lopez and T. Agapie, *J. Am. Chem. Soc.*, 2018, **140**, 11906–11910.

169   E. Tyrrell and P. Brookes, *Synthesis (Stuttg).*, 2003, 2003, 469–483.

170   W. Li, D. P. Nelson, M. S. Jensen, R. S. Hoerrner, D. Cai, R. D. Larsen and P. J. Reider, *J. Org. Chem.*, 2002, **67**, 5394–5397.

171   K. M. Clapham, A. E. Smith, A. S. Batsanov, L. McIntyre, A. Pountney, M. R. Bryce and B. Tarbit, *European J. Org. Chem.*, 2007, **2007**, 5712–5716.

172   R. F. Schinazi and W. H. Prusoff, *J. Org. Chem.*, 1985, **50**, 841–847.

173   T. K. Liao, E. G. Podrebarac and C. C. Cheng, *J. Am. Chem. Soc.*, 1964, **86**, 1869–1870.

174   A. Thakur, K. Zhang and J. Louie, *Chem. Commun.*, 2012, **48**, 203–205.

175   J. B. Grimm, K. J. Wilson and D. J. Witter, *J. Org. Chem.*, 2009, **74**, 6390–6393.

176   S. Wacharasindhu, S. Bardhan, Z. K. Wan, K. Tabei and T. S. Mansour, *J. Am. Chem. Soc.*, 2009, **131**, 4174–4175.

177   I. Kumar, R. Sharma, R. Kumar, R. Kumar and U. Sharma, *Adv. Synth. Catal.*, 2018, **360**, 2013–2019.

178   D. Dar'in and M. Krasavin, *J. Org. Chem.*, 2016, **81**, 12514–12519.

179   J. C. Vantourout, L. Li, E. Bendito-Moll, S. Chabbra, K. Arrington, B. E. Bode, A. Isidro-Llobet, J. A. Kowalski, M. G. Nilson, K. M. P. Wheelhouse, J. L. Woodard, S. Xie, D. C. Leitch and A. J. B. Watson, *ACS Catal.*, 2018, **8**, 9560–9566.

180   F. Menard and M. Lautens, *Angew. Chemie - Int. Ed.*, 2008, **47**, 2085–2088.

181   G. A. Molander, O. A. Argintaru, I. Aron and S. D. Dreher, *Org. Lett.*, 2010, **12**, 5783–5785.

182   R. Gómez-Bombarelli, J. Aguilera-Iparraguirre, T. D. Hirzel, D. Duvenaud, D. Maclaurin, M. A. Blood-Forsythe, H. S. Chae, M. Einzinger, D. G. Ha, T. Wu, G. Markopoulos, S. Jeon, H. Kang, H. Miyazaki, M. Numata, S. Kim, W. Huang, S. I. Hong, M. Baldo, R. P. Adams and A. Aspuru-Guzik, *Nat. Mater.*, 2016, **15**, 1120–1127.

183   A. J. J. Lennox and G. C. Lloyd-Jones, *J. Am. Chem. Soc.*, 2012, **134**, 7431–7441.

184   C. Simhadri, K. D. Daze, S. F. Douglas, N. Milosevich, L. Monjas, A. Dev, T. M. Brown, A. K. H. Hirsch, J. E. Wulff and F. Hof, *ChemMedChem*, 2019, **14**, 1444–1456.

185   Z. Cannone, A. M. Shaqra, C. Lorenc, L. Henowitz, S. Keshipeddy, V. L. Robinson, A. Zweifach, D. Wright and M. W. Peczuh, *ACS Comb. Sci.*, 2019, **21**, 192–197.

186   P. Devasthale, W. Wang, J. Mignone, K. Renduchintala, S. Radhakrishnan, J. Dhanapal, J. Selvaraj, R. Kuppusamy, M. A. Pelleymounter, D. Longhi, N. Huang, N. Flynn, A. V. Azzara, K. Rohrbach, J. Devenny, S. Rooney, M. Thomas, S. Glick, H. Godonis, S. Harvey, M. J. Cullen, H. Zhang, C. Caporuscio, P. Stetsko, M. Grubb, C. Huang, L. Zhang, C. Freeden, B. J. Murphy, J. A. Robl and W. N. Washburn, *Bioorganic Med. Chem. Lett.*, 2015, **25**, 4412–4418.

187   Y. D. Bodke, K. Kl and T. Venkatesh, *Pharma Chem.*, 2017, **9**, 29–34.

188   Q. Zeng, S. B. Rosenblum, Z. Yang, Y. Jiang, K. D. McCormick, R. G. Aslanian, L. Duguma, J. A. Kozlowski, N. Y. Shih, J. A. Hey, R. E. West, W. A. Korfmacher, M. Berlin and C. W. Boyce, *Bioorganic Med. Chem. Lett.*, 2013, **23**, 6001–6003.

189   S. Chowdhury, E. H. Sessions, J. R. Pocas, W. Grant, T. Schröter, L. Lin, C. Ruiz, M. D. Cameron, S. Schürer, P. Lograsso, T. D. Bannister and Y. Feng, *Bioorg. Med. Chem. Lett.*, 2011, **21**, 7107–7112.

190   E. H. Sessions, M. Smolinski, B. Wang, B. Frackowiak, S. Chowdhury, Y. Yin, Y. T. Chen, C. Ruiz, L. Lin, J. Pocas, T. Schröter, M. D. Cameron, P. LoGrasso, Y. Feng and T. D. Bannister, *Bioorg. Med. Chem. Lett.*, 2010, **20**, 1939–1943.

191   E. H. Sessions, Y. Yin, T. D. Bannister, A. Weiser, E. Griffin, J. Pocas, M. D. Cameron, C. Ruiz, L. Lin, S. C. Schürer, T. Schröter, P. LoGrasso and Y. Feng, *Bioorg. Med. Chem. Lett.*, 2008, **18**, 6390–6393.

192   S. Chowdhury, Y. T. Chen, X. Fang, W. Grant, J. Pocas, M. D. Cameron, C. Ruiz, L. Lin, H. Park, T. Schröter, T. D. Bannister, P. V. Lograsso and Y. Feng, *Bioorg. Med. Chem. Lett.*, 2013, **23**, 1592–1599.

193   G. Noronha, K. Barrett, A. Boccia, T. Brodhag, J. Cao, C. P. Chow, E. Dneprovskaia, J. Doukas, R. Fine, X. Gong, C. Gritzen, H. Gu, E. Hanna, J. D. Hood, S. Hu, X. Kang, J. Key, B. Klebansky, A. Kousba, G. Li, D. Lohse, C. C. Mak, A. McPherson, M. S. S. Palanki, V. P. Pathak, J. Renick, F. Shi, R. Soll, U. Splittgerber, S. Stoughton, S. Tang, S. Yee, B. Zeng, N. Zhao and H. Zhu, *Bioorg. Med. Chem. Lett.*, 2007, **17**, 602–608.

194   K. W. Woods, C. Lai, J. M. Miyashiro, Y. Tong, A. S. Florjancic, E. K. Han, N. Soni, Y. Shi, L. Lasko, J. D. Leverson, E. F. Johnson, A. R. Shoemaker and T. D. Penning, *Bioorg. Med. Chem. Lett.*, 2012, **22**, 1940–1943.

195   T. M. Chapman, S. A. Osborne, N. Bouloc, J. M. Large, C. Wallace, K. Birchall, K. H. Ansell, H. M. Jones, D. Taylor, B. Clough, J. L. Green and A. A. Holder, *Bioorg. Med. Chem. Lett.*, 2013, **23**, 3064–3069.

196   M. Atobe, K. Naganuma, M. Kawanishi, A. Morimoto, K. I. Kasahara, S. Ohashi, H. Suzuki, T. Hayashi and S. Miyoshi, *Bioorg. Med. Chem. Lett.*, 2014, **24**, 1327–1333.

197 S. Lin, F. Zhang, G. Jiang, S. A. Qureshi, X. Yang, G. G. Chicchi, L. Tota, A. Bansal, E. Brady, M. Trujillo, G. Salituro, C. Miller, J. R. Tata, B. B. Zhang and E. R. Parmee, *Bioorg. Med. Chem. Lett.*, 2015, **25**, 4143–4147.

198 J. T. Bagdanoff, R. Jain, W. Han, D. Poon, P. S. Lee, C. Bellamacina and M. Lindvall, *Bioorg. Med. Chem. Lett.*, 2015, **25**, 3626–3629.

199 J. E. Wilson, R. Kurukulasuriya, C. Sinz, M. Lombardo, K. Bender, D. Parker, E. C. Sherer, M. Costa, K. Dingley, X. Li, S. Mitelman, S. Tong, R. Bugianesi, A. Ehrhardt, B. Priest, K. Ratliff, F. Ujjainwalla, R. Nargund, W. K. Hagmann and S. Edmondson, *Bioorg. Med. Chem. Lett.*, 2016, **26**, 2947–2951.

200 N. R. Norcross, B. Baragaña, C. Wilson, I. Hallyburton, M. Osuna-Cabello, S. Norval, J. Riley, L. Stojanovski, F. R. C. Simeons, A. Porzelle, R. Grimaldi, S. Wittlin, S. Duffy, V. M. Avery, S. Meister, L. Sanz, B. Jiménez-Díaz, I. Angulo-Barturen, S. Ferrer, M. S. Martínez, F. J. Gamo, J. A. Frearson, D. W. Gray, A. H. Fairlamb, E. A. Winzeler, D. Waterson, S. F. Campbell, P. Willis, K. D. Read and I. H. Gilbert, *J. Med. Chem.*, 2016, **59**, 6101–6120.

201 Y. He, H. Dou, D. Gao, T. Wang, M. Zhang, H. Wang and Y. Li, *Bioorg. Med. Chem.*, 2019, **27**, 115015.

202 J. I. Montgomery, J. F. Smith, A. P. Tomaras, R. Zaniewski, C. J. McPherson, L. A. McAllister, S. Hartman-Neumann, J. T. Arcari, M. Lescoe, J. Gutierrez, Y. Yuan, C. Limberakis and A. A. Miller, *J. Antibiot. 2015 686*, 2014, **68**, 361–367.

203 T. Ku, N. Lopresti, M. Shirley, M. Mori, J. Marchant, X. Heng, M. Botta, M. F. Summers and K. L. Seley-Radtke, *Bioorganic Med. Chem.*, 2019, **27**, 2883–2892.

204 M. A. Larsen and J. F. Hartwig, *J. Am. Chem. Soc.*, 2014, **136**, 4287–4299.

205 O. R. Wauchope, M. Velasquez and K. Seley-Radtke, *Synth.*, 2012, **44**, 3496–3504.

206 W. S. Cheung, R. J. Patch and M. R. Player, *J. Org. Chem.*, 2005, **70**, 3741–3744.

207 J. Y. Wang, W. R. Zheng, L. L. Ding and Y. X. Wang, *New J. Chem.*, 2017, **41**, 1346–1362.

208 J. H. Kim, T. Constantin, M. Simonetti, J. Llaveria, N. S. Sheikh and D. Leonori, *Nat. 2021 5957869*, 2021, **595**, 677–683.

209 T. Taniguchi, *European J. Org. Chem.*, 2019, 2019, 6308–6319.

210 D. P. Curran, A. Solovyev, M. Makhlouf Brahmi, L. Fensterbank, M. Malacria and E. Lacôte, *Angew. Chemie - Int. Ed.*, 2011, 50, 10294–10317.

211 C. Wu, X. Hou, Y. Zheng, P. Li and D. Lu, *J. Org. Chem.*, 2017, **82**, 2898–2905.

212 S. H. Ueng, M. M. Brahmi, É. Derat, L. Fensterbank, E. Lacôte, M. Malacria and D. P. Curran, *J. Am. Chem. Soc.*, 2008, **130**, 10082–10083.

213 J. A. Baban and B. P. Roberts, *J. Chem. Soc. Perkin Trans. 2*, 1984, 1717–1722.

214 A. Staubitz, A. P. M. Robertson, M. E. Sloan and I. Manners, *Chem. Rev.*, 2010, **110**, 4023–4078.

215 B. Sheeller and K. U. Ingold, *J. Chem. Soc. Perkin Trans. 2*, 2001, **8**, 480–486.

216 H. Togo, K. Hayashi and M. Yokoyama, *Bull. Chem. Soc. Jpn.*, 1994, **67**, 2522–2527.

217 T. McCallum and L. Barriault, *Chem. Sci.*, 2016, **7**, 4754–4758.

218   J. Jin and D. W. C. MacMillan, *Nature*, 2015, **525**, 87–90.

219   J. D. Kirkham, S. J. Edeson, S. Stokes and J. P. A. Harrity, *Org. Lett.*, 2012, **14**, 5354–5357.

220   P. Fricero, L. Bialy, A. W. Brown, W. Czechtizky, M. Méndez and J. P. A. Harrity, *J. Org. Chem.*, 2017, **82**, 1688–1696.

221   P. Fricero, L. Bialy, W. Czechtizky, M. Méndez and J. P. A. Harrity, *ChemMedChem*, 2020, **15**, 1634–1638.

222   P. Fricero, L. Bialy, W. Czechtizky, M. Méndez and J. P. A. Harrity, *Org. Lett.*, 2018, **20**, 198–200.

223   G. A. Molander and B. Biolatto, *J. Org. Chem.*, 2003, **68**, 4302–4314.

224   W. Ren, J. Li, D. Zou, Y. Wu and Y. Wu, *Tetrahedron*, 2012, **68**, 1351–1358.

225   P. Ruiz-Castillo and S. L. Buchwald, *Chem. Rev.*, 2016, **116**, 12564–12649.

226   H. G. Bonacorso, A. Ferla, C. A. Cechinel, N. Zanatta and M. A. P. Martins, *J. Heterocycl. Chem.*, 2008, **45**, 483–487.

227   T. R. Jones, A. H. Calvert, A. L. Jackman, M. A. Eakin, M. J. Smithers, R. F. Betteridge, D. R. Newell, A. J. Hayter, A. Stocker, S. J. Harland, L. C. Davies and K. R. Harrap, *J. Med. Chem.*, 1985, **28**, 1468–1476.

228   N. Ando and S. Terashima, *Tetrahedron*, 2010, **66**, 6224–6237.

229   M. S. Bernatowicz, W. Youling and G. R. Matsueda, *J. Org. Chem.*, 1992, **57**, 2497–2502.

230   X. Z. Yang, R. Sun, X. Guo, X. R. Wei, J. Gao, Y. J. Xu and J. F. Ge, *Dye. Pigment.*, 2020, **173**, 107878.

231   Y. Q. Gu, W. Y. Shen, Y. Zhou, S. F. Chen, Y. Mi, B. F. Long, D. J. Young and F. L. Hu, *Spectrochim. Acta - Part A Mol. Biomol. Spectrosc.*, 2019, **209**, 141–149.

232   Y. Q. Gu, W. Y. Shen, Y. Mi, Y. F. Jing, J. M. Yuan, P. Yu, X. M. Zhu and F. L. Hu, *RSC Adv.*, 2019, **9**, 35671–35676.

233   R. N. Rao and K. Chanda, *Bioorg. Chem.*, 2020, 99, 103801.

234   E. J. Hanan, A. Van Abbema, K. Barrett, W. S. Blair, J. Blaney, C. Chang, C. Eigenbrot, S. Flynn, P. Gibbons, C. A. Hurley, J. R. Kenny, J. Kulagowski, L. Lee, S. R. Magnuson, C. Morris, J. Murray, R. M. Pastor, T. Rawson, M. Siu, M. Ultsch, A. Zhou, D. Sampath and J. P. Lyssikatos, *J. Med. Chem.*, 2012, **55**, 10090–10107.

235   N. Zidar, Ž. Jakopin, D. J. Madge, F. Chan, J. Tytgat, S. Peigneur, M. S. Dolenc, T. Tomašić, J. Ilaš, L. P. Mašič and D. Kikelj, *Eur. J. Med. Chem.*, 2014, **74**, 23–30.

236   R. F. Hunter, E. R. Parken and E. M. Short, *J. Chem. Soc.*, 1959, **10**, 784–788.

237   J. L. Mouton, M. Schmitt, C. G. Wermuth and J. J. Bourguignon, *Tetrahedron Lett.*, 1994, **35**, 6883–6886.

238   M. Bakherad, A. Keivanloo, Z. Kalantar and S. Jajarmi, *Tetrahedron Lett.*, 2011, **52**, 228–230.

239   P. M. Kochergin, I. A. Mazur, G. K. Rogul'chenko, E. V. Aleksandrova and B. E. Mandrichenko, *Chem. Heterocycl. Compd.*, 2001, **37**, 224–226.

240   D. Schilter, J. K. Clegg, M. M. Harding and L. M. Rendina, *Dalt. Trans.*, 2010, **39**, 239–247.

241 M. F. C. Santos, P. M. Harper, D. E. Williams, J. T. Mesquita, É. G. Pinto, T. A. Da Costa-Silva, E. Hajdu, A. G. Ferreira, R. A. Santos, P. J. Murphy, R. J. Andersen, A. G. Tempone and R. G. S. Berlinck, *J. Nat. Prod.*, 2015, **78**, 1101–1112.

242 H. C. Longuet-Higgins, *J. Chem. Phys.*, 1950, **18**, 275–282.

243 D. J. Brown and J. S. Harper, *J. Chem. Soc.*, 1963, **189**, 1276–1284.

244 E. S. H. El Ashry, Y. El Kilany, N. Rashed and H. Assafir, *Adv. Heterocycl. Chem.*, 1999, **75**, 79–165.

245 D. J. Brown and M. N. Paddon-Row, *J. Chem. Soc. C Org. Chem.*, 1967, 1928–1933.

246 S. Sakurai, T. Kato, R. Sakamoto and K. Maruoka, *Tetrahedron*, 2019, **75**, 172–179.

247 F. Li, L. Chen, Q. Kang, J. Cai and G. Zhu, *New J. Chem.*, 2013, **37**, 624–631.

248 Y. Watanabe, Y. Morisaki, T. Kondo and T. A. Mitsudo, *J. Org. Chem.*, 1996, **61**, 4214–4218.

249 M. Mastalir, G. Tomsu, E. Pittenauer, G. Allmaier and K. Kirchner, *Org. Lett.*, 2016, **18**, 3462–3465.

250 W. Erb, J. P. Hurvois, T. Roisnel and V. Dorcet, *Organometallics*, 2018, **37**, 3780–3790.

251 J. P. Collman and M. Zhong, *Org. Lett.*, 2000, **2**, 1233–1236.

252 P. Y. S. Lam, C. G. Clark, S. Saubern, J. Adams, M. P. Winters, D. M. T. Chan and A. Combs, *Tetrahedron Lett.*, 1998, **39**, 2941–2944.

253 D. N. Rao, S. Rasheed, S. Aravinda, R. A. Vishwakarma and P. Das, *RSC Adv.*, 2013, **3**, 11472–11475.

254 K. Rizwan, I. Karakaya, D. Heitz, M. Zubair, N. Rasool and G. A. Molander, *Tetrahedron Lett.*, 2015, **56**, 6839–6842.

255 S. S. AlNeyadi, A. A. Salem, M. A. Ghattas, N. Atatreh and I. M. Abdou, *Eur. J. Med. Chem.*, 2017, **136**, 270–282.

256 P. M. Arce, O. M. Khdour, R. Goldschmidt, J. S. Armstrong and S. M. Hecht, *ACS Med. Chem. Lett.*, 2011, **2**, 608–613.

257 Y. Yang, C. Su, X. Huang and Q. Y. Liu, *Tetrahedron Lett.*, 2009, **50**, 5754–5756.

258 WO/2001/000213, 2001.

259 C. Wang, J. Cai, M. Zhang and X. Zhao, , DOI:10.1021/acs.joc.6b02624.

260 N. Rozatian, I. W. Ashworth, G. Sandford and D. R. W. Hodgson, *Chem. Sci.*, 2018, **9**, 8692–8702.

261 D. M. Knapp, E. P. Gillis and M. D. Burke, 2009, 6961–6963.

262 G. A. Molander and A. R. Brown, *J. Org. Chem.*, 2006, **71**, 9681–9686.

263 R. A. Batey and T. D. Quach, *Tetrahedron Lett.*, 2001, **42**, 9099–9103.

264 J. Chen and A. Cammers-Goodwin, *Tetrahedron Lett.*, 2003, **44**, 1503–1506.

265 Y. Nishihara, H. Onodera and K. Osakada, *Chem. Commun.*, 2004, **4**, 192–193.

266 T. Korenaga, T. Kosaki, R. Fukumura, T. Ema and T. Sakai, *Org. Lett.*, 2005, **7**, 4915–4917.

267   D. Imao, B. W. Glasspoole, V. S. Laberge and C. M. Crudden, *J. Am. Chem. Soc.*, 2009, **131**, 5024–5025.

268   N. Mintcheva, Y. Nishihara, A. Mori and K. Osakada, *J. Organomet. Chem.*, 2001, **629**, 61–67.

269   N. Mintcheva, Y. Nishihara, M. Tanabe, K. Hirabayashi, A. Mori and K. Osakada, *Organometallics*, 2001, **20**, 1243–1246.

270   B. P. Carrow and J. F. Hartwig, *J. Am. Chem. Soc.*, 2011, **133**, 2116–2119.

271   J. P. Flemming, M. C. Pilon, O. Y. Borbulevitch, M. Y. Antipin and V. V. Grushin, *Inorganica Chim. Acta*, 1998, **280**, 87–98.

272   S. Gupta, P. Chaudhary, L. Seva, S. Sabiah and J. Kandasamy, *RSC Adv.*, 2015, **5**, 89133–89138.

273   M. M. Hussain, H. Li, N. Hussain, M. Urena, P. J. Carroll and P. J. Walsh, *J. Am. Chem. Soc.*, 2009, **131**, 6516–6524.

274   S. Gupta, P. Chaudhary, V. Srivastava and J. Kandasamy, *Tetrahedron Lett.*, 2016, **57**, 2506–2510.

275   G. A. Molander and L. N. Cavalcanti, *J. Org. Chem.*, 2011, **76**, 623–630.

276   A. W. Brown, J. Comas-Barceló and J. P. A. Harrity, *Chem. - A Eur. J.*, 2017, **23**, 5228–5231.

277   G. W. Gribble, 2009, pp. 9–348.

278   G. W. Kabalka and A. R. Mereddy, *Tetrahedron Lett.*, 2004, **45**, 343–345.

279   G. W. Kabalka and A. R. Mereddy, *Organometallics*, 2004, **23**, 4519–4521.

280   M. L. Yao, G. W. Kabalka, D. W. Blevins, M. S. Reddy and L. Yong, *Tetrahedron*, 2012, **68**, 3738–3743.

281   M. L. Yao, M. S. Reddy, Y. Li, I. Walfish, D. W. Blevins and G. W. Kabalka, *Org. Lett.*, 2010, **12**, 700–703.

282   D. W. Blevins, M. L. Yao, L. Yong and G. W. Kabalka, *Tetrahedron Lett.*, 2015, **56**, 3130–3132.

283   R. Pilli, V. Balakrishnan, R. Chandrasekaran and R. Rasappan, *Org. Biomol. Chem.*, 2019, **17**, 1749–1753.

284   H. C. Brown, M. M. Midland, A. B. Levy, H. C. Brown, R. B. Wetherill, A. Suzuki, S. Sono and M. Itoh, *Tetrahedron*, 1987, **43**, 4079–4088.

285   H. C. Brown, A. M. Salunkhe and B. Singaram, *J. Org. Chem.*, 1991, **56**, 1170–1175.

286   H. C. Brown, M. M. Midland and A. B. Levy, *J. Am. Chem. Soc.*, 1972, 94, 2114–2115.

287   D. S. Matteson and G. Y. Kim, *Org. Lett.*, 2002, **4**, 2153–2155.

288   J. Emsley, *Nature's building blocks. An A-Z guide to the elements*, Oxford University Press, New York, 2001.

289   K. K. Jason Chan and D. O'Hagan, in *Methods in Enzymology*, 2012, pp. 219–235.

290   D. O'Hagan, C. Schaffrath, S. L. Cobb, J. T. G. Hamilton and C. D. Murphy, *Nature*, 2002, **416**, 279.

291   D. B. Harper and D. O'Hagan, *Nat. Prod. Rep.*, 1994, **11**, 123–133.

292   J.-P. Bégué and D. Bonnet-Delpon, *Bioorganic and medicinal chemistry of fluorine*, John Wiley

& Sons, Ltd, New Jersey, 2008.

293   D. O'Hagan and D. B. Harper, *J. Fluor. Chem.*, 1999, **100**, 127–133.

294   D. O'Hagan, R. Perry, J. M. Lock, J. J. M. Meyer, L. Dasaradhi, J. T. G. Hamilton and D. B. Harper, *Phytochemistry*, 1993, **33**, 1043–1045.

295   R. J. HALL, *New Phytol.*, 1972, **71**, 855–871.

296   T. Okazoe, *Proc. Jpn. Acad. Ser. B. Phys. Biol. Sci.*, 2009, **85**, 276.

297   W. K. Hagmann, *J. Med. Chem.*, 2008, **51**, 4359–4369.

298   N. A. Meanwell, *J. Med. Chem.*, 2018, **61**, 5822–5880.

299   X.-H. Xu, K. Matsuzaki and N. Shibata, *Chem. Rev.*, 2014, **115**, 731–764.

300   S. Purser, P. R. Moore, S. Swallow and V. Gouverneur, *Chem. Soc. Rev.*, 2008, **37**, 320–330.

301   J. Fried and E. F. Sabo, *J. Am. Chem. Soc.*, 1954, **76**, 1455–1456.

302   D. O'Hagan, *J. Fluor. Chem.*, 2010, **131**, 1071–1081.

303   Y. Zhou, J. Wang, Z. Gu, S. Wang, W. Zhu, J. L. Aceña, V. A. Soloshonok, K. Izawa and H. Liu, *Chem. Rev.*, 2016, **116**, 422–518.

304   M. Inoue, Y. Sumii and N. Shibata, *ACS Omega*, 2020, **5**, 10633–10640.

305   A. Harsanyi and G. Sandford, *Green Chem.*, 2015, **17**, 2081–2086.

306   S. Caron, *Org. Process Res. Dev.*, 2020, **24**, 470–480.

307   Z. Wang, *Compr. Org. Name React. Reagents*, 2010, 2744–2747.

308   F. Swarts, *Bull. Akad. R. Belg.*, 1898, **35**, 375.

309   H. S. Booth, P. E. Burchfield and H. M. Elsey, *J. Am. Chem. Soc.*, 1935, **57**, 2066–2069.

310   575593, 1933.

311   2005705, 1935.

312   L. Zhu, K. Ploessl and H. F. Kung, *Science (80-.).*, 2013, **342**, 429–430.

313   S. Preshlock, M. Tredwell and V. Gouverneur, *Chem. Rev.*, 2016, **116**, 719–766.

314   K. M. Engle, L. Pfeifer, G. W. Pidgeon, G. T. Giuffredi, A. L. Thompson, R. S. Paton, J. M. Brown and V. Gouverneur, *Chem. Sci.*, 2015, **6**, 5293–5302.

315   J.-W. Lee, M. T. Oliveira, H. Bin Jang, S. Lee, D. Y. Chi, D. W. Kim and C. E. Song, *Chem. Soc. Rev.*, 2016, **45**, 4638–4650.

316   D. Landini, A. Maia and A. Rampoldi, *J. Org. Chem.*, 1989, **54**, 328–332.

317   S. Liang, G. B. Hammond and B. Xu, *Chem. – A Eur. J.*, 2017, **23**, 17850–17861.

318   J. H. Clark, *Chem. Rev.*, 1980, **80**, 429–452.

319   H. Suzuki and Y. Kimura, *J. Fluor. Chem.*, 1991, **52**, 341–351.

320   M. Lalonde and T. H. Chan, *Synthesis (Stuttg).*, 1985, 817–845.

321   E. J. Corey and A. Venkateswarlu, *J. Am. Chem. Soc.*, 1972, **94**, 6190–6191.

322   R. K. Sharma and J. L. Fry, *J. Org. Chem.*, 1983, **48**, 2112–2114.

323   H. S. And and S. G. DiMagno, *J. Am. Chem. Soc.*, 2005, **127**, 2050–2051.

324   H. Sun and S. G. DiMagno, *Angew. Chemie Int. Ed.*, 2006, **45**, 2720–2725.

325   H. Sun and S. G. DiMagno, *Chem. Commun.*, 2007, 528–529.

326   N. Yoneda, *Tetrahedron*, 1991, **47**, 5329–5365.

327   G. A. Olah, J. G. Shih and G. K. S. Prakash, *J. Fluor. Chem.*, 1986, **33**, 377–396.

328   S. Bowles, M. M. Campbell, M. Sainsbury and G. M. Davies, *Tetrahedron Lett.*, 1989, **30**, 3711–3714.

329   R. P. Singh and J. M. Shreeve, *Synthesis (Stuttg).*, 2002, **2002**, 2561–2578.

330   G. S. Lal, G. P. Pez, R. J. Pesaresi, F. M. Prozonic and H. Cheng, *J. Org. Chem.*, 1999, **64**, 7048–7054.

331   R. P. Singh and J. M. Shreeve, *J. Fluor. Chem.*, 2002, **116**, 23–26.

332   R. P. Singh, D. Chakraborty and J. M. Shreeve, *J. Fluor. Chem.*, 2001, **111**, 153–160.

333   M. Ichikawa and Y. Ichikawa, *Bioorg. Med. Chem. Lett.*, 2001, **11**, 1769–1773.

334   G. A. Guirgis, S. Bell and J. R. Durig, *J. Raman Spectrosc.*, 2000, **31**, 987–994.

335   * Gauri S. Lal, † and Elyse Lobach and A. Evans†, *J. Org. Chem.*, 2000, **65**, 4830–4832.

336   P. A. Messina, K. C. Mange and W. J. Middleton, *J. Fluor. Chem.*, 1989, **42**, 137–143.

337   W.-L. Hu, X.-G. Hu and L. Hunter, *Synthesis (Stuttg).*, 2017, **49**, 4917–4930.

338   M. K. Nielsen, C. R. Ugaz, W. Li and A. G. Doyle, *J. Am. Chem. Soc.*, 2015, **137**, 9571–9574.

339   E. W. Webb, J. B. Park, E. L. Cole, D. J. Donnelly, S. J. Bonacorsi, W. R. Ewing and A. G. Doyle, *J. Am. Chem. Soc.*, 2020, **142**, 9493–9500.

340   T. B. Patrick and R. Mortezania, *J. Org. Chem.*, 1988, **53**, 5153–5155.

341   S. T. Purrington, B. S. Kagen and T. B. Patrick, *Chem. Rev.*, 1986, **86**, 997–1018.

342   O. Lerman, Y. Tor and S. Rozen, *J. Org. Chem.*, 1981, **46**, 4629–4631.

343   S. D. Taylor, C. C. Kotoris and G. Hum, *Tetrahedron*, 1999, **55**, 12431–12477.

344   G. S. Lal, G. P. Pez and R. G. Syvret, *Chem. Rev.*, 1996, **96**, 1737–1755.

345   K. Kawada, in *Fluorination*, Springer, Singapore, 2018.

346   M. Rueda-Becerril, C. C. Sazepin, J. C. T. Leung, T. Okbinoglu, P. Kennepohl, J.-F. Paquin and G. M. Sammis, *J. Am. Chem. Soc.*, 2012, **134**, 4026–4029.

347   J.-D. Yang, Y. Wang, X.-S. Xue and J.-P. Cheng, *J. Org. Chem.*, 2017, **82**, 4129–4135.

348   M. Li, X. S. Xue and J. P. Cheng, *Acc. Chem. Res.*, 2020, **53**, 182–197.

349   B. Lantaño and A. Postigo, *Org. Biomol. Chem.*, 2017, 15, 9954–9973.

350   R. Szpera, D. F. J. Moseley, L. B. Smith, A. J. Sterling and V. Gouverneur, *Angew. Chemie Int. Ed.*, 2019, **58**, 14824–14848.

351 Z. Zou, W. Zhang, Y. Wang and Y. Pan, *Org. Chem. Front.*, 2021, **8**, 2786–2798.

352 K. Müller, C. Faeh and F. Diederich, *Science (80-.).*, 2007, **317**, 1881–1886.

353 E. Prchalová, O. Štěpánek, S. Smrček and M. Kotora, *Future Med. Chem.*, 2014, 6, 1201–1229.

354 V. C. R. Mcloughlin and J. Thrower, *Tetrahedron*, 1969, **25**, 5921–5940.

355 Y. Kobayashi and I. Kumadaki, *Tetrahedron Lett.*, 1969, **10**, 4095–4096.

356 G. G. Dubinina, H. Furutachi and D. A. Vicic, *J. Am. Chem. Soc.*, 2008, **130**, 8600–8601.

357 J.-A. Ma and D. Cahard*, *Chem. Rev.*, 2004, **104**, 6119–6146.

358 G. K. Surya Prakash and M. Mandal, *J. Am. Chem. Soc.*, 2002, **124**, 6538–6539.

359 S. Caron, N. M. Do, P. Arpin and A. Larivée, *Synthesis (Stuttg).*, 2003, **2003**, 1693–1698.

360 K. Iseki, T. Nagai and Y. Kobayashi, *Tetrahedron Lett.*, 1994, **35**, 3137–3138.

361 M. Oishi, H. Kondo and H. Amii, *Chem. Commun.*, 2009, 1909–1911.

362 G. Li, C. Zhang, C. Song and Y. Ma, *Beilstein J. Org. Chem. 1411*, 2018, **14**, 155–181.

363 Z. Weng, R. Lee, W. Jia, Y. Yuan, W. Wang, X. Feng and K.-W. Huang, *Organometallics*, 2011, **30**, 3229–3232.

364 T. Knauber, F. Arikan, G.-V. Röschenthaler and L. J. Gooßen, *Chem. – A Eur. J.*, 2011, **17**, 2689–2697.

365 Y. Li, T. Chen, H. Wang, R. Zhang, K. Jin, X. Wang and C. Duan, *Synlett*, 2011, **2011**, 1713–1716.

366 H. Kondo, M. Oishi, K. Fujikawa and H. Amii, *Adv. Synth. Catal.*, 2011, **353**, 1247–1252.

367 A. Zanardi, M. A. Novikov, E. Martin, J. Benet-Buchholz and V. V. Grushin, *J. Am. Chem. Soc.*, 2011, **133**, 20901–20913.

368 I. Popov, S. Lindeman and O. Daugulis, *J. Am. Chem. Soc.*, 2011, **133**, 9286–9289.

369 A. Lishchynskyi, G. Berthon and V. V. Grushin, *Chem. Commun.*, 2014, **50**, 10237–10240.

370 L. Chu and F.-L. Qing, *Org. Lett.*, 2010, **12**, 5060–5063.

371 D. A. Culkin and J. F. Hartwig, *Organometallics*, 2004, **23**, 3398–3416.

372 N. D. Ball, J. W. Kampf and M. S. Sanford, *J. Am. Chem. Soc.*, 2010, **132**, 2878–2879.

373 V. V. Grushin and W. J. Marshall, *J. Am. Chem. Soc.*, 2006, **128**, 12644–12645.

374 V. V. Grushin and W. J. Marshall, *J. Am. Chem. Soc.*, 2006, **128**, 4632–4641.

375 E. J. Cho, T. D. Senecal, T. Kinzel, Y. Zhang, D. A. Watson and S. L. Buchwald, *Science (80-.).*, 2010, **328**, 1679–1681.

376 F. Ozawa, K. Kurihara, M. Fujimori, T. Hidaka, T. Toyoshima and A. Yamamoto, *Organometallics*, 1989, **8**, 180–188.

377 J. M. Brown and P. J. Guiry, *Inorganica Chim. Acta*, 1994, **220**, 249–259.

378 J. F. Hartwig, *Organotransition Metal Chemistry*, University Science Books, 2010.

379 T. Furuya and T. Ritter, *J. Am. Chem. Soc.*, 2008, **130**, 10060–10061.

380   T. Furuya, D. Benitez, E. Tkatchouk, A. E. Strom, P. Tang, I. William A. Goddard and T. Ritter, *J. Am. Chem. Soc.*, 2010, **132**, 3793–3807.

381   P. Chen and G. Liu, *Synthesis (Stuttg).*, 2013, **45**, 2919–2939.

382   C. Alonso, E. M. de Marigorta, G. Rubiales and F. Palacios, *Chem. Rev.*, 2015, **115**, 1847–1935.

383   T. Furuya, A. S. Kamlet and T. Ritter, *Nature*, 2011, **473**, 470–477.

384   X. Wang, L. Truesdale and J.-Q. Yu, *J. Am. Chem. Soc.*, 2010, **132**, 3648–3649.

385   C. Ni, M. Hu and J. Hu, *Chem. Rev.*, 2015, 115, 765–825.

386   S. Barata-Vallejo, B. Lantaño and A. Postigo, *Chem. – A Eur. J.*, 2014, **20**, 16806–16829.

387   C. Zhang, *Org. Biomol. Chem.*, 2014, **12**, 6580–6589.

388   J. Charpentier, N. Früh and A. Togni, *Chem. Rev.*, 2015, 115, 650–682.

389   K. Natte, R. V. Jagadeesh, L. He, J. Rabeah, J. Chen, C. Taeschler, S. Ellinger, F. Zaragoza, H. Neumann, A. Brückner and M. Beller, *Angew. Chemie Int. Ed.*, 2016, **55**, 2782–2786.

390   V. L. Orkin and V. G. Khamaganov, *J. Atmos. Chem. 1993 162*, 1993, **16**, 169–178.

391   D. A. Nagib and D. W. C. MacMillan, *Nat. 2011 4807376*, 2011, **480**, 224–228.

392   B. R. Langlois, E. Laurent and N. Roidot, *Tetrahedron Lett.*, 1991, **32**, 7525–7528.

393   Y. Ji, T. Brueckl, R. D. Baxter, Y. Fujiwara, I. B. Seiple, S. Su, D. G. Blackmond and P. S. Baran, *Proc. Natl. Acad. Sci.*, 2011, **108**, 14411–14415.

394   Y. Fujiwara, J. A. Dixon, R. A. Rodriguez, R. D. Baxter, D. D. Dixon, M. R. Collins, D. G. Blackmond and P. S. Baran, *J. Am. Chem. Soc.*, 2012, **134**, 1494–1497.

395   H. Xiao, Z. Zhang, Y. Fang, L. Zhu and C. Li, *Chem. Soc. Rev.*, 2021, **50**, 6308–6319.

396   E. J. Cho, *Chem. Rec.*, 2016, **16**, 47–63.

397   A. Studer, *Angew. Chemie Int. Ed.*, 2012, **51**, 8950–8958.

398   F. D'Accriscio, P. Borja, N. Saffon-Merceron, M. Fustier-Boutignon, N. Mézailles and N. Nebra, *Angew. Chemie Int. Ed.*, 2017, **56**, 12898–12902.

399   E. A. Meucci, S. N. Nguyen, N. M. Camasso, E. Chong, A. Ariafard, A. J. Canty and M. S. Sanford, *J. Am. Chem. Soc.*, 2019, **141**, 12872–12879.

400   C. M. Kisukuri, V. A. Fernandes, J. A. C. Delgado, A. P. Häring, M. W. Paixão and S. R. Waldvogel, *Chem. Rec.*, 2021, 21, 2502–2525.

401   R. P. Bhaskaran and B. P. Babu, *Adv. Synth. Catal.*, 2020, **362**, 5219–5237.

402   D. F. Chicas-Baños and B. A. Frontana-Uribe, *Chem. Rec.*, 2021, **21**, 2538–2573.

403   A. G. O-Brien, A. Maruyama, Y. Inokuma, M. Fujita, P. S. Baran and D. G. Blackmond, *Angew. Chemie - Int. Ed.*, 2014, **53**, 11868–11871.

404   G.-Y. Dou, Y.-Y. Jiang, K. Xu and C.-C. Zeng, *Org. Chem. Front.*, 2019, **6**, 2392–2397.

405   Y. Qiu, A. Scheremetjew, L. H. Finger and L. Ackermann, *Chem. - A Eur. J.*, 2020, **26**, 3241–3246.

406   S. Liu, B. Chen, Y. Yang, Y. Yang, Q. Chen, X. Zeng and B. Xu, *Electrochem. commun.*, 2019,

109, 106583.

407 W. Wu and Z. Weng, *Synthesis (Stuttg).*, 2018, **50**, 1958–1964.

408 M. Grünebaum, A. Buchheit, C. Günther and H. D. Wiemhöfer, *Tetrahedron Lett.*, 2016, **57**, 1555–1559.

409 J. C. Sloop, C. L. Bumgardner and W. D. Loehle, *J. Fluor. Chem.*, 2002, **118**, 135–147.

410 S. V. Druzhinin, E. S. Balenkova and V. G. Nenajdenko, *Tetrahedron*, 2007, **63**, 7753–7808.

411 V. G. Nenajdenko, A. V. Sanin and E. S. Balenkova, *Mol. 1997, Vol. 2, Pages 186-232*, 1997, **2**, 186–232.

412 V. G. Nenaidenko, A. V. Sanin and E. S. Balenkova, *Russ. Chem. Rev.*, 1999, **68**, 437–458.

413 I. Katsuyama, O. Seiya, K. Yamaguchi, Yoshihiro Funabiki, M. Masaki and H. Shibata, Katsuyoshi Muramatsu, *Synthesis (Stuttg).*, 1997, 1321–1324.

414 A. Y. Rulev, V. M. Muzalevskiy, E. V. Kondrashov, I. A. Ushakov, A. R. Romanov, V. N. Khrustalev and V. G. Nenajdenko, *Org. Lett.*, 2013, **15**, 2726–2729.

415 V. M. Muzalevskiy, Y. A. Ustynyuk, I. P. Gloriozov, V. A. Chertkov, A. Y. Rulev, E. V. Kondrashov, I. A. Ushakov, A. R. Romanov and V. G. Nenajdenko, *Chem. – A Eur. J.*, 2015, **21**, 16982–16989.

416 I. P. Gloriozov, V. M. Muzalevskiy, A. Y. Rulev, E. V. Kondrashov, V. G. Nenajdenko and Y. A. Ustynyuk, *Russ. J. Org. Chem. 2016 528*, 2016, **52**, 1098–1111.

417 V. M. Muzalevskiy, A. Y. Rulev, E. V. Kondrashov, A. R. Romanov, I. A. Ushakov, V. A. Chertkov and V. G. Nenajdenko, *European J. Org. Chem.*, 2016, **2016**, 1612–1618.

418 A. Y. Rulev, A. R. Romanov, E. V. Kondrashov, I. A. Ushakov, A. V. Vashchenko, V. M. Muzalevskiy and V. G. Nenajdenko, *J. Org. Chem.*, 2016, **81**, 10029–10034.

419 A. R. Romanov, A. Y. Rulev, I. A. Ushakov, V. M. Muzalevskiy and V. G. Nenajdenko, *European J. Org. Chem.*, 2017, **2017**, 4121–4129.

420 V. M. Muzalevskiy, A. Y. Rulev, A. R. Romanov, E. V. Kondrashov, I. A. Ushakov, V. A. Chertkov and V. G. Nenajdenko, *J. Org. Chem.*, 2017, **82**, 7200–7214.

421 V. M. Muzalevskiy, M. N. Mamedzade, V. A. Chertkov, V. A. Bakulev and V. G. Nenajdenko, *Mendeleev Commun.*, 2018, **28**, 17–19.

422 V. M. Muzalevskiy, Z. A. Sizova, K. V. Belyaeva, B. A. Trofimov and V. G. Nenajdenko, *Molecules*, 2019, **24**, 3594.

423 V. M. Muzalevskiy, K. V. Belyaeva, B. A. Trofimov and V. G. Nenajdenko, *Green Chem.*, 2019, **21**, 6353–6360.

424 V. M. Muzalevskiy, Z. A. Sizova and V. G. Nenajdenko, *Org. Lett.*, 2021, **23**, 5973–5977.

425 F. Peng, Q. Zhao, W. Huang, S.-J. Liu, Y.-J. Zhong, Q. Mao, N. Zhang, G. He and B. Han, *Green Chem.*, 2019, **21**, 6179–6186.

426 Y.-L. Ji, X.-H. He, G. Li, Y.-Y. Ai, H.-P. Li, C. Peng and B. Han, *Org. Chem. Front.*, 2020, **7**, 563–570.

427 Q. Zhao, C. Peng, G. Zhan and B. Han, *RSC Adv.*, 2020, **10**, 40983–41003.

428   I. S. Kondratov, N. A. Tolmachova and G. Haufe, *European J. Org. Chem.*, 2018, **2018**, 3618–3647.

429   T. Hiyama and K. Sato, *Synlett*, 1990, 53–54.

430   M. Schlosser and H. Keller, *Liebigs Ann.*, 1995, **1995**, 1587–1589.

431   J.-N. Volle and M. Schlosser, *European J. Org. Chem.*, 2002, **2002**, 1490–1492.

432   R. G. Salomon, J. R. Burns and W. J. Dominic, *J. Org. Chem.*, 1976, **41**, 2918–2920.

433   K. Afarinkia, V. Vinader, T. D. Nelson and G. H. Posner, *Tetrahedron*, 1992, **48**, 9111–9171.

434   W. A. Boulanger and J. A. Katzenellenbogen, *J. Med. Chem.*, 1986, **29**, 1483–1487.

435   4 230 864, 1980.

436   M. B. Supurgibekov, G. K. S. Prakash and V. A. Nikolaev, *Synthesis (Stuttg).*, 2013, **45**, 1215–1226.

437   S. L. Clarke and G. P. McGlacken, *Tetrahedron*, 2015, **71**, 2906–2913.

438   P. Martin, J. Streith, G. Rihs, T. Winkler and D. Belluš, *Tetrahedron Lett.*, 1985, **26**, 3947–3950.

439   I. I. Gerus, N. A. Tolmachova, S. I. Vdovenko, R. Fröhlich and G. Haufe, *Synthesis (Stuttg).*, 2005, **2005**, 1269–1278.

440   N. A. Tolmachova, I. I. Gerus, S. I. Vdovenko, M. Essers, R. Fröhlich and G. Haufe, *European J. Org. Chem.*, 2006, **2006**, 4704–4709.

441   M. Tordeux, B. Langlois and C. Wakselman, *J. Chem. Soc. Perkin Trans. 1*, 1990, 2293–2299.

442   C. G. Béguin, *Enantiocontrolled Synthesis of FluoroOrganic Compounds: Stereochemical Challenges and Biomedical Targets*, John Wiley & Sons, Chichester, 1999.

443   G. H. Posner and D. G. Wettlaufer, *Tetrahedron Lett.*, 1986, **27**, 667–670.

444   K. Afarinkia and G. H. Posner, *Tetrahedron Lett.*, 1992, **33**, 7839–7842.

445   P. Gan, M. W. Smith, N. R. Braffman and S. A. Snyder, *Angew. Chemie Int. Ed.*, 2016, **55**, 3625–3630.

446   P. K. Mykhailiuk, *Chem. Rev.*, 2021, 121, 1670–1715.

447   P. L. McCormack, *Drugs*, 2011, 71, 2457–2489.

448   B. D. Maxwell, *J. Label. Compd. Radiopharm.*, 2000, **43**, 645–654.

449   A. K. Culbreath, T. B. Brenneman, R. C. Kemerait and G. G. Hammes, *Pest Manag. Sci.*, 2009, **65**, 66–73.

450   JP5830821B2, 2012.

451   WO/2019/030355, 2019.

452   S. Fustero, M. Sánchez-Roselló, P. Barrio and A. Simón-Fuentes, *Chem. Rev.*, 2011, **111**, 6984–7034.

453   G. Meazza, G. Zanardi and P. Piccardi, *J. Heterocycl. Chem.*, 1993, **30**, 365–371.

454   J. Lu, Y. Man, Y. Zhang, B. Lin, Q. Lin and Z. Weng, *RSC Adv.*, 2019, **9**, 30952–30956.

455   J. Comas-Barceló, R. S. Foster, B. Fiser, E. Gomez-Bengoa and J. P. A. Harrity, *Chem. - A Eur. J.*, 2015, **21**, 3257–3263.

456   R. S. Foster, H. Jakobi and J. P. A. Harrity, *Org. Lett.*, 2012, **14**, 4858–4861.

457   F. Dumitraşcu, C. Drâghici, D. Dumitrescu, L. Tarko and D. Râileanu, *Liebigs Ann.*, 1997, **1997**, 2613–2616.

458   R. Huisgen, *Angew. Chemie Int. Ed. English*, 1963, **2**, 633–645.

459   R. Fields and J. P. Tomlinson, *J. Fluor. Chem.*, 1979, **13**, 147–158.

460   E. Y. Slobodyanyuk, O. S. Artamonov, O. V. Shishkin and P. K. Mykhailiuk, *European J. Org. Chem.*, 2014, **2014**, 2487–2495.

461   J. F. Vivat, H. Adams and J. P. A. Harrity, *Org. Lett.*, 2009, **12**, 160–163.

462   J. D. Kirkham, R. J. Butlin and J. P. A. Harrity, *Angew. Chemie - Int. Ed.*, 2012, **51**, 6402–6405.

463   D. F. Crépin and J. P. A. Harrity, *Org. Lett.*, 2013, **15**, 4222–4225.

464   D. F. P. Crépin, J. P. A. Harrity, J. Jiang, A. J. H. M. Meijer, A.-C. M. A. Nassoy and P. Raubo, *J. Am. Chem. Soc.*, 2014, **136**, 8642–8653.

465   S. P. J. T. Bachollet, J. F. Vivat, D. C. Cocker, H. Adams and J. P. A. Harrity, *Chem. – A Eur. J.*, 2014, **20**, 12889–12893.

466   S. P. J. T. Bachollet, D. Volz, B. Fiser, S. Münch, F. Rönicke, J. Carrillo, H. Adams, U. Schepers, E. Gómez-Bengoa, S. Bräse and J. P. A. Harrity, *Chem. – A Eur. J.*, 2016, **22**, 12430–12438.

467   Y. P. Budiman, S. A. Westcott, U. Radius and T. B. Marder, *Adv. Synth. Catal.*, 2021, **363**, 2224–2255.

468   P. V. Ramachandran and W. Mitsuhashi, *J. Fluor. Chem.*, 2016, **190**, 7–11.

469   A. K. Brisdon, I. R. Crossley, R. G. Pritchard, G. Sadiq and J. E. Warren, *Organometallics*, 2003, **22**, 5534–5542.

470   A. K. Brisdon and I. R. Crossley, *Chem. Commun. (Camb).*, 2002, 2420–1.

471   V. V. Bardin, N. Y. Adonin and H. J. Frohn, *Organometallics*, 2005, **24**, 5311–5317.

472   T. Matsumoto, S. Harima, J.-K. Weng and K. Nihei, *Synth. Commun.*, 2020, **50**, 2981–2987.

473   N. Metanis, E. Keinan and P. E. Dawson, *J. Am. Chem. Soc.*, 2005, **127**, 5862–5868.

474   J. Sauer, D. K. Heldmann and G. R. Pabst, *European J. Org. Chem.*, 1999, 313–321.

475   E. Negishi, M. J. Idacavage, K.-W. Chiu, T. Yoshida, A. Abramovitch, M. E. Goettel, A. Silveira and H. D. Bretherick, *J. Chem. Soc. Perkin Trans. 2*, 1978, 1225–1232.

476   T. Lundrigan, S. M. Crawford, T. S. Cameron and A. Thompson, *Chem. Commun.*, 2012, **48**, 1003–1005.

477   T. E. Barder and S. L. Buchwald, *Org. Lett.*, 2004, **6**, 2649–2652.

478   Y. Yang, Q. Gao and S. Xu, *Adv. Synth. Catal.*, 2019, **361**, 858–862.

479   D. L. Cousins, P. Fricero, K. P. M. Kopf, E. J. McColl, W. Czechtizky, Y. H. Lim and J. P. A. Harrity, *Angew. Chemie - Int. Ed.*, 2021, **60**, 9412–9415.

480   A. Abo-Amer, H. J. Frohn, C. Steinberg and U. Westphal, *J. Fluor. Chem.*, 2006, **127**, 1311–

1323.

481   B. Duda and D. Lentz, *Org. Biomol. Chem.*, 2015, **13**, 5625–5628.

482   A. D. Becke, *Phys. Rev. A*, 1988, **38**, 3098.

483   A. D. Becke, *J. Chem. Phys.*, 1998, **98**, 1372.

484   C. Lee, W. Yang and R. G. Parr, *Phys. Rev. B*, 1988, **37**, 785.

485   M. J. Frisch, G. W. Trucks, H. B. Schlegel, G. E. . Scuseria, M. A. Robb, G. Cheeseman, J. R.; Scalmani, V. Barone, B. Mennucci, G. A. Petersson, H. Nakatsuji, M. Caricato, X. Li, H. P. Hratchian, A. F. Izmaylov, J. Bloino, G. Zheng, J. L. Sonnenberg, M. Hada, M. Ehara, K. Toyota, R. Fukuda, J. Hasegawa, M. Ishida, T. Nakajima, Y. Honda, O. Kitao, H. Nakai, T. Vreven, J. A. J. Montgomery, J. E. Peralta, F. Ogliaro, M. Bearpark, J. J. Heyd, E. Brothers, K. N. Kudin, V. N. Staroverov, R. Kobayashi, J. Normand, K. Raghavachari, A. Rendell, J. C. Burant, S. S. Iyengar, J. Tomasi, M. Cossi, N. Rega, J. M. Millam, M. Klene, J. E. Knox, J. B. Cross, V. Bakken, C. Adamo, J. Jaramillo, R. Gomperts, R. E. Stratmann, O. Yazyev, A. J. Austin, R. Cammi, C. Pomelli, J. W. Ochterski, R. L. Martin, K. Morokuma, V. G. Zakrzewski, G. A. Voth, P. Salvador, S. Dannenberg, J. J. Dapprich, A. D. Daniels, O. Farkas, J. B. Foresman, J. V. Ortiz, J. Cioslowski and D. J. Fox, 2009.

486   S. Grimme, S. Ehrlich and L. Goerigk, *J. Comput. Chem.*, 2011, **32**, 1456–1465.

487   C. Peng, P. Y. Ayala, H. B. Schlegel and M. J. Frisch, *J. Comput. Chem.*, 1996, **17**, 49–56.

488   E. Cancès, B. Mennucci and J. Tomasi, *J. Chem. Phys.*, 1998, **107**, 3032.

489   H. B. Schlegel, *J. Comput. Chem.*, 1982, **3**, 214–218.

490   G. Scalmani and M. J. Frisch, *J. Chem. Phys.*, 2010, **132**, 114110.

491   M. Cossi, N. Rega, G. Scalmani and V. Barone, *J. Comput. Chem.*, 2003, **24**, 669–681.

492   C. Hansch, A. Leo and R. W. Taft, *Chem. Rev.*, 1991, **91**, 165–195.

493   K. O. Christe, D. A. Dixon, D. McLemore, W. W. Wilson, J. A. Sheehy and J. A. Boatz, *J. Fluor. Chem.*, 2000, **101**, 151–153.

494   L. O. Müller, D. Himmel, J. Stauffer, G. Steinfeld, J. Slattery, G. Santiso-Quiñones, V. Brecht and I. Krossing, *Angew. Chemie Int. Ed.*, 2008, **47**, 7659–7663.

495   I. Krossing and I. Raabe, *Chem. - A Eur. J.*, 2004, **10**, 5017–5030.

496   E. W. Colvin, *Silicon in Organic Synthesis*, Elsevier Science, London, 1981.

497   Y. Okamoto and H. C. Brown, *J. Am. Chem. Soc.*, 1957, **79**, 1909–1912.

498   H. C. Brown and Y. Okamoto, *J. Am. Chem. Soc.*, 1958, **80**, 4979–4987.

499   D. D. Perrin and W. L. F. Armarego, *Purification of laboratory materials*, Pergamon, Oxford, 3rd edn., 1988.

500   B. Wrackmeyer and H. Noth, Springer Verlag, Berlin, 1978, pp. 6–7.

501   A. J. Blake, A. Cunningham, A. Ford, S. J. Teat and S. Woodward, *Chem. - A Eur. J.*, 2000, **6**, 3586–3594.

502   D. A. Petrone, M. Isomura, I. Franzoni, S. L. Rössler and E. M. Carreira, *J. Am. Chem. Soc.*, 2018, **140**, 4697–4704.

503   L. Burroughs, L. Eccleshare, J. Ritchie, O. Kulkarni, B. Lygo, S. Woodward and W. Lewis, *Angew. Chemie Int. Ed.*, 2015, **54**, 10648–10651.

504   Q. Deng, R. Shen, R. Ding and L. Zhang, *Adv. Synth. Catal.*, 2014, **356**, 2931–2936.

505   A. C. Götzinger, F. A. Theßeling, C. Hoppe and T. J. J. Müller, *J. Org. Chem.*, 2016, **81**, 10328–10338.

506   V. Yaziji, D. Rodríguez, H. Gutiérrez-de-Terán, A. Coelho, O. Caamaño, X. García-Mera, J. Brea, M. I. Loza, M. I. Cadavid and E. Sotelo, *J. Med. Chem.*, 2010, **54**, 457–471.

507   E. E. Wyatt, W. R. J. D. Galloway, G. L. Thomas, M. Welch, O. Loiseleur, A. T. Plowright and D. R. Spring, *Chem. Commun.*, 2008, 4962–4964.

508   L. Yin, J. Liebscher and F. Erdmann, *J. Heterocycl. Chem.*, 2005, **42**, 1369–1379.

509   R. B. Bedford, S. J. Durrant and M. Montgomery, *Angew. Chemie - Int. Ed.*, 2015, **54**, 8787–8790.

Appendix 1. ^{1}H and ^{19}F NMR data for the reaction of 166 with (4-chlorophenyl)guanidine

Preparation of a 2:1 mixture of aminopyrimidine-6-yl trifluoroborate salts from **166**

Crude mixture, ~2:1
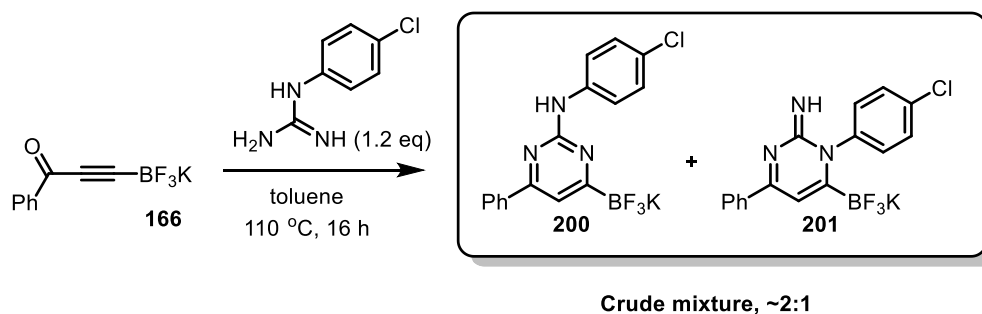
Following general procedure E (*cf* section **4.2.1**), using **166** (0.17 g, 0.74 mmol) and (4-chlorophenyl)guanidine (0.15 g, 0.88 mmol) a 2:1 mixture of products was obtained as a yellow solid. This mixture was tentatively assigned as **200:201** based on ^{1}H (*cf* spectrum 1) and ^{19}F (*cf* spectrum 2) NMR spectroscopy, LCMS (ESI) data showing two major peaks in negative mode of equal mass: [M-K]$^-$ found: 348.1 *m/z*.
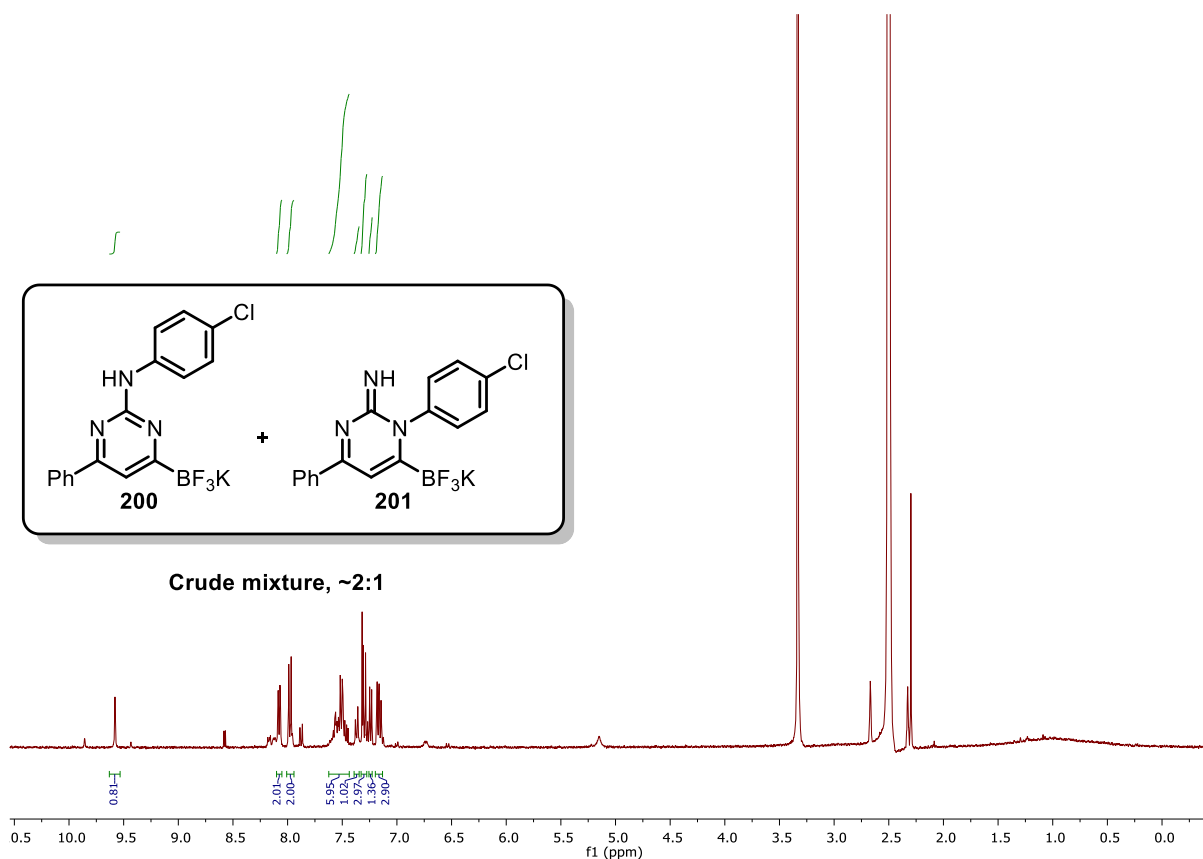
*Spectrum 1: ^{1}H NMR spectrum (400 MHz, DMSO-d^6) of the material obtained following the condensation of (4-chlorophenyl)guanidine with **166***
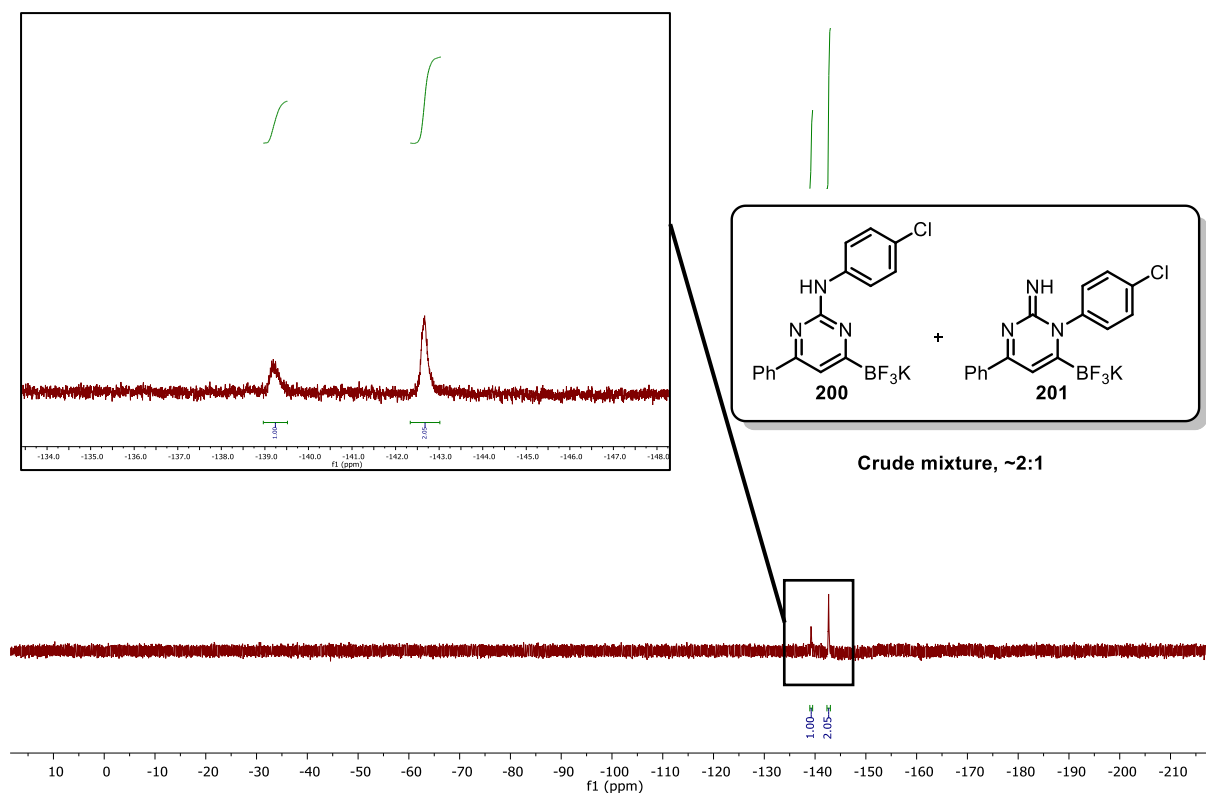
Spectrum 2: ^{19}F NMR spectrum (376 MHz, DMSO-d^6) of the material obtained following the condensation of (4-chlorophenyl)guanidine with 166

The pure aminopyrimidine-6-yl trifluoroborate **200** was obtained after precipitation from Acetone/Et$_2$O (0.18 g, 62%), as a yellow solid. See section **4.2.1** for details.
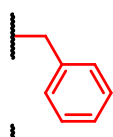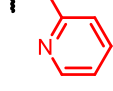
Appendix 2. supplementary NMR data relating to the assignment of substituted aminopyrimidin-6-yl trifluoroborate salts

Selectivity between exo- and endo-*N* substitution
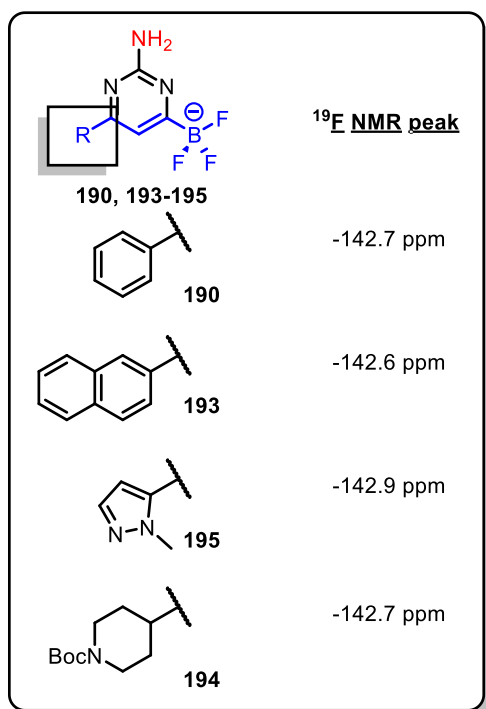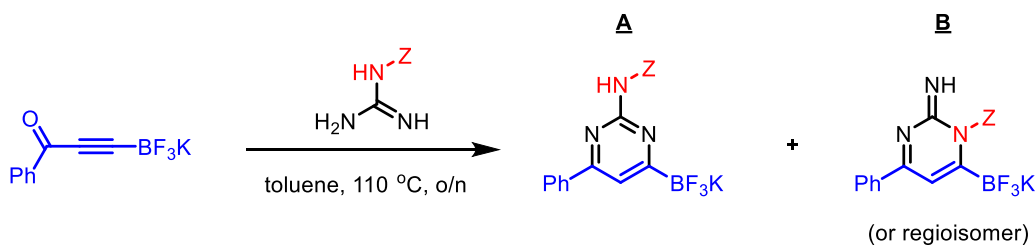
Z =	A:B ratio	2 peaks in ^{19}F NMR
—Me	3:1 (26% isol R$_x$)	-141.3 and **-142.5** ppm
(4-Cl-phenyl)	2:1 (62% isol R$_x$)	-139.3 and **-142.7** ppm
(benzyl)	6:1 (40% isol R$_x$)	-140.5 and **-142.6** ppm
(pyridylmethyl)	3:1	-141.4 and **-142.6** ppm

For substituted guanidines that provide the corresponding substituted pyrimidine products, two peaks are observed in the crude ^{19}F NMR spectrum. The major peak falls between **-142.5 and -142.7 ppm**, suggesting that the identity of the major product is an aminopyrimidine-type product **A**, based on the window described in the previous figure. The minor peak is shifted noticeably downfield, and is expected to describe the azopyrimidinone-type product **B**.
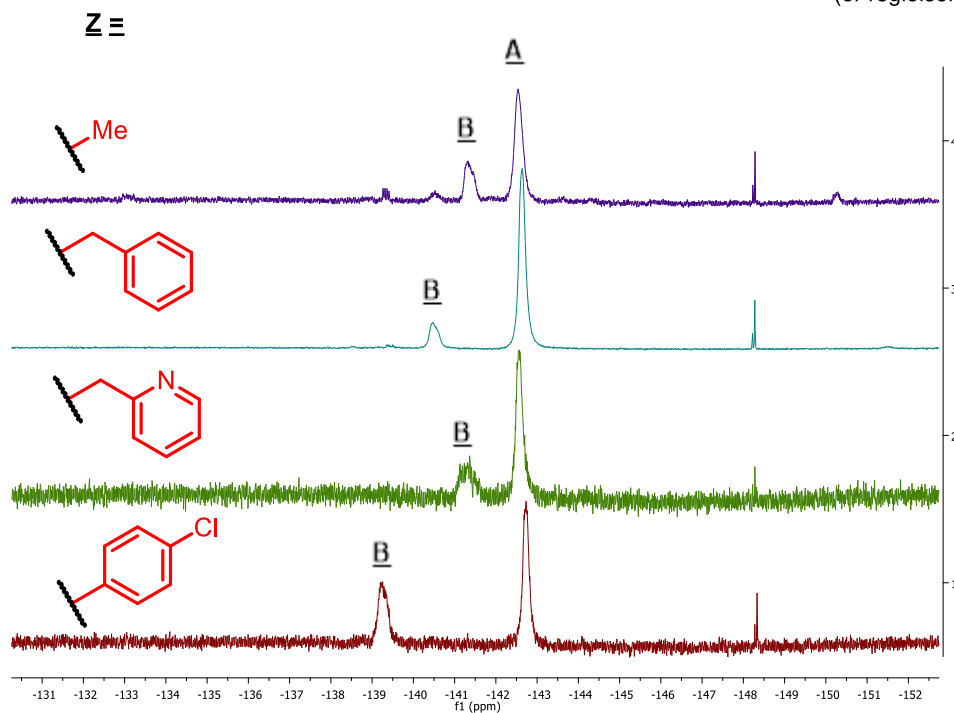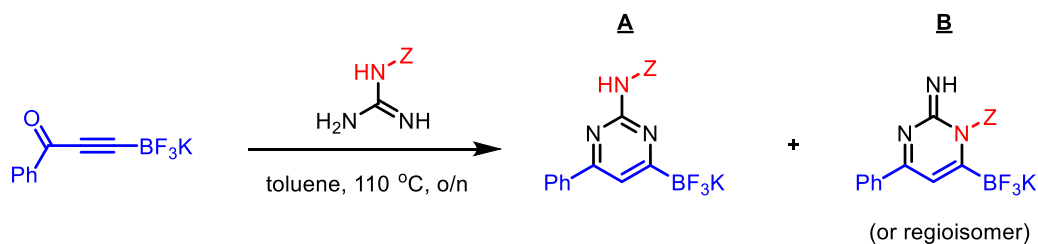
*Spectrum 3: Superimposed ^{19}F NMR spectra showing the similarity of chemical shift for aminopyrimidine-type products **A**.*

227

Selectivity between the two ring *N* atoms for methyl substitution

Comparison of crude NMR spectra for the two reactions of Route A and Route B shows that the minor isomer that was formed via Route A was the same product formed by the methylation of 190 (Route B), confirmed to be **228** by single crystal X-ray crystallographic analysis (see appendix 6).
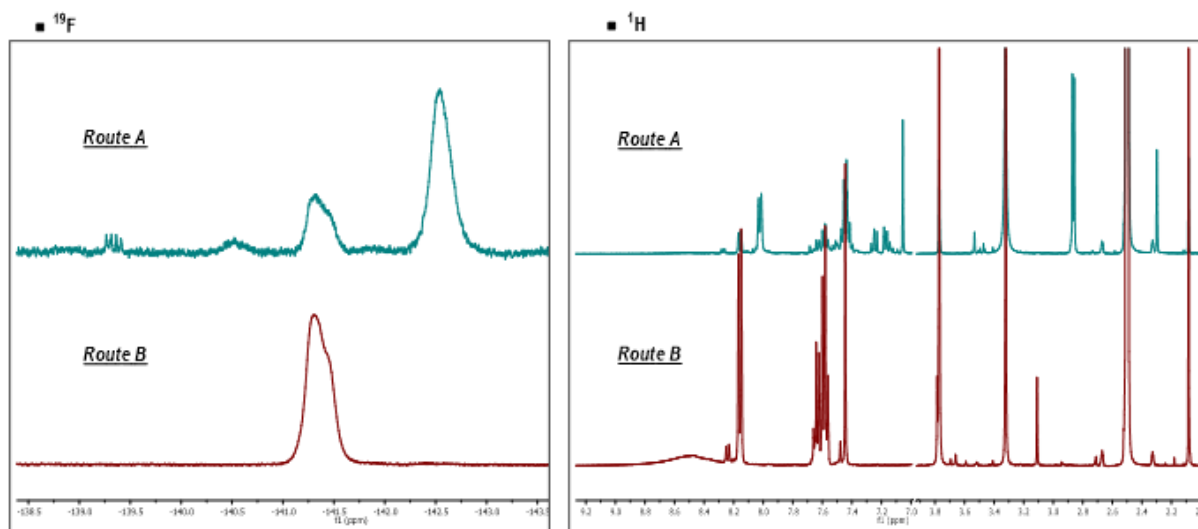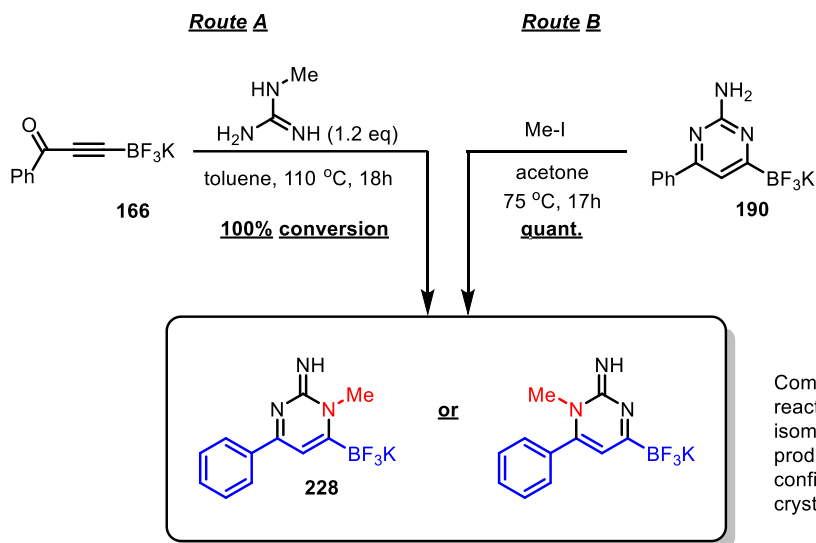
Spectrum 4: Superimposed ^{19}F (left) and ^{1}H (right) NMR spectra showing that the same product was formed by both routes A and B above.

Appendix 3. Data for substituted pyrazolo[1,5,*a*]pyrimidinyl trifluoroborates

Preparation of a 3:1 mixture of pyrazolo[1,5,a]pyrimidin-6-yl trifluoroborates from **166**

91% isolated, 3:1
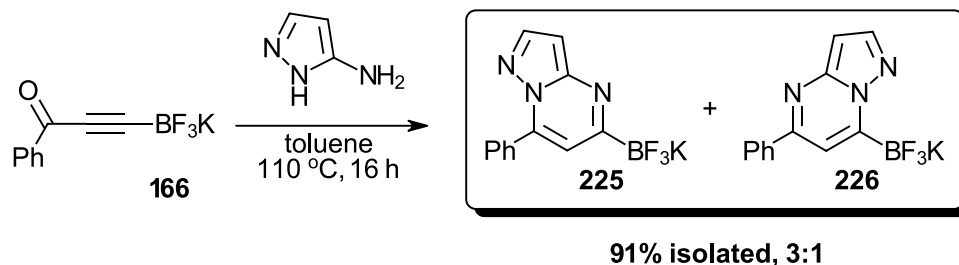
Following general procedure E (*cf* section **4.2.1**), using **166** (0.25 g, 1.06 mmol) and 3-aminopyrazole (0.26 g, 3.18 mmol) a 3:1 mixture of products was obtained as a yellow solid. This mixture was tentatively assigned as **225:226** based on ¹H (*cf* spectrum 5) and ¹⁹F (*cf* spectrum 6) NMR spectroscopy, LCMS (ESI) data showing two peaks in negative mode of equal mass: [M-K]⁻ found: 262.1 *m/z* and the results of the following protodeborylation study (289 mg, 91%). Recrystallisation of this mixture from EtOAc did not afford a single product, but a mixture that was slightly more biased in **225** (5:1).
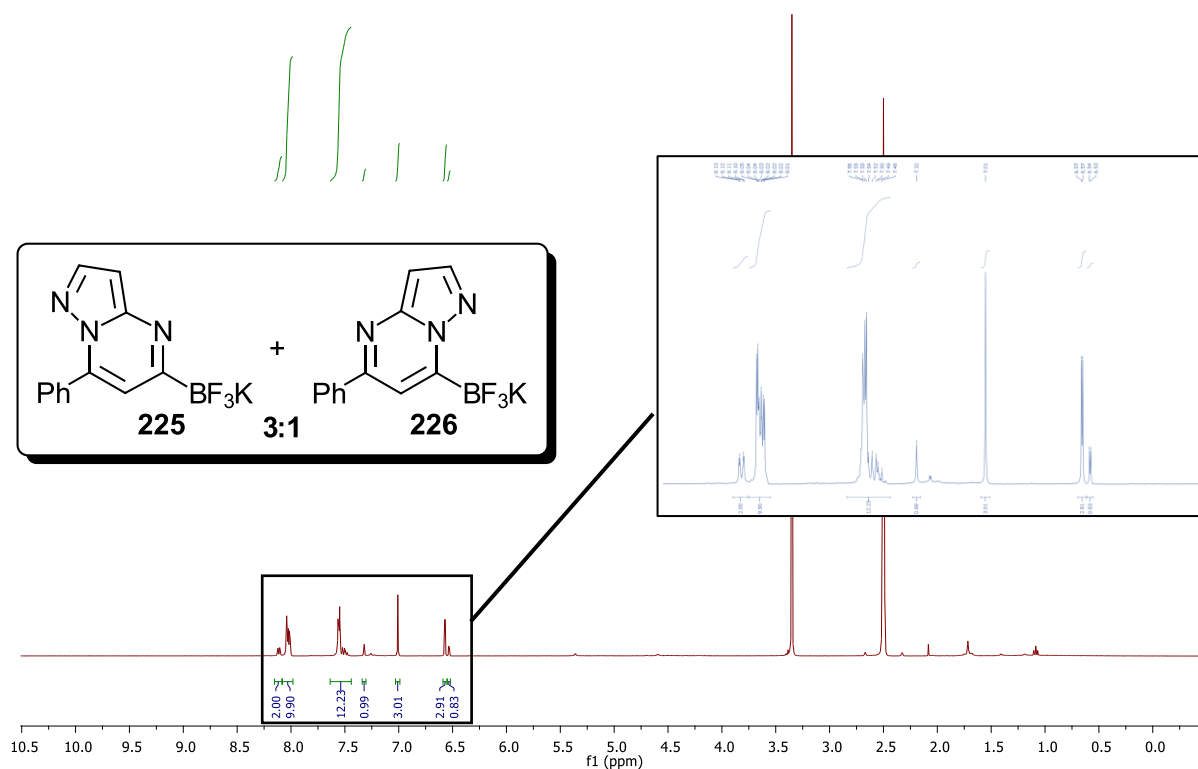
*Spectrum 5: ¹H NMR spectrum (400 MHz, DMSO-d⁶) of the purified material following the condensation of 3-aminopyrazole with **166***
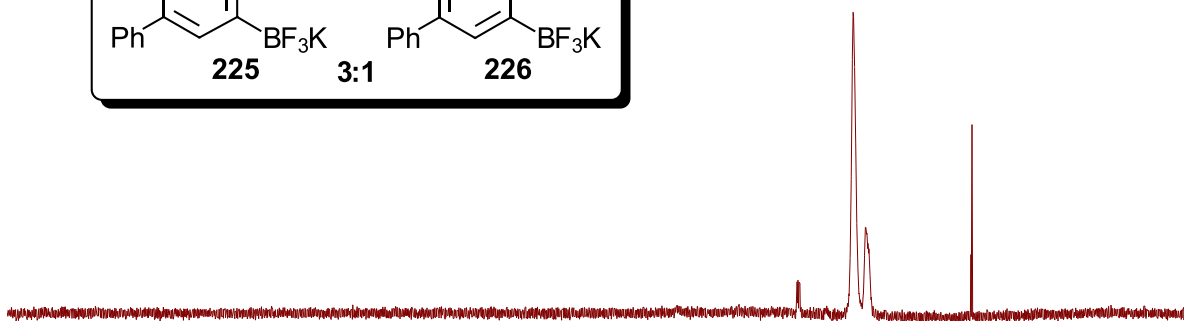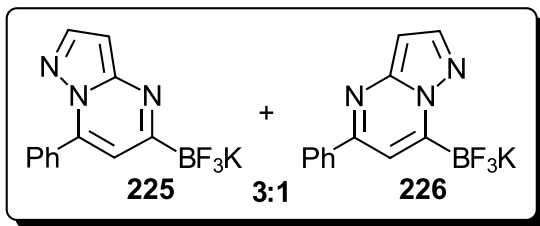
Spectrum 6: ^{19}F NMR spectrum (376 MHz, DMSO-d^6) of the purified material following the condensation of 3-aminopyrazole with 166

Probing the regiochemistry of the product pyrazolo[1,5,a]pyrimidin-6-yl trifluoroborates by derivatisation
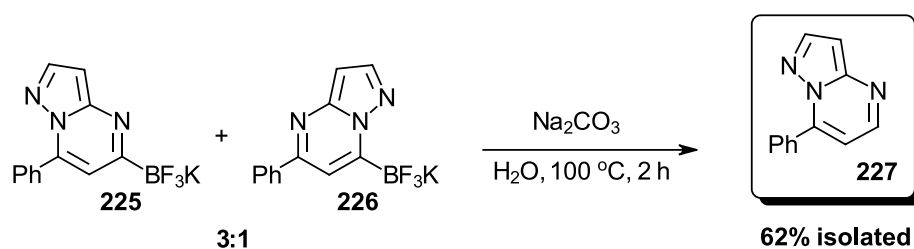
A solution of **225:226 (3:1)** (100 mg, 0.33 mmol) and Na_2CO_3 (70 mg, 0.66 mmol) in H_2O (2 mL) was heated at reflux for 2 hours then cooled to room temperature and extracted with CH_2Cl_2 (3 x 5 mL). The combined organic layers were dried over anhydrous $MgSO_4$ then filtered and concentrated, affording **227** as a yellow solid (40 mg, 62%). **^{1}H NMR (400 MHz, CDCl$_3$)** δ$_H$ ppm 6.78 (d, 1H, J = 2.5 Hz), 6.88 (d, 1H, J = 4.5 Hz), 7.52 – 7.59 (m, 3H), 7.97 – 8.06 (m, 2H), 8.17 (d, 1H, J = 2.5 Hz), 8.52 (d, 1H, J = 4.5 Hz). (The data were consistent with those published).[509]
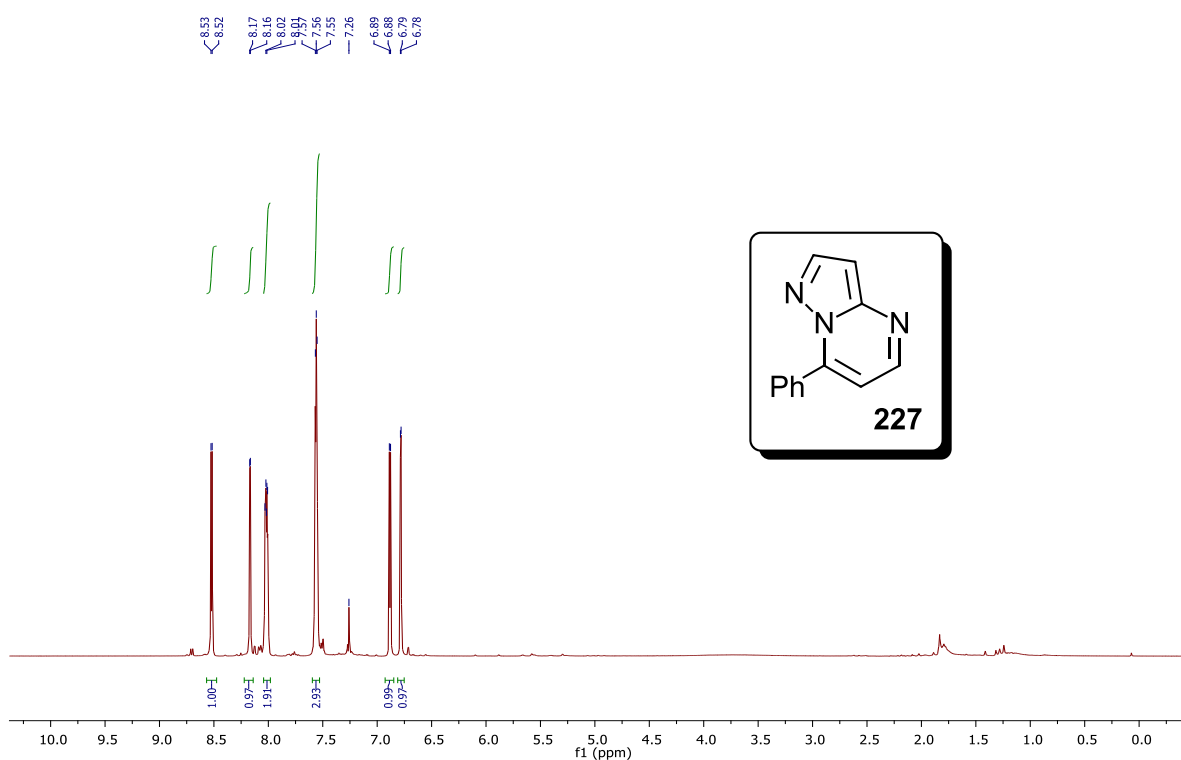
*Spectrum 7: ^{1}H NMR spectrum (400 MHz, DMSO-d^6) of the material obtained after base-promoted protodeborylation of the **225:226** mixture*

Appendix 4. NMR (2D) spectra and regiochemical assignment of 228 and 229

Regiochemistry of 228

MeI

acetone
50 °C, 16 h

100% conversion

or

Single isomer, 93% isolated
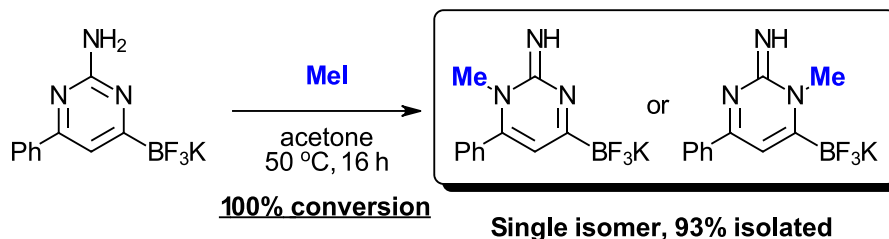
HSQC assignments:
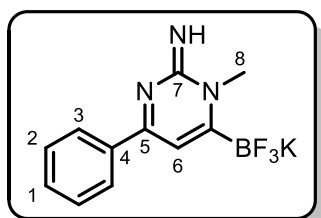
Compound 228

NB: The carbon atom attached to boron is not observed due to quadrupolar relaxation broadening

	^{1}H	^{13}C
1	7.64 ppm	134.6 ppm
2	7.58 ppm	127.8 ppm
3	8.15 ppm	129.2 ppm
4	-	132.5 ppm
5	-	166.3 ppm
6	7.44 ppm	109.4 ppm
7	-	156.5 ppm
8	3.77 ppm	38.6 ppm
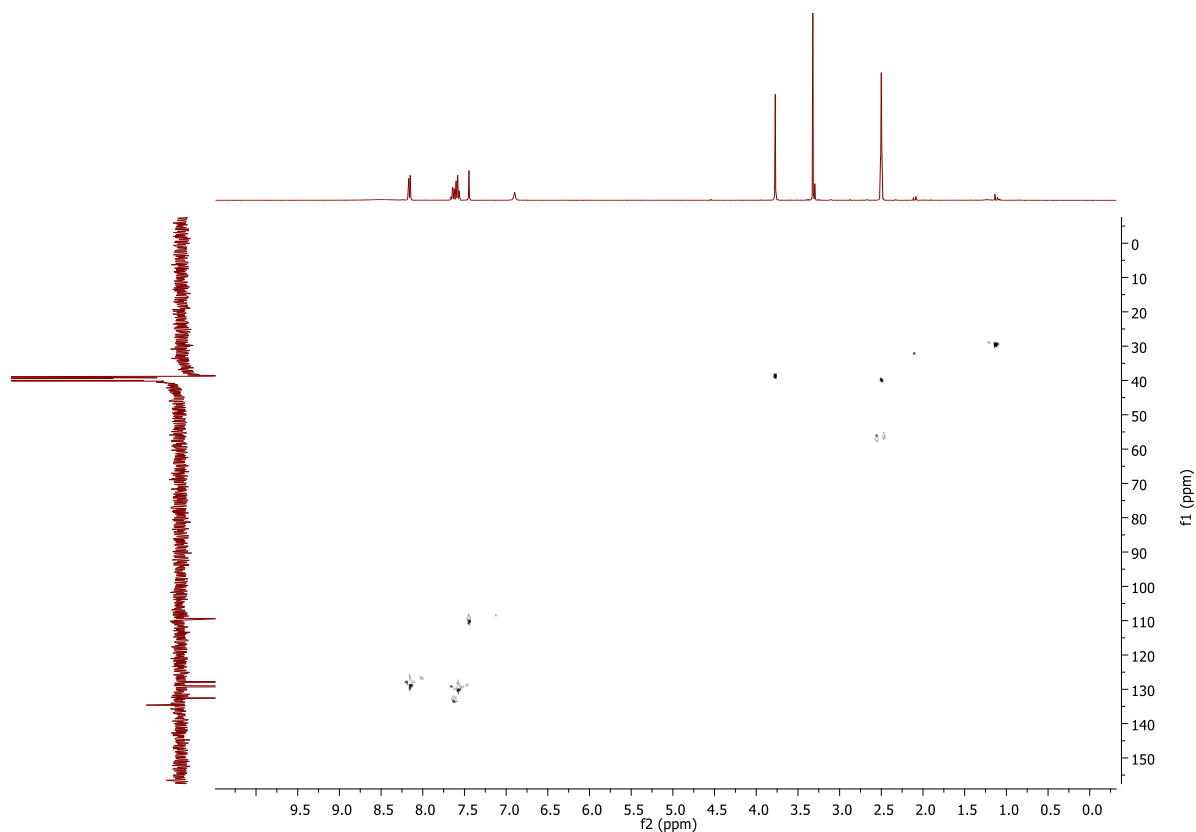
*Spectrum 8: ^{1}H-^{13}C HSQC spectrum of **228***

NOESY assignment:

No evidence of nOe between H3 and methyl group protons (H8)
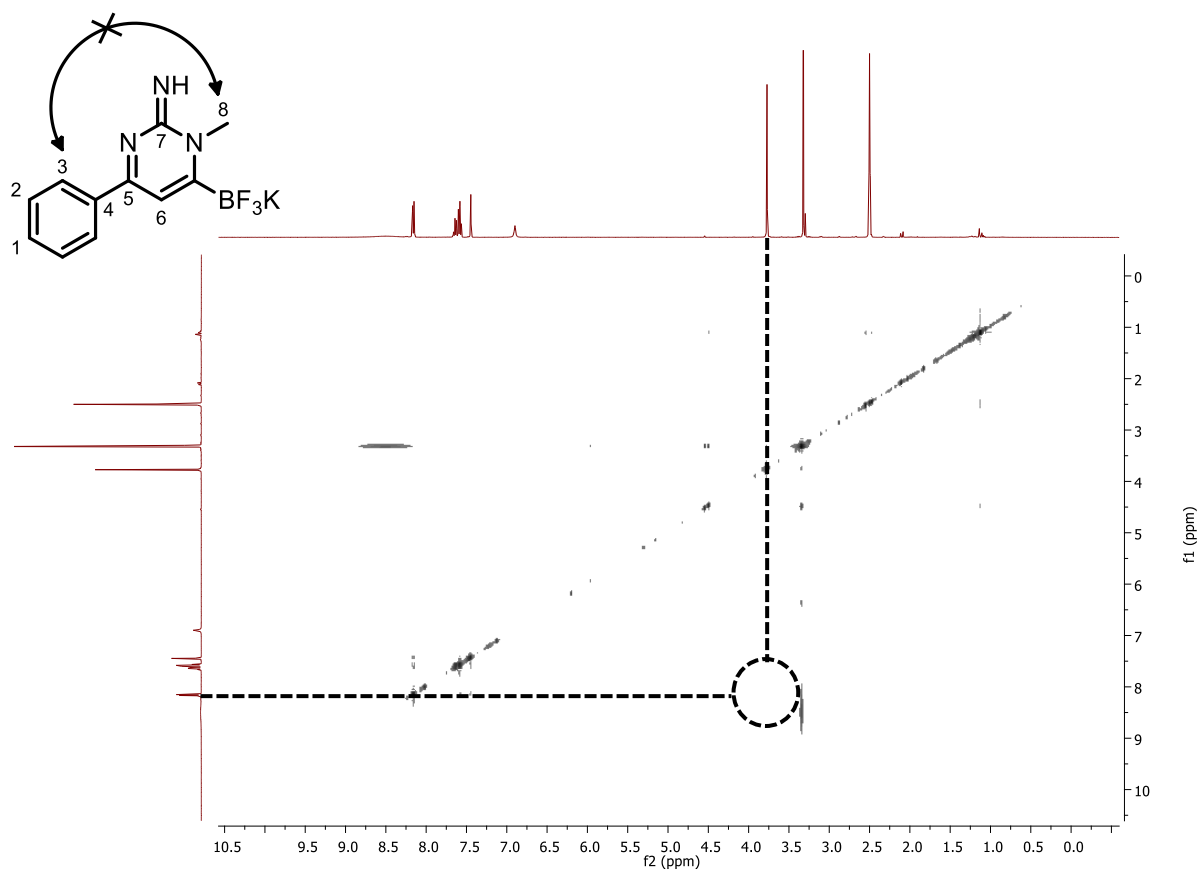
*Spectrum 9: ^1H-^1H NOESY spectrum of **228***

HMBC assignment:

Correlation of both H3 and H6 with C5 observed, no correlation of H8 with C5 observed.
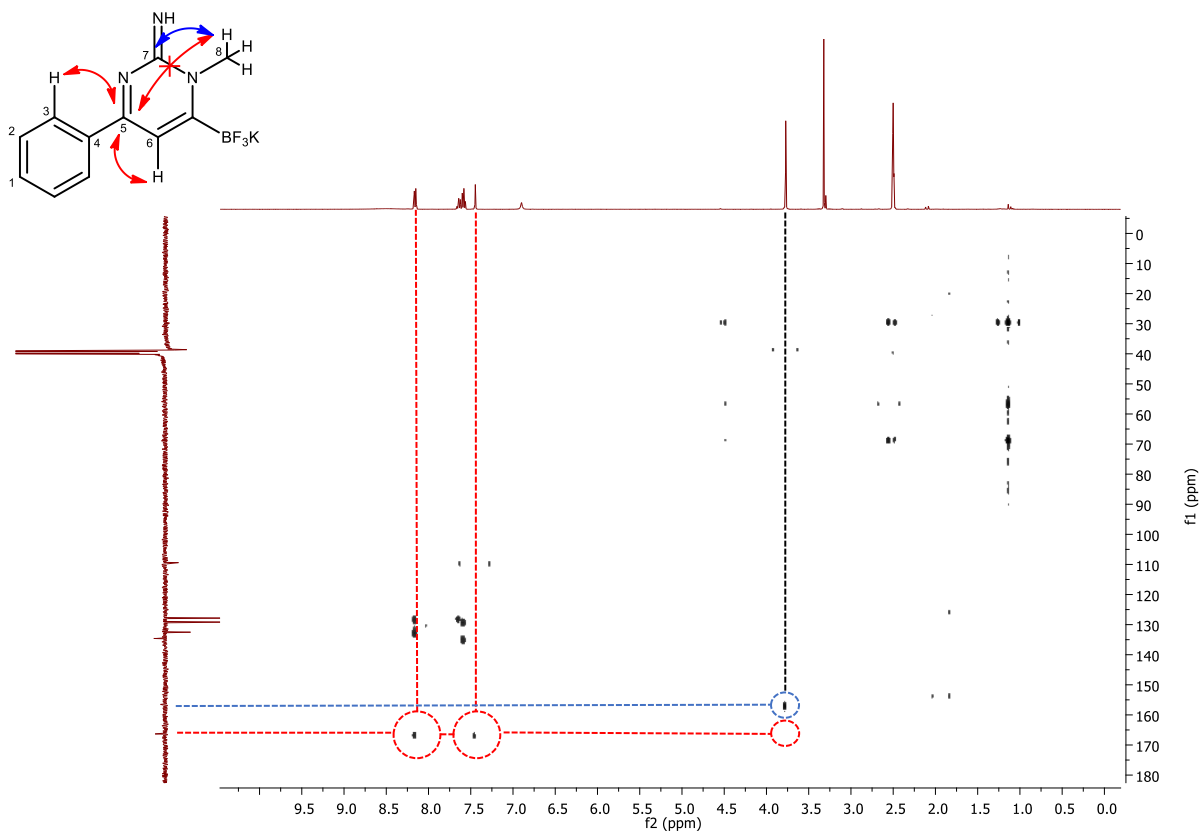
*Spectrum 10: ^1H-^{13}C HMBC spectrum of **228***

Regiochemistry of 229

100% conversion

Single isomer, 50% isolated
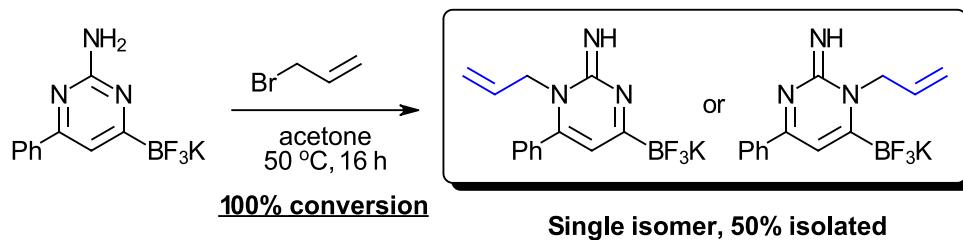
HSQC assignments:
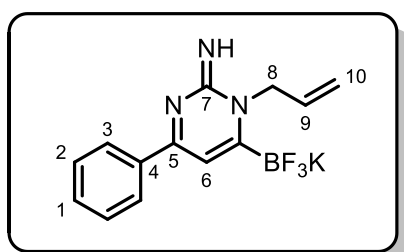
Compound 229

NB: The carbon atom attached to boron is not observed due to quadrupolar relaxation broadening

	^{1}H	^{13}C
1	7.64 ppm	132.8 ppm
2	7.58 ppm	129.3 ppm
3	8.16 ppm	128.0 ppm
4	-	134.5 ppm
5	-	166.8 ppm
6	7.49 ppm	109.9 ppm
7	-	155.7 ppm
8	4.96 ppm	52.1 ppm
9	5.90 ppm	130.4 ppm
10	5.25 ppm	118.5 ppm
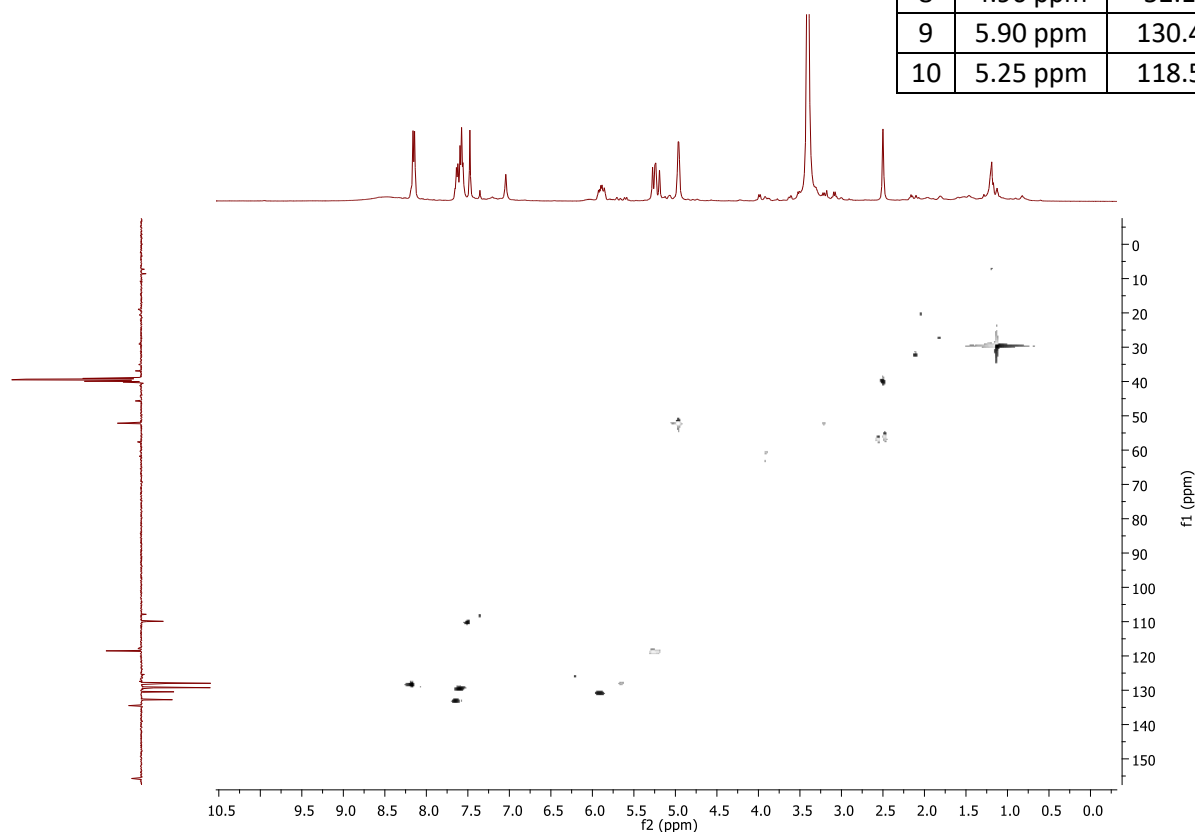
*Spectrum 11: ^{1}H-^{13}C HSQC spectrum of **229***

NOESY assignment:

No evidence of nOe between H3 and allylic methylene (H8)
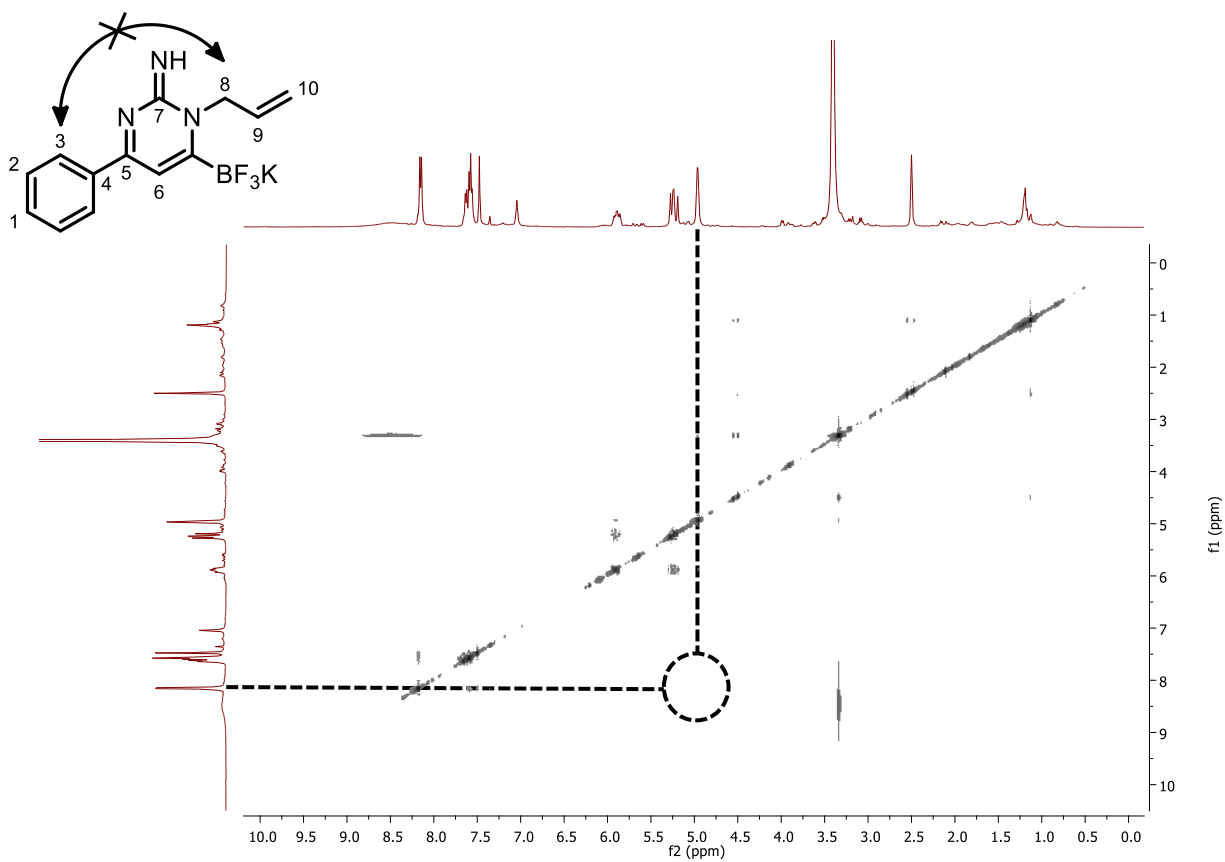
*Spectrum 12: ^{1}H-^{1}H NOESY spectrum of **229***

HMBC assignment:

Correlation of both H3 and H6 with C5 observed, no correlation of H8 with C5 observed.
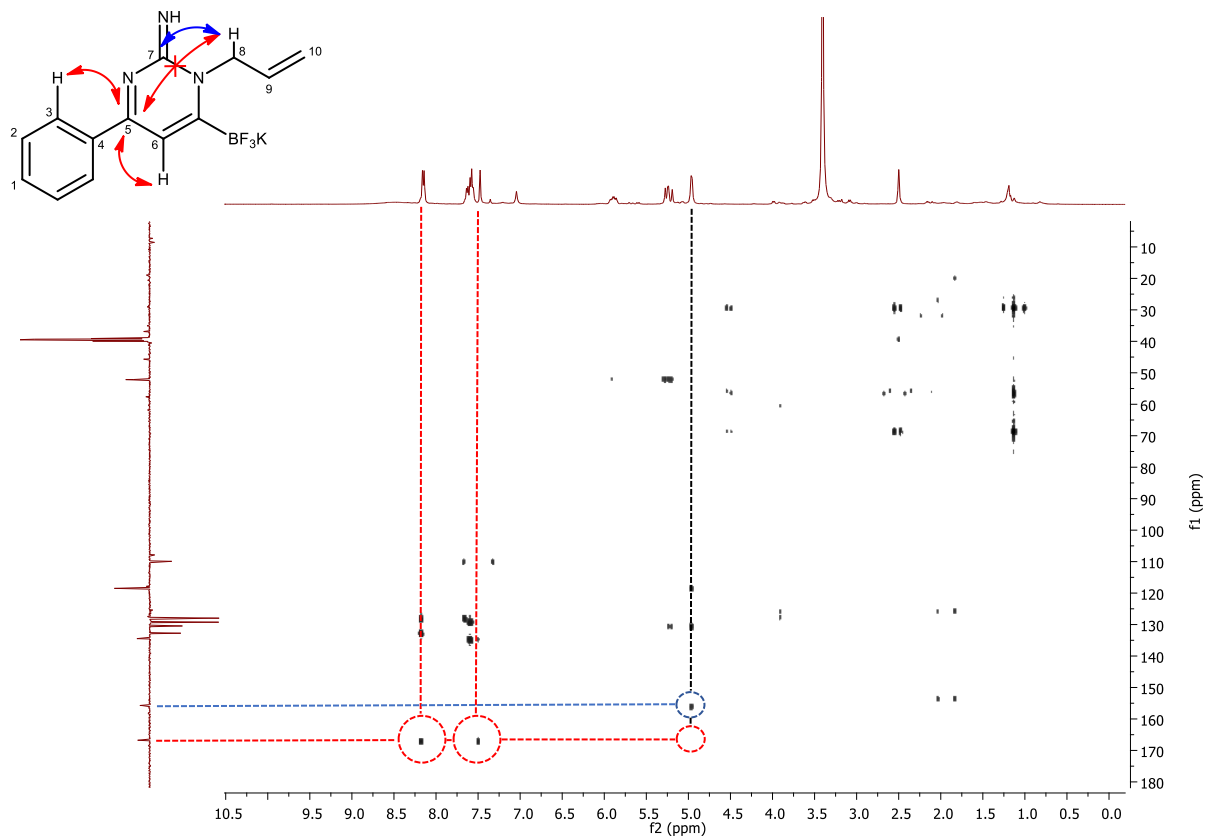
*Spectrum 13: ^1H-^{13}C HMBC spectrum of **229***

Appendix 5. Estimation of relative reaction rate *via* the Eyring equation

Determination of relative rates using the Eyring equation

For the reaction:
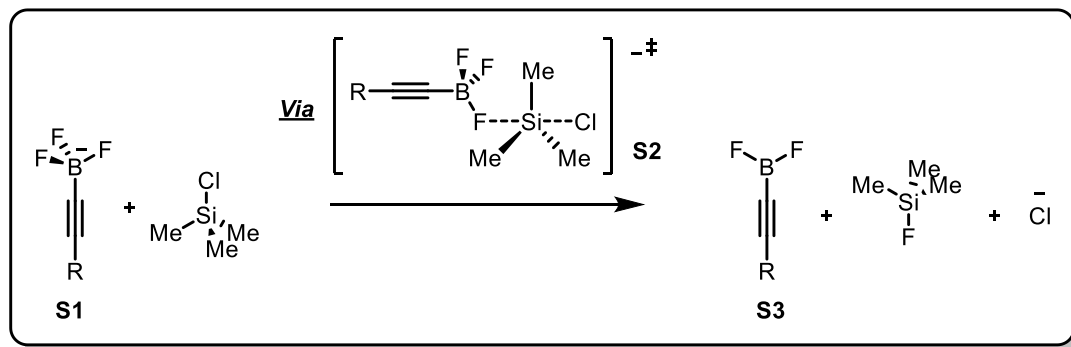
Where R = -**CF$_3$** or -**Ph**

Eyring equation:

$$k = \frac{k_B T}{h} e^{\frac{-\Delta G^{\ddagger}}{RT}}$$

Where: k   = rate constant

k$_B$ = Boltzmann's constant, 1.381 x 10^{-23} J K^{-1}

h   = Planck's constant, 6.626 x 10^{-34} J s

R   = Molar gas constant, 8.314 J mol^{-1} K^{-1}

$\Delta G^{\ddagger}$ = Gibbs energy of activation

$\Delta G^{\ddagger}$ can be obtained by taking the difference in free energy of the starting materials and transition states from their respective optimised structures.

Gibbs energy of activation (ΔG‡) for fluoride transfer using TMS-Cl

$$\Delta G^{\ddagger} = G(S2) - (G(S1) + G(TMSCl))$$

$\Delta G^{\ddagger}_{Ph}$ = 43.7 kJ mol^{-1}

$\Delta G^{\ddagger}_{CF3}$ = 59.5 kJ mol^{-1}

Calculation of relative rates, comparing alkyne side chains: Ph and CF$_3$

- When studying relative changes in rate, constant factors can be cancelled

$$\frac{k(Ph)}{k(CF3)} = \frac{\cancel{\frac{k_B T}{h}} e^{\frac{-\Delta G^{\ddagger}_{Ph}}{RT}}}{\cancel{\frac{k_B T}{h}} e^{\frac{-\Delta G^{\ddagger}_{CF3}}{RT}}}$$

- Calculation of the rate of fluoride abstraction for R = Ph, relative to R = CF$_3$ at room temperature (298 K) therefore becomes:

$$rel\ rate = \frac{k(Ph)}{k(CF3)} = \frac{e^{\frac{-43700}{8.314 \times 298}}}{e^{\frac{-59500}{8.314 \times 298}}}$$

R	ΔG‡ / kJ mol^{-1}	Rel rate (298 K)
-CF$_3$	59.5	1
-Ph	43.7	588

Appendix 6. X-ray crystallographic diffraction data

X-ray crystallographic analysis for compound 173
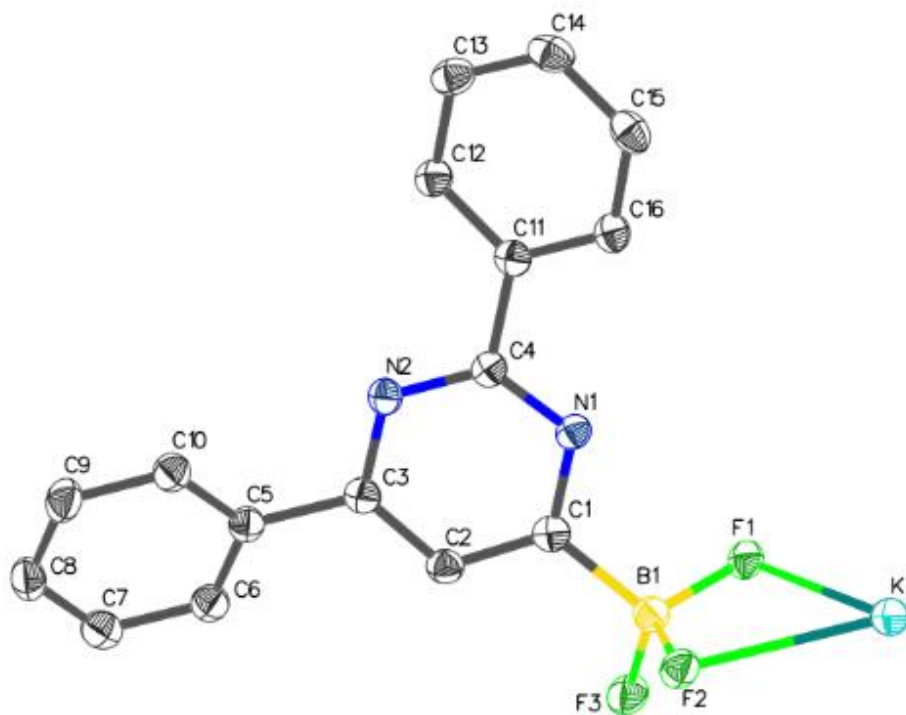
Figure 233: ORTEP of 173, thermal ellipsoids are shown at 50% probability

Crystal structure determination of 173 ($C_{16}H_{11}BF_3KN_2$).

Crystals of **173** were grown from a saturated acetone solution, allowing slow evaporation.

Crystal Data for $C_{16}H_{11}BF_3KN_2$ (*M* = 338.18 g/mol): orthorhombic, space group Pccn (no. 56), *a* = 27.2800(4) Å, *b* = 14.9160(2) Å, *c* = 7.17560(10) Å, *V* = 2919.81(7) Å^3, *Z* = 8, *T* = 100(2) K, μ(CuKα) = 3.487 mm^{-1}, *Dcalc* = 1.539 g/cm^3, 14282 reflections measured (6.48° ≤ 2Θ ≤ 136.502°), 2674 unique (R_{int} = 0.0379, R_{sigma} = 0.0290) which were used in all calculations. The final R_1 was 0.0291 (I > 2σ(I)) and wR_2 was 0.0794 (all data).

Table 1 Crystal data and structure refinement for 173.

Identification code	2018ncs0326s
Empirical formula	$C_{16}H_{11}BF_3KN_2$
Formula weight	338.18
Temperature/K	100(2)
Crystal system	orthorhombic

Space group	Pccn
a/Å	27.2800(4)
b/Å	14.9160(2)
c/Å	7.17560(10)
α/°	90
β/°	90
γ/°	90
Volume/Å^3	2919.81(7)
Z	8
ρ_{calc}g/cm^3	1.539
μ/mm^{-1}	3.487
F(000)	1376.0
Crystal size/mm^3	0.26 × 0.02 × 0.015
Radiation	CuKα (λ = 1.54184)
2Θ range for data collection/°	6.48 to 136.502
Index ranges	-32 ≤ h ≤ 24, -17 ≤ k ≤ 17, -8 ≤ l ≤ 8
Reflections collected	14282
Independent reflections	2674 [R_{int} = 0.0379, R_{sigma} = 0.0290]
Data/restraints/parameters	2674/0/208
Goodness-of-fit on F^2	1.023
Final R indexes [I>=2σ (I)]	R_1 = 0.0291, wR_2 = 0.0765
Final R indexes [all data]	R_1 = 0.0334, wR_2 = 0.0794
Largest diff. peak/hole / e Å^{-3}	0.34/-0.24

Table 2 Fractional Atomic Coordinates (×10^4) and Equivalent Isotropic Displacement Parameters (Å^2×10^3) for 2018ncs0326s. U$_{eq}$ is defined as 1/3 of of the trace of the orthogonalised U$_{IJ}$ tensor.

Atom	x	y	z	U(eq)
K1	8023.6(2)	3569.1(2)	6402.3(4)	20.94(11)
F1	7042.1(3)	3187.4(6)	5245.5(12)	22.6(2)
F2	7133.2(3)	4089.9(6)	7769.1(12)	25.3(2)
F3	6505.6(3)	3092.7(6)	7684.2(14)	30.0(2)
N1	6589.2(4)	4825.3(8)	4010.6(17)	19.1(3)
N2	5920.4(5)	5860.4(8)	4093.3(17)	19.3(3)
C1	6435.5(5)	4455.6(10)	5635(2)	19.6(3)
C2	6008.9(6)	4763.4(10)	6469(2)	20.9(3)
C3	5753.7(5)	5472.9(10)	5664(2)	19.4(3)
C4	6324.8(5)	5510.2(10)	3335(2)	18.3(3)
C5	5299.8(5)	5859.1(10)	6476(2)	20.0(3)
C6	4993.0(6)	5349.8(11)	7614(2)	22.4(3)
C7	4573.4(6)	5724.5(12)	8381(2)	24.9(4)
C8	4457.1(6)	6615.1(12)	8031(2)	27.0(4)
C9	4757.7(6)	7122.1(12)	6891(2)	28.1(4)

241

C10	5173.5(6)	6748.5(11)	6105(2)	23.9(3)
C11	6495.2(6)	5930.7(10)	1567(2)	19.6(3)
C12	6171.1(6)	6428.7(10)	470(2)	21.4(3)
C13	6335.4(6)	6869.2(11)	-1112(2)	25.5(4)
C14	6827.3(7)	6828.8(11)	-1610(2)	27.3(4)
C15	7150.7(6)	6330.8(10)	-538(2)	25.9(4)
C16	6985.3(6)	5869.4(10)	1019(2)	21.3(3)
B1	6776.6(7)	3697.0(12)	6579(2)	21.2(4)

Table 3 Anisotropic Displacement Parameters ($Å^2×10^3$) for 2018ncs0326s. The Anisotropic displacement factor exponent takes the form: $-2\pi^2[h^2a*^2U_{11}+2hka*b*U_{12}+...]$.

Atom	U_{11}	U_{22}	U_{33}	U_{23}	U_{13}	U_{12}
K1	24.30(19)	17.04(19)	21.48(19)	-1.34(12)	-0.45(12)	-1.02(12)
F1	27.3(5)	16.9(4)	23.6(5)	-1.0(3)	-0.8(4)	4.1(3)
F2	28.1(5)	24.3(5)	23.5(5)	-3.1(4)	-5.2(4)	3.9(4)
F3	28.1(5)	25.9(5)	36.0(5)	13.4(4)	4.7(4)	2.2(4)
N1	21.9(6)	15.4(6)	20.0(6)	-0.3(5)	-1.6(5)	0.4(5)
N2	21.3(6)	16.3(6)	20.4(6)	-1.6(5)	0.3(5)	0.8(5)
C1	22.8(7)	15.6(7)	20.3(7)	-1.2(6)	-1.1(6)	-2.5(6)
C2	24.3(8)	19.1(8)	19.4(8)	1.0(6)	1.0(6)	-0.3(6)
C3	22.3(7)	16.4(7)	19.5(7)	-2.1(6)	-0.2(6)	-1.5(6)
C4	20.7(7)	14.7(7)	19.5(7)	-2.1(6)	-1.8(6)	-1.1(6)
C5	19.7(7)	20.9(8)	19.4(7)	-2.3(6)	-2.0(6)	0.4(6)
C6	24.0(8)	21.9(8)	21.4(7)	-1.7(6)	-1.7(6)	0.5(6)
C7	22.4(8)	30.2(9)	22.2(8)	-1.7(7)	-1.0(6)	-3.8(6)
C8	20.2(7)	33.9(9)	26.7(8)	-7.3(7)	-1.2(7)	4.6(7)
C9	29.6(8)	23.4(8)	31.4(8)	-1.4(7)	-1.5(7)	7.8(7)
C10	25.0(8)	21.8(8)	24.9(8)	1.1(6)	1.3(6)	1.3(6)
C11	25.4(8)	13.8(7)	19.4(7)	-2.7(6)	0.6(6)	-0.8(6)
C12	24.6(8)	17.0(7)	22.7(8)	-0.2(6)	-0.3(6)	-0.1(6)
C13	33.6(9)	19.3(8)	23.6(8)	1.6(6)	-2.9(7)	-0.1(6)
C14	39.6(9)	19.5(8)	22.9(8)	1.2(6)	6.1(7)	-4.4(7)
C15	27.7(8)	22.0(8)	27.9(9)	-4.2(6)	6.9(7)	-2.7(6)
C16	23.6(8)	16.9(8)	23.5(8)	-2.7(6)	0.5(6)	0.4(6)
B1	23.6(9)	19.1(9)	20.8(9)	1.2(7)	1.5(7)	0.6(7)

Table 4 Bond Lengths for 2018ncs0326s.

Atom	Atom	Length/Å	Atom	Atom	Length/Å
K1	F1[1]	2.8216(9)	N2	C3	1.3455(19)
K1	F1	2.8603(9)	N2	C4	1.3364(19)
K1	F1[2]	2.7542(9)	C1	C2	1.387(2)

Atom	Atom	Length		Atom	Atom	Length
K1	F2	2.7323(9)		C1	B1	1.614(2)
K1	F2³	2.7537(9)		C2	C3	1.392(2)
K1	F3³	3.0451(11)		C3	C5	1.485(2)
K1	F3²	2.9394(10)		C4	C11	1.490(2)
K1	N1¹	2.8512(13)		C5	C6	1.395(2)
K1	C16¹	3.4422(16)		C5	C10	1.396(2)
K1	B1	3.4094(18)		C6	C7	1.388(2)
K1	B1²	3.4261(18)		C7	C8	1.389(2)
K1	B1³	3.5088(17)		C8	C9	1.383(2)
F1	K1³	2.8216(9)		C9	C10	1.384(2)
F1	K1²	2.7542(9)		C11	C12	1.398(2)
F1	B1	1.4206(19)		C11	C16	1.397(2)
F2	K1¹	2.7537(9)		C12	C13	1.386(2)
F2	B1	1.421(2)		C13	C14	1.390(2)
F3	K1¹	3.0451(11)		C14	C15	1.386(2)
F3	K1²	2.9394(10)		C15	C16	1.388(2)
F3	B1	1.4101(19)		C16	K1³	3.4422(16)
N1	K1³	2.8512(13)		B1	K1²	3.4261(18)
N1	C1	1.3556(19)		B1	K1¹	3.5088(17)
N1	C4	1.3413(19)				

¹3/2-X,+Y,1/2+Z; ²3/2-X,1/2-Y,+Z; ³3/2-X,+Y,-1/2+Z

Table 5 Bond Angles for 2018ncs0326s.

Atom	Atom	Atom	Angle/°	Atom	Atom	Atom	Angle/°
F1¹	K1	F1²	95.65(2)	K1¹	F1	K1³	118.84(3)

F1[1]	K1	F1	70.26(3)	K1[1]	F1	K1	99.37(3)
F1[2]	K1	F1	100.60(2)	K1[3]	F1	K1	107.64(3)
F1[1]	K1	F3[1]	47.20(2)	B1	F1	K1	100.09(8)
F1[2]	K1	F3[3]	146.72(3)	B1	F1	K1[1]	105.83(8)
F1[2]	K1	F3[1]	63.37(3)	B1	F1	K1[3]	121.20(8)
F1	K1	F3[3]	95.40(3)	K1	F2	K1[2]	113.44(3)
F1[1]	K1	F3[3]	62.71(3)	B1	F2	K1[2]	110.26(8)
F1	K1	F3[1]	109.39(3)	B1	F2	K1	106.00(8)
F1[1]	K1	N1[2]	147.90(3)	K1[1]	F3	K1[2]	106.66(3)
F1[2]	K1	N1[2]	60.96(3)	B1	F3	K1[2]	97.03(9)
F1[1]	K1	C16[2]	157.47(3)	B1	F3	K1[1]	97.70(8)
F1[2]	K1	C16[2]	106.19(3)	C1	N1	K1[3]	114.30(9)
F1	K1	C16[2]	99.71(3)	C4	N1	K1[3]	117.55(9)
F1[1]	K1	B1	89.97(4)	C4	N1	C1	117.01(12)
F1[1]	K1	B1[1]	23.51(3)	C4	N2	C3	116.87(13)
F1[2]	K1	B1[3]	170.03(4)	N1	C1	C2	119.74(13)
F1	K1	B1	24.22(3)	N1	C1	B1	117.89(13)
F1[1]	K1	B1[3]	76.38(3)	C2	C1	B1	122.30(13)
F1[2]	K1	B1[1]	76.99(3)	C1	C2	C3	119.45(14)
F1[2]	K1	B1	84.93(3)	N2	C3	C2	120.35(13)
F1	K1	B1[3]	82.53(3)	N2	C3	C5	116.35(13)
F1	K1	B1[1]	87.90(4)	C2	C3	C5	123.28(14)
F2	K1	F1[1]	108.71(3)	N1	C4	C11	117.43(13)
F2	K1	F1[2]	69.51(3)	N2	C4	N1	126.48(14)
F2[3]	K1	F1[1]	88.45(3)	N2	C4	C11	116.09(13)

F2³	K1	F1²	166.50(3)	C6	C5	C3	121.27(14)
F2³	K1	F1	68.66(3)	C6	C5	C10	118.76(14)
F2	K1	F1	47.83(3)	C10	C5	C3	119.97(14)
F2	K1	F2³	96.98(2)	C7	C6	C5	120.52(15)
F2³	K1	F3³	45.72(3)	C6	C7	C8	120.14(15)
F2	K1	F3³	139.10(3)	C9	C8	C7	119.64(15)
F2³	K1	F3¹	127.02(3)	C8	C9	C10	120.44(15)
F2	K1	F3¹	121.06(3)	C9	C10	C5	120.48(15)
F2	K1	N1²	84.66(3)	C12	C11	C4	120.39(14)
F2³	K1	N1²	119.58(3)	C16	C11	C4	120.74(14)
F2³	K1	C16²	69.02(3)	C16	C11	C12	118.80(14)
F2	K1	C16²	74.87(3)	C13	C12	C11	120.57(15)
F2	K1	B1¹	114.12(4)	C12	C13	C14	120.15(15)
F2	K1	B1³	118.47(4)	C15	C14	C13	119.68(15)
F2³	K1	B1¹	109.76(4)	C14	C15	C16	120.35(15)
F2	K1	B1	23.62(3)	C11	C16	K1³	92.06(9)
F2³	K1	B1³	22.33(3)	C15	C16	K1³	124.13(10)
F2³	K1	B1	82.21(3)	C15	C16	C11	120.38(15)
F3¹	K1	F3³	83.86(2)	K1	B1	K1²	83.03(4)
F3³	K1	C16²	99.53(3)	K1¹	B1	K1²	87.60(4)
F3¹	K1	C16²	150.30(3)	K1	B1	K1¹	77.57(4)
F3³	K1	B1	117.81(4)	F1	B1	K1	55.69(7)
F3¹	K1	B1³	106.66(4)	F1	B1	K1¹	50.66(7)
F3¹	K1	B1	118.13(4)	F1	B1	K1²	123.79(10)
F3¹	K1	B1¹	24.07(3)	F1	B1	F2	106.05(13)

F3³	K1	B1³	23.50(3)	F1	B1	C1	112.72(12)
F3³	K1	B1¹	74.64(3)	F2	B1	K1	50.39(7)
N1²	K1	F1	131.92(3)	F2	B1	K1¹	108.68(9)
N1²	K1	F3³	124.90(3)	F2	B1	K1²	47.41(7)
N1²	K1	F3¹	100.77(3)	F2	B1	C1	110.97(13)
N1²	K1	C16²	53.13(4)	F3	B1	K1¹	58.23(7)
N1²	K1	B1	107.96(4)	F3	B1	K1	120.55(10)
N1²	K1	B1³	123.66(4)	F3	B1	K1²	59.47(7)
N1²	K1	B1¹	124.41(4)	F3	B1	F1	107.71(13)
C16²	K1	B1³	82.42(4)	F3	B1	F2	106.54(12)
B1¹	K1	C16²	170.92(4)	F3	B1	C1	112.46(13)
B1	K1	C16²	86.57(4)	C1	B1	K1²	122.81(10)
B1	K1	B1¹	102.27(4)	C1	B1	K1¹	140.15(10)
B1¹	K1	B1³	93.75(4)	C1	B1	K1	126.78(10)
B1	K1	B1³	100.87(4)				

¹3/2-X,1/2-Y,+Z; ²3/2-X,+Y,1/2+Z; ³3/2-X,+Y,-1/2+Z

Table 6 Hydrogen Atom Coordinates (Å×10⁴) and Isotropic Displacement Parameters (Å²×10³) for 2.

Atom	x	y	z	U(eq)
H2	5892	4492	7582	25
H6	5072	4741	7867	27
H7	4365	5371	9146	30
H8	4173	6875	8571	32
H9	4678	7731	6646	34
H10	5374	7100	5308	29
H12	5835	6466	812	26
H13	6111	7199	-1857	31
H14	6941	7141	-2679	33
H15	7487	6305	-871	31
H16	7207	5510	1716	26

X-ray crystallographic analysis for compound 220
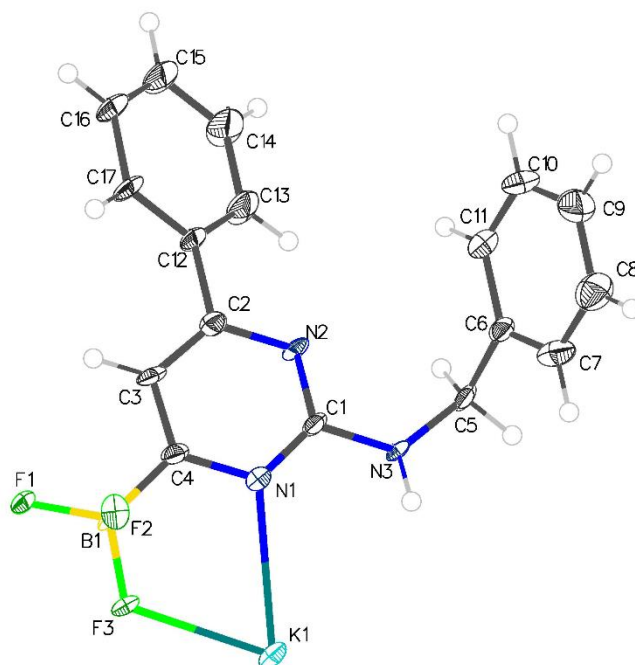
*Figure 234: ORTEP of **220**, thermal ellipsoids are shown at 50% probability*

Crystal structure determination of 220

Crystals of **220** were grown from a saturated acetone solution, allowing slow evaporation.

Crystal Data for $C_{17}H_{14}BF_3KN_3$ (M =367.22 g/mol): monoclinic, space group P2$_1$/c (no. 14), a = 18.251(5) Å, b = 10.005(3) Å, c = 9.1105(18) Å, β = 94.150(16)°, V = 1659.2(7) Å^3, Z = 4, T = 100 K, μ(MoKα) = 0.355 mm^{-1}, $Dcalc$ = 1.470 g/cm^3, 4270 reflections measured (4.476° ≤ 2Θ ≤ 46.598°), 2330 unique (R_{int} = 0.0897, R$_{sigma}$ = 0.1525) which were used in all calculations. The final R_1 was 0.0678 (I > 2σ(I)) and wR_2 was 0.1452 (all data).

Table 1 Crystal data and structure refinement for 220.

Identification code	ojH388k
Empirical formula	$C_{17}H_{14}BF_3KN_3$
Formula weight	367.22
Temperature/K	100
Crystal system	monoclinic
Space group	P2$_1$/c
a/Å	18.251(5)
b/Å	10.005(3)

c/Å	9.1105(18)
α/°	90
β/°	94.150(16)
γ/°	90
Volume/Å^3	1659.2(7)
Z	4
ρ_{calc}g/cm^3	1.470
μ/mm^{-1}	0.355
F(000)	752.0
Crystal size/mm^3	0.61 × 0.21 × 0.025
Radiation	MoKα (λ = 0.71073)
2Θ range for data collection/°	4.476 to 46.598
Index ranges	-14 ≤ h ≤ 20, -9 ≤ k ≤ 11, -10 ≤ l ≤ 10
Reflections collected	4270
Independent reflections	2330 [R_{int} = 0.0897, R_{sigma} = 0.1525]
Data/restraints/parameters	2330/199/226
Goodness-of-fit on F^2	1.021
Final R indexes [I>=2σ (I)]	R_1 = 0.0678, wR_2 = 0.1209
Final R indexes [all data]	R_1 = 0.1523, wR_2 = 0.1452
Largest diff. peak/hole / e Å^{-3}	0.44/-0.44

Table 2 Fractional Atomic Coordinates (×10^4) and Equivalent Isotropic Displacement Parameters (Å^2×10^3) for ojH388k. U$_{eq}$ is defined as 1/3 of of the trace of the orthogonalised U$_{IJ}$ tensor.

Atom	x	y	z	U(eq)
K1	4804.9(7)	2868.2(15)	5155.8(15)	20.5(4)
F1	5722.0(16)	4324(4)	727(3)	23.6(10)
N1	6075(3)	4493(5)	4782(5)	17.9(13)
C1	6653(3)	4283(6)	5805(6)	16.6(15)
B1	5562(4)	4735(8)	2153(8)	16.5(16)
F2	5350.8(17)	6104(4)	2087(4)	24.4(9)
N2	7360(3)	4100(6)	5533(5)	21.3(14)
C2	7517(3)	4156(7)	4114(7)	20.5(16)
F3	4923.1(17)	3994(4)	2490(3)	21.8(9)
N3	6485(2)	4228(5)	7237(5)	20.0(14)
C3	6962(3)	4334(6)	3002(7)	17.6(15)
C4	6240(3)	4500(6)	3351(6)	16.8(14)
C5	7052(3)	4058(7)	8443(6)	21.8(16)
C6	7437(3)	5366(7)	8943(6)	20.4(15)

Table 2 Fractional Atomic Coordinates (×10^4) and Equivalent Isotropic Displacement Parameters (Å^2×10^3) for ojH388k. U$_{eq}$ is defined as 1/3 of of the trace of the orthogonalised U$_{IJ}$ tensor.

Atom	x	y	z	U(eq)
C7	7084(4)	6267(7)	9760(7)	28.0(17)
C8	7439(4)	7439(8)	10294(8)	37.0(19)
C9	8161(4)	7658(9)	9991(8)	51(2)
C10	8512(4)	6751(10)	9158(8)	52(2)
C11	8157(4)	5597(9)	8628(7)	42(2)
C12	8301(3)	3998(8)	3825(7)	28.5(18)
C13	8770(3)	3262(8)	4785(7)	37(2)
C14	9508(4)	3134(10)	4535(8)	58(3)
C15	9791(4)	3781(10)	3362(8)	55(3)
C16	9328(3)	4536(9)	2420(8)	45(2)
C17	8585(3)	4647(8)	2643(7)	32(2)

Table 3 Anisotropic Displacement Parameters (Å^2×10^3) for ojH388k. The Anisotropic displacement factor exponent takes the form: -2π^2[h^{2}a*^{2}U$_{11}$+2hka*b*U$_{12}$+...].

Atom	U$_{11}$	U$_{22}$	U$_{33}$	U$_{23}$	U$_{13}$	U$_{12}$
K1	18.4(8)	25.5(9)	19.0(7)	1.5(8)	9.9(6)	-0.1(8)
F1	12.6(18)	44(3)	15.1(18)	-2.4(19)	6.6(15)	-1.8(18)
N1	16(3)	23(4)	16(2)	0(3)	5(2)	-3(3)
C1	16(3)	20(4)	15(3)	1(3)	8(2)	-3(3)
B1	15(4)	22(4)	13(3)	0(3)	10(3)	2(3)
F2	30(2)	23(2)	20(2)	-0.6(18)	0.3(17)	2.4(18)
N2	13(3)	32(4)	21(3)	-8(3)	12(2)	-1(3)
C2	16(3)	26(4)	20(3)	-5(3)	6(2)	-2(3)
F3	13.2(18)	34(3)	19.2(19)	1.0(19)	8.5(15)	-6.2(17)
N3	9(3)	36(4)	16(2)	-7(3)	9(2)	0(3)
C3	14(3)	16(4)	24(3)	-2(3)	11(2)	-6(3)
C4	14(3)	17(4)	20(3)	0(3)	6(2)	-5(3)
C5	17(3)	38(4)	12(3)	6(3)	8(3)	1(3)
C6	16(3)	31(4)	15(3)	8(3)	3(3)	-2(3)
C7	17(4)	31(4)	37(4)	8(3)	6(3)	1(3)
C8	41(4)	35(5)	36(4)	6(4)	8(3)	-4(3)
C9	46(4)	71(6)	35(5)	6(4)	-1(4)	-32(4)
C10	27(4)	93(7)	37(5)	2(5)	10(4)	-29(4)
C11	26(4)	80(6)	23(4)	0(4)	9(3)	-15(4)
C12	12(3)	57(5)	17(3)	-4(3)	7(3)	1(3)
C13	21(3)	66(6)	26(4)	2(4)	10(3)	13(4)
C14	21(4)	118(8)	34(4)	2(5)	6(3)	24(5)

Table 3 Anisotropic Displacement Parameters ($Å^2×10^3$) for ojH388k. The Anisotropic displacement factor exponent takes the form: $-2\pi^2[h^2a^{*2}U_{11}+2hka^*b^*U_{12}+...]$.

Atom	U_{11}	U_{22}	U_{33}	U_{23}	U_{13}	U_{12}
C15	20(4)	113(8)	33(4)	-9(5)	14(3)	6(4)
C16	19(4)	91(7)	28(4)	-9(4)	16(3)	-5(4)
C17	15(3)	59(6)	23(4)	1(4)	13(3)	-1(4)

Table 4 Bond Lengths for ojH388k.

Atom	Atom	Length/Å	Atom	Atom	Length/Å
K1	K1[1]	4.337(3)	B1	C4	1.607(9)
K1	K1[2]	4.6144(10)	N2	C2	1.346(7)
K1	K1[3]	4.6145(10)	C2	C3	1.390(8)
K1	F1[2]	2.785(4)	C2	C12	1.483(8)
K1	N1[1]	3.093(5)	N3	C5	1.464(7)
K1	N1	2.872(5)	C3	C4	1.387(7)
K1	B1[2]	3.412(8)	C5	C6	1.538(9)
K1	B1[1]	3.528(7)	C6	C7	1.361(9)
K1	F2[4]	2.700(4)	C6	C11	1.384(8)
K1	F2[1]	2.748(4)	C7	C8	1.408(9)
K1	F3[2]	2.824(4)	C8	C9	1.383(9)
K1	F3	2.699(3)	C9	C10	1.372(11)
F1	B1	1.413(7)	C10	C11	1.394(11)
N1	C1	1.372(7)	C12	C13	1.389(9)
N1	C4	1.359(7)	C12	C17	1.389(9)
C1	N2	1.343(7)	C13	C14	1.388(8)
C1	N3	1.363(7)	C14	C15	1.381(10)
B1	F2	1.423(9)	C15	C16	1.383(10)
B1	F3	1.434(8)	C16	C17	1.390(8)

[1]1-X,1-Y,1-Z; [2]+X,1/2-Y,1/2+Z; [3]+X,1/2-Y,-1/2+Z; [4]1-X,-1/2+Y,1/2-Z

Table 5 Bond Angles for ojH388k.

Atom	Atom	Atom	Angle/°	Atom	Atom	Atom	Angle/°
K1[1]	K1	K1[2]	94.63(5)	F3[3]	K1	B1[1]	86.16(15)
K1[1]	K1	K1[3]	103.49(5)	F3	K1	F2[1]	133.34(12)
K1[3]	K1	K1[2]	161.62(7)	F3	K1	F2[4]	66.60(11)
F1[3]	K1	K1[2]	90.91(8)	F3	K1	F3[3]	161.09(10)
F1[3]	K1	K1[1]	133.43(9)	B1	F1	K1[2]	103.8(4)
F1[3]	K1	K1[3]	74.50(7)	K1	N1	K1[1]	93.22(13)
F1[3]	K1	N1	89.35(13)	C1	N1	K1[1]	119.5(4)

Table 5 Bond Angles for ojH388k.

Atom	Atom	Atom	Angle/°	Atom	Atom	Atom	Angle/°
F1^3	K1	N1^1	167.08(13)	C1	N1	K1	114.9(4)
F1^3	K1	B1^1	123.17(15)	C4	N1	K1^1	99.5(4)
F1^3	K1	B1^3	23.72(13)	C4	N1	K1	110.7(4)
F1^3	K1	F3^3	47.75(9)	C4	N1	C1	116.1(5)
N1	K1	K1^2	85.17(10)	N2	C1	N1	126.6(5)
N1^1	K1	K1^3	94.65(9)	N2	C1	N3	117.2(5)
N1^1	K1	K1^1	41.39(9)	N3	C1	N1	116.1(5)
N1	K1	K1^3	105.37(10)	K1^2	B1	K1^1	143.1(2)
N1	K1	K1^1	45.39(10)	F1	B1	K1^1	154.0(5)
N1^1	K1	K1^2	101.04(10)	F1	B1	K1^2	52.4(3)
N1	K1	N1^1	86.78(13)	F1	B1	F2	108.3(5)
N1^1	K1	B1^1	44.12(15)	F1	B1	F3	105.8(5)
N1	K1	B1^3	101.31(16)	F1	B1	C4	112.4(5)
N1^1	K1	B1^3	146.37(15)	F2	B1	K1^1	46.4(3)
N1	K1	B1^1	83.86(15)	F2	B1	K1^2	127.9(4)
B1^3	K1	K1^2	112.07(13)	F2	B1	F3	106.5(5)
B1^1	K1	K1^3	53.77(13)	F2	B1	C4	111.2(6)
B1^1	K1	K1^2	143.90(13)	F3	B1	K1^1	90.3(3)
B1^3	K1	K1^3	51.72(12)	F3	B1	K1^2	54.2(3)
B1^3	K1	K1^1	136.35(14)	F3	B1	C4	112.2(5)
B1^1	K1	K1^1	54.36(12)	C4	B1	K1^1	78.7(3)
B1^3	K1	B1^1	103.78(7)	C4	B1	K1^2	120.9(4)
F2^4	K1	K1^2	32.43(8)	K1^5	F2	K1^1	115.78(13)
F2^4	K1	K1^3	129.44(10)	B1	F2	K1^1	111.5(3)
F2^1	K1	K1^1	73.74(9)	B1	F2	K1^5	132.4(3)
F2^4	K1	K1^1	127.04(9)	C1	N2	C2	116.5(5)
F2^1	K1	K1^2	165.81(10)	N2	C2	C3	120.7(5)
F2^1	K1	K1^3	31.79(8)	N2	C2	C12	116.2(6)
F2^1	K1	F1^3	102.97(11)	C3	C2	C12	123.1(5)
F2^4	K1	F1^3	69.84(10)	K1	F3	K1^2	113.30(13)
F2^4	K1	N1	108.79(13)	B1	F3	K1	121.8(3)
F2^1	K1	N1^1	64.89(12)	B1	F3	K1^2	101.5(3)
F2^1	K1	N1	91.96(12)	C1	N3	C5	121.8(5)
F2^4	K1	N1^1	123.06(13)	C4	C3	C2	120.1(5)
F2^1	K1	B1^1	22.03(15)	N1	C4	B1	116.0(5)
F2^4	K1	B1^3	85.47(15)	N1	C4	C3	119.9(6)
F2^4	K1	B1^1	162.85(15)	C3	C4	B1	124.0(5)
F2^1	K1	B1^3	82.12(14)	N3	C5	C6	114.0(5)
F2^4	K1	F2^1	157.58(11)	C7	C6	C5	120.1(6)
F2^4	K1	F3^3	97.86(11)	C7	C6	C11	119.7(7)
F2^1	K1	F3^3	64.26(11)	C11	C6	C5	120.1(6)

Table 5 Bond Angles for ojH388k.

Atom	Atom	Atom	Angle/°	Atom	Atom	Atom	Angle/°
F3[3]	K1	K1[2]	129.25(9)	C6	C7	C8	121.1(6)
F3[3]	K1	K1[1]	133.96(9)	C9	C8	C7	118.9(7)
F3[3]	K1	K1[3]	32.50(7)	C10	C9	C8	119.7(8)
F3	K1	K1[1]	60.44(8)	C9	C10	C11	121.0(7)
F3	K1	K1[3]	163.80(10)	C6	C11	C10	119.5(7)
F3	K1	K1[2]	34.20(8)	C13	C12	C2	120.2(6)
F3	K1	F1[3]	114.24(10)	C13	C12	C17	119.2(6)
F3[3]	K1	N1	116.39(13)	C17	C12	C2	120.4(6)
F3	K1	N1[1]	74.68(12)	C14	C13	C12	120.4(6)
F3	K1	N1	62.58(12)	C15	C14	C13	120.4(8)
F3[3]	K1	N1[1]	124.11(11)	C14	C15	C16	119.4(7)
F3[3]	K1	B1[3]	24.32(12)	C15	C16	C17	120.7(7)
F3	K1	B1[1]	111.90(15)	C12	C17	C16	119.9(7)
F3	K1	B1[3]	137.96(14)				

[1]1-X,1-Y,1-Z; [2]+X,1/2-Y,-1/2+Z; [3]+X,1/2-Y,1/2+Z; [4]1-X,-1/2+Y,1/2-Z; [5]1-X,1/2+Y,1/2-Z

Table 6 Torsion Angles for ojH388k.

A	B	C	D	Angle/°	A	B	C	D	Angle/°
K1[1]	F1	B1	K1[2]	-136.4(9)	N2	C1	N3	C5	3.7(9)
K1[1]	F1	B1	F2	-124.2(4)	N2	C2	C3	C4	2.1(10)
K1[1]	F1	B1	F3	-10.3(5)	N2	C2	C12	C13	27.9(10)
K1[1]	F1	B1	C4	112.5(5)	N2	C2	C12	C17	-148.2(7)
K1	N1	C1	N2	132.0(5)	C2	C3	C4	N1	0.2(9)
K1[2]	N1	C1	N2	-118.5(6)	C2	C3	C4	B1	179.0(6)
K1[2]	N1	C1	N3	63.1(7)	C2	C12	C13	C14	-178.7(7)
K1	N1	C1	N3	-46.4(7)	C2	C12	C17	C16	177.3(6)
K1	N1	C4	B1	46.3(6)	F3	B1	F2	K1[3]	-112.0(4)
K1[2]	N1	C4	B1	-50.8(6)	F3	B1	F2	K1[2]	74.0(5)
K1[2]	N1	C4	C3	128.1(5)	F3	B1	C4	N1	-42.5(8)
K1	N1	C4	C3	-134.8(5)	F3	B1	C4	C3	138.7(6)
K1[1]	B1	F2	K1[2]	131.2(3)	N3	C1	N2	C2	179.9(6)
K1[2]	B1	F2	K1[3]	174.0(5)	N3	C5	C6	C7	74.9(7)
K1[1]	B1	F2	K1[3]	-54.8(6)	N3	C5	C6	C11	-108.5(6)
K1[1]	B1	F3	K1	126.9(4)	C3	C2	C12	C13	-151.2(7)
K1[2]	B1	F3	K1[1]	169.27(12)	C3	C2	C12	C17	32.7(10)
K1[2]	B1	F3	K1	-63.8(3)	C4	N1	C1	N2	0.7(10)
K1[2]	B1	C4	N1	43.1(5)	C4	N1	C1	N3	-177.7(6)
K1[1]	B1	C4	N1	-103.0(6)	C4	B1	F2	K1[2]	-48.6(5)

Table 6 Torsion Angles for ojH388k.

A	B	C	D	Angle/°	A	B	C	D	Angle/°
K1[1]	B1	C4	C3	78.2(7)	C4	B1	F2	K1[3]	125.4(4)
K1[2]	B1	C4	C3	-135.7(6)	C4	B1	F3	K1	14.1(7)
F1	B1	F2	K1[2]	-172.6(3)	C4	B1	F3	K1[1]	-112.9(5)
F1	B1	F2	K1[3]	1.4(8)	C5	C6	C7	C8	176.7(6)
F1	B1	F3	K1[1]	10.0(5)	C5	C6	C11	C10	-176.4(6)
F1	B1	F3	K1	137.0(4)	C6	C7	C8	C9	-0.8(10)
F1	B1	C4	N1	-161.6(6)	C7	C6	C11	C10	0.2(10)
F1	B1	C4	C3	19.6(9)	C7	C8	C9	C10	1.3(11)
N1	C1	N2	C2	1.5(10)	C8	C9	C10	C11	-1.0(12)
N1	C1	N3	C5	-177.7(6)	C9	C10	C11	C6	0.3(11)
C1	N1	C4	B1	179.6(5)	C11	C6	C7	C8	0.1(10)
C1	N1	C4	C3	-1.6(9)	C12	C2	C3	C4	-178.9(6)
C1	N2	C2	C3	-2.9(10)	C12	C13	C14	C15	2.6(13)
C1	N2	C2	C12	178.0(6)	C13	C12	C17	C16	1.2(11)
C1	N3	C5	C6	82.9(7)	C13	C14	C15	C16	-1.3(13)
F2	B1	F3	K1[1]	125.1(4)	C14	C15	C16	C17	0.0(13)
F2	B1	F3	K1	-107.9(5)	C15	C16	C17	C12	0.1(12)
F2	B1	C4	N1	76.8(7)	C17	C12	C13	C14	-2.5(11)
F2	B1	C4	C3	-102.0(7)					

[1]+X,1/2-Y,-1/2+Z; [2]1-X,1-Y,1-Z; [3]1-X,1/2+Y,1/2-Z

Table 7 Hydrogen Atom Coordinates ($\text{Å}\times10^4$) and Isotropic Displacement Parameters ($\text{Å}^2\times10^3$) for ojH388k.

Atom	x	y	z	U(eq)
H3	6022.19	4295.73	7441.48	24
H3A	7077.71	4342.09	2002.16	21
H5A	7425.49	3422.76	8128.53	26
H5B	6824.36	3656.78	9294.03	26
H7	6590.36	6103.73	9974.37	34
H8	7186.3	8068.28	10852.51	44
H9	8412.32	8433.43	10358.26	61
H10	9005.74	6911.99	8938.58	62
H11	8406.14	4973.7	8055.25	51
H13	8584.13	2844.82	5618.07	45
H14	9819.85	2598.57	5173.73	69
H15	10297.86	3708.01	3202.93	66
H16	9520.79	4982.55	1611.93	54
H17	8272.35	5166.4	1989.25	39

X-ray crystallographic analysis for compound 228
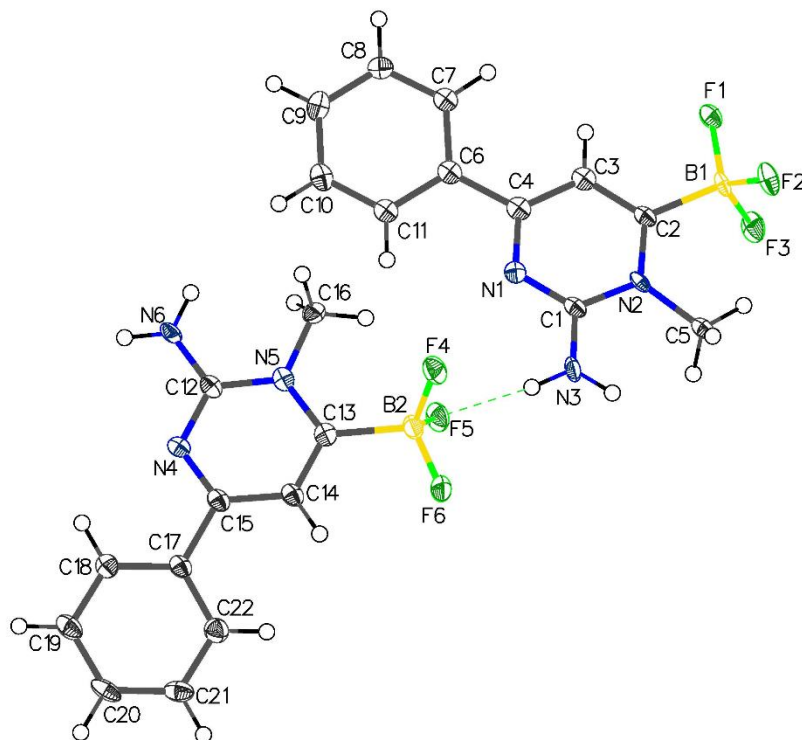
*Figure 235: ORTEP of **228**, thermal ellipsoids are shown at 50% probability*

Crystal structure determination of compound 228

Crystals of **228** were grown from a saturated acetone solution, allowing slow evaporation.

Crystal Data for $C_{11}H_{11}BF_3N_3$ (M =253.04 g/mol): monoclinic, space group P2$_1$/n (no. 14), a = 17.8400(7) Å, b = 6.8724(3) Å, c = 19.3259(8) Å, β = 102.492(2)°, V = 2313.33(17) Å^3, Z = 8, T = 100.03 K, μ(CuKα) = 1.055 mm^{-1}, $Dcalc$ = 1.453 g/cm^3, 12247 reflections measured (6.116° ≤ 2Θ ≤ 133.71°), 3735 unique (R_{int} = 0.0706, R$_{sigma}$ = 0.0683) which were used in all calculations. The final R_1 was 0.1587 (I > 2σ(I)) and wR_2 was 0.3409 (all data).

Table 1 Crystal data and structure refinement for OJH391v_0m.

Identification code	OJH391v_0m
Empirical formula	$C_{11}H_{11}BF_3N_3$
Formula weight	253.04
Temperature/K	100.03
Crystal system	monoclinic
Space group	P2$_1$/n

a/Å	17.8400(7)
b/Å	6.8724(3)
c/Å	19.3259(8)
α/°	90
β/°	102.492(2)
γ/°	90
Volume/Å^3	2313.33(17)
Z	8
ρ_{calc}g/cm^3	1.453
μ/mm^{-1}	1.055
F(000)	1040.0
Crystal size/mm^3	0.2 × 0.034 × 0.025
Radiation	CuKα (λ = 1.54178)
2Θ range for data collection/°	6.116 to 133.71
Index ranges	-21 ≤ h ≤ 21, -7 ≤ k ≤ 8, -22 ≤ l ≤ 22
Reflections collected	12247
Independent reflections	3735 [R_{int} = 0.0706, R_{sigma} = 0.0683]
Data/restraints/parameters	3735/282/279
Goodness-of-fit on F^2	1.419
Final R indexes [I>=2σ (I)]	R_1 = 0.1587, wR_2 = 0.3370
Final R indexes [all data]	R_1 = 0.1701, wR_2 = 0.3409
Largest diff. peak/hole / e Å^{-3}	0.58/-0.53

Table 2 Fractional Atomic Coordinates (×10^4) and Equivalent Isotropic Displacement Parameters (Å^2×10^3) for OJH391v_0m. U$_{eq}$ is defined as 1/3 of of the trace of the orthogonalised U$_{IJ}$ tensor.

Atom	x	y	z	U(eq)
F1	783(3)	4825(10)	4127(3)	31.3(15)
N1	3398(4)	3611(11)	3600(4)	15.2(15)
C1	3503(5)	3610(14)	4301(5)	16.7(11)
B1	1457(6)	4661(15)	4654(6)	15.0(18)
F2	1385(3)	3095(9)	5100(3)	27.9(14)
N2	2910(4)	3998(11)	4639(4)	13.7(15)
C2	2178(5)	4252(14)	4258(5)	16.7(11)
F3	1570(3)	6370(9)	5045(3)	27.0(14)
N3	4191(4)	3323(13)	4686(4)	21.9(18)
C3	2063(5)	4146(13)	3537(5)	16.1(8)
C4	2688(5)	3875(13)	3215(5)	16.1(8)
C5	3096(5)	4202(14)	5416(5)	16.7(11)
C6	2610(5)	3877(13)	2434(5)	16.1(8)
C7	1890(5)	3723(13)	1961(5)	16.1(8)

Table 2 Fractional Atomic Coordinates (×10⁴) and Equivalent Isotropic Displacement Parameters (Å²×10³) for OJH391v_0m. U$_{eq}$ is defined as 1/3 of of the trace of the orthogonalised U$_{IJ}$ tensor.

Atom	*x*	*y*	*z*	U(eq)
C8	1836(5)	3778(14)	1237(5)	17.9(19)
C9	2480(6)	3963(14)	958(5)	20.0(19)
C10	3193(6)	4094(14)	1417(5)	19.8(19)
C11	3267(5)	4061(13)	2146(5)	16.1(8)
B2	5799(6)	663(17)	3943(6)	19(2)
F4	5301(3)	−934(9)	3877(3)	27.7(14)
N4	6988(4)	972(11)	2157(4)	14.5(15)
F5	5386(3)	2399(9)	3956(3)	25.9(14)
N5	5838(4)	889(11)	2584(4)	15.4(15)
F6	6340(3)	487(11)	4562(3)	33.2(16)
N6	5824(4)	1077(12)	1378(4)	19.1(17)
C12	6220(5)	968(14)	2043(5)	16.3(17)
C13	6248(5)	744(13)	3276(5)	16.3(17)
C14	7024(5)	723(13)	3387(5)	17.2(11)
C15	7385(5)	873(14)	2814(5)	17.2(11)
C16	5001(5)	1022(15)	2411(5)	20(2)
C17	8231(5)	935(14)	2913(5)	17.2(11)
C18	8564(5)	786(14)	2328(5)	18.7(19)
C19	9352(5)	891(16)	2395(6)	25(2)
C20	9819(5)	1133(14)	3065(6)	22(2)
C21	9502(6)	1247(15)	3651(6)	24(2)
C22	8719(6)	1124(15)	3585(5)	23(2)

Table 3 Anisotropic Displacement Parameters (Å²×10³) for OJH391v_0m. The Anisotropic displacement factor exponent takes the form: -2π²[h²a*²U$_{11}$+2hka*b*U$_{12}$+…].

Atom	U$_{11}$	U$_{22}$	U$_{33}$	U$_{23}$	U$_{13}$	U$_{12}$
F1	13(3)	56(4)	26(3)	−5(3)	7(2)	3(3)
N1	20(3)	8(4)	19(3)	−1(3)	6(3)	−3(3)
C1	12(2)	16(3)	23(2)	−1(2)	5.5(18)	0(2)
B1	15(4)	13(4)	21(5)	0(3)	13(3)	0(4)
F2	30(3)	27(3)	33(3)	7(3)	20(3)	−1(3)
N2	11(3)	10(4)	21(3)	3(3)	7(3)	−2(3)
C2	12(2)	16(3)	23(2)	−1(2)	5.5(18)	0(2)
F3	28(3)	24(3)	34(3)	−6(2)	16(3)	4(3)
N3	16(3)	36(5)	17(4)	3(4)	10(3)	3(4)
C3	19.6(19)	6.4(17)	22.5(18)	0.9(16)	4.9(15)	0.2(16)
C4	19.6(19)	6.4(17)	22.5(18)	0.9(16)	4.9(15)	0.2(16)
C5	12(2)	16(3)	23(2)	−1(2)	5.5(18)	0(2)
C6	19.6(19)	6.4(17)	22.5(18)	0.9(16)	4.9(15)	0.2(16)

Table 3 Anisotropic Displacement Parameters ($Å^2 \times 10^3$) for OJH391v_0m. The Anisotropic displacement factor exponent takes the form: -$2\pi^2[h^2a^{*2}U_{11}+2hka^*b^*U_{12}+\dots]$.

Atom	U_{11}	U_{22}	U_{33}	U_{23}	U_{13}	U_{12}
C7	19.6(19)	6.4(17)	22.5(18)	0.9(16)	4.9(15)	0.2(16)
C8	17(4)	14(5)	22(4)	0(4)	1(3)	4(4)
C9	32(4)	10(4)	19(4)	5(4)	8(3)	5(4)
C10	25(4)	11(4)	26(4)	3(4)	11(3)	0(4)
C11	19.6(19)	6.4(17)	22.5(18)	0.9(16)	4.9(15)	0.2(16)
B2	19(5)	20(5)	20(4)	−1(4)	9(3)	−3(4)
F4	28(3)	29(3)	28(3)	2(3)	12(3)	−7(3)
N4	15(3)	8(4)	21(3)	0(3)	4(3)	−1(3)
F5	24(3)	27(3)	30(3)	−5(3)	13(3)	4(2)
N5	18(3)	8(4)	21(3)	0(3)	8(3)	2(3)
F6	21(3)	61(5)	19(3)	−4(3)	8(2)	1(3)
N6	9(4)	25(4)	24(3)	−3(3)	6(3)	2(3)
C12	16(4)	12(4)	21(4)	3(4)	6(3)	0(4)
C13	21(4)	7(4)	22(4)	−4(4)	8(3)	−1(3)
C14	18(2)	12(2)	23(2)	0(2)	7.2(18)	−3(2)
C15	18(2)	12(2)	23(2)	0(2)	7.2(18)	−3(2)
C16	19(4)	23(5)	19(5)	−7(4)	3(4)	−2(4)
C17	18(2)	12(2)	23(2)	0(2)	7.2(18)	−3(2)
C18	20(4)	15(5)	22(4)	−2(4)	7(3)	1(4)
C19	16(4)	26(6)	34(5)	−2(5)	9(4)	3(4)
C20	11(4)	15(5)	41(5)	4(4)	6(3)	3(4)
C21	15(4)	21(5)	32(5)	−5(4)	−1(4)	2(4)
C22	22(4)	23(5)	25(4)	−3(4)	7(3)	−1(4)

Table 4 Bond Lengths for OJH391v_0m.

Atom	Atom	Length/Å	Atom	Atom	Length/Å
F1	B1	1.402(13)	B2	F4	1.401(12)
N1	C1	1.327(12)	B2	F5	1.405(13)
N1	C4	1.335(12)	B2	F6	1.370(13)
C1	N2	1.384(11)	B2	C13	1.658(13)
C1	N3	1.304(12)	N4	C12	1.339(12)
B1	F2	1.403(12)	N4	C15	1.315(12)
B1	C2	1.657(13)	N5	C12	1.368(11)
B1	F3	1.387(12)	N5	C13	1.383(12)
N2	C2	1.364(12)	N5	C16	1.460(12)
N2	C5	1.474(11)	N6	C12	1.328(12)
C2	C3	1.365(13)	C13	C14	1.355(13)
C3	C4	1.402(13)	C14	C15	1.399(13)
C4	C6	1.486(13)	C15	C17	1.481(13)

Table 4 Bond Lengths for OJH391v_0m.

Atom	Atom	Length/Å	Atom	Atom	Length/Å
C6	C7	1.410(13)	C17	C18	1.390(13)
C6	C11	1.408(12)	C17	C22	1.405(14)
C7	C8	1.383(13)	C18	C19	1.385(13)
C8	C9	1.377(13)	C19	C20	1.389(15)
C9	C10	1.386(14)	C20	C21	1.373(14)
C10	C11	1.386(13)	C21	C22	1.377(14)

Table 5 Bond Angles for OJH391v_0m.

Atom	Atom	Atom	Angle/°	Atom	Atom	Atom	Angle/°
C1	N1	C4	118.5(8)	F4	B2	F5	110.0(8)
N1	C1	N2	121.8(8)	F4	B2	C13	111.0(8)
N3	C1	N1	119.3(8)	F5	B2	C13	109.2(8)
N3	C1	N2	118.8(8)	F6	B2	F4	108.9(9)
F1	B1	F2	109.3(8)	F6	B2	F5	109.4(8)
F1	B1	C2	107.8(7)	F6	B2	C13	108.3(8)
F2	B1	C2	109.7(8)	C15	N4	C12	118.4(8)
F3	B1	F1	109.2(8)	C12	N5	C13	119.7(8)
F3	B1	F2	109.7(8)	C12	N5	C16	118.5(8)
F3	B1	C2	111.1(8)	C13	N5	C16	121.8(7)
C1	N2	C5	118.1(7)	N4	C12	N5	122.4(8)
C2	N2	C1	120.7(8)	N6	C12	N4	118.1(8)
C2	N2	C5	121.1(7)	N6	C12	N5	119.4(8)
N2	C2	B1	121.3(8)	N5	C13	B2	120.7(8)
N2	C2	C3	117.3(8)	C14	C13	B2	121.8(8)
C3	C2	B1	121.4(8)	C14	C13	N5	117.5(8)
C2	C3	C4	120.1(9)	C13	C14	C15	120.2(9)
N1	C4	C3	121.3(8)	N4	C15	C14	121.7(8)
N1	C4	C6	115.8(8)	N4	C15	C17	116.3(8)
C3	C4	C6	122.8(8)	C14	C15	C17	122.0(8)
C7	C6	C4	122.0(8)	C18	C17	C15	119.7(8)
C11	C6	C4	119.9(8)	C18	C17	C22	118.0(9)
C11	C6	C7	118.0(8)	C22	C17	C15	122.2(8)
C8	C7	C6	120.6(9)	C19	C18	C17	121.5(9)
C9	C8	C7	121.1(9)	C18	C19	C20	119.1(9)
C8	C9	C10	118.9(9)	C21	C20	C19	120.3(9)
C11	C10	C9	121.5(9)	C20	C21	C22	120.6(9)
C10	C11	C6	119.9(9)	C21	C22	C17	120.4(9)

Table 6 Torsion Angles for OJH391v_0m.

A	B	C	D	Angle/°	A	B	C	D	Angle/°
F1	B1	C2	N2	−179.0(8)	B2	C13	C14	C15	−177.4(9)
F1	B1	C2	C3	0.7(12)	F4	B2	C13	N5	59.5(12)
N1	C1	N2	C2	5.0(14)	F4	B2	C13	C14	−122.3(10)
N1	C1	N2	C5	−172.7(8)	N4	C15	C17	C18	−10.0(13)
N1	C4	C6	C7	166.2(8)	N4	C15	C17	C22	170.6(9)
N1	C4	C6	C11	−14.6(13)	F5	B2	C13	N5	−62.0(11)
C1	N1	C4	C3	0.0(13)	F5	B2	C13	C14	116.3(10)
C1	N1	C4	C6	179.5(8)	N5	C13	C14	C15	0.9(13)
C1	N2	C2	B1	178.4(8)	F6	B2	C13	N5	179.0(8)
C1	N2	C2	C3	−1.3(13)	F6	B2	C13	C14	−2.8(13)
B1	C2	C3	C4	177.5(8)	C12	N4	C15	C14	1.4(14)
F2	B1	C2	N2	−60.1(12)	C12	N4	C15	C17	−178.4(8)
F2	B1	C2	C3	119.6(10)	C12	N5	C13	B2	179.5(8)
N2	C2	C3	C4	−2.9(14)	C12	N5	C13	C14	1.2(13)
C2	C3	C4	N1	3.6(14)	C13	N5	C12	N4	−2.2(13)
C2	C3	C4	C6	−175.8(9)	C13	N5	C12	N6	179.0(9)
F3	B1	C2	N2	61.4(12)	C13	C14	C15	N4	−2.3(15)
F3	B1	C2	C3	−118.9(10)	C13	C14	C15	C17	177.5(9)
N3	C1	N2	C2	−178.1(9)	C14	C15	C17	C18	170.2(9)
N3	C1	N2	C5	4.2(13)	C14	C15	C17	C22	−9.2(15)
C3	C4	C6	C7	−14.3(14)	C15	N4	C12	N5	0.8(14)
C3	C4	C6	C11	165.0(9)	C15	N4	C12	N6	179.7(9)
C4	N1	C1	N2	−4.3(13)	C15	C17	C18	C19	178.2(9)
C4	N1	C1	N3	178.9(9)	C15	C17	C22	C21	−177.6(9)
C4	C6	C7	C8	178.4(8)	C16	N5	C12	N4	175.9(9)
C4	C6	C11	C10	−179.0(9)	C16	N5	C12	N6	−2.9(13)
C5	N2	C2	B1	−4.0(13)	C16	N5	C13	B2	1.5(13)
C5	N2	C2	C3	176.4(8)	C16	N5	C13	C14	−176.8(8)
C6	C7	C8	C9	0.7(14)	C17	C18	C19	C20	0.6(16)
C7	C6	C11	C10	0.3(14)	C18	C17	C22	C21	2.9(15)
C7	C8	C9	C10	0.0(14)	C18	C19	C20	C21	0.7(16)
C8	C9	C10	C11	−0.6(15)	C19	C20	C21	C22	−0.1(16)
C9	C10	C11	C6	0.5(14)	C20	C21	C22	C17	−1.8(16)
C11	C6	C7	C8	−0.8(14)	C22	C17	C18	C19	−2.3(15)

Table 7 Hydrogen Atom Coordinates (Å×10⁴) and Isotropic Displacement Parameters (Å²×10³) for OJH391v_0m.

Atom	x	y	z	U(eq)
H3A	4578.98	3132.98	4479.7	26
H3B	4266.38	3319.69	5150.93	26
H3	1558.68	4255.6	3253.3	19

Table 7 Hydrogen Atom Coordinates (Å×10⁴) and Isotropic Displacement Parameters (Å²×10³) for OJH391v_0m.

Atom	x	y	z	U(eq)
H5A	3282.07	2954.72	5632.71	25
H5B	2635.13	4594.65	5578.72	25
H5C	3495.71	5193.5	5553.59	25
H7	1438.5	3580.37	2141.99	19
H8	1345.28	3686.14	926.16	22
H9	2437.64	4000.07	459.86	24
H10	3639.56	4208.7	1227.71	24
H11	3760.74	4162.97	2450.26	19
H6A	6065.43	1149.91	1027.74	23
H6B	5318.42	1076.72	1288.56	23
H14	7325.26	606.44	3854.59	21
H16A	4843.67	2161.79	2109.77	31
H16B	4812.27	1150.73	2848.92	31
H16C	4785.55	−155.97	2158.59	31
H18	8243.4	608.61	1871.02	22
H19	9569.43	797.36	1989.38	29
H20	10359.54	1220.86	3116.87	27
H21	9826.58	1411.6	4106.63	28
H22	8508.62	1167.24	3995.75	27
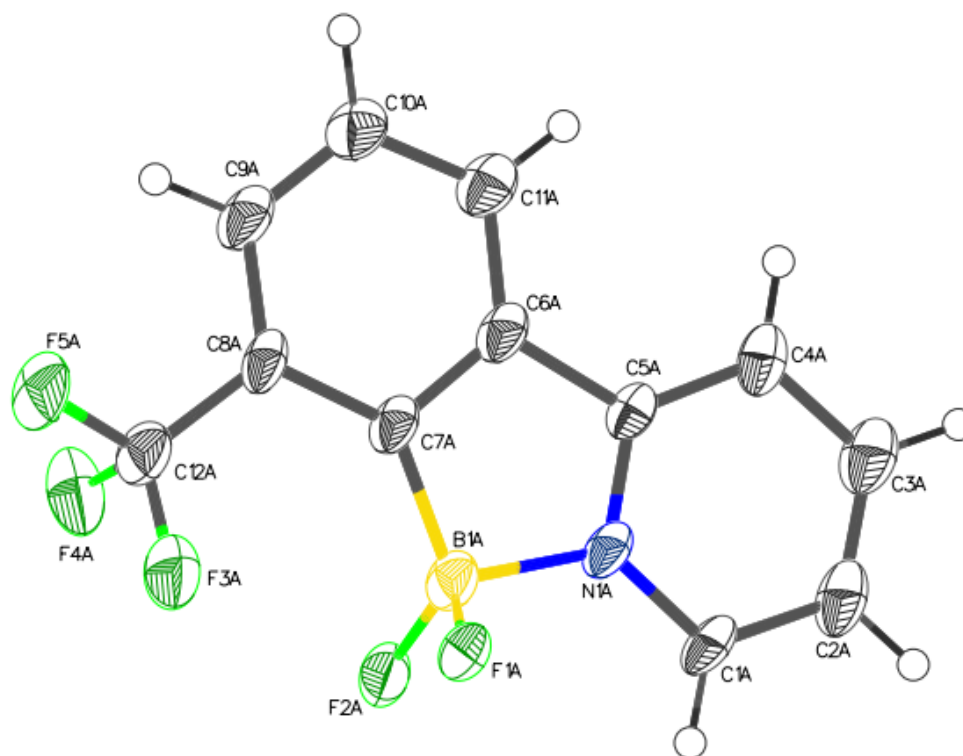
*Figure 236: ORTEP of **354**, ellipsoids are shown at 50% probability*

Table 1 Crystal data and structure refinement for 354.

Identification code	OJH376k_0m
Empirical formula	$C_{12}H_7BF_5N$
Formula weight	271.00
Temperature/K	100
Crystal system	triclinic
Space group	P-1
a/Å	7.934(5)
b/Å	10.500(7)
c/Å	13.898(9)
α/°	70.75(3)
β/°	89.77(3)
γ/°	89.88(3)
Volume/Å^3	1093.1(13)
Z	4
ρ_{calc}g/cm^3	1.647
μ/mm^{-1}	0.156
F(000)	544.0
Crystal size/mm^3	$0.416 \times 0.32 \times 0.223$

Radiation	MoKα (λ = 0.71073)	
2Θ range for data collection/°	3.104 to 55.47	
Index ranges	$-10 \le h \le 10, -10 \le k \le 13, -15 \le l \le 18$	
Reflections collected	13108	
Independent reflections	4964 [R_{int} = 0.2141, R_{sigma} = 0.3625]	
Data/restraints/parameters	4964/330/343	
Goodness-of-fit on F^2	1.012	
Final R indexes [I>=2σ (I)]	R_1 = 0.1296, wR_2 = 0.3321	
Final R indexes [all data]	R_1 = 0.3174, wR_2 = 0.4144	
Largest diff. peak/hole / e Å^{-3}	0.62/-0.66	

Experimental

Single crystals of $C_{12}H_7BF_5N$ 354 were grown from a saturated solution in CH_2Cl_2. A suitable crystal was selected and [MiTiGen microloop in fomblyn oil] on a 'Bruker APEX-II CCD' diffractometer. The crystal was kept at 100 K during data collection. Using Olex2 [1], the structure was solved with the XT [2] structure solution program using Intrinsic Phasing and refined with the XL [3] refinement package using Least Squares minimisation.

1. Dolomanov, O.V., Bourhis, L.J., Gildea, R.J, Howard, J.A.K. & Puschmann, H. (2009), J. Appl. Cryst. 42, 339-341.
2. Sheldrick, G.M. (2015). Acta Cryst. A71, 3-8.
3. Sheldrick, G.M. (2008). Acta Cryst. A64, 112-122.

Crystal structure determination of OJH376k_0m

Crystal Data for $C_{12}H_7BF_5N$ (*M* =271.00 g/mol): triclinic, space group P-1 (no. 2), *a* = 7.934(5) Å, *b* = 10.500(7) Å, *c* = 13.898(9) Å, *α* = 70.75(3)°, *β* = 89.77(3)°, *γ* = 89.88(3)°, *V* = 1093.1(13) Å^3, *Z* = 4, *T* = 100 K, μ(MoKα) = 0.156 mm^{-1}, *Dcalc* = 1.647 g/cm^3, 13108 reflections measured (3.104° ≤ 2Θ ≤ 55.47°), 4964 unique (R_{int} = 0.2141, R_{sigma} = 0.3625) which were used in all calculations. The final R_1 was 0.1296 (I > 2σ(I)) and wR_2 was 0.4144 (all data).

Table 2 Fractional Atomic Coordinates (×10^4) and Equivalent Isotropic Displacement Parameters (Å^2×10^3) for OJH376k_0m. U_{eq} is defined as 1/3 of of the trace of the orthogonalised U_{IJ} tensor.

Atom	x	y	z	U(eq)
F1A	8162(7)	4321(5)	2660(4)	34.6(14)
F2A	5696(7)	3208(5)	2444(4)	36.3(15)
F3A	5531(9)	4937(7)	3874(5)	58.1(19)
F4A	2925(8)	4909(6)	3489(5)	52.5(18)

F5A	3918(8)	6550(6)	3901(5)	50.7(18)
N1A	7297(10)	4509(8)	916(6)	28.3(17)
C1A	8212(12)	3583(10)	664(8)	31(2)
C2A	8703(13)	3851(11)	-353(8)	39(2)
C3A	8265(13)	5057(11)	-1084(9)	42(3)
C4A	7329(12)	6004(11)	-799(8)	34(2)
C5A	6859(11)	5687(9)	221(7)	23.8(19)
C6A	5863(12)	6496(10)	711(8)	30(2)
C7A	5657(12)	5801(9)	1745(8)	29(2)
C8A	4685(12)	6456(10)	2285(8)	31(2)
C9A	3953(13)	7699(10)	1817(8)	37(2)
C10A	4222(14)	8379(10)	794(9)	40(2)
C11A	5156(12)	7776(10)	213(9)	35(2)
C12A	4299(15)	5718(11)	3354(8)	39(2)
B1A	6666(16)	4422(12)	2027(9)	33(2)
F1B	9285(7)	-1788(5)	7438(4)	35.7(14)
F2B	6846(7)	-659(5)	7647(4)	32.3(14)
F3B	12056(9)	-97(7)	8496(5)	57.2(19)
F4B	11079(9)	1554(6)	8898(5)	52.7(18)
F5B	9452(8)	-66(7)	8874(5)	55.2(19)
N1B	7700(11)	-469(8)	5908(6)	33.1(19)
C1B	6778(13)	-1401(10)	5646(8)	35(2)
C2B	6334(13)	-1154(11)	4668(8)	37(2)
C3B	6737(13)	60(11)	3928(9)	39(2)
C4B	7661(12)	1009(11)	4205(8)	34(2)
C5B	8150(13)	704(10)	5211(8)	34(2)
C6B	9138(12)	1520(10)	5697(8)	32(2)
C7B	9335(12)	816(10)	6727(8)	29(2)
C8B	10345(13)	1433(10)	7294(8)	37(2)
C9B	11059(13)	2709(10)	6808(8)	35(2)
C10B	10771(13)	3373(11)	5789(8)	38(2)
C11B	9846(13)	2758(10)	5228(9)	36(2)
C12B	10715(14)	729(11)	8358(8)	38(2)
B1B	8339(16)	-612(12)	7027(10)	36(2)

Table 3 Anisotropic Displacement Parameters ($\text{Å}^2 \times 10^3$) for OJH376k_0m. The Anisotropic displacement factor exponent takes the form: -$2\pi^2[h^2a^{*2}U_{11}+2hka^*b^*U_{12}+\ldots]$.

Atom	U_{11}	U_{22}	U_{33}	U_{23}	U_{13}	U_{12}
F1A	44(3)	30(3)	34(3)	-17(3)	7(2)	6(3)

F2A	37(3)	33(3)	42(3)	-17(3)	14(2)	-1(2)
F3A	65(4)	70(5)	36(4)	-13(3)	13(3)	21(3)
F4A	59(4)	61(4)	43(4)	-25(3)	20(3)	-18(3)
F5A	71(4)	46(4)	49(4)	-34(3)	17(3)	-1(3)
N1A	28(4)	24(4)	39(4)	-19(3)	7(3)	0(3)
C1A	30(5)	27(5)	45(5)	-25(4)	3(4)	3(4)
C2A	40(6)	45(5)	45(5)	-33(4)	10(4)	-4(4)
C3A	43(6)	45(5)	50(5)	-32(4)	9(4)	-4(4)
C4A	30(5)	42(5)	39(4)	-26(4)	7(4)	-4(4)
C5A	20(4)	25(4)	34(4)	-19(3)	1(3)	-2(3)
C6A	33(5)	26(4)	39(4)	-21(3)	7(3)	-1(3)
C7A	32(5)	24(4)	38(4)	-19(3)	9(3)	-2(3)
C8A	31(5)	28(4)	43(4)	-24(3)	14(3)	-6(3)
C9A	37(6)	29(4)	55(5)	-25(4)	13(4)	-3(4)
C10A	48(6)	24(5)	53(5)	-20(4)	13(4)	-5(4)
C11A	34(5)	31(4)	46(5)	-21(4)	2(4)	-2(4)
C12A	48(5)	32(5)	42(4)	-20(3)	11(3)	2(4)
B1A	40(5)	29(4)	36(4)	-17(3)	8(3)	1(3)
F1B	41(3)	31(3)	38(3)	-16(3)	6(2)	5(2)
F2B	41(3)	30(3)	30(3)	-15(2)	12(2)	-7(2)
F3B	61(4)	66(4)	55(4)	-33(3)	2(3)	17(3)
F4B	79(5)	50(4)	41(4)	-32(3)	3(3)	-2(3)
F5B	58(4)	68(4)	41(4)	-20(3)	7(3)	-18(3)
N1B	41(5)	28(4)	39(4)	-23(3)	10(3)	0(3)
C1B	40(6)	27(5)	49(5)	-28(4)	11(4)	0(4)
C2B	34(6)	42(5)	50(5)	-37(4)	13(4)	5(4)
C3B	35(6)	44(5)	49(5)	-31(4)	5(4)	7(4)
C4B	32(5)	35(5)	42(5)	-22(4)	12(4)	6(4)
C5B	36(5)	31(4)	43(4)	-24(3)	9(3)	3(4)
C6B	37(5)	24(4)	40(4)	-20(3)	7(3)	5(4)
C7B	31(5)	27(4)	37(4)	-20(3)	11(3)	5(3)
C8B	41(5)	36(4)	40(4)	-22(3)	13(3)	-2(4)
C9B	30(5)	34(5)	48(5)	-24(4)	13(4)	-1(4)
C10B	43(6)	30(5)	48(5)	-22(4)	12(4)	2(4)
C11B	41(6)	29(4)	43(5)	-20(4)	10(4)	3(4)
C12B	44(5)	37(5)	39(4)	-23(3)	12(3)	-2(4)
B1B	42(5)	28(4)	41(5)	-16(3)	7(3)	3(4)

Table 4 Bond Lengths for OJH376k_0m.

Atom	Atom	Length/Å	Atom	Atom	Length/Å
F1A	B1A	1.464(14)	F1B	B1B	1.396(14)
F2A	B1A	1.438(12)	F2B	B1B	1.453(14)
F3A	C12A	1.327(13)	F3B	C12B	1.345(12)
F4A	C12A	1.357(12)	F4B	C12B	1.353(11)
F5A	C12A	1.367(12)	F5B	C12B	1.349(11)
N1A	C1A	1.347(12)	N1B	C1B	1.365(12)
N1A	C5A	1.341(12)	N1B	C5B	1.340(12)
N1A	B1A	1.594(14)	N1B	B1B	1.597(15)
C1A	C2A	1.400(14)	C1B	C2B	1.346(14)
C2A	C3A	1.381(15)	C2B	C3B	1.386(15)
C3A	C4A	1.397(14)	C3B	C4B	1.392(14)
C4A	C5A	1.394(13)	C4B	C5B	1.385(14)
C5A	C6A	1.479(13)	C5B	C6B	1.481(14)
C6A	C7A	1.389(14)	C6B	C7B	1.387(14)
C6A	C11A	1.410(14)	C6B	C11B	1.368(13)
C7A	C8A	1.402(13)	C7B	C8B	1.424(14)
C7A	B1A	1.585(15)	C7B	B1B	1.623(15)
C8A	C9A	1.380(14)	C8B	C9B	1.405(14)
C8A	C12A	1.463(14)	C8B	C12B	1.450(15)
C9A	C10A	1.380(15)	C9B	C10B	1.377(14)
C10A	C11A	1.390(15)	C10B	C11B	1.379(14)

Table 5 Bond Angles for OJH376k_0m.

Atom	Atom	Atom	Angle/°	Atom	Atom	Atom	Angle/°
C1A	N1A	B1A	127.1(9)	C1B	N1B	B1B	126.0(9)
C5A	N1A	C1A	121.7(9)	C5B	N1B	C1B	121.2(9)
C5A	N1A	B1A	111.2(8)	C5B	N1B	B1B	112.8(8)
N1A	C1A	C2A	119.2(10)	C2B	C1B	N1B	119.8(10)
C3A	C2A	C1A	120.2(10)	C1B	C2B	C3B	120.8(10)
C2A	C3A	C4A	119.4(11)	C2B	C3B	C4B	118.9(10)
C5A	C4A	C3A	118.3(10)	C5B	C4B	C3B	118.8(10)
N1A	C5A	C4A	121.2(9)	N1B	C5B	C4B	120.4(9)
N1A	C5A	C6A	109.8(8)	N1B	C5B	C6B	110.1(9)
C4A	C5A	C6A	128.9(9)	C4B	C5B	C6B	129.4(10)
C7A	C6A	C5A	110.6(9)	C7B	C6B	C5B	109.9(9)
C7A	C6A	C11A	123.6(9)	C11B	C6B	C5B	127.1(10)
C11A	C6A	C5A	125.8(10)	C11B	C6B	C7B	122.9(9)
C6A	C7A	C8A	115.6(9)	C6B	C7B	C8B	116.8(9)

C6A	C7A	B1A	108.9(8)	C6B	C7B	B1B	110.0(9)
C8A	C7A	B1A	135.5(10)	C8B	C7B	B1B	133.2(10)
C7A	C8A	C12A	117.9(9)	C7B	C8B	C12B	120.6(9)
C9A	C8A	C7A	122.2(10)	C9B	C8B	C7B	119.9(10)
C9A	C8A	C12A	119.6(9)	C9B	C8B	C12B	119.5(9)
C8A	C9A	C10A	120.6(10)	C10B	C9B	C8B	120.3(10)
C9A	C10A	C11A	119.9(11)	C9B	C10B	C11B	120.0(10)
C10A	C11A	C6A	117.9(11)	C6B	C11B	C10B	119.9(11)
F3A	C12A	F4A	105.7(9)	F3B	C12B	F4B	104.5(9)
F3A	C12A	F5A	104.5(9)	F3B	C12B	F5B	104.7(9)
F3A	C12A	C8A	115.3(9)	F3B	C12B	C8B	113.3(9)
F4A	C12A	F5A	103.5(8)	F4B	C12B	C8B	114.0(9)
F4A	C12A	C8A	113.9(9)	F5B	C12B	F4B	105.2(8)
F5A	C12A	C8A	112.8(9)	F5B	C12B	C8B	114.1(9)
F1A	B1A	N1A	107.5(8)	F1B	B1B	F2B	110.0(9)
F1A	B1A	C7A	116.0(8)	F1B	B1B	N1B	110.9(9)
F2A	B1A	F1A	108.3(9)	F1B	B1B	C7B	117.4(9)
F2A	B1A	N1A	108.4(8)	F2B	B1B	N1B	106.9(9)
F2A	B1A	C7A	116.4(9)	F2B	B1B	C7B	113.4(9)
C7A	B1A	N1A	99.3(8)	N1B	B1B	C7B	97.2(8)

Table 6 Hydrogen Atom Coordinates ($\text{Å}\times10^4$) and Isotropic Displacement Parameters ($\text{Å}^2\times10^3$) for OJH376k_0m.

| Atom	x	y	z	U(eq)
H1A	8520	2758	1169	37
H2A	9339	3202	-541	47
H3A	8597	5240	-1774	50
H4A	7021	6843	-1287	41
H9A	3258	8091	2203	45
H10A	3770	9258	488	48
H11A	5312	8213	-498	42
H1B	6451	-2220	6153	42
H2B	5738	-1821	4482	44
H3B	6389	242	3242	46
H4B	7950	1851	3713	41
H9B	11744	3116	7185	42
H10B	11209	4254	5472	46
H11B	9701	3194	4516	43

*Figure 237: ORTEP of **355**, ellipsoids are shown at 50% probability*

Table 1 Crystal data and structure refinement for 355

Identification code	OJH399v_0m
Empirical formula	$C_{15}H_7BF_7N$
Formula weight	345.03
Temperature/K	100.01
Crystal system	monoclinic
Space group	$P2_1/n$
a/Å	11.0976(5)
b/Å	8.9576(4)
c/Å	13.9824(6)
α/°	90
β/°	95.627(3)
γ/°	90
Volume/Å^3	1383.26(11)
Z	4

ρ_{calc}g/cm^3	1.657	
μ/mm^{-1}	1.461	
F(000)	688.0	
Crystal size/mm^3	0.204 × 0.158 × 0.02	
Radiation	CuKα (λ = 1.54178)	
2Θ range for data collection/°	9.724 to 133.54	
Index ranges	-13 ≤ h ≤ 11, -10 ≤ k ≤ 9, -15 ≤ l ≤ 16	
Reflections collected	21294	
Independent reflections	2410 [R_{int} = 0.1367, R_{sigma} = 0.0797]	
Data/restraints/parameters	2410/204/193	
Goodness-of-fit on F^2	1.267	
Final R indexes [I>=2σ (I)]	R_1 = 0.1308, wR_2 = 0.2202	
Final R indexes [all data]	R_1 = 0.1540, wR_2 = 0.2283	
Largest diff. peak/hole / e Å^{-3}	0.47/-0.54	

Table 2 Fractional Atomic Coordinates (×10^4) and Equivalent Isotropic Displacement Parameters (Å^2×10^3) for OJH399v_0m. U_{eq} is defined as 1/3 of of the trace of the orthogonalised U_{IJ} tensor.

Atom	x	y	z	U(eq)
F1	7003(3)	7916(4)	7128(3)	14.4(9)
F2	4296(4)	3994(5)	9202(3)	26.4(11)
F3	5043(4)	2365(5)	8304(3)	24.1(10)
F4	6187(4)	3462(5)	9413(3)	20.1(10)
F5	4754(4)	9083(5)	7672(3)	28.1(11)
F6	3227(4)	10289(5)	7021(3)	32.2(12)
F7	3066(4)	7963(5)	7351(3)	33.4(12)
N1	6852(5)	5939(6)	5926(4)	9.5(6)
C1	5124(6)	7610(7)	5942(5)	9.5(6)
C2	4144(6)	8558(8)	6030(5)	11.1(13)
C3	3436(7)	9091(8)	5229(5)	15.5(15)
C4	3659(6)	8658(8)	4311(5)	14.7(15)
C5	4618(6)	7694(8)	4202(5)	14.8(15)
C6	5324(6)	7204(7)	4997(5)	9.5(6)
C7	6379(6)	6200(7)	5014(5)	9.5(6)
C8	6879(7)	5507(8)	4253(5)	15.3(15)
C9	7865(7)	4599(8)	4453(5)	20.1(16)
C10	8338(7)	4367(8)	5392(5)	19.1(16)
C11	7807(6)	5051(8)	6129(5)	15.8(15)
C12	5754(6)	5742(8)	7477(5)	11.9(14)
C13	5507(6)	4856(8)	8062(5)	11.7(14)
C14	5267(6)	3679(7)	8743(5)	11.6(13)

Table 2 Fractional Atomic Coordinates (×10⁴) and Equivalent Isotropic Displacement Parameters (Å²×10³) for OJH399v_0m. U$_{eq}$ is defined as 1/3 of of the trace of the orthogonalised U$_{IJ}$ tensor.

Atom	x	y	z	U(eq)
C15	3805(6)	8989(8)	7014(5)	15.6(14)
B1	6164(7)	6888(8)	6688(5)	9.5(6)

Table 3 Anisotropic Displacement Parameters (Å²×10³) for OJH399v_0m. The Anisotropic displacement factor exponent takes the form: -2π²[h²a*²U₁₁+2hka*b*U₁₂+…].

Atom	U$_{11}$	U$_{22}$	U$_{33}$	U$_{23}$	U$_{13}$	U$_{12}$
F1	16(2)	12(2)	16(2)	−5.6(16)	6.1(16)	−3.6(16)
F2	19(2)	32(3)	32(3)	3(2)	21(2)	4(2)
F3	37(3)	12(2)	24(2)	−2.7(18)	8(2)	−12.2(19)
F4	18(2)	22(2)	19(2)	3.7(18)	−1.9(17)	0.0(18)
F5	20(2)	44(3)	20(2)	−13(2)	0.6(18)	6(2)
F6	38(3)	27(3)	32(3)	−10(2)	7(2)	20(2)
F7	41(3)	37(3)	25(3)	−9(2)	21(2)	−16(2)
N1	13.7(15)	4.3(14)	10.8(14)	−0.5(11)	3.5(12)	−3.2(11)
C1	13.7(15)	4.3(14)	10.8(14)	−0.5(11)	3.5(12)	−3.2(11)
C2	8(3)	8(3)	19(3)	1(2)	9(2)	−2(2)
C3	15(4)	12(4)	20(3)	3(3)	3(3)	−2(3)
C4	13(3)	18(4)	13(3)	5(3)	−1(3)	−2(3)
C5	15(4)	22(4)	8(3)	3(3)	5(3)	−2(3)
C6	13.7(15)	4.3(14)	10.8(14)	−0.5(11)	3.5(12)	−3.2(11)
C7	13.7(15)	4.3(14)	10.8(14)	−0.5(11)	3.5(12)	−3.2(11)
C8	22(4)	16(4)	7(3)	−6(3)	3(3)	−4(3)
C9	26(4)	15(4)	20(3)	−1(3)	11(3)	4(3)
C10	15(4)	18(4)	25(3)	1(3)	6(3)	3(3)
C11	16(4)	10(4)	21(4)	3(3)	3(3)	3(3)
C12	16(4)	10(3)	11(3)	−5(2)	5(3)	4(3)
C13	5(3)	12(3)	18(3)	−1(2)	1(3)	−2(3)
C14	11(3)	9(3)	16(3)	−4(2)	6(2)	−1(3)
C15	16(3)	14(3)	18(3)	−1(3)	4(3)	4(3)
B1	13.7(15)	4.3(14)	10.8(14)	−0.5(11)	3.5(12)	−3.2(11)

Table 4 Bond Lengths for OJH399v_0m.

Atom	Atom	Length/Å	Atom	Atom	Length/Å
F1	B1	1.408(8)	C2	C3	1.389(10)
F2	C14	1.337(7)	C2	C15	1.512(9)
F3	C14	1.340(8)	C3	C4	1.386(10)
F4	C14	1.331(8)	C4	C5	1.391(10)

Table 4 Bond Lengths for OJH399v_0m.

Atom	Atom	Length/Å	Atom	Atom	Length/Å
F5	C15	1.332(8)	C5	C6	1.368(10)
F6	C15	1.330(8)	C6	C7	1.476(9)
F7	C15	1.347(8)	C7	C8	1.393(9)
N1	C7	1.351(8)	C8	C9	1.371(10)
N1	C11	1.333(9)	C9	C10	1.380(10)
N1	B1	1.613(9)	C10	C11	1.379(10)
C1	C2	1.395(9)	C12	C13	1.190(10)
C1	C6	1.409(9)	C12	B1	1.605(10)
C1	B1	1.612(10)	C13	C14	1.463(9)

Table 5 Bond Angles for OJH399v_0m.

Atom	Atom	Atom	Angle/°	Atom	Atom	Atom	Angle/°
C7	N1	B1	111.5(5)	N1	C11	C10	119.7(7)
C11	N1	C7	122.1(6)	C13	C12	B1	176.5(7)
C11	N1	B1	126.3(6)	C12	C13	C14	175.3(7)
C2	C1	C6	115.8(6)	F2	C14	F3	106.4(5)
C2	C1	B1	134.6(6)	F2	C14	C13	111.6(6)
C6	C1	B1	109.6(6)	F3	C14	C13	111.9(6)
C1	C2	C15	120.1(6)	F4	C14	F2	107.0(5)
C3	C2	C1	121.5(6)	F4	C14	F3	106.8(5)
C3	C2	C15	118.3(6)	F4	C14	C13	112.8(6)
C4	C3	C2	120.8(7)	F5	C15	F7	105.7(6)
C3	C4	C5	118.9(7)	F5	C15	C2	113.2(6)
C6	C5	C4	119.6(6)	F6	C15	F5	106.8(6)
C1	C6	C7	109.9(6)	F6	C15	F7	106.5(6)
C5	C6	C1	123.3(6)	F6	C15	C2	113.1(6)
C5	C6	C7	126.8(6)	F7	C15	C2	111.0(6)
N1	C7	C6	110.8(6)	F1	B1	N1	107.3(5)
N1	C7	C8	119.8(6)	F1	B1	C1	114.9(6)
C8	C7	C6	129.4(6)	F1	B1	C12	109.7(6)
C9	C8	C7	118.5(7)	C1	B1	N1	98.0(5)
C8	C9	C10	120.3(7)	C12	B1	N1	107.6(5)
C9	C10	C11	119.5(7)	C12	B1	C1	117.9(6)

Table 6 Torsion Angles for OJH399v_0m.

A	B	C	D	Angle/°	A	B	C	D	Angle/°
N1	C7	C8	C9	-1.5(10)	C6	C1	B1	N1	-4.3(7)
C1	C2	C3	C4	2.0(11)	C6	C1	B1	C12	-119.1(6)
C1	C2	C15	F5	32.7(9)	C6	C7	C8	C9	-179.2(7)

Table 6 Torsion Angles for OJH399v_0m.

A	B	C	D	Angle/°	A	B	C	D	Angle/°
C1	C2	C15	F6	154.4(6)	C7	N1	C11	C10	−0.1(10)
C1	C2	C15	F7	−85.9(8)	C7	N1	B1	F1	−114.6(6)
C1	C6	C7	N1	0.5(8)	C7	N1	B1	C1	4.7(7)
C1	C6	C7	C8	178.4(7)	C7	N1	B1	C12	127.4(6)
C2	C1	C6	C5	0.1(10)	C7	C8	C9	C10	0.7(11)
C2	C1	C6	C7	−179.7(6)	C8	C9	C10	C11	0.4(11)
C2	C1	B1	F1	−67.8(10)	C9	C10	C11	N1	−0.7(11)
C2	C1	B1	N1	178.8(7)	C11	N1	C7	C6	179.3(6)
C2	C1	B1	C12	64.0(10)	C11	N1	C7	C8	1.2(10)
C2	C3	C4	C5	−0.9(11)	C11	N1	B1	F1	62.3(8)
C3	C2	C15	F5	−149.3(6)	C11	N1	B1	C1	−178.4(6)
C3	C2	C15	F6	−27.6(9)	C11	N1	B1	C12	−55.6(8)
C3	C2	C15	F7	92.1(8)	C15	C2	C3	C4	−176.0(6)
C3	C4	C5	C6	−0.5(10)	B1	N1	C7	C6	−3.6(7)
C4	C5	C6	C1	0.9(11)	B1	N1	C7	C8	178.3(6)
C4	C5	C6	C7	−179.3(6)	B1	N1	C11	C10	−176.7(6)
C5	C6	C7	N1	−179.3(6)	B1	C1	C2	C3	175.2(7)
C5	C6	C7	C8	−1.4(12)	B1	C1	C2	C15	−6.8(11)
C6	C1	C2	C3	−1.6(10)	B1	C1	C6	C5	−177.4(6)
C6	C1	C2	C15	176.4(6)	B1	C1	C6	C7	2.7(7)
C6	C1	B1	F1	109.1(6)					

Table 7 Hydrogen Atom Coordinates ($Å×10^4$) and Isotropic Displacement Parameters ($Å^2×10^3$) for OJH399v_0m.

Atom	x	y	z	U(eq)
H3	2790.13	9761.18	5310.79	19
H4	3164.25	9014.4	3765.32	18
H5	4781.9	7377.44	3579.05	18
H8	6544.23	5661.55	3608.61	18
H9	8225.35	4125.25	3943.9	24
H10	9024.35	3741.9	5529.6	23
H11	8119.86	4890.38	6777.23	19

Crystal structure determination of 355

Crystal Data for $C_{15}H_7BF_7N$ ($M =345.03$ g/mol): monoclinic, space group P2$_1$/n (no. 14), $a =$ 11.0976(5) Å, $b =$ 8.9576(4) Å, $c =$ 13.9824(6) Å, $\beta =$ 95.627(3)°, $V =$ 1383.26(11) Å^3, $Z =$ 4, $T =$ 100.01 K, μ(CuKα) = 1.461 mm^{-1}, $Dcalc$ = 1.657 g/cm^3, 21294 reflections measured (9.724° ≤ 2Θ ≤ 133.54°), 2410 unique (R_{int} = 0.1367, R$_{sigma}$ = 0.0797) which were used in all calculations. The final R_1 was 0.1308 (I > 2σ(I)) and wR_2 was 0.2283 (all data).
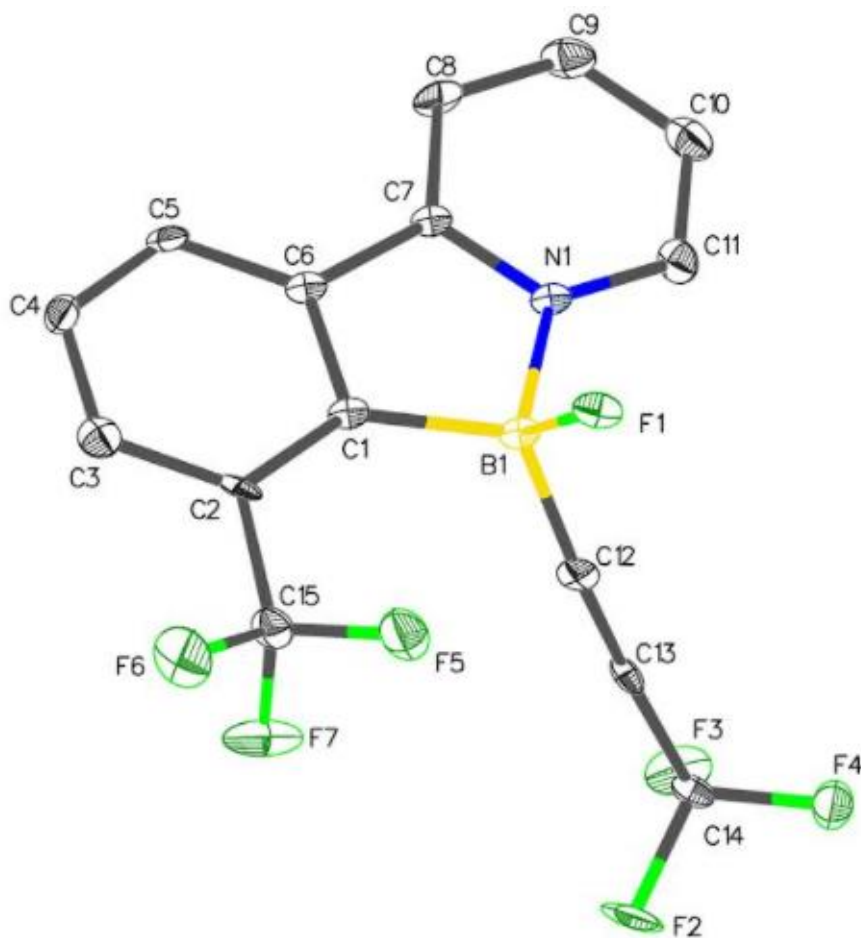
X-Ray crystallographic analysis for compound 356
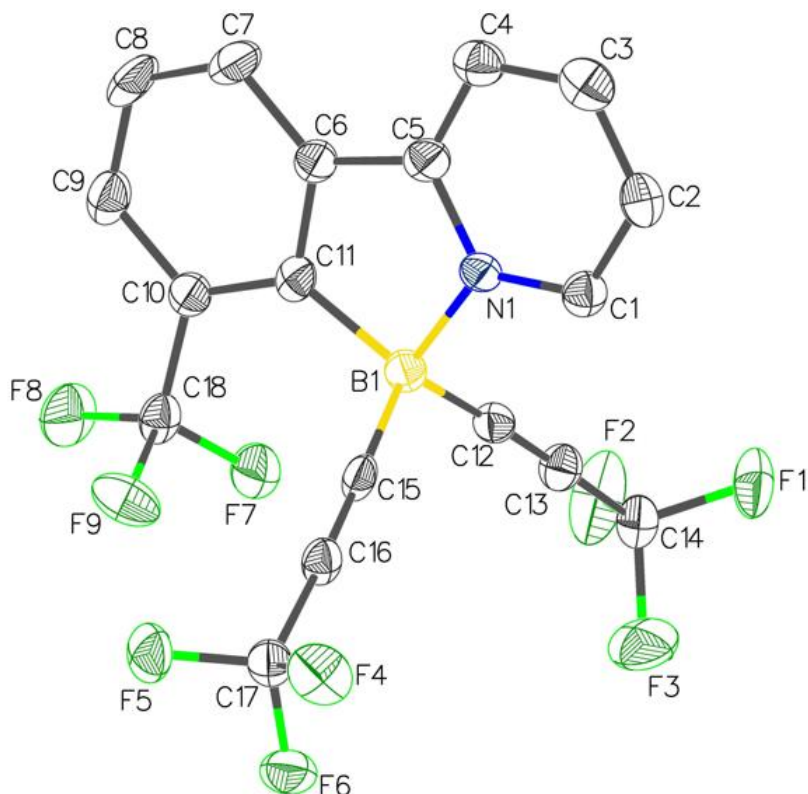
*Figure 238: ORTEP of **356**, ellipsoids are shown at 50% probability*

Table 1 Crystal data and structure refinement for 356.

Identification code	OJH401v_0m
Empirical formula	$C_{18}H_7BF_9N$
Formula weight	419.06
Temperature/K	100.0
Crystal system	monoclinic
Space group	$P2_1/c$
a/Å	8.7139(7)
b/Å	25.541(2)
c/Å	8.6369(7)
α/°	90
β/°	118.650(4)
γ/°	90
Volume/Å^3	1686.9(2)
Z	4
ρ_{calc}g/cm^3	1.650
μ/mm^{-1}	1.498
F(000)	832.0
Crystal size/mm^3	$0.388 \times 0.208 \times 0.08$

Radiation	CuKα (λ = 1.54178)		
2Θ range for data collection/°	6.922 to 134.36		
Index ranges	-7 ≤ h ≤ 10, -30 ≤ k ≤ 30, -10 ≤ l ≤ 9		
Reflections collected	8121		
Independent reflections	2925 [R_{int} = 0.0532, R_{sigma} = 0.0553]		
Data/restraints/parameters	2925/0/264		
Goodness-of-fit on F^2	1.077		
Final R indexes [I>=2σ (I)]	R_1 = 0.0715, wR_2 = 0.2040		
Final R indexes [all data]	R_1 = 0.0791, wR_2 = 0.2227		
Largest diff. peak/hole / e Å^{-3}	0.50/-0.46		

Table 2 Fractional Atomic Coordinates (×10^4) and Equivalent Isotropic Displacement Parameters (Å^2×10^3) for OJH401v_0m. U_{eq} is defined as 1/3 of of the trace of the orthogonalised U_{IJ} tensor.

Atom	x	y	z	U(eq)
F1	2350(5)	5126.6(12)	5973(4)	41.4(8)
F2	3395(7)	5819.9(14)	7472(5)	57.3(12)
F3	5085(5)	5252.0(17)	7263(5)	58.1(11)
F4	7975(5)	5677.6(14)	657(5)	42.2(8)
F5	8671(4)	6460.4(12)	1610(5)	40.4(8)
F6	9266(4)	5833.8(13)	3455(4)	37.6(8)
F7	5301(4)	6937.0(13)	5421(5)	41.2(8)
F8	5723(5)	7753.0(13)	5245(5)	46.0(9)
F9	6591(4)	7192.1(15)	4002(4)	41.7(8)
N1	1652(5)	6067.7(15)	139(5)	21.7(8)
C1	1341(6)	5571.5(18)	−409(7)	25.0(10)
C2	−148(7)	5439.1(19)	−1984(7)	28.3(10)
C3	−1285(7)	5838(2)	−2952(7)	33.6(11)
C4	−944(7)	6350(2)	−2381(7)	29.6(11)
C5	554(6)	6459.1(19)	−786(7)	26.2(10)
C6	1189(6)	6958.7(18)	99(7)	24.6(10)
C7	417(7)	7449(2)	−493(7)	31.7(11)
C8	1216(8)	7882.9(19)	503(8)	34.9(12)
C9	2801(7)	7835.8(19)	2097(8)	31.8(12)
C10	3554(6)	7345.3(18)	2655(7)	24.7(10)
C11	2764(6)	6893.7(18)	1684(6)	22.9(10)
C12	3326(6)	5987.4(17)	3560(6)	23.4(10)
C13	3416(7)	5757.5(17)	4813(7)	25.0(10)
C14	3552(7)	5495.7(19)	6360(7)	30.0(11)
C15	5019(6)	6160.6(16)	1828(7)	22.7(10)
C16	6372(7)	6082.4(17)	1815(7)	24.0(10)

Table 2 Fractional Atomic Coordinates (×10⁴) and Equivalent Isotropic Displacement Parameters (Å²×10³) for OJH401v_0m. U_{eq} is defined as 1/3 of of the trace of the orthogonalised U_{IJ} tensor.

Atom	x	y	z	U(eq)
C17	8043(7)	6017.8(19)	1873(7)	26.1(10)
C18	5274(7)	7309.5(18)	4328(7)	25.4(10)
B1	3298(7)	6278(2)	1929(7)	21.8(11)

Table 3 Anisotropic Displacement Parameters (Å²×10³) for OJH401v_0m. The Anisotropic displacement factor exponent takes the form: -$2\pi^2[h^2a^{*2}U_{11}+2hka^*b^*U_{12}+...]$.

Atom	U_{11}	U_{22}	U_{33}	U_{23}	U_{13}	U_{12}
F1	56(2)	31.6(16)	39.8(18)	1.8(14)	25.7(16)	−16.6(15)
F2	112(4)	36.1(18)	47(2)	−9.5(17)	57(2)	−15(2)
F3	45(2)	74(3)	48(2)	36.2(19)	16.8(17)	12.5(18)
F4	40.9(18)	47.0(18)	47(2)	−17.8(15)	27.9(15)	0.4(15)
F5	39.6(18)	33.0(16)	62(2)	6.8(14)	35.1(17)	−2.8(13)
F6	25.2(15)	43.8(17)	43.4(19)	11.2(14)	16.1(13)	6.6(13)
F7	36.8(18)	39.3(17)	42.9(19)	10.2(14)	15.4(14)	−4.6(13)
F8	54(2)	27.0(15)	49(2)	−13.5(14)	17.5(16)	−0.6(14)
F9	25.5(16)	65(2)	39.1(18)	−6.6(16)	19.1(13)	0.9(15)
N1	17.5(18)	23.5(18)	26(2)	2.0(15)	12.0(15)	1.6(15)
C1	26(2)	23(2)	29(2)	−0.8(18)	16(2)	1.5(18)
C2	31(3)	28(2)	30(3)	−3(2)	18(2)	−6(2)
C3	31(3)	41(3)	31(3)	−3(2)	16(2)	−2(2)
C4	26(2)	35(3)	26(2)	3(2)	12(2)	1(2)
C5	24(2)	28(2)	33(3)	5(2)	19(2)	4.7(19)
C6	23(2)	23(2)	33(3)	3.7(19)	18(2)	3.1(18)
C7	33(3)	28(2)	37(3)	12(2)	19(2)	12(2)
C8	46(3)	19(2)	50(3)	10(2)	31(3)	14(2)
C9	38(3)	21(2)	45(3)	0(2)	26(3)	1(2)
C10	24(2)	24(2)	33(3)	3.0(19)	18(2)	2.0(18)
C11	26(2)	23(2)	28(2)	5.8(19)	20(2)	1.8(18)
C12	19(2)	21(2)	30(2)	−0.5(19)	11.5(18)	0.9(17)
C13	28(2)	22(2)	26(2)	−1.0(19)	14.1(19)	−0.3(17)
C14	34(3)	24(2)	34(3)	1(2)	18(2)	−4(2)
C15	29(3)	12.5(18)	31(2)	1.4(17)	17(2)	0.3(17)
C16	27(2)	18(2)	33(3)	−1.6(17)	20(2)	0.4(17)
C17	26(2)	24(2)	32(3)	−2.0(19)	18(2)	0.3(19)
C18	32(3)	18(2)	34(3)	−2.7(19)	22(2)	0.5(18)
B1	21(3)	21(2)	25(3)	−1(2)	12(2)	0.1(19)

Table 4 Bond Lengths for OJH401v_0m.

Atom	Atom	Length/Å	Atom	Atom	Length/Å
F1	C14	1.328(6)	C5	C6	1.453(7)
F2	C14	1.324(7)	C6	C7	1.397(7)
F3	C14	1.334(6)	C6	C11	1.408(7)
F4	C17	1.342(6)	C7	C8	1.371(8)
F5	C17	1.322(6)	C8	C9	1.413(9)
F6	C17	1.352(6)	C9	C10	1.389(7)
F7	C18	1.333(6)	C10	C11	1.398(7)
F8	C18	1.329(6)	C10	C18	1.506(7)
F9	C18	1.340(6)	C11	B1	1.626(7)
N1	C1	1.334(6)	C12	C13	1.200(7)
N1	C5	1.349(6)	C12	B1	1.582(7)
N1	B1	1.615(7)	C13	C14	1.447(7)
C1	C2	1.398(7)	C15	C16	1.201(7)
C2	C3	1.388(8)	C15	B1	1.572(7)
C3	C4	1.378(8)	C16	C17	1.443(7)
C4	C5	1.399(7)			

Table 5 Bond Angles for OJH401v_0m.

Atom	Atom	Atom	Angle/°	Atom	Atom	Atom	Angle/°
C1	N1	C5	121.9(4)	F1	C14	C13	113.0(4)
C1	N1	B1	126.2(4)	F2	C14	F1	106.4(4)
C5	N1	B1	111.9(4)	F2	C14	F3	106.9(5)
N1	C1	C2	120.7(4)	F2	C14	C13	112.9(4)
C3	C2	C1	118.0(5)	F3	C14	C13	111.8(4)
C4	C3	C2	120.8(5)	C16	C15	B1	177.3(5)
C3	C4	C5	118.7(5)	C15	C16	C17	176.3(5)
N1	C5	C4	119.9(5)	F4	C17	F6	106.5(4)
N1	C5	C6	110.9(4)	F4	C17	C16	112.4(4)
C4	C5	C6	129.3(5)	F5	C17	F4	106.6(4)
C7	C6	C5	126.8(5)	F5	C17	F6	106.3(4)
C7	C6	C11	122.4(5)	F5	C17	C16	113.0(4)
C11	C6	C5	110.8(4)	F6	C17	C16	111.6(4)
C8	C7	C6	119.0(5)	F7	C18	F9	105.2(4)
C7	C8	C9	120.5(5)	F7	C18	C10	113.2(4)
C10	C9	C8	119.6(5)	F8	C18	F7	106.6(4)
C9	C10	C11	121.4(5)	F8	C18	F9	106.2(4)
C9	C10	C18	118.3(4)	F8	C18	C10	113.2(4)
C11	C10	C18	120.2(4)	F9	C18	C10	111.8(4)
C6	C11	B1	109.0(4)	N1	B1	C11	97.4(4)
C10	C11	C6	117.1(4)	C12	B1	N1	108.9(4)
C10	C11	B1	133.8(5)	C12	B1	C11	116.8(4)

Table 5 Bond Angles for OJH401v_0m.

Atom	Atom	Atom	Angle/°	Atom	Atom	Atom	Angle/°
C13	C12	B1	177.1(5)	C15	B1	N1	108.5(4)
C12	C13	C14	178.1(5)	C15	B1	C11	113.5(4)
F1	C14	F3	105.3(4)	C15	B1	C12	110.7(4)

Table 6 Torsion Angles for OJH401v_0m.

A	B	C	D	Angle/°	A	B	C	D	Angle/°
N1	C1	C2	C3	0.0(7)	C6	C11	B1	C15	113.7(5)
N1	C5	C6	C7	178.3(5)	C7	C6	C11	C10	-0.7(7)
N1	C5	C6	C11	-0.6(6)	C7	C6	C11	B1	-178.6(4)
C1	N1	C5	C4	-1.1(7)	C7	C8	C9	C10	0.1(8)
C1	N1	C5	C6	179.8(4)	C8	C9	C10	C11	-0.9(7)
C1	N1	B1	C11	-179.4(4)	C8	C9	C10	C18	178.0(5)
C1	N1	B1	C12	-57.8(6)	C9	C10	C11	C6	1.2(7)
C1	N1	B1	C15	62.7(6)	C9	C10	C11	B1	178.4(5)
C1	C2	C3	C4	0.6(8)	C9	C10	C18	F7	132.6(5)
C2	C3	C4	C5	-1.3(8)	C9	C10	C18	F8	11.1(7)
C3	C4	C5	N1	1.6(7)	C9	C10	C18	F9	-108.7(5)
C3	C4	C5	C6	-179.5(5)	C10	C11	B1	N1	-177.5(5)
C4	C5	C6	C7	-0.7(8)	C10	C11	B1	C12	67.0(7)
C4	C5	C6	C11	-179.7(5)	C10	C11	B1	C15	-63.6(7)
C5	N1	C1	C2	0.3(7)	C11	C6	C7	C8	-0.1(8)
C5	N1	B1	C11	-0.2(5)	C11	C10	C18	F7	-48.5(6)
C5	N1	B1	C12	121.4(4)	C11	C10	C18	F8	-170.0(4)
C5	N1	B1	C15	-118.1(4)	C11	C10	C18	F9	70.2(6)
C5	C6	C7	C8	-178.9(5)	C18	C10	C11	C6	-177.7(4)
C5	C6	C11	C10	178.3(4)	C18	C10	C11	B1	-0.5(8)
C5	C6	C11	B1	0.5(5)	B1	N1	C1	C2	179.4(4)
C6	C7	C8	C9	0.4(8)	B1	N1	C5	C4	179.7(4)
C6	C11	B1	N1	-0.2(5)	B1	N1	C5	C6	0.5(5)
C6	C11	B1	C12	-115.7(5)					

Table 7 Hydrogen Atom Coordinates (Å×10⁴) and Isotropic Displacement Parameters (Å²×10³) for OJH401v_0m.

Atom	x	y	z	U(eq)
H1	2139.27	5305.33	278.2	30
H2	-374.28	5086.37	-2379.12	34
H3	-2311.21	5757.84	-4021.42	40
H4	-1711.61	6623.75	-3058.87	36
H7	-645.7	7481.01	-1569.11	38
H8	698.67	8218.03	117.52	42

Table 7 Hydrogen Atom Coordinates ($Å\times10^4$) and Isotropic Displacement Parameters ($Å^2\times10^3$) for OJH401v_0m.

Atom	x	y	z	U(eq)
H9	3349.52	8137.73	2783.4	38

Crystal structure determination of 356

   Crystal Data for $C_{18}H_7BF_9N$ (M =419.06 g/mol): monoclinic, space group P2$_1$/c (no. 14), a = 8.7139(7) Å, b = 25.541(2) Å, c = 8.6369(7) Å, β = 118.650(4)°, V = 1686.9(2) Å^3, Z = 4, T = 100.0 K, μ(CuKα) = 1.498 mm^{-1}, $Dcalc$ = 1.650 g/cm^3, 8121 reflections measured (6.922° ≤ 2Θ ≤ 134.36°), 2925 unique (R_{int} = 0.0532, R$_{sigma}$ = 0.0553) which were used in all calculations. The final R_1 was 0.0715 (I > 2σ(I)) and wR_2 was 0.2227 (all data).

X-Ray crystallographic analysis for compound 377
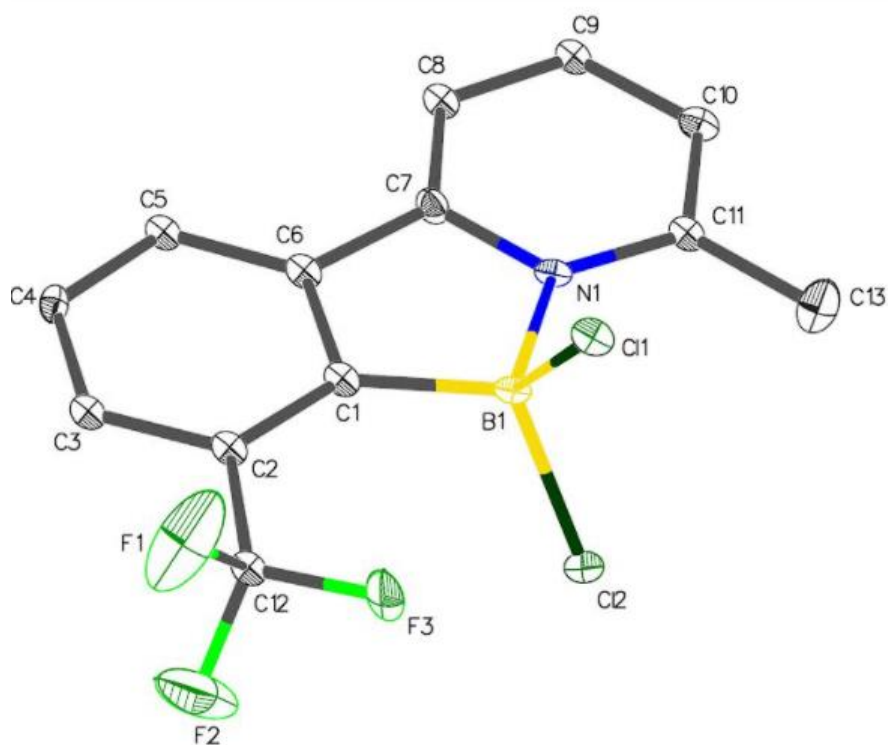
*Figure 239: ORTEP of **377**, ellipsoids are plotted at 50% probability*

Table 1 Crystal data and structure refinement for 377.

Identification code	OJH398v_0m
Empirical formula	$C_{13}H_9BCl_2F_3N$
Formula weight	317.92
Temperature/K	99.98
Crystal system	monoclinic
Space group	$P2_1/c$
a/Å	7.0180(4)
b/Å	11.5879(7)
c/Å	16.0847(9)
α/°	90
β/°	91.868(2)
γ/°	90
Volume/Å^3	1307.38(13)
Z	4
ρ_{calc}g/cm^3	1.615
μ/mm^{-1}	4.700
F(000)	640.0
Crystal size/mm^3	$0.5 \times 0.24 \times 0.22$

Radiation	CuKα (λ = 1.54178)		
2Θ range for data collection/°	5.498 to 133.514		
Index ranges	-8 ≤ h ≤ 8, 0 ≤ k ≤ 13, 0 ≤ l ≤ 19		
Reflections collected	3196		
Independent reflections	2142 [R_{int} = 0.0922, R_{sigma} = 0.0843]		
Data/restraints/parameters	2142/168/129		
Goodness-of-fit on F^2	2.792		
Final R indexes [I>=2σ (I)]	R_1 = 0.2109, wR_2 = 0.5471		
Final R indexes [all data]	R_1 = 0.2229, wR_2 = 0.5667		
Largest diff. peak/hole / e Å^{-3}	3.43/-1.84		

Table 2 Fractional Atomic Coordinates (×10^4) and Equivalent Isotropic Displacement Parameters (Å^2×10^3) for OJH398v_0m. U_{eq} is defined as 1/3 of of the trace of the orthogonalised U_{IJ} tensor.

Atom	x	y	z	U(eq)
Cl1	4767(4)	6212(2)	7109.6(19)	11.2(11)
Cl2	379(4)	6292(3)	7067.2(19)	10.9(11)
F1	4060(20)	9510(11)	5777(7)	59(4)
F2	969(19)	9403(11)	5797(8)	56(4)
F3	2709(16)	8528(7)	6698(5)	27(2)
N1	2491(15)	4689(9)	6180(6)	7.7(18)
C1	2567(19)	6615(11)	5584(8)	9.2(13)
C2	2616(18)	7763(11)	5317(8)	9.2(13)
C3	2606(18)	8022(11)	4475(8)	9.2(13)
C4	2636(18)	7166(11)	3879(7)	10(2)
C5	2567(18)	6006(11)	4116(8)	9.2(13)
C6	2563(18)	5769(11)	4960(7)	9.2(13)
C7	2517(19)	4591(11)	5322(8)	11(3)
C8	2468(18)	3551(11)	4932(8)	9.2(13)
C9	2412(17)	2550(10)	5393(7)	9.2(13)
C10	2397(18)	2635(11)	6276(8)	11(3)
C11	2399(19)	3712(10)	6658(8)	9.2(13)
C12	2580(19)	8784(10)	5888(8)	9.2(13)
C13	2350(30)	3818(11)	7588(9)	22(4)
B1	2530(20)	5977(12)	6459(8)	7.7(18)

Table 3 Anisotropic Displacement Parameters ($Å^2\times10^3$) for OJH398v_0m. The Anisotropic displacement factor exponent takes the form: -$2\pi^2[h^2a^{*2}U_{11}+2hka^*b^*U_{12}+...]$.

Atom	U_{11}	U_{22}	U_{33}	U_{23}	U_{13}	U_{12}
Cl1	10(2)	8.6(17)	15.1(18)	−3.3(11)	−3.7(13)	−2.7(11)
Cl2	9.3(19)	10.3(17)	13.3(18)	−2.2(10)	1.2(13)	−0.3(12)
F1	93(8)	50(7)	35(6)	−23(5)	22(6)	−59(6)
F2	70(6)	52(7)	44(7)	−24(6)	−25(5)	44(6)
F3	62(7)	6(4)	13(4)	−2(3)	0(4)	5(4)
N1	6(4)	7(4)	10(3)	−4(2)	−2(3)	−1(3)
C1	7(2)	8(2)	12(2)	−0.3(14)	−2.3(17)	−1.5(15)
C2	7(2)	8(2)	12(2)	−0.3(14)	−2.3(17)	−1.5(15)
C3	7(2)	8(2)	12(2)	−0.3(14)	−2.3(17)	−1.5(15)
C4	7(6)	14(4)	8(4)	2(3)	−2(4)	−2(4)
C5	7(2)	8(2)	12(2)	−0.3(14)	−2.3(17)	−1.5(15)
C6	7(2)	8(2)	12(2)	−0.3(14)	−2.3(17)	−1.5(15)
C7	14(7)	8(4)	12(4)	1(3)	0(4)	0(4)
C8	7(2)	8(2)	12(2)	−0.3(14)	−2.3(17)	−1.5(15)
C9	7(2)	8(2)	12(2)	−0.3(14)	−2.3(17)	−1.5(15)
C10	8(7)	10(5)	14(4)	−2(4)	−2(5)	0(4)
C11	7(2)	8(2)	12(2)	−0.3(14)	−2.3(17)	−1.5(15)
C12	7(2)	8(2)	12(2)	−0.3(14)	−2.3(17)	−1.5(15)
C13	45(10)	8(7)	14(5)	−6(4)	6(6)	−10(6)
B1	6(4)	7(4)	10(3)	−4(2)	−2(3)	−1(3)

Table 4 Bond Lengths for OJH398v_0m.

Atom	Atom	Length/Å	Atom	Atom	Length/Å
Cl1	B1	1.875(14)	C2	C3	1.388(18)
Cl2	B1	1.864(15)	C2	C12	1.498(17)
F1	C12	1.351(16)	C3	C4	1.379(17)
F2	C12	1.343(17)	C4	C5	1.399(17)
F3	C12	1.337(15)	C5	C6	1.386(16)
N1	C7	1.384(15)	C6	C7	1.484(17)
N1	C11	1.372(16)	C7	C8	1.358(18)
N1	B1	1.559(15)	C8	C9	1.377(17)
C1	C2	1.398(17)	C9	C10	1.425(16)
C1	C6	1.403(17)	C10	C11	1.391(17)
C1	B1	1.592(18)	C11	C13	1.50(2)

Table 5 Bond Angles for OJH398v_0m.

Atom	Atom	Atom	Angle/°	Atom	Atom	Atom	Angle/°
C7	N1	B1	111.4(10)	C7	C8	C9	120.0(12)

Table 5 Bond Angles for OJH398v_0m.

Atom	Atom	Atom	Angle/°	Atom	Atom	Atom	Angle/°
C11	N1	C7	119.6(10)	C8	C9	C10	118.7(11)
C11	N1	B1	129.0(10)	C11	C10	C9	120.2(12)
C2	C1	C6	116.5(12)	N1	C11	C10	119.5(12)
C2	C1	B1	135.6(11)	N1	C11	C13	119.6(10)
C6	C1	B1	107.9(10)	C10	C11	C13	120.9(11)
C1	C2	C12	124.2(12)	F1	C12	C2	112.5(11)
C3	C2	C1	120.4(12)	F2	C12	F1	107.4(13)
C3	C2	C12	115.4(11)	F2	C12	C2	112.7(11)
C4	C3	C2	121.5(12)	F3	C12	F1	103.8(11)
C3	C4	C5	120.0(11)	F3	C12	F2	104.7(11)
C6	C5	C4	117.3(12)	F3	C12	C2	114.9(10)
C1	C6	C7	111.2(11)	Cl2	B1	Cl1	110.9(7)
C5	C6	C1	124.2(12)	N1	B1	Cl1	107.9(9)
C5	C6	C7	124.6(11)	N1	B1	Cl2	109.3(9)
N1	C7	C6	108.5(10)	N1	B1	C1	101.0(9)
C8	C7	N1	122.1(11)	C1	B1	Cl1	113.0(10)
C8	C7	C6	129.4(11)	C1	B1	Cl2	114.1(10)

Table 6 Torsion Angles for OJH398v_0m.

A	B	C	D	Angle/°	A	B	C	D	Angle/°
N1	C7	C8	C9	−1(2)	C6	C1	B1	N1	−0.6(14)
C1	C2	C3	C4	−3(2)	C6	C7	C8	C9	−179.4(13)
C1	C2	C12	F1	125.6(15)	C7	N1	C11	C10	2.1(19)
C1	C2	C12	F2	−112.8(16)	C7	N1	C11	C13	−179.5(14)
C1	C2	C12	F3	7(2)	C7	N1	B1	Cl1	−118.1(10)
C1	C6	C7	N1	0.1(15)	C7	N1	B1	Cl2	121.2(10)
C1	C6	C7	C8	178.8(14)	C7	N1	B1	C1	0.6(14)
C2	C1	C6	C5	−1(2)	C7	C8	C9	C10	0.4(18)
C2	C1	C6	C7	179.7(12)	C8	C9	C10	C11	1.3(19)
C2	C1	B1	Cl1	−65(2)	C9	C10	C11	N1	−2.5(19)
C2	C1	B1	Cl2	63(2)	C9	C10	C11	C13	179.1(13)
C2	C1	B1	N1	−179.8(15)	C11	N1	C7	C6	178.4(11)
C2	C3	C4	C5	4(2)	C11	N1	C7	C8	0(2)
C3	C2	C12	F1	−57.5(16)	C11	N1	B1	Cl1	63.2(15)
C3	C2	C12	F2	64.1(16)	C11	N1	B1	Cl2	−57.5(15)
C3	C2	C12	F3	−176.0(12)	C11	N1	B1	C1	−178.1(12)
C3	C4	C5	C6	−3(2)	C12	C2	C3	C4	−180.0(12)
C4	C5	C6	C1	2(2)	B1	N1	C7	C6	−0.5(15)
C4	C5	C6	C7	−179.2(11)	B1	N1	C7	C8	−179.3(12)
C5	C6	C7	N1	−178.9(13)	B1	N1	C11	C10	−179.3(12)
C5	C6	C7	C8	0(2)	B1	N1	C11	C13	−1(2)

Table 6 Torsion Angles for OJH398v_0m.

A	B	C	D	Angle/°	A	B	C	D	Angle/°
C6	C1	C2	C3	2(2)	B1	C1	C2	C3	-179.1(14)
C6	C1	C2	C12	178.4(11)	B1	C1	C2	C12	-2(3)
C6	C1	B1	Cl1	114.4(11)	B1	C1	C6	C5	179.3(13)
C6	C1	B1	Cl2	-117.7(10)	B1	C1	C6	C7	0.4(15)

Table 7 Hydrogen Atom Coordinates ($Å×10^4$) and Isotropic Displacement Parameters ($Å^2×10^3$) for OJH398v_0m.

Atom	x	y	z	U(eq)
H3	2578.83	8807.21	4304.11	11
H4	2703.19	7365.28	3307.78	12
H5	2525.38	5404.91	3714.12	11
H8	2471.59	3514.69	4342.4	11
H9	2385.31	1818.44	5126.55	11
H10	2384.93	1954	6605.04	13
H13A	3243.76	4421.46	7777.11	33
H13B	2725.35	3080.51	7844.05	33
H13C	1060.82	4019.88	7749.49	33

Crystal structure determination of 377

Crystal Data for $C_{13}H_9BCl_2F_3N$ (M =317.92 g/mol): monoclinic, space group P2$_1$/c (no. 14), a = 7.0180(4) Å, b = 11.5879(7) Å, c = 16.0847(9) Å, β = 91.868(2)°, V = 1307.38(13) Å^3, Z = 4, T = 99.98 K, μ(CuKα) = 4.700 mm^{-1}, $Dcalc$ = 1.615 g/cm^3, 3196 reflections measured (5.498° ≤ 2Θ ≤ 133.514°), 2142 unique (R_{int} = 0.0922, R$_{sigma}$ = 0.0843) which were used in all calculations. The final R_1 was 0.2109 (I > 2σ(I)) and wR_2 was 0.5667 (all data).